



Oil Well Testing Handbook

Amanat U. Chaudhry



Oil Well Testing Handbook

Amanat U. Chaudhry

Advanced TWPSOM Petroleum Systems, Inc.
Houston, Texas



AMSTERDAM BOSTON HEIDELBERG LONDON
NEW YORK OXFORD PARIS SAN DIEGO
SAN FRANCISCO SINGAPORE SYDNEY TOKYO

Gulf Professional Publishing is an imprint of Elsevier



Gulf Professional Publishing is an imprint of Elsevier
200 Wheeler Road, Burlington, MA 01803, USA
Linacre House, Jordan Hill, Oxford OX2 8DP, UK

Copyright © 2004, Elsevier Inc. All rights reserved.

No part of this publication may be reproduced, stored in a retrieval system, or transmitted in any form or by any means, electronic, mechanical, photocopying, recording, or otherwise, without the prior written permission of the publisher.

Permissions may be sought directly from Elsevier's Science & Technology Rights Department in Oxford, UK: phone: (+44) 1865 843830, fax: (+44) 1865 853333, e-mail: permissions@elsevier.com.uk. You may also complete your request on-line via the Elsevier homepage (<http://elsevier.com>), by selecting "Customer Support" and then "Obtaining Permissions."

⊗ Recognizing the importance of preserving what has been written, Elsevier prints its books on acid-free paper whenever possible.

Library of Congress Cataloging-in-Publication Data

Application submitted.

British Library Cataloguing-in-Publication Data

A catalogue record for this book is available from the British Library.

ISBN: 0-7506-7706-6

For information on all Gulf Professional Publishing publications visit our website at www.gulfpp.com

03 04 05 06 07 08 10 9 8 7 6 5 4 3 2 1

Printed in the United States of America

This book is dedicated to my son Alhaj U. Chaudhry.

I am grateful to my parents for providing me with education, inspiration, and confidence. I am also indebted to my ex-wife (Nuraini Smith) who provided the encouragement, fortitude, and extraordinary understanding, which enabled me to steal many hours from my family while writing this book.

Foreword

Although elements of oil well testing methods have been practical almost since oil reservoirs were first recognized, the concept of oil well testing techniques took form only within the past three decades. Many individual monographs and at least one manual on the subject have been published in the open literature, and it is probable that proprietary presentations of oil well testing concepts are to be found within the internal libraries of some oil-producing companies. In the present volume, the author presents a treatment of the subject to be published in book form.

The roots of oil well testing are to be found in reservoir engineering taken in its broadest sense as the technology that deals with the well/reservoir behavior through the measuring and analysis of drill-stem tests, flow, and transient pressure responses in unfractured and fractured gas wells. The concepts related to oil well test data acquisition and interpretation are presented from a practical viewpoint. These concepts are emphasized throughout the book by means of examples and field case studies.

In *Oil Well Testing Handbook*, the author has presented a comprehensive study of the measuring and analysis of flow and transient pressure responses in oil wells. The basic principles are reviewed, and the applicability and limitations of the various testing techniques are critically discussed and illustrated with actual field examples. The material is presented in a form that will allow engineers directly involved in well behavior, pressure build-up, and flow testing to re-educate themselves in the subject. At the same time, with its up-to-date review of the literature and extensive bibliography, the book will serve as a useful guide and reference to engineers directly engaged in well pressure behavior work. The author has accomplished the intended objectives of the book in a thorough and excellent manner.

The author has illustrated field application examples and field case studies to describe the type of wells and reservoir behavior encountered in modern production practice. The source, nature, and precision of the data and studies on which the calculations and analysis are based are discussed subordinately. Numerous exercises are provided to develop an understanding of the principles and limitations of applied oil well testing methods.

The book is essential and important to engineers concerned with evaluating well/reservoir systems and the pressure performance of oil wells. The author has extensive experience in this field and is most qualified to treat the subject. It is a timely addition to the literature of petroleum technology.

Dilip Borthaker
Head of Gas Engineering Department
Gulf Indonesia Resources

Preface

The major purpose of writing this book is to provide a practical reference source for knowledge regarding state-of-the-art oil well testing technology. The book presents the use of oil well testing techniques and analysis methods for the evaluation of well conditions and reservoir characteristics. All techniques and data described in this book are “field-tested” and are published here for the first time. For example, this book contains new tables and comparisons of the various methods of well test analysis. Most of these techniques and applications are clearly illustrated in worked examples of the actual field data. Several actual field example calculations and field case studies are included for illustration purposes.

This text is a must for reservoir engineers, simulation engineers, practicing petroleum engineers and professional geologists, geophysicists, and technical managers and helps engineering professors better acquaint their students with “real-life” solution problems. This instructive text includes practical worked examples that the readers should find easy to understand and reproduce.

Fundamental concepts related to well test data acquisition and interpretation are presented from a practical viewpoint. Furthermore, a brief summary of the advances in this area is presented. Emphasis is given to the most common interpretation methods used at present. The main emphasis is on practical solutions and field application. More than 129 field examples are presented to illustrate effective oil well testing practices, most analysis techniques and their applications.

Many solutions, which are presented, are based upon author’s experience dealing with various well testing techniques and interpretation around the world. I am very thankful to the many companies with whom I had the opportunity to work in well test analysis for many years.

A properly designed, executed, and analyzed well test can provide information about formation permeability, reservoir initial or average pressure, sand-face condition (well damage or stimulation), volume of drainage area, boundary and discontinuities, reservoir heterogeneity, distance or extension of the fracture induced, validation of geological model, and system identification (type of reservoir and mathematical model).

Further, it is important to determine the ability of a formation to produce reservoir fluids and underlying reason for a well's productivity. These data, when combined with hydrocarbon, production data, and laboratory data on fluid and rock properties, afford the means to estimate the original hydrocarbon in-place and the recovery that may be expected from the reservoir under various modes of exploitation. In addition, well test data and IPR well performance equations, combined with production data, help to design, analyze, and optimize total well production system or production optimization.

The rigorous discussions, practical examples, and easy-to-read manner make this a valuable addition to every petroleum professional's library. Our colleagues' discussions and their suggestions were very valuable in making this book useful to a practicing engineer. Most users of this book will find it logically organized and readily applicable to many well testing problem solutions and field application.

One additional note should be made concerning this book. The author has inserted many personal opinions, evaluations, analysis, recommendations, conclusions, etc. He is often criticized for doing this without specifically stating that these are personal thoughts. If the reader does not find a reference or logical proof of a particular statement, he can safely assume that it is a personal opinion based on the author's experience and knowledge of the subject.

Suggestions of many readers were evaluated in preparing this book. Any further comment and suggestion for improvement of the book will be gratefully appreciated. Please feel free to contact me directly.

Amanat U. Chaudhry
Advanced TWPSOM Petroleum Systems, Inc.
10070 Westpark Drive # 905
Houston, TX 77042
1-713-783-1248

Acknowledgements

I would like to thank Dr. Furlow Fulton, Head of Petroleum Engineering Department at the University of Pittsburgh, for educating me in reservoir engineering. I am privileged to work with many professionals in the oil industry who have taught me many things and helped me grow and develop as an engineer. I am also thankful to A. C. Carnes, Jr., General manager, Integrated Technology Petroleum Consulting Services, Houston, who oriented me in the areas of reservoir simulation and well test analysis during my career. I am also thankful to many companies who were generous in providing the field histories and data which were used in the book. I am also thankful to Ambar Sudiono, General Manager of State Owned Oil Company of Indonesia, Jakarta, who was kind enough to read Chapters 3, 7, 8, 12, and 17 and provided many valuable suggestions.

Mr. Dilip Borthakur* has reviewed the material presented in this book. He has spent hundreds of hours reading, checking, and critically commenting on all aspects of the material and its presentation. There is no doubt that the book is a much better volume that it would have been without his aid.

The technical typing as well as figures and tables have been largely the work of Ms. Faiza Azam who is a graduate student in Physics and Mathematical Methods at Allama Iqbal Open University, Islamabad, Pakistan. Her highly accurate work has added substantially to this book.

* Presently Head of Gas Engineering Department with Gulf Indonesia Resources.

Amanat Chaudhry

Contents

<i>Foreword</i>	xiii
<i>Preface</i>	xv
<i>Acknowledgements</i>	xvii
1. Introduction	1
1.1 Role of Oil Well Tests and Information in Petroleum Industry	1
1.2 History of Oil Well Testing and Uses of Oil Well Tests	1
1.3 Oil Well Test Data Acquisition, Analysis, and Management	2
1.4 Selecting Oil Wells for Optimum Stimulation Treatment	2
1.5 Reservoir System Characterization Process	4
1.6 Scope and Objective	6
1.7 Organization	8
1.8 Unit's, Systems and Conversions	11
References	12
Additional Reading	12
2. Fundamentals of Reservoir Oil Flow Analysis	13
2.1 Introduction	13
2.2 Basic Fluid Flow Equations in Oil Reservoir	13

2.3	Numerical Models and Their Applications	26
2.4	Unsteady-state Pressure Distribution Calculations in Directional Well	33
2.5	Summary	41
	References	42
	Additional Reading	42
3.	Transient Well Testing Methods for Horizontal Oil Wells	44
3.1	Introduction	44
3.2	Flow Equations for Horizontal Oil Wells	44
3.3	Horizontal Oil Well Performance during Transient State	84
3.4	Transient Well Testing Techniques in Horizontal Oil Wells	86
3.5	Flow Time Equations and Solutions	88
3.6	Pressure Response Equations and Methods of Analysis	95
3.7	Horizontal Well Response and Normalized Pressure Derivative	103
3.8	Effects of Wellbore Storage	104
3.9	Summary	104
	References	105
	Additional Reading	106
4.	Pressure Drawdown Testing Techniques for Oil Wells	107
4.1	Introduction	107
4.2	Pressure-time History for Constant-rate Drawdown Test	108
4.3	Transient Analysis – Infinite-acting Reservoirs	108

4.4	Late Transient Analysis – Bounded (Developed) Reservoirs	111
4.5	Semi-steady-state Analysis – Reservoir Limit Test	115
4.6	Two-rate Flow Test Analysis	121
4.7	Variable-rate Flow Tests	129
4.8	Multi-rate Flow Test Analysis	137
4.9	Drawdown Rate Normalization Methods	146
4.10	Summary	150
	References	151
	Additional Reading	151
5.	Pressure Buildup Analysis Techniques for Oil Wells	153
5.1	Introduction	153
5.2	Ideal Pressure Buildup Test	153
5.3	Actual Buildup Tests – Infinite Reservoir	156
5.4	Pressure Buildup Test Analysis in Infinite-acting Reservoir	157
5.5	Pressure Buildup Testing Methods for Finite (Bounded) Reservoir	176
5.6	Multiphase Buildup Test Analysis	194
5.7	Afterflow Analysis Using Russel's Technique	199
5.8	Pressure Buildup Tests Preceded by Two Different Flow Rates	201
5.9	Variable-rate Pressure Buildup Analysis	206
5.10	Multi-phase, Multi-rate Buildup Analysis	210
5.11	Rate Normalization Techniques and Procedures (Pressure Buildup Data)	214
5.12	Summary	231
	References and Additional Reading	232

6.	Original and Average Reservoir Pressure Estimation Methods	234
6.1	Introduction	234
6.2	Original Reservoir Pressure in Infinite Reservoirs	234
6.3	Estimating Average and Initial Reservoir Pressure	235
6.4	Estimating Constant Pressure at Aquifer in Water-drive Reservoirs	244
6.5	Summary	252
	References and Additional Reading	252
7.	Well Testing Methods for Naturally Fractured Reservoirs	254
7.1	Introduction	254
7.2	Identification of Natural Fractures	254
7.3	Characteristics of Naturally Fractured Reservoirs	255
7.4	Typical Pressure Drawdown Behavior Curve Shapes	255
7.5	Pressure Buildup Behavior Characteristics	256
7.6	Well Test Interpretation Methods, Uses, and Limitations	257
7.7	Buildup Analysis Techniques for Tight Reservoir Matrix	270
7.8	Interpretation of Interference Tests in Matrix and Fractured Reservoirs	275
7.9	Horizontal Well Pressure Behavior Curve Shapes	278
7.10	Horizontal Well Production Forecasting – Dual-porosity Reservoir	284

7.11	Summary	285
	References and Additional Reading	285
8.	Fundamentals of Type Curve Matching	
	Methods for Oil Wells	287
8.1	Introduction	287
8.2	Application to Conventional Tests	287
8.3	Fracture Type Curve Matching Techniques	313
8.4	Type Curves – Horizontal Fractured Oil Wells	329
8.5	Summary	337
	References and Additional Reading	338
9.	Flow Regime Identification and Analysis Using	
	Special Methods	339
9.1	Introduction	339
9.2	Fracture Linear Flow Period	339
9.3	Bilinear Flow	341
9.4	Formation Linear Flow	345
9.5	Pseudo-radial Flow	346
9.6	Type Curve Matching Methods	346
9.7	Summary	356
	References	357
	Additional Reading	357
10.	Application of Pressure Derivative in Oil Well	
	Test Analysis	359
10.1	Introduction	359
10.2	Pressure Derivative Applications in Well Test Analysis	359
10.3	Pressure Derivative Analysis Methods	359
10.4	Fractured Reservoir Systems	365

xii Contents

10.5	Pressure Derivative Trends for Other Common Flow Regimes	370
10.6	Summary	371
	References	371
	Additional Reading	371

11. Massive Hydraulic-fractured Oil Well Behavior Analysis 372

11.1	Introduction	372
11.2	Methods of Evaluating MHF Oil Wells	372
11.3	Analyzing Infinite Flow Capacity Fractures	372
11.4	Analyzing Finite Flow Capacity Fractures	373
11.5	Estimating Formation Characteristics of Finite Conductivity Fractures	378
11.6	Pretreatment Testing of Hydraulically Fractured Candidate	384
11.7	Summary	385
	References	386
	Additional Reading	386

12. Drill-stem Testing Methods 387

12.1	Introduction	387
12.2	DST Equipment and Operational Procedures	388
12.3	Recommended Flow and Shut-in Time for Drill-stem Tests	389
12.4	Troubleshooting DST Pressure Charts	390
12.5	Checking Validity and Consistency of Reporting DST Data	391
12.6	Estimation of Average Flow Rate	392
12.7	DST Analysis Methods, Uses, and Limitations	396
12.8	Wireline Formation Test Data Evaluation	414

12.9	Summary	427
	References and Additional Reading	427
13.	Interference and Pulse Test Analysis Methods	429
13.1	Introduction	429
13.2	Interference Test Analysis Techniques	429
13.3	Analysis of Pulse Test Pressure Response	434
13.4	Vertical Pulse Test Design and Analysis Methods	445
13.5	Design and Analysis of Unequal Pulses	448
13.6	Summary	462
	References	462
	Additional Reading	462
14.	Injection Well Transient Testing and Analysis ...	463
14.1	Introduction	463
14.2	Injectivity Test Analysis Methods	463
14.3	Pressure Fall-off Test Analysis Methods	475
14.4	Two-rate Injectivity Test Analysis	492
14.5	Step-rate Injectivity Testing Technique	496
14.6	Summary	502
	References	502
	Additional Reading	503
15.	Well Testing Methods in Multilayered Oil Reservoir Systems	504
15.1	Introduction	504
15.2	Identification of Layered Oil Reservoir Systems ...	504
15.3	Analyzing Pressure Behavior in Multilayered Systems	505

15.4	Concept of Reservoir Layer Fracture Conductivity	509
15.5	Pressure Production Performance Response Equations	510
15.6	Investigating Degree of Communication and Type of Crossflow	512
15.7	Pressure Buildup Characteristics in Layered Reservoir Systems	512
15.8	Pressure Analysis Methods for Oil Wells Producing Commingled Zones	514
15.9	Factors Affecting Multilayered Reservoir Performance	520
15.10	Economic Aspects of Interlayer Crossflow	521
15.11	Summary	521
	References and Additional Reading	521

16.	Pressure Analysis Methods in Heterogeneous Oil Reservoir Systems	523
16.1	Introduction	523
16.2	Effect of Pressure on Rock Properties	523
16.3	Major Causes of Heterogeneities	524
16.4	Pressure Responses near No Flow Boundaries ...	524
16.5	Effect of Hydraulic Diffusivity on Reservoir Behavior	534
16.6	Simple Procedures and Guidelines to Estimate Reservoir Heterogeneity Properties	536
16.7	General Approach to Estimate Fracture Trends or Heterogeneity	536
16.8	Determination of Reservoir Parameters and Fracture Orientations	536

16.9	Defining Reservoir Heterogeneity by Multiple-well Tests	539
16.10	Method for Calculating Fracture Orientation	555
16.11	Estimating Two-dimensional Permeability with Vertical Interference Testing	556
16.12	Application of Pulse Tests to Describe Reservoir Heterogeneity	561
16.13	Validity of Various Models and Steps Used to Obtain Reservoir Description	573
16.14	Summary	574
	References and Additional Reading	574

Appendices

Appendix A:	Conversion Factors between Unit Systems	577
Appendix B:	Correlation Tables and Dimensionless Functions	585
	References and Additional Reading	594
Appendix C:	Pressure Drop through Vertical, Inclined, and Horizontal Oil Wells	595
	C.1 Hagedorn and Brown Method	596
	C.2 Beggs and Brill Method	602
	References and Additional Reading	606
Appendix D:	Oil and Water PVT Properties and Correlation Equations	607
	D.1 Oil PVT Properties and Correlations	608
	D.2 Solution Gas-oil Ratio	612
	D.3 Oil Formation Volume Factor	613
	D.4 Total Formation Volume Factor	616
	D.5 Oil Density	616
	D.6 Oil Viscosity	618
	D.7 Oil Compressibility	622

D.8 Reservoir Rock Properties	623
D.9 Reservoir PVT Water Properties	624
References and Additional Reading	639
Nomenclature	640
Bibliography	645
Index	661

Chapter 1

Introduction

1.1 Role of Oil Well Tests and Information in Petroleum Industry

Oil well test analysis is a branch of reservoir engineering. Information obtained from flow and pressure transient tests about in situ reservoir conditions are important to determining the productive capacity of a reservoir. Pressure transient analysis also yields estimates of the average reservoir pressure. The reservoir engineer must have sufficient information about the condition and characteristics of reservoir/well to adequately analyze reservoir performance and to forecast future production under various modes of operation. The production engineer must know the condition of production and injection wells to persuade the best possible performance from the reservoir.

Pressures are the most valuable and useful data in reservoir engineering. Directly or indirectly, they enter into all phases of reservoir engineering calculations. Therefore accurate determination of reservoir parameters is very important. In general, oil well test analysis is conducted to meet the following objectives:

- To evaluate well condition and reservoir characterization;
- To obtain reservoir parameters for reservoir description;
- To determine whether all the drilled length of oil well is also a producing zone;
- To estimate skin factor or drilling- and completion-related damage to an oil well. Based upon the magnitude of the damage, a decision regarding well stimulation can be made.

1.2 History of Oil Well Testing and Uses of Oil Well Tests

Two monographs^{1,3} and numerous additional oil well test analysis technical papers have been published. Those papers have extended the scope of oil well test analysis, publicized many new problems, provided

solutions for previously unsolved problems, and changed the approach to some phases of oil well test analysis. Thus, it is appropriate to provide an updated handbook dealing with advances in oil well test analysis in a manner that presents an up-to-date treatment of the state of the art. This book presents popular pressure transient test analysis techniques and estimates of the range of applicability. More than 100 actual field examples illustrate most analysis techniques. Figure 1-1 shows uses of well tests.

1.3 Oil Well Test Data Acquisition, Analysis, and Management

Throughout the life of an oil well, from exploration to abandonment, a sufficient amount of well test data are collected to describe well condition and behavior. It should be emphasized that the multidisciplinary professionals need to work as an integrated team to develop and implement the well test data management program.

Efficient Oil Well Test Analysis Programs

Initial bottom-hole pressure measurements should be made, preferably at each well and at selected "Key Oil Wells" periodically. Key oil wells represent 25% of the total wells². Reference 2 has also found that it is beneficial to measure pressure in all wells at least every 2-3 years to aid in calibrating reservoir models. It is essential to establish the specification of what and how much well test data need to be gathered, and the procedure and frequency to be followed. A logical, methodical, and sequential well test data acquisition and analysis program is shown in Figure 1-2.

1.4 Selecting Oil Wells for Optimum Stimulation Treatment

The key to determining whether or not a well is a good candidate for stimulation treatment is diagnosing the well to find the cause for its low productivity. Buildup, drawdown, or drill-stem tests, core analyses offset well data, and other information can be used to accomplish this. After diagnosis, the optimum well stimulation treatment, either small or massive hydraulic

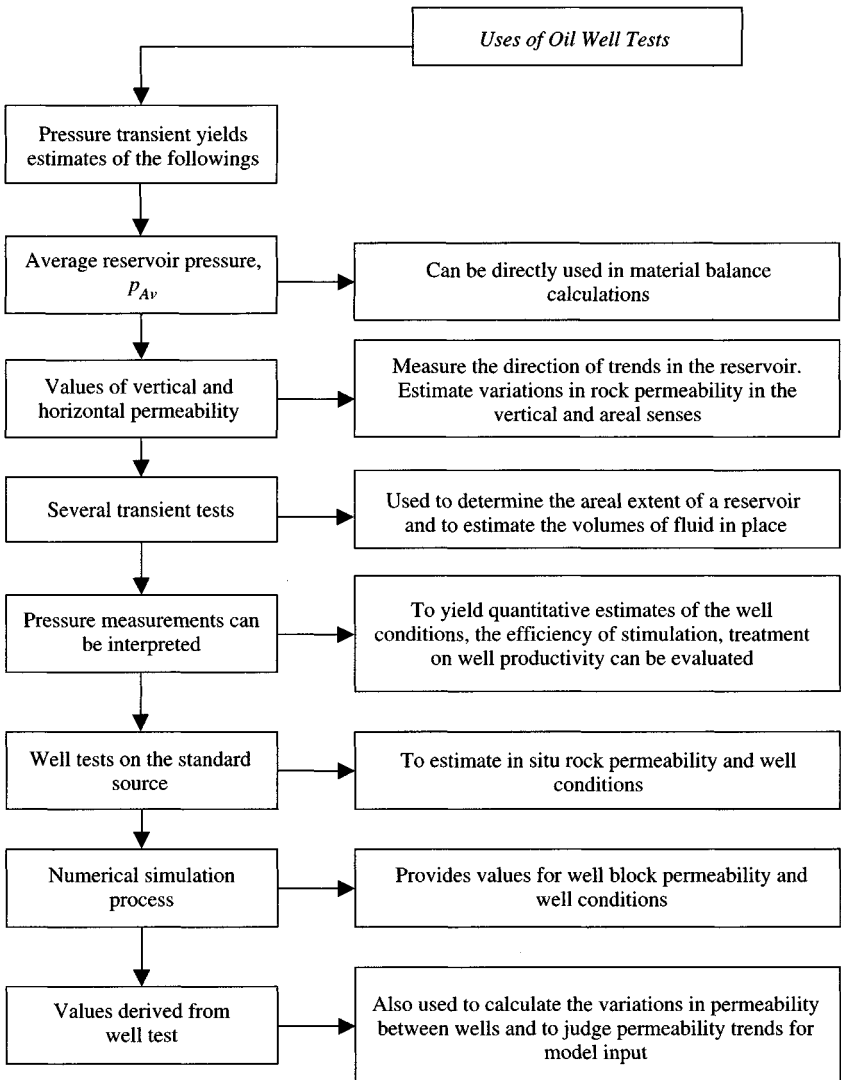


Figure 1–1. Various reservoir parameters and their uses.

fracturing, can be designed for the well. Figure 1–3 shows several sets of calculations designed to evaluate well/reservoir behavior, and to evaluate reservoir parameters, quality, and stimulation efforts to optimize completion methods for enhancing hydrocarbon oil recovery and maximizing profitability.

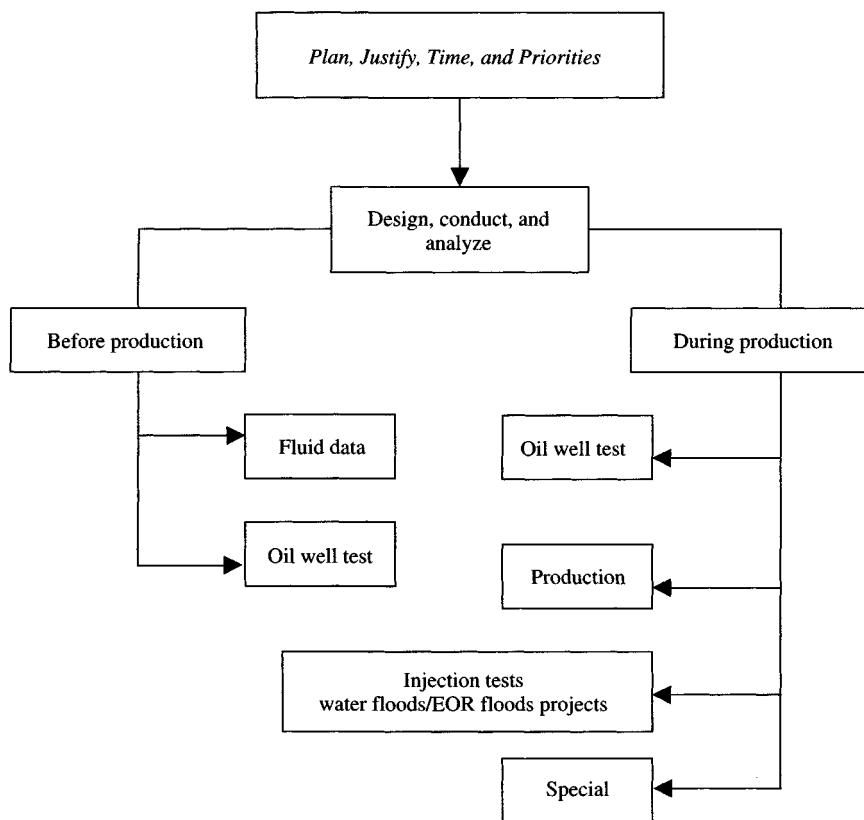


Figure 1-2. Logical well test data acquisition and analysis program.

1.5 Reservoir System Characterization Process

An efficient oil well test data acquisition and analysis program requires careful planning, designing, conducting, evaluation, and well-coordinated team efforts through an integrated approach. Figures 1-4 and 1-5 indicate general activities in reservoir description and inputs from various engineering disciplines (integrated approach). Core analysis measurements of samples selected by the geologist provide data for the preliminary identification of reservoir rock types. Well test results using various techniques were reasonable when compared with known geologic and core data. Well test studies aid in recognizing flow barriers, fractures, and variations in permeability. History matching of past production and pressure performance consists of adjusting the reservoir parameters of a model until the simulated

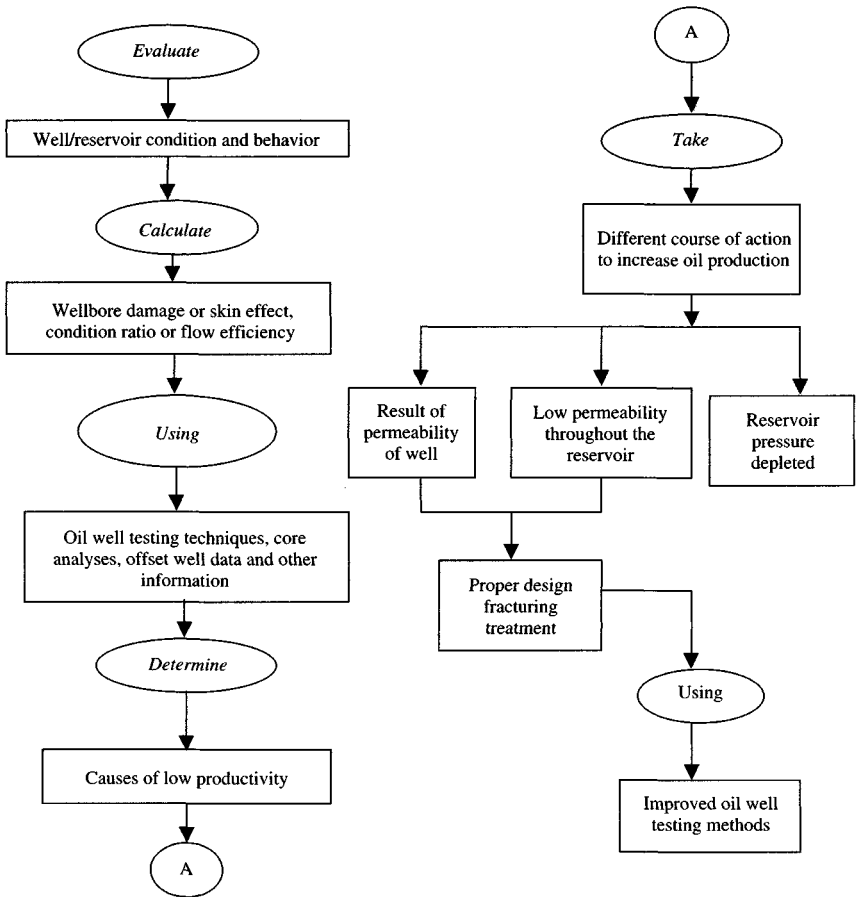


Figure 1-3. Selection of oil wells for optimum treatment.

performance matches the observed or historical behavior. The major goal is optimization of oil recovery through characterization of the reservoir system.

Most Common Oil Well Test Interpretation Methods

Figure 1-5 shows oil flow and pressure analysis methods. Theory and sample applications to illustrate effective well test analysis practices are discussed in the following chapters.

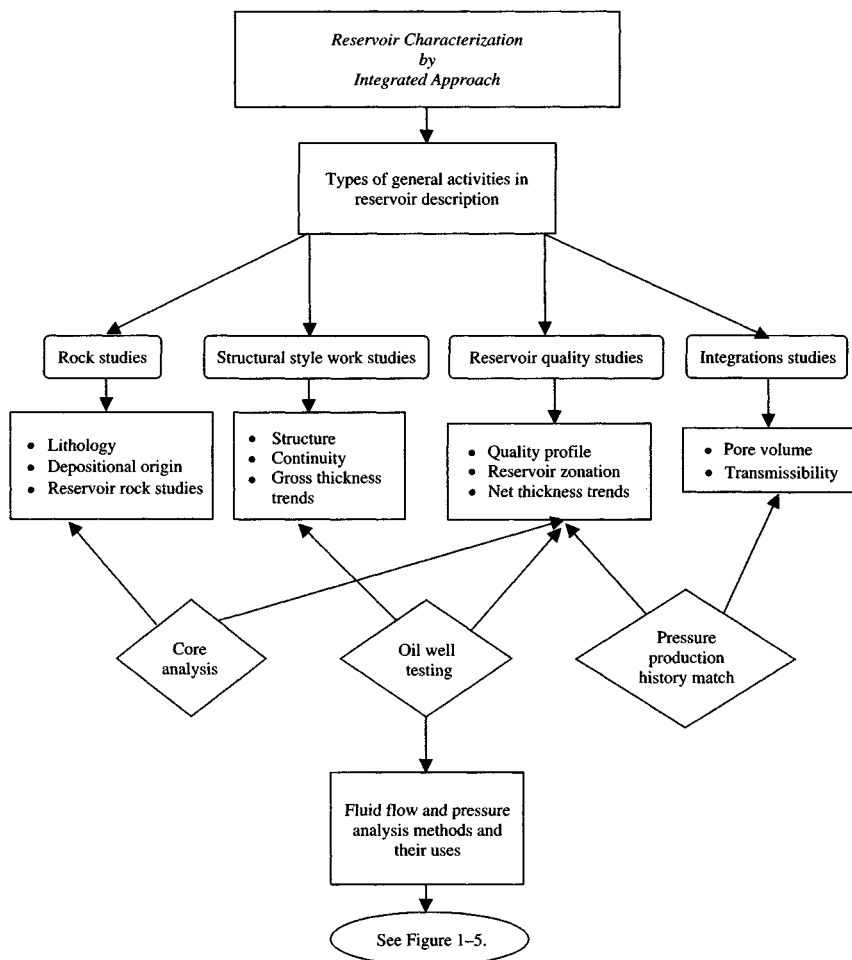


Figure 1-4. Reservoir system characterization flow chart process using integrated approach.

1.6 Scope and Objective

This book is very important to professional petroleum engineers, teachers, graduate students, and those who are concerned with evaluating well conditions and reservoir characterization. The data in this book should enable petroleum professionals to design and to conduct pressure transient tests and to analyze the results to obtain reliable information about well behavior. Emphasis is given to the most common interpretation methods used at present.

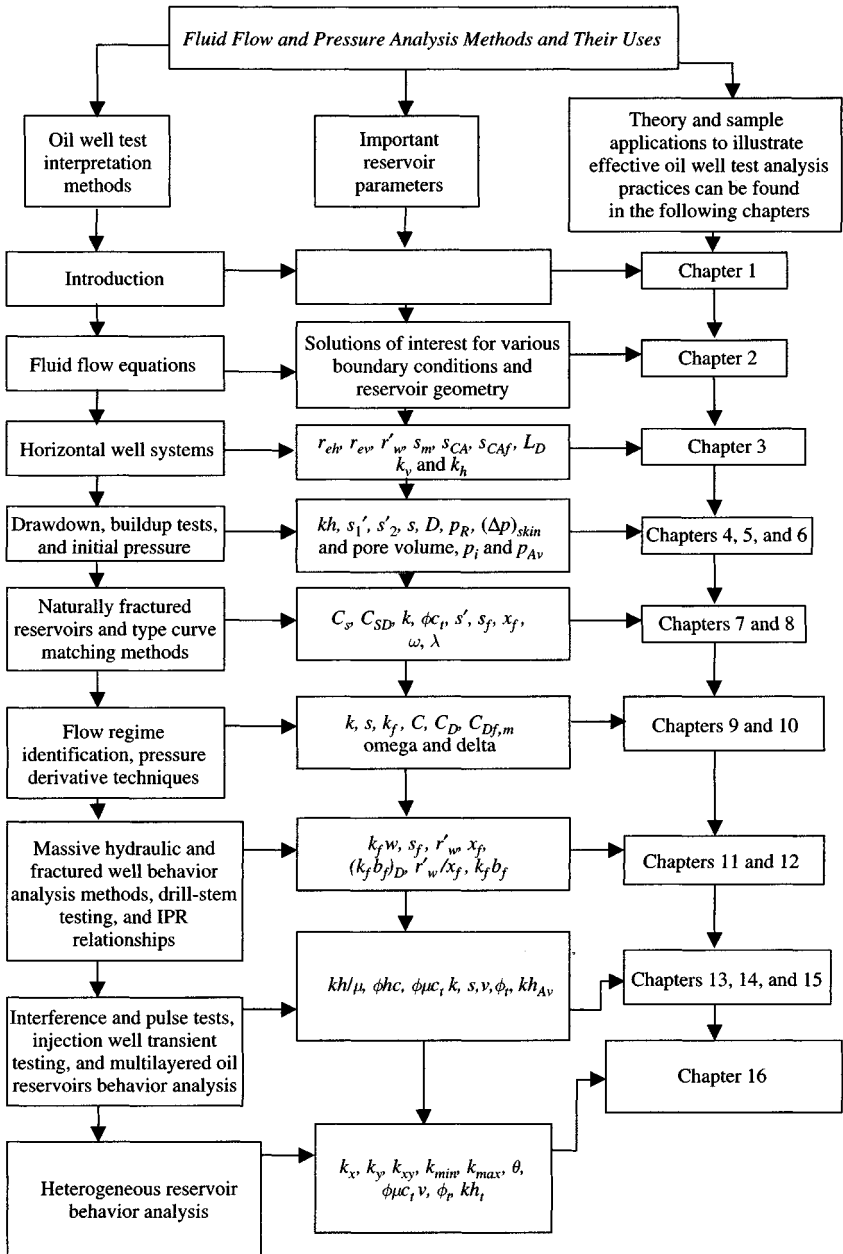


Figure 1-5. Various pressure analysis methods to determine important reservoir parameters.

1.7 Organization

This book presents:

- Outstanding instructive text source providing theory and practice of oil well testing methods and their role in petroleum industries.
- Valuable asset to technical libraries of petroleum industries, companies, academicians, petroleum professionals, and technical managers.
- Sound fundamental concepts/methodology related to oil well test data acquisition and interpretation from a practical viewpoint.
- Modern oil well testing methods and pressure transient test analysis techniques.
- Examples illustrating effective well test analysis techniques.
- Excellent practical reference source related to pressure transient analysis techniques and their interpretations.
- Theory and practices of testing methods and their roles in reservoir engineering management.
- Practical in-depth examples of real-life engineering problems with step-by-step solutions that are very easy to follow.
- Various charts, formulae, and tables for ready reference and quick solutions for oil well testing and analyses.
- New information, data, and technology and includes examples and problems illustrating the concepts, methods, interpretations, results, recommendations, and their engineering applications. Historical notes, summaries, and references are included in this highly practical edition.

Chapter 1 of this book is an overview of oil well testing and analysis methods. It also includes a short discussion of unit conversion factors and the SI (metric) unit system. Appendix A provides a list of conversion factors.

Chapter 2 deals with fundamental fluid flow equations, along with solutions of interest for various boundary conditions and reservoir geometry. These solutions are required in the design and interpretation of flow and pressure tests. This chapter provides analytical solutions of fluid flow equations. The equations are followed by a discussion of some of the most useful solutions to these equations such as exponential integral, finite difference, and graphical solutions, and the choice of the equation for flow analysis, with emphasis on the exponential-integral solutions, describing radial, unsteady-state flow. It also includes numerical models and their applications including unsteady-state pressure distribution calculations in directional oil wells.

Chapter 3 summarizes a discussion of horizontal wells in oil reservoirs. Horizontal wells enhance the drainage area in a given time period, while in high permeability oil reservoirs reduce near-wellbore turbulence and enhance well deliverability. Horizontal wells have high potential in oil reservoirs. This chapter also includes influence of turbulence, and turbulence

identification, comparison of inflow performance responses in vertical and horizontal oil wells, and time and transient pressure response analysis equations related to each of the flow regimes to solve for specific reservoir parameters using drawdown and buildup tests.

Chapter 4 deals with complete analysis of drawdown testing including transient, late transient, and semi-steady-state analysis including single, two-rate, variable-rate, reservoir limit test, and multi-phase and multiple-rate testing, and discusses how superposition may be used when variable rates are involved.

Chapter 5 treats pressure buildup test analysis and presents methods for estimating formation characteristics such as reservoir permeability, skin factor, wellbore damage, and improvement evaluation including average pressure for well drainage areas and the entire reservoir.

Chapter 6 presents estimation methods for original and average reservoir pressure using various techniques such as Horner and MBH method/MDH method/Dietz method/Ramey/Muskat and Arps methods. This chapter also includes constant pressure at aquifer in water-drive reservoir.

Chapter 7 presents identification of natural fractures, main characteristics, and brief review of the most widely used well testing models including their uses and limitations, typical pressure drawdown behavior curve shapes, and pressure buildup behavior characteristics. Buildup analysis techniques for tight reservoir matrix and horizontal well pressure behavior curve shapes, and identification of various flow periods, well test analysis equations, and solutions are presented. It also includes horizontal well production forecasting for dual-porosity reservoir.

Chapter 8 discusses the quantitative use of type curve analysis methods. The object of this chapter is to illustrate how a representative sample of type curves can be used for analysis aids. Fundamentals of type curve use are presented and will allow the reader to understand and to apply newer type curves as they appear in the literature. Many type curves can be used to determine the formation permeability and to characterize damage and stimulation of the tested well. Application to conventional tests and vertical and horizontal fractured well analysis is also presented.

Chapter 9 provides new techniques for analyzing pressure transient data for wells intercepted by a finite-conductivity vertical fracture. This method is based on the bilinear flow theory, which considers transient linear flow in both fracture and formation. These new type curves overcome the uniqueness problem exhibited by other type curves.

Chapter 10 deals with pressure derivative application to oil well test analysis and involves the combined use of existing type curves in both the conventional dimensionless pressure form (p_D) and the new dimensionless pressure derivative grouping ($p'_D \times t_D/C_D$). Thus this new approach has combined the most powerful aspects of the two previously distinct methods into a single-stage interpretive plot. Use of the pressure derivative with pressure behavior type curves reduces the uniqueness problem in type curve

matching and gives greater confidence in the results. Type curve match can be utilized to determine the reservoir parameter, and the pressure derivative plot helps to identify reservoir heterogeneity such as dual-porosity system for the case of pseudo-steady-state flow from matrix to fracture. The valley in the pressure derivative could also be indicative of a layered system.

Chapter 11 reviews advances in oil well stimulation techniques such as massive hydraulic fracturing (MHF). It is a proven technique for developing commercial wells in low-permeability or “tight” oil formations. Limitations of conventional analysis methods and alternative techniques for determining fracture length and fracture flow capacity on MHF wells are presented. It also discusses how to analyze past performance and forecast future performance of tight oil wells stimulated by MHF using finite fracture flow capacity type curves. The limitations of conventional pressure transient analysis and other methods of evaluating MHF treatment are discussed. The set of constant well rate and wellbore pressure type curves are also presented.

Chapter 12 discusses drill-stem testing (DST) equipment and operational procedures, recommended flow, and shut-in time for DST. It presents troubleshooting DST pressure charts for barrier detection, checking validity and consistency of reported DST data, DST analysis methods such as Horner’s plot, type curve matching techniques, and DST buildup test analysis with limited data. These methods are discussed in detail for their uses and limitations including wire line formation test data evaluation.

Chapter 13 reviews interference and pulse tests, also known as multiple-well testing. These types of tests can be used to obtain an adequate reservoir description for homogeneous (both isotropic and anisotropic) and heterogeneous systems. Numerical solutions must be used to analyze pressure transient data from heterogeneous reservoir systems. At the same time, it is one of the most important and useful tests to understand the well behavior in waterflood and EOR projects.

Chapter 14 presents pressure analysis techniques in injection wells. The injectivity test and the falloff tests are used to estimate the reservoir properties of injection wells in waterflood and EOR recovery projects. The knowledge of reservoir properties and near-wellbore conditions in injection wells is as important as in the producing wells. Injection well transient testing and analysis are simple as long as the mobility ratio between the injected and in situ fluids is about unity and the radius of investigation is not beyond the water-injected fluid bank.

Chapter 15 reviews various types of and testing of oil-layered reservoir systems including multilayered responses in fractured reservoirs. It also describes crossflow identification, and the nature and degree of communication between layers. Performance equations for cases of constant flowing pressure and constant producing rate are presented and discussed. It also reviews “layer effect” on pressure and/or production behavior including economic aspects of interlayer crossflow.

Chapter 16 discusses variations of heterogeneities in rock and fluid properties including causes and effects of pressure-dependent properties. It also analyzes and interprets pressure behavior in heterogeneous reservoirs near fault or other barriers and lateral changes in the hydraulic diffusivity that occur at fluid contacts. Pressure behavior analysis methods are discussed in brief to obtain adequate reservoir descriptions for isotropic, anisotropic, and heterogeneous systems including calculating fracture orientation and estimating two-dimensional permeability with vertical interference testing.

Details and supporting materials are presented in the appendices for the benefit of those who would like to learn more.

Appendix A shows conversion factors between unit systems. Appendix B presents correlation tables and charts for dimensionless functions. Appendix C helps to compute pressure drop calculations through vertical, inclined, and horizontal pipes. Appendix D presents methods and correlation equations for estimating fluid PVT and rock properties.

1.8 Unit's Systems and Conversions

In any book of this nature, it is worthwhile to include a comprehensive list of units' conversion factors, since data are often reported in units different from those used in the equations. Such factors are presented in Appendix A. Because of the possibility of eventual conversion of engineering calculations to a metric standard, I also include information about the "SI" system of weights and measures. Finally, I compare some important units and equations in five different unit systems. Table 1-1 shows that units are a hybrid system based on the CGS units. The only difference being that pressure is

Table 1-1
Absolute and Hybrid Systems of Units Used in Oil Well Testing Equations

Parameter	Symbol	Dimension	Absolute units		Hybrid units	
			CGS	SI	Darcy	Field
Pressure	P	$(ML/T^2)/L^2$	Dyne/cm ²	N/m ²	atm	psia
Time	t	T	sec	sec	sec	hr
Rate	q	L ³ /T	cm ³ /s	m ³ /s	cm ³ /s	stb/day
Viscosity	μ	M/LT	g/cm s	kg/m s	cP	cP
Permeability	k	L ²	cm ²	m ²	Darcy	mD
Velocity	u	L/T	cm/s	m/s	cm/s	ft/s
Mass	m	M	g	kg	g	lb
Length	l	L	cm	m	cm	ft
Density	ρ	M/L ³	g/cm ³	kg/m ³	g/cm ³	lb/ft ³

expressed in atmospheres, viscosity in cP (centipoises), and, as a consequence, the permeability in Darcies.

References

1. Matthews, C. S., and Russell, D. G., *Pressure Buildup and Flow Tests in Wells*, Monograph Series, No. 1, SPE, Dallas, TX 1967.
2. Ramey, H. J., Jr., Kumar, A., and Gulati, M. S., *Oil Well Test Analysis Under Water-drive Conditions*, AGA, Arlington, VA, 1973.
3. Earlougher, R. C., Jr., *Advances in Well Test Analysis*, Monograph Series, No. 5, SPE, Dallas, TX, 1977.

Additional Reading

1. Ramey, H. J., Jr., "Practical Use of Modern Well Test Analysis," paper SPE 5878 presented at the SPE 46th Annual California Regional Meeting, Long Beach, CA, April 8-9, 1976.
2. Raghavan, R., "Pressure Behavior of Wells Intercepting Fractures," Proc. Invitational Well-Testing Symposium, Berkeley, CA, Oct. 19-21, 1977.
3. Prats, M., Hazebrock, P., and Sticker, W. R., "Effect of Vertical Fractures on Reservoir Behavior - Compressible Fluid Case," *Soc. Pet. Eng. J.* (June 1962) 87-94; *Trans. AIME*, 225.
4. Gringarten, A. C., Ramey, H. J., and Raghavan, R., "Applied Pressure Analysis for Fractured Wells," *J. Pet. Tech.* (July 1975) 887-892; *Trans. AIME*, 259.
5. Fetkovich, M. J., "Multipoint Testing of Gas Wells," paper presented at the SPE-AIME Mid-Continent Section Continuing Education Course on Well Test Analysis (March 1975).
6. Campbell, J. M., "Report on Tentative SPE Metrication Standards," paper presented to the 51st Annual Fall Conference of the AIME, New Orleans, Oct. 1976.

Chapter 2

Fundamentals of Reservoir Oil Flow Analysis

2.1 Introduction

This chapter deals with the basic equations for flow of liquid through porous media along with solutions of interest for various boundary conditions and reservoir geometry. These solutions are required in the design and interpretation of flow and pressure tests. The applicable equations for liquid flow are presented in this section, including pressure transient behavior with dimensionless pressure solutions for the specific conditions. Some important dimensionless functions are presented and references to others are provided. The dimensionless pressure approach provides a way to calculate pressure response and to develop techniques for analyzing transient tests in a variety of systems.

2.2 Basic Fluid Flow Equations in Oil Reservoir

This section describes steady-state, pseudo-steady-state, and unsteady-state flow equations including oil radial diffusivity equation, basic oil flow equations, and various dimensional flow geometry.

Steady-State Flow Equations and Their Practical Applications

In steady-state flow, there is no change anywhere with time, i.e., the right-hand sides of all the continuity and diffusivity equations are zero. Solutions for steady state are, however, useful for certain unsteady-state problems. The steady-state flow equations can be derived from integrating and evaluating the integration constants from the boundary conditions. The steady-state flow equation and Darcy's equations accounting for specific geometry are

presented here. The steady-state flow equations are based on the following assumptions:

1. Thickness is uniform, and permeability is constant.
2. Fluid is incompressible.
3. Flow across any circumference is a constant.

Ideal Steady-State Flow Equation – Radial Flow

Let p_w be the pressure at the wellbore when the well is flowing q reservoir barrels per day and a pressure p_e is maintained at the external radius or drainage radius r_e . Let the pressure at any radius r be p . Then, at this radius r :

$$v = \frac{q_o}{A} = \frac{q_o}{2\pi r} = -1.127 \frac{k}{\mu} \frac{dp}{dr}$$

where position q_o is in the positive r -direction. Separating variables and integrating between any two radii, r_1 and r_2 , where the pressures are p_1 and p_2 , respectively,

$$\int_{r_1}^{r_2} \frac{q_o}{2\pi r} dr = - \int_{p_1}^{p_2} 1.127 \frac{k}{\mu} dp$$

$$q_o = - \frac{0.00708kh(p_2 - p_1)}{\mu\beta_o \ln(r_2/r_1)} \quad (2-1)$$

The minus sign is usually dispensed with; for where $p_2 > p_1$, the flow is known to be negative, i.e., in the negative r -direction, or toward the wellbore. Also it is customary to express q in surface units rather than reservoir units. Then, Eq. 2-1 becomes

$$q_o = \frac{0.00708kh(p_2 - p_1)}{\mu\beta_o \ln(r_2/r_1)} \quad (2-2)$$

Frequently, the two radii of interest are the wellbore radius r_w and the external or drainage radius r_e . Then, Eq. 2-1 becomes

$$q_o = \frac{0.00708kh(p_e - p_{wf})}{\mu\beta_o \ln(r_e/r_w)} \quad (2-3)$$

where

q_o = oil flow rate, stb/day

k = undamaged permeability, mD

h = thickness, ft

p_e = external pressure, psi

r_e = external radius, ft, and is calculated from well spacing

r_w = wellbore radius, ft

μ_o = viscosity of oil, cP

β_o = oil formation volume factor, rb/stb

In terms of the average pressure (i.e., $p = \bar{p}$ at $r = r_e$):

$$q_o = \frac{0.00708kh(\bar{p} - p_{wf})}{\mu_o\beta_o(\ln(r_e/r_w) - 0.5)} \quad (2-4)$$

For linear geometry:

$$q_o = \frac{0.001127kA(p_1 - p_2)}{\mu_o\beta_oL} \quad (2-5)$$

For hemispherical geometry:

$$q_o = \frac{0.00708kh(p_e - p_w)}{\mu_o\beta_o(1/r_1 - 1/r_2)} \quad (2-6)$$

For 5-spot waterflood:

$$q_o = \frac{0.003541kh(p_{wi} - p_{wp})}{\mu_o\beta_o[\ln(d/r_w) - 0.619]} \quad (2-7)$$

For 7-spot waterflood:

$$q_o = \frac{0.00472kh(p_{wf} - p_{wp})}{\mu_o\beta_o[\ln(d/r_w) - 0.569]} \quad (2-8)$$

To calculate undamaged permeability around the wellbore, pressure drop $(\Delta p)_{skin}$ (negative), due to damage or improvement could be incorporated into the above equations as

$$q_o = \frac{0.00708k_{imp}h(p_e - p_w - \Delta p_{skin})}{\mu_o\beta_o \ln(r_e/r_w)} \quad (2-9)$$

Practical Applications

Steady-state equations may be used without any significant error to analyze near the wellbore reservoir conditions, even in an unsteady-state system.

Example 2-1 *Calculating Improved Permeability from Steady-State Flow Equation*

A well is producing oil at a rate of 800 bbl/day with a bottom-hole pressure of 850 psi from a reservoir with very strong water drive (assume steady state). What is the improved permeability if a pressure drawdown analysis indicates that Δp_{skin} at this rate is 150 psi? Other data are: well spacing = 40 acres; $r_w = 6.5$ in.; $\mu_o = 2.0$ cP; $\beta_o = 1.255$ rb/stb; $h = 45$ ft; and $p_e = 1350$ psi.

Solution

$$r_w = \frac{6.5}{12 \times 2} = 0.27 \text{ ft}, \quad r_e = \sqrt{\frac{40 \times 43,560}{\pi}} = 745 \text{ ft}, \quad p_e = 1350 \text{ psi}$$

Using Eq. 2-8, we can calculate the improved permeability, k_{impr} :

$$k_{impr} = \frac{q_o \mu_o \beta_o \ln(r_e/r_w)}{0.00708 h (p_e - p_w - (\Delta p)_{skin})}$$

$$= \frac{800 \times 2.0 \times 1.255 \ln(745/0.27)}{0.00708 \times 45(1350 - 800 - 150)} = 124.83 \text{ mD}$$

Example 2-2 *Calculating Flow Rate and Pressure Drop Due to Skin from Steady-State Flow Equation in a Water-Drive Reservoir*

In a water-drive reservoir, the following data are known: boundary pressure = 2200 psia; flowing pressure = 950 psia; oil flow rate = 100 rb/day; well radius, $r_w = 0.39$ ft; effective drainage radius, $r_{eff} = 750$ ft; $h = 15$ ft; $\mu_o = 0.95$ cP; flow rate, $q_o = 75$ rb/day; and $\beta_o = 1.240$ rb/stb. Calculate (1) what is $(\Delta p)_{skin}$, (2) if $(\Delta p)_{skin} = 0$, find the oil flow rate, and (3) find $(\Delta p)_{skin}$, if $r_w = 5.5$ ft.

Solution

(1) Using Eq. 2-9, $(\Delta p)_{skin}$ is

$$q_o = \frac{0.00708 k h (p_e - p_w - (\Delta p)_{skin})}{\mu_o \beta_o \ln(r_e/r_w)}$$

$$75 = \frac{0.00708 \times 10 \times 15(2200 - 950 - (\Delta p)_{skin})}{0.95 \times 1.24 \ln(750/0.39)}$$

$$(\Delta p)_{skin} = 140.32 \text{ psi}$$

- (2) If the $(\Delta p)_{skin}$ is reduced to zero, the production rate would be (using Eq. 2-3)

$$q_o = \frac{0.00708kh(p_e - p_w)}{\mu_o\beta_o \ln(r_e/r_w)} = \frac{0.00708 \times 10 \times 15(2200 - 950)}{0.95 \times 1.24 \ln(750/0.39)} = 149.02 \text{ stb/day}$$

- (3) For $r_w = 5.5$ ft. Substituting this into Eq. 2-3, we get

$$149.02 = \frac{0.00708 \times 10 \times 15(2200 - 950 - (\Delta p)_{skin})}{0.95 \times 1.24 \ln(750/5.5)}$$

$$\therefore (\Delta p)_{skin} = 1327.5 - 862.83 = 464 \text{ psi}$$

Pseudo-Steady-State Flow Equations

When a reservoir is produced at a constant rate for a long enough period of time so that the entire drainage area of the reservoir is affected by the pressure disturbance, q constant change in pressure with time at all radii takes place. This constant pressure change results in parallel pressure distributions and corresponding constant rate distributions. This situation is called pseudo-steady-state flow. Many reservoirs spend most of their history in a pseudo-steady-state flow regime than in any other flow regime. This type of flow is also called depletion state or semi-steady state. Pseudo-steady-state flow problem can be solved using the following set of equations:

$$\left(\frac{\Delta p}{\Delta t}\right)_{pseudo} = \frac{5.615q_o}{\phi c_t V_b} \quad (2-10)$$

where V_b is equal to pore volume of reservoir in cubic ft and is equal to $\pi r_e^2 h$ or

$$\left(\frac{\Delta p}{\Delta t}\right)_{pseudo} = \frac{1.7866q_o}{\phi h c_t r_e^2} \quad (2-11)$$

Example 2-3 Calculating Porosity-Thickness, Permeability-Thickness from Pseudo-Steady-State Equation

Reservoir and well data are: $p_s = 2800$ psi; $p_e = 3350$ psi; $c_t = 10^{-6}$ psia⁻¹; $r_e = 2000$ ft; $r_w = 0.5$ ft; $c_t = 10^{-5}$ psi⁻¹; $\mu_o = 0.65$ cP; $p_w = 3.050$ psi; $q_o = 900$ stb/day; $\beta_o = 1.150$ rb/stb. The p_{wf} is declining at a constant rate of 2.2 psi/day. Determine the following:

- (1) Porosity-thickness
- (2) Permeability-thickness

- (3) Permeability–thickness. Assuming there is water drive (steady-state flow) and bottom hole pressure remains constant.

Solution

- (1) Using Eq. 2–11, porosity–thickness is

$$\phi h = \frac{1.7866 q_o \beta_o}{r_e^2 c_t} \left(\frac{\Delta t}{\Delta p} \right) = \frac{1.7866 \times 900 \times 1.15}{2000^2 \times 10^{-5}} \times \frac{1}{2.2} = 21 \text{ ft}$$

- (2) Using Eq. 2–13, permeability–thickness kh is

$$\begin{aligned} kh &= \frac{q_o \beta_o \mu_o [\ln(r_e/r_w) - 0.5]}{0.00708(p_e - p_w)} \\ &= \frac{900 \times 1.15 \times 0.65 [\ln(2000/0.5) - 0.5]}{0.00708(3350 - 3050)} = 2469 \text{ mD ft} \end{aligned}$$

- (3) Using Eq. 2–9, permeability–thickness in steady-state system is

$$\begin{aligned} kh &= \frac{q_o \beta_o \mu_o [\ln(r_e/r_w)]}{0.00708(p_e - p_w)} = \frac{900 \times 1.15 \times 0.65 [\ln(2000/0.5)]}{0.00708(3350 - 3050)} \\ &= 2627 \text{ mD ft} \end{aligned}$$

Flow Equations for Different Flow Regimes

Flow equations for pseudo-steady state for wells located centrally in the areal drainage plane are given below. It is important to note that the equations are based either on drainage boundary pressure p_e or average reservoir pressure \bar{p} . In general, reservoir pressure is estimated by using a DST test, a pressure bomb test, or a buildup test. These methods estimate average reservoir pressure \bar{p} . Eq. 2–12 can be applied to flow when other pressures and radii are evolved.

$$p - p_{wf} = \frac{141.2 q_o \mu_o \beta_o}{kh} \left(\ln \left(\frac{r}{r_w} \right) - \frac{r^2}{2r_e^2} \right) \quad (2-12)$$

Eq. 2–13 is a pseudo-steady-state equation written in terms of $p = p_e$ at $r = r_e$.

$$p - p_{wf} = \frac{141.2 q_o \mu_o \beta_o}{kh} \left(\ln \left(\frac{r}{r_w} \right) - 0.5 \right) \quad (2-13)$$

Eq. 2-13a is written in terms of the average reservoir pressure for a circular drainage area:

$$p - p_{wf} = \frac{141.2q_o\mu_o\beta_o}{kh} \left(\ln\left(\frac{r}{r_w}\right) - 0.75 \right) \quad (2-13a)$$

As an alternative, the skin factor can be accounted for in the flow equations by changing the wellbore radius, e.g., including the skin factor

$$p - p_{wf} = \frac{141.2q_o\mu_o\beta_o}{kh} \left(\ln\left(\frac{r}{r'_w}\right) - 0.75 \right)$$

in which

$$r'_w = r_w e^{-s}$$

- (a) Damaged well, $s > 0$
- (b) Stimulated well, $s < 0$.

Time to Reach Pseudo-Steady State

The time periods required to reach the pseudo-steady-state for different vertical well locations in the drainage plane and for various configurations of drainage areas are listed in Table B-1. Dimensionless time t_D , which is used to define various flow regimes, is given as

$$t_D = \frac{0.000264kt}{\phi\mu c_{ti}r_w^2} \quad (2-13b)$$

and area-based dimensionless time is defined as

$$t_{DA} = t_D \left(\frac{r_w^2}{A} \right) \quad (2-13c)$$

Thus

$$t_{DA} = \frac{0.000264kt}{\phi\mu c_{ti}A} \quad (2-13d)$$

where

- k = permeability, mD
- t = time, hr

ϕ = porosity in fraction

μ_o = oil viscosity, cP

c_{ii} = initial total compressibility, psi^{-1}

A = area, ft^2

r_w = wellbore radius, ft

As shown in Table B-1, for a vertical well located at the center of a drainage circle or a square to reach pseudo-steady-state requires $t_{DA} = 0.1$. Substituting this in Eq. 2-13d, we obtain

$$t_{DA} = 0.1 = \frac{0.000264kt}{\phi\mu c_{ii}A} \quad (\text{hour}) \quad (2-13e)$$

$$t_{pss} = \frac{379\phi\mu c_{ii}A}{k} \quad (\text{days}) \quad (2-13f)$$

where t_{pss} is the time to reach pseudo-steady state. Generally, oil wells are developed on 40-acres spacing and gas wells are developed on 160-acres spacing.

$$40 \text{ acres} = 43,560 \times 40 = 1.7424 \times 10^6 \text{ ft}^2$$

$$160 \text{ acres} = 43,560 \times 160 = 6.9696 \times 10^6 \text{ ft}^2$$

Eqs. 2-13e and 2-13f show that transient time depends on the basic reservoir properties such as k , ϕ , and c_{ii} . Time to reach pseudo-steady state does not depend on well stimulation. In the case of oil wells, time to reach pseudo-steady state normally is on the order of a few days to months. In contrast, for gas wells in low-permeability reservoirs, time to reach pseudo-steady state could be very long; in some cases as long as a few years.

Example 2-4 Determining the Time to Reach Pseudo-Steady-State

For an oil well drilled at 40-acre spacing, calculate the time to reach pseudo-steady state. Given: $\mu = 3.75$ cP; $k = 45$ mD; $c_{ii} = 5.5 \times 10^{-5}$ psi^{-1} ; $\phi = 12.5\%$; $A = 40$ acres.

Solution Using Eq. 2-13f, time to reach pseudo-steady state is calculated as

$$\begin{aligned} t_{pss} &= \frac{379\phi\mu c_{ii}A}{k} = \frac{379 \times 0.125 \times 3.75 \times 5.5 \times 10^{-5} \times 40 \times 43,560}{45} \\ &= 37 \text{ hours} = 15.6 \text{ days} \end{aligned}$$

Example 2-5 Calculating the Time to Reach Pseudo-Steady State (20- and 160-Acre Spacing)

Calculate the time required to reach pseudo-steady state for an oil well drilled at either 20- or 160-acre spacing in a reservoir with an

initial pressure of 1550 psi. The following reservoir properties are given: $\phi = 0.125$ fraction; $\mu_o = 3.75$ cP; $c_{ii} = 55 \times 10^{-5}$ psi $^{-1}$; $k = 45$ mD

Solution

$$t_{pss} = \frac{379\phi\mu c_{ii}A}{k} = \frac{379 \times 0.09 \times 0.0145 \times 6.9 \times 10^{-4} \times A}{0.05} = 0.00683A$$

For 20 acres, $t_{pss} = 0.00683 \times 20 \times 43,560$ hr = 5946 hr = 248 days = 0.68 years

For 160 acres, $t_{pss} = 0.00683 \times 160 \times 43,560 = 47,602$ hr = 1983 days = 5.43 years

Unsteady-State (Transient) Flow Equations

Unsteady-state flow is a flow that occurs while the pressures and/or rate changes with time. Reservoir conditions that are not described by the steady-state flow above are described by unsteady-state flow. The greater the compressibility of the fluid, the more pronounced the unsteady-state effect of the reservoir fluid. The engineers use the diffusivity equation for studying the unsteady-state flow of fluid in porous media. The equations used to describe unsteady-state flow are derived from hydraulic diffusivity equation and presented in the next section.

Radial Diffusivity Equation

The basic differential equation will be derived in radial form thus simulating the flow of fluids in the vicinity of a well. Analytical solutions of the equation can then be obtained under various boundary and initial conditions for use in the description of well testing and well inflow, which have considerable practical application in reservoir engineering. The radial cell geometry is shown in Figure 2-1 and the following assumptions will be made to develop diffusivity equation:

1. Homogeneous and isotropic porous media of uniform thickness;
2. Rock and fluid properties are pressure-independent;
3. Pressure gradients are small;
4. Flow is radial;
5. Darcy's law is applicable;
6. Gravity forces are negligible;
7. The flow is along a radial path toward the wellbore;

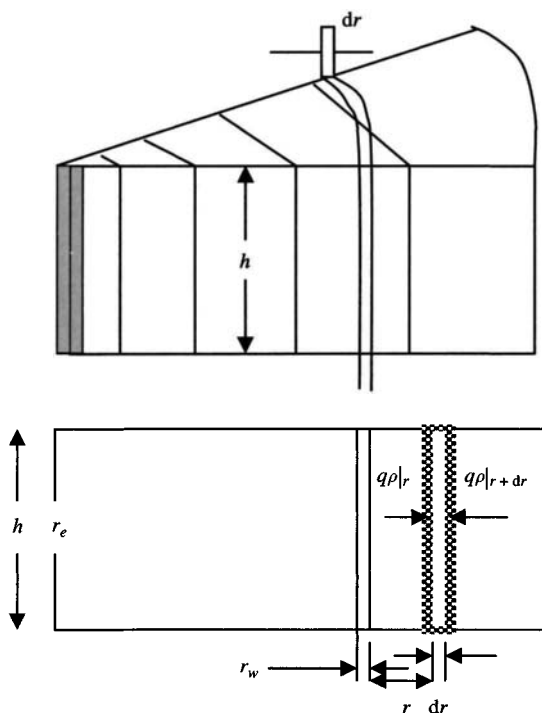


Figure 2-1. Radial flow of a single-phase fluid in the vicinity of a producing well.

8. The fluid flow is single phase and fluid saturation in the system is constant;
9. The porosity and permeability are constant in space and time; and
10. Viscosity and compressibility of the fluid are constant.

Consider the flow through a volume element of thickness, dr , situated at a distance r from the center of the radial cell. Then applying the principle of mass conservation, Mass flow rate – mass flow rate = rate of change of mass in volume element

Input = Output

$$q\rho|_{r+dr} - q\rho|_r = 2\pi rh\phi \, dr \frac{\partial \rho}{\partial t}$$

where $2\pi rh\phi$ is the volume of the small element of thickness dr . The left-hand side of the equation can be expressed as

$$\left(q\rho|_r + \frac{\partial(q\rho)}{\partial t} dr - q\rho|_r \right) = 2\pi rh\phi \, dr \frac{\partial \rho}{\partial t}$$

which simplifies to

$$\frac{\partial(q\rho)}{\partial t} = 2\pi rh\phi \frac{\partial\rho}{\partial t} \quad (2-14)$$

By applying Darcy's law for radial, horizontal flow it is possible to substitute for the flow rate, q , in Eq. 2-14, since

$$q = \frac{2\pi khr}{\mu} \frac{\partial p}{\partial r}$$

Therefore

$$\frac{\partial}{\partial r} \left(\frac{2\pi khr}{\mu} \rho \frac{\partial\rho}{\partial r} \right) = 2\pi rh\phi \frac{\partial\rho}{\partial t}$$

or

$$\frac{1}{r} \frac{\partial}{\partial r} \left(\frac{k\rho}{\mu} r \frac{\partial\rho}{\partial r} \right) = \phi \frac{\partial\rho}{\partial t} \quad (2-15)$$

The time derivative of the density appearing on the right-hand side of Eq. 2-15 can be expressed in terms of a time derivative of the pressure by using the definition of isothermal compressibility:

$$c = -\frac{1}{V} \frac{\partial V}{\partial p}$$

and since

$$\rho = \frac{m}{V}$$

the compressibility can be alternatively expressed as

$$c = -\frac{\rho}{m} \frac{\partial(m/\rho)}{\partial\rho} = \frac{1}{\rho} \frac{\partial\rho}{\partial p} \quad (2-16)$$

Differentiating Eq. 2-16 with respect to time, we get

$$c\rho \frac{\partial p}{\partial t} = \frac{\partial\rho}{\partial t} \quad (2-17)$$

Finally, substituting Eq. 2-17 into Eq. 2-16 leading to

$$\frac{1}{r} \frac{\partial}{\partial r} \left(k \rho r \frac{\partial p}{\partial r} \right) = \phi c \rho \frac{\partial p}{\partial t} \quad (2-18)$$

Eq. 2-18 is nonlinear, since the coefficients on both sides are themselves functions of a dependent variable, the pressure. This equation has to be presented in linear form in order to obtain analytical solutions, i.e., Eq. 2-18 is reduced to the radial form. For a radial flow toward a well in a circular reservoir, if we combine the law of conservation of mass and Darcy's law for the isothermal flow of fluids of small and constant compressibility, Eq. 2-18 simplifies to

$$\frac{\partial^2 p}{\partial r^2} + \frac{1}{r} \frac{\partial p}{\partial r} = \frac{\phi \mu c_t}{0.00264k} \frac{\partial p}{\partial t} \quad (2-19)$$

This equation is called the radial diffusivity equation; the term $0.000264k/\phi\mu c_t$ is called the hydraulic diffusivity. Analytical solutions of this equation are obtained under various boundary and initial conditions for use in well testing and well inflow performance calculations.

Various Dimensional Flow Geometry

Eq. 2-19 may be expressed in terms of linear, cylindrical, or spherical coordinates.

$$\nabla^2 p = \frac{\phi \mu c}{k} \frac{\partial p}{\partial t} \quad (2-20)$$

where $\nabla^2 p$ is the Laplacian of p . Expression "one-dimensional" referred to a specified coordinate system?

Linear Flow

Flow lines are parallel, and the cross-sectional area of flow is constant and represented by Eq. 2-21, which is the rectangular coordinate system in the one-dimensional form of Eq. 2-20:

$$\frac{\partial^2 p}{\partial x^2} = \frac{\phi \mu c_t}{0.000264k} \frac{\partial p}{\partial t} \quad (2-21)$$

Linear flow occurs in some reservoirs with long, highly conductive vertical fractures. Consider a situation with linear flow (in the x -direction) of a

slightly compressible fluid in an infinite, homogeneous reservoir, initially at uniform pressure, p_i . Fluid is produced at constant rate $q\beta_o$ over an area A_f (ft^2). If the area A_f represented a vertical fracture with two equal-length wings of length L_f (ft) and height h (ft), $A_f = 4hL_f$, with flow entering both sides of each wing of the fracture. This situation is modeled by the diffusivity equation in the form of Eq. 2-21. For the conditions stated, the solution to this equation at $x = 0$ is

$$p_i - p_{wf} = 16.26 \frac{q\beta_o}{A_f} \left(\frac{\mu t}{k\phi c_t} \right)^{0.5} \quad (2-22)$$

For linear flow into vertical fracture, $A_f = 4hL_f$, and

$$p_i - p_{wf} = 4.064 \frac{q\beta_o}{hL_f} \left(\frac{\mu t}{k\phi c_t} \right)^{0.5} \quad (2-23)$$

Radial-Cylindrical Flow

For radial flow, the corresponding equation is

$$\frac{1}{r} \frac{\partial}{\partial r} \left(r \frac{\partial p}{\partial r} \right) = \frac{\phi\mu c}{0.000264k} \frac{\partial p}{\partial t} \quad (2-24)$$

Eq. 2-24 is a diffusivity equation. Analytical solutions to Eq. 2-24 are known for several simple boundary conditions; these solutions are used for most well test analyses. Eq. 2-24 is based on several important assumptions, including:

- (1) The single-phase liquid flowing has small and constant compressibility;
- (2) k is constant and the same in all directions (isotropic);
- (3) ϕ is constant; and
- (4) Pressure gradients are small.

Radial-Spherical Flow

For radial-spherical flow, the corresponding equation is

$$\frac{1}{r^2} \frac{\partial}{\partial r} \left(r^2 \frac{\partial p}{\partial r} \right) = \frac{\phi\mu c}{0.000264k} \frac{\partial p}{\partial t} \quad (2-25)$$

2.3 Numerical Models and Their Applications

Numerical models utilize large computers to solve the mathematical equations, which govern the behavior of the fluids in porous media. They provide a generalized approach using a gridded format that can accommodate a reservoir description just by a reordering of the indices of the grids. The procedure involved consists of decomposing the reservoir into blocks and performing mass and energy balances on all these blocks simultaneously. This gridding of cells shows a more realistic representation of rock and fluid properties which can vary in any manner. The block diagram shown in Figure 2-2 can visualize the technique of reservoir modeling and the role played by the engineer.

Purpose and Objective of Reservoir Simulation

The simulation program can be used to study a reservoir containing a single well, a group of wells, or several wells interacting as a complex. Figure 2-3 shows the objectives of simulation.

Reservoir Model Development Process

Different types of data have been processed separately, leading to several different models. Indicator geostatistics provide an approach to merge all the information to produce an integrated reservoir model. Figure 2-4 shows the reservoir model construction process.

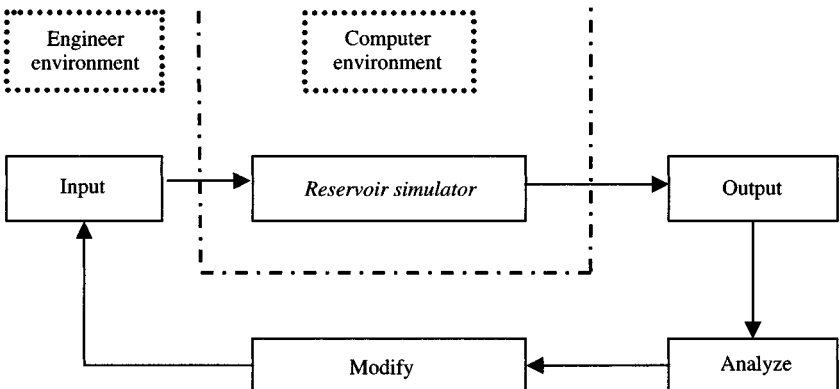


Figure 2-2. Reservoir modeling.

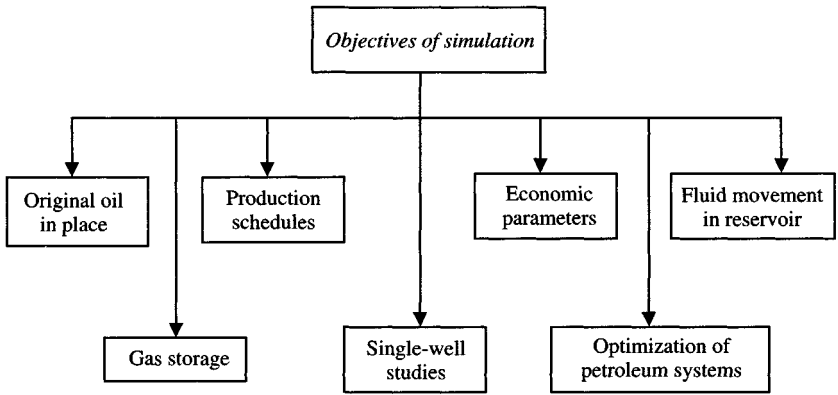


Figure 2-3. Objectives of simulation.

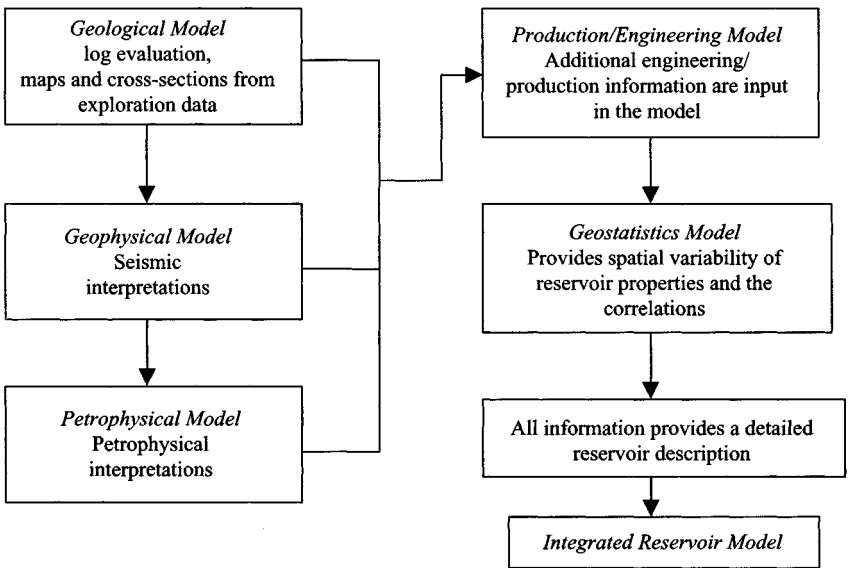


Figure 2-4. Reservoir model construction process.

Selection of Numerical Simulation Models and Applications

Most common numerical simulators such as black oil, coning and cross-sectional, and n -component are used for modeling petroleum reservoirs. The

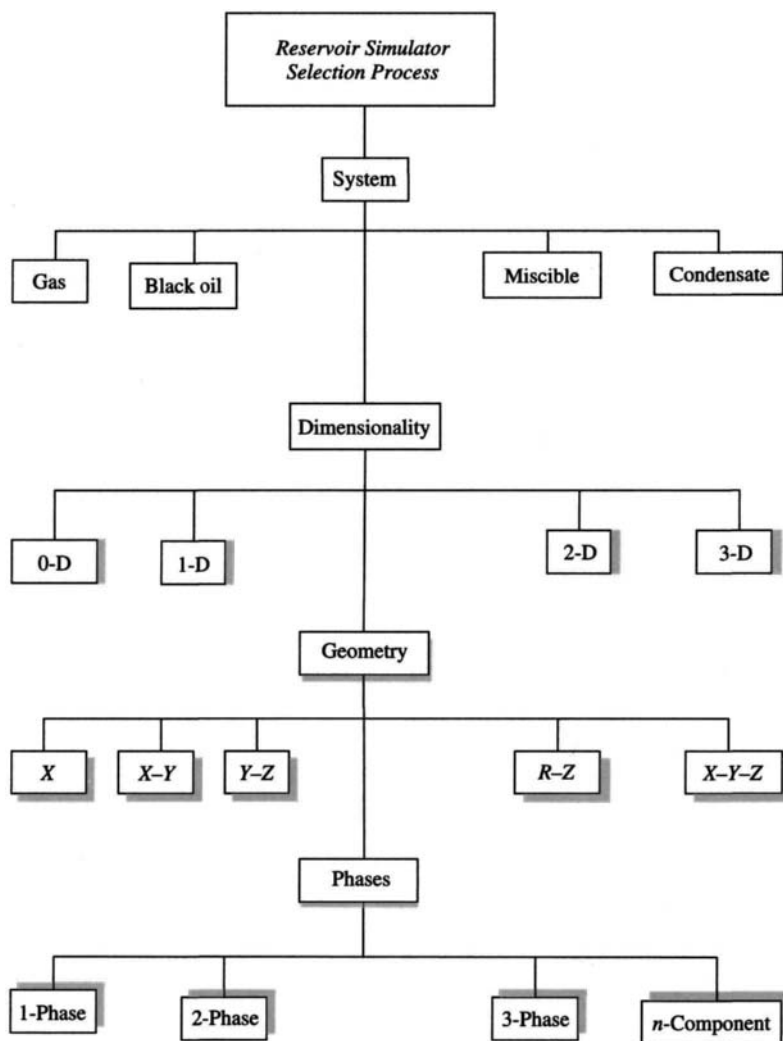


Figure 2-5. Model selection process of optimum selection.

engineer has to make a decision in selecting the optimum model to simulate the reservoir under study. The selection must be made systematically and with an analysis of all the parameters involved. The model study using a simulator is obviously too sophisticated and expensive. Figure 2-5 shows the selection process. The parameters that are important in a model selection are the following:

- Reservoir type;
- Reservoir geometry and dimensionality;
- Data availability;
- Type of secondary or tertiary process being modeled;
- Manpower requirement;
- Computer availability; and
- Cost effectiveness of model.

Figures 2-6 through 2-13 illustrate various models and their applications.

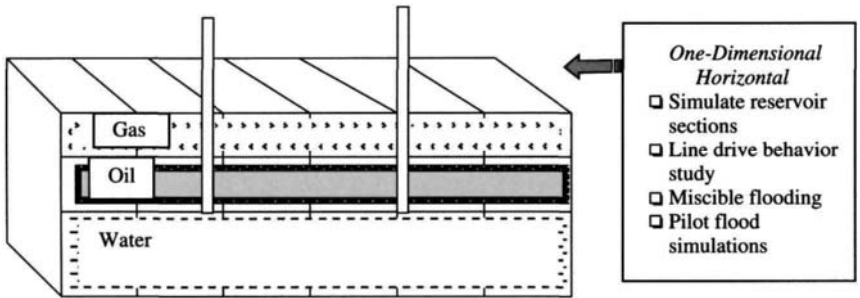


Figure 2-6. Block diagram showing one-dimensional horizontal model and its applications.

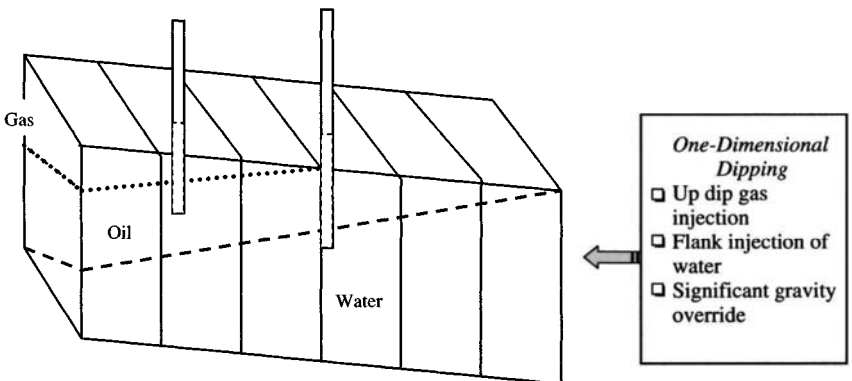


Figure 2-7. Block diagram showing one-dimensional dipping model and its applications.

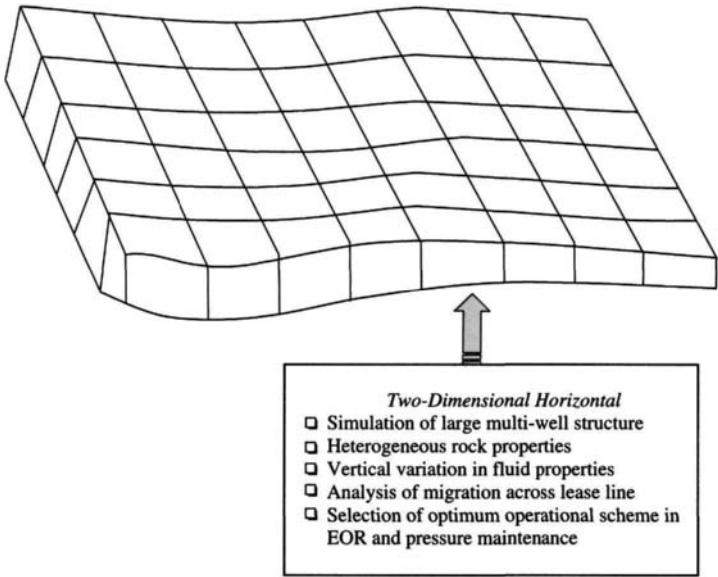


Figure 2-8. Block diagram showing two-dimensional horizontal model and its applications.

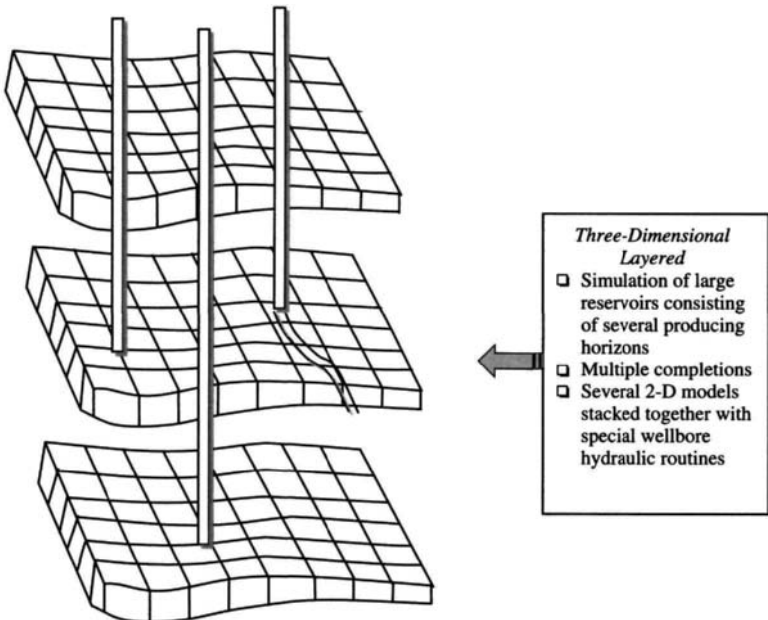


Figure 2-9. Block diagram showing three-dimensional layered model and its applications.

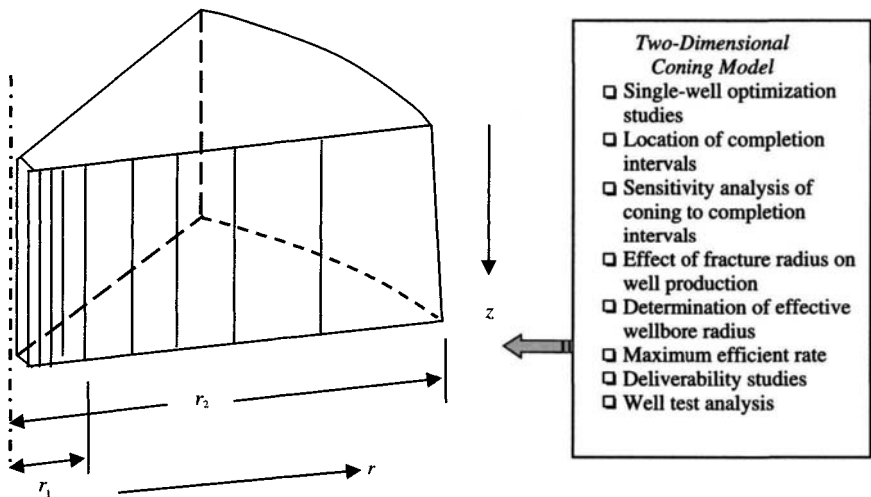


Figure 2-10. Block diagram showing two-dimensional coning model and its applications.

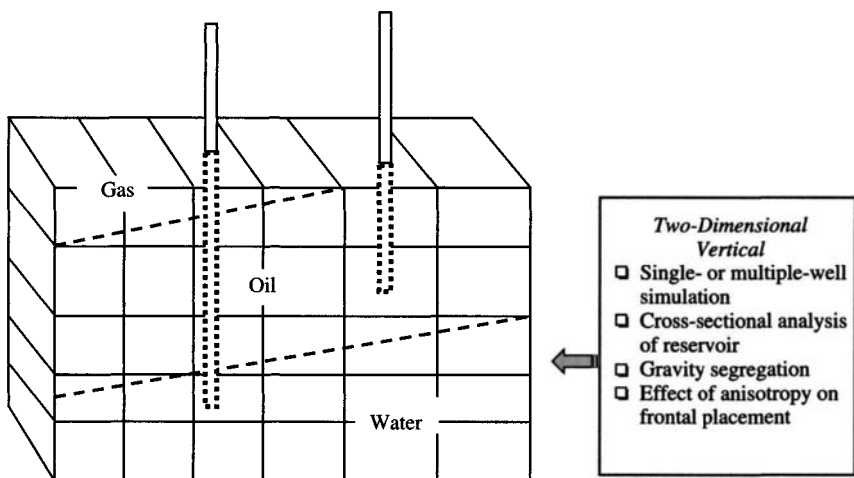


Figure 2-11. Block diagram showing two-dimensional vertical model and its applications.

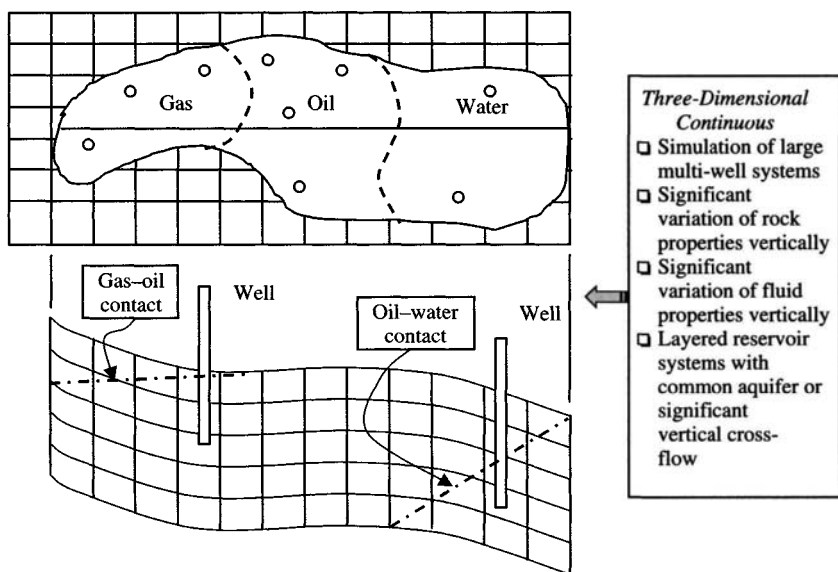


Figure 2-12. Block diagram showing three-dimensional continuous model and its applications.

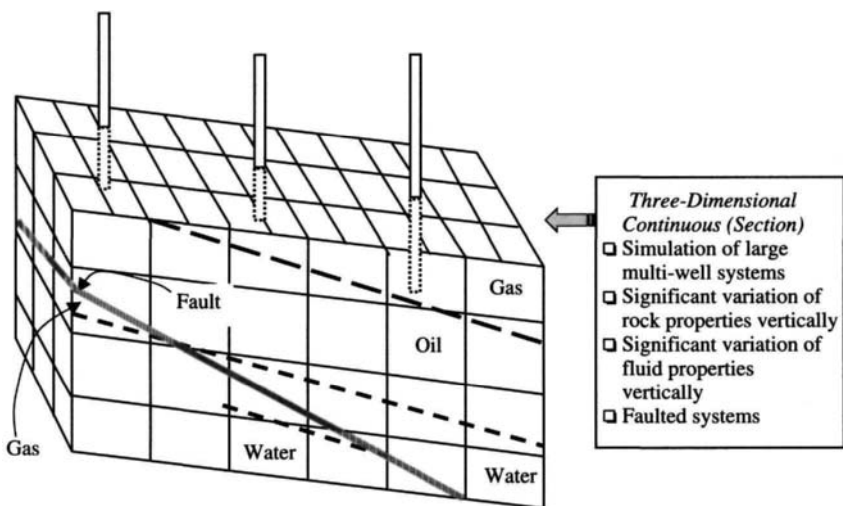


Figure 2-13. Block diagram showing three-dimensional continuous (section) model and its applications.

2.4 Unsteady-State Pressure Distribution Calculations in Directional Well

Cinco et al.² have presented a solution for unsteady-state pressure distribution created by a directional drilled well. They have also presented the equations to calculate skin factors for slanted wells. Figure 2-14 shows infinite slab reservoir with slanting well. The equation in dimensionless form is

$$p_D(r_D, \theta, z_D, t_D, \theta'_w, z_{wD}, h_{wD}, h_D) = \frac{k_r \sqrt{k_r/k_z} h \Delta p(r, \theta, z, t, \theta'_w, z_w, h_w, h)}{141.2 q_w \mu \beta} \quad (2-26)$$

where

$$t_D = \frac{0.000264 k_r t}{\phi \mu c_t r_w^2} \quad (2-27)$$

$$h_D = \frac{h}{r_w} \sqrt{\frac{k_r}{k_z}} \quad (2-28)$$

$$r_D = \frac{r}{r_w} \quad (2-29)$$

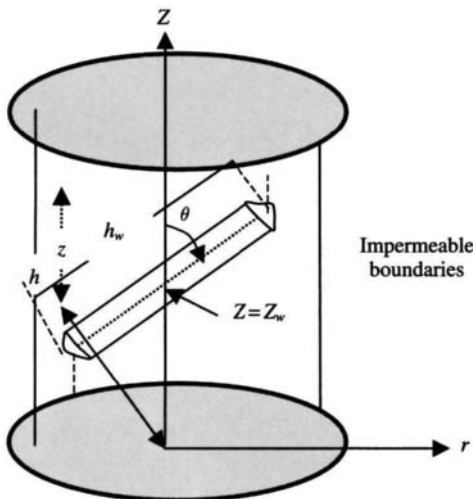


Figure 2-14. Infinite slab reservoir with slanting well.¹⁵

$$z_D = \frac{z}{r_w} \sqrt{\frac{k_r}{k_z}} \quad (2-30)$$

$$z_{wD} = \frac{z_w}{r_w} \sqrt{\frac{k_r}{k_z}} \quad (2-31)$$

$$h_{wD} = \frac{h_w}{r_w} \sqrt{\cos^2 \theta_w \frac{k_r}{k_z} + \sin^2 \theta_w} \quad (2-32)$$

$$\theta'_w = \tan^{-1} \left(\sqrt{\frac{k_z}{k_r}} \tan \theta_w \right) \quad (2-33)$$

For fully penetrated wells:

$$z_{wD} = 0.5h_D \quad \text{and} \quad h_{wD} = \frac{h_D}{\cos \theta'_w} \quad (2-34)$$

For Long-Time Approximation

At large values of the dimensionless time, the dimensionless pressure at any point in the reservoir may be expressed as

$$p_D(r_D, \theta, z_D, t_D, \theta'_w, h_D) = 0.5 \left[\ln \left(\frac{t_D}{r_D^2} \right) + 0.80907 \right] + s_\theta(r_D, \theta, z_D, \theta'_w, h_D) \quad (2-35)$$

The pseudo-skin factor term For $t_D > t_{D1}$, where

$$s_\theta(r_D, \theta, z_D, \theta'_w, h_D) = p_D(r_D, \theta, z_D, t_D, \theta'_w, h_D) - 0.5 \left[\ln \left(\frac{t_D}{r_D^2} \right) + 0.80907 \right] \quad (2-36)$$

and

$$t_{D1} = \max \left[\begin{array}{l} 70r_D^2 \\ \frac{25}{3} \left(r_D \cos \theta + \frac{h_D}{2} \tan \theta'_w \right)^2 \\ \frac{25}{3} \left(r_D \cos \theta - \frac{h_D}{2} \tan \theta'_w \right)^2 \end{array} \right] \quad (2-37)$$

the pseudo-skin factor may be approximated as

$$s_{\theta}(\theta'_w, h_D) = -\left(\frac{\theta'_w}{41}\right)^{2.06} - \left(\frac{\theta'_w}{56}\right)^{1.865} \times \log\left(\frac{h_D}{100}\right) \quad (2-38)$$

For $0 \leq \theta'_w \leq 75^\circ$ and $t_D \geq t_{D1}$

$$s_t = s_d + s_{\theta} \quad (2-39)$$

where

s_t = total skin factor, obtained from conventional pressure analysis of field data, that includes the true skin factor, s_d

s_d = sum of many factors, such as partial penetration, perforation, non-Darcy flow, etc.

s_{θ} = pseudo-skin factor caused by the inclination of the well.

Eq. 2-34 is discussed further in Ref. 1; however, the validity of this equation may be checked by means of Tables 2-1 through 2-5, which present evaluations of Eq. 2-37 and 2-38. Computation of the effect of directional drilling on the performance of a well is illustrated in the following example.

Example 2-6 *Calculating Pseudo-skin Factor in a Slanted Well and Evaluating Actual Well Condition*

A pressure buildup test indicates that the skin factor 0.72 indicates mild damage. The semilog straightline slope is 110 psi/cycle. Average angle of inclination = 45° , $h = 85$ ft, $r_w = 0.29$ ft, and core analysis indicates that the $k_r/k_z = 5$. Determine the apparent skin factor caused by directional drilling. The well fully penetrates the formation.

Solution *Pressure drop due to skin* $= (\Delta p)_{skin} = 0.869 \text{ ms} = 0.869(110)(0.72) = 68.82 \text{ psi}$.

From Eq. 2-27,

$$h_D = \frac{h}{r_w} \sqrt{\frac{k_r}{k_z}} = \frac{85}{0.29} \sqrt{5} = 655.4$$

From Eq. 2-32,

$$\begin{aligned} \theta'_w &= \tan^{-1} \left[\sqrt{\frac{k_z}{k_r}} \tan \theta_w \right] = \tan^{-1} \left[\sqrt{\frac{1}{5}} \tan 60^\circ \right] \\ &= \tan^{-1} [(0.4472 \times 0.5774)] = \tan^{-1}(0.7582) = 14.48^\circ \end{aligned}$$

(text continued on page 41)

Table 2-1
 p_{wD} Versus t_D With h_D ($h_D = 100$) as a Parameter²

t_D	15°	30°	45°	60°	75°
1×10^{-1}	0.0120	0.0108	0.0088	0.0062	0.0032
2×10^{-1}	0.0707	0.0634	0.0518	0.0366	0.0189
5×10^{-1}	0.2703	0.2424	0.1979	0.1399	0.0724
7×10^{-1}	0.3767	0.3378	0.2758	0.1950	0.1009
1	0.5043	0.4522	0.3602	0.2611	0.1351
2	0.7841	0.7030	0.5740	0.4059	0.2101
5	1.1919	1.0686	0.8725	0.6170	0.3194
7	1.3477	1.2083	0.9866	0.6976	0.3611
1×10	1.5148	1.3581	1.1089	0.7841	0.4059
2×10	1.8436	1.6529	1.3496	0.9543	0.4940
5×10	2.2829	2.0472	1.6714	1.1816	0.6116
7×10	2.4452	2.1937	1.7914	1.2659	0.6551
1×10^2	2.6179	2.3507	1.9211	1.3571	0.7017
2×10^2	2.9551	2.6612	2.1841	1.5473	0.7981
5×10^2	3.4032	3.0796	2.5508	1.8319	0.9528
7×10^2	3.5681	3.2344	2.6879	1.9421	1/0183
1×10^3	3.7431	3.3991	2.8338	2.0597	1.0911
2×10^3	*	3.7227	3.1228	2.2912	1.2375
5×10^3	A	4.1617	3.5291	2.6291	1.4506
7×10^3		4.3259	3.6859	2.7678	1.5432
1×10^4		4.5012	3.8555	2.9225	1.6528
2×10^4		*	4.1916	3.2397	1.9005
5×10^4		B	4.6434	3.6793	2.2855
7×10^4			*	3.8439	2.4382
1×10^5			C	4.0195	2.6046
2×10^5				*	2.9368
5×10^5				D	3.3861
7×10^5					3.5526
1×10^6					*
2×10^6					E
5×10^6					
7×10^6					

* Line-source solution at the wellbore $p_D(1, t_D) - [A, B, C, D, \text{ and } E]$,
 $A = -0.123 = -0.516$, $C = -1.175$, $D = -2.148$, and $E = -3.586$.

Table 2-2
 p_{wD} Versus t_D With h_D ($h_D = 200$) as a Parameter²

t_D	15°	30°	45°	60°	75°
1×10^{-1}	0.0120	0.0108	0.0088	0.0062	0.0032
2×10^{-1}	0.0707	0.0634	0.0518	0.0366	0.0189
5×10^{-1}	0.2703	0.2424	0.1979	0.1399	0.0724
7×10^{-1}	0.3767	0.3378	0.2758	0.1950	0.1009
1	0.5043	0.4522	0.3692	0.2611	0.1351
2	0.7841	0.7030	0.5740	0.4059	0.2101
5	1.1919	1.0686	0.8725	0.6170	0.3194
7	1.3477	1.2083	0.9866	0.6976	0.3611
1×10	1.5148	1.3581	1.1089	0.7841	0.4059
2×10	1.8436	1.6529	1.3496	0.9543	0.4940
5×10	2.2825	2.0465	1.6709	1.1815	0.6116
7×10	2.4443	2.1915	1.7894	1.2653	0.6550
1×10^2	2.6161	2.3455	1.9151	1.3542	0.7010
2×10^2	2.9506	2.64589	2.1602	1.5273	0.7905
5×10^2	3.4950	3.0495	2.4937	1.7623	0.9107
7×10^2	3.5590	3.2007	2.6221	1.8553	0.9578
1×10^3	3.7332	3.3625	2.6618	1.9599	1.0117
2×10^3	4.0726	3.6798	3.0409	2.1785	1.1322
5×10^3	4.5222	4.1029	3.4159	2.4801	1.3171
7×10^3	4.6879	4.2601	3.5567	2.5925	1.3883
1×10^4	4.8640	4.4286	3.7090	2.7153	1.4655
2×10^4	*	4.7620	4.0193	2.9757	1.6301
5×10^4	<i>A</i>	5.2117	4.4531	3.3692	1.9071
7×10^4		5.3783	4.6166	3.5239	2.0289
1×10^5		*	4.7913	3.6919	2.1685
2×10^5		<i>B</i>	5.1336	4.0260	2.4649
5×10^5			*	4.4765	2.8900
7×10^5			<i>C</i>	*	3.0516
1×10^6				<i>D</i>	3.2249
2×10^6					3.5656
5×10^6					*
7×10^6					<i>E</i>

* Line-source solution at the wellbore $p_D(1, t_D) - [A, B, C, D, \text{ and } E]$,
A = -0.152, *B* = -0.608, *C* = -1.378, *D* = -2.494, and *E* = -4.099.

Table 2-3
 p_{wD} Versus t_D With h_D ($h_D = 500$) as a Parameter²

t_D	15°	30°	45°	60°	75°
1×10^{-1}	0.0120	0.0108	0.0088	0.0062	0.0032
2×10^{-1}	0.0707	0.0634	0.518	0.0366	0.0189
5×10^{-1}	0.2703	0.2424	0.0979	0.1399	0.0724
7×10^{-1}	0.3767	0.3378	0.2758	0.1950	0.1009
1	0.5043	0.4522	0.3692	0.2611	0.1351
2	0.7841	0.7030	0.5740	0.4059	0.2101
5	1.1919	1.0686	0.8725	0.6170	0.3194
7	1.3477	1.2083	0.9866	0.6976	0.3611
1×10	1.5148	1.3581	1.1089	0.7841	0.4059
2×10	1.8436	1.6529	1.3496	0.9543	0.4940
5×10	2.2829	2.0465	1.6709	1.1815	0.6116
7×10	2.4443	2.1915	1.7894	1.2653	0.6550
1×10^2	2.6161	2.3455	1.9151	1.3542	0.7010
2×10^2	2.9503	2.6541	2.1597	1.5272	0.7905
5×10^2	3.3924	3.0416	2.4834	1.7560	0.9090
7×10^2	3.5549	3.1873	2.6024	1.8401	0.9525
1×10^3	3.7272	3.3419	2.7286	1.9293	0.9987
2×10^3	4.0629	3.6448	2.9766	2.1037	1.0886
5×10^3	4.5091	4.0545	3.3218	2.3518	1.2145
7×10^3	4.0736	4.2076	3.4588	2.4525	1.2671
1×10^4	4.8483	4.3708	3.5982	2.5646	1.3282
2×10^4	5.1880	4.6897	3.8805	2.7909	1.4618
5×10^4	5.6388	5.1165	4.2609	3.0960	1.6541
7×10^4	5.8051	5.2761	4.4063	3.2138	1.7279
1×10^5	*	5.4474	4.5853	3.3463	1.8111
2×10^5	A	5.7853	4.8872	3.6297	1.9994
5×10^5		*	5.3298	4.0446	2.3171
7×10^5		B	5.4950	4.2040	2.4521
1×10^6			5.6710	4.3757	2.6036
2×10^6			*	4.7144	2.9167
5×10^6			C	*	3.3534
7×10^6				D	3.5175
1×10^7					3.6927
2×10^7					E*

* Line-source solution at the wellbore $p_D(1, t_D) = [A, B, C, D, \text{ and } E]$,
 $A = -0.183$, $B = -0.731$, $C = -1.647$, $D = -2.953$, and $E = -4.778$.

Table 2-4
 p_{wD} Versus t_D With h_D ($h_D = 1000$) as a Parameter²

t_D	15°	30°	45°	60°	75°
1×10^{-1}	0.0120	0.0108	0.0088	0.0062	0.0032
2×10^{-1}	0.0707	0.0634	0.518	0.0366	0.0189
5×10^{-1}	0.2703	0.2424	0.1979	0.1399	0.0724
7×10^{-1}	0.3767	0.3378	0.2758	0.1950	0.1009
1	0.5043	0.4522	0.3692	0.2611	0.1351
2	0.7841	0.7030	0.5740	0.4059	0.2101
5	1.1919	1.0686	0.8725	0.6170	0.3194
7	1.3477	1.2083	0.9866	0.6976	0.3611
1×10	1.5148	1.3581	1.1089	0.7841	0.4059
2×10	1.6436	1.6529	1.3496	0.9543	0.4940
5×10	2.2825	2.0465	1.6709	1.1815	0.6116
7×10	2.4443	2.1915	1.7894	1.2653	0.6550
1×10^2	2.6161	2.3455	1.9151	1.3542	0.7010
2×10^2	2.9503	2.6451	2.1597	1.5272	0.7905
5×10^2	3.3924	3.0416	2.4834	1.7560	0.9090
7×10^2	3.5549	3.1872	2.6023	1.8401	0.9525
1×10^3	3.7271	3.3416	2.7284	1.9293	0.9987
2×10^3	4.0618	3.6417	2.9734	2.1025	1.0884
5×10^3	4.5046	4.0392	3.2979	2.3317	1.2069
7×10^3	4.6676	4.1863	3.4183	2.4163	1.2506
1×10^4	4.8408	4.3437	3.5485	2.5078	1.2973
2×10^4	5.1787	4.6548	3.8119	2.6984	1.3939
5×10^4	5.6271	5.0736	4.1789	2.9832	1.5487
7×10^4	5.7921	5.2284	4.3160	3.0934	1.6143
1×10^5	5.9671	5.3931	4.4620	3.2111	1.6871
2×10^5	6.3084	5.7168	4.7511	3.4426	1.8335
5×10^5	*	6.1559	5.1574	3.7805	2.0467
7×10^5	<i>A</i>	6.3201	5.3142	3.9192	2.1392
1×10^6		6.4954	5.4838	4.0739	2.2488
2×10^6		*	5.8199	4.3911	2.4965
5×10^6		<i>B</i>	6.2717	4.8307	2.8815
7×10^6			*	4.9953	3.0343
1×10^7			<i>C</i>	5.1709	3.2006
2×10^7				<i>D*</i>	<i>E*</i>

* Line-source solution at the wellbore $p_D(1, t_D) - [A, B, C, D, \text{ and } E]$, $A = -0.207$, $B = -0.824$, $C = -1.850$, $D = -3.299$, and $E = -5.292$.

Table 2-5
 p_{wD} Versus t_D With h_D ($h_D = 5000$) as a Parameter²

t_D	15°	30°	45°	60°	75°
1×10^{-1}	0.0120	0.0108	0.0088	0.0062	0.0032
2×10^{-1}	0.0707	0.0634	0.0518	0.0366	0.0189
5×10^{-1}	0.2703	0.2424	0.1979	0.1399	0.0724
7×10^{-1}	0.3767	0.3378	0.2758	0.1950	0.1009
1	0.5043	0.4522	0.3692	0.2611	0.1351
2	0.7841	0.7030	0.5740	0.4059	0.2101
5	1.1919	1.0686	0.8725	0.3170	0.3194
7	1.3477	1.7083	0.9866	0.6976	0.3611
1×10	1.5148	1.3581	1.1089	0.7841	0.4059
2×10	1.8436	1.6529	1.3496	0.9643	0.4940
5×10	2.2825	2.0465	1.6709	1.1815	0.6116
7×10	2.4443	2.1915	1.7894	1.2653	0.6550
1×10^2	2.6161	2.3455	1.9151	1.3542	0.7010
2×10^2	2.9503	2.6451	2.1597	1.5272	0.7905
5×10^2	3.3924	3.0416	2.4834	1.7560	0.9090
7×10^2	3.5549	3.1872	2.6023	1.8401	0.9525
1×10^3	3.7271	3.3416	2.7284	1.9293	0.9987
2×10^3	4.0616	3.6417	2.9734	2.1025	1.0889
5×10^3	4.5043	4.0384	3.2974	2.3316	1.2069
7×10^3	4.6668	4.1841	3.4163	2.4157	1.2505
1×10^4	4.8390	4.3386	3.5424	2.5049	1.2965
2×10^4	5.1736	4.6387	3.7875	2.6781	1.3863
5×10^4	5.6163	5.0355	4.1114	2.9072	1.5049
7×10^4	5.7789	5.1812	4.2304	2.9913	1.5484
1×10^5	5.9512	5.3359	4.3567	3.0805	1.5946
2×10^5	6.2870	5.6389	4.6047	3.2550	1.6845
5×10^5	6.7332	6.0486	4.9500	3.5031	1.8105
7×10^5	6.8976	6.2017	5.0829	3.6038	1.8630
1×10^6	7.0724	6.3649	5.2264	3.7159	1.9242
2×10^6	7.4122	6.6838	5.5086	3.9422	2.0578
5×10^6	7.8630	7.1106	5.8891	4.2473	2.2500
7×10^6	8.0293	7.2702	6.0345	4.3651	2.3238
1×10^7	A*	7.4415	6.1935	4.4976	2.4070
5×10^7		B*	C*	D*	E*

* Line-source solution at the wellbore $p_D(1, t_D) = [A, B, C, D, \text{ and } E]$,
 $A = -0.261$, $B = -1.040$, $C = -2.321$, $D = -4.104$, and $E = -4.2886$.

Table 2-6

Well angle (°)	s_θ	s_d	$(\Delta p)_{skin}$ (psi)
0	0	+0.7200	68.82
30	-0.1828	+0.9030	86.32
45	-0.5040	+1.2240	117.00
60	-1.2355	+1.9555	186.92
70	-2.2411	+2.9611	283.05
75	-3.0237	+3.7437	357.86

(text continued from page 35)

From Eq. 2-37,

$$\begin{aligned}
 s_\theta(\theta'_w, h_D) &= -\left(\frac{\theta'_w}{41}\right)^{2.06} - \left(\frac{\theta'_w}{56}\right)^{1.865} \times \log\left(\frac{h_D}{100}\right) \\
 &= -\left(\frac{14.48}{41}\right)^{2.06} - \left(\frac{14.48}{56}\right)^{1.865} \times \log\left(\frac{655.4}{100}\right) \\
 &= -0.1172 - 0.0803 \times 0.8165 = -0.1828
 \end{aligned}$$

After rearranging, Eq. 2-38 becomes $s_d = s_t - s_\theta = 0.72 - (-0.1828) = +0.903$. This indicates that the well is more damaged than originally thought and that it is a candidate for stimulation. The true pressure drop across the skin is $= 0.869 \times 110 \times 0.903 = 86.32$ psi rather than the pressure value of 68.82 psi.

Calculated values of pressure drop across skin for various values of slant angle are summarized in Table 2-6. This table indicates a significant effect on well condition.

2.5 Summary

This chapter discusses the basic flow theory for oil well testing and analysis techniques. A general equation is used for transient pressure behavior with dimensionless pressure solutions desired. Some important dimensionless pressure functions are presented and references to others are provided. The dimensionless pressure approach provides a way to calculate the pressure response and to apply techniques for analyzing transient tests in a variety of systems. Section 2.4 presents unsteady-state pressure distribution calculations in directional oil wells.

References

1. Ramey, H. J., Jr., and Cobb, W. M., "A General Buildup Theory for a Well in Closed Drainage Area," *J. Pet. Tech.* (Dec. 1971) 1493–1505.
2. Cinco, H., Miller, F. G., and Ramey, H. J., Jr., "Unsteady-state Pressure Distribution Created by a Directionally Drilled Well," SPE-AIME, 1975.

Additional Reading

1. Al-Hussainy, R., Ramey, H. J., Jr., and Crawford, P. B., "The Flow of Real Gases Through Porous Media," *J. Pet. Tech.* (May 1966) 624–636; *Trans. AIME*, 237.
2. Lee, J., *Well Testing*, SPE Textbook Series, Vol. 1, Society of Petroleum Engineers of AIME, Richardson, TX, 1982.
3. Van Everdingen, A. F., and Hurst, W., "The Application of Laplace Transformation to Flow Problems in Reservoirs," *Trans. AIME* (1949) 186, 305–324.
4. Amyx, J. W., Bass, D. M., Jr., and Whiting, R. L., *Petroleum Reservoir Engineering: Physical Properties*, McGraw-Hill, New York, 1960, pp. 78–79.
5. Wattenbarger, R. A., and Ramey, H. J., Jr., "Gas Well Testing With Turbulence, Damage and Wellbore Storage," *J. Pet. Tech.* (Aug. 1968) 877–887; *Trans. AIME*, 243.
6. Ramey, H. J., Jr., "Non-Darcy Flow and Wellbore Storage Effects in Pressure Buildup and Drawdown of Gas Wells," *J. Pet. Tech.* (1965) 223–233; 234.
7. Chen, H.-K., and Brigham, W. E., "Pressure Buildup for a Well With Storage and Skin in a Closed Square," paper SPE 4890 presented at the SPE-AIME 44th Annual California Regional Meeting, San Francisco, April 4–5, 1974.
8. Earlougher, R., Jr., and Ramey, J., Jr., "Interference Analysis in Bounded Systems," *J. Pet. Tech.* (Oct.–Dec. 1973) 33–45.
9. Earlougher, R. C., Jr., Ramey, H. J., Jr., Miller F. G., and Mueller T. D., "Pressure Distributions in Rectangular Reservoirs," *J. Pet. Tech.* (1968) 20, 199–208.
10. Van Poolen, H. K., "Radius of Investigation and Stabilization Time Equations," *Oil Gas J.* (1964) 63 (51), 71–75.
11. Hurst, W., "Establishment of the Skin Effect and Its Impediment to Fluid Flow Into a Wellbore," *Pet. Eng.* (Oct. 1953) B-16.
12. Miller, C. C., Dyes, A. B., and Hutchinson, C. A., Jr., "The Estimation of Permeability and Reservoir Pressure From Bottom Hole Pressure Buildup Characteristic," *Trans. AIME* (1950) 189, 91–104. Also Reprint

- Series, No. 9 – Pressure Analysis Methods, Society of Petroleum Engineers of AIME, Dallas, 1967, pp. 11–24.
13. Horner, D. R., “Pressure Buildup in Wells,” Proc; Third World Pet. Cong; Vol. II, E. J. Brill, Leiden, 1951, p. 503.
 14. Saidikowski, R. M., “Numerical Simulation of the Combined Effects of Wellbore Damage and Partial Penetration,” paper SPE 8204, Sept. 23–26, 1979.
 15. Van Everdingen, A. F., “The Skin Effect and Its Influence on the Productive Capacity of a Well,” *Trans. AIME* (1953) 198, 171–176.
 16. Carter, R. D., “Solutions of Unsteady-State Radial Gas Flow,” *J. Pet. Tech.* (1962) 14, 549–554.
 17. Carter, R. D., “Performance Predictions for Gas Reservoirs Considering Two-Dimensional Unsteady-state Flow,” *Soc. Pet. Eng. J.* (1966) 6, 35–43.
 18. Bruce, G. H., Peaceman, D. W., Richford, A. A., Jr., and Rice, J. D., “Calculations of Unsteady-state Gas Flow Through Porous Media,” *Trans. AIME* (1953) 198, 79–92.
 19. Craft, B. C., and Hawkins M. F., *Applied Petroleum Reservoir Engineering*, Prentice-Hall, Englewood Cliffs, NJ, 1959 (Chapter 6).
 20. Collins, R. E., *Flow of Fluids Through Porous Materials*, Reinhold Publishing Corporation, New York, 1961.
 21. De Wiest, R. J. M. (ed.), *Flow Through Porous Media*, Academic Press, New York, 1969.
 22. Muskat, M., *The Flow of Homogeneous Fluids Through Porous Media*, McGraw-Hill, New York, 1937.
 23. Janicek, J., and Katz, D. L., *Applications of Unsteady-state Gas Flow Calculations*, Preprint, University of Michigan Publishing Services, Ann Arbor, MI, 1955.
 24. Derradii, S., *Bessel Functions, Laplace Transforms and Their Application*, MS Report, University of Tulsa, Tulsa, OK 1983.
 25. Jones, L. G., “An Approximate Method for Computing Non-steady-state Flow of Gases in Porous Media,” *Soc. Pet. Eng. J.* (1961) 1, 264–276.
 26. Watson, E. J., *Laplace Transforms and Applications*, van Nostrand Reinhold Company, New York, 1981, p. 89.
 27. Watson, G. N., *Theory of Bessel Functions*, Cambridge University Press, London, 1944, p. 44.
 28. Abramowitz, M., and Stegun, I. A. (eds.), *Handbook of Mathematical Functions With Formulas, Graphs and Mathematical Tables*, National Bureau of Standards Applied Mathematics Series-55, June 1964, pp. 227–253.
 29. Van Poollan, H. K., Bixel, H. C., and Jargon, J. R., “Reservoir Modeling – 1: What It Is, What It Does.” *Oil and Gas Journal* (July 28, 1969) 158–160.
 30. Chatas, A. T., “A Practical Treatment of Non-steady-state Flow Problems in Reservoir Systems,” *Pet. Eng.*, Part 1 (May 1953) B-42–B-50; Part 2 (June 1953) B-38–B-50, Part 3 (Aug. 1953) B-44–B-56.

Chapter 3

Transient Well Testing Methods for Horizontal Oil Wells

3.1 Introduction

Transient pressure analysis of horizontal wells is more complex than that of vertical wells because of the following reasons:

- Most horizontal well models assume that horizontal wells are perfectly horizontal and are parallel to the top and bottom boundaries of the reservoir. In general, the drilled horizontal wellbores are rarely horizontal, with many variations in the vertical plane along the well length, affecting pressure gauge inserted at the producing end of a horizontal well.
- Calculation is not straightforward because horizontal wells exhibit negative skin factors.
- It is difficult to estimate exact production length of a long horizontal well.

3.2 Flow Equations for Horizontal Oil Wells

This section describes steady-state fluid flow through a reservoir. Mathematical equations are included for horizontal oil wells. In oil wells, normally pressure instead of pressure squared and pseudo-pressure methods are used to describe the relationship between pressures and flow rates.

Steady-State Flow Equations and Solutions

Steady-state flow rate can be predicted by using several solutions which are available in the literature.¹⁶⁻¹⁸ These solutions in US Oilfield Units are given as follows.

Josh¹⁸ Method

$$q_h = \frac{0.007078k_h h(\bar{p}_R - p_{wf})/(\mu_o\beta_o)}{\ln\left[\frac{a + \sqrt{a^2 - (L/2)^2}}{L/2}\right] + (h/L)\ln[h/(2r_w)]} \quad (3-1)$$

where

$$a = (L/2)\left[0.5 + \sqrt{0.25 + (2r_{eh}/L)^4}\right]^{0.5} \quad (3-2)$$

Giger et al.¹⁶ Method

$$q_h = \frac{0.007078k_h L(\bar{p}_R - p_{wf})/(\mu_o\beta_o)}{(L/h)\ln\left[\frac{1 + \sqrt{1 - [L/(2r_{eh})]^2}}{L/(2r_{eh})}\right] + \ln[h/(2\pi r_w)]} \quad (3-3)$$

Borisov¹⁷ Method

$$q_h = \frac{0.007078k_h h(\bar{p}_R - p_{wf})/(\mu_o\beta_o)}{[\ln(4r_e/L) + (h/L)\ln(h/(2\pi r_w))]} \quad (3-4)$$

Giger et al.¹⁶ Method

$$J_h/J_v = \frac{\ln(r_{ev}/r_w)}{\ln\left[\frac{1 + \sqrt{1 - (L/(2r_{eh})^2}}{L/(2r_{eh})}\right] + (h/L)\ln[h/(2\pi r_w)]} \quad (3-5)$$

Renard and Dupay¹⁹ Method

$$q_h = \frac{2\pi k_h(\bar{p}_R - p_{wf})}{\mu_o\beta_o} \left[\frac{1}{\cosh^{-1}(x) + (h/L)\ln(h/(2\pi r_w))} \right] \quad (3-6)$$

where

- $x = 2a/L$ for ellipsoidal drainage area
- $a =$ half the major axis of drainage ellipse (see Eq. 3-2).

Giger et al.¹⁶ Method

$$q_h = \frac{2\pi k_h L(\bar{p}_R - p_{wf})}{\mu_o \beta_o} \left[\frac{1}{(L/h) \ln[1 + \sqrt{1 - (L/(2r_{eh}))^2}]} \right] + \ln[h/(2\pi r_w)] \quad (3-7)$$

In Eqs. 3-1 through 3-7

L = horizontal well length, ft

h = reservoir height, ft

r_w = wellbore radius, ft

r_{ev} = drainage radius of vertical well, ft = $\sqrt{(\text{acres} \times 43,560)/\pi}$

r_{eh} = drainage radius of horizontal well, ft = $\sqrt{(2 \times \text{acres} \times 43,560)/\pi}$

μ_o = oil viscosity, cP

β_o = oil formation volume factor, rb/stb

$\Delta p = (\bar{p}_R - p_{wf})$ = pressure drop from drainage boundary to the wellbore, psi

q_h = horizontal well flow rate, stb/day

$J_h = q_h/\Delta p$ = productivity index for horizontal oil well, stb/(day/psi)

$J_v = q_v/\Delta p$ = productivity index for unstimulated vertical index, stb/(day/psi)

$$J_h = \frac{0.007078 k_h h / (\mu_o \beta_o)}{\ln(r_{ev}/r_w)} \quad (3-8)$$

$$J_{v|\text{Stimulated}} = \frac{0.007078 k_h h / (\mu_o \beta_o)}{\ln(r_{ev}/r_w) + s} = \frac{0.007078 k_h h / (\mu_o \beta_o)}{\ln(r_{ev}/r'_w)} \quad (3-8a)$$

where

$$r'_w = r_w \exp(-s) \quad (3-8b)$$

$$s = -\ln\left(\frac{r'_w}{r_w}\right) \quad (3-8c)$$

For damaged well, $s > 0$ and for stimulated well, $s < 0$.

Example 3-1 *Calculating Steady-state Horizontal Well Productivity Using Various Methods*

A horizontal oil well which is 1250-ft long is drilled in a reservoir with the following characteristics: $h = 170$ ft; $r_w = 0.39$ ft; $\phi = 4.9\%$; $\beta_o = 1.275$ rb/stb;

and $\mu_o = 0.75$ cP. Calculate the steady-state horizontal well productivity using different methods if a vertical well drains 80 acres; $k_v = k_h = 85$ mD.

Solution If a vertical well spacing is 80 acres, then a 1250-ft long horizontal well would drain about 160 acres. For a vertical well draining 80 acres, drained radius, r_{ev} , for a circular drainage area is

$$\text{Area of a circle} = \pi r_{ev}^2 = 80 \text{ acres} \times 43,560 \text{ ft}^2/\text{acre} \Rightarrow r_{ev} = 1053 \text{ ft}$$

The productivity index for a vertical well can be calculated from Eq. 3-8:

$$J_v = \frac{0.007078 k_h h}{\mu_o \beta_o \ln(r_{ev}/r_w)} = \frac{0.007078(85)(170)}{0.75(1.275) \ln(1053/0.39)} = 13.54 \text{ stb}/(\text{day}/\text{psi})$$

For a horizontal well draining 160 acres, the drainage radius of a circular draining area is

$$\text{Area of a circle} = \pi r_{eh}^2 = 160 \times 43,560 \text{ ft}^2/\text{acre} \Rightarrow r_{eh} = 1489 \text{ ft}$$

*Joshi Method*¹⁸

From Eq. 3-2

$$\begin{aligned} a &= (L/2) \left[0.5 + \sqrt{0.25 + (2r_{eh}/L)^4} \right]^{0.5} \\ &= (1250/2) \left[0.5 + 0.25 + (2r_{eh}/L)^4 \right]^{0.5} \cong 1556 \end{aligned}$$

From Eq. 3-1

$$\begin{aligned} J_h &= q_h / (\bar{p}_R - p_{wf}) = \frac{0.007078 k_h h (\bar{p}_R - p_{wf}) / (\mu_o \beta_o)}{\ln \left[\frac{a + \sqrt{a^2 - (L/2)^2}}{L/2} \right] + (h/L) \ln[h/(2r_w)]} \\ &= \frac{0.007078 \times 85 \times 170 / (0.75 \times 1.275)}{\ln \left[\frac{1556 + \sqrt{1556^2 - (1250/2)^2}}{1250/2} \right] + (170/1250) \ln[170/(2 \times 0.39)]} \\ &= \frac{106.96}{1.5658 + 0.7323} = 46.54 \text{ stb}/(\text{day}/\text{psi}) \end{aligned}$$

Giger et al. Method¹⁶

From Eq. 3-3

$$\begin{aligned}
 J_h = q_h / (\bar{p}_R - p_{wf}) &= \frac{0.007078 k_h L / (\mu_o \beta_o)}{(L/h) \ln \left[\frac{1 + \sqrt{1 - [L/(2r_{eh})]^2}}{L/(2r_{eh})} \right] + \ln [h/(2\pi r_w)]} \\
 &= \frac{0.007078 \times 85 \times 1250 / (0.75 \times 1.275)}{(1250/170) \ln \left[\frac{1 + \sqrt{1 - [1250/(2 \times 1489)]^2}}{1250/(2 \times 1489)} \right] + \ln [170/(2 \times (22/7) \times 0.39)]} \\
 &= \frac{786.44}{7.3529 \ln \left[\frac{2.9076}{0.4197} \right] + \ln(69.3473)} = \frac{786.44}{7.3529 \times 1.5141 + 4.2391} \\
 &= 51.16 \text{ stb}/(\text{day}/\text{psi})
 \end{aligned}$$

Borsov Method¹⁷

From Eq. 3-4

$$\begin{aligned}
 J_h = q_h / (\bar{p}_R - p_{wf}) &= \frac{0.007078 k_h h / (\mu_o \beta_o)}{\ln(4r_e/L) + (h/L) \ln(h/(2\pi r_w))} \\
 &= \frac{0.007078 \times 85 \times 170 / (0.75 \times 1.275)}{\ln(4 \times 1489/1250) + (170/1250) \ln(170/(2 \times (22/7) \times 0.39))} \\
 &= \frac{106.95}{1.5613 + 0.1360 \times 4.2391} = 49.89 \text{ stb}/(\text{day}/\text{psi})
 \end{aligned}$$

The productivity ratios for a 160-acre spacing horizontal well and an 80-acre spacing vertical well by different methods are listed in Table 3-1.

Table 3-1
 J_h/J_v by Different Methods

Methods	Productivity index, J_h (stb/day/psi)	J_h/J_v ratio	Aerial productivity index, J_h/acre (stb/(day/psi/acre))
Joshi	46.54	3.44	0.582
Giger	51.16	3.78	0.640
Borosov	49.89	3.68	0.624

Note: Above productivity index comparison assumes an unstimulated vertical well ($s = 0$).

Unsteady-State Flow Equations and Solutions

References 18 and 19 have presented the equations to include the effect of reservoir anisotropy. Their equations in US Oilfield Units are given below.

Renard and Dupuy¹⁹ Method (Eq. 3-6)

$$J_h = \frac{0.007078k_h h}{\mu_o \beta_o} \left[\frac{1}{\cosh^{-1}(x) + (\beta h/L) \ln[h/(2\pi r'_w)]} \right] \quad (3-9)$$

Joshi¹⁸ Method

$$q_h = \frac{q_h}{\Delta p} = \frac{0.007078k_h h}{\mu_o \beta_o \ln \left[\frac{a + \sqrt{a^2 - (L/2)^2}}{L/2} \right] + (\beta h/L) \ln[\beta h/(2r_w)]} \quad (3-10)$$

$$q_h = \frac{q_h}{\Delta p} = \frac{0.007078k_h h}{\mu_o \beta_o \ln \left[\frac{a + \sqrt{a^2 - (L/2)^2}}{L/2} \right] + (\beta^2 h/L) \ln[h/(2r_w)]} \quad (3-11)$$

where

$$r'_w = \frac{1 + \beta}{2\beta}, \quad \beta = \sqrt{\frac{k_h}{k_v}}, \quad x = \frac{2a}{L}$$

The following example shows how to use these equations.

Example 3-2 Calculating Horizontal Well Productivity Index Including Effect of Reservoir Anisotropy

Given well and other reservoir parameters are: $L = 2000$ -ft long horizontal well; $A = 160$ acres; $k_h = 10$ mD; $h = 45$ ft; $\mu_o = 0.45$ cP; $\beta_o = 1.225$ rb/stb; $r_w = 0.39$ ft. Calculate horizontal well productivity index at various values of vertical and horizontal permeability ratios of $k_v/k_h = 0.1, 0.5$ and 1.0 .

Solution Preliminary calculations are:

For $k_v/k_h = 0.1$; $k_v/k_h = 0.5$; and $k_v/k_h = 1$

$$\beta = \sqrt{\frac{k_h}{k_v}} = \sqrt{\frac{1}{0.1}} = 3.162, \quad \beta = \sqrt{\frac{k_h}{k_v}} = \sqrt{\frac{1}{0.5}} = 1.414,$$

$$\beta = \sqrt{\frac{k_h}{k_v}} = \sqrt{\frac{1}{1}} = 1$$

$$r'_w = \frac{1 + \beta}{2\beta} r_w = \frac{1 + 3.162}{2(3.162)} (0.39) = 0.2567,$$

$$r'_w = \frac{1 + \beta}{2\beta} r_w = \frac{1 + 1.414}{2(1.414)} (0.39) = 0.3329,$$

$$r'_w = \frac{1 + \beta}{2\beta} r_w = \frac{1 + 1}{2(1)} (0.39) = 0.39$$

$$\frac{\beta h}{2r_w} = \frac{3.162(45)}{2 \times 0.39} = 182.42, \quad \frac{\beta h}{2r_w} = \frac{1.414(45)}{2 \times 0.39} = 81.58,$$

$$\frac{\beta h}{2r_w} = \frac{1.0(45)}{2 \times 0.39} = 57.69$$

$$\frac{\beta h}{L} = \frac{3.162(45)}{2000} = 0.0711, \quad \frac{\beta h}{L} = \frac{1.414(45)}{2000} = 0.0318,$$

$$\frac{\beta h}{L} = \frac{1(45)}{2000} = 0.0225$$

$$x = \frac{2a}{L} = \frac{2(1665)}{2000} = 1.665, \quad \frac{h}{2\pi r_w} = \frac{45}{2 \times (22/7) \times 0.39} = 18.3566$$

Substituting these values in the following equations we get:

*Renard and Dupuy*¹⁹ method (Eq. 3-9)

For $k_v/k_h = 0.1$

$$J_h = \frac{0.007078 \times 10 \times 45}{0.45(1.225)} \left[\frac{1}{\cosh^{-1}(1.665) + (0.0711) \ln[27.89]} \right]$$

$$= 5.778 \left[\frac{1}{1.0974 + 0.0711(3.3283)} \right] = 4.33 \text{ stb}/(\text{day}/\text{psi})$$

For $k_v/k_h = 0.5$

$$J_h = \frac{0.007078 \times 10 \times 45}{0.45(1.225)} \left[\frac{1}{\cosh^{-1}(1.665) + (0.0318) \ln[21.51]} \right]$$

$$= 5.778 \left[\frac{1}{1.0974 + 0.0318(3.0685)} \right] = 4.84 \text{ stb}/(\text{day}/\text{psi})$$

For $k_v/k_h = 1.0$

$$J_h = \frac{0.007078 \times 10 \times 45}{0.45(1.225)} \left[\frac{1}{\cosh^{-1}(1.665) + (0.0225) \ln[18.3566]} \right]$$

$$= 5.778 \left[\frac{1}{1.0974 + 0.0225(2.9100)} \right] = 4.97 \text{ stb}/(\text{day}/\text{psi})$$

Joshi¹⁸ method (Eq. 3-10)

For $k_v/k_h = 0.1$

$$q_h = \frac{q_h}{\Delta p} = \frac{0.007078 \times 10 \times 45}{0.45(1.225) \ln \left[\frac{1665 + \sqrt{1665^2 - (2000/2)^2}}{2000/2} \right] + (0.0711) \ln[182.42]} = \frac{5.778}{1.0974 + 0.3702} = 3.94 \text{ stb}/(\text{day}/\text{psi})$$

For $k_v/k_h = 0.5$

$$q_h = \frac{q_h}{\Delta p} = \frac{0.007078 \times 10 \times 45}{0.45(1.225) \ln \left[\frac{1665 + \sqrt{1665^2 - (2000/2)^2}}{2000/2} \right] + (0.0318) \ln[81.58]} = 4.67$$

For $k_v/k_h = 1.0$

$$q_h = \frac{q_h}{\Delta p} = \frac{0.007078 \times 10 \times 45}{0.45(1.225) \ln \left[\frac{1665 + \sqrt{1665^2 - (2000/2)^2}}{2000/2} \right] + (0.0225) \ln[57.69]} = 4.86$$

Horizontal well productivity index values, J_h (stb/(day/psi)), are summarized below.

Method	Reservoir anisotropy		
	$k_v/k_h = 0.1$	$k_v/k_h = 0.5$	$k_v/k_h = 1.0$
Renard and Dupuy	4.43	4.86	4.97
Joshi	3.94	4.67	4.86

Figure 3-1 shows that the influence of reservoir anisotropy on horizontal well production increases as anisotropy ratio k_v/k_h increases.

Calculating Effective Wellbore Radius for Horizontal Oil Well

Joshi Technique¹⁸

The effective wellbore radius is defined by Eq. 3-8b. Assuming equal drainage volumes, $r_{eh} = r_{ev}$, and equal productivity indices, $(q/\Delta p)_{\text{vertical}} = (q/\Delta p)_{\text{horizontal}}$. This gives

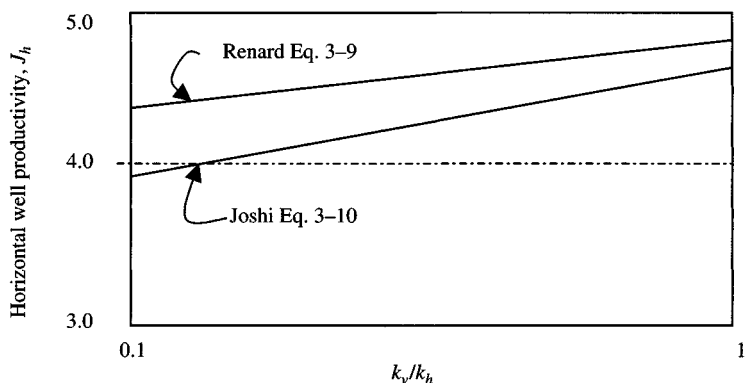


Figure 3-1. Influence of reservoir anisotropy on horizontal well performance.

$$\left| \frac{0.007078k_h h / (\mu_o \beta_o)}{\ln(r_{ev}/r'_w)} \right|_{\text{Eq. 3-8a}}^{\text{Vertical}} = \left| \frac{0.007078k_h h / (\mu_o \beta_o)}{\ln(4r_e/L) + (h/L) \ln(h/(2\pi r_w))} \right|_{\text{Eq. 3-1}}^{\text{Horizontal}}$$

Solving Eqs. 3-1 and 3-8a for r'_w gives

$$r'_w = \frac{r_{eh}(L/2)}{a \left[1 + \sqrt{1 - (L/(2a))^2} \right] \left[h/(2r_w) \right]^{h/L}} \quad (3-12)$$

For anisotropic reservoir, r'_w is

$$r'_w = \frac{r_{eh}(L/2)}{a \left[1 + \sqrt{1 - (L/(2a))^2} \right] \left[\beta h/(2r_w) \right]^{\beta h/L}} \quad (3-13)$$

Van Der Vlis et al. Method²⁰

$$r'_w = \frac{L}{4} \left[\sin\left(\frac{4r_w}{h} \times 90^\circ\right) \cos\left(\frac{\delta}{h} \times 180^\circ\right) \right]^{h/L} \quad (3-14)$$

where δ = vertical distance between reservoir mid-height and well center;
 $\delta = 0$ if well is drilled at the elevation center of the reservoir height.

Skin factor, s , is given by

$$s = -\ln\left(\frac{r'_w}{r_w}\right) \quad (3-8c)$$

Example 3-3 *Calculating Effective Wellbore Radius for Horizontal Well*

Given data and other reservoir parameters: $L = 2000$ -ft long horizontal well; $A = 160$ acres; $k_h = 40$ mD; $h = 80$ ft; $\mu_o = 0.75$ cP; $\beta_o = 1.350$ rb/stb; $r_w = 0.39$ ft; $\delta = 0$. Calculate effective wellbore radius of horizontal well.

Solution Preliminary calculations are

$$r_{eh} = \sqrt{160 \times \frac{43560}{\pi}} = 1489 \text{ ft}$$

$$a = \frac{L}{2} \left[0.5 + \sqrt{0.25 + \left(\frac{2r_{eh}}{L} \right)^4} \right]^{0.5}$$

Using Van Der Vlis et al. method²⁰ (Eq. 3-14)

$$r'_w = \frac{L}{4} \left[\sin \left(\frac{4r_w}{h} \times 90^\circ \right) \cos \left(\frac{\delta}{h} \times 180^\circ \right) \right]^{h/L}$$

$$= \frac{2000}{4} \left[\sin \left(\frac{4 \times 0.33}{80} \times 90^\circ \right) \cos \left(\frac{0}{80} \times 180^\circ \right) \right]^{80/2000}$$

$$= 500[0.0259]^{0.04} = 432.02 \text{ ft}$$

From Eq. 3-8c, skin factor, s , is

$$s = -\ln \left(\frac{r'_w}{r_w} \right) = -\ln \left(\frac{432.02}{0.33} \right) = -7.18$$

Using Eq. 3-12, the effective wellbore radius is

$$r'_w = \frac{r_{eh}(L/2)}{a \left[1 + \sqrt{1 - (L/(2a))^2} \right] \left[h/(2r_w) \right]^{h/L}}$$

$$= \frac{1489(2000/2)}{1665 \left[1 + \sqrt{1 - (2000/(2 \times 1665))^2} \right] [80/(2 \times 0.33)]^{80/2000}} = 410.15 \text{ ft}$$

From Eq. 3-8c, skin factor, s , is

$$s = -\ln \left(\frac{r'_w}{r_w} \right) = -\ln \left(\frac{410.15}{0.33} \right) = -7.13$$

For anisotropic reservoir, term β is given by

$$\beta = \sqrt{\frac{k_h}{k_v}} = \sqrt{\frac{1}{0.5}} = \sqrt{2} = 1.414, \quad \frac{\beta h}{L} = \frac{1.414 \times 80}{2000} = 0.0566$$

and

$$\frac{\beta h}{2r_w} = \frac{1.414 \times 80}{2 \times 0.33} = 171.39$$

Substituting these values in Eq. 3-11, we get

$$\begin{aligned} r'_w &= \frac{r_{eh}(L/2)}{a \left[1 + \sqrt{1 - (L/(2a))^2} \right] \left[\beta h / (2r_w) \right]^{\beta h / L}} \\ &= \frac{1489(2000/2)}{1665 \left[1 + \sqrt{1 - (2000/(2 \times 1665))^2} \right] [171.39]^{0.0566}} = 371.4 \text{ ft} \end{aligned}$$

From Eq. 3-8c, skin factor, s , is

$$s = -\ln\left(\frac{r'_w}{r_w}\right) = -\ln\left(\frac{371.4}{0.33}\right) = -7.03$$

Effect of Formation Damage on Horizontal Well Productivity

Refs. 21-23 have reported the following equations for isotropic reservoir to determine flow rate from damaged horizontal well. Figure 3-2 shows a schematic view of a skin zone near wellbore.

$$\frac{q_{\text{damage}}}{q_h} = \frac{(h/L) \ln[h/(2r_w)] + \ln(c)}{(k/k_{\text{Avg-Vert}})(h/L) \ln[h/(2r_w)] + (k/k_{\text{Avg-Hor}}) \ln(c)} \quad (3-15)$$

where

$$k_{\text{Avg-Vert}} = \frac{k_s k \ln[h/(2r_w)]}{k \ln[(r_w + d)/r_w] + k_s \ln(2r_w + 2d)} \quad (3-16)$$

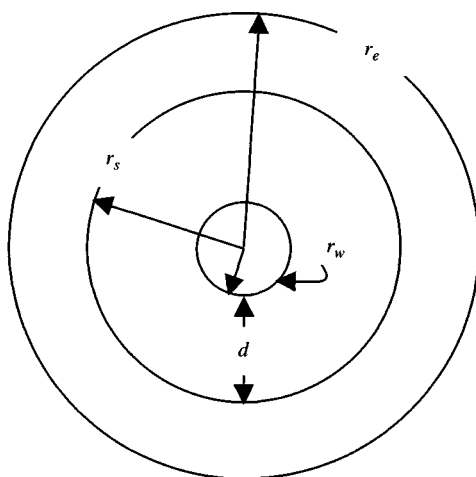


Figure 3-2. View of a skin zone near wellbore.

$$k_{Avg-Hor} = \frac{k_s k \ln[r_e/r_w]}{k \ln[(r_w + d)/r_w] + k_s \ln(r_e/r_w + d)} \quad (3-17)$$

$$c = \frac{r_{eh} + (r_{eh}^2 - (L/2)^2)^{0.5}}{L/2} \quad (3-18)$$

q_{damage} = flow rate of a damaged horizontal well

q_h = flow rate of an undamaged horizontal well

k = formation permeability, mD

k_s = damage zone permeability, mD

d = damage zone thickness, ft

Ref. 15 presented a solution to estimate productivity index of a damaged horizontal well.

$$J_{h,damage} = \frac{0.007078 k_h h}{\mu_o \beta_o \left[\cosh^{-1}(x) + (\beta h/L) \ln[h/(2\pi r'_w)] + s_h \right]} \quad (3-19)$$

where

$$x = \frac{2a}{L}, \quad r'_w = \frac{1 + \beta}{2\beta} r_w$$

s_h = skin factor near wellbore damage given by

$$s_h = \frac{\beta h}{L} \left[\frac{k}{k_s} - 1 \right] \ln\left(\frac{r_s}{r_w}\right) \quad (3-20)$$

$$\frac{s_h}{s_v} = \frac{\beta h}{L}, \quad s_v = \frac{s_h L}{\beta h} \quad (3-21)$$

$$r'_w = \frac{1 + \beta}{2\beta} r_w \quad (3-22)$$

Combining Eqs. 3-9 and 3-20 we can derive the following relationship:

$$\frac{J_{h,damage}}{J_h} = \beta''(\beta'' + s_v) \quad (3-22a)$$

where

$$\beta'' = \left[\frac{L}{h\beta} \right] \cosh^{-1}(x) + \ln \left[\frac{h}{2\pi r'_w} \right] \quad (3-23)$$

The following example will show how to use these equations.

Example 3-4 *Calculating the Effect of Formation Damage on Horizontal Well Productivity for Anisotropic Reservoir*

Horizontal oil well is 2000-ft long and well/reservoir data are: $d = 2$ ft; $k_s = 25$ mD; $k = 100$ mD; $h = 50$ ft; $r_w = 0.33$ ft; $A = 320$ acres. Calculate the effect of formation damage with $d = 0.5, 1, 2,$ and 3 on ratio of q_{damage}/q_h .

Solution $r_{eh} = \sqrt{320 \times 43,560/\pi} = 2106$ ft

From Eq. 3-16

$$\begin{aligned} k_{Avg-Vert} &= \frac{k_s k \ln[h/(2r_w)]}{k \ln[(r_w + d)/r_w + k_s \ln(2r_w + 2d)]} \\ &= \frac{25(100) \ln[50/(2 \times 0.33)]}{100 \ln[(0.33 + 2)/0.33 + 25 \ln(2 \times 0.33 + 2 \times 2)]} = 42.46 \text{ mD} \end{aligned}$$

From Eq. 3-17

$$\begin{aligned} k_{Avg-Hor} &= \frac{k_s k \ln[r_e/r_w]}{k \ln[(r_w + d)/r_w + k_s \ln(r_e/r_w + d)]} \\ &= \frac{25(100) \ln[2106/0.33]}{100 \ln[(0.33 + 2)/0.33 + 25 \ln(2106/(0.33 + 2))]} = 59.9 \text{ mD} \end{aligned}$$

From Eq. 3-18

$$c = \frac{r_{eh} + (r_{eh}^2 - (L/2)^2)^{0.5}}{L/2}$$

$$= \frac{2106 + (2106^2 - (2000/2)^2)^{0.5}}{2000/2} = 4.0676$$

Substituting these values in Eq. 3-15, we get

$$\frac{q_{damage}}{q_h} = \frac{(h/L) \ln[h/(2r_w)] + \ln(c)}{(k/k_{Avg-Vert})(h/L) \ln[h/(2r_w)] + (k/k_{Avg-Hor}) \ln(c)}$$

$$= \frac{(50/2000) \ln[50/(2 \times 0.33)] + \ln(4.0676)}{(42.46)(50/2000) \ln[50/(2 \times 0.33)] + (59.91) \ln(4.0676)} = 0.593$$

Eqs. 3-16 through 3-18 are for isotropic reservoirs only. Eq. 3-18 represents a loss in production for a horizontal well due to wellbore damage. The set of calculations is similar to those reported in Eqs. 3-16 through 3-18; the only difference is that one has to estimate equivalent damage zone thickness, d . The results are shown in Table 3-2 and plotted in Figures 3-3 and 3-4. Table 3-2 shows a significant drop in deliverability of a horizontal well due to near wellbore damage.

Example 3-5 *Determining the Effect of Vertical Well Damage and Reservoir Anisotropy on Horizontal Well Productivity Ratio*

Horizontal oil well is 2000-ft long and well/reservoir data are: $d = 2$ ft; $k_s = 25$ mD; $k = 100$ mD; $h = 50$ ft; $r_w = 0.33$ ft; $A = 160$ acres; $r_{eh} = 1665$ ft. Calculate the effect of formation damage with ratios of $k_v/k_h = 0.1$, 0.5, and 1.0.

Table 3-2
Effect of Formation Damage on q_{damage}/q_h Ratio Calculation

d (ft)	k_s (mD)	$k_{Avg-Vert}$ (mD)	$k_{Avg-Hor}$ (mD)	q_{damage}/q_h
0.5	25	53.86	70.84	0.736
1	25	48.16	65.37	0.666
2	25	42.46	59.90	0.593
3	25	36.76	54.42	0.561

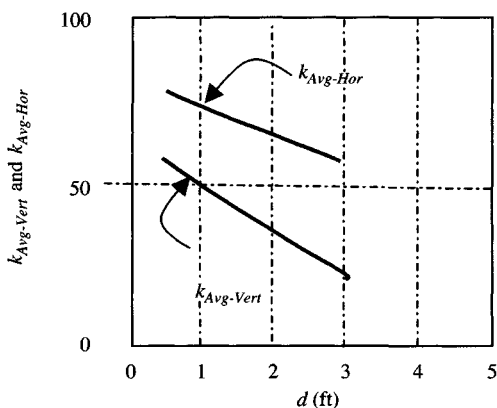


Figure 3-3. Effect of damage zone thickness on k_v and k_h .

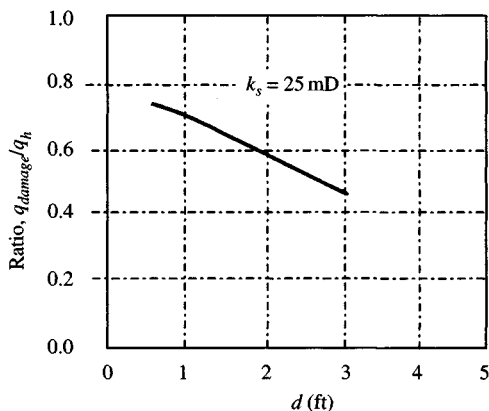


Figure 3-4. Effect of damage zone thickness on q_{damage}/q_h .

Solution

From Eq. 3-21

$$\text{For } \beta = 3.162, \quad s_h = \frac{s_v \times \beta h}{L} = \frac{s_v \times 3.162 \times 50}{2000}$$

$$\text{For } \beta = 1.414, \quad s_h = \frac{s_v \times \beta h}{L} = \frac{s_v \times 1.414 \times 50}{2000}$$

$$\text{For } \beta = 1.000, \quad s_h = \frac{s_v \times \beta h}{L} = \frac{s_v \times 1.000 \times 50}{2000}$$

Table 3-3 is prepared by substituting the values of s_v in the above equations and the results are plotted in Figure 3-5.

Table 3-3
Effect of s_v on Effective Formation Damage, s_h

Skin factor vertical, s_v	s_h		
	$\beta = 3.162$	$\beta = 1.414$	$\beta = 1.000$
1	0.0791	0.0354	0.0250
2	0.1582	0.0707	0.0500
4	0.3164	0.1380	0.1000
6	0.4746	0.2124	0.1500
8	0.6328	0.2832	0.2000
10	0.7910	0.3450	0.2500
15	1.1865	0.5310	0.3750
20	1.5820	0.7080	0.5000

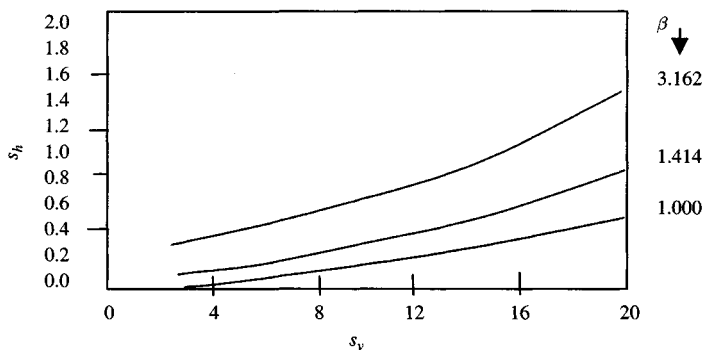


Figure 3-5. Effect of s_v on effective formation damage, s_h .

Investigating Effect of s_v and β on Horizontal Well Productivity Ratio

$$x = \frac{2a}{L} = \frac{2 \times 1665}{2000} = 1.665$$

For $\beta = 3.162$

$$r'_w = \frac{1 + \beta}{2\beta} r_w = \frac{1 + 3.162}{2(3.162)} \times 0.33 = 0.6581$$

From Eq. 3-23

$$\beta'' = \left[\frac{L}{h\beta} \right] \cosh^{-1}(x) + \ln \left[\frac{h}{2\pi r'_w} \right]$$

$$\begin{aligned}
 &= \frac{2000}{50 \times 3.162} \left[\cosh^{-1}(1.665) + \ln \left(\frac{50}{2 \times (22/7) \times 0.6581} \right) \right] \\
 &= 12.65[1.0774 + 2.4921] = 45.41 \\
 r'_w &= \frac{1 + \beta}{2\beta} r_w = \frac{1 + 1.414}{2(1.414)} \times 0.33 = 0.2827
 \end{aligned}$$

From Eq. 3-23

$$\begin{aligned}
 \beta'' &= \left[\frac{L}{h\beta} \right] \cosh^{-1}(x) + \ln \left[\frac{h}{2\pi r'_w} \right] \\
 &= \frac{2000}{50 \times 1.414} \left[\cosh^{-1}(1.665) + \ln \left(\frac{50}{2 \times (22/7) \times 0.2827} \right) \right] \\
 &= 28.29[1.0974 + 3.3371] = 125.45 \\
 r'_w &= \frac{1 + \beta}{2\beta} r_w = \frac{1 + 1.000}{2(1.000)} \times 0.33 = 0.1650
 \end{aligned}$$

From Eq. 3-23

$$\begin{aligned}
 \beta'' &= \left[\frac{L}{h\beta} \right] \cosh^{-1}(x) + \ln \left[\frac{h}{2\pi r'_w} \right] \\
 &= \frac{2000}{50 \times 1.000} \left[\cosh^{-1}(1.665) + \ln \left(\frac{50}{2 \times (22/7) \times 0.1650} \right) \right] \\
 &= 40[1.0974 + 3.8756] = 198.92
 \end{aligned}$$

Calculate $J_{d,h}/J_h$ by substituting the values of s_v in Eq. 3-22a:
 For example, if $s_v = 4$, $\beta = 3.162$, $\beta'' = 45.41$

$$\frac{J_{d,h}}{J_h} = \frac{\beta''}{\beta'' + s_v} = \frac{45.41}{45.41 + 4} = 0.919$$

Tables 3-4 through 3-6 summarize the results obtained using Eqs. 3-20 through 3-23.

Pseudo-Steady-State Equations and Solutions

When the fluid mass situated at the drainage boundary starts moving towards the producing well, the pseudo-steady state begins. This

Table 3-4
Effects of s_v and β on Effective Formation Damage, s_h

Skin factor vertical, s_v	s_h		
	$\beta = 3.162;$ $\beta'' = 45.41$	$\beta = 1.414;$ $\beta'' = 94.19$	$\beta = 1.000;$ $\beta'' = 126.85$
1	0.979	0.989	0.992
2	0.958	0.979	0.985
4	0.919	0.959	0.969
6	0.883	0.940	0.955
8	0.850	0.922	0.941
10	0.820	0.904	0.927
15	0.754	0.863	0.894
20	0.694	0.825	0.864

Table 3-5
Effects of s_v and β on Horizontal Well Productivity Ratio

Skin factor vertical, s_v	Productivity Ratio, $J_{d,h}/J_h$		
	$\beta = 3.162;$ $\beta'' = 45.41$	$\beta = 1.414;$ $\beta'' = 94.19$	$\beta = 1.000;$ $\beta'' = 126.85$
1	0.979	0.989	0.992
2	0.958	0.979	0.985
4	0.919	0.959	0.969
6	0.883	0.940	0.955
8	0.850	0.922	0.941
10	0.820	0.904	0.927
15	0.754	0.863	0.894
20	0.694	0.825	0.864

Table 3-6
Effects of s_h and β on Horizontal Well Productivity Ratio

s_h	s_v	k_v/k_h	$\beta = \sqrt{k_h/k_v}$	β''	$J_{d,h}/J_h$
0.3159	4.0	0.1	3.162	45.41	0.919
0.1412	4.0	0.5	1.414	94.19	0.959
0.0999	4.0	1.0	1.000	126.85	0.969

pseudo-steady-state is also called as semi-steady-state or a depletion state. In other words, it tells us that the reservoir has reached a point where the pressure at all reservoir boundaries and also the average reservoir pressure will decrease over time as more and more fluid is withdrawn from the reservoir. Time to reach pseudo-steady-state, t_{pss} , is calculated as follows:

Dimensionless time, t_D , is

$$t_D = \frac{0.000264 kt}{\phi \mu c_t r_w^2} \quad (3-24)$$

Area-based dimensionless time is defined as

$$t_{DA} = \frac{t_D}{(r_w^2/A)}, \quad A = \text{acre} \times 43,560 \text{ ft}^2 \quad (3-25)$$

Therefore

$$t_{DA} = \frac{0.000264 kt}{\phi \mu c_t A} \quad (3-26)$$

and

$$t_{pss} = \frac{\phi \mu c_t A}{0.000264 k} [t_{DA}]_{Table\ 3-10} \quad (3-27)$$

Drainage area of horizontal well is $\pi ab/43,560$ acre, where a is half major axis of an ellipse and b is half minor axis of an ellipse. (See Figures 3-6 and 3-7.)

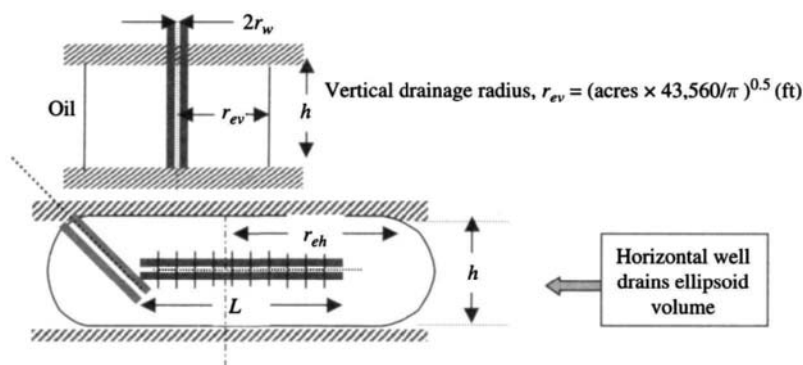


Figure 3-6. Horizontal and vertical well drainage areas.

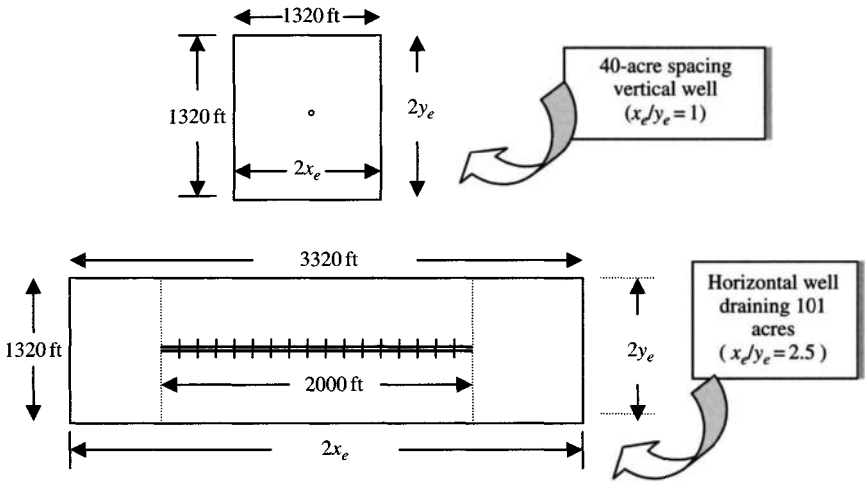


Figure 3-7. Horizontal and vertical well drainage areas for a given time.

Example 3-6 Calculating Drainage Area of Horizontal Well Using Figure 3-7

Solution Half major axis of an ellipse, $a = 2000/2 + 660 = 1660$ ft; half minor axis of an ellipse, $b = 660$ ft; drainage area of horizontal well = $\pi ab/43,560 = (22/7 \times 1660 \times 660)/43,560 \cong 80$ acres.

The pseudo-steady-state equations for vertical wells, fracture vertical wells, and horizontal oil wells on the basis of circular drainage area are

$$\bar{p}_R - p_{wf} = \frac{141.2q\mu\beta}{kh} \left[\ln\left(\frac{r_e}{r_w}\right) - AC' + s + s_m + s_{CA} - C' + Dq \right] \quad (3-28)$$

where

$$D = \frac{2.222 \times 10^{-15} \times \gamma_g k_a h \beta'}{\mu_{pwf} r_w h_p^2} \quad (3-29)$$

$$\beta' = 2.73 \times 10^{10} k_a^{-1.1045} \quad (3-30)$$

or

$$\beta' = 2.33 \times 10^{10} k_a^{-1.201} \quad (3-31)$$

where

s = equivalent negative skin factor due to either well stimulation or due to horizontal well

s_m = mechanical skin factor, dimensionless

s_{CA} = shape-related skin factor, dimensionless

- C' = shape factor conversion constant, dimensionless
 k = permeability, mD
 h = reservoir height, ft
 p_R = average reservoir pressure, psia
 p_{wf} = well flowing pressure, psia
 q = oil flow rate, stb/day
 $\bar{\mu}$ = oil viscosity evaluated at some average pressure between \bar{p}_R and p_{wf}
 β' = high-velocity flow coefficient, 1/ft
 γ_g = gas gravity, dimensionless
 r_w = wellbore radius, ft
 h_p = perforated interval, ft
 k_a = permeability in the near wellbore region, mD
 AC' = 0.75 for a circular drainage area and 0.738 for rectangular drainage area.

Eq. 3-30 for β' is given in Ref. 7 while Eq. 3-31 is given in References 2 and 7. Depending upon β' definition used a somewhat different answer will be obtained. We can also write similar equations on the basis of square drainage area as

$$\bar{p}_R - p_{wf} = \frac{141.2q\mu\beta}{kh} \left[\ln\left(\frac{r_e}{r_w}\right) - 0.738 + s + s_m + s_{CA} - C' + Dq \right] \quad (3-31a)$$

Shape-Related Skin Factors for Vertical and Fractured Oil Wells

In the above equations, definitions of s_{CA} and C' depend upon the type of well as listed below.

Vertical well: $C' = 0$ and s_{CA} from Table 3-10.

Fractured vertical well (Figure 3-8 is an aerial view of a fractured vertical well): $C' = 1.386$ and $s_{CA} = s_{CA,f}$.

$$s_{CA,f} = \ln \sqrt{\frac{30.88}{c_f}}$$

c_f is obtained from Tables 3-7 through 3-9.

Shape Factors for Horizontal Oil Wells

Horizontal well (Figure 3-9 shows a horizontal well located in a rectangular drainage volume): $C' = 1.386$ and $s_{CA} = s_{CA,h}$, where $s_{CA,h}$ is obtained from Table 3-10 or from Figures 3-10 through 3-13.⁸ Dq is a turbulence

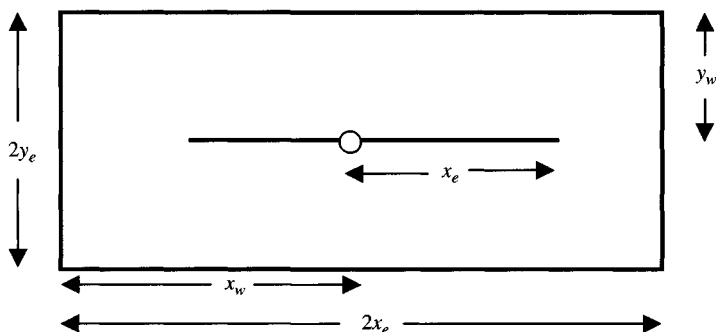


Figure 3-8. An aerial view of fractured vertical oil well.

Table 3-7
Shape Factors c_f for Fractured
Vertical Wells in a Square
Drainage Area³

x_f/x_e	Shape factor, c_f
0.1	2.6541
0.2	2.0348
0.3	1.9986
0.5	1.6620
0.7	1.3127
1.0	0.7887

term and is called turbulence skin or rate-dependent skin factor. Eqs. 3-28 and 3-31a can be used for different well flowing pressures to calculate oil flow rates. Eq. 3-31a can be rewritten as

$$q = \frac{0.007078kh(\bar{p}_R - p_{wf})}{\left[\ln\left(\frac{r_e}{r_w}\right) - 0.75 + s + s_m + s_{CA} - C' + Dq_g \right]}$$

$$= \frac{CC'}{BB' + Dq_g} \quad (3-32)$$

Eqs. 3-31a and 3-32 are quadratic equations and can be written as

$$Dq_g^2 + BB'q_g - CC' = 0 \quad (3-33)$$

$$Dq_g^2 + BB'q_g - CC' = 0 \quad (3-34)$$

and

Table 3-8
Shape Factors, c_f , for Off-Centered-Fractured
Vertical Wells⁸

y_w/y_e	x_f/x_e	Influence of y_w/y_e^*		
		0.25	0.50	1.00
$x_e/y_e = 1$	0.1	0.2240	0.8522	2.0200
	0.3	0.2365	0.7880	1.8220
	0.5	0.2401	0.7165	1.6040
	0.7	0.2004	0.5278	1.3170
	1.0	0.1451	0.3606	0.7909
$x_e/y_e = 2$	0.1	0.2272	0.7140	1.4100
	0.3	0.3355	0.7700	1.3610
	0.5	0.4325	0.8120	1.2890
	0.7	0.4431	0.7460	1.1105
	1.0	0.2754	0.4499	0.6600
$x_e/y_e = 5$	0.1	0.0375	0.09185	0.2110
	0.3	0.1271	0.20320	0.2864
	0.5	0.2758	0.38110	0.4841
	0.7	0.3851	0.49400	0.5960
	1.0	0.2557	0.31120	0.3642
x_w/x_e	x_f/x_e	Influence of x_w/x_e^*		
		0.50	0.75	1.00
$x_e/y_e = 1$	0.1	0.9694	1.7440	2.0200
	0.3	1.1260	1.7800	1.8200
	0.5	1.2708	1.7800	1.6000
$x_e/y_e = 2$	0.1	0.3679	1.0680	1.4098
	0.3	0.5630	1.2980	1.3611
	0.5	0.8451	1.5470	2.2890
$x_e/y_e = 5$	0.1	0.0058	0.0828	0.2110
	0.3	0.0317	0.2540	0.2864
	0.5	0.1690	0.7634	0.6050

* x_w and y_w represent the distance of the fracture center from the nearest y - and x -boundary, respectively (see Figure 3-7).






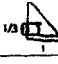

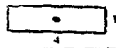
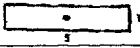

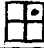
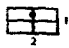
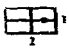
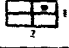
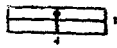
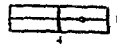
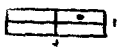
Table 3-9
Shape Factors, c_f , for Fractured Vertical Wells Located Centrally
in the Rectangular Drainage Area⁹

$c_f, x_f/x_e$	1	2	3	5	10	20
0.1	2.020	1.4100	0.751	0.2110	0.0026	0.000005
0.3	1.820	1.3611	0.836	0.2860	0.0205	0.000140
0.5	1.600	1.2890	0.924	0.6050	0.1179	0.010550
0.7	1.320	1.1100	0.880	0.5960	0.3000	0.122600
1.0	0.791	0.6662	0.528	0.3640	0.2010	0.106300

Table 3-9a
Values of Dimensionless Function, F , for Estimation
of Horizontal Well Productivity¹¹

← $y_w/2y_e = 0.50$ and $x_w/2x_e = 0.50$ →						
← $L/4x_e$ →						
$y_e/x_e \sqrt{k_x/k_y}$	0.1	0.2	0.3	0.4	0.5	
0.25	3.80	2.11	1.09	0.48	0.26	
0.50	3.25	1.87	1.12	0.69	0.52	
1.00	3.62	2.30	1.60	1.21	1.05	
2.00	4.66	3.34	2.65	2.25	2.09	
4.00	6.75	5.44	4.74	4.35	4.19	
← $y_w/2y_e = 0.25$ and $x_w/2x_e = 0.50$ →						
0.25	4.33	2.48	1.36	0.70	0.46	
0.50	3.89	2.42	1.58	1.10	0.92	
1.00	4.47	3.13	2.41	2.00	1.83	
2.00	6.23	4.91	4.22	3.83	3.67	
4.00	9.90	8.58	7.88	7.49	7.33	
← $y_w/2y_e = 0.25$ and $x_w/2x_e = 0.25$ →						
0.25	9.08	7.48	6.43	5.65	5.05	
0.50	6.97	5.56	4.71	4.12	3.71	
1.00	6.91	5.54	4.76	4.24	3.90	
2.00	8.38	7.02	6.26	5.76	5.44	
4.00	11.97	10.61	9.85	9.36	9.04	
← $y_w/2y_e = 0.50$ and $x_w/2x_e = 0.25$ →						
0.25	8.44	6.94	5.98	5.26	4.70	
0.50	6.21	4.83	4.02	3.47	3.08	
1.00	5.86	4.50	3.73	3.23	2.90	
2.00	6.73	5.38	4.62	4.12	3.81	
4.00	8.82	7.46	6.71	6.21	5.89	

Table 3-10
Shape Factor-Dependent Skin Factors, s_{CA} ,
for Vertical Wells (after Fetkovich and Vienot, Feb. 1985)⁴

Geometry	C_A	s_{CA}	t_{DApss}
	31.62	0.000	0.1
	30.88	0.012	0.1
	31.60	0.000	0.1
	27.60	0.068	0.2
	27.10	0.077	0.2
	21.90	0.184	0.4
	21.84	0.185	0.3
	5.379	0.886	0.8
	2.361	1.298	1.0
	12.98	0.445	0.7
	4.513	0.973	0.6
	10.84	0.535	0.4
	4.514	0.973	2.5
	2.077	1.362	1.7
	2.690	1.232	0.8
	0.232	2.458	4.0
	0.115	2.806	4.0

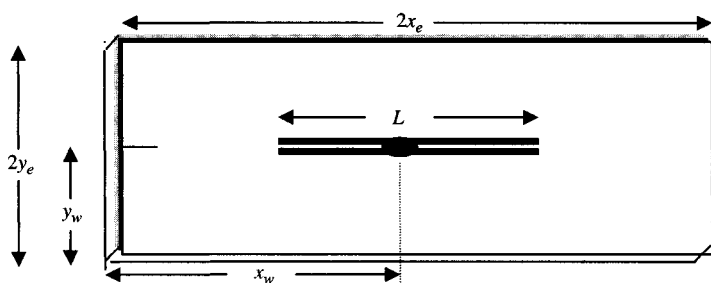


Figure 3-9. A schematic of a horizontal well located in a rectangular drainage volume.

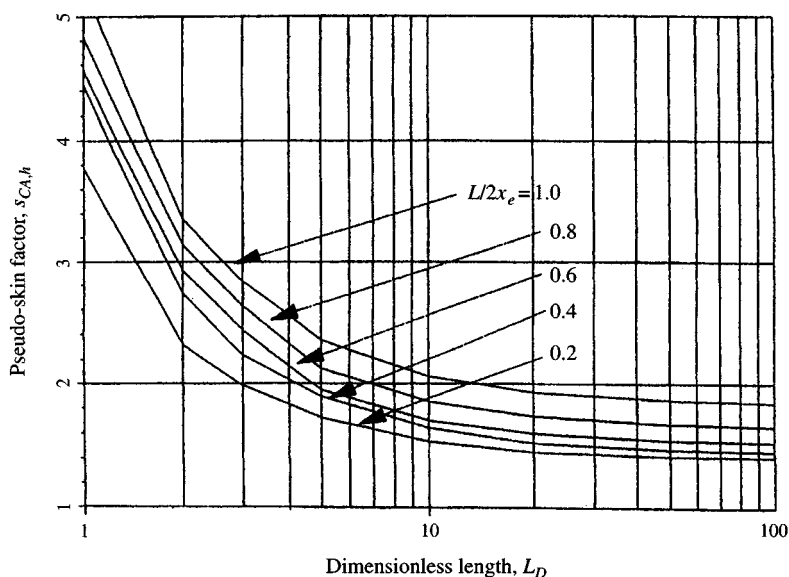


Figure 3-10. Shape-related skin factor, $s_{CA,h}$, for a horizontal well in a square drainage area ($x_e/y_e = 1$).⁸

$$q_g = \frac{-BB + \sqrt{(BB)^2 + 4D(CC)}}{2D} \quad (3-35)$$

$$q_g = \frac{-BB' + \sqrt{(BB')^2 + 4D(CC')}}{2D} \quad (3-36)$$

To solve Eqs. 3-35 and 3-36 we need to calculate turbulence factor D using Eqs. 3-29 and 3-30 and assuming $k = k_a$.

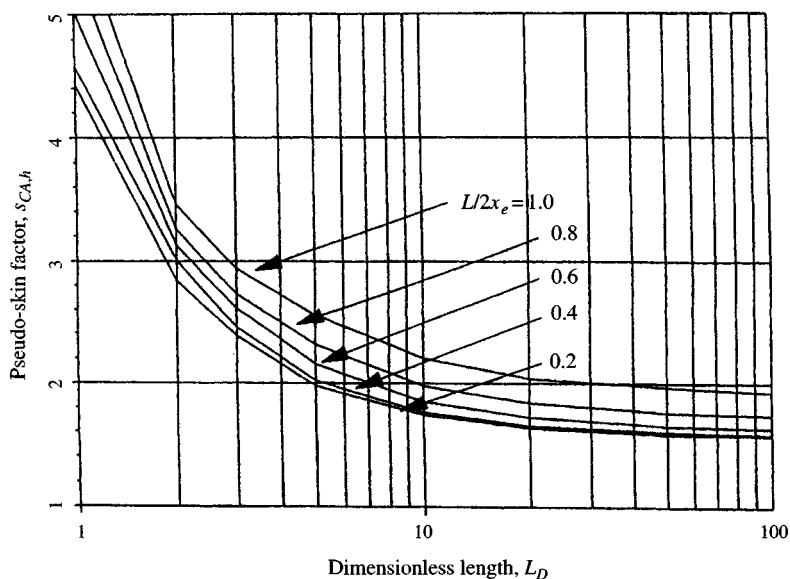


Figure 3-11. Shape-related skin factor, $s_{CA,h}$, for a horizontal well located in a rectangular drainage area ($x_e/y_e = 2$).⁸

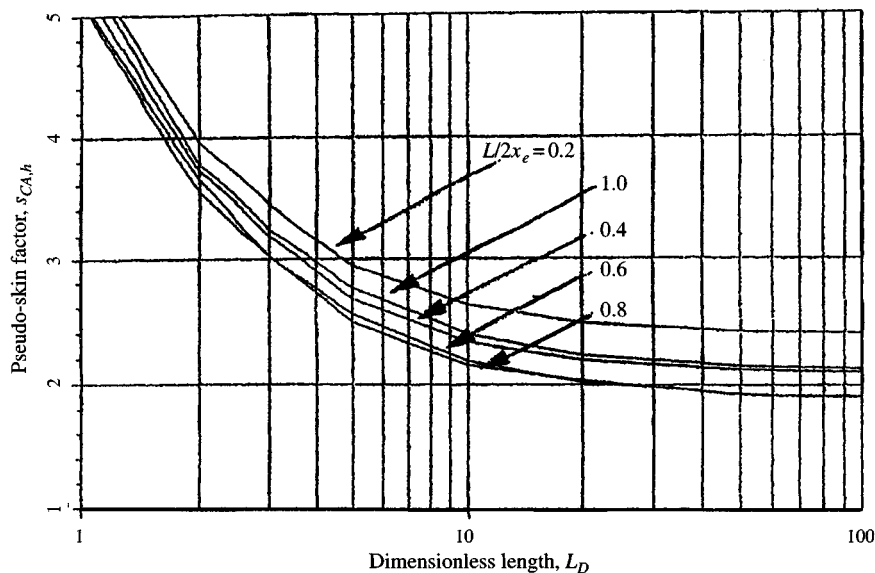


Figure 3-12. Shape-related skin factor, $s_{CA,h}$, for a horizontal well located in a rectangular drainage area ($x_e/y_e = 5$).⁸

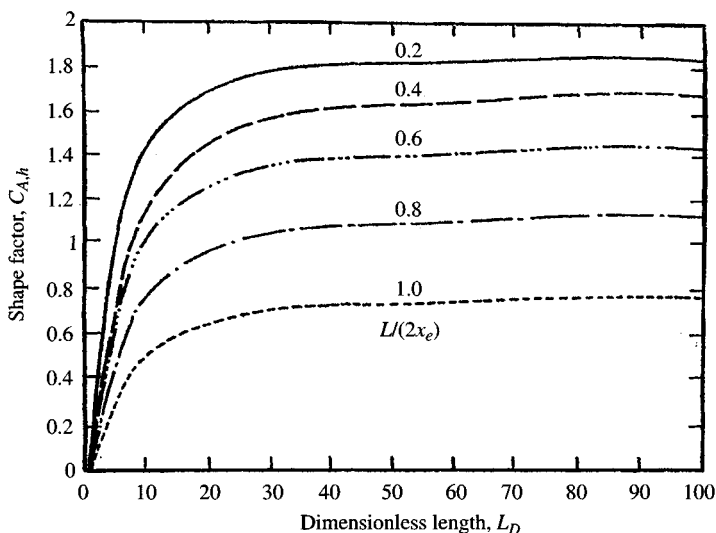


Figure 3-13. Shape factor, $C_{A,h}$, for a horizontal well located in a square drainage area for different dimensionless length.⁸

Calculation of Skin Factor for Horizontal Oil Well

$$r'_w = \frac{L}{4} \quad (3-37)$$

$$s = -\ln\left(\frac{r'_w}{r_w}\right) \quad (3-38)$$

Figure 3-14 shows a graphic correlation for shape factor c'_f ; to convert this shape factor c'_f to c_f , the following equation can be used: $c_f = 0.25c'_f$. Instead of calculating shape factors, one can adjust effective wellbore radius of a fractured vertical well to account for both fracture length as well as shape factor. Figure 3-15 shows a plot of effective wellbore radius for vertical wells with uniform flux and infinite-conductivity fractures for different fracture penetrations. The effective wellbore radius, r'_w , calculated from Figure 3-15 can be directly substituted in place of r_w in the following equations to calculate gas flow rate in fractured vertical wells, where the vertical well is located centrally in a square drainage area. These results can also be extended to rectangular drainage boundaries for varying $(2x_e/2y_e)$ ratios by replacing (x_f/x_e) with $(2x_f/\sqrt{A})$ on the x -axis in Figure 3-15.

$$q_g = \frac{0.007078kh[\bar{p}_R - p_{wf}]}{\mu\beta[\ln(r_e/r_w) - 0.75]} \quad (3-39)$$

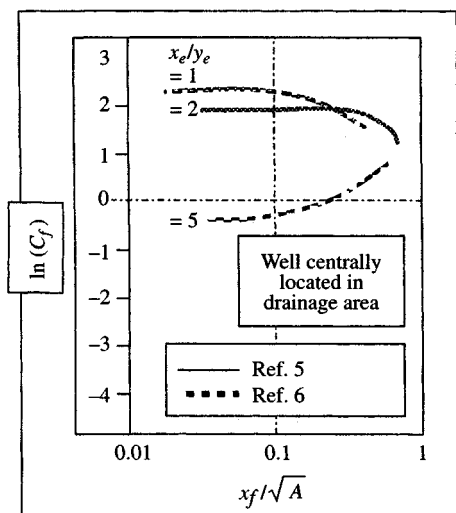


Figure 3-14. Shape factors for fractured vertical wells for different fractured penetration (after Gringarten, Oct. 1978).⁹

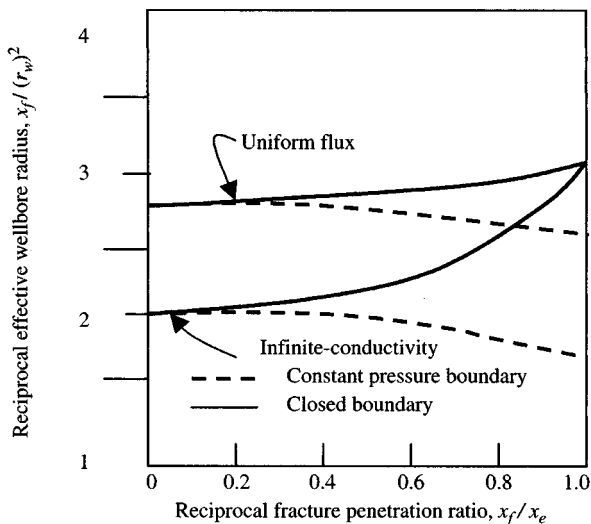


Figure 3-15. Effective wellbore radius for fractured vertical wells for different fracture penetration (after Gringarten, Aug. 1974).¹⁰

Calculation of s_{CA}

Assuming a square drainage area with each side being $2x_e$ for 640 acres, we have

$$2x_e = \sqrt{\text{acre} \times 43,560} \quad (\text{ft}) \quad (3-40)$$

First find $L/2x_e$ and k_v/k_h ; then calculate L_D using the following equation:

$$L_D = \frac{L}{2h} \sqrt{\frac{k_v}{k_h}} \quad (3-41)$$

From Figure 3-13 or Table 3-9, corresponding to L_D and $L/2x_e$, find s_{CA} .

Pseudo-Steady-State Productivity Calculation Methods

Method 1 (Mutalik et al.⁸ Method)

This method assumes a horizontal well drilled in a bounded reservoir as an infinite-conductivity well. Mutalik et al.⁸ have reported the shape factors and the corresponding equivalent skin factors, $s_{CA,h}$, for horizontal wells located at various positions within the drainage volume. The pseudo-skin factors, $s_{CA,h}$, for centrally located wells within drainage area with ratios of sides $2x_e/2y_e = 1, 2$ and 5 are plotted in Figures 3-10 through 3-13 and are summarized in Table 3-11. The following equation can be used to calculate the productivity of a horizontal oil well.

$$J_h = \frac{q_o}{\bar{p}_R - p_{wf}} = \frac{kh}{141.2\beta_o\mu_o} \left(\frac{1}{\ln(r'_e/r_w) - A' + s_f + s_m + s_{CA,h} - C' + Dq_o} \right) \quad (3-42)$$

where

$$r'_e = \sqrt{A/\pi}, \text{ ft}$$

r_w = wellbore radius, ft

$$A' = \text{drainage area constant} = \frac{1}{2} [\ln(2.2458\pi) - \ln(C_A)] \quad (3-42a)$$

C_A = shape factor, dimensionless; the values are listed in Table 3-10

s_m = mechanical skin factor, dimensionless

$s_f = -\ln \left[\frac{L}{4r_w} \right]$ = negative skin factor of an infinite-conductivity, fully penetrating fracture of length, L

Tables 3-11
Shape-Related Skin Factors, $s_{CA,h}$, for Horizontal Wells
for Various Well Penetrations and Different Rectangular
Drainage Area⁸

t_D	$L/2x_e$				
	0.2	0.4	0.6	0.8	1.0
$x_e/y_e = 1$					
1	3.772	4.439	4.557	4.819	5.250
2	2.231	2.732	2.927	3.141	3.354
3	1.983	2.240	2.437	2.626	2.832
5	1.724	1.891	1.948	2.125	2.356
10	1.536	1.644	1.703	1.851	2.061
20	1.452	1.526	1.598	1.733	1.930
50	1.420	1.471	1.546	1.672	1.863
100	1.412	1.458	1.533	1.656	1.845
$x_e/y_e = 2$					
1	4.425	4.578	5.025	5.420	5.860
2	2.840	3.010	3.130	3.260	3.460
3	2.380	2.459	2.610	2.730	2.940
5	1.982	2.020	2.150	2.310	2.545
10	1.740	1.763	1.850	1.983	2.198
20	1.635	1.651	1.720	1.839	2.040
50	1.584	1.596	1.650	1.762	1.959
100	1.572	1.582	1.632	1.740	1.935
$x_e/y_e = 5$					
1	5.500	5.270	5.110	5.140	5.440
2	3.960	3.720	3.540	3.650	3.780
3	3.440	3.190	3.020	3.020	3.250
5	2.942	2.667	2.554	2.493	2.758
10	2.629	2.343	2.289	2.155	2.399
20	2.491	2.196	2.022	2.044	2.236
50	2.420	2.120	1.934	1.925	2.150
100	2.408	2.100	1.909	1.903	2.136

$s_{CA,h}$ = shape-related skin factor or pseudo-skin factor that can be determined from Table 3-11 or using Figures 3-10 through 3-13

C' = shape factor conversion constant = $(1/2) \ln 16 = 1.386$.

The calculation of various parameters using Eq. 3-32 involves the following steps:

1. Determine A' as $1/2[\ln(2.2458\pi) - \ln(C_A)]$.
2. Calculate negative skin factor, s_f , as $-\ln(L/(4r_w))$.

3. Determine the value of $s_{CA,h}$ from Table 3-10 or Figures 3-10 through 3-13.
4. Knowing the values of A', s_f and $s_{CA,h}$ the productivity can then be calculated by using Eq. 3-42.

Method 2 (Kuchuk et al.¹¹ Method)

Kuchuk et al. used an approximate infinite-conductivity solution, where the constant wellbore pressure is calculated by averaging pressure values of the uniform-flux solution along the well length. They derived the following equation for horizontal well pseudo-steady-state productivity:

$$J_h = \frac{q_o}{\bar{p}_R - p_{wf}} = \frac{k_h h / (70.6 \beta_o \mu_o)}{F + (h/0.5L) \sqrt{k_h/k_v s_x}} \quad (3-43)$$

F is a dimensionless function and depends upon the values of $y_w/2y_e$, $x_w/2x_e$, $L/4x_e$ and $(y_e/x_e) \sqrt{k_x/k_y}$. Typical values of the function F are listed in Table 3-9a. The value of s_x is calculated using the following equation:

$$s_x = -\ln \left[\left(\frac{\pi r_w}{h} \right) \left(1 + \sqrt{\frac{k_v}{k_h}} \right) \sin \left(\frac{\pi z_w}{h} \right) \right] - \sqrt{\frac{k_h}{k_v}} \left(\frac{2h}{L} \right) \left[\frac{1}{3} - (z_w/h) + (z_w/h)^2 \right] \quad (3-44)$$

Method 3 (Odeh and Babu¹² Method)

This method assumes uniform-flux boundary conditions. They derived the expression $q_h = (\text{PI})/(\bar{p}_R - p_{wf})$ from the analytical solution of their mathematical model, and therefore they need an independent method to evaluate s_R . Babu and Odeh use a material balance equation for this purpose. Here PI is the productivity index and \bar{p}_R is the average reservoir pressure at pseudo-steady-state condition. In the Odeh and Babu method, all boundaries are no-flow boundaries. They consider a uniform-flux solution given by the equation (see Figure 3-15):

$$J_h = \frac{q_o}{\bar{p}_R - p_{wf}} = \frac{(2x_e) \sqrt{k_y k_v}}{141.2 \beta_o \mu_o} \left(\frac{1}{\ln(\sqrt{A_1}/r_w) - A' + \ln C_H + s_R} \right) \quad (3-45)$$

where

q_o = constant rate of production, stb/day
 \bar{p}_R = average reservoir pressure, psi

p_{wf} = flowing bottomhole pressure, psi

r_w = wellbore radius, ft

β_o = oil formation volume factor

μ_o = oil viscosity, cP

C_H = geometric factor

s_R = pseudo-skin factor due to fractional penetration; 0 if $L = 2x_e$

A' = drainage area constant given by Eq. 3-42a

A_1 = horizontal well drainage area in the vertical plane = $2y_e h$

$2x_e, 2y_e$ = reservoir dimensions shown in Figure 3-8

k_y = horizontal permeability in the direction perpendicular to the wellbore.

Eq. 3-45 includes no formation damage, but it can be included as an additive term in the denominator.

Estimation of $\ln C_H$

$$\ln C_H = 6.28 \left(\frac{2y_e}{h} \right) \sqrt{\frac{k_v}{k_y}} \left[\frac{1}{3} - \frac{y_w}{2y_e} + (y_w/2y_e)^2 \right] - \ln \left[\sin(180^\circ) \times \frac{z_w}{h} \right] - 0.5 \ln \left[\frac{2y_e}{h} \sqrt{\frac{k_v}{k_y}} \right] - 1.088 \quad (3-46)$$

where

z_w = vertical distance between the horizontal and the bottom boundary (see Figure 3-8)

y_w = the distance from the horizontal well to the closest boundary in the y -direction.

Estimation of s_R

$s_R = 0$ when $L = 2x_e$. If $L < 2x_e$, then the value of partial penetration skin factor s_R depends upon the following two conditions:

1. $2y_e/\sqrt{k_y} \geq 1.5x_e/\sqrt{k_x} \gg 0.75h/\sqrt{k_y}$
2. $2x_e/\sqrt{k_x} \geq 2.66y_e/\sqrt{k_y} \gg 1.33h/\sqrt{k_y}$

Case 1:

$$s_R = \text{PXYZ} + \text{PXY}' \quad (3-47)$$

Here

$$\text{PXYZ} = \left[\frac{2x_e}{L} - 1 \right] \left[\ln \left(\frac{h}{r_w} \right) + 0.25 \ln \left(\frac{k_y}{k_x} \right) - \ln(\sin 180^\circ z_w) - 1.84 \right] \quad (3-48)$$

$$PXY' = \left(\frac{2(2x_e)^2 \sqrt{\frac{k_v}{k_y}}}{Lh} \right) \left[\int \left(\frac{L}{4x_e} \right) + 0.5 \left[\int \left(\frac{4x_w + L}{4x_e} \right) - \int \left(\frac{4x_w - L}{4x_e} \right) \right] \right] \quad (3-49)$$

If $\frac{4x_w + L}{4x_e}$ or $\frac{4x_w - L}{4x_e} > 1.0$, then the following equation can be used:

$$\int \left(\frac{4x_w + L}{4x_e} \right) = \left(2 - \frac{4x_w + L}{4x_e} \right) \left[0.145 + \ln \left(2 - \frac{4x_w + L}{4x_e} \right) - 0.137 \left(2 - \frac{4x_w + L}{4x_e} \right)^2 \right] \quad (3-50)$$

If $\frac{4x_w - L}{4x_e} > 1.0$, then use the following equation:

$$\int \left(\frac{4x_w - L}{4x_e} \right) = \left(2 - \frac{4x_w - L}{4x_e} \right) \left[0.145 + \ln \left(2 - \frac{4x_w - L}{4x_e} \right) - 0.137 \left(2 - \frac{4x_w - L}{4x_e} \right)^2 \right] \quad (3-51)$$

If $(4x_w + L)/4x_e \leq 1.0$, then use the equation:

$$\int \left(\frac{4x_w + L}{4x_e} \right) = - \left(\frac{4x_w + L}{4x_e} \right) \left[0.145 + \ln \left(2 - \frac{4x_w + L}{4x_e} \right) - 0.137 \left(\frac{4x_w + L}{4x_e} \right)^2 \right] \quad (3-52)$$

If $(4x_w - L)/4x_e \leq 1.0$, then use the equation:

$$\int \left(\frac{4x_w - L}{4x_e} \right) = - \left(\frac{4x_w - L}{4x_e} \right) \left[0.145 + \ln \left(\frac{4x_w - L}{4x_e} \right) - 0.137 \left(\frac{4x_w - L}{4x_e} \right)^2 \right] \quad (3-53)$$

The function $\int (L/4x_e)$ is calculated by using the following equation:

$$\int \left(\frac{L}{4x_e} \right) = - \frac{L}{4x_e} \left[0.145 + \ln \left(\frac{L}{4x_e} \right) - 0.137 \left(\frac{L}{4x_e} \right)^2 \right] \quad (3-54)$$

where x_w is the distance from the horizontal well mid-point to the closet boundary in the x -direction (see Figure 3-8). Additionally, pressure computations are made at the mid-point along the well length.

Case 2:

$$s_R = PXYZ + PY + PXY \quad (3-55)$$

The three components in the above Eq. 3-55 are given below:
The PXYZ component is calculated using Eq. 3-48.

$$\begin{aligned} \text{The PY component} = & 6.28 \frac{(2x_e)^2 \sqrt{k_y k_v}}{2y_e h} \left[\left\{ \frac{1}{3} - \left(\frac{x_w}{2x_e} \right) + \left(\frac{x_w}{2x_e} \right)^2 \right\} \right. \\ & \left. + \frac{L}{48x_e} \left(\frac{L}{2x_e} - 3 \right) \right] \end{aligned} \quad (3-56)$$

where x_w is the mid-point coordinate of the well.

$$\begin{aligned} \text{The PXY component} = & \left(\frac{2x_e}{L} - 1 \right) \frac{6.28(2y_e)}{h} \sqrt{\frac{k_v}{k_y}} \left[\frac{1}{3} - \left(\frac{y_w}{2y_e} \right) + \left(\frac{y_w}{2y_e} \right)^2 \right] \\ & \quad (3-57) \end{aligned}$$

$$[\min\{y_w(2y_e - y_w)\} \geq 0.5y_e]$$

Eq. 3-57 is an approximation of the rigorous solution given below:

$$\begin{aligned} PXY = & \left(\frac{2x_e}{L} - 1 \right) \frac{6.28(2y_e)}{h} \sqrt{\frac{k_v}{k_y}} \left[\frac{1}{3} - \left(\frac{y_w}{2y_e} \right) + \left(\frac{y_w}{2y_e} \right)^2 \right] - \left[\frac{4(2x_e)(2y_e)}{\pi L h} \right] \\ & \sqrt{\frac{k_v}{k_y}} \sum_1^3 \left[\frac{1}{n^2} \cos^2 \left(\frac{n\pi y_w}{2y_e} \right) \exp \left(\frac{n\pi L}{4y_e} \sqrt{\frac{k_y}{k_x}} \right) \right] \end{aligned} \quad (3-58)$$

Although Eq. 3-58 gives more accurate results, Eq. 3-57 is an adequate approximation for many field applications. The following example will illustrate how to use these equations.

Example 3-7 *Calculating Pseudo-Steady-State Horizontal Oil Well Productivity Using Various Methods*

A horizontal oil well which is 2000 ft long is drilled in a reservoir with the following characteristics: $h = 100$ ft; $r_w = 0.39$ ft; $\phi = 4.9\%$; $\beta_o = 1.215$ rb/stb; $\mu_o = 0.45$ cP; $s_m = 0$; $D = 0$; $z_w = 30$ ft; $kh = k_x = k_y = 1.0$ mD; and $k_v/k_h = 0.5$. Assuming square drainage area = 160 acres, calculate the pseudo-steady-state horizontal well productivity using various methods.

Solution

Method 1:

$$r'_w = \sqrt{\frac{A}{\pi}} = \sqrt{\frac{160 \times 43,560}{\pi}} = 1489 \text{ ft} \quad (3-58a)$$

$$s_f = -\ln\left[\frac{L}{4r'_w}\right] = -\ln\left[\frac{2000}{4 \times 0.39}\right] = -7.1562 \quad (3-58b)$$

 Calculation of $s_{CA,h}$

$$L_D = \frac{L}{2h} \sqrt{\frac{k_v}{k_h}} = \frac{2000}{2 \times 100} \sqrt{1.0} = 10 \quad (3-58c)$$

 For a square drainage shape, $2x_e = 2y_e$. Therefore

$$2x_e = \sqrt{160 \times 43,560} = 2640 \text{ ft}, \quad \frac{L}{2x_e} = \frac{2000}{2640} = 0.757$$

 From Figure 3-10 (using the values of $L_D = 10$, $L/2x_e = 0.757$) shape-related pseudo-skin factor $s_{CA,h} = 1.82$.

$$\begin{aligned} A' &= 0.5[\ln(C_A)_{Table\ 2-1} - \ln(2.2458\pi)] \\ &= 0.5[\ln(31.62)_{Table\ 2-1} - \ln(2.2458 \times 22/7)] = 0.738 \end{aligned}$$

$$s_f = -7.1562, \quad s_m = 0, \quad D = 0, \quad C_1 = 1.386$$

Using Eq. 3-42

$$\begin{aligned} J_h &= \frac{q_o}{\bar{p}_R - p_{wf}} \\ &= \frac{kh}{141.2\beta_o\mu_o} \left(\frac{1}{\ln(r'_e/r_w) - A' + s_f + s_m + s_{CA,h} - C' + Dq_o} \right) \\ &= \frac{1 \times 100}{141.2 \times 0.45 \times 1.215} \\ &\quad \left(\frac{1}{\ln(1489/0.39) - 0.738 + (-7.1562) + 0 + 1.82 - 1.386 + 0} \right) \\ &= \frac{1.2946}{8.2475 - 0.738 - 7.1562 + 1.82 - 1.386} = 1.644 \text{ stb}/(\text{day}/\text{psi}) \end{aligned}$$

Method 2:

In order to calculate the value of F , first estimate the following parameters:

$$\frac{L}{4x_e} = \frac{2000}{4 \times 1320} = 0.3788, \quad \frac{x_w}{2x_e} = \frac{1320}{2640} = 0.5$$

$$\frac{y_w}{2y_e} = \frac{1320}{2640} = 0.5, \quad \frac{y_e}{x_e} \sqrt{\frac{k_x}{k_y}} = 1 \times \sqrt{1} = 1.0$$

From Table 3-9a, for these sets of values, $F = 1.05$.

Calculation of s_x

$$\frac{k_v}{k_y} = \frac{k_v}{k_h} = 0.1, \quad \frac{k_y}{k_x} = 1, \quad \frac{k_h}{k_v} = \frac{1}{0.1} = 10, \quad \frac{z_w}{h} = \frac{30}{100} = 0.3,$$

$$\frac{h}{0.5L} = \frac{100}{0.5(2000)} = 0.10$$

Using Eq. 3-44

$$\begin{aligned} s_x &= -\ln \left[\left(\frac{\pi r_w}{h} \right) \left(1 + \sqrt{\frac{k_v}{k_h}} \right) \sin \left(\frac{\pi z_w}{h} \right) \right] - \sqrt{\frac{k_h}{k_v}} \left(\frac{2h}{L} \right) \left[\frac{1}{3} - \left(\frac{z_w}{h} \right) + \left(\frac{z_w}{h} \right)^2 \right] \\ &= -\ln \left[\left(\frac{\pi \times 0.39}{100} \right) \left(1 + \sqrt{0.1} \right) \sin \left(\frac{180 \times 0.3}{100} \right) \right] - \sqrt{10} (0.10) \\ &\quad [0.333 - 0.3 + 0.3^2] \\ &= -\ln [0(0.0123)(1 + \sqrt{0.1}) \sin(0.54)] - 0.0389 \\ &= -\ln [0.0123 \times 1.8090] - 0.0389 = 3.767 \end{aligned}$$

From Eq. 3-43, with values of $k_v/k_h = 0.5$ and $k_h/k_v = 2$

$$\begin{aligned} J_h &= \frac{k_h h / (70.6 \beta_o \mu_o)}{F + (h/0.5L) \sqrt{k_h/k_v} s_x} \\ &= \frac{1 \times 100 / (70.6 \times 0.45 \times 1.215)}{1.05 + (100 / (0.5 \times 2000)) \sqrt{2} \times 3.767} = 1.638 \end{aligned}$$

Method 3 ($k_v/k_y = k_v/k_h = 0.5$):

Estimation of $\ln C_H$

$$\frac{z_w}{h} = \frac{30}{100} = 0.333, \quad \frac{y_w}{2y_e} = \frac{1320}{2640} = 0.50$$

From Eq. 3-46

$$\begin{aligned} \ln C_H &= 6.28 \left(\frac{2y_e}{h} \right) \sqrt{\frac{k_v}{k_y} \left[\frac{1}{3} - \frac{y_w}{2y_e} + \left(\frac{y_w}{2y_e} \right)^2 \right]} - \ln \left[\sin(180^\circ) \frac{z_w}{h} \right] \\ &\quad - 0.5 \ln \left[\frac{2y_e}{h} \sqrt{\frac{k_v}{k_y}} \right] - 1.088 \\ &= 6.28 \left(\frac{2640}{100} \right) \sqrt{0.1 \left[\frac{1}{3} - 0.5 + (0.5)^2 \right]} - \ln [\sin(180^\circ) \times 0.333] \\ &\quad - 0.5 \ln \left[\left(\frac{2640}{100} \right) \sqrt{0.5} \right] - 1.088 \\ &= (52.428)(0.083) - \ln(0.8655)^{-0.14444} - 0.5(2.968) - 1.088 \\ &= 1.9445 \end{aligned}$$

Estimation of s_R

$$k_y = k_x = 1 \text{ mD}, \quad k_v = 0.5 \text{ mD}$$

$$\frac{2y_e}{\sqrt{k_y}} = \frac{2640}{\sqrt{1}} = 2640, \quad \frac{1.5x_e}{\sqrt{k_x}} = \frac{1.5 \times 1320}{\sqrt{1}} = 1980,$$

$$\frac{0.75h}{\sqrt{k_v}} = \frac{0.75 \times 100}{\sqrt{0.5}} = 106.066$$

Hence

$$\frac{2y_e}{\sqrt{k_y}} > \frac{1.5x_e}{\sqrt{k_x}} > \frac{0.75h}{\sqrt{k_v}}$$

Therefore, one should use Case 1 where

$$s_R = \text{PXYZ} + \text{PXY}'$$

PXYZ component can be calculated from Eq. 3-48:

$$\begin{aligned} \text{PXYZ} &= \left[\frac{2x_e}{L} - 1 \right] \left[\ln \left(\frac{h}{r_w} \right) + 0.25 \ln \left(\frac{k_y}{k_v} \right) - \ln(\sin(180^\circ)z_w) - 1.84 \right] \\ &= \left[\frac{2640}{2000} - 1 \right] \left[\ln \left(\frac{100}{0.39} \right) + 0.25 \ln \left(\frac{1}{0.5} \right) - \ln(\sin(180^\circ) \times 0.3) - 1.84 \right] \\ &= 1.320[5.5468 + 0.1733 - 0.809 - 1.84] = 4.0539 \end{aligned}$$

To calculate PXY' component first calculate the following parameters:

$$x = \frac{L}{4x_e} = \frac{2000}{4 \times 1320} = 0.3788$$

$$\begin{aligned} \int \left(\frac{L}{4x_e} \right) &= -\frac{L}{4x_e} \left[0.145 + \ln \left(\frac{L}{4x_e} \right) - 0.137 \left(\frac{L}{4x_e} \right)^2 \right] \\ &= -0.3788[0.145 + \ln(0.3788) - 0.137(0.3788)^2] = 0.3202 \end{aligned}$$

$$y_1 = \frac{4x_w + L}{4x_e} = \frac{4 \times 1320 + 2000}{4 \times 1320} = 1.3788$$

Since $y_1 > 1$, the function $\int (4x_w + L)/4x_e$ is calculated from Eq. 3-50 with $y = y_1$:

$$\begin{aligned} \int \left(\frac{4x_w + L}{4x_e} \right) &= \left(2 - \frac{4x_w + L}{4x_e} \right) \left[0.145 + \ln \left(2 - \frac{4x_w + L}{4x_e} \right) \right. \\ &\quad \left. - 0.137 \left(2 - \frac{4x_w + L}{4x_e} \right)^2 \right] \\ &= (2 - y)[0.145 + \ln(2 - y) - 0.137(2 - y)^2] \\ &= (2 - 1.3788)[0.145 + \ln(2 - 1.3788) - 0.137(2 - 1.3788)^2] \\ &= 0.6212[0.145(-0.4761) - 0.0529] = -0.2385 \end{aligned}$$

$$y_2 = \frac{4x_w - L}{4x_e} = \frac{4 \times 1320 - 2000}{4 \times 1320} = 0.6212$$

Since $y_2 < 1.0$, the function $\int(4x_w - L)/4x_e$ is calculated from Eq. 3-53 with $y = y_2$:

$$\begin{aligned} \int\left(\frac{4x_w - L}{4x_e}\right) &= -\left(\frac{4x_w - L}{4x_e}\right) \left[0.145 + \ln\left(\frac{4x_w - L}{4x_e}\right) - 0.137\left(\frac{4x_w - L}{4x_e}\right)^2\right] \\ &= -y[0.145 + \ln(y) - 0.137(y)^2] \\ &= -0.6212[0.145 + \ln(0.6212) - 0.137(0.6212)^2] = 0.240 \end{aligned}$$

From Eq. 3-49

$$\begin{aligned} \text{PXY}' &= \left(\frac{2(2x_e)^2}{Lh} \sqrt{\frac{k_v}{k_y}}\right) \left[\int\left(\frac{L}{4x_e}\right) + 0.5\left[\int\left(\frac{4x_w + L}{4x_e}\right) - \int\left(\frac{4x_w - L}{4x_e}\right)\right]\right] \\ &= \frac{2 \times 2640^2}{2000 \times 100} \sqrt{0.5}[0.3202 + 0.5(-0.2385 - 0.240)] = 3.99 \end{aligned}$$

Using Eq. 3-47

$$s_R = \text{PXYZ} + \text{PXY}' = 4.0539 + 3.99 = 8.044$$

From Eq. 3-45, with $A_1 = 2y_e h$ and $A' = 0.750$

$$\begin{aligned} J_h &= \frac{q_o}{\bar{p}_R - p_{wf}} \\ &= \frac{(2x_e)\sqrt{k_y k_v}}{141.2\beta_o\mu_o} \left(\frac{1}{\ln(\sqrt{A_1}/r_w) - A' + \ln C_H + s_R}\right) \\ &= \frac{2640\sqrt{1 \times 0.5}}{141.2 \times 1.215 \times 0.45 [\ln(\sqrt{2640 \times 100}/0.39) - 0.750 + 1.9445 + 8.044]} \\ &= \frac{24.1663}{7.1835 + 1.9445 - 0.750 + 8.044} = 1.472 \text{ stb}/(\text{day}/\text{psi}) \end{aligned}$$

A comparison of the horizontal well productivity obtained by three methods is shown below:

Method 1	$J_h = 1.644 \text{ stb}/(\text{day}/\text{psi})$
Method 2	$J_h = 1.638 \text{ stb}/(\text{day}/\text{psi})$
Method 3	$J_h = 1.472 \text{ stb}/(\text{day}/\text{psi})$

3.3 Horizontal Oil Well Performance During Transient State

Refs. 6, 13, 14 have presented the solution for a horizontal well in an infinite reservoir (see Figure 3-16). The equation is given below:

$$p_D(x_D, y_D, z_D, z_{WD}, L_D, t_D) = \frac{\sqrt{\pi}}{4} \sqrt{\frac{k_h}{k_y}} \int_0^{t_D} \left[\operatorname{erf} \left(\frac{\sqrt{k_h/k_x + x_D}}{2\sqrt{\tau}} \right) \right] \times \left[\exp \left(\frac{-y_D^2}{4\tau} \right) \right] \times \left[1 + 2 \sum_{n=1}^{\infty} \exp(-n^2 \pi^2 L_D^2 \tau) \cos n\pi z_D \cos n\pi z_{WD} \right] \frac{d\tau}{\sqrt{\tau}} \quad (3-59)$$

where

$$x_D = \frac{2x}{L} \sqrt{\frac{k_h}{k_x}} \quad (3-60)$$

$$y_D = \frac{2y}{L} \sqrt{\frac{k_h}{k_y}} \quad (3-61)$$

$$L_D = \frac{L}{2h} \sqrt{\frac{k_y}{k_h}} \quad (3-62)$$

$$r_{WD} = \frac{2r_w}{L} \sqrt{\frac{k_h}{k_y}} \quad (3-63)$$

$$z_D = \frac{z}{h} \quad (3-64)$$

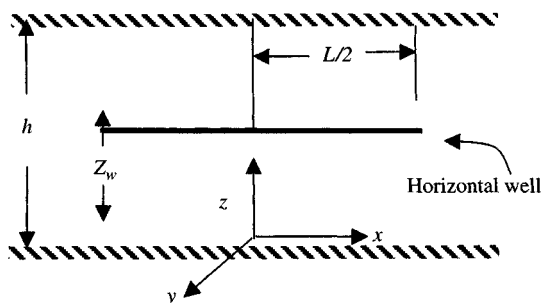


Figure 3-16. Horizontal well model.

$$z_{WD} = \frac{z_w}{h} \tag{3-65}$$

$$ct_D = \frac{0.001055k_h t}{\phi\mu c_i L^2} \tag{3-66}$$

$$k_h = \sqrt{k_x k_y} \tag{3-67}$$

z_w = vertical distance measured from the bottom boundary of the pay zone to the well.

- Uniform-flux solution.
- Infinite-conductivity solution.
- Uniform-flux solutions with wellbore pressure averaging.

For an infinite-conductivity wellbore, Figure 3-17 is a log-log plot of p_{WD} versus t_D with a dimensionless wellbore length, L_D , as a parameter. Figure 3-17 shows that:

- Bottom curve represents the pressure response of a vertical well with a fully penetrating infinite-conductivity fracture.
- Time between dashed lines AA and BB represents transitional flow period from early-time radial flow (vertical radial flow) to pseudo-radial flow.
- Once the pseudo-radial flow starts, horizontal well solution for $L_D \geq 10$ is practically the same as the vertically fractured well solution.

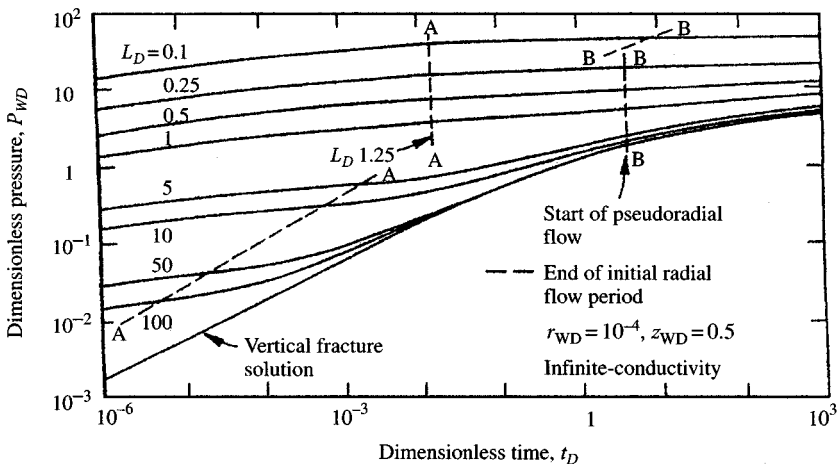


Figure 3-17. Pressure response of horizontal well.

3.4 Transient Well Testing Techniques in Horizontal Oil Wells

Horizontal well testing is complex and on many occasions it is difficult to interpret. In this chapter the limitations and use of horizontal well testing are outlined. There are four transient flow regimes that are theoretically possible with a buildup or drawdown test in a horizontal well, which are as follows.

Early-Time Radial Flow

The flow is radial and is equivalent to that of a fully penetrating vertical well in an infinite reservoir. (See Figure 3-18.)

Intermediate-Time Linear Flow

A horizontal well will generally be long compared to the formation thickness; a period of linear flow may develop once the pressure transient reaches the upper and lower boundaries. (See Figure 3-19.)

Late-Time Radial Flow

If the horizontal well length is sufficiently small as compared to the reservoir size, a second radial flow known as a pseudo-radial flow will develop at late times. (See Figure 3-20.)

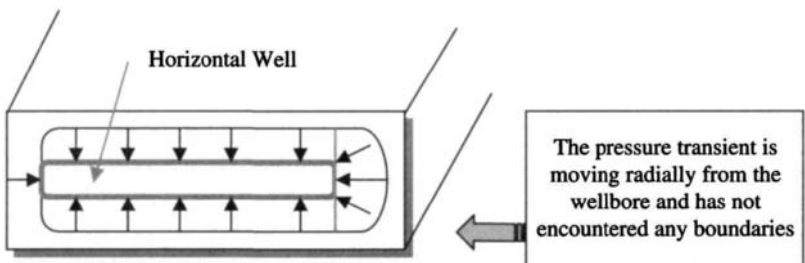


Figure 3-18. Early-time radial flow.

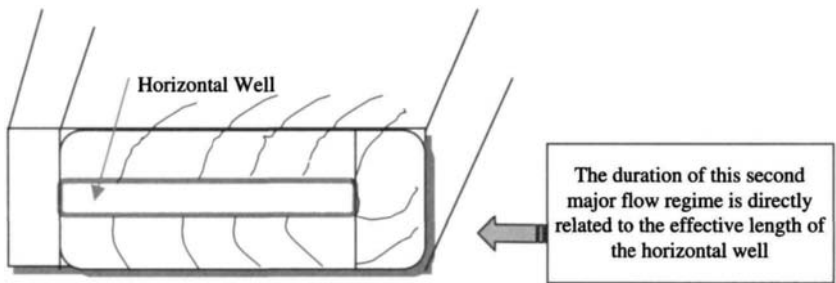


Figure 3-19. Intermediate-time linear flow.

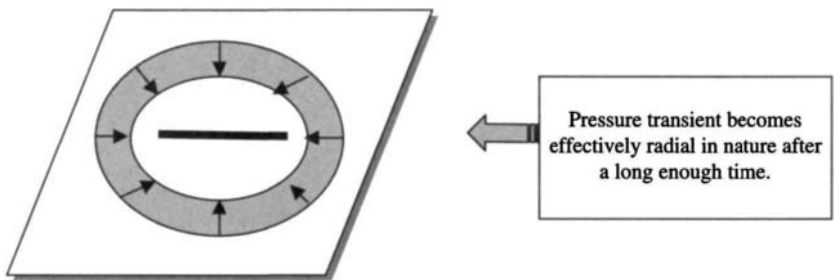


Figure 3-20. Late-time radial flow (pseudo-radial flow).

Late-Time Linear Flow

This flow period occurs when the pressure transient reaches the lateral extremities of the reservoir. This second and final linear flow period develops only for reservoir of finite width. The identification of these flow regimes is critical to the proper interpretation of a horizontal well test. (See Figure 3-21.)

Possible Flow Regimes and Analytical Solutions

Figures 3-18 through 3-21 show four possible transient flow regimes depending on the well length relative to the reservoir thickness and drainage area.^{5,12} Under certain circumstances, permeability, k , anisotropy, and skin factors can be estimated by analyzing these transient flow pressure data. Time and pressure response equations relating to each of the flow regimes to solve specific reservoir parameters for drawdown and buildup tests can

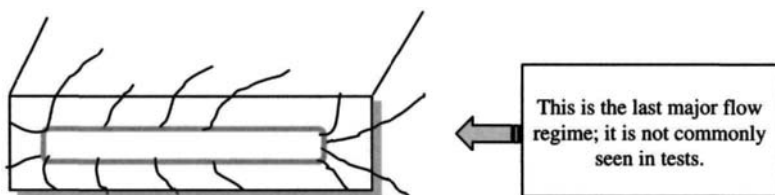


Figure 3-21. Late-time linear flow (pseudo-steady state).

be found in the next sections. Figure 3-22 shows transient flow regime and analytical solutions.

3.5 Flow Time Equations and Solutions

These sets of equations are presented here for estimating the various flow regimes based on the concepts of Goode and Thambynayagam,⁵ Odeh and Babu,¹² and Joshi.¹⁸

Method 1 – Goode and Thambynayagam's Equations⁵

Early-Time Radial Flow

The early-time radial flow period ends at

$$t_{e1} = \frac{190.0d_z^{2.095}r_w^{-0.095}\phi\mu_o c_t}{k_v} \quad (3-68)$$

Intermediate-Time Linear Flow

Intermediate-time linear flow is estimated to end at

$$t_{e2} = \frac{20.8\phi\mu_o c_t L^2}{k_v} \quad (3-69)$$

The intermediate-time linear flow may not develop if the time estimated from Eq. 3-69 is less than the time calculated for the early-time radial flow to end (Eq. 3-68).

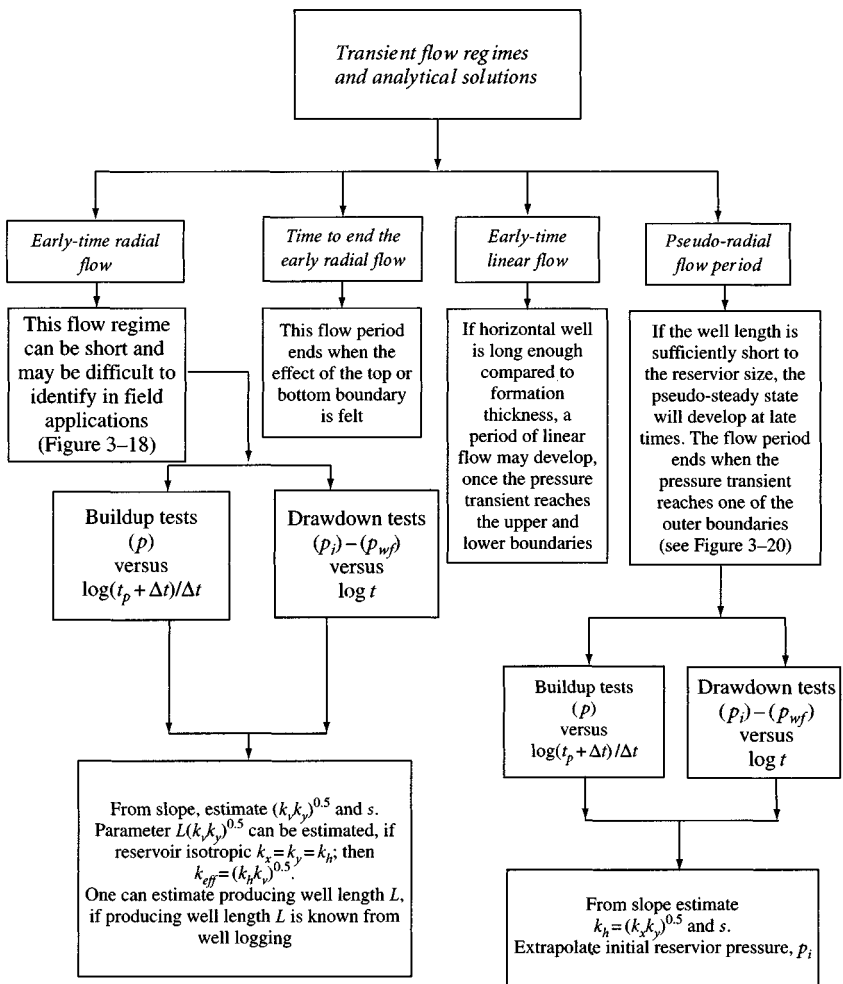


Figure 3-22. Flow regimes and horizontal wellbore pressure responses during flow period.

Late-Time Radial Flow or Pseudo-Radial Flow

If late-time radial flow or pseudo-radial flow develops, it will begin at approximately

$$t_{e3} = \frac{1230.0L^2\phi\mu_o c_t}{k_v} \tag{3-70}$$

Ref. 5 suggested the following equation to determine the beginning of pseudo-radial flow:

$$t_{e3} = \frac{1480L^2\phi\mu_o c_t}{k_x} \quad (3-71)$$

For a reservoir of finite width, this would end at

$$t_{e3} = \frac{297.0(L_{x1} + L_{xd})^{2.095} L^{-0.095} \phi\mu_o c_t}{k_x} \quad (3-72)$$

where

d_z = distance from the upper reservoir boundary to the center of the horizontal well, ft

k_v = permeability in vertical direction, mD

L = effective length of horizontal well, ft

k_x = permeability in x -direction, mD

L_{x1} = distance in x -direction to beginning of horizontal wellbore, ft

L_{xd} = distance in x -direction to end of horizontal wellbore, ft.

This radial flow period will not develop if the estimated time at the end of late-time radial flow (Eq. 3-72) is less than that calculated at the beginning of pseudo-radial flow (Eq. 3-70). It also means that the reservoir is smaller than anticipated. A plot of p_{wf} versus \sqrt{t} can be used to calculate L_{x1} and L_{xd} in Eq. 3-72.

Method 2 – Odeh and Babu's Equations¹²

Early-Time Radial Flow

The duration of this period may be approximated by the minimum of the following two terms:

$$t_{e1} = \frac{1800d_z^2\phi\mu_o c_t}{k_v} \quad (3-73)$$

or

$$t_{e1} = \frac{125L^2\phi\mu_o c_t}{k_v} \quad (3-74)$$

Intermediate-Time Linear Flow

Time durations for the start and end of linear flow can be found by

$$t_{e2} = \frac{1800D_z^2\phi\mu_o c_t}{k_v} \quad (3-75)$$

and

$$t_{e2} = \frac{160\phi\mu_o c_t L^2}{k_x} \quad (3-76)$$

Late-Time Radial Flow

This flow period starts at

$$t_{e3} = \frac{1480L^2\phi\mu_o c_t}{k_x} \quad (3-77)$$

and ends at minimum of

$$t_{e3} = \frac{2000\phi\mu_o c_t (d_x + \frac{L}{4})^2}{k_x} \quad (3-78)$$

or

$$t_{e3} = \frac{1650\phi\mu_o c_t d_y^2}{k_y} \quad (3-79)$$

Late-Time Linear Flow

The flow ends at the maximum of

$$t_{e4} = \frac{4800\phi\mu_o c_t D_x^2}{k_x} \quad (3-80)$$

or

$$t_{e4} = \frac{1800D_z^2\phi\mu_o c_t}{k_z} \quad (3-81)$$

where

- d_z = the shortest distance between the well and the z -boundary, ft
 $D_z = h - d_z$; the longest distance between the well and the z -boundary, ft,
 and h is the reservoir height
 k_y = permeability in y -direction, mD
 d_x = the shortest distance between the well and the x -boundary, ft
 D_x = the longest distance between the well and the x -boundary, ft.

Method 3 – Ozkan et al.'s Equations¹⁴

Early-Time Radial Flow

$$L_D = \frac{L}{2h} \sqrt{\frac{k_y}{k_h}} \quad (3-82)$$

$$r_{wD} = \frac{2r_w}{L} \sqrt{\frac{k_h}{k_y}} \quad (3-83)$$

Assuming isotropic reservoir, i.e., $k_x = k_y$, Eq. 3-83 reduces to

$$r_{wD} = \frac{2r_w}{L} \quad (3-84)$$

After estimating the value of L_D and r_{wD} , and using Figure 3-17, one can find t_D (dashed line AA) and duration of the early-time radial flow and is given by

$$t_{e1} = \frac{t_D \phi \mu_o c_t L_w^2}{0.001055 k_h} \quad (3-85)$$

where

- L_D = dimensionless length
 h = reservoir thickness, ft
 r_{wD} = dimensionless radius
 t_D = dimensionless time.

Late-Time Radial Flow

Start of this radial (pseudo-radial) flow can be calculated by using Eqs. 3-82 and 3-83. Find t_D from Figure 3-17 (dashed line BB) and then substitute in Eq. 3-85.

Example 3-8 *Calculating the Time Required to End Early-Time Radial Flow*

A horizontal oil well, which is 2000-ft long, is drilled in a reservoir with the following characteristics: $h = 120$ ft; $r_w = 0.354$ ft; $\phi = 15.0\%$; $\beta_o = 1.235$ rb/stb; $\mu_o = 0.35$ cP; $c_t = 10.0 \times 10^{-6}$ psi $^{-1}$; $k = 0.8$ mD (from well test data), $k_v = 0.2$ mD (from core data). The Well is in the central elevation of the reservoir, and the distance from the upper reservoir boundary to center of horizontal well is 20 ft. Estimate the time required to end initial radial flow.

Solution $d_z = (120/2) - 20 = 40$ ft.

Method 1 – using Eq. 3-68

$$\begin{aligned}
 t_{el} &= \frac{190.0 d_z^{2.095} r_w^{-0.095} \phi \mu_o c_t}{k_v} \\
 &= \frac{190.0 \times 40^{2.095} \times 0.354^{-0.095} \times 0.15 \times 0.35 \times 10.0 \times 10^{-6}}{0.2} = 1.25 \text{ hr}
 \end{aligned}$$

Method 2 – using Eq. 3-73

$$\begin{aligned}
 t_{el} &= \frac{1800 d_z^2 \phi \mu_o c_t}{k_v} \\
 &= \frac{1800 \times 40^2 \times 0.15 \times 0.35 \times 10.0 \times 10^{-6}}{0.2} = 7.56 \text{ hr}
 \end{aligned}$$

$$t_{el} = \frac{125 L^2 \phi \mu_o c_t}{k_y} = \frac{125 \times 2000^2 \times 0.15 \times 0.35 \times 10.0 \times 10^{-6}}{0.8} = 328.0 \text{ hr}$$

The minimum of these two values is 1.25 hr. Thus, initial radial flow period will end in 1.25 hr.

Method 3 – using Figure 3-17

$$L_D = \frac{2000}{2 \times 120} \sqrt{\frac{0.2}{0.8}} = 4.17 \text{ (Eq. 3-58c), assuming isotropic reservoir}$$

$$(k_x = k_y = k_h)$$

$$r_{wD} = \frac{2r_w}{L} \sqrt{\frac{k_h}{k_y}} = \frac{2 \times 0.354}{2000} \times 1 = 3.54 \times 10^{-4} \text{ (Eq. 3-63)}$$

Knowing L_D , r_{wD} , time to end initial radial flow period given by dotted line AA ($t_D = 1.5 \times 10^{-3}$) and after rearranging and substituting these values in Eq. 3-85

$$t_{e1} = \frac{\phi\mu c_t L^2}{0.001055k_h} t_D = \frac{0.15 \times 0.35 \times 10.0 \times 10^{-6} \times 2000^2}{0.001055 \times 0.8} (1.5 \times 10^{-3})$$

$$= 3.73 \text{ hr}$$

Therefore, the initial time required to end initial radial flow would last between 1.25 and 3.73 hours. The reservoir engineers will have to use down hole shut-in devices to enhance the chances of measuring the early radial flow regime.

Example 3-9 *Calculating the Time to Start and Time to End Early-Time Linear Flow*

For the well described in Example 3-8, assuming $k_x = k_y = 0.8$ mD, calculate time to start and time to end early-time linear flow.

Solution Maximum distance of well from either top or bottom boundary is

$$D_z = h - d_z = 120 - 40 = 80 \text{ ft}$$

From Eq. 3-73

$$t_{e2} = \frac{1800D_z^2\phi\mu c_t}{k_v} = \frac{1800 \times 80^2 \times 0.15 \times 0.35 \times 10 \times 10^{-6}}{0.2} = 30.24 \text{ hours}$$

From Eq. 3-76

$$t_{e2} = \frac{160\phi\mu c_t L^2}{k_x} = \frac{160 \times 0.15 \times 0.35 \times 10 \times 10^{-6} \times 2000^2}{0.8} = 420 \text{ hours}$$

From Eq. 3-69

$$t_{e2} = \frac{20.8\phi\mu c_t L^2}{k_x} = \frac{20.8 \times 0.15 \times 0.35 \times 10 \times 10^{-6} \times 2000^2}{0.8} = 54.6 \text{ hours}$$

Thus, this flow period will end in about 55–420 hours. This indicates that the current well is sufficiently long compared to the reservoir height. Therefore, it is possible to analyze pressure data of the flow period.

Example 3-10 *Calculating the Time Required to Start a Pseudo-Radial Flow*

For the well/reservoir data given in Example 3-9, calculate time to start and time to end early-time linear flow.

Solution

Method 1 – from Eq. 3–70

$$t_{e2} = \frac{1230\phi\mu c_t L^2}{k_x} = \frac{1230 \times 0.15 \times 0.35 \times 10 \times 10^{-6} \times 2000^2}{0.8} = 3229 \text{ h}$$

$$= 134.5 \text{ days}$$

Method 2 – from Eq. 3–71

$$t_{e2} = \frac{1480\phi\mu c_t L^2}{k_x} = \frac{1480 \times 0.15 \times 0.35 \times 10 \times 10^{-6} \times 2000^2}{0.8}$$

$$= 3885 \text{ h} = 162 \text{ days}$$

Method 3 – from Figure 3–17, time to start pseudo-radial flow (dashed line BB) is $t_D = 3.0$; thus

$$t_{e1} = \frac{\phi\mu c_t L^2}{0.001055k_h} t_D = \frac{0.15 \times 0.35 \times 10.0 \times 10^{-6} \times 2000^2}{0.001055 \times 0.8} (3.0) = 7465 \text{ h}$$

$$= 311 \text{ days}$$

It will take 135 to 311 days to reach pseudo-radial flow. It will be economically difficult to shut-in a well for such a long time. In this case one will have to obtain the necessary information from an early time radial or linear flow period.

3.6 Pressure Response Equations and Methods of Analysis

Certain reservoir parameters can only be approximated during particular flow regimes; therefore, it is important to calculate the times relating to each of the flow regimes. Goode et al.⁵ developed pressure response function at the horizontal wellbore for conditions of both pressure drawdown and pressure buildup. These pressure response equations published in 1985 assumed an effective pressure point along the horizontal wellbore. Later work by Kuchuk et al.¹¹ was based on pressure averaging under conditions of pressure drawdown. These equations provide pressure response during each flow regime.

Under the Condition of Pressure Drawdown Test

Early-Time Radial Flow

The wellbore pressure response during this flow period is given by

$$p_i - p_{wf} = \frac{162.6q_o\beta_o\mu_o}{\sqrt{k_y k_y L}} \left[\log \left(\frac{\sqrt{k_y k_y t}}{\phi\mu_o c_t r_w^2} \right) - 3.23 + 0.868s \right] \quad (3-86)$$

where s is mechanical skin damage due to drilling and completion. Eq. 3-86 indicates that a plot of wellbore pressure, p_{wf} or $(p_i - p_{wf})$, versus $\log t$ will exhibit a semilog straight line with slope given by

$$m_1 = \frac{162.6q_o\beta_o\mu_o}{\sqrt{k_v k_y} L} \quad (3-87)$$

The equivalent permeability in a vertical plane around the wellbore can be calculated as

$$\sqrt{k_v k_y} = \frac{162.6q_o\beta_o\mu_o}{m_1 L} \quad (3-88)$$

Extrapolating the semilog straight line to $t = 1$ hr, the following equation is obtained:

$$p_i - p_{1hr} = m_1 \left[\log \left(\frac{k_v k_y}{\phi \mu_o c_t r_w^2} \right) - 3.23 + 0.868s \right] \quad (3-89)$$

where p_i is the initial reservoir pressure and p_{1hr} the pressure obtained at $t = 1$ hr. Rearranging the above Eq. 3-89 gives

$$s = 1.151 \left[\frac{p_i - p_{1hr}}{m_1} - \log \left(\frac{\sqrt{k_v k_y}}{\phi \mu_o c_t r_w^2} + 3.23 \right) \right] \quad (3-90)$$

Using Eq. 3-90 one can estimate skin factor, s . If the reservoir is aerial isotropic ($k_x = k_y = k_h$), then using Eq. 3-87, we have

$$L\sqrt{k_v k_y} = Lk_{eff} = \frac{162.6q_o\beta_o\mu_o}{m_1} \quad (3-91)$$

where k_{eff} ($=\sqrt{k_h k_v}$) is the effective reservoir permeability. Thus, if k_{eff} is known, one can estimate producing well length, L_w . Vice versa, if producing well length, L , is known by well logging, then one can calculate the effective reservoir permeability. As mentioned earlier, this flow regime can be of short duration and may be difficult to identify in field applications.

Intermediate-Time Linear Flow

Pressure response during this flow period is given by

$$p_i - p_{wf} = \frac{8.128q_o\beta_o}{Lh} \sqrt{\frac{t}{k_y \phi \mu_o c_t}} + \frac{141.2q_o\mu_o\beta_o}{L\sqrt{k_y k_v}} (s_z + s) \quad (3-92)$$

where s_z is the pseudo-skin factor caused by partial penetration in the vertical direction, and is given by⁸

$$s_z = \ln\left(\frac{h}{r_w}\right) + 0.25 \ln\left(\frac{k_y}{k_v}\right) - \ln\left(\sin 180^\circ\left(\frac{z_w}{h}\right)\right) - 1.838 \quad (3-93)$$

where

z_w = vertical location of well, ft

h = reservoir height, ft.

Eq. 3-92 indicates that a plot of $\Delta p = p_i - p_{wf}$ versus \sqrt{t} will exhibit a straight line with slope given by

$$m_2 = \frac{8.128q_o\beta_o}{Lh} \sqrt{\frac{\mu_o}{\phi c_t k_y}} \quad (3-94)$$

Hence, the product of producing well length square L^2 and permeability k_y can be obtained from the slope given by

$$L^2 k_y = \left(\frac{8.128q_o\beta_o}{hm_2}\right)^2 \frac{\mu_o}{\phi c_t} \quad (3-95)$$

Additionally, extrapolating the straight line to $\sqrt{t} = 0$ gives

$$\Delta p|_{t=0} = \frac{141.2q_o\beta_o\mu_o}{L\sqrt{k_y k_v}} (s_z + s) \quad (3-96)$$

where

$$s = \frac{0.058}{h} \sqrt{\frac{k_v}{\phi\mu_o c_t}} \left(\frac{p_i - p_{wf}(0h)}{m_2}\right) - s_z \quad (3-97)$$

Late-Time Radial Flow

Pressure response during this radial (pseudo-radial) flow period is given by

$$p_i - p_{wf} = \frac{162.6q_o\beta_o\mu_o}{k_x k_y h} \left[\log\left(\frac{k_x t}{\phi\mu_o c_t L^2}\right) - 2.023 \right] + \frac{141.2q_o\mu_o\beta_o}{L\sqrt{k_y k_v}} (s_z + s) \quad (3-98)$$

Eq. 3-98 indicates that a plot of p_{wf} or $(p_i - p_{wf})$ versus $\log t$ will exhibit a semilog straight line of slope m_3 given by

$$m_3 = \frac{162.6q_o\beta_o\mu_o}{\sqrt{k_x k_y} h} \quad (3-99)$$

The equivalent horizontal permeability $\sqrt{k_x k_y}$ can be estimated as

$$k_h = \sqrt{k_x k_y} = \frac{162.6q_o\beta_o\mu_o}{m_3 h} \quad (3-100)$$

Skin factor can also be obtained by

$$s = \frac{1.151L}{h} \sqrt{\frac{k_v}{k_x}} \left[\frac{p_i - p_{1hr}}{m_3} - \log \left(\frac{k_x}{\phi\mu_o c_t L_w^2} \right) + 2.023 \right] - s_z \quad (3-101)$$

where p_{1hr} is obtained by extrapolating the late-time radial flow semilog straight line to $t = 1$ hour. Eq. 3-93 gives pseudo-skin factor, s_z . This can also be estimated using Spencer function⁵:

$$s_z = \frac{0.07958h_z}{r_{wa}} [\psi(\xi_1) + \psi(\xi_2) - \psi(\xi_3) - \psi(\xi_4)] \quad (3-102)$$

where

$$\xi_1 = \frac{0.52\pi r_{wa}}{h_z}$$

$$\xi_2 = \frac{\pi}{h_z} (2h_s + 3.48r_{wa})$$

$$\xi_3 = \frac{3.38\pi r_{wa}}{h_z}$$

$$\xi_4 = \frac{\pi}{h_z} (2h_s - 0.52r_{wa})$$

r_{wa} = apparent wellbore radius, ft

h_s = horizontal well in center of reservoir, ft

h_z = partial penetration in vertical direction, ft.

If the bottom and top boundaries are maintained at constant pressure then the pseudo-radial or late-time radial flow period will not develop and there will be steady-state flow at the late time.

Late-Time Linear Flow

Pressure response during this period, also known as pseudo-steady-state, is given by

$$p_i - p_{wf} = \frac{8.128q_o\beta_o}{2x_e h} \sqrt{\frac{\mu_o t}{k_y \phi c_t}} + \frac{141.2q_o\beta_o\mu_o}{L\sqrt{k_y k_v}} (s_x + s_z + s) \quad (3-103)$$

where

$2x_e$ = width of reservoir, ft

s_z = pseudo-skin factor due to partial penetration in a vertical direction (Eq. 3-93 or 3-102)

s_x = pseudo-skin factor due to partial penetration in the x -direction given by

$$s_x = \frac{0.6366h_x^2 L_w}{h\sqrt{k_y/k_x}} \sum_{n=1}^{\infty} \frac{\Xi n^2}{n} \quad (3-104)$$

h = reservoir height, ft

h_x = height between the well and the x -boundary, ft.

Eq. 3-103 indicates that a plot of $p_{wf}(p_i - p_{wf})$ versus \sqrt{t} will exhibit a straight line of slope m_4 given by

$$m_4 = \frac{8.128q_o\beta_o\mu_o}{h_x h \sqrt{\phi c_t k_y}} \quad (3-105)$$

Reservoir parameter h_x or $\sqrt{\pi c_t k_y / \mu_o}$ can be obtained as

$$h_x = \frac{8.128q_o\beta_o\mu_o}{m_4 h \sqrt{\phi c_t k_y}} \quad (3-106)$$

or

$$\sqrt{\frac{\phi c_t k_y}{\mu_o}} = \frac{8.128q_o\beta_o\mu_o}{m_4 h \sqrt{\phi c_t k_y}}$$

Skin factor, s , can be found from

$$s = \frac{0.058L}{hh_x} \sqrt{\frac{k_v}{\phi \mu_o c_t}} \left(\frac{p_i - p_{wf(0hr)}}{m_4} \right) - (s_x + s_z) \quad (3-107)$$

where $p_{wf(0hr)}$ is the pressure obtained at $t = 0$ hr.

Under the Condition of Pressure Buildup Test

Early-Time Radial Flow

Pressure buildup response during this flow period is given by:
For infinite reservoir

$$p_i - p_{ws} = \frac{162.6q_o\beta_o\mu_o}{\sqrt{k_zk_yL_w}} \left[\log\left(\frac{t_p + \Delta t}{\Delta t}\right) + \gamma_1 \right] \quad (3-108)$$

where

$$\begin{aligned} \gamma_1 = & \frac{L}{h} \sqrt{\frac{k_v}{k_x}} \left[\log\left(\frac{k_x t}{\phi\mu_o c_t L_w^2}\right) - 2.023 \right] - \log(t) - \log\left(\frac{\sqrt{k_v k_y}}{\phi\mu_o c_t r_w^2}\right) \\ & + 3.227 + 0.869s_z \end{aligned}$$

Eq. 3-108 indicates that a plot of Δp versus $\log\left(\frac{t_p + \Delta t}{\Delta t}\right)$ will exhibit a semilog straight line with slope, m_{1r} , given by

$$m_{1r} = \frac{162.6q_o\beta_o\mu_o}{\sqrt{k_v k_y L}} \quad (3-109)$$

The equivalent permeability in the vertical plane can be estimated by

$$k_v k_y = \left(\frac{162.6q_o\beta_o\mu_o}{m_{1r} L} \right)^2 \quad (3-110)$$

Extrapolating the semilog straight line to $t = 1$ hour, the following equation is obtained to estimate s :

$$s = 1.151 \left[\frac{p_{1hr} - p_{wf}}{m_{1r}} - \log\left(\frac{k_v k_y}{\phi\mu_o c_t r_w^2}\right) + 3.23 \right] \quad (3-111)$$

For finite (bounded) reservoir

$$p_i - p_{ws} = \frac{162.6q_o\beta_o\mu_o}{\sqrt{k_y k_v L}} \left[\log\left(\frac{t_p + \Delta t}{\Delta t}\right) + \gamma_2 \right] \quad (3-112)$$

where

$$\gamma_2 = \frac{0.05L}{hh_x} \sqrt{\frac{k_v t}{\phi \mu_o c_t}} - \log \left(\frac{\sqrt{k_y k_v t}}{\phi \mu_o c_t r_w^2} \right) + 3.227 + 0.868(s_x + s_z)$$

Eq. 3-111 gives s_m .

Intermediate-Time Linear Flow

Pressure buildup response during this flow period is given by:
For infinite reservoir (first linear flow)

$$p_i - p_{ws} = \frac{8.128q_o\beta_o}{hL} \sqrt{\frac{\mu_o \Delta t}{k_y \phi c_t}} + \gamma_3 \quad (3-113)$$

where

$$\gamma_3 = \frac{162.6q_o\beta_o\mu_o}{h\sqrt{k_x k_y}} \left[\log \left(\frac{k_x t}{\phi \mu_o c_t L^2} \right) - 2.023 \right]$$

A plot of Δp versus $\sqrt{\Delta t}$ will exhibit a slope given by

$$m_{1l} = \frac{8.128q_o\beta_o}{h\sqrt{k_v k_y}} \quad (3-114)$$

The equivalent permeability in the vertical plane can be calculated by

$$k_v k_y = \left(\frac{8.128q_o\beta_o}{m_{1l}h} \right)^2 \quad (3-115)$$

Skin factor, s , is given by

$$s = \frac{0.058}{h} \sqrt{\frac{k_v}{\phi \mu_o c_t}} \left[\frac{p_{1h} - p_{wf}}{m_{1l}} \right] - s_z \quad (3-116)$$

For finite (bounded) reservoir

$$p_i - p_{ws} = \frac{8.128q_o\beta_o}{hL} \sqrt{\frac{\mu_o}{k_y \phi c_t}} \left(\sqrt{\Delta t} - \frac{L\sqrt{t}}{h_x} \right) + \frac{141.2q_o\beta_o\mu_o}{L\sqrt{k_y k_x}} s_x \quad (3-117)$$

Eq. 3-116 gives s .

Late-Time Radial Flow

Pressure buildup response during this flow period is given by:
For infinite reservoir

$$p_i - p_{ws} = \frac{162.6q_o\beta_o\mu_o}{h\sqrt{k_xk_y}} \left[\log\left(\frac{t_p + \Delta t}{\Delta t}\right) \right] \quad (3-118)$$

A plot of p_{ws} versus $\log\left(\frac{t_p + \Delta t}{\Delta t}\right)$ will exhibit a straight line with slope given by

$$m_{2r} = \frac{162.6q_o\beta_o\mu_o}{h\sqrt{k_xk_y}} \quad (3-119)$$

Skin factor, s , is given by

$$s_m = \frac{1.151L}{h} \sqrt{\frac{k_v}{k_x}} \left[\frac{p_{1hr} - p_{wf}}{m_{2r}} - \log\left(\frac{k_v}{\phi\mu_o c_t L^2}\right) + 2.023 \right] - s_z \quad (3-120)$$

For finite (bounded) reservoir

$$p_i - p_{ws} = \frac{162.6q_o\beta_o\mu_o}{h\sqrt{k_xk_y}} \left[\log\left(\frac{t_p + \Delta t}{\Delta t}\right) + \gamma_4 \right] \quad (3-121)$$

where

$$\gamma_4 = \frac{0.05}{h} \sqrt{\frac{k_x t}{\phi\mu_o c_t}} - \log\left(\frac{k_x t}{\phi\mu_o c_t L^2}\right) + 2.023 + 0.868s_z$$

Calculate s_m using Eq. 3-120. Generally, only the initial part of the Horner plot generated by Eq. 3-121 will be a straight line.

Late-Time Linear Flow

During this flow period (infinite reservoir case does not exist) (pseudo-radial flow) the pressure buildup response for finite (bounded) reservoir is given by

$$p_i - p_{ws} = \frac{8.128q_o\beta_o}{hh_x} \sqrt{\frac{\mu_o}{k_y\phi c_t}} (\sqrt{t} - \sqrt{\Delta t}) \quad (3-122)$$

A plot of p_{ws} versus $(\sqrt{t} - \sqrt{\Delta t})$ will produce a straight line that will extrapolate to p_i while a plot of Δp versus $(\sqrt{t} - \sqrt{\Delta t})$ will exhibit a straight line of slope, m_{4l} , given by

$$m_{4l} = \frac{8.128q_o\beta_o}{h_z h_x \sqrt{\frac{\phi c_t k_y}{\mu_o}}} \quad (3-123)$$

or

$$\sqrt{\frac{\phi c_t k_y}{\mu_o}} = \frac{8.128q_o\beta_o}{m_{4l} h h_x} \quad (3-124)$$

Skin factor, s , is given by

$$s = \frac{0.058L}{hk_x} \sqrt{\frac{k_v}{\phi\mu_o c_t} \left(\frac{p_{1h} - p_{wf}}{m_{4l}} \right)} - (s_z + s_x) \quad (3-125)$$

3.7 Horizontal Well Response and Normalized Pressure Derivative

Horizontal well tests are best interpreted using log-log representation of the pressure-time data in conjunction with the derivative curve. This will provide the best identification between the various flow regimes, which improves the ability to correctly identify the flow regimes and also maximizes the chances of obtaining a unique solution of the data. Figure 3-23 shows the type curves for infinite-conductivity horizontal wells.¹⁴ The dash curves represent the pressure responses and solid curves represent the pressure derivative group.

At early times, the pressure/pressure derivative solutions show that the influence of dimensionless well length L_D is negligible. As time increases, these solutions diverge and ultimately merge with the appropriate p_{WD} curves after the onset of pseudo-steady-state flow. Thus, Figure 3-23 can also be used to identify the appropriate semilog straight lines. Pressure derivative can also be used to determine the time at which pseudo-steady-state flow begins for bounded reservoirs. Once the slope of the Cartesian plot of p_{WD} versus t_{DA} becomes 2π , pseudo-steady-state begins. Many investigators use the following equation to determine the beginning of the pseudo-steady-state flow:

$$\frac{dp_{WD}}{dt_{DA}} = 2\pi \quad (3-126)$$

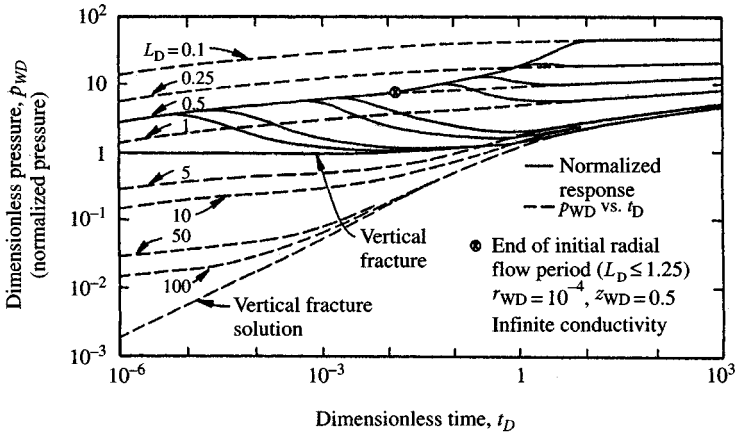


Figure 3-23. Horizontal well response and normalized pressure derivative.¹⁴

3.8 Effects of Wellbore Storage

Wellbore storage effects can have serious consequences on the effectiveness of a pressure transient test. In Ref. 1, it was shown that the first semilog straight line associated with early-time radial flow almost always disappears because of the effect of wellbore storage. Goode and Thambynayagam⁶ noted that the storage effect in a horizontal well lasts longer than that in a vertical well in the same formation because of greater wellbore volume and because anisotropy reduces the effective permeability, k_z , for a horizontal well.

First semilog straight line (early-time radial flow) commonly does not appear due to wellbore storage because true wellbore damage, s_m , and horizontal permeability, k_z , can only be estimated during that time.

3.9 Summary

This Chapter summarizes a discussion of horizontal wells in oil reservoirs. Horizontal wells enhance the drainage area in a given time period while in-high permeability oil reservoirs reduce near-wellbore turbulence and enhance well deliverability. Horizontal wells have high potential in oil reservoirs. Also, it includes the influence of turbulence and turbulence identification, comparison of inflow performance responses in vertical and horizontal oil wells, and time and transient pressure response analysis equations related to each of the flow regimes to solve for specific reservoir parameters using drawdown and buildup tests.

References

1. Smith, R. V., *Practical Natural Gas Engineering*. PennWell Publishing Co, Tulsa, OK, 1983.
2. Brown, K. E., *The Technology of Artificial Methods*. PennWell Publishing Co, Tulsa, OK, 1984.
3. Earlougher, R. C., Jr., *Advances in Well Test Analysis*. Monograph Vol. 5 of the Henry L. Doherty Series in Society of Petroleum Engineers of AIME, 1977.
4. Fetkovich, M. J., and Vienot, M. E., "Shape Factors, C_A , Expressed as a Skin, s_{CA} ," *J. Pet. Technol.* (Feb. 1985), 321–322.
5. Goode, P. A., and Thambynayagam, R. K. M., "Pressure Drawdown and Buildup Analysis for Horizontal Wells in Anisotropic Media," *SPE Formation Eval.* (Dec. 1987), 683–697.
6. Daviau, F., Mouronval, G., Bourdarot, G., and Curutchet, P., "Pressure Analysis for Horizontal Wells," SPE 14251, presented at the SPE Annual Technical Conference and Exhibition, Las Vegas, NV, Sept. 22–25, 1985.
7. Golan, M., and Whitson, C. H., *Well Performance*. International Human Resources Development Corporation, Boston, MA, 1986.
8. Mutalik, P. N., Godbole, S. P., and Joshi, S. D., "Effect of Drainage Area Shapes on Horizontal Well Productivity," paper SPE 18301, presented in the SPE 63rd Annual Technical Conference, Houston, TX, Oct. 2–5, 1988.
9. Gringarten, A. C., "Reservoir Limit Testing for Fractured Wells," paper SPE 7452, presented at the SPE 53rd Annual Fall Technical Conference and Exhibition, Houston, TX, Oct. 1–3, 1978.
10. Gringarten, A. C., Ramey, H. J., Jr., and Raghavan, R., "Unsteady-State Pressure Distribution Created by a Well with a Single Infinite-Conductivity Vertical Fracture," *Soc. Pet. Eng. J.* (Aug. 1974), 347–360.
11. Kuchuk, F. J., Goode, P. A., Wilkinson, D. J., and Thambynayagam, R. K. M., "Pressure Transient Behavior of Horizontal Wells With and Without Gas Cap or Aquifer," paper SPE 17413, presented at the SPE California Regional Meeting, Long Beach, CA, March 23–25, 1988.
12. Odeh, A. S., and Babu, D. K., "Transient Flow Behavior of Horizontal Wells Pressure Drawdown and Buildup Analysis," *SPE Formation Eval.* (March 1990), 7–15.
13. Clonts, M. D., and Ramey, H. J., Jr., "Pressure Transient Analysis for Wells with Horizontal Drainage Holes," paper SPE 15116, presented at the SPE California Regional Meeting, Oakland, CA, April 2–4, 1986.
14. Ozkan, E., Raghavan, R., and Joshi, S. D., "Horizontal Well Pressure Analysis," *SPE Formation Eval.* (Dec. 1989), 567–575.

15. Celier, G. C. M. R., Jouault, P., de Montigny, O. A. M. C. Z., "A Gas Field Development with Horizontal Wells," paper SPE 19826, presented at the SPE 64th Annual Technical Conference and Exhibition of the Society of Petroleum Engineers, San Antonio, TX, Oct. 8–11, 1989.
16. Giger, F. M., Reiss, L. H., and Jourdan, A. P., "The Reservoir Engineering Aspect of Horizontal Drilling," paper SPE 13024, presented at the SPE 59th Annual Technical Conference and Exhibition, Houston, TX, Sept. 16–19, 1984.
17. Borisov, Ju. P., *Oil Production Using Horizontal and Multiple Deviation Wells*. Nedra, Moscow, 1964. Translated Strauss, S. D. Joshi (ed.), Phillips Petroleum Co, the R&D Library Translation, Bartlesville, OK, 1984.
18. Joshi, S. D., "Argumentation of Well Productivity Using Slant and Horizontal Wells," *J. Pet. Technol.* (June 1988), 729–739.
19. Renard, G. I., and Dupuy, J. M., "Influence of Formation Damage on the Flow Efficiency of Horizontal Wells," paper SPE 19414, presented at the Formation Damage Control Symposium, Lafayette, LA, Feb. 22–23, 1990.
20. Van Der Vlis, A. C., Duns, H., and Luque, R. F., "Increasing Well Productivity in Tight Chalk Reservoir," Vol. 3, Proc. 10th World Petroleum Conference, Bucharest, Romania, 1979, 71–78.
21. Van Everdingen, A. F., and Hurst, W., "The Application of the Laplace Transformation to Flow Problems in Reservoirs," *Trans. AIME* (1949) 186, 305–324.
22. Van Everdingen, A. F., "The Skin Effect and Its Influence on the Production Capacity of a Well," *Trans. AIME* (1953) 198, 171.
23. Hurst, W., "Establishment of the Skin Effect and Its Impediment to Fluid Flow into a Wellbore," *Pet. Eng.* (Oct. 1953).

Additional Reading

1. Al-Hussainy, R., Ramey, H. J., Jr., and Crawford, P. B., "The Flow of Real Gases Through Porous Media," *J. Pet. Technol.* (1966), 624–636; *Trans. AIME*, 237.
2. Duda, J. R., Aminian, K., and Ameri, S., "Predicting Horizontal Well Production Performance Using Type Curves," papers SPE 18993, 19342, presented at the SPE Eastern Regional Meeting, Morgantown, West Virginia, Oct. 24–27, 1989.

Chapter 4

Pressure Drawdown Testing Techniques for Oil Wells

4.1 Introduction

A pressure drawdown test is simply a series of bottom-hole pressure measurements made during a period of flow at constant production rate. Usually the well is closed prior to the flow test for a period of time sufficient to allow the pressure to stabilize throughout the formation, i.e., to reach static pressure. As discussed by Odeh and Nabor,¹ transient flow condition prevails to a value of real time approximately equal to

$$t \approx \frac{\phi\mu_o r_e^2}{0.00264k} \quad (4-1)$$

Semi-steady-state conditions are established at a time value of

$$t \approx \frac{\phi\mu_o c r_e^2}{0.00088k} \quad (4-2)$$

In this section, we will discuss drawdown tests in infinite-acting reservoirs and developed reservoirs including two-rate, variable, multiphase, multi-rate drawdown tests. An analysis technique applicable to pressure drawdown tests during each of these periods including other types of tests is presented in the following sections.

4.2 Pressure–Time History for Constant-Rate Drawdown Test

Figure 4–1 shows the flow history of an oil well and can be classified into three periods for analysis:

- Transient or early flow period is usually used to analyze flow characteristics;
- Late transient period is more completed; and
- Semi-steady-state flow period is used in reservoir limit tests.

4.3 Transient Analysis – Infinite-Acting Reservoirs

An ideal constant-rate drawdown test in an infinite-acting reservoir is modeled by the logarithmic approximation to the E_i -function solution:

$$p_{wf} = p_i - 141.2 \frac{q_o \mu_o \beta_o}{kh} [p_D(t_D) + s] \quad (4-3)$$

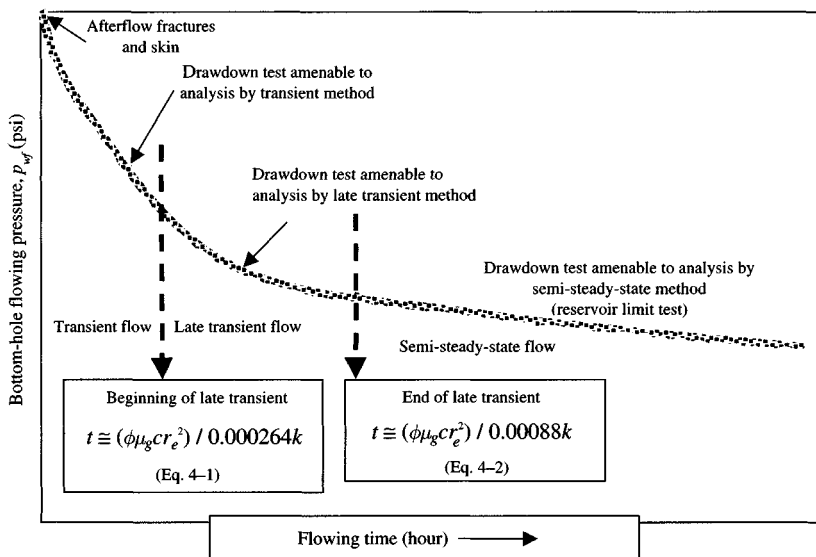


Figure 4–1. Schematic pressure–time histories for a constant-rate drawdown test (after Odeh and Nabor, *J. Pet. Tech.*, Oct. 1966).

Assuming initially the reservoir at initial pressure, p_i , the dimensionless pressure at the well ($r_D = 1$) is given as

$$p_D = 0.5[\ln(t_D) + 0.80907] \tag{4-4}$$

After the wellbore storage effects have diminished and $t_D/r_D^2 > 100$, dimensionless time is given by

$$t_D = \frac{0.0002637kt}{\phi\mu_o c_t r_w^2} \tag{4-5}$$

Combining and rearranging Eqs. 4-3 through 4-5, we get a familiar form of the pressure drawdown equation

$$p_{wf} = p_i - \frac{162.6q_o\mu_o\beta_o}{kh} \left[\log t + \log \left(\frac{k}{\phi\mu_o c_t r_w^2} \right) - 3.23 + 0.869s \right] \tag{4-6}$$

Eq. 4-6 describes a straight line with intercept and slope term together and it may be written as

$$p_{wf} = m \log t + p_{1hr} \tag{4-7}$$

A plot of flowing bottom-hole pressure data versus the logarithm of flowing time should be a straight line with slope m and intercept p_{1hr} (Figure 4-2). Semilog straight line does appear after wellbore damage

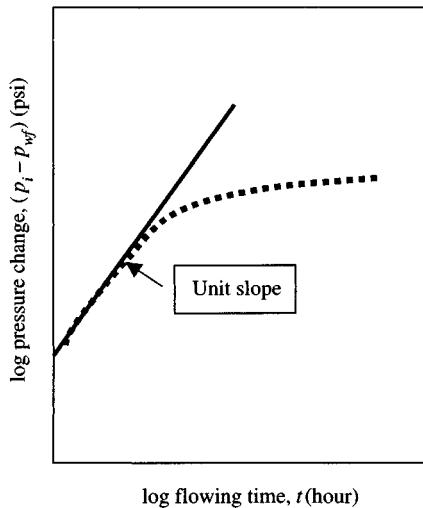


Figure 4-2. Semilog pressure drawdown data plot.

and storage effects have diminished. The slope of the semilog straight line may be given by

$$m = -\frac{162.6q_o\mu_o\beta_o}{kh} \quad (4-8)$$

The intercept at $\log t = 0$, which occurs at $t = 1$, is also determined from Eq. 4-6:

$$p_{1h} = p_i + m \left[\log \left(\frac{k}{\phi\mu_o\beta_o c_t r_w^2} \right) - 3.23 + 0.869s \right] \quad (4-9)$$

The skin factor is estimated from a rearranging form of Eq. 4-9:

$$s = 1.151 \left[\frac{p_i - p_{1hr}}{m} - \log \left(\frac{k}{\phi\mu_o c_t r_w^2} \right) + 3.23 \right] \quad (4-10)$$

The beginning time of the semilog straight line may be estimated from log-log plot of $[\log(p_i - p_{wf})]$ versus $\log t$ (Figure 4-3); when the slope of the plot is one cycle in Δp per cycle in t , wellbore storage dominates and test data give no information about the formation. The wellbore storage coefficient may be estimated from the unit-slope straight line using the following equation:

$$C = \frac{q_o\beta_o}{24} \cdot \frac{\Delta t}{\Delta p} \quad (4-11)$$

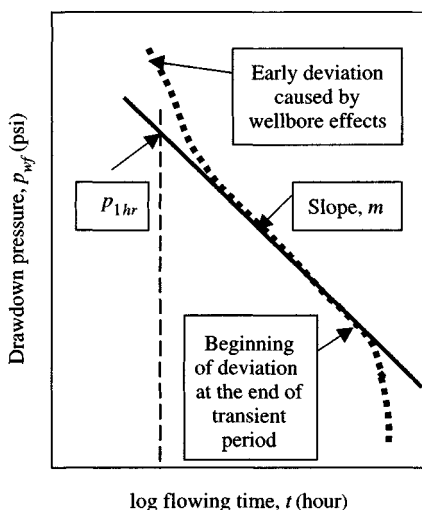


Figure 4-3. log-log pressure drawdown data plot.

where Δt and Δp are the values read from a point on the log-log unit slope straight line. C is calculated using Eq. 4-11, and should agree with C calculated from Eq. 4-12:

$$C = \frac{V_u}{(\rho/144g)g_c} \quad (4-12)$$

where V_u is the wellbore volume per unit length in barrels per foot. Duration of wellbore unloading can be estimated from Eq. 4-13:

$$t_{wbs} = \frac{(200,000 + 120,005)C_s}{kh/\mu_o} \quad (\text{hr}) \quad (4-13)$$

where

$$C_s = \frac{25.65A_{wb}}{\rho} \quad (4-14)$$

The apparent wellbore radius r_{wa} may be estimated by

$$r_{wa} = r_w e^{-s} \quad (4-15)$$

Radius of investigation at the beginning and end of the apparent middle time line may be checked by the following equation:

$$r_i = \left(\frac{kt}{848\phi\mu_o c_t} \right)^{0.5} \quad (4-16)$$

4.4 Late Transient Analysis – Bounded (Developed) Reservoirs

Pressure behavior at constant rate in a bounded reservoir can be represented by²

$$\log(p_{wf} - \hat{p}) = \log(b_1) - (\beta_1)t \quad (4-17)$$

From this we see that a plot of $\log(p_{wf} - \hat{p})$ versus t should be linear with slope magnitude:

$$\beta_1 = \frac{0.00168k}{\phi\mu_o c r_e} \quad (4-18)$$

and intercept

$$b_1 = 118.6 \frac{q_o \mu_o \beta_o}{kh} \quad (4-19)$$

The plot of $\log(p_{wf} - \hat{p})$ versus t will be linear provided the value of \hat{p} is known. Usually it is not. This means that a trial-and-error plot must be made using assumed \hat{p} values. That value which yields the best straight line on the $\log(p_{wf} - \hat{p})$ versus t plot is chosen as the correct \hat{p} value. A schematic late transient drawdown analysis plot is shown in Figure 4-4.

After determining the correct \hat{p} value, kh can be estimated from the intercept value b by

$$kh = \frac{118.6q_o\mu_o\beta_o}{b} \quad (4-20)$$

The pore volume (drainage volume) of the well V_p can be determined from the slope of plot (Figure 4-4). This value, in barrels, is given by

$$V_p = 0.1115 \frac{q_o\beta_o}{\beta_1 b_1 c_t} \quad (4-21a)$$

The equivalent drainage radius r_e is given by

$$r_e = \left[\frac{A \times 43,560}{\pi} \right]^{0.5} \quad (4-21b)$$

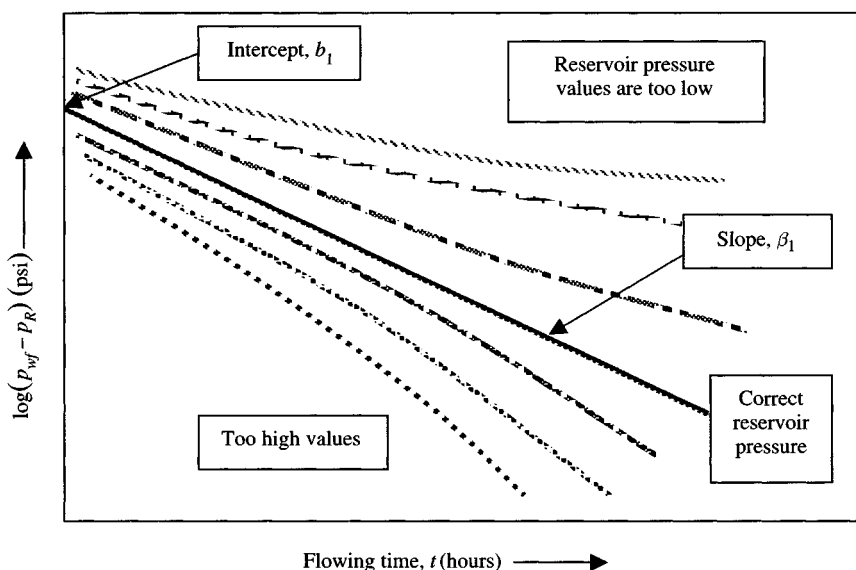


Figure 4-4. Schematic late-transient drawdown analysis plot.

The skin factor can be found from

$$s = 0.84 \left[\frac{\bar{p} - \hat{p}}{b_1} \right] - \ln \left(\frac{r_e}{r_w} \right) + 0.75 \quad (4-22)$$

where \bar{p} is the average reservoir pressure. The pressure drop across skin zone is given by

$$(\Delta p)_{skin} = \frac{b_1 s}{0.84} \quad (4-23)$$

Example 4-1 Analyzing Late Transient Drawdown Test

The pressure drawdown data were obtained from a 50-hours drawdown test in an oil well. Before this test, the well has been shut-in and the pressure is allowed to build up to a stabilized value of 1895 psi. Other data pertinent to the test are as follows: $q_o = 750$ stb/day; $h = 15$ ft; $\mu_o = 0.90$ cP; $\phi = 0.12$; $r_w = 0.29$ ft; $c_t = 17.5 \times 10^{-6}$ psi $^{-1}$; $\beta_o = 1.245$ rb/stb. Find the average reservoir pressure, intercept, slope, permeability k , pore volume, skin factor and pressure drop across skin.

Solution To prepare this late transient analysis plot, follow these steps:

1. Choose various values of average pressure, $p_R = 1300, 1400, 1460,$ and 1490 psi.
2. Plot $\log(p_{wf} - p_R)$ versus time in hours on semilog paper.
3. If the curve is concave downward, estimated value of p_R is too low. Conversely, if the curve is concave upward, the estimated value of p_R is too large. Thus a trial-and-error procedure is involved until a straight line is obtained.
4. Find the intercept and slope of the straight line.

From Figure 4-5, we find the intercept and slope values as

$$b' = 320 \text{ psi} \quad \text{and} \quad \beta' = \frac{\log(320) - \log(32)}{7.4} = 0.135 \text{ hr}^{-1}$$

From Eq. 4-20, we find

$$kh = \frac{118.6 q_o \mu_o \beta_o}{b'} = \frac{118.6 \times 750 \times 0.9 \times 1.245}{320} = 311.46 \text{ mD-ft}$$

$$k = \frac{311.46}{15} = 20.76 \text{ mD}$$

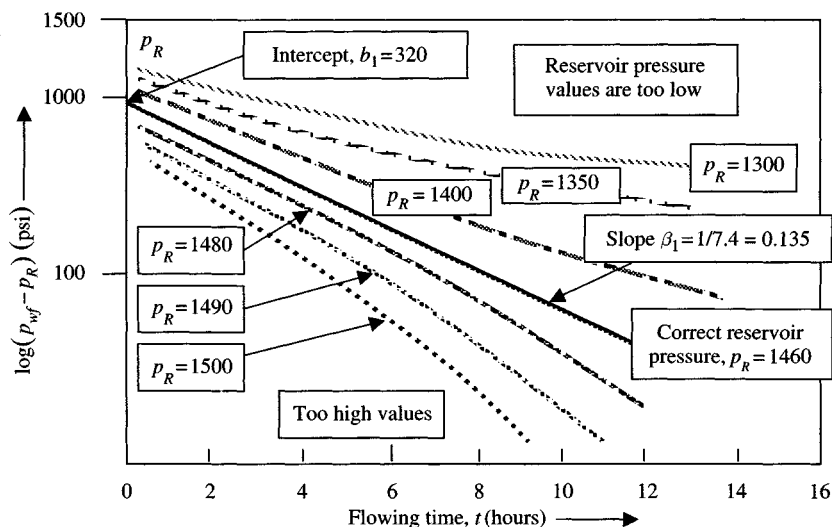


Figure 4-5. Semilog late-transient analysis plot, extended pressure drawdown test.

From Eq. 4-21a, we find

$$V_p = 0.1115 \frac{q_o \beta_o}{\beta' b_1 c_t} = 0.1115 \times \frac{750 \times 1.245}{0.135 \times 320 \times 17.5 \times 10^{-6}} = 1.38 \times 10^5 \text{ rbbbl}$$

$$\text{Area, } A = \frac{V_p \times 5.615}{43,560 \times h} = \frac{1.38 \times 10^5 \times 5.615}{43,560 \times 15} = 12 \text{ acres}$$

From Eq. 4-21b, we find

$$r_e = \sqrt{\frac{A \times 43,560}{\pi}} = \sqrt{\frac{12 \times 43,560}{22/7}} = 410 \text{ ft}$$

From Eq. 4-22, we find

$$\begin{aligned} s &= 0.84 \left[\frac{\bar{p} - \bar{p}}{b'} \right] - \ln \left(\frac{r_e}{r_w} \right) + 0.75 = 0.84 \left[\frac{1895 - 1460}{320} \right] - \ln \left(\frac{410}{0.29} \right) + 0.75 \\ &= 0.84 \times 1.3593 - 7.254 + 0.75 = -5.36 \end{aligned}$$

From Eq. 4-23, we find

$$(\Delta p)_{\text{skin}} = \frac{b's}{0.84} = \frac{3209 - 5.36}{0.84} = -2041 \text{ psi}$$

4.5 Semi-Steady-State Analysis – Reservoir Limit Test

If a pressure drawdown test is run for a long period of time, the pressure follows semi-steady-state behavior, which starts when the curve for that shape presented by Matthews et al.² may be combined with Eqs. 4-24 and 4-26 and simplified to Eq. 4-29:

$$p_D(t_D, \dots) = 2\pi t_{DA} + \frac{1}{2} \ln\left(\frac{A}{r_w^2}\right) + \frac{1}{2} \ln\left(\frac{2.2458}{C_A}\right) \quad (4-24)$$

$$p_D = \ln\left(\frac{r_e}{r_w}\right) \quad (4-25a)$$

$$t_D = \frac{0.000264kt}{\phi\mu_o c_t r_w^2} \quad (4-25b)$$

$$t_D\left(\frac{r_w^2}{A}\right) = t_{DA} = \frac{0.000264kt}{\phi\mu_o c_t A} \quad (4-26)$$

$$p_{wf} = m^* t + p_o \quad (4-27)$$

where

$$m^* = -\frac{0.233q_o\beta_o}{\phi c_t h A} \quad (4-28)$$

$$p_{Int} = p_i - \frac{70.6q_o\beta_o\mu_o}{kh} \left[\ln\left(\frac{A}{r_w^2}\right) + 0.80907 + 2s \right] \quad (4-29)$$

where

A = drainage area, ft²

C_A = Dietz's shape factor

m^* = negative slope of the linear part of the plot of p_{wf} versus t ,
in psi/hr

p_{Int} = intercept of the straight line when it is extrapolated to $t = 0$.

Eq. 4-27 indicates that a Cartesian plot of bottom-hole flowing pressure versus time should be a straight line during semi-steady-state flow, with slope m^* given by Eq. 4-28 and intercept p_{Int} given by Eq. 4-29; the slope can be used to estimate the reservoir drainage volume:

$$V_p = \phi h A = -\frac{0.23395q_o\beta_o}{c_t m^*} \quad (\text{ft}^3) \quad (4-30)$$

or

$$V_p = \phi h A = -\frac{0.23395q_o\beta_o}{c_t m^*(5.615)} \quad (\text{bbl}) \quad (4-31)$$

If ϕ and h are known, the drainage area may be estimated and if pressure drawdown test data are available during both the infinite period and semi-steady-state period, it is possible to estimate drainage shape. The semilog plot is used to determine m and p_{1hr} , the Cartesian plot is used to get m^* and p_{Int} . The system shape factor is estimated from⁴

$$C_A = 5.456 \frac{m}{m^*} \exp \left[\frac{2.303(p_{1hr} - p_{Int})}{m} \right] \quad (4-32)$$

or, using common logarithms:

$$C_A = 5.456 \frac{m}{m^*} \text{antilog} \left[\frac{(p_{1hr} - p_{Int})}{m} \right] \quad (4-33)$$

The dimensionless time used by Dietz to define the beginning of semi-steady-state behavior is calculated from

$$(t_{DA})_{pss} = 0.1833 \frac{m^*}{m} t_{pss} \quad (4-34)$$

where t_{pss} is the time at the start of the semi-steady-state period (hours), \Rightarrow that is time at the start of the straight line of the plot of p_{wf} versus t .

We can use the above material to analyze reservoir limit test. The technique is as follows:

- Plot both p_{wf} versus $\log t$ and p_{wf} versus t .
- From semilog plot determine m and p_{1hr} (extrapolate if necessary). If desired, these quantities may be used to calculate kh/μ and skin factor s using standard techniques.
- From the linear plot find slope, m^* , p_{Int} , and t_{pss} .

Estimation of Reservoir Limit

Calculate the drainage volume, $V_p = \phi h A = -0.233 q_o \beta_o / c_t m^*$ in ft^3 . If ϕ , h , and c_t are known, then the drainage area A and reservoir size r_e can be estimated as

$$A \text{ (ft}^2\text{)} = \pi r^2 = \sqrt{\frac{V_p \text{ (ft}^3\text{)}}{\phi h}} \quad \text{or} \quad A \text{ (acres)} = \sqrt{\frac{V_p \text{ (ft}^3\text{)}}{\phi h}} \frac{1}{43,560 \text{ (ft}^2\text{/acre)}}$$

$$r_e = \sqrt{\frac{A \text{ (acres)} \times 43,560}{\pi}} \quad (\text{ft})$$

Estimation of Reservoir Geometry

- Calculate C_A using Table B-2 or Figure B-8.
- Estimate the drainage shape and well location.

To illustrate the technique outlined above, the following example will clarify the analysis.

Example 4-2 Analyzing Single-Rate, Single-Phase Pressure Drawdown Test

A constant-rate drawdown test was run in an oil well with the following characteristics: $q_o = 250$ stb/day, $\mu_o = 0.8$ cP, $\beta_o = 1.136$ rb/stb, $c_o = 17.0 \times 10^{-6}$ psi⁻¹, $\phi = 0.039$, $h = 69$ ft, $p_i = 4412$ psi, and $r_w = 0.198$ ft. Last flowing time = 460 hr. From the test data given in Table 4-1, estimate the formation permeability, skin factor, pressure drop across skin, flow efficiency and reservoir pore volume.

Solution To estimate the reservoir parameters, follow these steps:

Plot $(p_i - p_{wf})$ versus log time (semilog data plot, Figure 4-7)

Plot $(p_i - p_{wf})$ versus log time (log-log data plot, Figure 4-6)

Plot p_{wf} versus time (Cartesian data plot, Figure 4-8)

From log-log data plot, Figure 4-6, determine

MTR1 → time at the beginning of transient period = 12 hours

MTR2 → time at the end of transient period = 150 hours

Show the value of MTR on semilog plot, Figure 4-7.

Estimate the formation permeability k using Eq. 4-8 as

$$k = \frac{162.6q_o\beta_o\mu_o}{mh} = \frac{162.6 \times 250 \times 1.136 \times 0.8}{70 \times 69} = 7.65 \text{ mD}$$

Check the radius of investigation at the beginning and end of the apparent middle time line to ensure that we are sampling a representative portion of the formation.

$$r_i \text{ at 12 hours} = \left(\frac{kt}{948\phi\mu c_i} \right)^{0.5} = \left(\frac{7.65 \times 12}{948 \times 0.039 \times 0.8 \times 17.0 \times 10^{-6}} \right)^{0.5} = 427 \text{ ft}$$

$$r_i \text{ at 150 hours} = \left(\frac{7.65 \times 150}{948 \times 0.039 \times 0.8 \times 17.0 \times 10^{-6}} \right)^{0.5} = 1510 \text{ ft}$$

Table 4-1
Drawdown Test Data (Single-Rate and Single-Phase Pressure Drawdown Test)

Time, t (hr)	Pressure, p_{wf} (psig)	$(p_i - p_{wf})$ (psig)
0.00	4412	0
0.12	3812	600
1.94	3699	713
2.79	3653	759
4.01	3636	776
4.82	3616	796
5.78	3607	805
6.94	3600	812
9.32	3593	819
9.99	3586	826
14.40	3573	839
17.30	3567	845
20.70	3561	851
24.90	3555	857
29.80	3549	863
35.80	3544	868
43.00	3537	875
51.50	3532	880
61.80	3526	886
74.20	3521	891
89.10	3515	897
107.00	3509	903
128.00	3503	909
154.00	3497	915
185.00	3490	922
222.00	3481	931
266.00	3472	940
319.00	3460	952
383.00	3446	966
460.00	3429	983

Estimate the skin factor s using Eq. 4-10 as

$$s = 1.151 \left[\frac{4412 - 3652}{70} - \log \left(\frac{7.65}{0.039 \times 0.8 \times 17.0 \times 10^{-6} \times 0.198^2} \right) + 3.23 \right]$$

$$= 6.36$$

This means the well is damaged and needs to be stimulated. Find pressure drop due to skin using the following equation:

$$(\Delta p)_{skin} = 0.869 \text{ ms} = 0.869 \times 70 \times 6.36 = 386.9 \text{ psi}$$

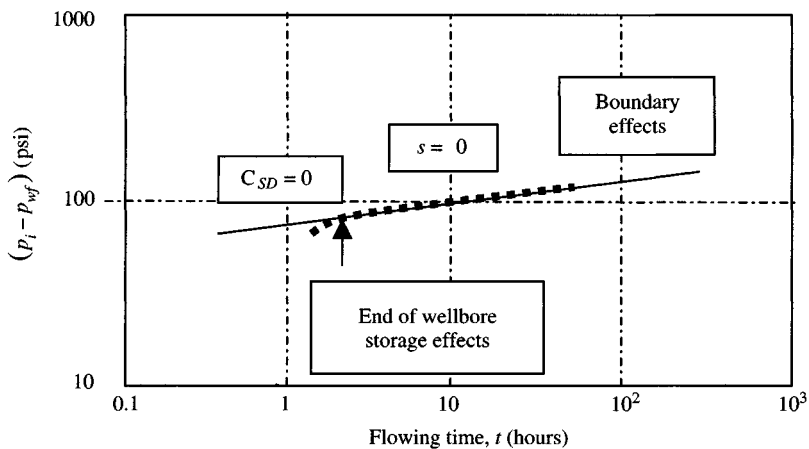


Figure 4-6. Single-rate drawdown test – log-log data plot.

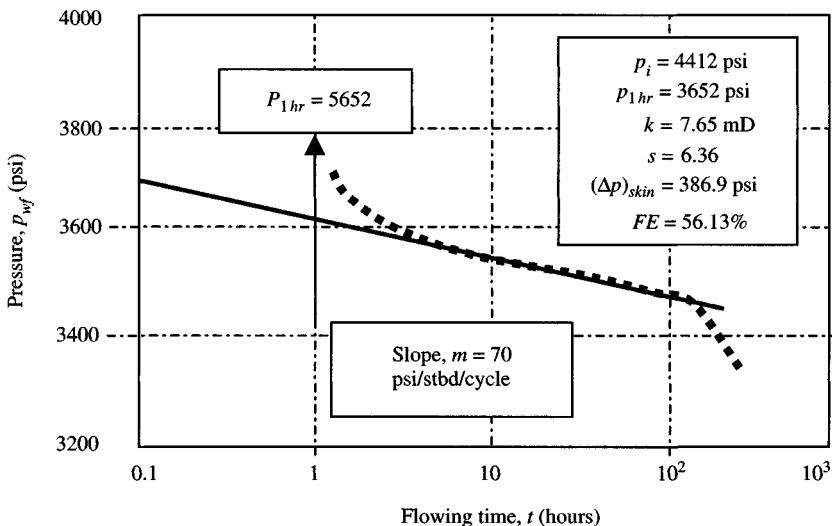
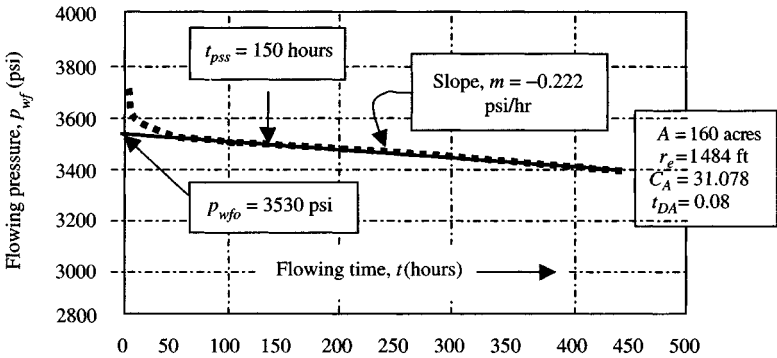


Figure 4-7. Single-rate drawdown test – semilog data plot.

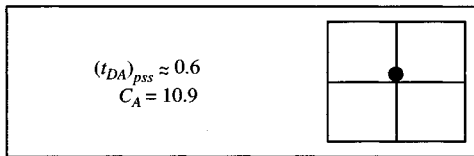
The flow efficiency is

$$FE = \frac{p_i - p_{wf,t=0} - (\Delta p)_{skin}}{p_i - p_{wf,t=0}} = \frac{4412 - 3530 - 386.9}{4412 - 3530} = \frac{495.1}{882} \times 100$$

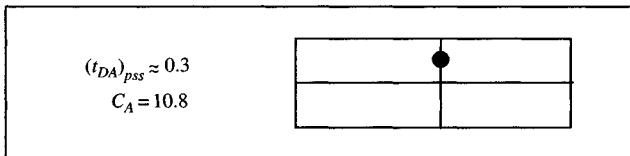
$$= 56.13\%$$



(a)



(b)



(c)

Figure 4-8. (a) Single-drawdown test – linear data plot; (b) Well location in a square drainage area; and (c) Well location in a 4×1 rectangular area.

Estimation of Reservoir Drainage Volume

To estimate the reservoir (drainage) volume V_p , find slope of the curve from linear plot, Figure 4-8.

$$\frac{\partial p_{wf}}{\partial t} = \frac{3530 - 3420}{0 - 500} = -0.222 \text{ psi/hr}$$

Thus, using Eq. 4-30, we find

$$\begin{aligned} V_p &= -\frac{0.23395q_o\beta_o}{c_t m^*} = -\frac{0.23395 \times 250 \times 1.136}{17.0 \times 10^{-6} \times (-0.222)} = 17,605,140.43 \text{ ft}^3 \\ &= \frac{3,315,376.75}{5.615} = 3,315,376.75 \text{ bbl} \end{aligned}$$

Estimation of Reservoir Size

Also V_p is equal to $\phi h A = \pi \phi h r_e^2$ and reservoir limits (size) are

$$r_e = \sqrt{\frac{V_p \times 5.615}{\pi \phi h}} = \sqrt{\frac{3,315,376.75/5.615}{22/7 \times 0.039 \times 69}} = 1484 \text{ ft}$$

$$\text{Area (acres)} = \pi r_e^2 = \frac{22}{7} \times 1484^2 \approx 160 \text{ acres}$$

Estimation of Reservoir Shape

Using Eq. 4-32 or 4-33, shape factor C_A is

$$\begin{aligned} C_A &= 5.456 \frac{m}{m^*} e^{[2.303(p_{1h} - p_o)/m]} \\ &= 5.456 \frac{-70.0}{-0.222} e^{[2.303(3652 - 3530/20)]} = 10.9 \end{aligned}$$

From Table B-2, we find:

More likely is one of the two shapes.

Discussion: If both short- and long-time pressure drawdown test data are available, we can estimate reservoir size and geometry from conventional reservoir limit test. The method does not need knowledge of the μ_o , r_w , s , or initial reservoir pressure. It is also applicable to gas reserves and injection testing.

4.6 Two-Rate Flow Test Analysis

To analyze the two-rate test, two cases will be discussed: when the initial pressure is not known and when the initial pressure is known.

When Initial Pressure Is not Known

This type of test can be used to estimate the permeability, skin factor, and reservoir pressure. The flow test does not have to be shut-in; thus no income is lost. The second rate could be increased or decreased; however, both the rates have to be stabilized. Two-rate flow test can be modeled as⁴

$$p_i - p_{wf} = 162.6 \frac{q_o \mu_o \beta_o}{kh} \left[\frac{q_1}{q_2} \log t + \left(\frac{q_2 - q_1}{q_2} \right) \log(t - t_1) \right. \\ \left. + \log \left(\frac{k}{\phi \mu_o c_t r_w^2} \right) - 3.23 + 0.869s \right] \quad (4-35)$$

Rearranging and introducing specialized nomenclature, $t_1 = t_{p1}$ and $t - t_{p1} = \Delta t'$, Eq. 4-35 becomes

$$p_{wf} = p_i - \frac{162.6 q_2 \mu_o \beta_o}{kh} \left[\log \left(\frac{k}{\phi \mu_o c_t r_w^2} \right) - 3.23 + 0.869s \right] \\ - 162.6 \frac{q_1 \mu_o \beta_o}{kh} \left[\log \left(\frac{t_{p1} + \Delta t'}{\Delta t'} \right) + \frac{q_2}{q_1} \log(\Delta t') \right] \quad (4-36)$$

Duration of wellbore storage distortion is essentially the same as in any buildup or drawdown test. However, the test procedure may minimize the effects of phase segregation in the wellbore. The following steps can be used to analyze the two-rate flow test:

- Plot p_{wf} versus $[\log((t_{p1} + \Delta t')/\Delta t') + (q_2/q_1) \log(\Delta t')]$
- Determine the slope m from the plot and use it to calculate the permeability k from the relationship

$$k = 162.6 \frac{q_1 \mu_o \beta_o}{mh} \quad (4-37)$$

- Calculate the skin factor s from the equation

$$s = 1.151 \left[\frac{q_1}{q_1 - q_2} \left(\frac{p_{1hr} - p_{wf1}}{m} \right) - \log \left(\frac{k}{\phi \mu_o c_t r_w^2} \right) + 3.23 \right] \quad (4-38)$$

- Pressure drop due to skin:

$$(\Delta p)_{skin} = 0.869ms \text{ at rate } q_1 \quad (4-38a)$$

$$(\Delta p)_{skin} = 0.869 \frac{q_2}{q_1} ms \text{ at rate } q_2 \quad (4-38b)$$

- p_i (or, more generally, p^*) is obtained by solving for p_i (p^*) from the drawdown equation written to model conditions at the time of the rate change:

$$p^* = p_{int} - \frac{q_2}{q_1 - q_2} [p_{wf}(\Delta f=0) - p_{1hr}] \quad (4-39)$$

$$p_i \text{ or } p^* = p_{wf1} + m \left[\log \left(\frac{kt_{p1}}{\phi \mu_o c_t r_w^2} \right) - 3.23 + 0.869s \right] \quad (4-40)$$

This false pressure p^* may be used to determine the average drainage region pressure. The following example will clarify the method of analysis.

Example 4-3 *Analyzing Two-Rate Drawdown Test When Initial Pressure Is not Known*

A two-rate flow test was run by stabilizing the flow rate at 105 stb/day for several days and then reducing the flow rate to 75 stb/day. The pressure data during the second rate are shown in Figure 4-9. Other pertinent data are: $h = 65$ ft, $c_t = 10.0 \times 10^{-5}$ psi⁻¹, $V_p = 32,000$ stb (cumulative volume produced at last rate change), $p_{wf}(\Delta t = 0) = 3200$ psi, $\phi = 0.10$, $\mu_o = 0.75$, $\beta_o = 1.65$ rb/stb, $r_w = 0.3$.

Solution $t_{p1} = 24(32,000)/105 = 7314.29$ hr. The pressure data during the second flow rate are shown in Figure 4-9. Calculate the formation permeability k using Eq. 4-37:

$$k = 162.6 \frac{q_1 \mu_o \beta_o}{mh} = 162.6 \times \frac{105 \times 0.75 \times 1.75}{105 \times 65} = 3.28 \text{ mD}$$

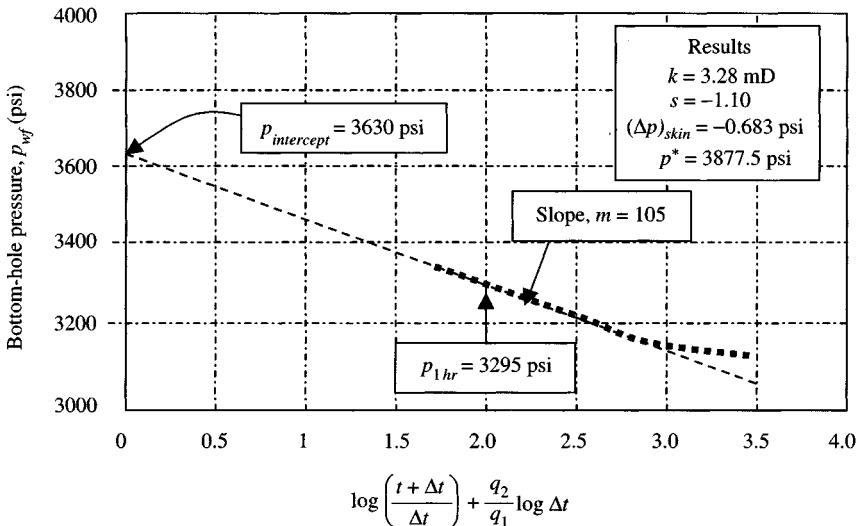


Figure 4-9. Two-rate drawdown test – when p_i is not known.

Estimate the skin factor s using Eq. 4-38:

$$\begin{aligned}
 s &= 1.151 \left[\frac{q_1}{q_1 - q_2} \left(\frac{p_{1hr} - p_{wf1}}{m} \right) - \log \left(\frac{k}{\phi \mu_o c_t r_w^2} \right) + 3.23 \right] \\
 &= 1.151 \left[\frac{105}{105 - 75} \left(\frac{3295 - 3220}{105} \right) - \log \left(\frac{3.28}{0.1 \times 0.75 \times 10 \times 10^{-5} \times 0.3^2} \right) \right. \\
 &\quad \left. + 3.23 \right] \\
 &= 1.151 [3.5 \times (-0.7143) - 6.687 + 3.23] = -1.10
 \end{aligned}$$

Estimate the pressure drop due to skin using Eqs. 4-38a and 4-38b:

$$(\Delta p)_{skin} = 0.869 ms \text{ at rate } q_1 = 0.869 \times 105(-1.10) = -100.37 \text{ psi}$$

$$(\Delta p)_{skin} = 0.869 \frac{q_2}{q_1} ms \text{ at rate } q_2 = 0.869 \left(\frac{75}{105} \right) (-1.10) = -0.683 \text{ psi}$$

The minus sign indicates that, because of an enlarged well radius, the pressure drop near wellbore is less than normal. The false pressure, p^* , is determined from Eq. 4-39:

$$\begin{aligned}
 p_i \text{ or } p^* &= p_{Int} - \frac{q_2}{q_1 - q_2} [p_{wf}(\Delta t=0) - p_{1hr}] \\
 &= 3630 - \frac{75}{105 - 75} [3220 - 3295] \\
 &= 3690 + 187.5 = 3877.5 \text{ psi}
 \end{aligned}$$

The p^* value may be used with the material in Chapter 5 to determine the average drainage region pressure.

When Initial Pressure Is Known

The general equation for an n -rate flow test is

$$\begin{aligned}
 \frac{p_i - p_{wf}}{q_n} &= 162.6 \frac{\mu_o \beta_o}{kh} \left[\sum_{j=1}^n \frac{q_j - q_{j-1}}{q_n} \right] \log(t_n - t_{j-1}) \\
 &\quad + 162.6 \frac{\mu_o \beta_o}{kh} \left[\log \left(\frac{k}{\phi \mu_o c_t r_w^2} \right) - 3.23 + 0.869s \right] \quad (4-41)
 \end{aligned}$$

If Eq. 4-41 is plotted as $[(p_i - p_{wf})/q_n]$ versus $\sum_{j=1}^n ((q_j - q_{j-1})/q_n) \log(t_n - t_{j-1})$ on Cartesian coordinate paper, it should give a straight line of slope, m' , from which the formation permeability can be estimated:

$$k = 162.6 \frac{q_1 \mu_o \beta_o}{m' h} \quad (4-42)$$

The intercept b' of the straight line is obtained when the plotting function is zero,

$$b' = m' \left[\log \left(\frac{k}{\phi \mu_o c_i r_w^2} \right) - 3.23 + 0.869s \right] \quad (4-43)$$

where b' is the value of $(p_i - p_{wf})/q_n$, when plotting function is zero. By solving for s in Eq. 4-41, we obtain

$$s = 1.151 \left[\frac{b'}{m'} - \log \left(\frac{k}{\phi \mu_o c_i r_w^2} \right) + 3.23 \right] \quad (4-44)$$

The method of analysis has the disadvantage that the initial reservoir pressure p_i and the entire flow rate history must be known; frequently, they are not. In such cases, the analysis technique may be modified so that the initial pressure is not used. The following section will present modified analysis techniques proposed by Russell⁴ for a two-rate test.

$$p_{wf} = m'_1 \left[\log \left(\frac{t_1 + \Delta t}{\Delta t} \right) + \frac{q_2}{q_1 \log \Delta t} \right] + p_{int} \quad (4-45)$$

Eq. 4-43 assumes a constant flow rate q_1 , from time 0 to time t_1 , at start of the test. t_1 should be calculated from the following equation:

$$t_1 = 24 \frac{V_p}{q_1} \quad (4-46)$$

where V_p is the cumulative volume produced since last rate stabilization. Eq. 4-45 indicates that a plot of p_{wf} versus $[\log((t_1 + \Delta t)/\Delta t) + (q_2/q_1) \log \Delta t]$ should be a straight line with slope

$$m'_1 = - \frac{162.6 q_1 \mu_o \beta_o}{k h} \quad (4-47)$$

and the intercept (extrapolated to zero) is

$$p_{int} = p_i + m'_1 \frac{q_2}{q_1} \left[\log \left(\frac{k}{\phi \mu_o c_t r_w^2} \right) - 3.23 + 0.869s \right] \quad (4-48)$$

Once the slope of the straight line is determined from the data plot, the reservoir permeability may be estimated from

$$k = - \frac{162.6 q_1 \mu_o \beta_o}{m'_1 h} \quad (4-49)$$

The skin factor is estimated from

$$s = 1.151 \left[\frac{q_1}{q_1 - q_2} \left(\frac{p_{wf}(\Delta t = 0) - p_{1hr}}{m'_1} \right) - \log \left(\frac{k_2}{\phi \mu_o c_t r_w} \right) + 3.23 \right] \quad (4-50)$$

The intercept of the data plot may be used to estimate the false pressure,²

$$p^* = p_{int} - \frac{q_2}{q_1 - q_2} [p_{wf}(\Delta t = 0) - p_{1hr}] \quad (4-51a)$$

which is used to estimate the average reservoir pressure using the method given in Chapter 5. The initial reservoir pressure can be calculated as

$$p_i = p_{wf1} + m \left[\log \left(\frac{k t_{p1}}{\phi \mu_o c_t r_w^2} \right) - 3.23 + 0.869s \right] \quad (4-51b)$$

where p_{wf1} is the flowing pressure at the first rate change ($\Delta t = 0$) and p_{1hr} is the flowing pressure at $\Delta t = 1$ hr or the MTR line. p_{int} is the intercept extrapolated to zero.

Example 4-4 *Analyzing Two-Rate Drawdown Test When Initial Pressure Is Known*

A two-rate flow test was run on an oil well with the given properties. From these properties and the data given in Table 4-2, determine k , s , and p^* . The well depth is 7550 ft. $\mu_o = 0.805$ cP, $\beta_o = 1.137$ rb/stb, $p_i = 4412$ psi, $\phi = 0.039$, $r_w = 0.198$ ft, $A_{wb} = 0.0218$ ft², $\rho_m = 52.7$ lb/ft³, $h = 69$ ft, $T_R = 162^\circ$ F, pressure at time of rate change = 3490 psi, $t_{p1} = 184.7$ h, $q_1 = 250$ stb/day and $q_2 = 125$ stb/day.

Solution The plotting function X is tabulated in Table 4-2, and a plot of p_{wf} versus X is shown in Figure 4-10. The MTR line of the plot p_{wf} versus X has the following characteristics:

Beginning of MTR at $\Delta t = 6$ hr, $X = 1.9$

End of MTR at $\Delta t = 50$ hr, $X = 1.5$

Table 4-2
Two-Rate Drawdown Test Data

Time, t (hr)	Flowing pressure, p_{wf} (psig)	Flowing pressure, p_{wf} (psia)	$\frac{t + \Delta t}{\Delta t}$	$\frac{\log(t + \Delta t)}{\Delta t} + \frac{q_2}{q_1} \times \log(\Delta t)$
0.11	3528	3523	1680.09	2.7460
0.15	3549	3564	1232.33	2.6769
0.22	3577	3592	840.55	2.5983
0.31	3612	3627	596.81	2.5190
0.45	3654	3669	411.44	2.4405
0.65	3702	3717	285.15	2.3618
0.93	3751	3766	199.60	2.2831
1.34	3795	3810	138.84	2.2050
1.94	3831	3846	96.40	2.1272
2.79	3853	3868	67.25	2.0500
4.01	3867	3882	47.06	1.9739
5.78	3876	3891	32.96	1.8985
8.32	3882	3897	23.20	1.8252
12.00	3888	3903	16.39	1.7539
17.30	3893	3908	11.68	1.6860
24.90	3897	3912	8.42	1.6230
35.80	3900	3915	6.16	1.5662
51.50	3903	3918	4.59	1.5171
74.20	3904	3919	3.49	1.4777
89.10	3903	3918	3.07	1.4622
107.00	3902	3917	2.73	1.4500
128.00	3901	3916	2.44	1.4413
154.00	3898	3913	2.20	1.4358
184.70	3895	3910	2.00	1.4340

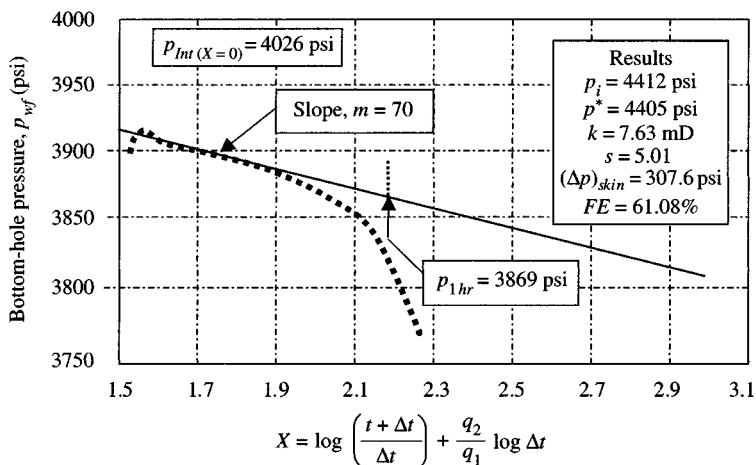


Figure 4-10. Two-rate drawdown test – when p_i is known.

Slope of MTR line, $m_1 = 70.65$ psi

Intercept of MTR line at $X = 0$, $p_{Int} = 4026$ psi

$p_{1\text{ hr}}$ (at $\Delta t = 1$ hr), $X = 2.270 = 3869$ psi

Estimate the formation permeability using Eq. 4-49:

$$k = \frac{162.6q_1\mu_o\beta_o}{m'_1h} = \frac{162.6 \times 250 \times 1.137 \times 0.805}{70.65 \times 69} = 7.63 \text{ mD}$$

Determine the skin factor from Eq. 4-50:

$$\begin{aligned} s &= 1.151 \left[\frac{q_1}{q_1 - q_2} \left(\frac{p_{wf}(\Delta f=0) - p_{1\text{ hr}}}{m'_1} \right) - \log \left(\frac{k}{\phi\mu_o c_f r_w} \right) + 3.23 \right] \\ &= 1.151 \left[\frac{250}{250 - 125} \frac{(3490 - 3869)}{70.65} \right. \\ &\quad \left. - \log \left(\frac{7.63}{0.039 \times 0.805 \times 7.01 \times 10^{-6} \times 0.198^2} \right) + 3.23 \right] = 5.01 \end{aligned}$$

The pressure drops across the skin at rates q_1 and q_2 , respectively,

$$(\Delta p)_{skin} = 0.869ms = 0.869 \times 70.65 \times 5.01 = 307.6 \text{ psi}$$

$$(\Delta p)_{skin} = 0.869 \frac{q_2}{q_1} ms = 0.869 \times \frac{125}{250} \times 70.65 \times 5.01 = 153.8 \text{ psi}$$

The false pressure p^* is determined from Eq. 4-51a:

$$\begin{aligned} p^* &= p_{Int} - \frac{q_2}{q_1 - q_2} [p_{wf}(\Delta f=0) - p_{1\text{ hr}}] = 4026 - \frac{125}{250 - 125} (3490 - 3869) \\ &= 4405 \text{ psi} \end{aligned}$$

Check if we have chosen the proper range of MTR.

$$C_S = 25.65 \frac{A_{wb}}{\rho_m} = 25.65 \frac{0.0218}{52.7} = 0.0106 \text{ bbl/psi}$$

$$t_{wbs} = \frac{(200,000 + 12,000s)C_S}{kh/\mu} = \frac{200,000 + 12,000 \times 5.88}{(7.65 \times 69)/0.805} = 4.45 \text{ hours}$$

At this time the plotting function X is 1.95. This confirms our choice of the start of the MTR line.

4.7 Variable-Rate Flow Tests

It is impossible to maintain a constant rate long enough to complete a drawdown test. In such cases, variable (multiple)-rate testing analysis techniques are applicable. A variable-rate test may include one with several variable rates or one with a series of constant rates. Accurate flow rate and pressure measurements are essential for the successful analysis. Rate measurements are much more critical in variable-rate well tests than in conventional constant-rate well test. Variable rate testing has the following advantages:

- Provide transient test data while production continues;
- Trends to minimize changes in wellbore storage coefficient and phase segregation effects.

To obtain a meaningful and useable information from variable-rate tests, good flow rate data are much more critical than the conventional constant-rate well tests. In this section, we will discuss the n -rate flow test. The method assumes an infinite-acting reservoir during the entire test period.

Modified Variable-Rate Cases

This section will present transient and semi-steady-state cases.

Transient Case When $t_p < t_{pss}$

Refs. 6 and 7 have provided a technique to analyze the n -rate flow test; a plot of the following variables on semilog graph paper is required.

$$\frac{(p_i - p_{wf})}{q_n} \text{ versus } \log t \quad (4-52)$$

The slope (m') and intercept (b') of the appropriate straight line in the plot above are used to estimate the formation permeability and skin factor. The following equations are used to estimate the reservoir parameters:

$$k = \frac{162.6\mu_o\beta_o}{m'h} \quad (4-53)$$

$$s = 1.151 \left[\frac{b'}{m'} - \log \left(\frac{k}{\phi\mu_o cr_w^2} \right) + 3.23 \right] \quad (4-54)$$

$$(\Delta p)_{skin} = 0.869(q_o)_{average}(m')(s) \quad (4-55)$$

Calculation of Average Reservoir Pressure, \bar{p}

Assume that if the well was producing in the semi-steady state, then \bar{p} can be calculated by the following equation:

$$\begin{aligned}\bar{p} - p_{wf} &= 2m' \log\left(\frac{0.472r_e}{r_w}\right) + 0.869s \\ &= 2m' \left[\log\left(\frac{0.223r_e^2}{r_w}\right) + 0.435s \right] \\ &= 2m' \left[\log\left(\frac{0.223C_A \pi r_e^2}{\pi C_A r_w^2}\right) + 0.435s \right]\end{aligned}\quad (4-55a)$$

or

$$\bar{p} = 2m' \left[\log\left(\frac{2.241A}{C_A r_w^2}\right)^{0.5} + 0.435s \right] + p_{wf}(\Delta t=0) \quad (4-55b)$$

Flow efficiency FE is

$$FE = \frac{\bar{p} - p_{wf} - (\Delta p)_{skin}}{\bar{p} - p_{wf}} \times 100$$

Example 4-5 Analyzing Variable-Rate Pressure Drawdown Test Assuming Transient Flow

A variable-flow-rate test was run on an oil well. The test data are given in Table 4-3. To interpret the test, the following reservoir, PVT, and flow parameters are given: Pressure at ($t = 0$) = 4412 psig, $\beta_o = 1.136$ rb/stb, $\mu_o = 0.80$ cP, $h = 69$ ft, $c_t = 17.0 \times 10^{-6}$ psi $^{-1}$, $API = 35^\circ$, $r_w = 0.198$ ft, $\phi = 0.039$ fraction, $A = 40$ acres.

Assume circular drainage area. Determine the following:

1. Formation permeability, k
2. Skin factor, s
3. Pressure drop due to skin
4. Average reservoir pressure, \bar{p}
5. Flow efficiency, FE .

Solution A plot of $\Delta p/q_n$ versus plotting function (rate-time function) is given in Figure 4-11. From this plot the following results are obtained: slope, $m' = 0.288$ psi/cycle, intercept, $b' = 3.04$ psi/(stb/day) at $q_n = 166$ stb/day $\rightarrow (p_i - p_{if})/q_n = (4412 - 4099)/166 = 1.8855$ psi/(stb/day).

Table 4-3
Variable-Flow-Rate Drawdown Test Data

Time, t (hr)	Rate (stb/day)	$\Delta q = q_i - q_n$ (stb/day)	Pressure (psig)	$(p_i - p_{wf})$ (psig)	$(p_i - p_{wf})/q_i$ (psi/(stb/day))
0.105	180	0	4332.0	80.0	0.4444
0.151	177	3	4302.0	110.0	0.6215
0.217	174	6	4264.0	148.0	0.8506
0.313	172	8	4216.0	196.0	1.1395
0.450	169	11	4160.0	252.0	1.4911
0.648	166	16	4099.0	313.0	1.8855
0.934	163	17	4039.0	373.0	2.2883
1.340	161	19	3987.0	425.0	2.6398
1.940	158	22	3952.0	460.0	2.9114
2.790	155	25	3933.0	479.0	3.0903
4.010	152	28	3926.0	486.0	3.1974
5.780	150	30	3926.0	486.0	3.2400
8.320	147	33	3927.0	485.0	3.2993
9.990	145	35	3928.0	484.0	3.3379
14.400	143	37	3931.0	481.0	3.3636
20.700	140	40	3934.0	478.0	3.4143
29.800	137	43	3937.0	475.0	3.4672
43.000	134	46	3941.0	471.0	3.5149

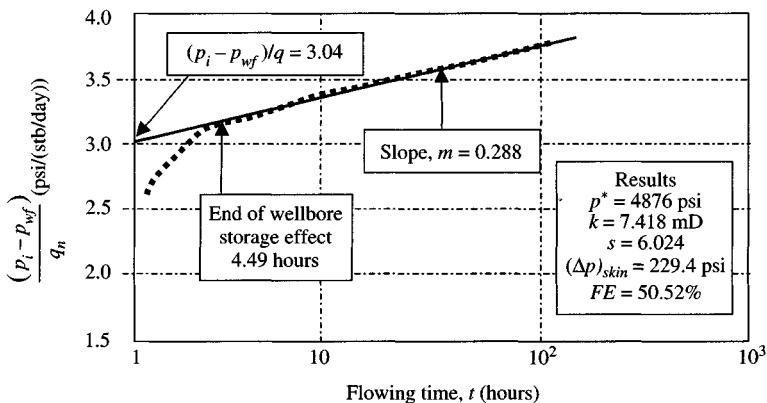


Figure 4-11. Variable-rate drawdown test – transient case.

1. From the slope of 0.288 psi/cycle, the permeability, k , is found from Eq. 4-53:

$$k = \frac{162.6\beta_o\mu_o}{m'h} = \frac{162.6 \times 1.136 \times 0.80}{0.288 \times 69} = 7.44 \text{ mD}$$

2. The skin factor, s , is obtained from Eq. 4-54:

$$s = 1.151 \left[\frac{3.04}{0.288} - \log \left[\frac{7.44}{0.039 \times 0.8 \times 17.0 \times 10^{-6} \times 0.198^2} + 3.23 \right] \right] = 6.02$$

It means the well is damaged and needs stimulation.

3. The pressure drop due to skin factor is

$$(\Delta p)_{skin} = 0.869(q)_{Av}(s)(m') = 0.869 \times 151 \times 6.02 \times 0.288 = 227 \text{ psi}$$

4. The average reservoir pressure, \bar{p} , can be calculated using Eq. 4-55b:

$$\begin{aligned} \bar{p} &= 2m' \left[\log \left(\frac{2.241A}{C_A r_w^2} \right)^{0.5} + 0.435s \right] + p_{wf}(\Delta t = 0) \\ &= 2 \times 0.288 \left[\log \left(\frac{2.241 \times 40 \times 43,560}{31.6 \times 0.198^2} \right)^{0.5} + 0.435 \times 6.02 \right] + 4412 \\ &= 0.576[3.249 \times 0.435 \times 6.024] + 4412 = 4416 \text{ psi} \end{aligned}$$

5. Flow efficiency, $FE = \frac{4416 - 4412 - 227}{5020 - 4412} \times 100 = 62.66\%$.

Semi-Steady-State Case⁴ When $t_p < t_{pss}$

The method assumes an infinite-acting oil reservoir with a well located at $r = 0$ and produced at a constant rate. The point source solution is

$$p_{wf} = p_i + \frac{162.6q\mu_o\beta_o}{kh} E_i \left(-\frac{r_w^2 \phi \mu_o c_t}{4kt} \right) \quad (4-56)$$

where p_i is the original pressure at $t = 0$, p_{wf} the pressure at any t and wellbore radius r_w . Eq. 4-56 shows the pressure formation around it is neither damaged nor improved. If a condition of permeability damage and improvement exists, the equation must be corrected for these effects. Van Everdingen and Hurst⁸ introduced an additional term:

$$p_i - p_{wf} = \frac{162.6q_o\mu_o\beta_o}{kh} \left(\ln \left(\frac{kt}{\phi\mu_o c_t r_w^2} \right) + 0.809 + 2s \right) \quad (4-57)$$

where s is the skin factor and is dimensionless. If the well is produced at a variable rate, then using the superposition principle and solution, we have

$$\begin{aligned}
 p_i - p_{wf} = & \frac{162.6\mu_o\beta_o}{kh} \left\{ q_1 \left[\ln \left(\frac{kt_n}{\phi\mu_o c_t r_w^2} \right) + 0.809 + 2s \right] \right. \\
 & + (q_2 - q_1) \left[\ln \left(\frac{k(t_n - t_1)}{\phi\mu_o c_t r_w^2} \right) + 0.809 + 2s \right] \left. \right\} \\
 & + \dots + (q_n - q_{n-1}) \left[\ln \left(\frac{k(t_n - t_{n-1})}{\phi\mu_o c_t r_w^2} \right) + 0.809 + 2s \right] \quad (4-58)
 \end{aligned}$$

where t_n is the total flowing time for n constant rate flow periods $t_1 - t_0, t_2 - t_1, \dots, t_n - t_{n-1}$ with rates q_1, q_2, \dots, q_n . If we use Eq. 4-58 in its present form to construct a straight line pressure drawdown plot, k, ϕ, μ, c_t, r_w , and s must be known. This is so because for every t_n , a variable factor $q_n(\ln(k/\phi\mu_o c_t r_w^2) + 0.809 + 2s)$ is left at the right-hand side of the equation. Hence this has been a problem in analyzing a variable-rate pressure drawdown. Odeh and Jones⁷ used the superposition principle to arrive at a variable-rate procedure for appraising wellbore damage in water-injection wells. To construct a straight-line pressure drawdown plot, divide both sides of Eq. 4-58 by q_n , and after simplification and summation give

$$\frac{p_i - p_{wf}}{q_n} = \frac{70.6\mu_o}{kh} \left[\sum_{i=0}^{n-1} \frac{\Delta q_i}{q_n} \ln(t_n - t_i) - 7.432 + 2s + \ln \frac{k}{\phi\mu_o c_t r_w^2} \right] \quad (4-59)$$

or

$$\frac{p_i - p_{wf}}{q_n} = \frac{162.6\mu_o}{kh} \left[\sum_{i=0}^{n-1} \frac{\Delta q_i}{q_n} \log(t_n - t_i) - 3.23 + 0.869s + \log \left(\frac{k}{\phi\mu_o c_t r_w^2} \right) \right] \quad (4-60)$$

When p is in psi, q in bbl/day, μ in cP, kh in mD-ft, t in h, r in ft, ϕ in fraction, c in psi^{-1} , $t_0 = 0$, t is the time when the change in rate was initiated, $\Delta q_i = q_{i+1} - q_i$, and $q_0 = 0$. Thus, a plot of $(p_i - p_{wf})/q_n$ versus $(1/q_n) \sum_{i=0}^{n-1} \Delta q_i \ln(t_n - t_i)$ should result in a straight line with a slope, m is

$$m = \frac{70.6\mu_o\beta_o}{kh} \quad (4-61)$$

Solving Eqs. 4-59 and 4-61 for s , we get

$$s = 0.5 \left[\frac{b'}{m} - \ln \left(\frac{k}{\phi\mu_o c_t r_w^2} \right) + 7.432 \right] \quad (4-62a)$$

and

$$(\Delta p)_{skin} = 2msq_n \quad (4-62b)$$

If log is used, then

$$m = \frac{162.6\mu_o\beta_o}{kh} \quad (4-63)$$

$$s = 1.151 \left[\frac{b'}{\bar{m}} - \log \left(\frac{k}{\phi\mu_o c_i r_w^2} \right) + 3.23 \right] \quad (4-64)$$

and total pressure drop due to the skin effect for the drawdown test then will be

$$(\Delta p)_{skin} = 0.869 msq_n \quad (4-65)$$

Method of Applications

To analyze variable-rate drawdown test, follow these steps:

1. Plot production rate versus time on regular paper.
2. Divide the time axis into time increments and calculate the average flow rate for each increment.
3. Calculate $\Delta p = p_i - p_{wf}$ as a function of time, and divide each Δp log the average rate existing at that time at which p_{wf} was read. p_i and p_{wf} are, respectively, the initial and bottom-hole pressures in psi.
4. Calculate the plotting function $X = (1/q_n) \sum_{i=0}^{n-1} \Delta q_i \log(t_n - t_i)$ as a function of time and plot it against $\Delta p/q_n$ calculated in step (3) on rectangular coordinate paper. t_n is the total flow time, t_i the time when each change in rate was initiated, $t_n = 0$, q_i the flow rate in stb/day during $(t_i - t_{i-1})$ time interval, $\Delta q_i = q_{i+1} - q_i$, $q_o = 0$, and q_n the flow rate during $(t_n - t_{n-1})$ time interval.
5. Calculate the slope m of the resulting straight-line plot of step (4).
6. Calculate kh using Eq. 4-63.
7. Calculate skin factor s using Eq. 4-64.
8. Calculate pressure drop due to skin effect using Eq. 4-65.

Example 4-6 Analyzing Variable-rate Pressure Drawdown Test Using Odeh and Jones Method

A 3-hours drawdown test was conducted on a new well. The average flow rate during the first, the second, and the third hour were, respectively, 478.5,

Table 4-4
Variable Drawdown Test Analysis

Plotting functions							
n	t (min)	q_i (stb/day)	p_{wf} (psi)	Δp (psi)	$\frac{\Delta p}{q_n}$ (psi/stb/day)	$\frac{1}{q_n} \sum_{i=0}^{n-1}$ $\Delta q_i \ln(t_n - t_i)$	$\frac{1}{q_n} \sum_{i=1}^{n-1}$ $\Delta q_i \log(t_n - t_i)$
1	0		3000	0	0	—	—
1	20	478.5	999	2001	4.1818	2.9957	1.3010
1	40	478.5	857	2143	4.4786	3.6889	1.6021
1	60	478.5	779	2222	4.6437	4.0943	1.7782
2	120	319.0	1378	1622	5.0846	5.1341	2.2297
3	140	159.5	2043	957	6.0000	7.4552	3.2342
3	160	159.5	2077	924	5.7131	6.9287	3.0103
3	180	159.5	2094	906	5.6767	6.6872	3.8157

319, and 159.5 reservoir bbl/day. The original reservoir pressures were 3000 psi. Drawdown test data are given in Table 4-4, the reservoir and well data are:

$$h = 27 \text{ ft}, \phi = 0.17, r_w = 0.29 \text{ ft}, \mu_o = 0.60 \text{ cP}, \text{ and } \beta_o = 1.2172 \text{ rb/stb},$$

$$c_t = 7.5 \times 10^{-6} \text{ psi}^{-1}.$$

Solution Table 4-4 shows the calculated data and plotting functions and Figure 4-12 shows a plot of these functions.

Calculation of Plotting Functions

For $n = 3$, $q_n = 159.5$ stb/day, $q_0 = 0$, $t_n = 140$, and $t_0 = 0$:

$$\begin{aligned} & \frac{1}{159.5} [(478.5 \log(140 - 0) + (319 - 478.5) \log(140 - 60) \\ & + (159.5 - 319) \log(140 - 120)] \\ & = \frac{1}{159.5} [478.5(2.416) + (-159.5)(1.9031) + (-159.5)(1.3010)] \\ & = \frac{1}{159.5} [1026.91 + (-303.54) - 207.51] = 3.2342 \end{aligned}$$

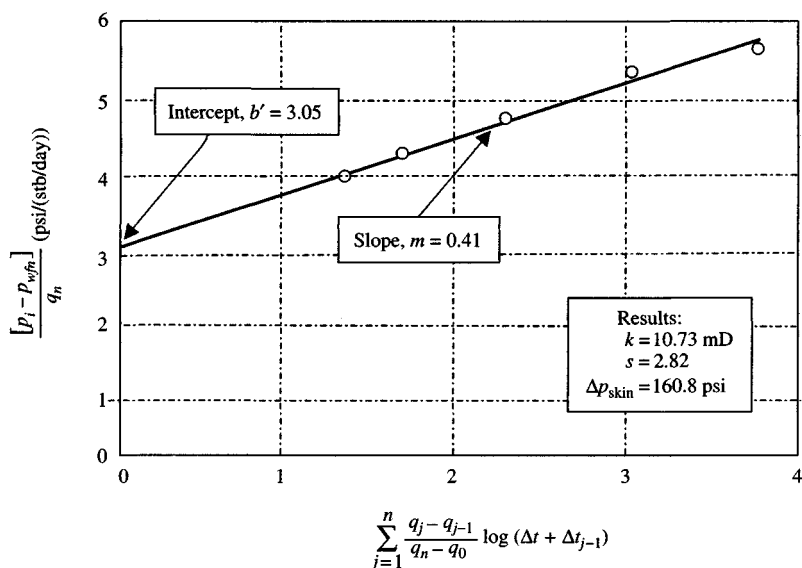


Figure 4-12. Variable-rate case using Odeh and Jones plot.

For $n = 3$, $q_n = 159.5$ stb/day, $q_0 = 0$, $t_n = 160$, and $t_0 = 0$:

$$\begin{aligned} & \frac{1}{159.5} [(478.5 \log(160 - 0) + (319 - 478.5) \log(160 - 60) \\ & + (159.5 - 319) \log(160 - 120))] \\ &= \frac{1}{159.5} [478.5(2.2041) + (-159.5)(2.000) + (-159.5)(1.6021)] \\ &= \frac{1}{159.5} [1054.67 + (-319.0) + (-255.53) + (-159.5)(1.6021)] \\ &= 3.0103 \end{aligned}$$

For $n = 3$, $q_n = 159.5$ stb/day, $q_0 = 0$, $t_n = 180$, and $t_0 = 0$:

$$\begin{aligned} & \frac{1}{159.5} [(478.5 \log(180 - 0) + (319 - 478.5) \log(180 - 60) \\ & + (159.5 - 319) \log(180 - 120))] \\ &= \frac{1}{159.5} [478.5(2.2553) + (-159.5)(2.0792) + (-159.5)(1.7782)] \\ &= \frac{1}{159.5} [1222.71 + (-331.63) + (-283.62)] = 3.8157 \end{aligned}$$

For $n = 2$, $q_n = 319$ stb/day, $q_0 = 0$, $t_n = 120$, and $t_0 = 0$:

→ ln

$$\begin{aligned} & \frac{2}{319} [(478.5 - 0) \ln(120 - 0) + (319 - 478.5) \ln(120 - 60)] \\ &= \frac{1}{319} [478.5 \times 4.7875 + (-159.5) \times 4.0943] \\ &= \frac{1}{319} [2290.82 - 653.04] = 5.1341 \end{aligned}$$

→ log

$$\begin{aligned} & \frac{1}{319} [(478.5 - 0) \log(120 - 0) + (319 - 478.5) \log(120 - 60)] \\ &= \frac{1}{319} [478.5(2.0792) + (-159.5)(1.7782)] \\ &= \frac{1}{319} [994.90 - 283.62] = 2.2297 \end{aligned}$$

Calculate the permeability k from Eq. 4-63:

$$k = \frac{162.6 \mu_o \beta_o}{mh} = \frac{162.6(0.60)(1.2172)}{0.41(27)} = 10.727 \text{ mD}$$

Determine the skin factor s from Eq. 4-64:

$$\begin{aligned} s &= 1.151 \left[\frac{b'}{m} - \log \left(\frac{k}{\phi \mu_o c_t r_w^2} \right) + 3.23 \right] \\ &= 1.151 \left[\frac{3.05}{0.41} - \log \left(\frac{10.727}{0.17(0.60)(7.5 \times 10^{-6})(0.29)^2} \right) \right] \\ &= 1.151 [7.439 - 8.222 + 3.23] = 2.82 \end{aligned}$$

Estimate the pressure drop due to skin from Eq. 4-65:

$$(\Delta p)_{skin} = 0.869 m s q_n = 0.869 \times 0.41 \times 2.82 \times 159.5 = 160.8 \text{ psi.}$$

4.8 Multi-Rate Flow Test Analysis

Multi-rate testing^{7,9} has the advantage of providing transient test data while production continues. It tends to minimize changes in wellbore storage coefficient and phase segregation (humping) effects and thus may provide

good results when drawdown or buildup testing would not. Rate measurements are more critical in multi-rate testing than conventional, constant-rate well tests. In this section, we will discuss both single and multiphase, multi-rate drawdown tests.

Multi-Rate, Single-Phase Test

The general equation for drawdown test analysis is

$$\frac{p_i - p_{wf}}{q_n} = \frac{162.6 \mu_o \beta_o q_n}{kh} \sum_{j=1}^n \left[\frac{q_j - q_{j-1}}{q_n} \log(t - t_{j-1}) \right] + \frac{162.6 \mu_o \beta_o}{kh} \left[\log \left(\frac{k}{\phi \mu_o c_i r_w^2} \right) - 3.2275 + 0.869s \right] \quad (4-66)$$

This equation is that of a straight line of the form $y = b + mx$, where

$$y = \frac{p_i - p_{wf}}{q_n}, \quad x = \frac{1}{q_n} \sum_{j=1}^n (q_j - q_{j-1}) \log(t - t_{j-1}) \quad (4-67)$$

$$\text{Slope, } m = \frac{162.6 q_n \mu_o \beta_o}{kh} \quad (4-68)$$

$$\text{Intercept, } b = m \left[\log \left(\frac{k}{\phi \mu_o c_i r_w^2} \right) - 3.23 + 0.869s \right] \quad (4-69)$$

To make that plot correctly it is important to understand that the rate corresponding to each plotted pressure point is q_n , the last rate that can affect that pressure. As time increases the number of rates may increase and the last rate may change; but each pressure point is identified with the rate occurring when that pressure was measured. There may be several pressure points associated with a given rate. Once the data plot of

$$\left(\frac{p_i - p_{wf}}{q_n} \right) \text{ versus } \sum_{j=1}^n \left[\frac{(q_j - q_{j-1})}{q_n} \log(t - t_{j-1}) \right]$$

is made, the straight-line slope and intercept are measured. The permeability, skin factor, $(\Delta p)_{skin}$, and FE are estimated using the following equations:

$$k = \frac{162.6 \mu_o \beta_o}{mh} \quad (4-70)$$

$$s = 1.151 \left[\frac{b}{\bar{m}} - \log \left(\frac{k}{\phi \mu_o c_t r_w^2} \right) + 3.23 \right] \quad (4-71)$$

$$(\Delta p)_{skin} = 0.869ms \quad (4-72)$$

$$FE = \frac{p_i - p_{wf}(t=0) - (\Delta p)_{skin}}{p_i - p_{wf}(t=0)} \quad (4-73)$$

The following example illustrates how the summation term in this plotting technique is calculated.

Example 4-7 *Analyzing Multi-Rate, Single-Phase Drawdown Test*

Production rate during a 48-hours drawdown test declined from 1580 to 983 stb/day. Rate and pressure data appear in Table 4-5. Reservoir, PVT, and rock data are: $p_i = 2906$ psi, $\mu_o = 0.6$ cP, $\beta_o = 1.270$ rb/stb, $h = 40$ ft, $\phi = 12\%$, $c_t = 17.5 \times 10^{-6}$, and $r_w = 0.29$ ft.

Solution Figure 4-13 is a plot of $((p_i - p_{wf})/q_n)$ versus $\sum_{j=1}^n [(q_j - q_{j-1})/q_n] \log(t - t_{j-1})$. This plot exhibits two straight lines. The first slope is used to estimate the formation permeability k . The slope of the second line is greater than that of the first, possibly indicating transition to pseudo-steady state, faulting or decreasing in permeability away from the well. To illustrate the method of computing the time summation, we calculate it at 5.50 and 12.0 hours. At 5.50 hours, $q = 1440$ stb/day is the third rate observed, so $n = 3$, $t_n = 5.5$.

Computing the summation term:

$$\begin{aligned} \frac{1}{q_n} \sum_{j=1}^n (q_i - q_{j-1}) \log(t - t_{j-1}) &= \frac{1}{1440} \left\{ [(1580 - 0) \log(5.5 - 0)]_{j=1} \right. \\ &+ \left. [(1490 - 1580) \log(5.5 - 2.40)]_{j=2} + [(1490 - 1490) \log(5.5 - 4.8)]_{j=3} \right\} \\ &= \frac{1}{1440} \left\{ [1580 \log(5.5)]_{j=1} + [-90 \log(3.1)]_{j=2} + [(-50) \log(0.70)]_{j=3} \right\} \\ &= \frac{1}{1440} \{ 1169.77 - 44.22 + 7.75 \} = 0.7869 \end{aligned}$$

At $n = 3$, $t_n = 12.0$ hours, the summation term is

$$\frac{1}{q_n} \sum_{j=1}^n (q_i - q_{j-1}) \log(t - t_{j-1})$$

Table 4-5
Multiphase Drawdown Test Data

Time (hr)	Flow rate (stb/day)	Tubing pressure (psig)	$\frac{(p_i - p_{if})}{q}$ (psig/(stb/day))	$\sum \left[\left(\frac{q_i - q_{(i-1)}}{q_n} \right) \times \log(t - t(i-1)) \right]$ function
1.00	1580	2023.0	0.5589	0.0000
1.50	1580	1968.0	0.5937	0.1761
1.89	1580	1941.0	0.6108	0.2764
2.40	1580	1941.0	0.6108	0.3801
3.00	1580	1892.0	0.6872	0.5192
3.45	1490	1882.0	0.6872	0.5689
3.98	1490	1873.0	0.6933	0.6240
4.50	1490	1867.0	0.6973	0.6731
4.80	1490	1867.0	0.6973	0.6993
5.50	1490	1853.0	0.7067	0.7869
6.05	1440	1843.0	0.7382	0.8191
6.55	1440	1834.0	0.7444	0.8484
7.00	1440	1830.0	0.7472	0.8738
7.20	1440	1830.0	0.7472	0.8847
7.50	1370	1827.0	0.7876	0.9735
8.95	1370	1821.0	0.7920	1.0089
9.60	1370	1821.0	0.7920	1.0320
10.00	1300	1815.0	0.8392	1.1240
12.00	1300	1797.0	0.8531	1.1533
14.40	1190	1797.0	0.9319	1.2274
15.00	1190	1775.0	0.9504	1.3371
18.00	1190	1771.0	0.9538	1.3551
19.20	1160	1771.0	0.9784	1.3721
20.00	1160	1772.0	0.9776	1.4223
21.60	1137	1772.0	0.9974	1.4345
24.00	1106	1756.0	1.0398	1.4848
28.80	1106	1756.0	1.0398	1.5596
30.00	1080	1751.0	1.0694	1.6064
33.60	1080	1751.0	1.0694	1.6267
36.00	1000	1751.0	1.1550	1.7438
36.20	983	1756.0	1.1699	1.7850
48.00	983	1743.0	1.1831	1.7974

$$\begin{aligned}
 &= \frac{1}{1300} \left\{ [(1580 - 0) \log(12.0 - 0)]_{j=1} + [(1490 - 1580) \log(12.0 - 2.40)]_{j=2} \right. \\
 &+ [(1440 - 1490) \log(12.0 - 4.8)]_{j=3} + [(1370 - 1440) \log(12.0 - 7.2)]_{j=4} \\
 &\left. + [(1300 - 137) \log(12.0 - 9.60)]_{j=5} \right\}
 \end{aligned}$$

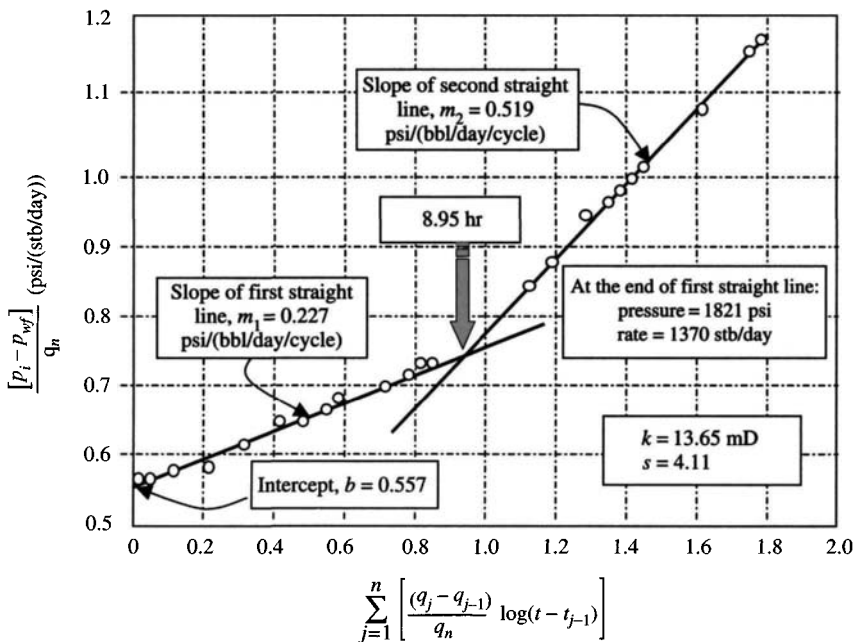


Figure 4-13. Multi-rate drawdown test.

$$\begin{aligned}
 &= \frac{1}{1300} \left\{ [1580 \log(12.0)]_{j=1} + [-90 \log(9.6)]_{j=2} + [(-50) \log(7.2)]_{j=3} \right. \\
 &\quad \left. + (-70) \log(4.8)_{j=4} + [(-70) \log(2.4)]_{j=5} \right\} \\
 &= \frac{1}{1300} \{1705.11 - 88.40 - 42.87 - 47.69 - 26.61\} = 1.1540
 \end{aligned}$$

From this plot, the following results are obtained:

$m_1 = 0.227$ psi/(stb/(day/cycle)) → first slope

$m_2 = 0.513$ psi/(stb/(day/cycle)) → second slope and intercept, $b = 0.557$ psi/(stb/day)

From the first slope of 0.227 psi/(stb/day/cycle), the permeability k is found as follows:

$$k = \frac{162.6}{m_1 h} \mu_o \beta_o = \frac{262.6 \times 0.6 \times 1.270}{0.227 \times 40} = 13.65 \text{ mD}$$

From Figure 4-13, the intercept b is 0.557. Thus using Eq. 4-71, we obtain

$$s = 1.151 \left[\frac{b}{\bar{m}} - \log \left(\frac{k}{\phi \mu_o c_t r_w^2} \right) + 3.23 \right]$$

$$= 1.151 \left[\frac{0.557}{0.227} - \log \left(\frac{13.65}{0.12 \times 0.6 \times 17.7 \times 10^{-6} \times 0.29^2} + 3.23 \right) \right] = 4.11$$

The positive skin factor indicates that the well is damaged and needs stimulation.

Multi-Rate, Multi-Phase Test

The general equation for drawdown analysis is

$$p_{wf} = p_i - \frac{162.6 \mu_o \beta_o q_n}{kh} \left[\sum_{j=1}^n \frac{\Delta q_j}{q_n} \log(t - t_{j-1}) \right] - \frac{162.6 \mu_o \beta_o q_n}{kh} \left[\log \left(\frac{k}{\phi \mu_o c_t r_w^2} \right) - 3.23 + 0.869s \right] \quad (4-74)$$

This equation is that of a straight line of the form $y = a + mx$:

$$y = p_{wf} \quad (4-75)$$

$$x = \sum \frac{\Delta q_j}{q_n} \log(t - t_{j-1}) \quad (4-76)$$

$$x = \frac{1}{q_n} \sum_{j=1}^n \Delta q_j \log(t - t_{j-1}) \quad (4-77)$$

$$m = - \frac{162.6 \mu_o \beta_o q_n}{kh}$$

$$a = p_i - \frac{162.6 \mu_o \beta_o q_n}{kh} \left[\log \left(\frac{k}{\phi \mu_o c_t r_w^2} \right) - 3.23 + 0.869s \right] \quad (4-78)$$

where

$$\Delta q_j = q_j - q_{j-1}$$

$$\Delta q_1 = q_1$$

$$t_j = 0.$$

A plot of the dimensionless function X versus p_{wf} results in a straight line of slope m , which can be used to calculate the formation permeability k . The

intercept b of the straight line is obtained by setting $x = 0$ and calculating p_{wf} . Since the permeability and intercept are known, the skin factor may be evaluated by solving in Eq. 4-78. Thus

$$k = \frac{162.6\mu_o\beta_o}{mh} \quad (4-79)$$

$$s = 1.151 \left[\frac{b}{m} - \log \left(\frac{k}{\phi\mu_o c_t r_w^2} \right) + 3.23 \right] \quad (4-80)$$

$$(\Delta p)_{skin} = 0.869 ms \quad (4-81)$$

The lower boundary of the proper straight-line portion of the curve is arbitrarily selected at a t_{Dw} of 89,000. The upper boundary varies according to the shape of the drainage area and the location of the well within the area. References 7 and 9 have proposed various shapes, locations and the values of t_{De} at which boundary effects are first detected. By definition

$$t_{Dw} = \frac{0.000264k(t - t_{n-1})}{\phi\mu_o c_t r_w^2} \quad (4-82a)$$

$$t_{De} = \frac{0.000264kt}{\phi\mu_o c_t r_e^2} \quad (4-82b)$$

The maximum radius reached is computed by

$$r_{max} = \left(\frac{0.00105kt}{\phi\mu_o c_t} \right)^{0.5} \quad (4-82c)$$

The drawdown test equations are modified to account for multiphase flow in the same way as we discussed for buildup tests. The following example will clarify the analysis.

Example 4-8 Analyzing Multi-Rate, Multi-Phase Drawdown Test

Table 4-6 shows the rate record up to stabilization. The rate and pressure-time data are given in Table 4-7. Input data and preliminary calculations are shown in Table 4-8. Other reservoir and well data follow. Fluid and reservoir properties: $\phi = 0.09$, $r_w = 0.67$ ft, $h = 25$ ft, $\mu_o = 0.95$ cP, $\beta_o = 1.20$ rb/stb, $c_t = 8.64 \times 10^{-6}$ psi⁻¹ and area shape = circular, $A = 160$, shut-in pressure = 5500 psi.

Solution Calculated results are

For points used 3-6:

Average slope m and intercept a are calculated using a computer program and are 33.385 psi and 5337.33, respectively. The permeability k is

Table 4-6
Rate Record up to Stabilization

Rate No.	Rate (stb/day)	Rate duration (hr)	Flow time to end of period	Cumulative production at the end of pressure (stb)
1	440	0.15	0.1	2.8
2	387	0.15	0.3	5.2
3	355	0.40	0.7	10.1
4	337	0.50	1.2	18.1
5	327	0.30	1.5	22.2
6	325	—	—	—

Table 4-7
Bottom-Hole Pressures at Corresponding Flowing Time

Point No.	Time, t (hr)	Pressure, p_{wf} (psi)	$\frac{1}{q_n} \sum_{j=1}^n \Delta q_j$ $\log(t - t_{j-1})$
1	1.66	5327	0.272
2	2.49	5322	0.425
3	3.31	5318	0.541
4	4.14	5315	0.633
5	4.97	5312	0.709
6	5.80	5309	0.775
7	6.63	5308	0.831
8	7.45	5306	0.881
9	8.29	5305	0.926
10	12.42	5299	1.099
11	17.39	5295	1.244

$$k = \frac{162.6\mu_o\beta_o q_{o1}}{mh} = \frac{162.6 \times 0.95 \times 1.2 \times 325}{36.704 \times 25} = 65.7 \text{ mD}$$

The skin factor s is

$$\begin{aligned} s &= 1.151 \left[\frac{a - p_i}{m} - \log \left(\frac{k}{\phi\mu_o c_i r_w^2} \right) + 3.23 \right] \\ &= 1.151 \left[\frac{5337.33 - 5500}{36.704} - \log \left(\frac{65.7}{0.09 \times 0.95 \times 8.64 \times 10^{-6} \times 0.67^2} \right) \right] \\ &= 1.151 [4.4319 - 8.2964 + 3.23] = -0.65 \end{aligned}$$

Table 4-8
Calculated Results

Points used	Average slope, m	Intercept of curve, a	Permeability, k (mD)	Skin factor, s	$(\Delta p)_{skin}$ (psi)	Dimensionless time, t_{Dw}	Dimensionless time, t_{De}	Maximum radius reached (ft)
1-4	30.298	79.5	5333.78	0.38	10.0	105,108	0.05304	684.1
2-5	32.916	73.2	5335.10	0.12	-4.0	145,124	0.05861	719.1
3-6*	36.704	65.7	5337.33	-0.73	-23.0	173,005	0.06134	735.7
4-7	35.536	67.8	5336.75	-0.56	-17.0	223,498	0.07242	799.4
5-8	32.608	73.7	5334.52	-0.70	-2.0	291,686	0.08847	883.5
6-9	26.922	89.5	5329.72	1.29	-30.0	413,293	0.11953	1027.0
7-10	32.634	73.8	5334.74	-0.07	-2.0	389,747	0.14773	1141.7
8-11	30.460	79.1	5332.66	0.40	10.0	469,218	0.22161	1398.4

The pressure drop due to skin is

$$(\Delta p)_{skin} = 0.869 ms = 0.869 \times 36.676 \times (-0.65) = -20.72 \text{ psi}$$

The dimensionless time is

$$t_{Dw} = \frac{0.000264k(t - t_{n-1})}{\phi\mu_o c_t r_w^2} = \frac{0.000264 \times 65.7 \times 3.31}{0.09 \times 0.95 \times 8.64 \times 10^{-6} \times (0.67)^2} = 173,005$$

$$r_e = \sqrt{\frac{160 \times 43,560 \times 7}{22}} = 1489 \text{ ft}$$

The dimensionless time is

$$t_{De} = \frac{0.000264kt}{\phi\mu_o c_t r_e^2} = \frac{0.000264 \times 65.7 \times 5.792}{0.09 \times 0.95 \times 8.64 \times 10^{-6} \times (1489)^2} = 0.06134$$

The maximum radius reached is

$$r_{max} = \left(\frac{0.00105kt}{\phi\mu_o c_t} \right)^{0.5} = \left(\frac{0.00105 \times 65.7 \times 5.792}{0.09 \times 0.95 \times 8.64 \times 10^{-6}} \right) = 735.7 \text{ ft}$$

4.9 Drawdown Rate Normalization Methods

Methods to analyze afterflow-dominated pressure buildup data are presented. Total afterflow fluid rate should be used in multiphase flow analysis. The logarithm of time approximation to p_D for analysis of low-permeability stimulated oil wells is often invalid. Normalized type curve analysis identifies whether the semilog straight line exists and suggests the proper p_D-t_D model for analysis purposes. Additional detailed discussions of the normalization methods were given by Gladfelter et al.,¹¹ Winestock and Colpitts,¹² and Odeh and Jones.^{7,13}

Analysis Methods, Their Applications and Limitations

Figure 4-14 shows various methods of analysis and their applications and limitations.

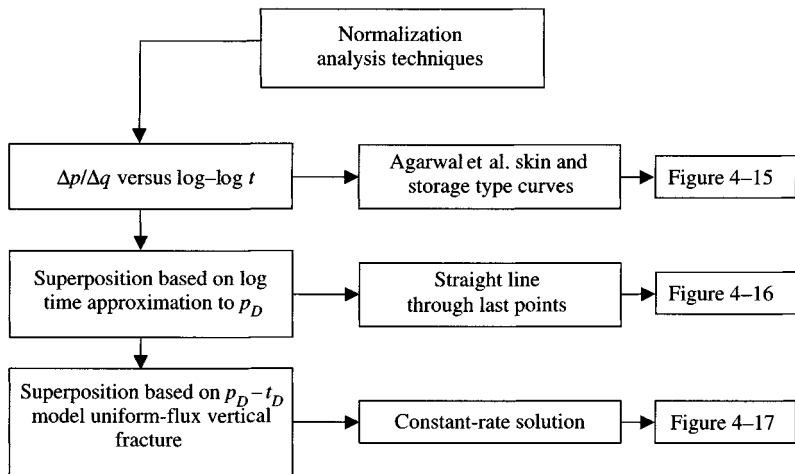


Figure 4-14. Various analysis techniques, their applications, and their limitations.

Drawdown Rate Normalization Equations and Solutions

The drawdown rate variation generally lasts much longer than the after-flow rate variation. The rate normalization equation by Odeh and Jones¹³ for an oil well drawdown analysis can be written as

$$\frac{p_i - p_{wf} - D'q_n^2}{q_n} = \frac{141.2\mu_o}{kh} [\ln t_D + 0.809 + 2s] \quad (4-83)$$

where

$$t_D = \frac{0.000264kt}{\phi\mu_o c_t r_w^2} \quad (4-84)$$

and the constant D' is related to the non-Darcy flow constant and is given by

$$D' = \frac{141.2\mu_o}{kh} D \quad (4-85)$$

where

D = non-Darcy flow constant

$D' = Dm$

Eq. 4-83 represents an approximation to superposition for a gradually changing flow rate condition. A superposition equation for any variation

of rate was given by Gladfelter et al.¹¹ with p_D being approximated by the logarithm of time as

$$\frac{p_i - p_{wfn} - D'q_n^2}{q_n} = \frac{141.2}{kh} \left\{ \frac{1}{q_n} \left[\sum_{i=1}^n (q_i - q_{i-1}) \ln(t_n - t_{i-1}) \right] + \ln \left(\frac{k}{\phi \mu_o c_t r_w^2} \right) - 7.432 - 2s \right\} \quad (4-86)$$

A plot of $(p_i - p_{wfn})/q_n$ versus $(1/q_n) \sum_{i=1}^n (q_i - q_{i-1}) \ln(t_n - t_{i-1})$ should be linear, if $D' = 0$, with slope, m' , and intercept, b , yielding kh and s , respectively. Flow capacity is evaluated from the slope m' as

$$kh = \frac{141.2\mu_o}{m'h} \quad (4-87)$$

and the skin from intercept b by

$$s = -0.5 \left(\frac{b}{m'} - \ln \left(\frac{k}{\phi \mu_o c_t r_w^2} \right) + 7.432 \right) \quad (4-88a)$$

The fracture half-length x_f is given by

$$x_f = 2r_w \exp[-(S)] \quad (4-88b)$$

If the plot bows, the data should be corrected for the quadratic effect $D'q^2$ until the plot is made linear. When this method even is not applicable, the logarithm of time approximation to p_D is made. A more general form of Eq. 4-86 in terms of $p_D - t_D$ by Cornett¹⁰ is

$$\frac{p_i - p_{wfn} - D'q_n^2}{q_n} = \frac{141.2}{kh} \left\{ \frac{1}{q_n} \left[\sum (q_i - q_{i-1}) p_D(t_n - t_{i-1})_D \right] + s \right\} \quad (4-89)$$

where

$$p_D(t_D) = \frac{kh(p_i - p_{wfn})}{141.2q\mu\beta} \quad (4-90)$$

A plot of $(p_i - p_{wfn})/q_n$ versus $(1/q_n) \sum_{i=1}^n (q_i - q_{i-1}) p_D(t_n - t_{i-1})_D$ should be plotted as a straight line if $D' = 0$, with slope m' , from which kh can be evaluated by

$$kh = \frac{141.2\mu_o}{m'} \quad (4-91)$$

and the skin from intercept b is

$$s = \frac{k h b}{141.2 \mu_o} = \frac{b}{m'} \quad (4-92)$$

Example 4-9 Normalization of Drawdown Pressure by Using Afterflow Data

The oil well is a low-permeability oil well. It was hydraulically fractured and a 72-hours drawdown test was conducted. The test is neither a constant rate nor a constant wellbore pressure situation; various techniques are presented to demonstrate the validity and utility of normalization in well test analysis. Table 4-9 summarizes the results from all methods of analysis.

- Figure 4-15 is an afterflow rate normalization log-log plot
- Figure 4-16 is a superposition plot based on straight line passing through last points.
- Figure 4-17 represents a superposition analysis based on value of $p_D - t_D$ model.

Table 4-9
Summary of Analysis Results

Various analysis techniques	$\left(\frac{kh}{\mu}\right)_T$ (mD-ft/cP)	Skin, s	Fracture length x_f (ft)
Afterflow rate normalization log-log graph model – Figure 4-15	161.0	-5.1	95.4
Superposition based on logarithm of time approximation to $p_D - t_D$ – Figure 4-16	165.3	-5.3	116.20
Superposition based on uniform-flux vertical fracture – Figure 4-17	163.4	-5.2	105.0

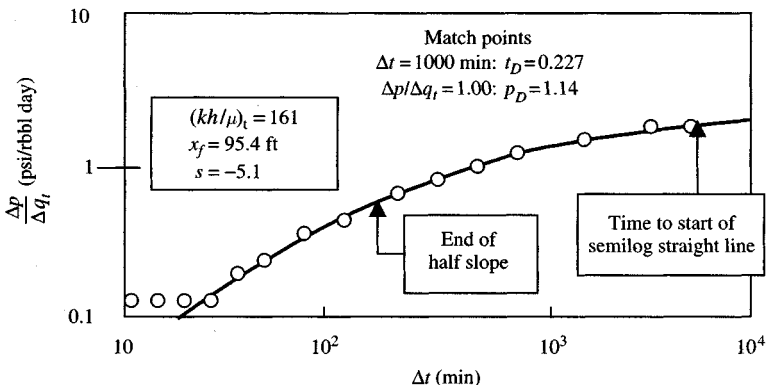


Figure 4-15. Afterflow rate normalization log-log graph model.⁷

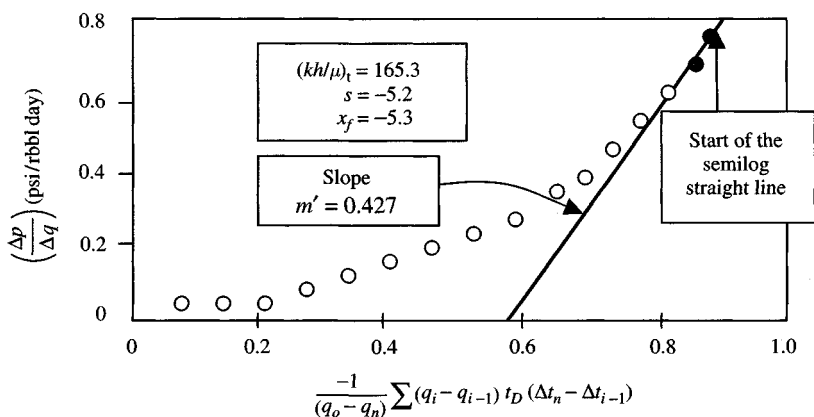


Figure 4-16. Superposition based on logarithm of time approximation to p_D .⁷

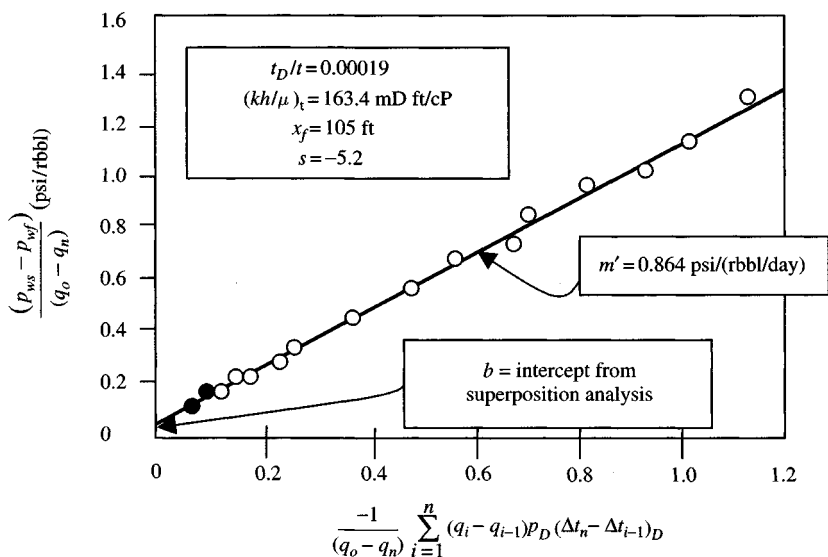


Figure 4-17. Superposition based on uniform-flux vertical fracture - $p_D - t_D$ model.⁷

4.10 Summary

This chapter deals with the complete analysis of drawdown test including transient, late transient, and semi-steady-state analysis including single, two-rate, variable-rate, reservoir limit test, and multiphase and multiple-rate testing and discusses how superposition may be used when variable rates are involved.

References

1. Odeh, A. S., and Nabor, G. W., "The Effect of Production History on Determination of Formation Characteristics From Flow Tests," *J. Pet. Tech.* (Oct. 1966) 1343–1350.
2. Matthews, C. S., Brons, F., and Hazebroek, P., "A Method for Determination of Average Pressure in a Bounded Reservoir," *Trans. AIME* (1954) 201, 182–191.
3. Earlougher, R. C., Jr., and Kersch, K. M., "Analysis of Short-time Transient Test Data by Type-curve Matching," *J. Pet. Tech.* (July 1974) 793–800; *Trans. AIME*, 257.
4. Russell, D. G., "Determination of Formation Characteristics from Two-Rate Flow Tests," *J. Pet. Tech.* (Dec. 1963) 1347–1355; *Trans. AIME*, 228.
5. Earlougher, R. C., Jr., "Variable Flow Rate Reservoir Limit Testing," *J. Pet. Tech.* (Dec. 1972) 1423–1429.
6. Kazemi, H., "Discussion of Variable Flow Rate Reservoir Limit Testing," *J. Pet. Tech.* (Dec. 1972) 1429–1430.
7. Odeh, A. S., and Jones, L. G., "Pressure Drawdown Analysis Variable-Rate Case," *J. Pet. Tech.* (1965) 217, 960–964.
8. Van Everdingen, A. F., and Hurst, W., "The Application of the Laplace Transformation to Flow Problems in Reservoirs," *Trans. AIME* (1949) 186, 305–324.
9. Matthews, C. S., and Russell, D. G., *Pressure Buildup and Flow Tests in Wells*, Monograph, AIME, 1967.
10. Cornett, J. E., "How to Locate Reservoir Limits," *Pet. Eng. J.* (1961) 33, B19–B24.
11. Gladfelter, R. E., Tracy, G. W., and Wilsey, L. E., "Selecting Wells Which Will Respond to Production-Stimulation Treatment," *Drill. Prod. Prac. API* (1955) 117–129.
12. Winestock, A. G., and Colpitts, G. P., "Advances in Estimating Gas Well Deliverability," *J. Can. Pet. Tech.* (July–Sept. 1965) 11–119.
13. Odeh, A. S., and Jones, L. G., "Two-rate Flow Test, Variable-rate Case – Application to Gas-lift and Pumping Wells," *J. Pet. Tech.* (Jan. 1974) 93–99; *Trans. AIME*, 257.

Additional Reading

1. Dietz, D. N., "Determination of Average Reservoir Pressure From Build-Up Surveys," *J. Pet. Technol.* (Aug. 1965) 955–959; *Trans. AIME*, 234.
2. Fetkovich, M. J., "The Isochronal Testing of Oil Wells," paper SPE 4529 presented at the SPE-AIME 48th Annual Fall Meeting, Las Vegas, NV Sep. 30–Oct. 3, 1973.

3. Jones, L. G., Blount, E. M., and Glaze, O. H., "Use of Short-term Multiple Rate Flow Tests to Predict Performance of Wells Having Turbulence," paper SPE 6133 presented at the SPE 51st Annual Meeting, New Orleans, Oct. 3–6, 1976.
4. Dake, L. P., *Fundamentals of Reservoir Engineering*, Elsevier, Amsterdam, 1978.
5. Slider, H. C., "A Simplified Method of Pressure Analysis for a Stabilized Well," *J. Pet. Tech.* (1971) 23, 1155–1160.
6. Earlougher, R. C., Jr., "Estimating Drainage Shapes from Reservoir Limit Tests," *J. Pet. Tech.* (1971) 23, 1266–1268.

Chapter 5

Pressure Buildup Analysis Techniques for Oil Wells

5.1 Introduction

Pressure buildup testing is the most familiar transient well-testing technique, which has been used extensively in the petroleum industry. Basically, the test is conducted by producing a well at constant rate for some time, shutting the well in (usually at the surface), allowing the pressure to build up in the wellbore, and recording the down-hole pressure in the wellbore as a function of time. From these data, it is possible to estimate the formation permeability and current drainage area pressure, and to characterize damage or stimulation and reservoir heterogeneity or boundaries frequently.

Knowledge of surface and subsurface mechanical conditions is important in buildup test data interpretation. Therefore it is recommended that testing and casing sizes, well depth, packer condition, etc., be determined before data interpretation starts. Usually, short-time pressure observations are necessary for the complete delineation of wellbore storage effects. Data may be needed at intervals as short as 15 seconds for the first few minutes of some buildup tests. As the test progresses, the data collection interval can be expended.

In this chapter we will discuss ideal, actual buildup tests, buildup tests in infinite-acting reservoirs and in developed (finite) reservoirs; we will also discuss multiphase buildup tests and the variable-flow-rate test analysis.

5.2 Ideal Pressure Buildup Test

In an ideal situation, we assume that the test is conducted in an infinite-acting reservoir in which no boundary effects are felt during the entire flow and later shut-in period. The reservoir is homogeneous and containing in a

slightly compressible, single-phase fluid with uniform properties so that the E_i function and its logarithmic approximation apply. Horner's approximation is applicable. Wellbore damage and stimulation is concentrated in a skin of zero thickness at the wellbore. Flow into the wellbore ceases immediately at shut-in. If a well is shut-in after it has produced at rate q for time t_p and the bottom-hole pressure p_{ws} is recorded at time Δt , then a plot of p_{ws} versus $\log(t_p + \Delta t)\Delta t$ will give a straight line, which is represented by the following equation:

$$p_{ws} = p_i - \frac{162.6 q_o \mu_o \beta_o}{kh} \log \left[\frac{t_p + \Delta t}{\Delta t} \right] \quad (5-1)$$

where the slope m is $162.6 q_o \mu_o \beta_o / kh$ and p_i (initial reservoir pressure) is the intercept at $(t_p + \Delta t) / \Delta t = 1.0$. The absolute value of the slope m is used in analyzing the test result. The formation permeability k can be calculated from the slope and given by

$$k = \frac{162.6 q_o \mu_o \beta_o}{mh} \quad (5-2)$$

and the skin factor is

$$s = 1.151 \left[\frac{p_{1hr} - p_{ws}(\Delta t=0)}{m} - \log \left(\frac{k}{\phi \mu_o c_t r_w^2} \right) + 3.23 \right] \quad (5-3)$$

Example 5-1 Analyzing Ideal Pressure Buildup Test

A new oil well produced 400 stb/day for $2\frac{1}{2}$ days; then it was shut-in for a pressure buildup test, during which the data in Table 5-1 were recorded. The other data were: $\beta_o = 1.25$ rb/stb, $h = 20$ ft, $\phi = 0.20$, $r_w = 0.29$ ft,

Table 5-1
Ideal Pressure Buildup Data

Shut-in time, Δt (hr)	$\frac{(t_p + \Delta t)}{\Delta t}$	p_{ws} (psig)	p_{ws} (psia)
0	—	1150	1165
2	37.0	1795	1801
4	19.0	1823	1838
8	10.0	1850	1865
16	5.5	1876	1891
24	4.0	1890	1905
48	2.5	1910	1925

$c_t = 19.5 \times 10^{-6}$, and $\mu_o = 1.1$ cP. From these data, estimate the formation permeability, k , p_i , and skin factor s .

Solution To estimate k , p_i , and s , follow these steps:

1. Plot shut-in BHP, p_{ws} versus $\log(t_p + \Delta t)/\Delta t$, as shown in Figure 5-1.
2. Measure the slope m that is equal to 100 psi/cycle.
3. Calculate the formation permeability using Eq. 5-2.

$$k = 162.6 \frac{q_o \mu_o \beta_o}{mh} = 162.6 \frac{400 \times 1.25 \times 1.1}{100 \times 20} = 44.72 \text{ mD}$$

4. Read original reservoir pressure p_i at $(t_p + \Delta t)/\Delta t = 1.0 \Rightarrow p_i = 1960$ psi.
5. Calculate the skin factor s from Eq. 5-3.

$$s = 1.151 \left[\frac{p_{1hr} - p_{ws(\Delta t=0)}}{m} - \log \left(\frac{k}{\phi \mu_o c_t r_w^2} \right) + 3.23 \right]$$

$$= 1.151 \left[\frac{1779 - 1165}{100} - \log \left(\frac{44.72}{0.20 \times 1.1 \times 19.5 \times 10^{-6} (0.29)^2} \right) + 3.23 \right]$$

$$= 1.151 [6.14 - 8.093 + 3.23] = 1.37$$

6. Read original reservoir pressure $p_i = 1960$ psia.

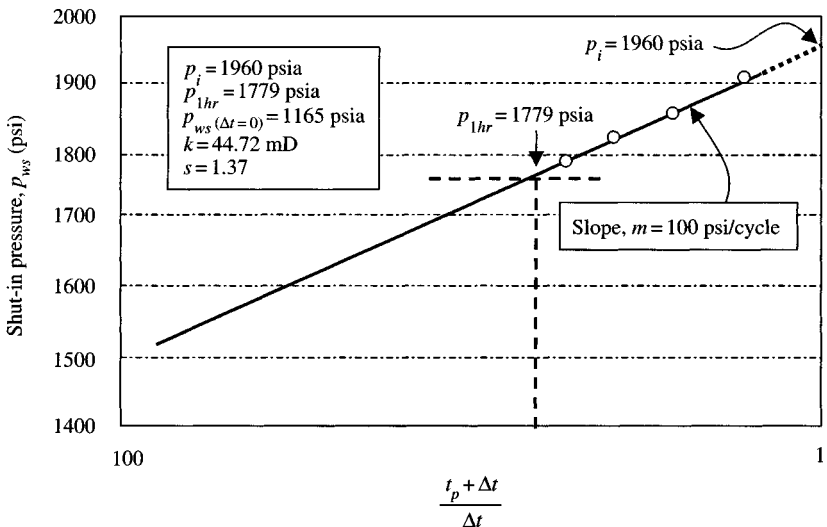


Figure 5-1. Ideal pressure buildup graph.

5.3 Actual Buildup Tests – Infinite Reservoir

Instead of a single straight line for all times, we obtain a curve with a complicated shape, which indicates the effect of afterflow, we can logically divide a buildup curve into three regions (see Figure 5–2):

Early-time region (ETR). In this region, a pressure transient is moving through the formation nearest the wellbore.

Middle-time region (MTR). In this region, the pressure transient has moved away from the wellbore into the bulk formation.

Late-time region (LTR). In this region, the pressure transient has reached the drainage boundaries well.

MTR is a straight line. This is the portion of the buildup curve that we must identify and analyze. Analysis of this portion only will provide reliable reservoir properties of the tested well. The reasons for the distortion of the straight line in the ETR and LTR are as follow: In the ETR, the curve is affected by:

- Altered permeability near the wellbore;
- Wellbore storage.

Using a packer in the hole and shutting-in the well at the packer can minimize this effect. In the LTR, the pressure behavior is influenced by boundary configuration, interferences from nearby wells, reservoir heterogeneities, and fluid/fluid contacts.

Analyzing a pressure buildup in an infinite-acting reservoir using Horner's technique involves the following steps:

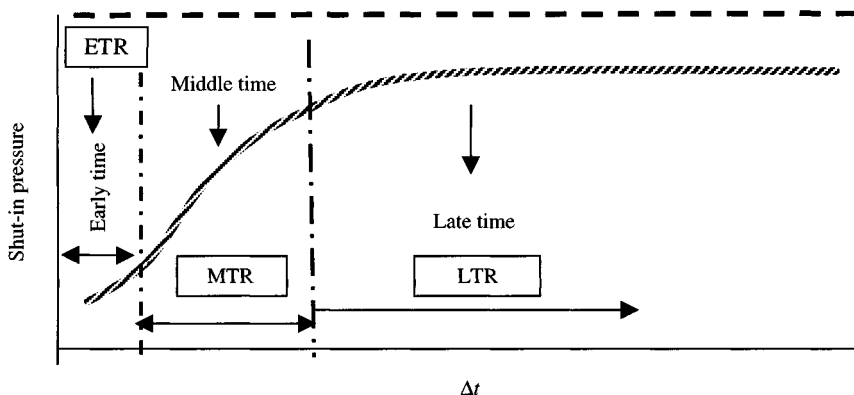


Figure 5–2. Behavior of the static pressure on shut-in oil well.

- Find t_p , the cumulative production since completion divided by the rate, immediately before shut-in (when rate varies). As a matter of general practice to approximate, t_p using cumulative production since last pressure equalization:

$$t_p = \frac{24V_p}{q_o} \quad (5-4)$$

- Plot p_{ws} versus $\log(t_p + \Delta t)/\Delta t$ on semilog graph paper.
- Plot $\Delta p_{ws} = (p_{ws} - p_{wf}(\Delta t = 0))$ versus Δt on log-log graph paper to identify wellbore effects, i.e., identify ETR and beginning of MTR which can be found using type curves. The MTR ends when the radius of investigation begins to detect the drainage boundaries of the tested well; at this time the buildup curve starts to deviate from the straight line.
- Find slope m of the straight-line portion of the Horner plot (MTR) and extrapolate the line to infinite time at $\log((t_p + \Delta t)/\Delta t) = 1$ to find p^* . Once the MTR is identified, determine the slope and intercept.
- On straight-line portion of the curve or the extrapolated portion read p_{ws} at $\Delta t = 1$ hour, referred to as p_{1hr} .
- Calculate the reservoir properties by using the equation in the following section.

5.4 Pressure Buildup Test Analysis in Infinite-Acting Reservoir

For any pressure buildup testing situation, the bottom-hole shut-in pressure, p_{ws} , in the test well may be expressed using the principle of superposition for a well producing at rate q_o until time t_p , and at zero rate thereafter. At any time after shut-in

$$p_{ws} = p_i - \frac{141.2q_o\mu_o\beta_o}{kh} [p_D(t_p + \Delta t)_D - p_D(\Delta t_D)] \quad (5-5)$$

where p_D is the dimensionless pressure function and t_D the dimensionless time and is defined by the following equation:

$$t_D = \frac{0.000264kt}{\phi\mu_o c_t r_w^2} \quad (5-6)$$

During the infinite-acting time period, after wellbore storage effects have diminished and assuming there are no major indeed fractures, p_D in Eq. 5-5

may be replaced by the logarithmic approximation to the exponential integral:

$$p_D = 0.5(\ln t_D + 0.80907) \quad (5-7)$$

Eq. 5-7 applies when $t_D > 100$, which occurs after a few minutes for most unfractured systems. Eqs. 5-5 through 5-7 may be rewritten as

$$p_{ws} = p_i - 70.6 \frac{q_o \mu_o \beta_o}{kh} \ln \left(\frac{t_p + \Delta t}{\Delta t} \right)$$

or

$$p_{ws} = p_i - 162.6 \frac{q_o \mu_o \beta_o}{kh} \log \left(\frac{t_p + \Delta t}{\Delta t} \right) \quad (5-8)$$

Eq. 5-8 gives the pressure response during shut-in BHP, p_{ws} . This equation indicates that plotting p_{ws} versus $(t_p + \Delta t)/\Delta t$ on semilog coordinates will exhibit a semilog straight line of slope m , where

$$m = \frac{162.6 q_o \mu_o \beta_o}{kh} \quad (5-9)$$

Effects and Duration of Afterflow

To recognize the MTR is essential for the successful buildup curve analysis based on the Horner plotting method, because the line must be identified to estimate the reservoir properties. The following methods can be used to determine when (if ever) afterflow ceased.

log-log Curve Matching Procedures

The following steps should be used to estimate the beginning of MTR:

- Plot p_{ws} versus $\log(t_p + \Delta t)/\Delta t$ on semilog graph paper.
- Plot $(p_{ws} - p_{wf})$ versus Δt_e on log-log graph paper, where

$$\Delta t_e = \frac{\Delta t}{1 + \Delta t/t_p} \quad (5-10)$$

- From the graph, find approximately at what shut-in time (Δt) does afterflow cease and boundary effects appear.

- Find a uniform slope region (45° line at earliest time), choose any point on the unit slope line and calculate the wellbore storage constant, C_S :

$$C_S = \frac{q_o \beta_o}{24} \left(\frac{\Delta t}{\Delta p} \right)_{\text{unit-sloped line}} \quad (5-11)$$

where Δt and Δp are the values read from a point on the unit-slope line. Using actual mechanical properties of the well, we can also establish

$$C_S = 25.65 \frac{A_{wb}}{\rho_{wb}} \quad (5-12)$$

for a well with a rising liquid/gas interface, where A_{wb} = wellbore area (ft²) and ρ_{wb} = density. Also $C_S = C_{wb} V_{wb}$ for a wellbore containing only single-phase fluid (liquid only), where C_{wb} is the compressibility of the liquid in wellbore (psi⁻¹) and V_{wb} the wellbore volume (bbl).

- Establish dimensionless wellbore storage constant C_{SD} that characterizes the actual test from curve match or using the following equation:

$$C_{SD} = \frac{0.894 C_S}{\phi c_i h r_w^2} \quad (5-13)$$

- Determine k and the skin factor s .
- Find the end of wellbore storage effects, t_{wbs} (h), after selecting the proper Ramey's curve.
- Verify the time, t_{wbs} , marking the end of wellbore storage distortion using empirical relationships:

$$t_D \cong 50 C_S \exp(0.14s) \quad (5-14)$$

or

$$t_{wbs} \cong \frac{170,000 C_S \exp(0.14s)}{kh/s} \quad (5-15)$$

Calculation of Flow Capacity and Formation Permeability

The formation permeability k can be obtained as

$$k = \frac{162.6 q_o \mu_o \beta_o}{mh} \quad (5-16)$$

and kh is the flow capacity (mD ft). Both Theis and Horner proposed the estimating permeability in this manner. The p_{ws} versus $\log[(t_p + \Delta t)/\Delta t]$ plot is commonly called the Horner plot (graph method) in the petroleum industry. Extrapolation of the straight-line section to an infinite shut-in time $[(t_p + \Delta t)/\Delta t] = 1$ gives a pressure and we will denote this as p^* throughout this book. In this case $p^* = p_i$, the initial pressure. However, the extrapolated pressure value is useful for estimating the average reservoir pressure, as indicated in Chapter 6.

Estimation of Skin Factor

The skin factor does affect the shape of the pressure buildup data. In fact, an early-time deviation from the straight line can be caused by skin factor as well as by wellbore storage. Positive skin factor indicates a flow restriction, i.e., wellbore damage. A negative skin factor indicates stimulation. To calculate skin factor, s from the data available in the idealized pressure buildup test. At the instant a well is shut-in, the flowing BHP, p_{wf} , is

$$p_{wf} = p_i + m \left[\log \left(\frac{16.88 \phi \mu_o c_t r_w^2}{k t_p} \right) - 0.869s \right] \quad (5-17)$$

At shut-in time Δt in the buildup test

$$p_{wf} = p_i + m \left[\log \left(\frac{t_p + \Delta t}{\Delta t} \right) \right] \quad (5-18)$$

Combining Eqs. 5-17 and 5-18 and solving for the skin factor s , we have

$$s = 1.151 \left(\frac{p_{ws} - p_{wf}}{m} \right) + 1.151 \log \left(\frac{1688 \phi \mu_o c_t r_w^2}{k \Delta \Delta} \right) + 1.151 \log \left(\frac{t_p + \Delta t}{\Delta t} \right) \quad (5-19)$$

It is a convenient practice in the petroleum industry to choose a fixed shut-in time Δt of 1 hour and the corresponding shut-in pressure, p_{1hr} , to use in this equation. The pressure, p_{1hr} , must be on the straight line on its extrapolation. Assuming further that $\log(t_p + \Delta t)/\Delta t$ is negligible. p_{wf} is the pressure measured before shut-in at $\Delta t = 0$. With these simplifications, the skin factor is

$$s = 1.151 \left[\frac{p_{1hr} - p_{wf}(\Delta t=0)}{m} - \log \left(\frac{k}{\phi \mu_o c_t r_w^2} \right) + 3.23 \right] \quad (5-20)$$

Pressure Drop Due to Skin

Pressure drop due to skin is also called an additional pressure drop $(\Delta p)_{skin}$ across the altered zone near the wellbore. Calculation of this pressure drop due to skin is meaningful in describing the effect of skin on actual production. In terms of the skin factor s and the slope m of the middle-time line

$$(\Delta p)_{skin} = 0.869 ms \quad (5-21)$$

For example, a well may be producing 200 stb/day oil with a drawdown of 1200 psi. Analysis of a buildup test might show that $(\Delta p)_{skin}$ is 1000 psi and thus that 1000 psi of the total drawdown occurs across the altered zone. This implies that if the damage was removed, the well could produce much more fluid with the same drawdown or, alternatively, could produce the same 200 stb/day with a much smaller drawdown.

Determination of Effective Wellbore Radius

The effective wellbore radius r_{wa} is defined as

$$r_{wa} = r_w e^{-s} \quad (5-22)$$

If s is positive, the effective wellbore radius r_{wa} is smaller than r_w , then fluid must theoretically travel through additional formation to give the required pressure drop. If s is negative, the effective wellbore radius is larger than r_w . For example, s values of -4 and -6 correspond to the effective well radii of 14 and 101 ft, respectively, for $r_w = 0.25$ ft. This effective wellbore radius concept is especially useful in hydraulic fracturing.

Flow Efficiency and Damage Ratio

The flow efficiency is defined as the ratio of the actual productivity index of a well to its productivity index if there were no skin ($s = 0$):

$$\text{Flow efficiency} = FE = \frac{J_{actual}}{J_{ideal}}$$

Since

$$J_{actual} = \frac{q_o}{\bar{p} - p_{wf}}$$

and

$$J_{ideal} = \frac{q_o}{\bar{p} - p_{wf} - (\Delta p)_{skin}}$$

therefore

$$FE = \frac{\bar{p} - p_{wf} - (\Delta p)_{skin}}{\bar{p} - p_{wf}} \quad (5-23)$$

The quantity $(\Delta p)_{skin}$ is obtained from Eq. 5-21. The flow efficiency is also known as productivity ratio, condition ratio, and/or completion factor.¹ When subtracted from unity it gives the damage factor² which is also a relative indicator of the wellbore condition and is the inverse of the flow efficiency. The following example will clarify the use of these equations.

Example 5-2 *Analyzing Single-Phase and Single-Rate Pressure Buildup Test*

A single-phase and single-rate pressure buildup test was conducted on an oil well. The data in the first two columns of Table 5-2 were recorded. The following well/reservoir parameters are given: $\beta_o = 1.224$ rb/stb, $h = 55$ ft, $\phi = 0.06$, $r_w = 0.21$ ft, $c_o = 1.5 \times 10^{-6}$, and $\mu_o = 0.65$ cP, $p_{sc} = 14.65$ psia, $T = 200^\circ\text{F}$, $r_e = 1520$ ft, and $\rho_o = 53.5$ lb_m/ft³.

Assume the well is draining from the center of a square. Well depth = 4500 ft, $q_f =$ final production rate at shut-in time = 250 stb/day, and cumulative production at shut-in time = 141,979 stb. Determine the following:

1. At what shut-in time Δt does afterflow cease and boundary effect appear?
2. Formation permeability, k
3. Skin factor, s
4. Additional pressure drop near the wellbore, $(\Delta p)_{skin}$
5. Effective wellbore radius, r_{wa}
6. Flow efficiency FE using p^*
7. Damage ratio DR using p^*
8. Productivity index, PI
9. Radius of investigation by the shut-in transient at the start and end of the MTR
10. End of wellbore storage distortion.

Table 5-2
Pressure Buildup Test Data – Single-Phase Test ($t_p = 13,629.99$ h)

Time, Δt (hr)	$\frac{(t_p + \Delta t)}{\Delta t}$	$\frac{\Delta t}{(1 + \Delta t/t_p)}$ single-phase	P_{ws} (psig)	$P_{ws} - P_{wf}$ (psig)	P_{ws} (psia)	$P_{ws} - P_{wf}$ (psia)	r_i (ft)
0.00	—	—	3519	0	3534	0	0
0.15	90,867.56	0.15	3680	161	3695	161	48
0.20	68,150.93	0.20	3723	204	3738	204	55
0.30	45,434.28	0.30	3800	281	3815	281	68
0.40	34,075.96	0.40	3866	347	3881	347	78
0.50	27,260.97	0.50	3920	401	3935	401	87
1.00	13,630.99	1.00	4103	584	4118	584	123
2.00	6815.99	2.00	4250	731	4265	731	174
4.00	3408.50	4.00	4320	801	4335	801	247
6.00	2272.66	6.00	4340	821	4355	821	302
7.00	1948.14	7.00	4344	825	4359	825	326
8.00	1704.75	8.00	4350	831	4365	831	349
12.00	1136.83	11.99	4364	845	4379	845	427
16.00	852.87	15.98	4373	854	4388	854	493
20.00	682.5	19.97	4379	860	4394	860	552
24.00	568.92	23.96	4384	865	4399	865	604
30.00	455.33	29.93	4393	874	4408	874	676
40.00	341.75	39.88	4398	879	4413	879	780
50.00	273.60	49.82	4402	883	4417	883	872
60.00	228.17	59.74	4405	886	4420	886	955
72.00	190.31	71.62	4407	888	4422	888	1047

Solution First estimate the pseudo-producing time, t_p ,

$$t_p = \frac{24 \times 141,979}{250} = 13,630 \text{ hours}$$

Horner time ratio $(t_p + \Delta t)/\Delta t$ and equivalent time Δt_e are calculated and listed in Table 5-2. A semilog graph p_{ws} versus $\log(t_p + \Delta t)/\Delta t$ of these data is shown in Figure 5-4, and log-log graph $(p_{wf} - p_{ws})$ versus Δt_e in Figure 5-3. From these graphs answer the following questions:

1. At what shut-in time Δt does afterflow cease distortion the pressure buildup test data?
2. At what shut-in time Δt do boundary effects appear?

From the semilog graph (Figure 5-4), it seems that afterflow distortion disappears at $(t_p + \Delta t)/\Delta t = 2280$ or $\Delta t = 6.25$ hours, because of the end

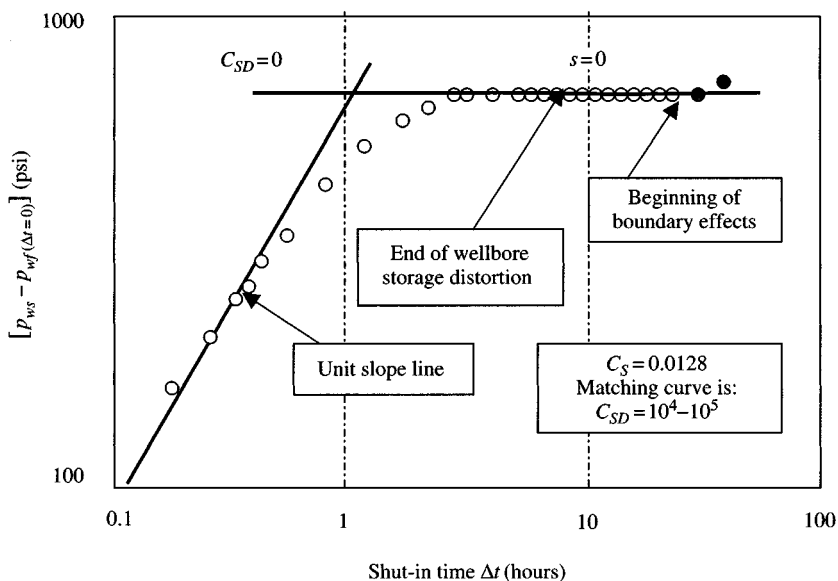


Figure 5-3. log-log single-rate buildup data plot.

of the characteristic S-shaped curve. Confirm the result with the log-log graph. After plotting $\Delta p = (p_{ws} - p_{wf})$ versus $\Delta t_e = \Delta t / (1 + \Delta t / t_p)$ on log-log paper, we find that the actual data fit well for curves for $s = 5$ for several values of C_{SD} (e.g., $C_{SD} = 10^3$, 10^4 , and 10^5). In each case, the curve fitting the earliest data coincides with $C_{SD} = 0$, curve for $s = 5$ at $\Delta t_e = 4-6$ hours. This, then, is the end of wellbore effects: $t_{wbs} = 6$ hours. The data begin to deviate from the semilog straight line at $(t_p + \Delta t) / \Delta t = 225$ or $\Delta t = 50$ hours. On the log-log graph, data begin falling below the fitting curve at $\Delta t = \Delta t_e = 40$ hours, consistent with the semilog graph.

Also determine the beginning and end of the MTR by matching Ramey's curve; the solution is a critically important part of the analysis. The log-log curve-matching analysis was performed without the knowledge of C_{SD} . Note that C_{SD} can be established in this case, at least approximately: from the curve match, we note that the data are near the unit-slope line on the graph of Ramey's solution; the points $\Delta p = 100$ and $\Delta t = 0.1$ are essentially on this line. Thus, from Eq. 5-11:

$$C_S = \frac{q_o \beta_o}{24} \left(\frac{\Delta t}{\Delta p} \right)_{\text{unit-slope line}}$$

$$= \frac{250 \times 1.224}{24} \times \frac{0.1}{100} = 0.0128$$

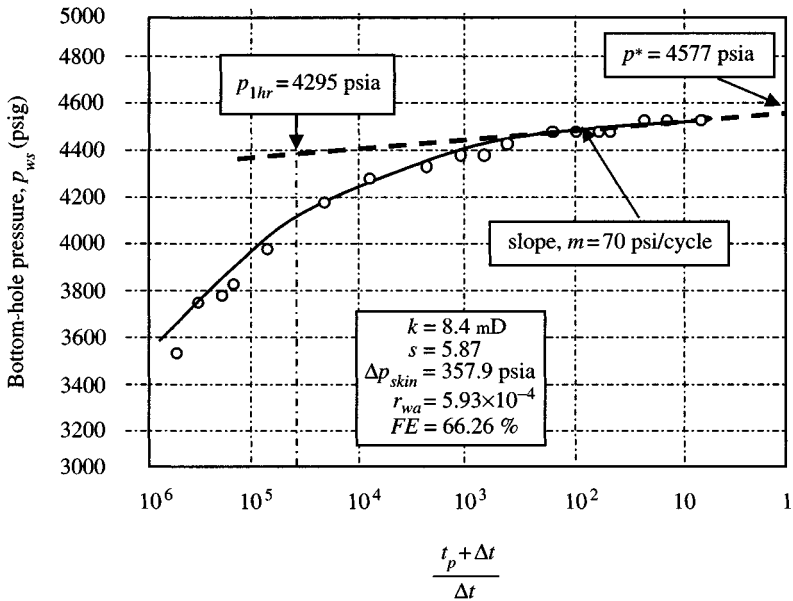


Figure 5-4. Semilog single-rate buildup data plot.

Then, from Eq. 5-13:

$$C_{SD} = \frac{0.894C_S}{\phi c_i h r_w^2} = \frac{0.894 \times 0.0218}{0.06 \times 55 \times 17.5 \times 10^{-6} \times (0.21)^2} = 7653$$

Thus matching should be attempted in the range $10^3 < C_{SD} < 10^4$. From Figure 5-4, there appears to be a well-defined semilog straight line. Find the following parameters:

Slope of Horner's plot = $m = 70$ psia/cycle

From log-log plot \rightarrow time at the beginning of MTR = 6.00 hours

From semilog plot \rightarrow time at the end of MTR = 50 hours

$p_{1hr} = 4295$ psia and p^* at $(t_p + \Delta t)/\Delta t = 4577$ psia

2. From Eq. 5-16, the formation permeability is

$$k = \frac{162.6 \times 250 \times 1.224 \times 0.65}{70 \times 55} = 8.4 \text{ mD}$$

3. From Eq. 5-20, the skin factor is

$$s = 1.151 \left[\frac{4295 - 3519}{70} - \log \left(\frac{8.4}{0.06 \times 0.65 \times 17.5 \times 10^{-6} \times (0.21)^2} \right) + 3.23 \right] = 5.87$$

This means that the well is damaged and needs stimulation treatment.

4. Calculate the additional pressure drop near the wellbore using Eq. 5-21:

$$(\Delta p)_{skin} = 0.869 \times 70 \times 5.87 = 357.9 \text{ psia}$$

5. Estimate the effective wellbore radius from Eq. 5-22:

$$r_{wa} = 0.21 e^{-5.87} = 5.93 \times 10^{-4}$$

6. Determine the flow efficiency using Eq. 5-23:

$$FE = \frac{p^* - p_{wf} - (\Delta p)_{skin}}{p^* - p_{wf}} = \frac{4577 - 3519 - 357}{4577 - 3519} \\ = 0.6626 \times 100 = 66.26\%$$

This means that the well is producing at approximately 66% of the rate it would have been producing if the well was not damaged.

7. Damage ratio is estimated as

$$DR = \frac{1}{FE} = \frac{1}{0.6626} = 1.51$$

The damage ratio also shows the production rate would have been approximately twice the present rate if the well was not damaged.

8. Productivity index is

$$PI = \frac{q_o}{p^* - p_{wf} - (\Delta p)_{skin}} = \frac{250}{4577 - 3519 - 357} = 0.3566 \text{ bbl/psi}$$

9. Determine the radius of investigation using the following equation:

$$r_i = \left(\frac{kt}{948\phi\mu_o c_t} \right)^{0.5}$$

Thus at $\Delta t = 6$ hours

$$r_i = \left(\frac{8.4 \times 6}{948 \times 0.06 \times 0.65 \times 17.5 \times 10^{-6}} \right)^{0.5} = 279 \text{ ft}$$

and at $\Delta t = 50$ hours

$$r_i = \left(\frac{8.4 \times 50}{948 \times 0.06 \times 0.65 \times 17.5 \times 10^{-6}} \right)^{0.5} = 806 \text{ ft}$$

Thus, a significant fraction of the well's drainage area has been sampled; its permeability is 8.4 mD.

10. End of the wellbore storage distortion can be found using Eq. 5-15 such as

$$t_{wbs} = \frac{170,000 C_S e^{0.145}}{kh/\mu_o} = \frac{170,000 \times 0.0218 e^{0.145}}{8.4 \times 55/0.65} = 6.1 \text{ hours}$$

This agrees closely.

Estimation of Skin Effects of Incompletely Perforated Interval

The damage is caused by drilling or completion operation and stimulation by attempting to improve the well productivity using acidizing or fracturing treatments. In addition, nonradial flow near the wellbore will also cause apparent skin factor. The reasons are:

- The well does not completely penetrate the production interval;
- The well is perforated only in a portion of production interval as in the case of gas cap.

In such cases Saidikowski³ found that the total skin factor, s , determined from the pressure transient test is related to the true skin factor, s_d , caused by the formation damage and the apparent skin factor, s_p , caused by an incomplete perforated interval. The relationship between these skin factors is given:

$$s = \frac{h_t}{h_p} s_d + s_p \quad (5-24)$$

where h_t is the total interval height (ft) and h_p the perforated interval (ft). Saidikowski³ also verified that s_p can be estimated from the equation such as

$$s_p = \left(\frac{h_t}{h_p} - 1 \right) \left[\ln \left(\frac{h_t}{hr_w} \left(\frac{k_h}{\bar{k}_v} \right)^{0.5} \right) - 2 \right] \quad (5-25)$$

where k_h is the horizontal permeability (mD) and k_v the vertical permeability (mD).

Papatzacos⁴ presented the following equation to calculate the pseudo-skin factor for a well with restricted flow entry where infinite conductivity is taken into account:

$$s_p = \left(\frac{1}{h_{pD}} - 1 \right) \ln \left(\frac{1.5714}{r_D} \right) + \frac{1}{h_{pD}} \ln \left[\frac{h_{pD}}{2 + h_{pD}} \sqrt{\frac{A-1}{B-1}} \right] \quad (5-26)$$

where

$$h_{pD} = \frac{h_p}{h_t}$$

$$r_D = \frac{r_w}{h_t} \left[\frac{k_v}{k_h} \right]$$

$$A = \frac{1}{(h_{iD} + h_{pD}/4)}$$

$$B = \frac{1}{(h_{iD} + 3h_{pD}/4)}$$

$$h_{iD} = \frac{h_1}{h'_t}$$

where h_1 is the height from top of the reservoir to top of the producing interval (ft).

Odeh⁵ presented an equation for calculating the skin factor due to restricted entry, and the skin factor is a function of sand thickness, location of open interval, and the wellbore radius:

$$s_r = 1.35 \left[\left(\frac{h_t}{h_p} \right)^{0.825} \ln \left\{ \left(h_t \sqrt{\frac{k_h}{k_v}} + 7 \right) - \left[0.49 + 0.1 \ln \left(h_t \sqrt{\frac{k_h}{k_v}} \right) \right] \ln r_{wc} - 1.9 \right\} \right] \quad (5-27)$$

where

s_r = skin due to restricted entry

r_{wc} = corrected wellbore radius (ft) and is equal to

$$r_{wc} = r_w e^{0.2126(z_m/h_i + 2.753)} \quad (5-28)$$

z_m = distance between the top of the sand and middle of the open interval (ft) and = $Y + h_p/2$

Y = distance between the top of the sand and top of the open interval (ft).

If $Y > 0$, then $r_{wc} = r_w$. Use of these equations is best illustrated with an example.

Example 5-3 Analyzing Incomplete Perforated Interval

An oil well is perforated in the bottom 12 ft of the total formation thickness of 33 ft. Assuming ratio of horizontal to vertical permeability, $k_h/k_v = 1.0$. A pressure buildup test was run on this well; results and basic properties are: $p_{wf} = 1450$ psi, $p_{1hr} = 2000$ psi, $k = 4.5$ mD, $m = 48$ psi/cycle, $r_w = 0.30$ ft, $c_t = 1.6 \times 10^{-5}$ psi $^{-1}$, $\phi = 0.18$, $\mu_o = 0.45$ cP.

Calculate the following:

1. Total true skin factor, s
2. Skin due to formation damage, s_d
3. Skin due to incompletely perforated interval, s_p
4. Determine whether the productivity problem results from formation damage or from other causes.

Solution

1. Find the skin factor using Eq. 5-20:

$$\begin{aligned} s &= 1.151 \left[\frac{p_{1hr} - p_{wf}}{m} - \log \left(\frac{k}{\phi \mu_o c_t r_w^2} \right) + 3.23 \right] \\ &= 1.151 \left[\frac{2000 - 1450}{48} - \log \left(\frac{4.5}{0.18 \times 0.45 \times 1.6 \times 10^{-5} (0.3)^2} \right) \right] \\ &= 1.151 [11.4583 - 7.5864 + 3.23] = 8.17 \end{aligned}$$

Using Eq. 5-25, estimate s_p :

$$s_p = \left(\frac{33}{12} - 1 \right) \left[\ln \left(\frac{33}{0.30} \sqrt{1} \right) - 2 \right] = 1.7500(4.7005 - 2) = 4.73$$

Using Eq. 5-24, estimate the skin factor due to formation damage, s_D :

$$s_D = \frac{h_p}{h_t} (s - s_p) = \frac{12}{33(8.17 - 4.73)} = 1.25$$

If s_p is greater than s , s_D will be negative but this will not mean that the formation is stimulated. In this case the well is neither damaged nor stimulated. The observed productivity problem is caused entirely by the effects of an incomplete perforated interval.

Determination of Skin Effects in a Partially Completed Damaged Well

When a well is partially completed, Hawkins' equation⁶ may be applied. The results should be of value to all who are concerned with well testing and estimating well productivity. Using Hawkins' approach, for an undamaged well completed over the entire length of producing interval the pressure drop from outer radius of the damage zone r_s to well radius r_w is

$$\Delta p_1 = \frac{141.2q_o\mu_o\beta_o}{kh} \ln \left[\frac{r_s}{r_w} \right] \quad (5-29)$$

If the permeability is altered in region from r_w to r_s , this pressure drop becomes

$$\Delta p_1 = \frac{141.2q_o\mu_o\beta_o}{kh} \ln \left[\frac{r_s}{r_w} \right] \quad (5-30)$$

The pressure drop due to skin is

$$\Delta p_2 - \Delta p_1 = \Delta p_s = \frac{141.2q_o\mu_o\beta_o}{kh} \left[\left(\frac{k - k_s}{k_s} \right) \ln \left(\frac{r_s}{r_w} \right) \right] \quad (5-31)$$

where s_t is the skin as defined by Hawkins' equation⁶

$$s_t = \left(\frac{k - k_s}{k_s} \right) \ln \left(\frac{r_s}{r_w} \right) \quad (5-32)$$

The pressure drop due to damage then becomes

$$\Delta p_s = \frac{141.2}{kh} \frac{h}{h_p} \left(\frac{k - k_s}{k_s} \right) \ln \left(\frac{r_s}{r_w} \right) \quad (5-33)$$

Therefore the true skin due to formation damage is

$$s_t = \frac{h}{h_p} \left(\frac{k - k_s}{k_s} \right) \ln \left(\frac{r_s}{r_w} \right) \quad (5-34)$$

If h_p is small compared with h and when the partially perforated interval is in the center of the productive zone, then Eq. 5-34 can be corrected to Eq. 5-35:

$$s_t = \frac{h}{h_p} \left[1 - 0.2 \left(\frac{r_e - r_w}{h_p} \right) \right] \left(\frac{k - k_s}{k_s} \right) \ln \left(\frac{r_s}{r_w} \right) \quad (5-35)$$

The pseudo-steady-state equation relating flow rate to pressure drop is

$$q_o = \frac{0.00708kh(\bar{p} - p_{wf})}{\mu_o\beta_o \left[\ln \frac{0.472r_e}{r_w} + s \right]} \quad (5-36)$$

Example 5-4 Analyzing Partially Completed Damage Well

Sand control measure is required to allow production from a highly permeable formation. The pressure buildup test was run in the well; results and basic properties are: $p_i - p_{wf} = 150$ psi, $k = 950$ mD, $r_w = 0.38$ ft, $r_e = 1450$ ft, $k_s/k = 0.25$, $h_p = 10$ ft, $r_s = 1.4$ ft, $k_s = 0.25 \times 950 = 237.5$ mD, $c_t = 2.0 \times 10^{-5}$ psi⁻¹, $\phi = 0.20$, $\mu_o = 0.754$ cP, $\beta = 1.07$ rb/stb, $m = 35$ psi/cycle, and $(p_{1h} - p_{wf}) = 810$ psi.

Calculate the following:

1. Total true skin factor, s_t
2. Apparent skin factor, s_a
3. Flow rate if entire zone is perforated
4. Flow rate if middle 10 ft is perforated
5. Theoretical skin factor, s .

Solution Find oil flow rate using pseudo-steady-state flow rate equation 5-36:

$$\begin{aligned} q_o &= \frac{0.00708kh(\bar{p} - p_{wf})}{\mu_o\beta_o \left[\ln \frac{0.472r_e}{r_w} + s \right]} \\ &= \frac{0.00708 \times 950 \times 35 \times 150}{0.754(1.07) \left[\ln \left(\frac{0.472 \times 1450}{0.38} \right) + s \right]} = \frac{43,768.44}{7.50 + s} \end{aligned}$$

where $s = s_a + s_t$ and s_a is the apparent skin due to partial completion. Since h_p is small compared to h , therefore using Eq. 5-35, we get

$$s_t = \frac{35}{10} \left[1 - 0.2 \left(\frac{1.4 - 0.38}{10} \right) \right] \left(\frac{950 - 237.5}{237.5} \right) \ln \left(\frac{1.4}{0.38} \right) = 13.42$$

If the middle 19 ft are perforated we calculate, s_a from Eq. 5-27

$$\begin{aligned}
 s_r &= 1.35 \left[\left(\frac{h_t}{h_p} \right)^{0.825} \ln \left\{ \left(h_t \sqrt{\frac{k_h}{k_v}} + 7 \right) \right. \right. \\
 &\quad \left. \left. - \left[0.49 + 0.1 \ln \left(h_t \sqrt{\frac{k_h}{k_v}} \right) \right] \ln r_{wc} - 1.9 \right\} \right] \\
 &= 1.35 \left[\left(\frac{35}{10} \right)^{0.825} \left\{ \ln(35\sqrt{0.2} + 7) \right. \right. \\
 &\quad \left. \left. - 0.49 + 0.1 \ln 35\sqrt{0.2} \ln(0.38) - 1.95 \right\} \right] = 7.25
 \end{aligned}$$

If the entire productive zone is perforated and no permeability reduction is present, $s = 0$ and from Eq. 5-36:

$$q_o = \frac{43,768.44}{7.50} = 5836.0 \text{ stb/day}$$

If the middle 10 ft are perforated when no permeability reduction (damage) is present,

$$q_o = \frac{43,768.44}{7.50 + 7.25} = 2967 \text{ stb/day}$$

When permeability reduction is present to the extent that $k_s/k = 0.2$, then

$$q_o = \frac{43,768.44}{7.50 + 7.25 + 13.42} = 1554 \text{ stb/day}$$

Using Eq. 5-32,

$$s_t = \frac{950 - 237.5}{237.5} \ln \left(\frac{1.4}{0.38} \right) = 3.91$$

If we use Hawkins' equation 5-32 without correction, s_t would be 3.91 and flow rate would have been estimated as

$$q_o = \frac{43,768.44}{7.50 + 7.25 + 3.91} = 2346 \text{ stb/day}$$

Using Eq. 5-20, theoretical skin factor s is

$$s = 1.151 \left[\frac{747}{35} - \log \left(\frac{950}{0.2 \times 0.754 \times 2.0 \times 10^{-5} (0.38)^2} \right) \right] = 17.54$$

After backing out 7.25 for the skin due to partial completion, the true skin would be 13.42. If it is known that the sand has been consolidated to a radius of 1.4 ft, the ratio of skin permeability to formation permeability calculated using Eq. 5-33 would be $k_s/k = 0.097$ instead of the actual value of 0.25.

Estimation of Reservoir Size from Two Pressure Buildup Tests

The results of pressure buildup tests can sometimes be used to estimate the reservoir size. The basic idea is to compare the average static reservoir pressure before and after production of a known quantity of fluid from a closed, volumetric reservoir, with compressibility, c_t . If V_{Res} is the reservoir volume (barrels), ΔN_p is the stock – tank barrels of oil produced between times 1 and 2, and p_{Av1} and p_{Av2} are the average reservoir pressures before and after oil production, respectively, then a material balance on the reservoir shows that

$$\bar{p}_{Av2} = \bar{p}_{Av1} - \frac{\Delta N_p \beta_o}{V_{Res} c_t \phi} \quad (5-37)$$

or

$$V_{Res} = \frac{\Delta N_p \beta_o}{(\bar{p}_{Av1} - \bar{p}_{Av2}) c_t \phi} = \frac{43,560 \text{ (acres)} h}{5.615} \quad (5-38)$$

$$A_{Res} = \frac{V_{Res} \times 5.615}{h \times 43,560} \quad \text{(acres)} \quad (5-39)$$

Example 5-5 Estimating Reservoir Size from Two Pressure Buildup Tests

The following data were recorded from two pressure buildup tests: $p_{Av1} = 3900$ psi, $p_{Av2} = 3000$ psi, oil produced between two tests in 6 months $= q_{Av} = 250$ stb/day; average formation volume factor, $\beta_o = 1.292$ rb/stb, total compressibility, $c_t = 9.52 \times 10^{-6}$ psi⁻¹; $\phi = 21.5\%$, average sand thickness, $h = 12.5$ ft. Estimate the reservoir size in acres.

Solution

From Eq. 5-39,

$$\begin{aligned} V_{Res} &= \frac{\Delta N_p \beta_o}{(\bar{p}_{Av1} - \bar{p}_{Av2}) c_t \phi} \\ &= \frac{(250 \text{ stb/day})(6 \times 31.5 \text{ days})(1.292 \text{ rb/stb})}{(3900 - 3000)(9.5 \times 10^{-6})(0.215)} = 33.14 \times 10^6 \text{ bbl} \end{aligned}$$

Thus, from Eq. 5-39,

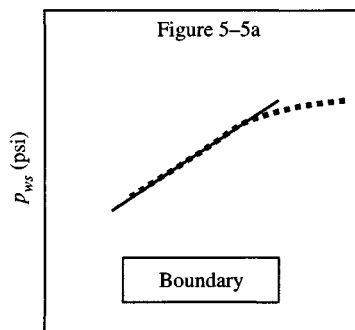
$$V_{Res} = \frac{(3314 \times 10^6)(5.615 \text{ ft}^3/\text{bbl})}{125 \times 43,560 \text{ ft}^2/\text{acre}} = 342 \text{ acres}$$

The reservoir size is

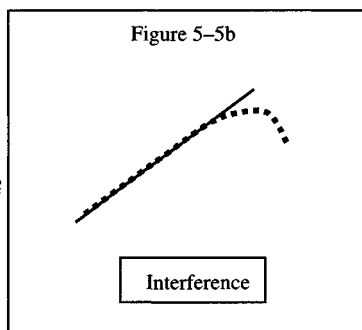
$$r_e = \sqrt{\frac{\text{Acres} \times 43,560}{\pi}} = \sqrt{\frac{342 \times 43,560}{22/7}} = 2177 \text{ ft}$$

Typical Shapes of Buildup Curves

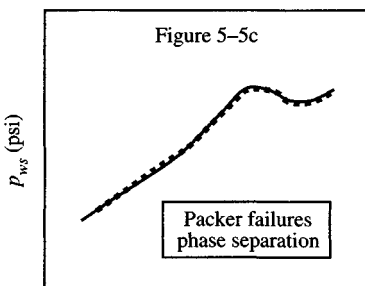
Downtrending Horner plots are shown in Figures 5-5a through 5-5d. These curves tend to bend downward because of:



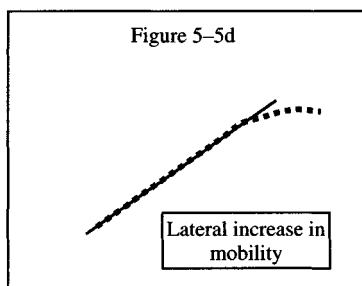
$$\log \left[\frac{t + \Delta t}{\Delta t} \right]$$



$$\log \left[\frac{t + \Delta t}{\Delta t} \right]$$



$$\log \left[\frac{t + \Delta t}{\Delta t} \right]$$



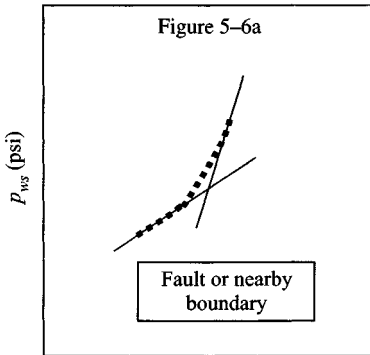
$$\log \left[\frac{t + \Delta t}{\Delta t} \right]$$

Figure 5-5. Horner plots showing downtrending.⁷

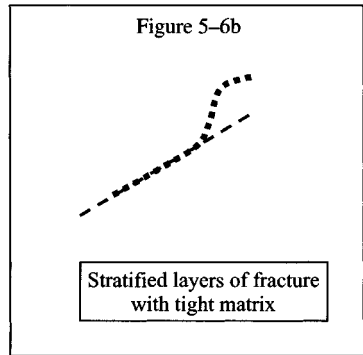
1. Reservoirs bounded;
2. Well interference is present;
3. Phase separation occurs;
4. Fluid mobility increases;
5. Porosity or permeability decreases;
6. As time increases.

Uptrending Horner plots are shown in Figures 5-6a through 5-6d. These curves tend to bend upward because of:

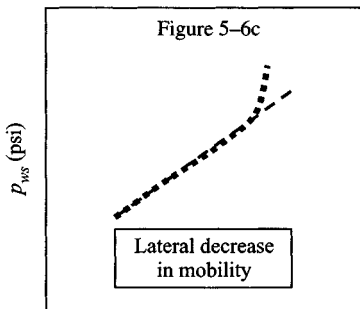
1. Faults, partial boundaries, stratified layers without crossflow;
2. Lateral decrease in mobility;
3. Increases in ϕ and k ;
4. Lenses, irregular well locations or drainage areas;



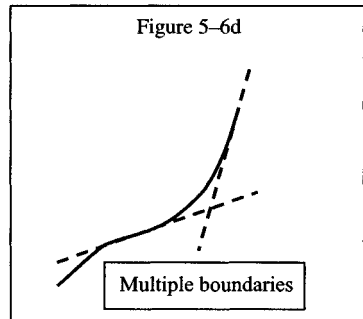
$$\log \left[\frac{t + \Delta t}{\Delta t} \right]$$



$$\log \left[\frac{t + \Delta t}{\Delta t} \right]$$



$$\log \left[\frac{t + \Delta t}{\Delta t} \right]$$



$$\log \left[\frac{t + \Delta t}{\Delta t} \right]$$

Figure 5-6. Horner plots showing downtrending.⁷

5. Unconnected zones with widely differing pressure;
6. Use of improved flow times.

5.5 Pressure Buildup Testing Methods for Finite (Bounded) Reservoir

In this section, we consider pressure buildup testing of a single well in an finite (bounded) and of a well in a developed (old) reservoir using methods commonly referred to as Horner,⁸ MDH,⁹ Muskat,¹⁰ and Slider.¹¹

Horner and MBH Methods

The Horner and MBH methods are used to analyze the buildup data only for infinite-acting reservoirs. This is not true; Horner's method can be used to estimate the reservoir parameters in finite reservoirs just as in infinite-acting reservoirs. The difference occurs only in late-time data when boundary effects influence the data as shown in Figure 5-7.

$$\log \left[\frac{t_p + \Delta t}{\Delta t} \right]$$

For an infinite-acting reservoir, an estimate of p_i is obtained by extrapolating the straight-line section of the Horner plot to infinite shut-in time. For finite and developed reservoirs, the extrapolated pressure is not a good estimate of p_i and generally has been called the false pressure, p^* . As shown

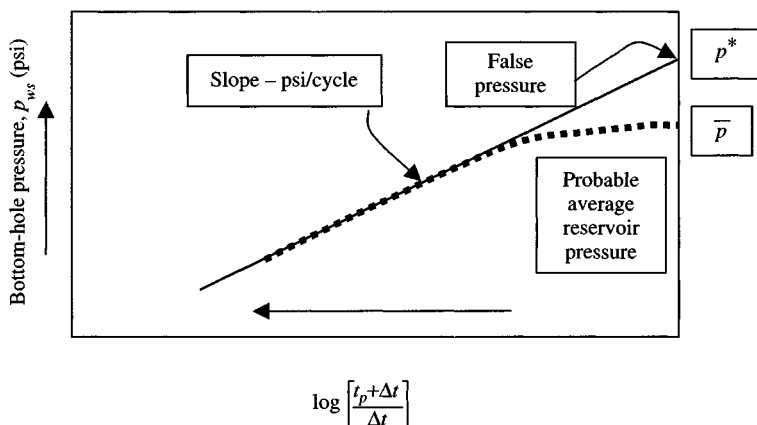


Figure 5-7. Horner plot of pressure buildup data from a well in a finite reservoir.

in Figure 5-7, the extrapolated false pressure, p^* , is higher than the average reservoir pressure at the instant of shut-in unless the drainage region is highly skewed. Using the concept of the false pressure, we may rewrite Eq. 5-18 as

$$p_{ws} = p^* - m \log \left(\frac{t_p + \Delta t}{\Delta t} \right) \quad (5-40)$$

Ramey and Cobb¹² show that p^* is related to p_i by

$$p^* = p_i - \frac{142.2q_o\mu_o\beta_o}{kh} [p_D(t_{pDA}) - 0.5(\ln t_{pD} + 0.8907)] \quad (5-41)$$

where

$$t_{pDA} = \frac{0.0002637kt_p}{\phi\mu_o c_t r_w^2} \quad (5-42)$$

Although it is commonly believed that the Horner plot should be used only for new wells or when t_p is relatively small, Ramey and Cobb¹² and Cobb and Smith¹³ indicate that Horner plot may always be used for pressure buildup analysis. However, since it requires more work than the MDH method, the Horner plot is generally not used unless $t_p < t_{pss}$, where, t_{pss} is the pseudo-steady-state time and is given by Eq. 5-43:

$$t_{pss} = \frac{\phi\mu_o c_t A}{0.0002637k} (t_{DA})_{pss} \quad (5-43)$$

and $(t_{DA})_{pss}$ is given in the "for $t_{DA} >$ " column of Table B-2. Both C_A and $(t_{DA})_{pss}$ depend on reservoir shape and well location. If $t_p \gg t_{pss}$, then t_p should be replaced by t_{pss} to improve the accuracy.

Miller-Dyes-Hutchinson (MDH) Method

The MDH method is best for older wells in bounded depleting reservoirs; when the producing time is not known, or can be estimated only roughly, MDH plotting can be used. This or it can tend to yield estimates that are too high for short producing periods. The method is applicable for the initial transient period of buildup. The MDH buildup requires a plot of buildup pressures versus the logarithm of buildup time. The Horner plot may be simplified if $\Delta t \ll t_p$. In that case, $t_p + \Delta t \cong t_p$ and

$$\log\left(\frac{t_p + \Delta t}{\Delta t}\right) \cong \log t_p - \log \Delta t \quad (5-44)$$

If we use Eq. 5-44 in Eq. 5-40, then we have

$$p_{ws} = p_{1hr} + m \log \Delta t \quad (5-45)$$

Eq. 5-45 indicates that a plot of p_{ws} versus $\log \Delta t$ should be a straight line with slope, $+m$, where Eq. 5-9 gives m . Permeability k may be estimated from Eq. 5-16 and the skin factor may be estimated from Eq. 5-20. The p_{ws} versus $\log \Delta t$ plot is commonly called the MDH plot.⁹ The false pressure may be estimated from the MDH plot using

$$p^* = p_{1hr} + m \log(t_p + 1) \approx p_{1hr} + m \log(t_p) \quad (5-46)$$

The beginning of the MDH semilog straight line may be estimated by making the log-log data plot and observing when the data points reach slowly curving low-slope line, about 1–1.5 cycles in time after the end of unit-slope straight line. Alternatively, the time to the beginning of the semilog straight line for either the Horner or the MDH plot can be estimated in exactly the same way as mentioned earliest.

Example 5-6 Analyzing Pressure Buildup Test Using Horner, MBH and MDH Methods

Analyze pressure buildup and well/reservoir data given in Table 5-3 using the MDH method.

Table 5-3
Extended Muskat Analysis of Late Pressure Buildup Data

Shut-in time, Δt (hr)	Shut-in pressure, p_{ws} (psi)	$p_i - p_{ws}$ (psi) for		
		$p_i = 4510$	$p_i = 4518$	$p_i = 4535$
0	3576	934	942	959
10	4402	108	116	133
20	4447	63	71	88
30	4472	38	46	63
40	4488	22	30	47
50	4501	9	17	34
60	4503	7	15	32
70	4506	4	14	29
80	4508	1	10	27

Solution Figure 5–8 shows the Horner plot for the data. The slope of the straight line is in psi/cycle and p_{1hr} is in psi. The permeability k is calculated using Eq. 5–16:

$$k = \frac{162.6q_o\mu_o\beta_o}{mh} = \frac{162.6 \times 350 \times 0.8 \times 1.136}{152 \times 49} = 6.94 \text{ mD}$$

Skin effect from Eq. 5–20:

$$s = 1.151 \left[\frac{p_{1hr} - p_{wf}}{m} - \log \left(\frac{k}{\phi\mu_o c_t r_w^2} \right) + 3.23 \right] = 1.151 \left[\frac{4235 - 3561}{152} - \log \left(\frac{6.94}{0.23 \times 0.80 \times 17 \times 10^{-6} \times 0.29^2} \right) + 3.23 \right] = 0.28$$

From Eq. 5–21, we obtain

$$(\Delta p)_{skin} = 0.869 \times 0.28 \times 152 = 37 \text{ psi}$$

Find dimensionless well producing time before shut-in from Eq. 5–42:

$$t_{DA} = 0.000264 \times \frac{6.94 \times 4320}{0.23 \times 0.80 \times 17 \times 10^{-6} \times 7.723 \times 43,560} = 7.53$$

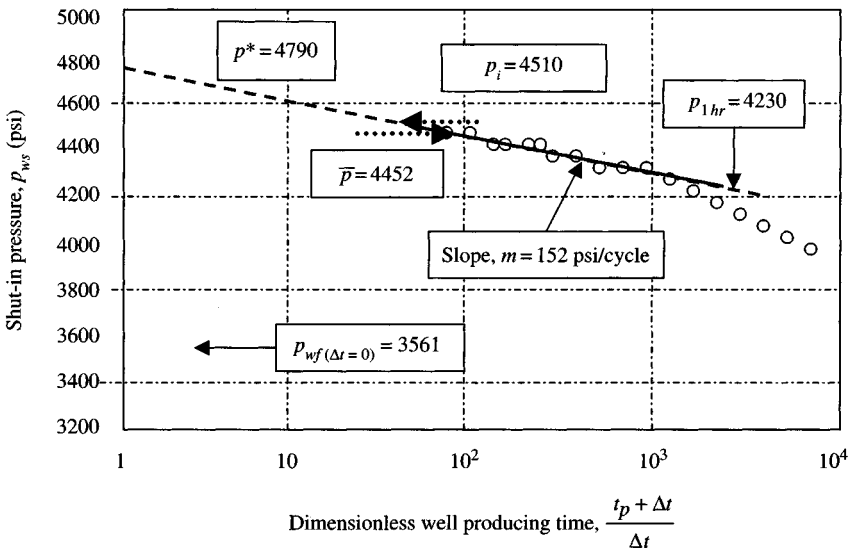


Figure 5–8. Horner plot.

Find false pressure p^* at unit time ratio by extrapolating, which is 4785 psia and calculate the average pressure, \bar{p} , from Figure 5-9. For $t_{DA} = 7.53$:

$$\frac{kh}{70.65q_o\mu_o\beta_o}(p^* - \bar{p}) = 5.00$$

$$\frac{kh}{70.65q_o\mu_o\beta_o}(p^* - p_i) = 4.08$$

$$(\Delta p)_{skin} = 0.869ms = 0.869 \times 0.28 \times 150 = 42 \text{ psi}$$

Using Figure 5-9, the average and initial pressures are

$$\bar{p} = 4785 - 5.0 \times \frac{70.65 \times 350 \times 0.8 \times 1.136}{340.3} = 4455 \text{ psia}$$

and

$$p_i = 4785 - 4.08 \times \frac{70.65 \times 350 \times 0.8 \times 1.136}{340.3} = 4515 \text{ psia}$$

The values of average and initial pressures can also be determined by using Figure 5-10. Reading the dimensionless buildup pressure at a value of the time ratio at which p_{ws} is known, for a line selected for the proper dimensionless

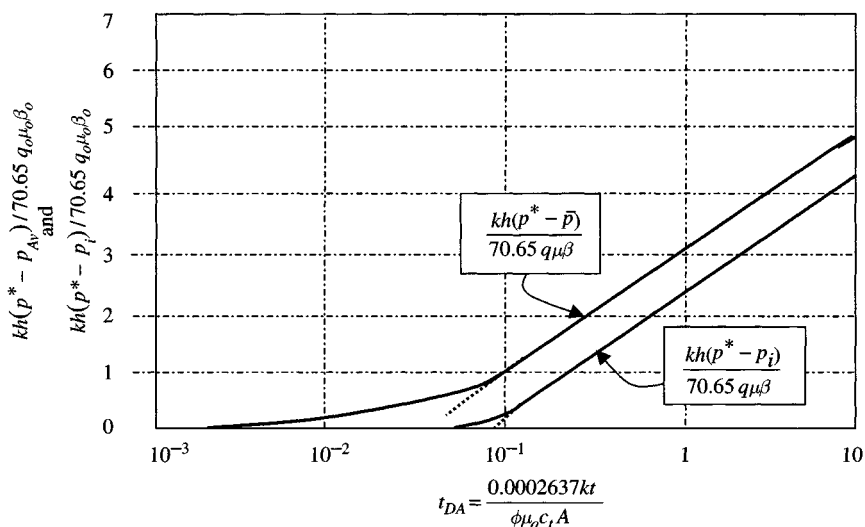


Figure 5-9. MBH graph for a well producing in the center of a constant pressure.¹⁴

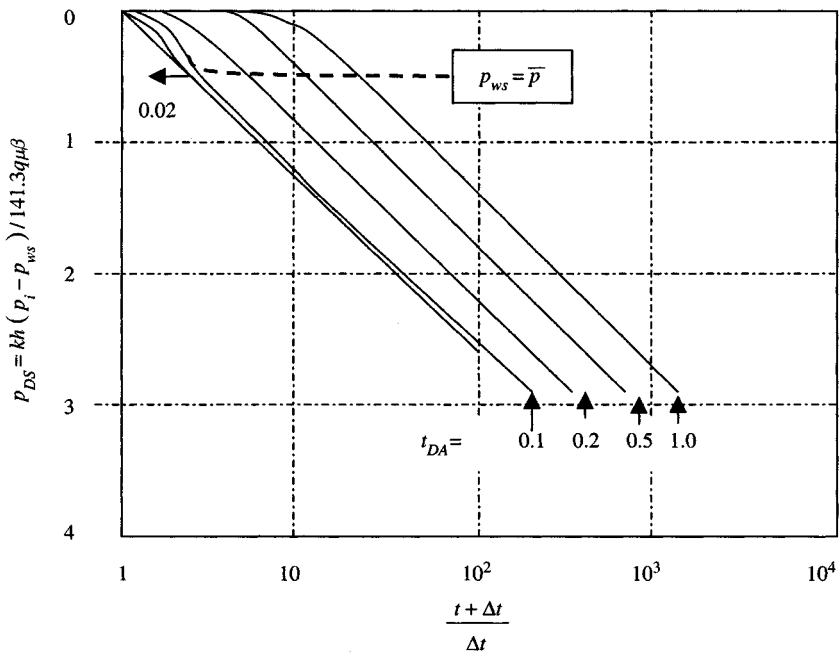


Figure 5-10. Horner plot for a well producing in the center of a constant pressure.⁹

producing time, t_{DA} , p_i may be determined. The value of $(p_i - \bar{p})$ may then be read from the dashed line and \bar{p} is calculated. This cannot be done with the existing Figure 5-10 for $t_{DA} = 7.53$ because the highest value of t_{DA} shown in Figure 5-10 is unity. Hence it is easier to use the MDH type graph, Figure 5-11, because only one line exists for the long producing times.

MDH Method

Figure 5-12 shows the MDH graph. The appearance of the graph is similar to that of the Horner plot, and also the slope and p_{1hr} values are the same. It is clear that the Horner and MDH methods will yield the same permeability and skin effect values. Figure 5-11 shows the MDH data plot.

To estimate the initial pressure by means of MDH method, Figure 5-12 can be used. The pressure of 4432 psi at a shut-in time of 20 hr will be corrected to p_i by means of Figure 5-12.

Dimensionless producing time,

$$t_{DA} = \frac{0.0002637 kt}{\phi \mu_o c_t A} = 7.53 \text{ for } t \text{ of } 4320 \text{ hours}$$

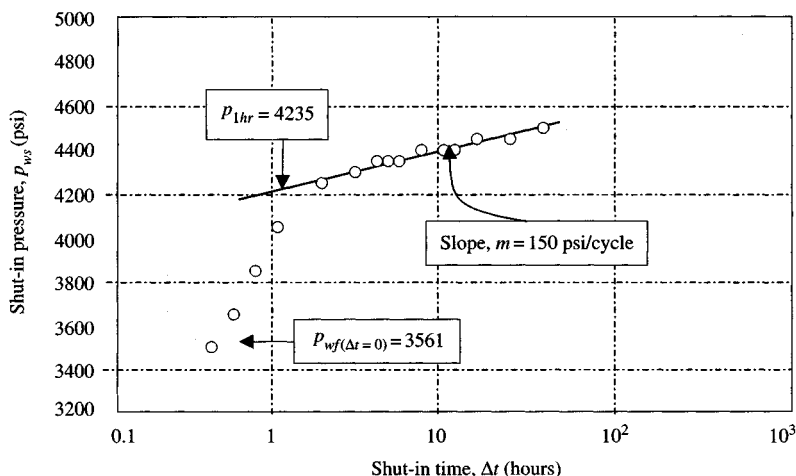
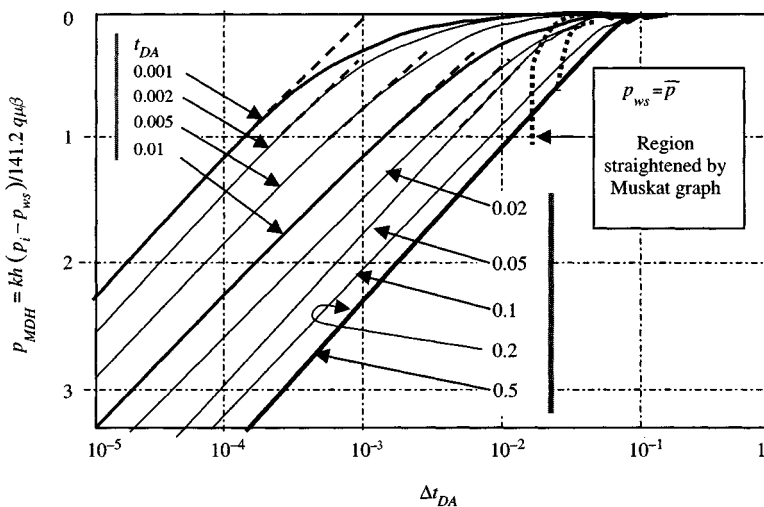


Figure 5-11. MDH data plot.

Figure 5-12. MDH graph for a well in the center of a constant-pressure square.⁹

$$\Delta t_{DA} = \frac{7.53 \times 20}{4370} = 0.0349$$

From Figure 5-12,

$$P_{MDH} = \frac{kh(p_i - p_{ws})}{141.3q\mu\beta} = 0.66$$

$$\frac{141.3q\mu\beta}{kh} = 0.869 \text{ (slope, } m)$$

Therefore

$$\frac{(p_i - 4432)}{0.869 \times 150} = 0.66 \quad \text{or} \quad p_i = 4518 \text{ psi}$$

This is a close check of the value of 4516 psi obtained by the Horner plot.

Extended Muskat Method

In 1937, Muskat¹⁵ proposed the plotting pressure buildup data as $\log(\bar{p} - p_{ws})$ versus Δt . Subsequent theoretical studies^{16,17} indicate that this graph should be used with caution and only as a late-time analysis method. Because of the long shut-in times, usually required for pressure buildup data to reach the Muskat straight line, the method has limited application for pressure buildup test analysis. However, it appears to be more practical for analyzing pressure buildup data in producing wells, water-drive reservoirs, and filled-up waterfloods because of the longer duration of the Muskat straight line in those systems.^{18,19}

The Muskat method uses a trial-and-error plot with several \bar{p} estimates; a straight line is obtained for the correct \bar{p} . Figure 5-13 is a schematic illustration of the extended Muskat plot.¹⁵ If the assumed \bar{p} is too high, the plot will be concave upward; if \bar{p} is too low, the plot will be concave downward. The following equations may be used to estimate the permeability, porosity-total system effective compressibility.

$$k = \frac{141.3q\mu\beta(1.34)}{h(p_i - p_{ws})_{\Delta t=0}} \quad (5-47)$$

$$\phi c_t = -0.0559 \frac{k}{\mu A} \text{ (slope, } \log_{10} \text{ cycle/day)} \quad (5-48)$$

Table 5-3 presents this additional buildup data. Use these data to estimate the initial pressure p_i using Muskat method. Figure 5-13 shows the Muskat data plot.

Estimate the permeability using Eq. 5-47:

$$k = \frac{141.3q\mu\beta(1.34)}{h(p_i - p_{ws})_{\Delta t=0}} = \frac{141.3 \times 350 \times 0.8 \times 1.136 \times 1.34}{175 \times 49} = 7.02 \text{ mD}$$

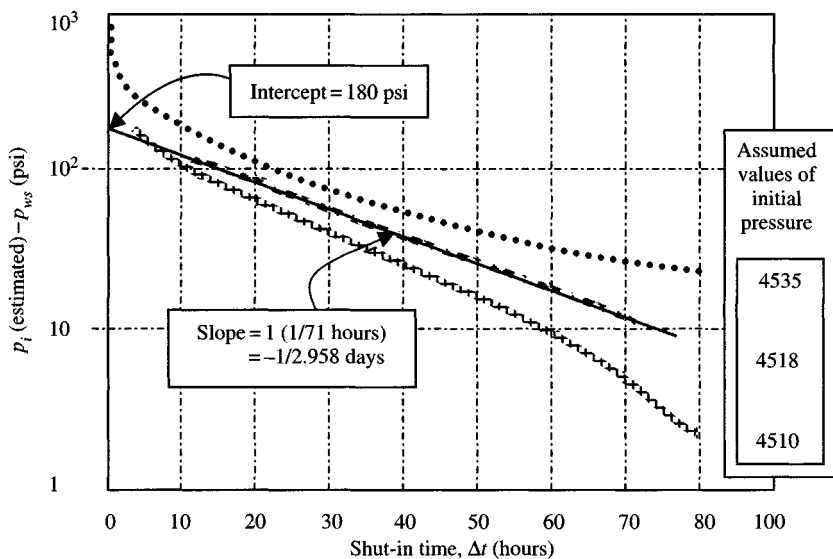


Figure 5-13. Muskat data plot.

$$\begin{aligned} \phi c_t &= -0.0559 \frac{k}{\mu A} (\text{slope, } \log_{10} \text{ cycle/day}) \\ &= -0.0559 \frac{7.02 \times 2.958}{0.8 \times 7.72 \times 43560} = 3.95 \times 10^{-6} \text{ psi}^{-1} \end{aligned}$$

Check: $\phi c_t = 0.23 \times 17.0 \times 10^{-6} \cong 3.91 \times 10^{-6}$ psi.

The skin effect can be computed using Muskat method using the following equation:

$$s = 1.151 \left[\frac{(p_i - p_{1hr})}{-m} - \log \left(\frac{k}{\phi \mu c_t r_w^2} \right) + 3.23 \right] \quad (5-49)$$

$$\begin{aligned} s &= 1.151 \left[\frac{(4345 - 3576)}{150} - \log \left(\frac{7.04}{0.23 \times 0.8 \times 17 \times 10^{-6} (0.29)^2} \right) + 3.23 \right] \\ &= 0.33 \end{aligned}$$

$$(\Delta p)_{skin} = 0.869ms = 0.869 \times 150 \times 0.33 = 43 \text{ psi}$$

Calculate p^* using the following equation:

$$p^* = p_{1hr} + m \log(t_p) = 4235 + 150 \log(4320) = 4780 \text{ psi}$$

The slope of the Muskat plot at straight line may be used to estimate the drainage area. For a close square:¹⁰

$$A = -\frac{0.00472k}{\phi\mu_o c_t m_m} \quad (5-50)$$

$$A = -\frac{0.00472 \times 5.24}{0.23 \times 0.8 \times 17 \times 10^{-6} \times (-0.01538)} = 513,014 \text{ ft}^2$$

and for a square with constant pressure boundaries (water-drive system)

$$A = -\frac{0.00233k}{\phi\mu_o c_t m_m} \quad (5-51)$$

where A is the area in ft^2 and is equal to πr_e^2 and r_e can be estimated. In Eqs. 5-50 and 5-51, m_m is the slope of the Muskat plot and is negative number in cycle/hr. The following equation may be used to estimate the physical time range during which Muskat straight line will occur:

$$\frac{250\phi\mu_o c_t r_e^2}{k} \leq \Delta t \leq \frac{750\phi\mu_o c_t r_e^2}{k} \quad (5-52)$$

Example 5-7 *Analyzing Single-Phase and Single-Rate Pressure Buildup Test Using Horner Plot and MDH Method in Finite Reservoir*

A buildup test was conducted on an oil well. The well was produced for an effective time of 180 days at the final rate. The buildup and other pertinent reservoir data are: $q_o = 350$ stb/day, $\mu_o = 0.8$ cP, $\beta_o = 1.136$ rb/stb, $c_t = 17.0 \times 10^{-6}$ psi^{-1} , $h = 49$ ft, $r_w = 0.29$ ft, $\phi = 0.23$, $A = 11.55$ acres.

Table 5-4 shows the pressure buildup and calculated data. Assuming the well is in the center of a closed square, determine:

1. k , s , pressure drop due to skin and p^* using Horner plot.
2. k , s , pressure drop due to skin and p^* using MDH method.
3. k , ϕc_t and drainage area.

Solution

$$t_p = 180 \times 24 = 4320 \text{ hours}$$

A Horner graph for this test is shown in Figure 5-14. It has the following characteristics:

- Slope of buildup straight line, $m = 152$ psi/ log cycle;
- $p_{1hr} = 4510$ psi;
- $p^* = 4978$ psi.

Table 5-4
Pressure Buildup Test Data

Shut-in time, Δt (hr)	Shut-in pressure, p_{ws} (psi)	$\frac{(t_p + \Delta t)}{\Delta t}$
0	3561	—
0.333	3851	12,974
0.500	3960	8641
0.668	4045	6478
0.833	4104	4893
1.000	4155	4321
2.000	4271	2161
3.000	4306	1441
4.000	4324	1081
5.000	4340	860
6.000	4352	721
7	4363	618
8	4371	541
9	4380	481
10	4387	433
20	4432	217
40	4473	109
50	4486	87
60	4495	73
70	4500	62
80	4506	55

Permeability–thickness product, using Eq. 5-14:

$$kh = \frac{162.6q_o\mu_o\beta_o}{m} = \frac{162.6 \times 350 \times 1.136 \times 0.8}{152} = 340.3 \text{ mD ft}$$

$$k = \frac{340.3}{49} = 6.94 \text{ mD}$$

Skin effect from Eq. 5-17:

$$s = 1.151 \left[\frac{4510 - 3561}{152} - \log \left(\frac{6.94}{0.23 \times 0.8 \times 17.0 \times 10^{-6} (0.29)^2} \right) + 3.23 \right]$$

$$= 5.07$$

From Eq. 5-19:

$$(\Delta p)_{skin} = 0.869ms = 0.869 \times 152 \times 5.07 = 669.9 \text{ psi}$$

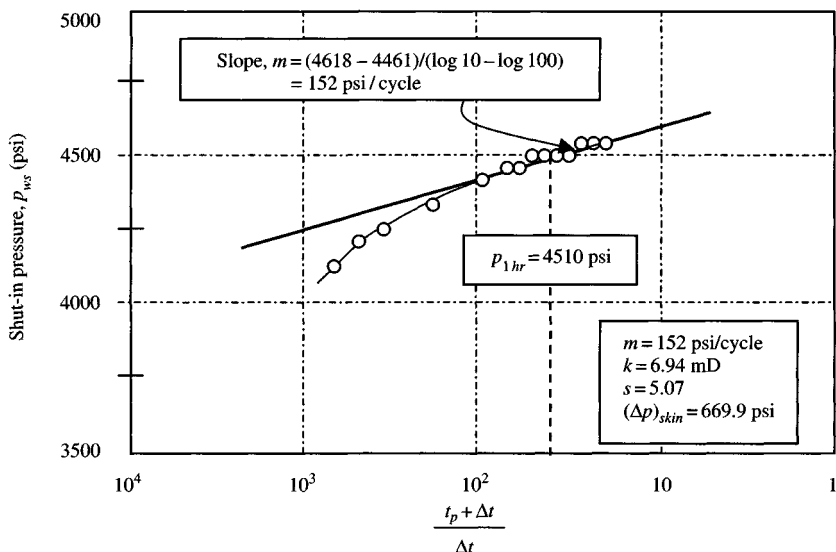


Figure 5-14. Horner's plot.

Figure 5-15 presents an MDH type buildup graph for data of Example 5-7. The appearance of the graph is similar to that of the Horner graph (Figure 5-14).

The slope of the straight-line portion is 150 psi/cycle (from MDH graph). The p_{1hr} is 4510 psi. Find the formation permeability from Eq. 5-14:

$$k = \frac{162.6 \times 350 \times 1.136 \times 0.8}{150 \times 49} = 7.04 \text{ mD}$$

The difference in permeability between the two methods is only 1%.

Calculate the skin factor using Eq. 5-17:

$$\begin{aligned} s &= 1.151 \left[\frac{p_{1hr} - p_{wfo}}{m} - \log \left(\frac{k}{\phi \mu_o c_r r_w^2} \right) + 3.23 \right] \\ &= 1.151 \left[\frac{4510 - 3561}{150} - \log \left(\frac{7.04}{0.23 \times 0.8 \times 17.0 \times 10^{-6} (0.29)^2} \right) + 3.23 \right] \\ &= 4.98 \end{aligned}$$

$$(\Delta p)_{skin} = 0.869 ms = 0.869 \times 150 \times 4.98 = 657.8 \text{ psi}$$

From Eq. 5-46:

$$p^* = p_{1hr} + m \log(t_p) = 4510 + 150 \log 4320 = 5055 \text{ psi}$$

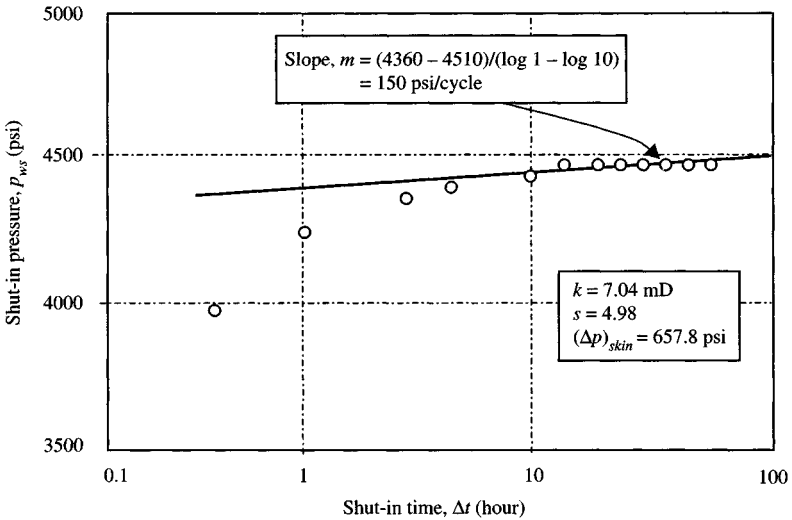


Figure 5-15. MDH data plot.

Example 5-8 Analyzing Single-Phase and Single-Rate Pressure Buildup Test Using Muskat's Method in Finite Reservoir

Rework Example 5-7 using Muskat method.

Solution A Muskat plot of the pressure data of Table 5-5 is shown in Figure 5-16. Only three points define the straight line in Figure 5-16. From Figure 5-16, we find

Intercept = $(\bar{p} - p_w)_{int} = b = 175$ psi and slope, $m_M = -0.01538$ cycle/day

$$t_{pDA} = \frac{0.000264 \times 6.94 \times 4320}{0.23 \times 0.8 \times 17.0 \times 10^{-6} \times 7.72 \times 43,560} = 7.54$$

For closed square system using Eq. 5-47:

$$k = \frac{141.2 \times 350 \times 1.136 \times 0.8}{49 \times 175} [0.67] = 5.24 \text{ mD}$$

From Eq. 5-48,

$$\phi c_t = -0.0559 \times \frac{5.24}{0.8(7.72)(43,560)} \left(-\frac{1}{0.3690} \right) = 2.95 \times 10^{-6} \text{ psi}^{-1}$$

This checks the values given:

$$\phi c_t = 0.23(17.0 \times 10^{-6}) = 3.91 \times 10^{-6} \text{ psi}^{-1}$$

Table 5-5
Pressure Buildup Test Data Using Muskat Method

Shut-in time Δt (hr)	$p_i - p_{ws}(\text{psi})$ for			
	p_{ws} (psi)	$\bar{p} = 4507$ psi	$\bar{p} = 4516$ psi	$\bar{p} = 4525$ psi
0	3561	946	955	964
10	4387	120	129	128
20	4432	75	84	93
30	4455	52	61	70
40	4473	34	43	52
50	4486	21	30	39
60	4495	12	21	30
70	4501	6	15	24
80	4506	1	10	19

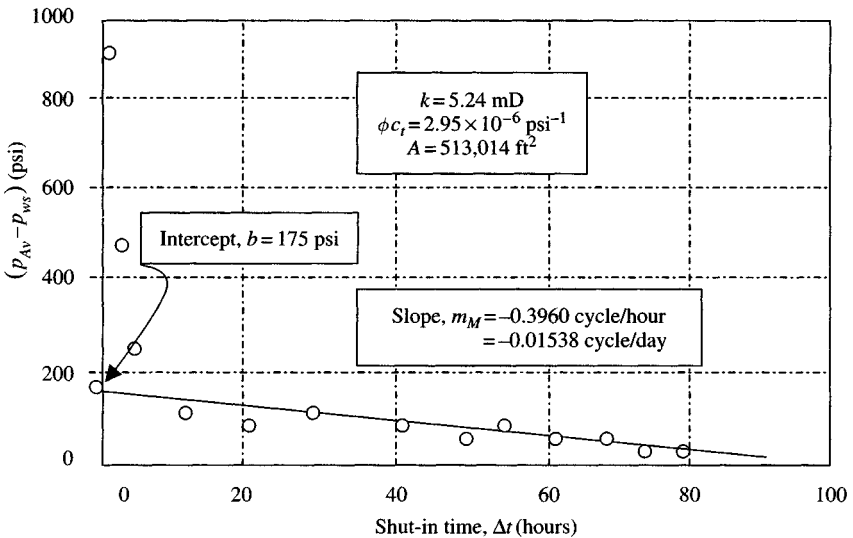


Figure 5-16. Muskat plot.

The drainage area is calculated using Eq. 5-50:

$$A = \frac{-0.00471k}{\phi\mu_o c_t m_M} = \frac{-0.00471(5.24)}{(0.23)(0.8)(17.0 \times 10^{-6})(-0.01538)} = 513,014 \text{ ft}^2$$

For data provided in Example 5-8, we find $A = 7.72 \times 43,560 = 336,283 \text{ ft}^2$.

Example 5-9 *Analyzing Single-Phase and Single-Rate Pressure Buildup Test Using Muskat's Method in Finite Reservoir Assuming Well in Center of Constant Pressure Square (Water-Drive System)*

Rework the buildup data in Example 5-8.

Solution For constant pressure square, permeability and porosity-total system effective compressibility product are estimated using Eqs. 5-47 and 5-48.

For closed square system using Eq. 5-47,

$$k = \frac{141.2(350)(1.136)(0.8)}{49(175)} [1.34] = 7.02 \text{ mD}$$

From Eq. 5-48,

$$\phi c_t = -0.0559 \frac{7.02}{0.8(7.72)(43560)} \left(-\frac{1}{0.3690} \right) = 3.95 \times 10^{-6} \text{ psi}^{-1}$$

This checks the values given

$$\phi c_t = 0.23(17.0 \times 10^{-6}) = 3.91 \times 10^{-6} \text{ psi}^{-1}$$

The drainage area is calculated using Eq. 5-51:

$$A = \frac{-0.002331k}{\phi \mu_o c_t m_M} = \frac{-0.00233(7.02)}{(0.23)(0.8)(17.0 \times 10^{-6})(-0.01538)} = 339,993 \text{ ft}^2$$

For data provided in Example 5-8, we find $A = 7.72 \times 43,560 = 336,283 \text{ ft}^2$.

Slider's Technique For Analyzing Buildup Test

Slider¹¹ presented in 1971 an entirely new approach to transient pressure behavior termed as negative superposition. Slider's analysis was based on the following assumptions:

- If the well had been shut-in, no appreciable or measurable change would have occurred during the shut-in time.
- Based on the distance to the nearest boundary, the shut-in time, Δt , must be less than the stabilization time, t_s .

In the case of pseudo-steady-state, the change in pressure with time is estimated using the following equations:

$$\left(\frac{\Delta p}{\Delta t}\right)_{pseudo} = \frac{0.0744q_o\beta_o}{\phi h c_t r_e^2} \quad (\text{psi/hr})$$

or

$$\left(\frac{\Delta p}{\Delta t}\right)_{pseudo} = \frac{0.234q_o\beta_o}{c_t v_p} \quad (\text{psi/hr}) \quad (5-53)$$

where

$$v_p = \pi r_e^2 h \phi \quad \text{ft}^3$$

In case of a well that is infinite-acting at shut-in, the change in pressure during the shut-in period, if the well had not been shut-in, is estimated from the following equation:

$$(\Delta p)_{max} = m \log \frac{t_p + \Delta t_{max}}{t_p} \quad (5-54)$$

If the unchanging pressure assumption is satisfied, then the following equations are used to analyze a buildup test regardless of whether the well is infinite-acting, in pseudo-steady state or steady state at time of shut-in:

$$(\Delta p)_{skin} = p_{ws} - p_{wf}(\Delta t = 0) - 0.869m(0.5)[\ln(\Delta t_D) + 0.809] \quad (5-55)$$

where Δt_D is the dimensionless time and is given by

$$\Delta t_D = \frac{0.000264k\Delta t}{\phi\mu_o c_t r_w^2} \quad (5-56)$$

where

m = estimated slope from Horner plot

Δt = shut-in time on the straight line or its extrapolation at $\Delta t = 10$ min, i.e., $\log = 1.0$, and Δt is in hours from MDH plot.

The permeability and skin factor are estimated using the following equations:

$$k = \frac{162.6q_o\mu_o\beta_o}{mh} \quad (5-57)$$

$$s = \frac{(\Delta p)_{skin}}{0.869m} \quad (5-58)$$

In cases where the unchanged pressure assumption is not valid, Horner's method for analyzing buildup test should be used in an infinite-acting reservoir. For the analysis for buildup test in a bounded (finite) reservoir, when the unchanging pressure assumption is not valid, Slider introduced a method in which Δp_q is plotted versus Δt on semilog graph paper. The use of Δp_q plot for analyzing buildup is used for a well that is in pseudo-steady state at shut-in. The approximate time when pseudo-steady-state flow began is given by

$$t_s = 948 \frac{\phi \mu_o c_t r_e^2}{k} \quad (5-59)$$

The Δp_q term may also be calculated using the following equation:

$$\Delta p_q = p_{ws} - p_{wf}(\Delta t=0) + \Delta t \left(\frac{\Delta p}{\Delta t} \right)_{pseudo} \quad (5-60)$$

where $(\Delta p / \Delta t)_{pseudo}$ is estimated using Eq. 5-53 or from field data. The following example will clarify the Δp_q plot type of solution.

Example 5-10 *Analyzing Single-Phase and Single-Rate Pressure Buildup Test Using Δp Plot in Finite Reservoir*

Rework the buildup data in Example 5-2 using Δp_q plotting technique, assuming the well was in pseudo-steady state at time of shut-in and that the flowing tubing head pressure decline was about 45 psi/day (1.66 psi/hr). The well will drain a 45-acre drainage area. Determine the following:

1. Permeability, k
2. Pressure drop due to skin, $(\Delta p)_{skin}$
3. Skin factor.

Solution First prepare a plot of Δp_q versus Δt on semilog graph paper and find slope m of the straight-line portion of the plot. The Δp plot is shown in Figure 5-17. The Δp_q values were calculated using Eq. 5-59; sample calculations are shown below and results are tabulated in Table 5-6.

$$\Delta t = 1 \text{ hr}, \quad p_{ws} = 4103 \text{ psi}$$

$$\Delta p_q = 4203 - 3519 + (1)(1.88) = 685.88 \text{ psi at 1 hr}$$

$$\Delta t = 2 \text{ hours}, \quad p_{ws} = 4250 \text{ psi}$$

$$\Delta p_q = 4250 - 3519 + (2)(1.88) = 734.76 \text{ psi at 2 hours}$$

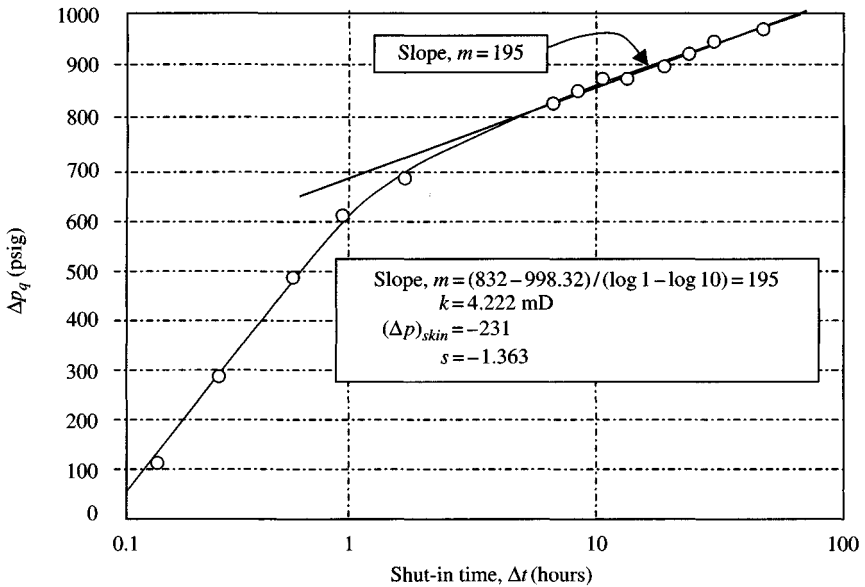


Figure 5-17.

1. Calculate the permeability k using Eq. 5-57:

$$k = \frac{162.6(350)(0.65)(1.224)}{55(195)} = 4.222 \text{ mD}$$

2. Using Eq. 5-60 and

$$(\Delta p)_{skin} = p_{ws} - p_{wf}(\Delta t = 0) - 0.869(m)(0.5)[\ln(\Delta t_D) + 0.809]$$

where m is the slope of the straight line and

$$\Delta t_D = \frac{0.000264k \Delta t}{\phi \mu_o c_t r_w^2} = \frac{0.000264(4.222)(1)}{0.1(0.65)(17.7 \times 10^{-6})(0.21)^2} = 21,968.32$$

$$\begin{aligned} \text{Therefore, } (\Delta p)_{skin} &= 4203 - 3519 - 0.869(195)(0.5)[\ln(21968.32)] \\ &= -231 \end{aligned}$$

3. Calculate the skin factor using Eq. 5-58:

$$s = \frac{(\Delta p)_{skin}}{0.869m} = \frac{-231}{0.869 \times 195} = -1.363$$

Table 5-6
Pressure Buildup Data

Time Δt (hr)	Time Δt (min)	Shut-in pressure, p_{ws} (psig)	$p_{ws} - p_{wf}$ (psig)	$\Delta p_q = p_{ws} - p_{wf} + \Delta t \left(\frac{\Delta p}{\Delta t} \right)_{pseudo}$ (psig)
0	0	3519	0	0.0
0.15	9	3680	161	161.3
0.20	12	3723	204	204.4
0.30	18	3800	281	281.6
0.40	24	3866	347	347.8
0.50	30	3920	601	601.9
1	60	4103	689	686.0*
2	100	4250	731	735.0*
4	240	4320	801	808.5
6	360	4340	821	832.3
7	420	4344	825	838.2
8	480	4350	821	836.0
12	720	4364	845	867.6
16	960	4373	854	884.1
20	1200	4379	860	897.6
24	1440	4384	865	910.0
30	1800	4393	869	925.4
40	2400	4398	879	954.2
50	3000	4402	883	977.0
60	3600	4405	886	998.8
72	4320	4407	888	1023.4

4. For the beginning of pseudo-steady state using Eq. 5-59:

$$t_s = 948 \frac{\phi \mu_o c_t r_e^2}{k} = 948 \frac{0.1(0.65)(17.7 \times 10^{-6})(1520)^2}{4.222} = 619.52 \text{ hours}$$

5.6 Multiphase Buildup Test Analysis

Basic buildup equations can be modified to model multiphase flow. For an infinite-acting reservoir, the buildup equation becomes

$$p_{ws} = p_i - \frac{162.6q_t}{\lambda_i h} \log \left(\frac{t_p + \Delta t}{\Delta t} \right) \quad (5-61)$$

Table 5-6
Pressure Buildup Data

Time Δt (hr)	Time Δt (min)	Shut-in pressure, p_{ws} (psig)	$p_{ws} - p_{wf}$ (psig)	$\Delta p_q = p_{ws} - p_{wf} + \Delta t \left(\frac{\Delta p}{\Delta t} \right)_{pseudo}$ (psig)
0	0	3519	0	0.0
0.15	9	3680	161	161.3
0.20	12	3723	204	204.4
0.30	18	3800	281	281.6
0.40	24	3866	347	347.8
0.50	30	3920	601	601.9
1	60	4103	689	686.0*
2	100	4250	731	735.0*
4	240	4320	801	808.5
6	360	4340	821	832.3
7	420	4344	825	838.2
8	480	4350	821	836.0
12	720	4364	845	867.6
16	960	4373	854	884.1
20	1200	4379	860	897.6
24	1440	4384	865	910.0
30	1800	4393	869	925.4
40	2400	4398	879	954.2
50	3000	4402	883	977.0
60	3600	4405	886	998.8
72	4320	4407	888	1023.4

4. For the beginning of pseudo-steady state using Eq. 5-59:

$$t_s = 948 \frac{\phi \mu_o c_t r_e^2}{k} = 948 \frac{0.1(0.65)(17.7 \times 10^{-6})(1520)^2}{4.222} = 619.52 \text{ hours}$$

5.6 Multiphase Buildup Test Analysis

Basic buildup equations can be modified to model multiphase flow. For an infinite-acting reservoir, the buildup equation becomes

$$p_{ws} = p_i - \frac{162.6q_t}{\lambda_i h} \log \left(\frac{t_p + \Delta t}{\Delta t} \right) \quad (5-61)$$

where

q_t = total flow rates of oil, gas, and water (bbl/day) and is given by

$$q_t = q_o\beta_o + \left(q_g - \frac{q_o R_s}{1000} \right) \beta_g + q_w\beta_w \quad (5-62)$$

q_o = oil flow rate (stb/day)

β_o = oil formation volume factor (rb/stb)

q_g = gas flow rate (mscf/day)

R_s = solution gas oil ratio (scf/stb)

β_g = gas formation volume factor (rb/mscf)

q_w = water flow rate (stb/day)

β_w = water formation volume factor (rb/stb)

λ_t = total mobility (mD/cP) and is given by

$$\lambda_t = \frac{k_o}{\mu_o} + \frac{k_g}{\mu_g} + \frac{k_w}{k_w} \quad (5-63)$$

Total system compressibility c_t is estimated by using the equation:

$$c_t = s_o c_o + s_w c_w + s_g c_g + c_f \quad (5-64)$$

It can be determined from the slope m of a buildup test run on a well that produces two or three phases simultaneously by the following equation:

$$\lambda_t = \frac{162.6q_{Rt}}{mh} \quad (5-65)$$

Perrine¹⁶ has shown that it is also possible to estimate the permeability to each phase flowing from the same slope, m :

$$k_o = \frac{162.6q_o\mu_o}{mh} \quad (5-66)$$

$$k_g = \frac{162.6 \left[q_g - \frac{q_o R_s}{1000} \right] \beta_g \mu_g}{mh} \quad (5-67)$$

and

$$k_w = \frac{162.6q_w\mu_w}{mh} \quad (5-68)$$

The skin factor s is estimated using the following equation:

$$s = 1.151 \left[\frac{p_{1hr} - p_{wf}}{m} - \log \left(\frac{\lambda_t}{\phi c_t r_w^2} \right) + 3.23 \right] \quad (5-69)$$

where c_o is given by

$$c_o = \frac{\beta_g}{\beta_o} \frac{dR_s}{dp} - \frac{1}{\beta_o} \frac{d\beta_o}{dp} \quad (\text{psi}^{-1}) \quad (5-70)$$

Values of (dR_s/dp) and $(d\beta_o/dp)$ are obtained as the slopes of laboratory determined curves of R_s and β_o versus p ; the slope is drawn at the estimated average pressure:

$$\lambda_t = \left[\frac{k}{\mu} \right]_t = \frac{162.6}{m} [q_t] \quad (5-71)$$

Applications of these equations are illustrated by the following example. Average reservoir pressure, \bar{p} , is calculated just as for a single-phase reservoir.

Example 5-11 Analyzing Multiphase Pressure Buildup Test

A buildup test is run in an oil well that is below saturation pressure and producing oil, gas, and water simultaneously. Well, rock, and fluid properties evaluated at average reservoir pressure during the test include the following. The pressure buildup data were recorded in Table 5-7.

Table 5-7
Multiphase Pressure Buildup Analysis (Single-Rate Test; $t_p = 3232.65$ h)

Time, Δt (hr)	$\frac{(t_p + \Delta t)}{\Delta t}$	$\frac{\Delta t}{[(1 + \Delta t)/t_p]}$	P_{ws} (psig)	$(P_{ws} - P_{wfo})$ (psig)	P_{ws} (psia)	$(P_{ws} - P_{wfo})$ (psia)	r_i (ft)
0.00	—	—	497	0	512	0	0
0.25	12,931.61	0.25	558	61	573	61	25
0.40	8082.63	0.40	637	140	652	140	32
0.60	5388.76	0.60	667	170	682	170	39
1.00	3233.65	1.00	696	199	711	199	51
2.00	1617.33	2.00	734	237	749	237	72
3.00	1078.55	3.00	759	262	774	262	88
4.00	809.16	4.00	779	282	794	282	102
5.00	647.53	4.99	793	296	808	296	114
6.00	539.78	5.99	806	309	821	309	125
7.00	462.81	6.98	818	321	833	321	135
8.00	405.08	7.98	827	330	842	330	144
9.00	360.18	8.98	837	340	852	340	153
10.00	324.27	9.97	845	348	860	348	161
11.00	294.88	10.96	854	357	869	357	169
12.00	270.39	11.96	861	364	876	364	176

$q_o = 245$ stb/day, $q_g = 489$ mscf/day, $q_w = 38$ stb/day, $R_s = 685$ scf/stb, $\beta_o = 1.300$ rb/stb, $\beta_g = 1.4801$ rb/mscf, $\beta_w = 1.02$ rb/stb, $c_o = 8.64 \times 10^{-6}$ psi⁻¹, $c_g = 3.70 \times 10^{-4}$ psi⁻¹, $c_w = 3.60 \times 10^{-6}$ psi⁻¹, $c_f = 3.50 \times 10^{-6}$ psi⁻¹, $s_o = 64\%$, $s_g = 2\%$, $s_w = 34\%$, $h = 38$ ft, $\phi = 17\%$, $r_w = 0.30$ ft, $r_e = 1520$ ft, $\mu_o = 1.5$ cP, $\mu_g = 0.0299$ cP, and $\mu_w = -0.70$ cP. Estimate the multi-phase flow permeabilities, s , and flow efficiency based on the average pressure.

Solution From plots of β_o , R_s versus pressure at average pressure in the buildup test:

$$\frac{dR_s}{dp} = 0.0776 \text{ scf}/(\text{stb}/\text{psi}) \quad \text{and} \quad \frac{d\beta_o}{dp} = 2.48 \times 10^{-6} \text{ rb}/(\text{stb}/\text{psi})$$

The production rates prior to the buildup test were given. From the plot of p_{ws} versus $\log((t_p + \Delta t)/\Delta t)$ (Figure 5-18), the slope of the MTR, m , is 120 psi/cycle and that p_{1hr} , at the instant of shut-in, was 497 psig. From these data, the following reservoir parameters can be estimated as follows:

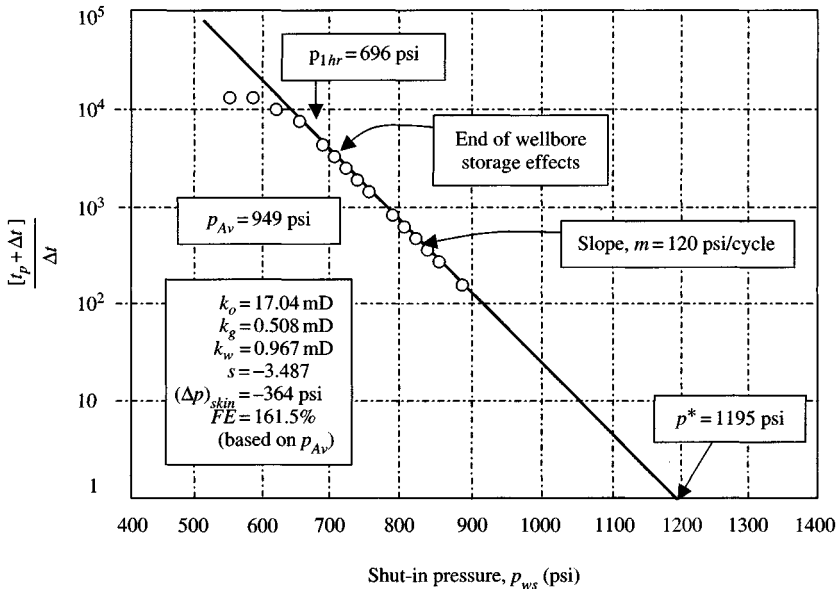


Figure 5-18. Multiphase pressure buildup data plot.

Permeability to each phase can be determined from the slope of the MTR using Eqs. 5-66 through 5-68

$$k_o = \frac{162.6q_o\mu_o\beta_o}{mh} = \frac{162.6(245)(1.300)(1.5)}{120(38)} = 17.04 \text{ mD}$$

$$k_w = \frac{162.6q_w\mu_w\beta_w}{mh} = \frac{162.6(38)(1.02)(0.70)}{120(38)} = 0.967 \text{ mD}$$

$$k_g = \frac{162.6\left(q_g - \frac{q_o R_s}{1000}\right)\mu_g\beta_g}{mh} = \frac{162.6\left(489 - \frac{245(685)}{1000}\right)(1.300)(1.5)}{120(38)} = 0.508 \text{ mD}$$

To calculate the total mobility, λ_t , we first need the total flow rate q_t using Eq. 5-62:

$$\begin{aligned} q_t &= q_o\beta_o + \left(q_g - \frac{q_o R_s}{1000}\right)\beta_g + q_w\beta_w \\ &= 245 \times 1.3 + \left(489 - \frac{(245 \times 685)}{1000}\right) \times 1.480 + 38 \times 1.02 \\ &= 793.84 \text{ rb/day} \end{aligned}$$

Then using Eq. 5-65,

$$\lambda_t = \frac{162.6q_t}{mh} = \frac{162.6(793.84)}{120(38)} = 28.31 \text{ mD/cP}$$

To calculate the skin factor s , we first need c_o and c_f :

$$\begin{aligned} c_o &= \frac{\beta_g}{\beta_o} \frac{dR_s}{dp} - \frac{1}{\beta_o} \frac{d\beta_o}{dp} = \frac{1.480}{1.30} (0.0776) - \frac{1}{1.30} (2.48 \times 10^{-6}) \\ &= 9.64 \times 10^{-6} \text{ psi}^{-1} \end{aligned}$$

Then from Eq. 5-64,

$$\begin{aligned} c_t &= s_o c_o + s_g c_g + s_w c_w + c_f = 0.64(8.64 \times 10^{-6}) + 0.02(3.90 \times 10^{-4}) \\ &\quad + 0.34(3.60 \times 10^{-6} + 3.5 \times 10^{-6}) = 6.78 \times 10^{-5} \text{ psi}^{-1} \end{aligned}$$

and from Eq. 5-69,

$$\begin{aligned} s &= 1.151 \left[\frac{p_{1h} - p_{wf}}{m} - \log \left(\frac{\lambda_t}{\phi c_t r_w^2} \right) + 3.23 \right] \\ &= 1.151 \left[\frac{696 - 497}{120} \log \left(\frac{28.31}{0.17 \times 6.78 \times 10^{-5} \times (0.3)^2} \right) + 3.23 \right] = -3.49 \end{aligned}$$

5.7 Afterflow Analysis Using Russel's Technique

Russell² presented a theoretical method for analyzing the pressure response during the afterflow period in order to determine kh and s . In some cases, however, afterflow analysis provides a valuable means of obtaining information about the reservoir. For instance, in several areas in the Middle East, wells are capable of producing in excess of 50,000 mbbbl from limestone reservoirs. Because of very high kh values, which lead to very rapid pressure buildups, and the fact that in many cases the wells produce through casing, the afterflow period can completely dominate the pressure buildup and afterflow analysis is the only method of determining the essential reservoir parameters. Figure 5-19 shows the pressure buildup dominated by afterflow which distorts the early part of the Horner buildup plot.

McKinly,^{18,21} Ramey and Cobb,¹² and Earlougher and Kersch¹⁹ have also presented afterflow analysis technique relying on the use of type curves. Of all these methods, which is the most reliable is a question that is still unanswered. Afterflow analysis by type curves matching techniques as discussed in Chapter 7. The analysis method that will be described in this section is of Russell.² He developed a theoretical equation describing how the bottom-hole pressure should increase as fluid accumulates in the well-bore during the buildup. As a result of this, he determined that the correct way of plotting the pressure during the part of the buildup influenced by the afterflow was

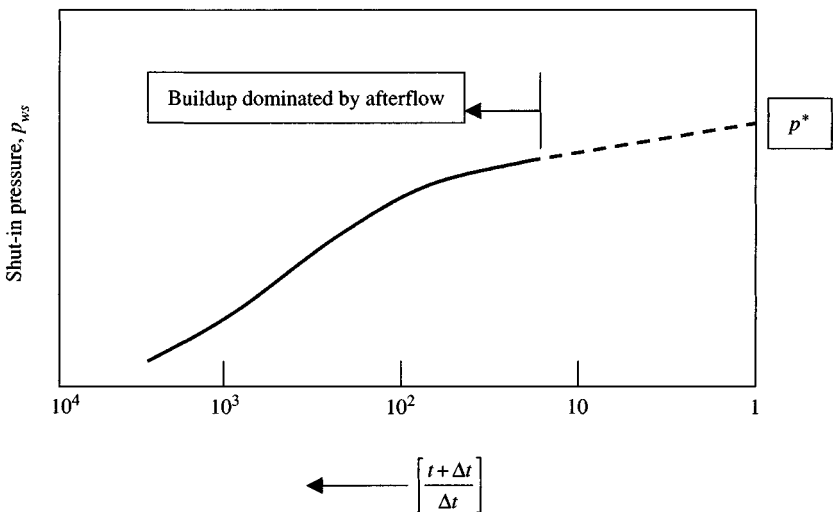


Figure 5-19. Pressure buildup plot dominated by afterflow.

$$\frac{\Delta p}{1 - \frac{1}{CF\Delta t}} \text{ versus } \log \Delta t \quad (5-72)$$

in which $\Delta p = p_{ws} - p_{wf}(\Delta t = 0)$, CF is a correction factor to allow for the gradually decreasing flow into the wellbore. This correction factor, CF , must be selected by trial and error so that the resulting plot is linear. The plot should be made only for values of Δt measured after 1 hour of closed I time. Having chosen the correct values of CF , the slope of the straight line is measured ($m = \text{psi}/\log \text{ cycle}$) and the formation permeability can be determined using the following equation:

$$kh = \frac{162.6q_o\mu_o\beta_o}{m} \quad (5-73)$$

The skin factor s can be calculated using Eq. 5-74:

$$s = 1.151 \left[\frac{p_{ws}(1 \text{ hr}) - p_{wf}}{\frac{1-CF\Delta t}{m}} - \log \left(\frac{k}{\phi\mu_o c_t r_w^2} \right) + 3.23 \right] \quad (5-74)$$

The following example illustrates the use of this method.

Example 5-12 *Analyzing Afterflow Pressure Buildup Test Using Russell's Technique*

The pressure-time data were recorded in a 12-hours pressure buildup test and are listed in Table 5-8. The production data, reservoir, and fluid properties are as follows: $N_p = 30,655$ stb, $q_o = 225$ stb/day, $\beta_o = 1.295$, $\mu_o = 0.58$ cP, $\phi = 0.19$, $c_t = 18.5 \times 10^{-6}$ psi⁻¹, $h = 12$ ft, $r_w = 0.29$ ft.

Horner plot versus $\log((t_p + \Delta t)/\Delta t)$ does not become linear, even for the largest values of Δt , and therefore the afterflow analysis techniques must be used to analyze this test. Estimate the formation permeability and skin factor s using Russell's technique.

Solution This technique to analyze afterflow as suggested by Russell² (1966) can only be applied for pressures measured after $\Delta t = 1$ hour. In Table 5-9, several values of the parameters or correlation factor c have been selected in an attempt to liberalize the plot of Eq. 5-72.

As shown in Figure 5-20, the correct value of parameter c to obtain a linear Russell's plot is $c = 2.1$. Since the slope of this line is 151 psi/log cycle, then the formation permeability k can be evaluated using Eq. 5-73 as

$$k = \frac{162.6q_o\mu_o\beta_o}{mh} = \frac{162.6 \times 225 \times 0.58 \times 1.295}{151 \times 12} = 15.17 \text{ mD}$$

Table 5-8
Pressure Buildup Data for Afterflow Analysis

Shut-in time, Δt (min)	Shut-in pressure, p_{ws} (psi)
0	1600
20	1920
40	2160
60	2350
90	2525
120	2650
150	2726
180	2779
210	2822
240	2852
270	2879
300	2910
360	2935
420	2960
480	2980
540	2998
600	3011
660	3022
720	3035

The value of $(\Delta p/(1 - 1/c\Delta t))$ at $\Delta t = 1$ hour can be read from the linear plot as 1329 psi. Therefore the skin factor can be calculated using Eq. 5-74 as

$$\begin{aligned}
 s &= 1.151 \left[\frac{p_{ws}(\Delta t=1 \text{ hr}) - p_{wf}}{\frac{1 - \frac{1}{c\Delta t}}{m}} - \log \left(\frac{k}{\phi \mu_o c_t r_w^2} \right) + 3.23 \right] \\
 &= 1.151 \left[\frac{1329}{151} - \log \left(\frac{15.17}{0.19(0.58)(18.5 \times 10^{-6})(0.29)^2} \right) \right] = 4.70
 \end{aligned}$$

5.8 Pressure Buildup Tests Preceded by Two Different Flow Rates

Pressure buildup behavior preceded by two different flow rates can be described as

$$p_{ws} = p_i - \frac{162.6q_2\mu_o\beta_o}{kh} \left[\frac{q_1}{q_2} \log \left(\frac{t}{t-t_1} \right) + \log \left(\frac{t-t_1}{t-t_2} \right) \right] \quad (5-75)$$

Table 5-9
Afterflow Analysis Using Russell's Techniques

$$F = \frac{\Delta p}{1 - \frac{c}{c\Delta t}}$$

Δt (min)	p_{ws} (psig)	Δt (hr)	$\log \Delta t$	$\Delta = (p_{ws} - p_{wf})$ (psig)	$c = 1.50$	$c = 1.70$	$c = 2.0$	$c = 2.1$	$c = 2.5$	$c = 3.0$
0	1600	0	-	0	-	-	-	-	-	-
60	2350	1.00	0	750	2250	1820	1500	1431	1250	1125
90	2525	1.50	0.1761	925	1665	1522	1388	1355	1261	1189
120	2650	2.50	0.3010	1050	1575	1488	1400	1378	1303	1260
150	2726	3.00	0.3929	1126	1535	1472	1408	1391	1270	1299
180	2777	3.50	0.4770	1179	1516	1467	1415	1401	1360	1326
210	2827	3.50	0.5440	1222	1510	1469	1426	1414	1380	1351
240	2852	4.00	0.6020	1252	1502	1468	1431	1421	1391	1366
270	2879	4.50	0.6531	1279	1501	1471	1439	1430	1404	1380
300	2900	5.00	0.6988	1300	1500	1473	1444	1432	1413	1393
360	2935	6.00	0.7780	1335	1502	1480	1456	1450	1430	1414
420	2960	7.00	0.8449	1360	1503	1485	1465	1459	1442	1428
480	2980	8.00	0.9020	1380	1505	1490	1472	1467	1453	1440
540	2998	9.00	0.9541	1378	1510	1496	1480	1476	1463	1452
600	3011	10.00	0.9998	1400	1512	1490	1485	1482	1470	1460
660	3022	11.00	1.0412	1422	1514	1502	1490	1486	1476	1466
720	3035	12.00	1.0790	1435	1519	1509	1497	1494	1484	1476

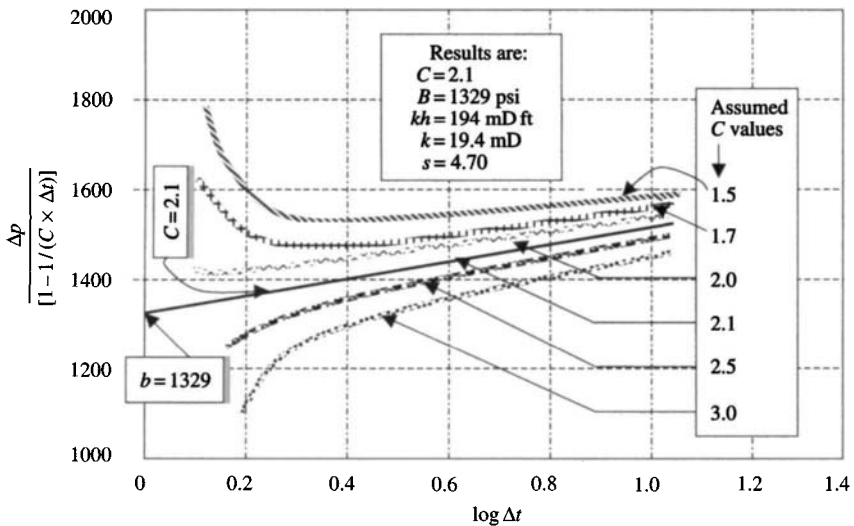


Figure 5-20. Russell afterflow analysis plot.

where

$$t - t_2 = \Delta t,$$

$$t_1 = t_{p1},$$

$$t_2 = t_{p1} + t_{p2}, \text{ and}$$

$$t - t_1 = t_{p2} + \Delta t, \text{ then}$$

$$p_{ws} = p_i - \frac{162.6q_2\mu_o\beta_o}{kh} \left[\frac{q_1}{q_2} \log \left(\frac{t_{p1} + t_{p2} + \Delta t}{t_{p2} + \Delta t} \right) + \log \left(\frac{t_{p2} + \Delta t}{\Delta t} \right) \right] \quad (5-76)$$

Eq. 5-76 can be used, when the producing rate is changed a short time before the buildup test begins, so that there is not sufficient time for Horner's approximation to be valid. All production before time t_1 is at rate q_1 for time t_{p1} and production just before the test to have been at rate q_2 for time t_{p2} . Upon simplification, Eq. 5-76 becomes

$$p_{ws} = p_i - \frac{162.6q_2\mu_o\beta_o}{kh} \left[\frac{q_1}{q_2} \log \left(\frac{t_{p1} + t_{p2} + \Delta t}{t_{p2} + \Delta t} \right) + \log \left(\frac{t_{p2} + \Delta t}{\Delta t} \right) \right] \quad (5-77)$$

Hence a plot of

$$p_{ws} \text{ versus } \left[\frac{q_1}{q_2} \log \left(\frac{t_{p1} + t_{p2} + \Delta t}{t_{p2} + \Delta t} \right) + \log \left(\frac{t_{p2} + \Delta t}{\Delta t} \right) \right]$$

on Cartesian coordinates should give a straight line of slope, m , from which

$$k = \frac{162.6q_1\mu_o\beta_o}{mh} \quad (5-78)$$

Extrapolation of this line to zero will give $p_{ws} = p_i$ to calculate the skin factor, s ; note that at the end of the flow period just before shut-in

$$p_i - p_{wf} = m \left[\frac{q_1}{q_2} \log \left(\frac{t_{p1} + t_{p2}}{t_{p2}} \right) + \log(t_{p2}) + s \right] \quad (5-79)$$

The equation of the MTR line on the buildup test plot is

$$p_i - p_{ws} = m \left[\frac{q_1}{q_2} \log \left(\frac{t_{p1} + t_{p2} + \Delta t}{t_{p2} + \Delta t} \right) + \log \left(\frac{t_{p2} - \Delta t}{\Delta t} \right) \right] \quad (5-80)$$

Subtracting Eq. 5-80 from Eq. 5-79, we get

$$p_{ws} - p_{wf} = m \left\{ \frac{q_1}{q_2} \log \left[\frac{(t_{p1} + t_{p2})(t_{p2} + \Delta t)}{(t_{p1} + t_{p2} + \Delta t)(t_{p2})} + \log \left[\frac{(t_{p2})(\Delta t)}{t_{p2} + \Delta t} \right] + s \right] \right\} \quad (5-81)$$

Assuming $t_{p1} + t_{p2} + \Delta t = t_{p1} + t_{p2}$ and $t_{p2} + \Delta t = t_{p2}$ for small Δt (e.g., $\Delta t = 1$ hr), then $p_{ws} - p_{wf} = m(\log \Delta t + s)$.

If we choose $\Delta t = 1$ hr, $p_{ws} = p_{1hr}$ (on the MTR line) and, for $t_{p2} \gg 1$,

$$s = 1.151 \left[\left(\frac{q_1}{q_1 - q_2} \right) \frac{p_{1hr} - p_{wf}}{m} - \log \left(\frac{k}{\phi\mu_o c_t r_w^2} \right) + 3.23 \right] \quad (5-82)$$

and

$$p_i = p_{ws(\Delta t=0)} + m \left[\log \left(\frac{kt_p}{\phi\mu_o c_t r_w^2} \right) - 3.23 + 0.869s \right] \quad (5-83)$$

The duration of wellbore storage distortion is calculated as in the previous analysis for buildup test.

Example 5-13 Analyzing Two-Rate Pressure Buildup Test

A two-rate flow test was run on a well with properties given below. From these properties and the data given in Table 5-10, determine k , s , and p_i .

Cumulative oil production = 32,000 stb, first stabilization oil rate, $q_1 = 85$ stb/day, stabilized gas rate, $q_{g1} = 590$ mscf/day, second stabilized oil rate, $q_2 = 50$ stb/day, second gas rate, $q_{g2} = 390.2$ mscf/day, pressure at

Table 5-10
Two-Rate Buildup Test Analyses

Shut-in time, Δt , (hr)	Shut-in pressure, p_{ws} (psig)	Shut-in pressure, p_{ws} , (psia)	$\frac{(t_p + \Delta t)}{\Delta t}$	$\frac{\log(t_p + \Delta t)}{\Delta t} + \frac{q_2}{q_1} \log(\Delta t)$
0.50	3245	3260	18,071.59	4.0792
1.00	3285	3300	9036.29	3.9553
1.50	3310	3325	6024.53	3.8828
2.00	3330	3345	4518.65	3.8314
3.00	3355	3370	3012.76	3.7589
4.00	3375	3390	2259.82	3.7076
5.00	3390	3405	1808.06	3.6677
6.00	3405	3420	1506.88	3.6352
7.00	3425	3440	1291.76	3.6076
8.00	3440	3455	1130.41	3.5838
10.00	3465	3480	904.53	3.5440
15.00	3515	3530	603.35	3.4718
20.00	3545	3560	452.76	3.4206

time of rate change, $p_{wf} = 3200$ psia, $\phi = 0.14$, $h = 11$ ft, $\mu_o = 0.43$ cP, $\beta_o = 1.450$ rb/stb, $c_t = 5.72 \times 10^{-5}$ psi $^{-1}$, $r_w = 0.33$, $r_e = 550$ ft.

Solution Apparent producing time, t_p , is $t_p = (32,000/85) \times 24 = 9035.29$ h. Well pressure at time rate changed from q_1 to q_2 is 3200 psia. Figure 5-21 is a plot of well pressure versus plotting function X of the data of Table 5-10. From Figure 5-21, the following information is obtained: $m = 650$ psi/cycle and $p_{1hr} = 3212$ psia. Substituting the given reservoir and fluid properties in the expression for m , and by Eq. 5-78:

$$k = \frac{162.6q_1\mu_o\beta_o}{mh} = \frac{162.6(85)(1.450)(0.43)}{650(11)} = 1.21 \text{ mD}$$

Using Eq. 5-82, the skin factor is

$$\begin{aligned}
 s &= 1.515 \left[\left(\frac{q_1}{q_1 - q_2} \right) \frac{p_{1hr} - p_{ws \text{ at rate changed}}}{m} - \log \left(\frac{k}{\phi \mu_o c_t r_w^2} \right) + 3.23 \right] \\
 &= 1.515 \left[\frac{85}{85 - 50} \frac{3212 - 3200}{650} - \log \left(\frac{1.21}{(0.14)(0.43)(5.72 \times 10^{-5})(0.21)^2} \right) \right. \\
 &\quad \left. + 3.23 \right] = -4.18
 \end{aligned}$$

Using Eq. 5-83, calculate the initial pressure p_i as

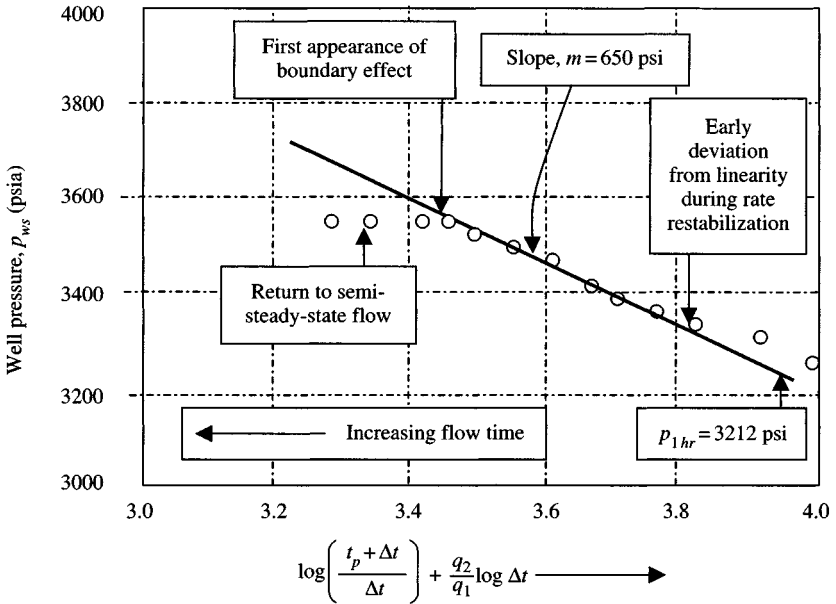


Figure 5-21. Plot of well pressure versus plotting function X.

$$\begin{aligned}
 p_i &= 3200 + 650 \left[\log \left(\frac{1.21(9035.29)}{0.14(0.43)(5.72 \times 10^{-5})(0.21)^2} \right) \right. \\
 &\quad \left. - 3.23 + 0.869(-4.18) \right] \\
 &= 3200 + 650[10.86 - 3.23 - 3.63] = 5800 \text{ psia}
 \end{aligned}$$

5.9 Variable-Rate Pressure Buildup Analysis

The pressure buildup behavior is described by

$$\begin{aligned}
 p_i - p_{ws} &= 162.6 \frac{q_{n-1} \mu_o \beta_o}{kh} \left[\frac{q_1}{q_{n-1}} \log \left(\frac{t}{t-t_1} \right) + \frac{q_2}{q_{n-1}} \log \left(\frac{t-t_1}{t-t_2} \right) + \dots \right. \\
 &\quad \left. + \frac{q_{n-2}}{q_{n-1}} \log \left(\frac{t-t_{n-3}}{t-t_{n-2}} \right) + \log \left(\frac{t-t_{n-2}}{t-t_{n-1}} \right) \right] \quad (5-84)
 \end{aligned}$$

where $t - t_{n-1} = \Delta t$, time after shut-in and q_{n-1} is the production rate just before shut-in. Eq. 5-84 is based on the fact that for $t = t_{p1} + t_{p2} + \dots + t_{pn-1} + (t - t_{n-1})$ the reservoir is infinite-acting. The following analysis

procedure can be used. Plot p_{ws} versus X on ordinary (Cartesian coordinate) graph paper, where plotting function X is

$$X = \sum_{j=1}^n \frac{q_j}{q_n} \log \left(\frac{t_n - t_{j-1} + \Delta t}{t_n - t_j + \Delta t} \right) \quad (5-85)$$

Determine the slope m of the plot and calculate the formation permeability by the equation

$$k = \frac{162.6 q_{n-1} \mu_o \beta_o}{m h} \quad (5-86)$$

Calculate the skin factor s from the equation

$$s = 1.151 \left[\frac{p_{1hr} - p_{ws}(\Delta t = 0)}{m} - \log \left(\frac{k}{\phi \mu_o c_t r_w^2} \right) + 3.23 \right] \quad (5-87)$$

The original reservoir pressure p_i is the value of p_{ws} on the MTR line extrapolated to $X = 0$. Figure 5-22 shows the schematic representation of rate variation preceding a pressure buildup test.

Example 5-14 Analyzing Variable-Rate Pressure Buildup Test

A variable-rate flow test was run on a well with the given properties. From these properties and the data in Tables 5-11 and 5-12, determine k , s ,

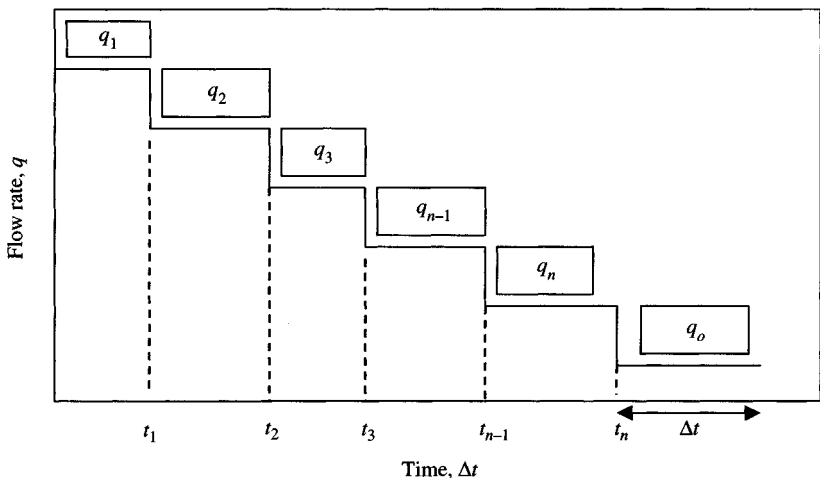


Figure 5-22. Schematic representation of rate variation preceding a pressure buildup test.

Table 5-11
Variable-Rate Buildup Test Analysis
(Pressure and Rate Data for Plotting)

Time, t_i (hr)	Rate, q_i (stb/day)
0.000	0.000
3.000	479.0
6.000	319.0
9.000	160.0
12.000	125.0
14.000	100.0
18.000	75.00

Table 5-12
Variable-Rate Buildup Test and Computations

Time, Δt (hr)	Shut-in pressure, p_{ws} (psig)	Pressure change, $p_{ws} - p_{wfo}$ (psia)	Function X $\sum \frac{q_j}{q_n} \times \log \left[\frac{(t_n - t_j - t + \Delta t)}{(t_n - t_j + \Delta t)} \right]$
0.150	2675	10.00	3.12822
0.250	2697	32.00	2.90002
0.300	2736	71.00	2.81772
0.350	2758	93.00	2.74769
0.400	2772	107.00	2.68666
0.500	2794	129.00	2.58376
0.750	2813	148.00	2.39333
1.000	2838	173.00	2.25486
1.500	2872	207.00	2.05392
2.000	2895	230.00	1.90673
3.000	2913	248.00	1.69252
5.000	2924	259.00	1.41352
7.000	2935	270.00	1.22770
9.000	2945	280.00	1.09051
11.000	2951	286.00	0.98348
13.000	2957	292.00	0.89696
15.000	2962	297.00	0.82523
17.000	2967	302.00	0.76462
19.000	2971	306.00	0.71263
21.000	2976	311.00	0.66747
23.000	2980	315.00	0.62785
25.000	2983	318.00	0.59278
27.000	3012	347.00	0.56150
29.000	3031	366.00	0.53341
31.000	3042	377.00	0.50804

$(\Delta p)_{skin}$, p^* , and flow efficiency. Well and reservoir data: depth = 5250 ft; average pressure = 3000 psi; $\mu_o = 0.80$ cP; $\beta_o = 1.136$ rb/stb; $h = 11$ ft; $\phi = 0.12$; $c_t = 17.0 \times 10^{-6}$ psi $^{-1}$; $r_w = 0.198$ ft.

Solution The plotting function X is tabulated in Table 5–12 and a plot of p_{ws} versus X is shown in Figure 5–23. Figure 5–23 shows the end of wellbore storage effects. The MTR line of the plot p_{ws} versus X has the following characteristics:

Slope in Figure 5–23 gives $m = -116.8$ psi/cycle. Using Eq. 5–86 with the last rate

$$k = \frac{162.6q_{n-1}\mu_o\beta_o}{mh} = \frac{162.6(75)(1.136)(0.80)}{116.8(11)} = 8.63 \text{ mD}$$

p_{1h} at $\Delta t = 1$ hour, $X = 2.2549 = 2823$ psi. Using Eq. 5–87,

$$\begin{aligned}
 s &= 1.151 \left[\frac{p_{1hr} - p_{ws}(\Delta t=0)}{m} - \log \left(\frac{k}{\phi\mu_o c_t r_w^2} \right) + 3.23 \right] \\
 &= 1.151 \left[\frac{2823 - 2665}{116.8} - \log \left(\frac{8.63}{0.12(0.8)(17.0 \times 10^{-6})(0.198)^2} \right) + 3.23 \right] \\
 &= -4.08
 \end{aligned}$$

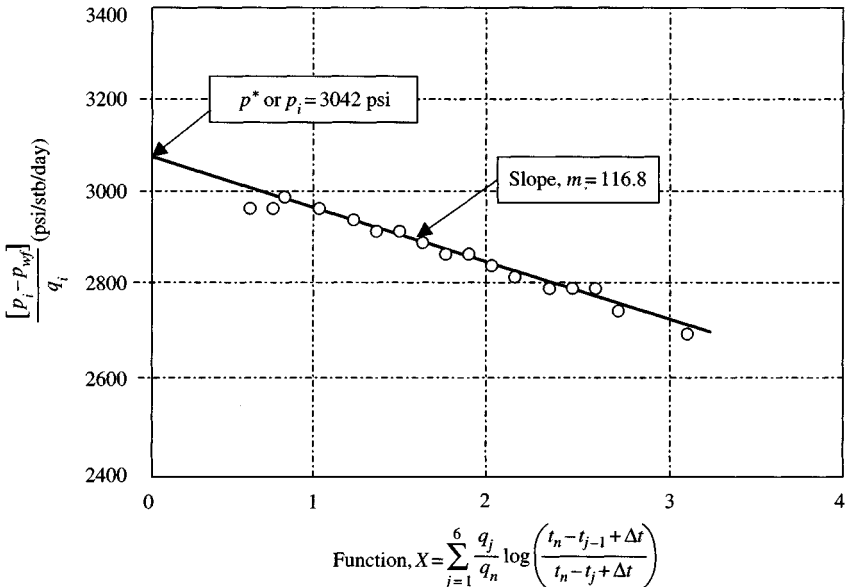


Figure 5–23. Variable-rate pressure buildup analysis plot.

Original reservoir pressure p_i at $X = 0$ is 3042 psi. The pressure drop due to skin is

$$(\Delta p)_{skin} = 0.869ms = 0.869(116.8)(-4.08) = -414.12$$

Flow efficiency based on p_i is

$$FE = \frac{p_i - p_{ws} - (\Delta p)_{skin}}{p_i - p_{ws}} = \frac{3042 - 2665 - (-414.12)}{3042 - 26,655} \times 100 = 210.0\%$$

5.10 Multi-phase, Multi-Rate Buildup Analysis

The basic equations used for multi-phase pressure buildup analysis are quite similar to those used for single phase. The basic equation is

$$p_{ws} = p_i - \frac{162.6q_n}{h(k/\mu_o)_t} \sum_{j=1}^n \frac{q_j}{q_n} \log \left[\frac{t_n + t_s - t_{j-1}}{t_n + t_s - t_j} \right] \quad (5-88)$$

where the flow rates q_1 through q_n are re-expressed in total fluids q_t (stb) as

$$q_t = q_o\beta_o + \left(q_t - \frac{q_o R_S}{1000} \right) \beta_g + q_w\mu_w$$

Eq. 5-88 is that of a straight line of the form $Y = b + mX$ where $Y = p_{ws}$ where

$$m = - \frac{162.6q_n}{h(k/\mu_o)_t}$$

$$X = \sum_{j=1}^n \frac{q_j}{q_n} \log \left(\frac{t_n + t_s - t_{j-1}}{t_n + t_s - t_j} \right)$$

$$b = p_i$$

Figure 5-24 shows a hypothetical flow history of a well. Upon shut-in, a plot of the bottom-hole shut-in pressure versus the dimensionless summation Cartesian (Eq. 5-88) assumes a characteristic shape given in Figure 5-25. After the wellbore effects have dissipated, the straight-line relationship holds and the observed slope can be translated into values of total mobility:

$$\left(\frac{k}{\mu_o} \right)_t = \frac{162.6}{mh} [q_o\beta_o + (q_g t - q_o R_S)\beta_g + q_w\beta_w] \quad (5-89)$$

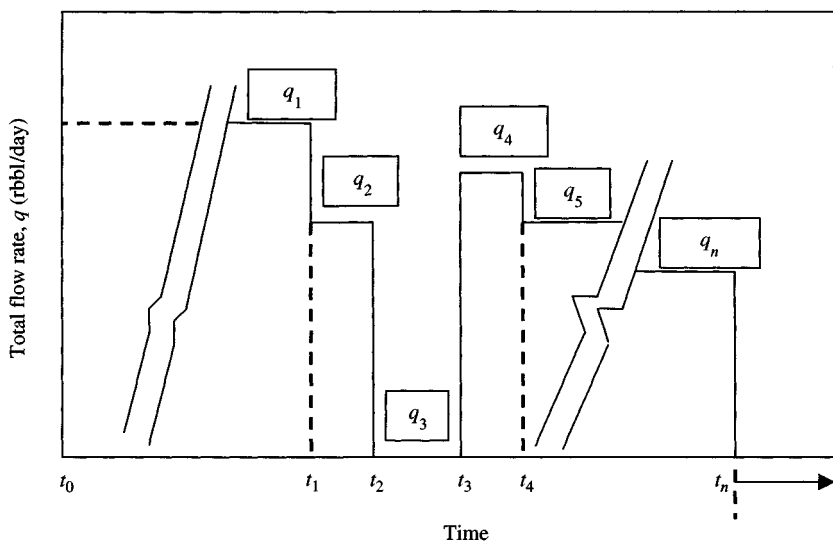


Figure 5-24. Flow history of an oil well.

The gas and oil formation volume factors are pressure-dependent. It is recommended that as a first approximation they may be selected at the highest observed pressure. Later, for subsequent runs if desired they may be selected at average pressures given below:

$$\bar{p} = \frac{p_{wf} + p^*}{2} \quad (5-90)$$

$$\beta_g = 5.01 \frac{zT}{p} \quad (\text{rb/mscf}) \quad (5-91)$$

To calculate the skin factor and its associated pressure drop, the following equations are used:

$$s = 1.151 \left[\frac{p_{1hr} - p_{wf}}{m} - \log \left(\frac{(k/\mu_o)_t F}{\phi c_i r_w^2} \right) + 3.23 \right] \quad (5-92)$$

$$(\Delta p)_{skin} = 0.869ms \quad (5-93)$$

The factor, F , in Eq. 5-92 corrects for short flow times. In most other cases, F will equal or approach to 1.

$$F = \frac{t_n}{t_n + t_s} \approx 1.0 \quad (5-94)$$

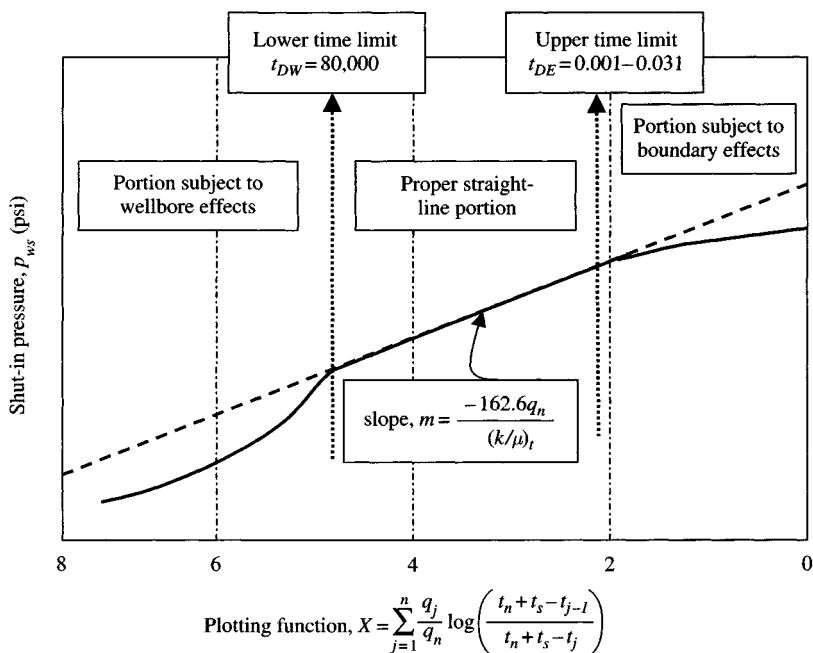


Figure 5-25. Typical pressure buildup.

In Eq. 5-92, the total compressibility, c_t , is

$$c_t = s_o c_o + s_g c_g + s_w c_w + c_f \quad (5-95)$$

For multiphase flow, below the saturation or bubble point pressure:

$$c_o = \frac{\beta_g}{\beta_o} \frac{\partial R_S}{\partial p} - \frac{1}{\beta_o} \frac{\partial \beta_o}{\partial p} \quad (5-96)$$

The gas compressibility may be estimated from correlation charts such as those given in Ref. 1. The flow efficiencies are computed on a reservoir barrel per psi basis:

$$J_{actual} = \frac{q_n}{\bar{p} - p_{wf}} \quad (5-97)$$

$$J_{ideal} = \frac{q_n}{\bar{p} - p_{wf} - (\Delta p)_{skin}} \quad (5-98)$$

The flow efficiency is the ratio of the two productivity indices:

$$FE = \frac{J_{actual}}{J_{ideal}} \times 100\% \quad (5-99)$$

The maximum radius reached by the transient test is computed at a t_{De} of 0.25 using Van Poollen's equation:²⁰

$$r_{inv} = \left(\frac{0.00105(k/\mu_o)_t t_s}{\phi c_t} \right)^{0.5} \quad (5-100)$$

Dimensionless times calculated to select the proper straight-line limits are computed from:

$$\text{Upper time limit: } t_{De} = \frac{0.000264(k/\mu_o)_t t_s}{\phi c_t r_e^2} \quad (5-101)$$

$$\text{Lower time limit: } t_{De} = \frac{0.000264(k/\mu_o)_t t_s}{\phi c_t r_w^2} \quad (5-102)$$

Example 5-15 *Analyzing MultiPhase, Multi-Rate Pressure Buildup Test*

Rate history and pressure buildup data are given in Tables 5-13 through 5-19. Other reservoir and well data follow: $\phi = 0.235$, $r_w = 0.23$ ft, $h = 13$ ft, $\mu_o = 1.27$ cP, $\mu_g = 0.016$ cP, $\mu_w = 0.30$ cP, drainage area = 17.8 acres, bottom-hole pressure = 1253 psi, total compressibility, $c_t = 3.2 \times 10^{-6}$ psi⁻¹, last flowing bottom-hole pressure = 1257 psi, cumulative oil production = 997,567 stb at shut-in, cumulative water production = 50,000 stb at shut-in, cumulative gas production = 1,200,000 mscf at shut-in.

Solution Lower and upper limits can be found by plotting $\log(p_{ws} - p_{wf})$ versus log time. The beginning of the straight line can be estimated by one of the two methods:

- By the one and one-half log cycle rule or by the type curve overlay method;

Table 5-13
Rate History

Flowing time (days)	Oil rate (rb/day)	Gas rate (mscf/day)	Water rate (stb/day)	Solution GOR (mscf/stb)	Oil FVF (rb/stb)	Gas FVF (rb/mscf)	Water FVF (rb/stb)
27	126	369	154	250	1.181	1.617	1.02
61	109	938	162	250	1.156	1.970	1.02
31	68	734	115	250	1.156	1.970	1.02
31	63	625	94	250	1.156	1.970	1.02
10	77	468	95	250	1.156	1.970	1.02

Table 5-14
Pressure Buildup Data

Shut-in time, Δt (hr)	Bottom-hole pressure, p_{ws} (psig)
0.25	1391
0.50	1401
1.00	1415
2.00	1431
3.00	1446
4.00	1455
5.00	1467
6.00	1483
12.00	1510
18.00	1522
24.00	1531
30.00	1536
36.00	1538
48.00	1548

Table 5-15
Reservoir Voidage History Calculations

Length (days)	q_o (rb/day)	q_g (rb/day)	q_w (rb/day)	Total (rb/day)	Cumulative voidage (rb)	Observed flowing time (hr)
27	148.8	545.7	157.1	851.6	4,290,679	120,917.7
61	128.0	1794.2	165.2	2085.4	4,417,890	122,381.7
31	78.6	1412.5	117.3	1608.4	4,467,750	123,125.7
31	72.8	1200.2	95.9	1368.9	4,510,187	123,869.7
10	89.0	884.0	96.9	1069.9	4,520,886	124,109.7

- The area shape selected has an upper limit for the straight line of $t_{De} \cong 0.0240$. Results with calculated t_{De} higher than this should be disregarded or used with caution.

From Figure 5-26, lower and upper limits are 65,000 and 0.024. Figure 5-27 is a Cartesian plot showing calculated results.

5.11 Rate Normalization Techniques and Procedures (Pressure Buildup Data)

Methods to analyze afterflow-dominated pressure buildup data are presented. Total afterflow fluid rate should be used in multiphase flow analysis.

Table 5-16
Bottom-Hole Pressure at Corresponding Shut-In Times

Pressure buildup test data			Computed data	
Test point No.	Shut-in time, Δt (hr)	Shut-in pressure, p_{ws} (psi)	Computed dimensionless summation function X	$\Delta p = (p_{ws} - 1253)$ (psi)
1	0.25	1391	5.92	138.2
2	0.50	1401	5.62	148.0
3	1.00	1405	5.32	162.0
4	2.00	1434	5.01	181.0
5	3.00	1446	4.84	193.0
6	4.00	1455	4.71	202.0
7	5.00	1467	4.61	214.0
8	6.00	1483	4.54	230.0
9	12.00	1510	4.23	252.0
10	18.00	1522	4.05	269.0
11	24.00	1538	3.92	278.0
12	30.00	1536	3.82	283.0
13	36.00	1538	3.74	285.0
14	42.00	1541	3.67	288.0
15	48.00	1543	3.61	290.0

Table 5-17
Pressure Buildup Test Data — Calculated Results by Computer

Point used	Slope m (psi/cycle)	Total mobility (mD/cP)	p^* (psi)	\bar{p} (psi)	PI		FE (%)	Skin factor, s
					Actual	Ideal		
1-4	47.50	32.41	1669	1480	4.702	3.74	126	-1.41
2-5	57.90	26.59	1724	1490	4.350	3.09	142	-2.03
3-6	60.05	23.31	1765	1512	4.130	2.69	154	-2.41
4-7	80.14	19.21	1834	1533	3.810	2.23	192	-2.30
5-8	119.43	12.88	2021	1573	3.140	1.49	211	-3.65
6-9	112.90	13.64	1989	1580	3.250	1.57	207	-3.57
7-10	94.05	26.37	1925	1558	3.500	1.89	185	-3.19
8-11	78.59	19.59	1840	1540	3.600	2.26	162	-2.66
9-12	68.72	23.79	1784	1535	3.790	2.24	138	-1.91
10-13	52.48	29.24	1735	1579	3.870	3.30	114	-0.88
12-14	38.48	40.21	1680	1526	3.900	4.60	85	1.23
12-15	33.48	45.99	1663	1526	3.920	5.30	74	2.44

Table 5-18
Average Values

Slope, m (psi/cycle)	70.31
Total mobility, λ_t (mD/cP)	26.10
False pressure, p^* (psi)	1804.42
Average reservoir pressure, \bar{p}	1533.00
Productivity index (actual)	3.83
Productivity index (ideal)	2.87
Flow efficiency (%)	149.00
Skin factor, s	-2.00

Table 5-19
Calculated Parameters

Pressure drop, (Δp) _{skin} (psi)	t_{De}	t_{Dw}	k_o (mD)	k_w (mD)	k_g (mD)	Maximum radius reached (ft)
-58.3	0.00924	5433	3.42	0.88	0.43	95
-102.4	0.01137	8916	2.81	0.70	0.35	106
-138.6	0.01328	15,630	2.46	0.63	0.31	114
-201.9	0.01369	25,765	2.03	0.52	0.25	116
-379.2	0.01102	25,935	1.36	0.35	0.17	104
-350.9	0.02332	365,580	1.44	0.37	0.18	151
-260.8	0.04198	54,887	1.73	0.45	0.22	203
-181.7	0.06699	78,825	2.07	0.53	0.26	257
-107.7	0.10169	191,438	2.51	0.65	0.32	316
-40.1	0.15047	354,096	3.10	0.80	0.39	384
41.0	0.23943	643,948	4.23	1.08	0.53	485
71.0	0.31452	925,193	4.86	1.25	0.61	556

The logarithm of time approximation to p_D for analysis of low-permeability stimulated oil wells is often invalid. Normalized type curve analysis identifies whether the semilog straight line exists and suggests the proper $p_D - t_D$ model for analytical purposes. Additional detailed discussions of the normalization methods were given by Gladfelter et al.,²² Winestock and Colpitts,²³ and Odeh and Jones.^{24,25}

Analysis Methods: Their Applications and Limitations

Figure 5-28 shows various methods of analysis, their applications, and their limitations.

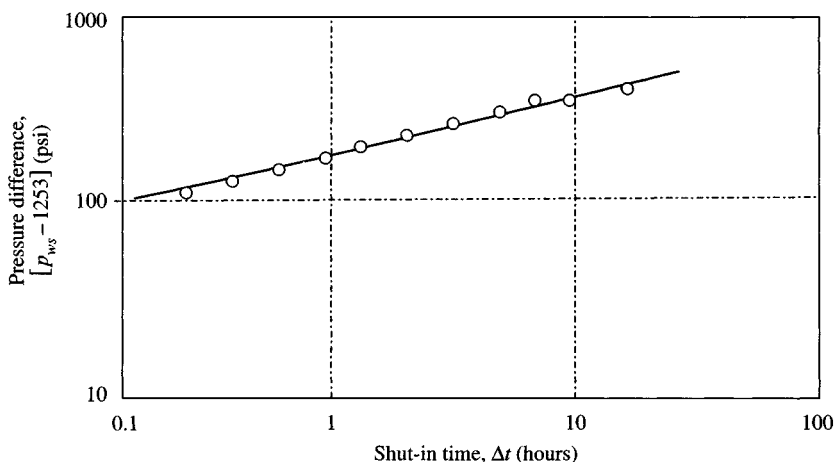


Figure 5-26. log-log type plot.

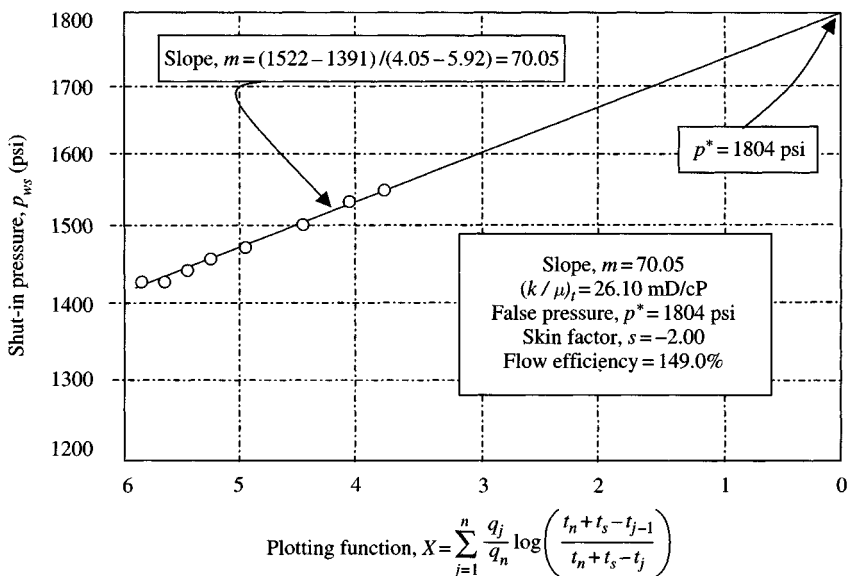


Figure 5-27. Multiphase and multi-rate pressure buildup data plot.

Buildup Rate Normalization Equations and Solutions

The afterflow rate normalized pressure equations proposed by Gladfelter et al.²² to analyze pressure buildup data dominated by afterflow were given as

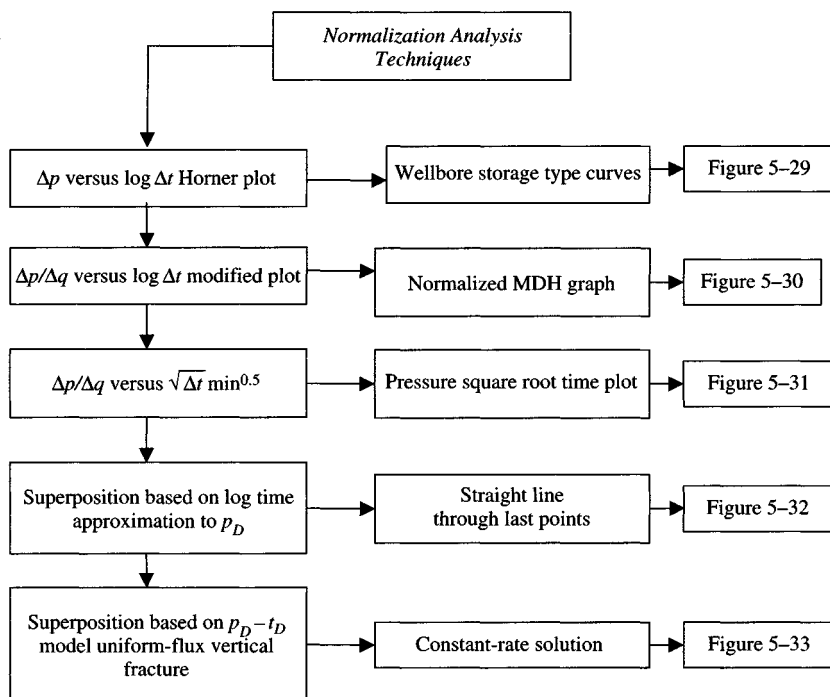


Figure 5-28. Various analysis techniques, their applications, and their limitations.

$$\frac{[p_{ws}(\Delta t) - p_{wf,s}]q_o}{(q_o - q(\Delta t))} = \frac{70.6q_o\mu_o}{kh} \left[\ln \left(\frac{0.000264k(\Delta t)}{\phi\mu_o c_t r_w^2} \right) + 0.809 + 2s \right] \quad (5-103)$$

Canceling q_o and expressing in the familiar logarithm form, the rate normalized MDH equation is

$$\frac{p_{ws(\Delta t)} - p_{wf,s}}{q_o - q(\Delta t)} = \frac{162.6\mu_o}{kh} \left[\log \left(\frac{k(\Delta t)}{\phi\mu_o c_t r_w^2} \right) - 3.23 + 0.869s \right] \quad (5-104)$$

Eq. 5-103 indicates that a plot of $(p_{ws(\Delta t)} - p_{wf,s})/(q_o - q(\Delta t))$ versus $\log \Delta t$ should be linear with slope equal to

$$m' = \frac{162.6\mu_o}{kh} \quad (5-105)$$

from which k can be calculated as

$$k = \frac{162.6\mu_o}{m'} \quad (5-106)$$

The skin is determined from

$$s = 1.151 \left[\frac{P_{ws}(\Delta t) - P_{wf,s}}{m'(q_o - q_{at}(\Delta t))} - \log \left(\frac{k(\Delta t)}{\phi \mu_o c_t r_w^2} \right) + 3.23 \right] \quad (5-107)$$

In 1974, Odeh and Jones²⁵ presented a method to analyze buildup after rates following a constant rate semi-steady-state production period at rate, q_o . The general equation describing the pressure change at any shut-in time, Δt_n , is

$$P_{ws}(\Delta t) - P_{wf,s} = \frac{70.6\mu_o}{kh} \left[-(q_i - q_{i-1}) \ln(\Delta t_n - \Delta t_{i-1}) + (q_o - q_n) \sum_{i=1}^n \left\{ \ln \left(\frac{0.000264k}{\phi \mu_o c_t r_w^2} \right) + 0.809 + 2s + D(q_o - q_n) \right\} \right] \quad (5-108)$$

The linearized form of Eq. 5-108 is

$$P_{ws}(\Delta t_n) - P_{wf,s} - D'(q_o - q_n)^2 = \frac{70.6\mu_o}{kh} \left\{ -\frac{1}{(q_o - q_n)} \ln(\Delta t_n - \Delta t_{i-1}) + \ln \left(\frac{0.000264k}{\phi \mu_o c_t r_w^2} \right) + 0.809 + 2s \right\} \quad (5-109)$$

where

$$D' = \frac{70.6\mu_o}{kh} (2D) \quad (5-110)$$

If non-Darcy flow is zero, a plot of

$$\frac{P_{ws}(\Delta t_n) - P_{wf,s}}{q_o - q_n} \text{ versus } -\frac{1}{q_o - q_n} \sum_{i=1}^n (q_i - q_{i-1}) \ln(\Delta t_n - \Delta t_{i-1})$$

will give a straight line with slope m' is

$$m' = \frac{70.6\mu_o}{kh} \quad (5-111)$$

and the intercept b , from which the skin can be calculated and is given by

$$s = 0.5 \left(\frac{b}{m'} - \ln \left(\frac{0.000264k}{\phi \mu_o c_t r_w^2} \right) - 0.809 \right) \quad (5-112)$$

A more general form of Eq. 5-109, expressed in terms of dimensionless pressure p_D and dimensionless time t_D is

$$\frac{p_{ws}(\Delta t_n) - p_{wf,s} - D'(q_o - q_n)^2}{q_o - q_n} = \frac{141.2\mu_o}{kh} \left\{ -\frac{1}{q_o - q_n} \left[\sum_{i=1}^n (q_i - q_{i-1}) p_D(\Delta t_n - \Delta t_{i-1})_D + s \right] \right\} \quad (5-113)$$

When non-Darcy flow is zero, Eq. 5-113 should be linear when plotted as

$$\frac{p_{ws}(\Delta t_n) - p_{wf,s}}{q_o - q_n} \text{ versus } \frac{-1}{q_o - q_n} \sum_{i=1}^n (q_i - q_{i-1}) p_D(\Delta t_n - \Delta t_{i-1})_D$$

having slope such as

$$m' = \frac{141.2\mu_o}{kh} \quad (5-114)$$

and intercept

$$b = m's \quad (5-115)$$

Normalized Pressure-Modified MDH Plot Analysis

Figure 5-31 is a rate-normalized pressure-modified MDH plot and a straight line drawn through the last group of points of the continuously sweeping data curve. From known value of the slope, the permeability and skin factor can be determined using the following equations:

$$k = \frac{162.6\mu_o}{m'h} \quad (5-116)$$

$$s = 1.151 \left[\frac{p_{ws}(\Delta t) - p_{wf,s}}{m'[q_o - q(\Delta t)]} - \log \left(\frac{k}{\phi\mu_o c_t r_w^2} \right) + 3.23 \right] \quad (5-117)$$

Figure 5-32 is a pressure versus shut-in time log-log graph. The curve does not match to any of the published wellbore storage type curves. So this technique proved unsuccessful. However, the total fluid afterflow rate-normalized pressure versus shut-in time log-log graph was matched to the uniform-flux vertical

fracture solution. From match points, permeability, skin factor, and half fracture length can be estimated by using the following equations:

$$k = \frac{141.2\mu_o}{h} \left(\frac{p_D}{\frac{\Delta p}{\Delta q_t}} \right)_{MP} \quad (5-118)$$

$$x_f = \left[\frac{0.000264k}{\phi\mu_o c_t} \left(\frac{\Delta t_1 h}{t_{Dxf}} \right)_{MP} \right]^{0.5} \quad (5-119)$$

Calculate the skin factor s as follows:

$$r_{wa} = \frac{x_f}{2} = r_w \exp(-s) \quad (5-120)$$

Normalized Average Reservoir Pressure Equation

Odeh and Jones²⁵ have suggested estimating p_R from an equation based on total fluid withdrawal basis. The equation is

$$\bar{p}_R = \frac{141.2q_t \left[\ln \sqrt{\frac{2.25A}{CAr_w^2}} + s \right]}{\left(\frac{kh}{\mu} \right)_t} + p_{wf(\Delta t=0)} \quad (5-121)$$

Example 5-16 Normalizing Afterflow Rate and Analyzing Pressure Buildup Test

A 67-hours buildup test was run and all the pressure and afterflow data are appearing in Tables 5-20 and 5-21. The wellbore storage coefficient has been calculated and added following the procedures appearing in Ref. 8. Cumulative production is 75,800 bbl. Well/reservoir data are: $T = 123^\circ\text{F}$, $\text{API} = 35^\circ$, $\mu_o = 3.18$ cP, $\mu_w = 0.56$ cP, $\mu_g = 0.0155$ cP, $f_w = 30\%$, casing ID, in = 4.953, tubing ID, in = 2.375, $c_t = 20.0 \times 10^{-6}$ psi⁻¹, well spacing = 40 acres, $r_w = 0.31$ ft, $h = 47$ ft, $\phi = 14\%$, $q_{T(\Delta t=0)} = 328$ rbd.

Find the flow capacity and skin factor using the following techniques:

- Conventional Horner buildup analysis.
- $\Delta p/\Delta q_t$ versus $\log t$ modified MDH method.
- $\Delta p/\Delta q_t$ versus \log - \log graph uniform-flux vertical fracture constant-rate solution.
- Superposition based on logarithm of time approximation to $p_D - t_D$ (straight line through last point).
- Average reservoir pressure.

Table 5-20
Pressure Buildup Data

Shut-in time, Δt (min)	Shut-in pressure, p_{ws} (psi)	$\frac{\Delta t}{t_p + \Delta t}$
0	90	—
3	103	0.0005
5	105	0.0009
10	111	0.0018
15	116	0.0027
20	122	0.0036
25	128	0.0045
30	133	0.0054
35	139	0.0063
40	145	0.0072
45	151	0.0080
50	156	0.0089
55	162	0.0098
60	168	0.0107
70	180	0.0125
80	192	0.0142
90	202	0.0160
100	212	0.0177
110	222	0.0194
120	231	0.0212
173	272	0.0303
236	315	0.0408
308	356	0.0528
390	395	0.0657
583	472	0.0951
694	505	0.1112
814	536	0.1280
945	564	0.0923
1034	591	0.0963
1234	621	0.1007
1393	648	0.1046
1562	674	0.1084
1741	700	0.1121
1929	726	0.1158
2127	752	0.1194
2334	777	0.1229
2552	830	0.1302
2778	828	0.1313
3015	853	0.1333
3180	867	0.1352
3240	873	0.1360
3300	878	0.1367

Table 5-20 (continued)

Shut-in time, Δt (min)	Shut-in pressure, p_{ws} (psi)	$\frac{\Delta t}{t_p + \Delta t}$
3360	883	0.1373
3420	888	0.1380
3480	899	0.1395
3540	904	0.1402
3600	908	0.1407
3660	913	0.1414
3720	917	0.1419
3780	922	0.1425
3840	926	0.1431
3900	930	0.1436
3960	935	0.1443
4020	939	0.1448

Solution *Conventional Horner Buildup Analysis*

Figure 5-29 is the conventional Horner plot, which shows no clear straight-line sections. A straight line drawn through the last group of points gives reasonable calculated results. The plot has the following characteristics: $t_p = 5546$ hours, $m = 700$ psi/cycle, and $p_{1\text{ hr}} = 340$ psi.

From Eq. 5-2, k is

$$k = \frac{162.6q_o\mu_o}{mh} = \frac{162.6(328)(3.18)(1.0)}{700(47)} = 5.16 \text{ mD}$$

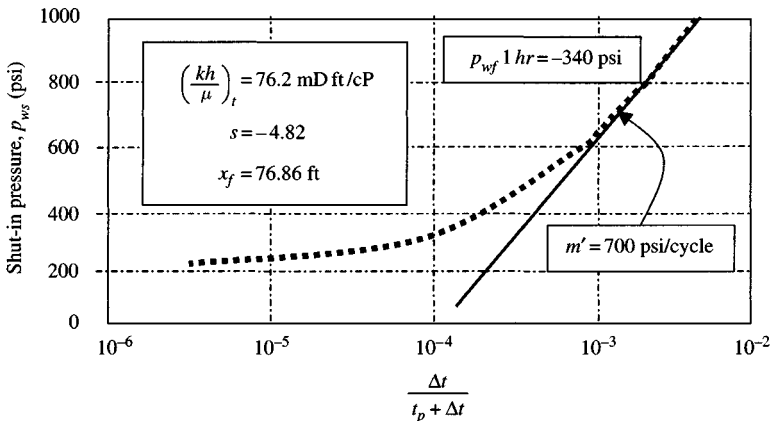


Figure 5-29. Conventional Horner buildup plot.

Table 5-21
Pressure Buildup Test and Afterflow Rates

Time, Δt (min)	Time, $\sqrt{\Delta t}$ (min)^{0.5}	Liquid level (ft)	Pressure, p_{wh} (psi)	Pressure, p_{wf} (psi)	Gas rate (rb/day)	Liquid rate (rb/day)	Total rate (rb/day)	Δp (psi)	$\left(\frac{\Delta p}{\Delta q}\right)_t$ (psi/rb/day)	Wellbore storage coefficient (bbl/psi)
0	—	7277	40.9	90	257	71	328	0	0	0
3	1.732	7269	41.3	103	229	59	288	4	0.100	0.161
5	2.236	7263	41.5	105	219	59	278	6	0.120	0.197
10	3.162	7248	42.1	111	202	60	262	12	0.182	0.156
15	3.873	7234	42.8	116	183	61	244	17	0.202	0.176
20	4.472	7219	43.4	122	168	61	229	23	0.232	0.137
25	5.000	7205	43.9	128	154	62	226	29	0.259	0.129
30	5.477	7190	44.5	133	142	62	204	34	0.274	0.146
35	5.916	7176	45.0	139	131	63	194	40	0.299	0.115
40	6.324	7160	45.6	145	122	63	185	46	0.322	0.110
45	6.708	7147	46.1	151	112	64	176	52	0.342	0.105
50	7.071	7132	46.6	156	105	64	169	57	0.358	0.120
55	7.416	7118	47.1	162	98	64	162	63	0.380	0.094
60	7.746	7103	47.6	168	91	65	156	69	0.401	0.092
70	8.367	7074	48.6	180	82	65	147	81	0.448	0.088
80	8.944	7045	49.5	192	72	66	138	93	0.489	0.083
90	9.487	7019	50.4	202	67	61	128	103	0.515	0.092
100	10.000	6994	51.3	212	62	57	119	113	0.541	0.086

Table 5-21 (continued)

Time, Δt (min)	Time, $\sqrt{\Delta t}$ (min) ^{0.5}	Liquid level (ft)	Pressure, p_{wh} (psi)	Pressure, p_{wf} (psi)	Gas rate (rb/day)	Liquid rate (rb/day)	Total rate (rb/day)	Δp (psi)	$\left(\frac{\Delta p}{\Delta q}\right)_t$ (psi/rb/day)	Wellbore storage coefficient (bbl/psi)
110	10.488	6970	52.1	222	58	55	113	123	0.572	0.081
120	10.955	6948	42.9	231	55	50	105	132	0.592	0.084
173	13.153	6851	56.8	272	41	43	84	173	0.709	0.085
236	15.362	6756	60.5	315	27	36	63	216	0.815	0.075
308	17.550	6665	64.0	356	19	31	50	257	0.924	0.069
390	19.748	6579	67.5	395	15	26	41	296	1.031	0.066
583	24.145	6413	74.3	472	9	20	29	323	1.247	0.061
694	26.344	6341	77.4	505	7	16	23	406	1.331	0.061
814	28.531	6274	80.4	536	6	14	20	437	1.419	0.058
945	30.741	6213	83.3	564	5	12	17	465	1.495	0.060
1034	32.156	6155	86.1	591	4	11	15	492	1.572	0.037
1234	35.128	6098	8.5	621	3	10	13	522	1.657	0.065
1393	37.323	6040	90.0	648	2	9	11	549	1.732	0.049
1562	39.522	5983	92.7	674	2	9	11	575	1.814	0.050
1741	41.725	5926	94.7	700	2	8	10	601	1.890	0.050
1929	43.920	5868	96.6	726	1	8	9	627	1.966	0.048
2127	46.119	5811	98.4	752	1	8	9	653	2.047	0.048
2334	48.312	5754	100.0	777	0	8	8	678	2.119	0.049
2552	50.517	5696	102.1	830	0	7	8	704	2.200	0.047
2778	52.707	5639	103.8	828	0	6	7	729	2.271	0.046
3015	54.909	5582	105.6	853	1	6	7	754	2.349	0.053

Table 5-21 (continued)

Time, Δt (min)	Time, $\sqrt{\Delta t}$ (min) ^{0.5}	Liquid level (ft)	Pressure, p_{wh} (psi)	Pressure, p_{wf} (psi)	Gas rate (rb/day)	Liquid rate (rb/day)	Total rate (rb/day)	Δp (psi)	$\left(\frac{\Delta p}{\Delta q}\right)_t$ (psi/rb/day)	Wellbore storage coefficient (bbl/psi)
3180	56.392	5547	106.8	867	0	5	6	768	2.385	0.042
3240	56.921	5535	107.2	873	1	5	6	774	2.404	0.050
3300	57.446	5523	107.6	878	1	5	6	779	2.419	0.050
3360	57.966	5511	108.0	883	1	5	6	784	2.435	0.050
3420	58.481	5499	108.4	888	1	5	6	789	2.450	0.021
3480	58.992	5488	108.6	899	0	5	5	800	2.477	0.042
3540	59.498	5477	108.9	904	0	5	5	805	2.492	0.042
3600	60.000	5466	109.1	908	0	5	5	809	2.505	0.052
3660	60.498	5466	109.3	913	0	5	5	814	2.520	0.042
3720	60.992	5455	109.5	917	0	5	5	818	2.533	0.052
3780	61.482	5444	109.7	922	0	5	5	823	2.548	0.042
3840	61.968	5423	109.9	926	0	5	5	827	2.560	0.052
3900	62.450	5413	110.1	930	0	4	5	831	2.573	0.052
3960	62.929	5493	110.4	935	0	4	4	836	2.580	0.038
4020	63.404	5383	110.5	939	0	2	4	840	2.593	0.042

From Eq. 5-3, s is

$$\begin{aligned} s &= 1.151 \left[\frac{p_{1hr} - p_{wf}}{m} - \log \left(\frac{k}{\phi \mu_o c_t r_w^2} \right) + 3.23 \right] \\ &= 1.151 \left[\frac{-340 - 99}{700} - \log \left(\frac{5.15}{0.14(3.18)(20.0 \times 10^{-6})(0.31)^2} \right) + 3.23 \right] \\ &= 1.151[-0.6271 - 6.7809 + 3.23] = -4.19 \end{aligned}$$

From Eq. 5-120,

$$x_f = 2r_{wa} \exp(-s) = 2 \times 0.31 \exp[-(-4.19)] = 40.93 \text{ ft}$$

Normalized Pressure-Modified MDH Analysis

Figure 5-30 is a rate-normalized pressure-modified MDH plot and a straight line drawn through the last group of points of the continuously sweeping data curve. The plot has the following characteristics:

$$\begin{aligned} m' &= 1.9 \text{ psi}/(\text{rb}/\text{stb}) \quad \text{and} \quad \frac{\Delta p}{\Delta q_t}, 1 \text{ hour} = -0.90 \text{ psi}(\text{rb}/\text{stb}) \\ &= \frac{p_{ws}(\Delta t) - p_{wf}(\Delta t=0)}{q_o - q(\Delta t)} \end{aligned}$$

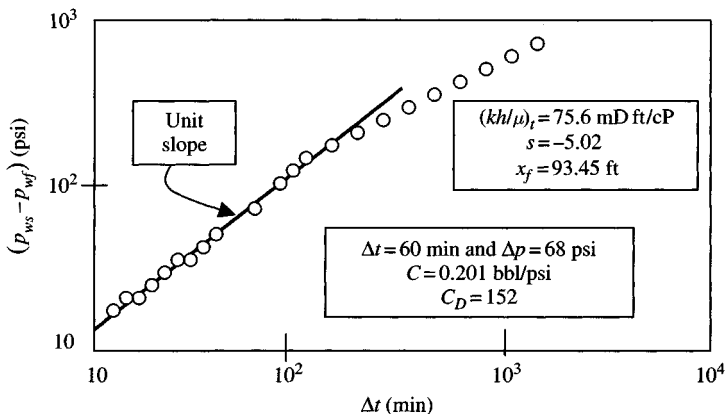


Figure 5-30. Conventional pressure-time log-log graph.

From Eq. 5-105,

$$k = \frac{162.6\mu_o}{m'h} = \frac{162.6(3.18)}{1.9(47)} = 5.79 \text{ mD}$$

From Eq. 5-107,

$$\begin{aligned} s &= 1.151 \left[\frac{p_{ws}(\Delta t) - p_{wf,s}}{m' [q_o - q(\Delta t)]} - \log \left(\frac{k}{\phi\mu_o c_t r_w^2} \right) + 3.23 \right] \\ &= 1.151 \left[\frac{-0.90}{1.9} - \log \left(\frac{5.79}{0.14(3.18)(20.0 \times 10^{-6})(0.31)^2} \right) + 3.23 \right] \\ &= 1.151 [-0.4737 - 6.8304 + 3.23] = -4.69 \end{aligned}$$

From Eq. 5-120,

$$x_f = 2 \times 0.31 \exp[-(-4.69)] = 67.49 \text{ ft}$$

Figure 5-30 is a pressure versus shut-in time log-log graph. The curve does not match to any of the published wellbore storage type curves.¹⁹ So this technique proved unsuccessful. The plot has the following characteristics:

$$\Delta t = 60 \text{ min}, \quad \Delta p = 68 \text{ psi} \rightarrow C = 0.201 \text{ bbl/psi}, \quad \text{and} \quad C_D = 152$$

However, the total fluid afterflow rate-normalized pressure versus shut-in time log-log graph was matched to the uniform-flux vertical fracture solution.

Match points are

$$\Delta t = 1000 \text{ min}, \quad t_{Dxf} = 0.335, \quad \frac{\Delta p}{\Delta q_t} = 1.0 \text{ psi/rb/stb}, \quad \text{and} \quad p_D = 0.62$$

Calculate the permeability k from Eq. 8-39:

$$k = \frac{141.2\mu_o\beta_o}{h} \left(\frac{p_D}{\frac{\Delta p}{\Delta q_t}} \right)_{MP} = \frac{141.2(3.18)(1.0)}{47} \left(\frac{0.62}{1.0} \right) = 5.92 \text{ mD}$$

Estimate the fracture half-length x_f from Eq. 8-40:

$$\begin{aligned} x_f &= \left[\frac{0.000264k}{\phi\mu_o c_t} \left(\frac{\Delta t_{1hr}}{t_{Dxf}} \right)_{MP} \right]^{0.5} = \left[\frac{0.000264(5.92)}{0.14(3.18)(20.0 \times 10^{-6})} \left(\frac{1000/60}{0.335} \right) \right]^{0.5} \\ &= [175.53 \times 7.0535]^{0.5} = 93.45 \text{ ft} \end{aligned}$$

Calculate the skin factor s as follows:

$$r_{wa} = \frac{x_f}{2} = r_w \exp^{(-s)}$$

Therefore, $s = -\ln(x_f/2r_w) = -\ln[93.2/(2 \times 0.31)] = -5.02$

Odeh–Jones Logarithm of Time Superposition Plot (Straight Line Through Last Points)

Figure 5–31 is an Odeh–Jones logarithm of time superposition plot. Normally, in looking for a linear flow period a pressure versus $\sqrt{\Delta t}$ graph is made. In this case, a Δp versus $\sqrt{\Delta t}$ does not result in a straight line but a total fluid afterflow rate-normalized pressure plot, $\Delta p/\Delta q_T$ versus $\sqrt{\Delta t}$, does. This can be seen in Figure 5–32. The plot has the following characteristics:

$$\text{Slope, } m' = \frac{0.120 - 0.541}{3.162 - 10} = 0.062$$

Figure 5–32 is an Odeh–Jones logarithm of time superposition plot. Straight line is drawn through the last group of points on this plot, which will give reasonable calculated results. The plot has the following characteristics:

$$m' = 0.83 \text{ psi}/(\text{rb}/\text{stb})$$

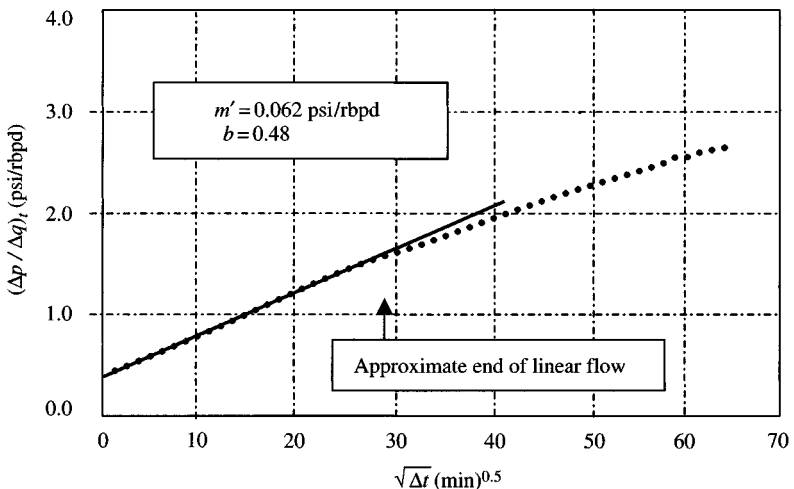


Figure 5–31. Afterflow rate-normalized pressure – square root of time plot.

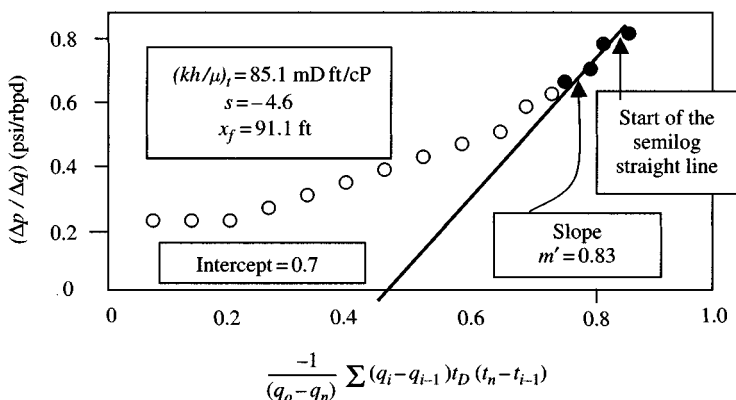


Figure 5-32. Superposition based on uniform-flux vertical fracture $p_D - t_D$ (straight line through last points).

Estimate the permeability k from Eq. 5-111:

$$k = \frac{70.6\mu_o}{m'h} = \frac{70.6(3.18)}{(0.83)(47)} = 5.76 \text{ mD}$$

Determine the skin factor s from Eq. 5-112:

$$s = 0.5 \left[\frac{b}{m'} - \ln \left(\frac{0.000264k}{\phi\mu_o c_t r_w^2} \right) - 0.809 \right]$$

$$= 0.5 \left[\frac{-0.70}{0.83} - \ln \left(\frac{0.000264(5.76)}{0.14(3.18)(20.0 \times 10^{-6})(0.31)^2} \right) - 0.809 \right] = -4.99$$

$$x_f = 2 \times r_{wa} = 2 \times 0.31 \exp[-(-499)] = 91.1 \text{ ft}$$

Superposition Based on $p_D - t_D$ Model (Uniform-Flux Vertical Fracture Constant-Rate Solution)

From Figure 5-33, find the following:

$$m' = 1.6 \text{ psi(rb/stb/cycle)}, \quad \frac{t_D}{t} = 0.00034$$

From Eq. 5-89,

$$\left[\frac{kh}{\mu} \right]_t = \frac{141.2}{1.6} = 88.0 \text{ mD (ft/cP)}$$

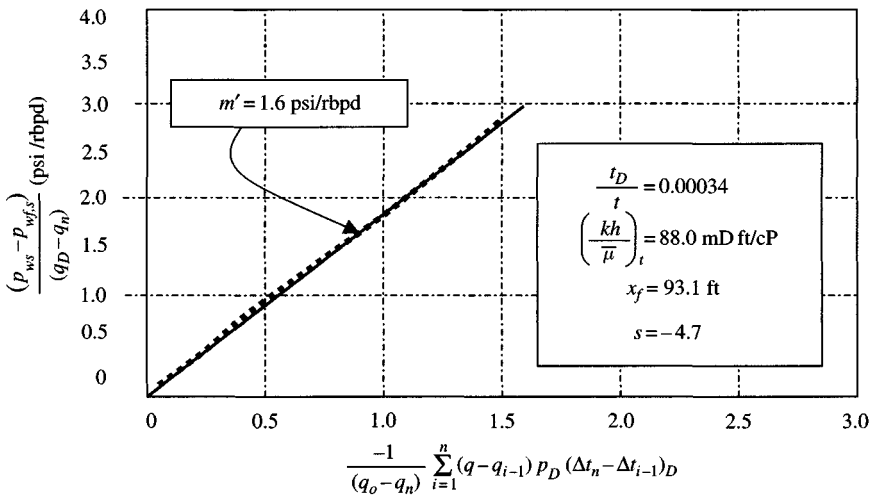


Figure 5-33. Superposition based on uniform-flux vertical fracture p_D-t_D model.

Average Reservoir Pressure

Find p_R , using Eq. 5-121:

$$\begin{aligned} \bar{p}_R &= \frac{141.2q_T \left[\ln \sqrt{\frac{2.25A}{CA_w^2}} + s \right]}{\left(\frac{kh}{\mu} \right)_t} + p_{wf}(\Delta t=0) \\ &= \frac{141.2 \times 328 \left[\ln \sqrt{\frac{2.25 \times 40 \times 43,560}{30.883 \times 0.31^2}} - 4.7 \right]}{88.0} + 99.0 = 1235 + 99 = 1334 \text{ psi} \end{aligned}$$

Table 5-22 summarizes the results from all methods of analysis.

5.12 Summary

This chapter treats pressure buildup test analysis and presents methods for estimating formation characteristics such as the reservoir permeability, skin factor, wellbore damage, and improvement evaluation including average pressure for well drainage areas and the entire reservoir. In addition, analysis methods for afterflow-dominated pressure buildup data are presented to identify linear flow, near-wellbore permeability changes or boundaries using both accurate pressure and total afterflow fluid rate.

Table 5-22
Summary of Analysis Results

Methods of analysis	$\left(\frac{kh}{\mu}\right)_T$ (mD ft/cP)	Skin s	x_f (ft)
Conventional Horner buildup analysis (Figure 5-29)	76.2	-4.80	76.86
$\frac{\Delta p}{\Delta q_T}$ versus $\log \Delta t$, modified MDH analysis (Figure 5-30)	75.6	-5.02	93.45
Approximation on $p_D - t_D$ (straight line through last points) (Figure 5-32)	85.6	-4.99	91.1
Superposition based on $p_D - t_D$, uniform flux vertical fracture constant rate solution (Figure 5-33)	88.0	-4.7	93.6

References and Additional Reading

1. Matthews, C. S., "Analysis of Pressure Build-Up and Flow Test Data," *J. Pet. Tech.* (Sept. 1961) 862-870. Also Reprint Series, No. 9 - Pressure Analysis Methods, Society of Petroleum Engineers of AIME, Dallas, TX, 1967, pp. 111-119.
2. Russell, D. G., "Extensions of Pressure Buildup Analysis Methods," *J. Pet. Tech.* (Dec. 1966) 1624-1636; *Trans. AIME*, 237. Also Reprint Series, No. 9 - Pressure Analysis Methods, Society of Petroleum Engineers of AIME, Dallas, TX, 1967, pp. 175-187.
3. Saidikowski, R. M., "Numerical Simulations of the Combined Effects of Wellbore Damage and Partial Penetration," paper SPE 8204 (Sept. 1979).
4. Papatzacos, P., "Approximation Partial-Penetration Pseudo-Skin for Infinite-Conductivity Wells," SPE Reservoir Engineering, pp. 227-234, May 1988; *Trans. AIME*, Vol. 237, pp. 518, 1966.
5. Odeh, A. S., "An Equation for Calculating Skin Factor Due to Restricted-Entry," *J. Pet. Tech.* (June 1980), 964-965.
6. Hawkins, M. F., Jr., "A Note on the Skin Effect," *Trans. AIME* (1956) 267, 356-357.
7. Matthews, C. S., and Russell, D. G., *Pressure Buildup and Flow Tests in Wells*, Monograph Series, Vol. 1, Society of Petroleum Engineers of AIME, Dallas, TX, 1967.
8. Horner, D. R., Pressure Build-Up in Wells, Proceedings, Third World Pet. Congress - Sect. II, 1951, pp. 503-521.
9. Miller, C. C., Dyes, A. B., and Hutchinson, C. A., Jr., "The Estimation of Permeability and Reservoir Pressure from Bottom-Hole Pressure Buildup Characteristics," *Trans. AIME* (1950) 189, 91-104.

10. Muskat, M., *Physical Principles of Oil Production*, McGraw-Hill, New York, 1949, p. 378.
11. Slider, H. C., "A Simplified Method of Pressure Buildup Analysis for a Stabilized Well," *J. Pet. Tech.* (Sept. 1971) 1155–1160; *Trans. AIME*, 251.
12. Ramey, H. J., Jr., and Cobb, W. M., "A General Buildup Theory for a Well in a Closed Drainage Area," *J. Pet. Tech.* (Dec. 1971) 1493–1505; *Trans. AIME*, 251.
13. Cobb, W. M., and Smith, J. T., "An Investigation of Pressure Buildup Tests in Bounded Reservoirs," paper SPE 5133 presented at the SPE-AIME 49th Annual Fall Meeting, Houston, Oct. 6–9, 1974 (an abridged version appears in *J. Pet. Tech.* (Aug. 1975) 991–996; *Trans. AIME*, 259).
14. Kumar, A., and Ramey, H. J., Jr., "Well Test Analysis for a Well in a Constant-Pressure Square," paper SPE 4054 presented at the SPE-AIME 47th Annual Fall Meeting, San Antonio, TX, Oct. 8–11, 1972 (an abridged version appears in *Soc. Pet. Eng. J.* (April 1974), 107–116).
15. Muskat, M., "Use of Data on the Build-Up of Bottom-Hole Pressures," *Trans. AIME* (1937) 123, 44–48. Also Reprint Series No. 9 – Pressure Analysis Methods, Society of Petroleum Engineers of AIME, Dallas, TX, 1967, pp. 5–9.
16. Perrine, R. L., "Analysis of Pressure Buildup Curves," *Drill. Prod. Prac. API* (1956) 482–509.
17. Ramey, H. J., Jr., Kumar, A., and Gulati, M. S., *Gas Well Test Analysis Under Water-Drive Conditions*, AGA, Arlington, VA, 1973 (Chapters 4–7).
18. McKinley, R. M., "Wellbore Transmissibility from Afterflow-Dominated Pressure Buildup Data," paper SPE 2416, 45th Fall Meeting of AIME, Houston, TX.
19. Earlougher, R. C., Jr., and Kersch, K. M., "Field Examples of Automatic Transient Test Analysis," *J. Pet. Tech.* (Oct. 1972) 1271–1277.
20. Van Poolen, H. K., "Radius-of-Drainage and Stabilization-Time Equations," *Oil Gas J.* (1964) 62, 138–146.
21. McKinley, R. M., "Estimating Flow Efficiency from Afterflow-Distorted Pressure Buildup Data," *J. Pet. Tech.*, (1974) 26(6), 696–697.
22. Gladfelter, R. E., Tracy, G. W., and Wilsey, L. E., "Selecting Wells which will Respond to Production-Stimulation Treatment," *Drill. Prod. Prac. API* (1955) 117–128.
23. Winestock, A. G., and Colpitts, G. P., "Advances in Estimating Gas Well Deliverability," *J. Cdn. Pet. Tech.* (July–Sept. 1965) 111–119.
24. Odeh, A. S., and Jones, L. G., "Pressure Drawdown Analysis – Variable-Rate Case," *J. Pet. Tech.* (Aug. 1965) 960–964; *Trans. AIME*, 234.
25. Odeh, A. S., and Jones, L. G., "Two-Rate Flow Test, Variable-Rate Case – Application to Gas-Lift and Pumping Wells," *J. Pet. Tech.* (Jan. 1974) 93–99; *Trans. AIME*, 257.

Chapter 6

Original and Average Reservoir Pressure Estimation Methods

6.1 Introduction

Average reservoir pressure, p'_R , can be determined from a pressure buildup test. Also, p'_R is referred to as static drainage area pressure in the formation surrounding a tested well. Average reservoir pressure is used:

1. To compute rock and fluid characteristics.
2. To estimate oil in-place.
3. To predict future reservoir behavior in primary/secondary recovery and pressure maintenance projects.

Note that initial or original reservoir pressure is different from average reservoir pressure. Average reservoir pressure is determined for reservoirs that have experienced some pressure depletion. Several methods are available to estimate average reservoir pressure.

6.2 Original Reservoir Pressure in Infinite Reservoirs

Original reservoir pressure, p_i , is found as suggested by ideal theory. We simply identify the middle-time line, extrapolate it to infinite shut-in time, and read the pressure that is the original reservoir pressure as shown in Figure 6-1.

This technique is possible only for a well in a new reservoir, i.e., one in which there has been negligible pressure depletion. For a reservoir with one

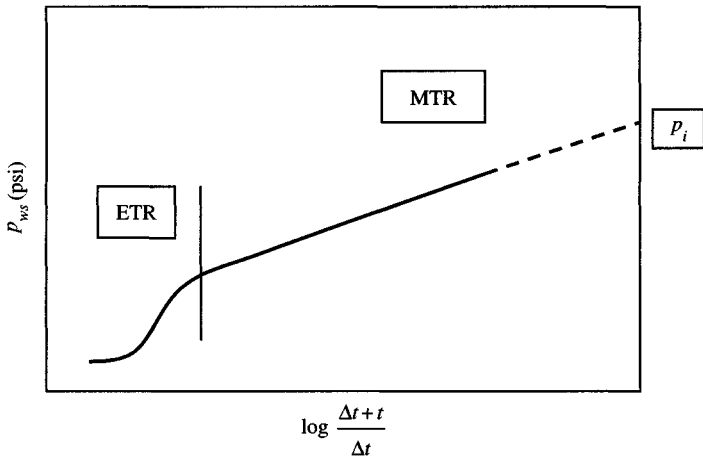


Figure 6-1. Buildup test graph for infinite-acting reservoir.

or more boundaries relatively near a tested well, the late-time line must be extrapolated to find p_i (Figure 6-2).

6.3 Estimating Average and Initial Reservoir Pressure

In this section we will discuss various methods to estimate average \bar{p} and initial p_i in both closed (no flow) and water-drive (constant pressure) oil reservoirs.

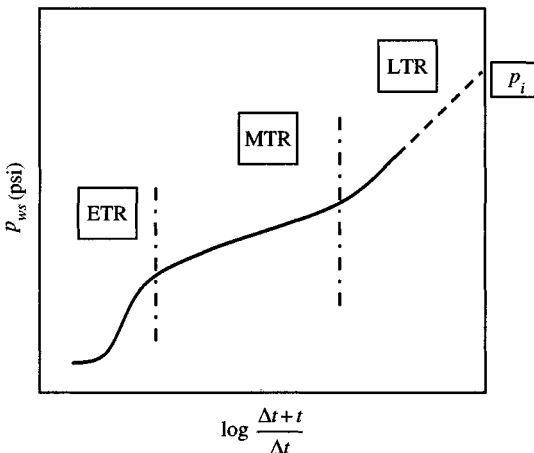


Figure 6-2. Buildup test graph for well near reservoir limit.

Horner and MBH Methods

The Horner and MBH methods⁶ are also known as the p^* method, as these methods use the pressure p^* obtained from the straight-line extrapolation of Horner and MDH plots. Using the imaging technique and the principle of superposition, Mathews et al. developed buildup curves for wells at various positions in the drainage area of various shapes.² These curves are presented as Figures B-2 through B-8 or Table B-1. The following steps are followed to calculate average reservoir pressure using the MBH method:

1. Find false pressure from Horner or MDH plot.
2. Estimate the drainage area and shape.
3. Select the proper curve type from Figures B-2 through B-8 or Table B-1.
4. Using Eq. 6-1 calculate t_{DA} , and find the corresponding ordinate value, p_{DMBH} , using the appropriate MBH plot.

$$t_{pDA} = \frac{0.000264kt_p}{\phi\mu_o c_t A} \quad (6-1)$$

5. Calculate the average reservoir pressure, \bar{p} , using Eq. 6-2:

$$\bar{p} = p^* - \frac{m[p_{DMBH}(t_{pDA})]_{\text{Figures B-2 to B-8}}}{2.303} \quad (6-2)$$

where p_{DMBH} is the corresponding ordinate value using the appropriate MBH series of plots of $kh(p^* - \bar{p})/(70.6q_o\mu_o\beta_o)$ versus $0.000264kt_p/(\phi\mu_o c_t A)$. Note that $kh(p^* - \bar{p})/70.6q_o\mu_o\beta_o$ can be written as $2.303(p^* - \bar{p})/m$. Accuracy of the p^* method may be improved by using t_{pss} , producing time required to achieve pseudo-steady state, in the Horner plot and in the abscissa of the MBH curves in Figures B-2 through B-8 or Table B-1. In principle, results should be identical for any $t_p > t_{pss}$:

$$t_p = \frac{24V_p}{q_o} \quad (6-3)$$

$$t_{pss} = \frac{\phi\mu_o c_t A}{0.000264k} (t_{DA}) \quad (6-4)$$

If $t_p \gg t_{pss}$, then t_{pss} should be replaced.

MDH Method⁷

The average reservoir pressure \bar{p} may be estimated for closed circular or square drainage regions from the MDH data plot (p_{ws} versus $\log \Delta t$). The MDH average reservoir pressure analysis method applies directly only to wells operating at pseudo-steady state before the buildup test. To use the MDH method, choose any convenient time on the semilog straight line, Δt , and read the corresponding pressure, p_{ws} . Then calculate the dimensionless shut-in time based on the drainage area:

$$\Delta t_{DA} = \Delta t_D \left(\frac{r_w^2}{A} \right) = \frac{0.000264k(\Delta t)}{\beta\phi\mu_o c_t A} \quad (6-5)$$

$$\bar{p} = p_{ws} + \frac{mp_{DMDH}(\Delta t_{DA})_{\text{upper curve, Figure 6-3}}}{1.1513} \quad (6-6)$$

$$p_i = p_{ws} + \frac{mp_{DMDH}(\Delta t_{DA})_{\text{lower curve, Figure 6-3}}}{1.1513} \quad (6-6a)$$

where Δt and its corresponding p_{ws} are read from the straight-line portion of the MDH plot and p_{DMDH} is obtained from Figure 6-3.

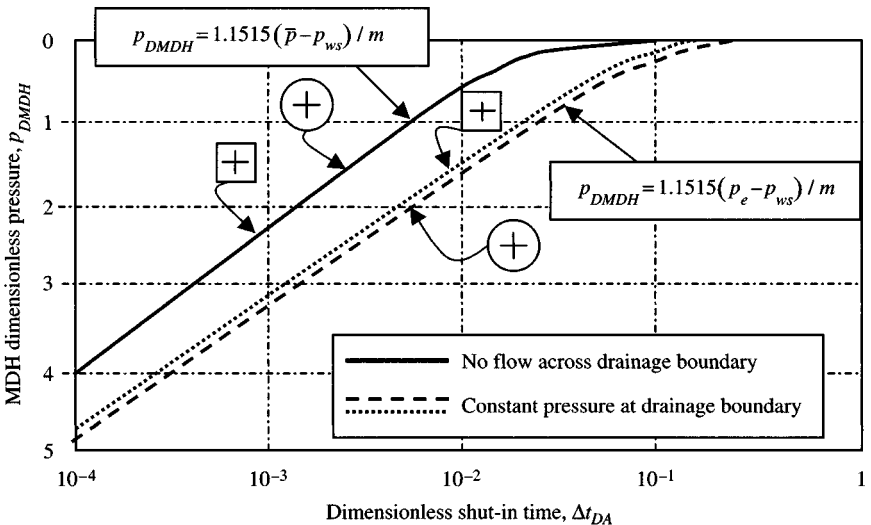


Figure 6-3. MDH dimensionless pressure for circular and square areas.²

Dietz Method¹

The Dietz method requires MDH plot and is preferred for oil wells with negative skin factor ($s < -3$ or $r_{ws} > 0.05r_e$) caused by acidizing or fracturing. The well should be in pseudo-steady state before shut-in. Dietz determined the time, $(\Delta t)_{\bar{p}}$, when \bar{p} may be read directly from the extrapolated semilog straight line:

$$(\Delta t)_{\bar{p}} = \frac{t_p}{C_A t_{pDA}} = \frac{\phi \mu_o c_l A}{0.000264 C_A k} \quad (6-7)$$

where C_A is the Dietz shape factor¹ given in Table B-2. This method is very simple and quick.

Ramey et al. Method

The Ramey et al. method³ also uses Table B-2 except that it is used to extrapolate a Horner straight line to \bar{p} instead of an MDH straight line. For $t_p \geq t_{pss}$, they show that

$$\left(\frac{t_p + \Delta t}{\Delta t} \right)_{\bar{p}} = C_A t_{pDA} = \frac{0.000264 k t_p C_A}{\phi \mu_o c_l A} \quad (6-8)$$

Eq. 6-8 reduces to Eq. 6-7 when $(t_p + \Delta t) \cong t_p$. When $t_p < t_{eia}$, which may be estimated

$$t_{eia} = \frac{\phi \mu_o c_l A}{0.000264 k} (t_{DA})_{Table\ B-2} \quad (6-9)$$

where t_{eia} is the duration of the infinite-acting period where $(t_{DA})_{eia}$ is given in the "for $t_{DA} <$ " column of Table B-2. For a well in the center of a closed circular reservoir, $(t_{DA})_{eia} = 0.1$ and

$$t_{eoa} \cong \frac{379 \phi \mu_o c_l A}{k} \quad (6-10)$$

Ramey et al.³ show that if $t_p < t_{eia}$, then

$$\left(\frac{t_p + \Delta t}{\Delta t} \right)_{\bar{p}} = e^{4\pi t_{pDA}} \quad (6-11)$$

Example 6-1 *Calculating Average and Initial Reservoir Pressures Using Pressure BuildUp Data by Various Methods in Circular Drainage Area*

Using the pressure buildup data of Example 5-2, calculate the average and initial reservoir pressures by using the following methods: (1) the MBH method, (2) the MDH method, and (3) the Dietz method. Assume that the well is draining from the center of a circular area of 167 acres.

Solution

(1) MBH method:

$$p^* = 4577, \quad t_p = 13,630 \text{ hours}, \quad k = 8.4 \text{ mD}$$

Using Eq. 6-4, calculate t_{pDA} such that

$$t_{pDA} = \frac{0.000264kt_p}{\phi\mu_o c_1 A} = \frac{0.000264 \times 8.4 \times 13,630}{0.1 \times 0.65 \times 17.5 \times 10^{-6} \times 167 \times 43,560} = 3.65$$

From Figure B-1, the corresponding ordinate value p_{MBH} is 4.75.

$$\bar{p} = \frac{p^* - mp_{DMBH}}{2.303} = \frac{4577 - 70(4.75)}{2.303} = 4433 \text{ psig}$$

Accuracy of the p^* method may be improved by using t_{pss} , producing time required to achieve pseudo-steady state, in the Horner plot and in the abscissa of the MBH curves. In principle, results should be identical for any $t_p > t_{pss}$; in practice, use of the smallest possible t_p may reduce the error. Time to reach pseudo-steady state can be calculated after formation permeability, k , has been established, given the drainage size and shape. Values are given in Table B-2 for common drainage area. As an example, for conditions in Example 6-1, in the column "for t_{DA} " we read 0.1 for a well centered in a circular drainage area. This means that

$$t_{DA} = \frac{0.000264kt_{pss}}{\phi\mu_o c_1 A} = 0.1$$

or for this case with $A = 167 \text{ acres} \Rightarrow 167 \times 43,560 \text{ ft}^2$

$$t_{pss} = \frac{\phi\mu_o c_1 A}{0.000264k} (t_{DA}) = \frac{0.1 \times 0.65 \times 17.4 \times 10^{-6}}{0.000264 \times 8.4} (0.1) = 373.14 \text{ hours}$$

The reader can verify that use of t_{pss} in the Horner plot and in the p^* method leads to the same results as in Examples 5-2 and 6-1.

(2) MDH method:

We consider the same buildup test as in Examples 5–2. The drainage area of the well is 1520 ft. We choose $\Delta t = 20$ hr on the straight-line section of the MDH plot in Figure 5–4. From Eq. 6–5

$$\Delta t_{DA} = \frac{0.000264k\Delta t}{\phi\mu_o c_t A} = \frac{0.000264 \times 8.4 \times 20}{0.1(0.65)(17.5 \times 10^{-6}) \times \pi(1520)^2} = 0.00537$$

From the upper curve in Figure 6–3, at $\Delta t_{DA} = 0.00537$, the value of $p_{MDH} = 0.94$. From MDH plot (Figure 5–3), p_{ws} at $\Delta t = 20$ hr is 4379 in psig and m is 70.0 in psig/cycle. Then, using Eq. 6–6

$$\bar{p} = p_{ws} + m \frac{p_{DMDH}(t_{pDA})}{1.1513} = 4379 + 70 \times 0.94/1.1513 = 4436 \text{ psig}$$

(3) Dietz method:

From MDH plot given in Figure 5–4 (Example 5–2) $m = 70.0$ psi/cycle, $k = 8.4$ mD, and $p^* = 4577$ psi.

The shape factor, C_A , for a closed circular reservoir is 31.62 (from Table B–1).

$$\begin{aligned} (\Delta t)_{\bar{p}} &= \frac{t_p}{C_A t_{pDA}} = \frac{\phi\mu_o c_t A}{0.000264 C_A k} \\ &= \frac{0.09 \times 0.65 \times 17.5 \times 10^{-6} \times 22/7 \times (1520)^2}{0.000264 \times 31.62 \times 8.4} = 94.23 \text{ hours} \end{aligned}$$

The MDH plot, Figure 5–3, does not extend to 94.23 hours, but the straight line may be extrapolated to that time. From Figure 5–3, $p_{ws} = 4407$ psig at 72 hours, so extrapolated one cycle to 94.23 hours.

$$\bar{p} = 4518 \text{ psig}$$

Modified Muskat Method

The modified Muskat method⁴ is based on the solution to flow equation for a well producing from a closed, constant rate. Muskat showed that a plot of $\log(\bar{p} - p_{ws})$ versus Δt should give a straight line that can be used to estimate \bar{p} . The method also requires that Δt and its corresponding p_{ws} value should be chosen in the range given by relationship:

$$\frac{250\phi\mu_o c_t r_e^2}{k} \leq \Delta t \leq \frac{750\phi\mu_o c_t r_e^2}{k} \quad (6-12)$$

Note that Eq. 5-40 has the form

$$\log(\bar{p} - p_{ws}) = A + B\Delta t \quad (6-13)$$

where A and B are constants. Follow these steps to apply Eq. 6-13:

- Assume a value of \bar{p} and plot $\log(\bar{p} - p_{ws})$ versus Δt until a straight line results.
- Extrapolating this straight line to zero provides an estimate of \bar{p} (Figure 6-4).

The Muskat method is quite sensitive. It gives satisfactory \bar{p} value for hydraulically fractured wells, and no crossflow occurs between the layers. The well should be centered in its drainage area. In some cases, the Δt range given above may take long shut-in times for the straight line to develop, particularly when dealing with low-permeability reservoirs.

Arps and Smith Method

The Arps and Smith method is based on Muskat's work.⁴ Arps and Smith⁵ suggest plotting of $\partial p_{ws}/\partial t$ versus p_{ws} during the late-transient buildup period to estimate average reservoir pressure, \bar{p} . The plot should yield a straight line that, when extrapolated to zero, provides an estimate of \bar{p} .

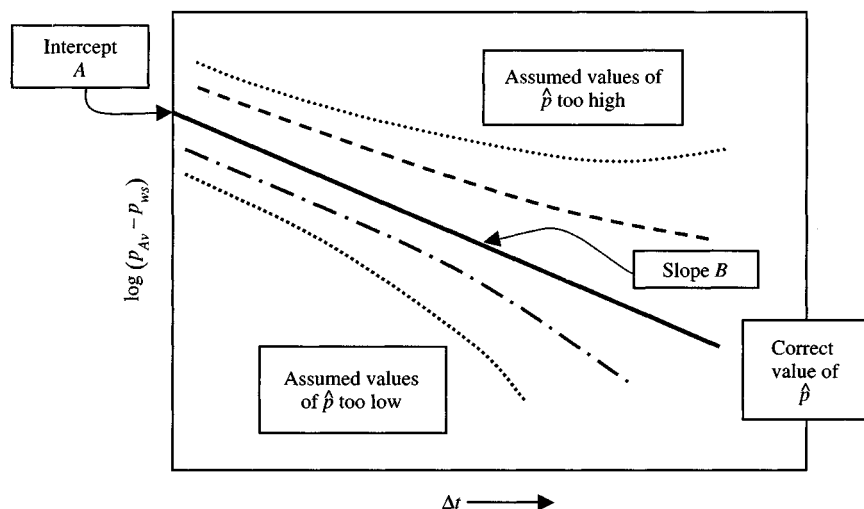


Figure 6-4. Technique to estimate \bar{p} using the modified Muskat method.

Example 6-2 *Calculating Average and Initial Reservoir Pressures in Square Drainage Area (Closed Reservoirs – No Flow Boundary)*

Assume that the well is draining from the center of a square drainage area of 20 acres. Calculate average reservoir pressure using MBH method.

Solution The following values are obtained from Example 5-7:

$$p^* = 4978 \text{ psi}, \quad t_p = 4320 \text{ hours}, \quad m = 152 \text{ psi/cycle}$$

Calculate t_{DA} using Eq. 6-1:

$$t_{pDA} = \frac{0.000264 \times 6.94 \times 4320}{0.23 \times 0.8 \times 17.0 \times 10^{-6} (7.72 \times 43,560)} = 7.54$$

To see if we should use $t_p = 4320$ hours, we estimate t_{pss} from Eq. 6-4 using $(t_{DA})_{pss} = 0.1$ (from Table B-2):

$$\begin{aligned} t_{pss} &= \frac{\phi \mu_o c_t A}{0.000264k} (t_{DA})_{pss} \\ &= \frac{0.23 \times 0.8 \times 17.0 \times 10^{-6} \times 7.72 \times 43,560}{0.000264 \times 6.94} \times 0.1 = 57.4 \text{ hours} \end{aligned}$$

Thus, $t_p > t_{pss}$; therefore, use t_p in the analysis. From Figure B-1

$$p_{DMBH}(t_{pDA}) = 5.25 \quad (\text{the corresponding ordinate value at } 7.54)$$

Calculate average reservoir pressure using Eq. 6-2:

$$\bar{p} = p^* - \frac{mp_{DMBH}(t_{pDA})}{2.303} = 4978 - \frac{152 \times 5.25}{2.303} = 4978 - 347 = 4631 \text{ psi}$$

Example 6-3 *Calculating Average Reservoir Pressure Using Muskat, and Arps and Smith Methods*

The following data in Table 6-1 were obtained during a pressure buildup test of an oil well. Table 6-2 shows calculations at various assumed values of average pressure.

Estimate average reservoir pressure in the drainage area of the well using the Muskat, and Arps and Smith methods.

Solution Columns 3 through 7 of Table 6-2 show computations necessary for the Muskat method. Each of these columns is plotted versus column 1 in Figure 6-5. For $\bar{p} = 2145$ psig a straight line is obtained showing this to be the correct reservoir pressure.

Table 6-1

Shut-in time, Δt (hr)	Well pressure, p_{ws} (psig)
0	1600
1	1984
3	2023
7	2052
10	2064
20	2087
30	2101
40	2109
50	2116
60	2121
70	2125
80	2128
90	2131
100	2133
110	2135
130	2138

Table 6-2
Average Reservoir Pressure Calculations Using Muskat Method
($\bar{p} - p_{ws}$ at $\Delta t = 0$)

Time, Δt (min)	Well pressure (psi)	$\bar{p} = 2145$ psi	$\bar{p} = 2150$ psi	$\bar{p} = 2155$ psi	$\bar{p} = 2160$ psi	$\bar{p} = 2140$ psi
40	2109	36	41	46	51	31
50	2116	29	34	39	44	24
60	2121	24	29	34	39	19
70	2125	20	25	30	35	15
80	2128	17	22	27	32	12
90	2131	14	19	24	29	9
100	2133	12	17	22	27	7
110	2135	10	15	20	25	5
130	2138	7	12	17	22	2

Intercept b at $\Delta t = 0$ is 38.5716 psig and slope $m = -0.24286$ psi/hr = -0.01012 psi/day.

Rework the buildup data in Example 6-3 using the Arps and Smith method. Table 6-3 shows average reservoir pressure calculations.

Columns 3 through 6 of Table 6-3 show computations necessary for the Arps and Smith method. Here, increments of pressure, Δp , and time, Δt , are used

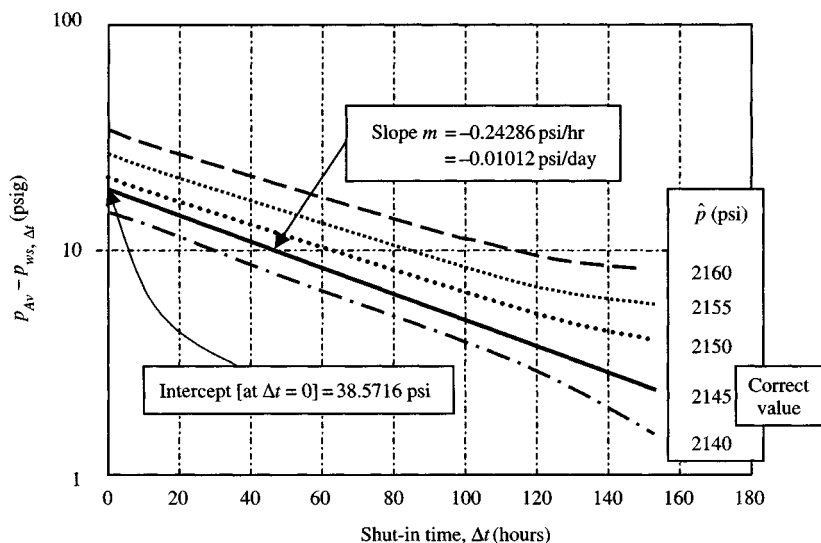


Figure 6-5. Determination of average reservoir pressure, p_{Av} , by Muskat method.

Table 6-3
Average Reservoir Pressure Calculations Using Arps and Smith Method

Δt (min)	Well pressure (psi)	Δp (psig)	Δt (hr)	$\Delta p/\Delta t$	Average $p_{ws\Delta t}$
40	2109	—	—	—	—
50	2116	7	10	0.70	2113
60	2121	5	10	0.50	2119
70	2125	4	10	0.40	2123
80	2128	3	10	0.30	2127
90	2131	3	10	0.30	2130
100	2133	2	10	0.20	2132
110	2135	2	10	0.20	2134
130	2138	3	20	0.15	2137

to approximate $\partial p/\partial t \approx \Delta p/\Delta t$. These values are plotted in Figure 6-6 against the average pressure, p_{ws} , for each respective increment.

6.4 Estimating Constant Pressure at Aquifer in Water-Drive Reservoirs

In water-drive systems, the initial and average pressures are important. The average pressure as a function of time at the original water-oil contact may be used for past-performance matching and prediction. Several techniques

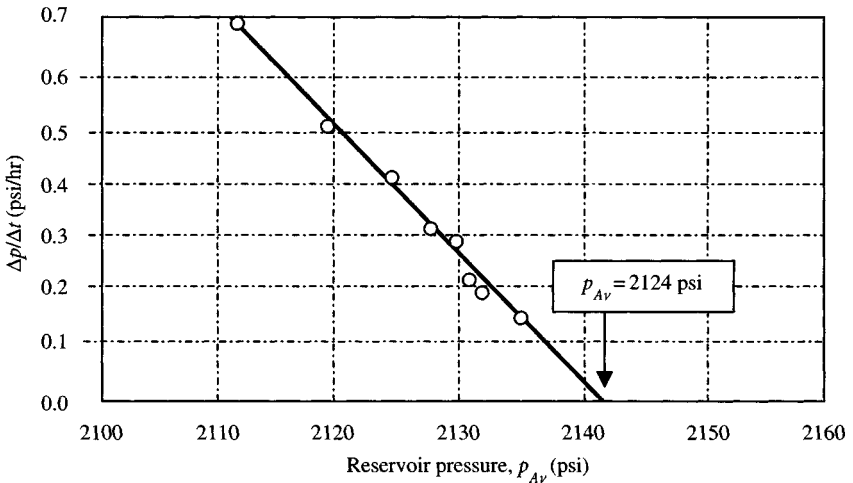


Figure 6-6. Determination of average reservoir pressure, p_{Av} , by Arps and Smith method.

may be used to estimate average and boundary pressures for water-drive systems. For short production times, the Horner and MBH methods are probably the best. The Dietz and MDH methods both apply for $t_{pDA} > 0.25$ and $s > -3$. The Muskat method also applies and may have more utility for water-drive systems than for closed systems. In this section we will discuss various methods to analyze and estimate initial and average pressures for water-drive systems.

Boundary and Average Pressure Estimation Using Various Methods

In this section we will discuss the estimation of boundary and average pressures using various techniques.

MBH Method

Pressure buildup data are plotted on semilog paper versus $(t_p + \Delta t)/\Delta t$. The resulting semilog straight line is extrapolated to $(t_p + \Delta t)/\Delta t = 1$ to obtain p^* . Then, the boundary or initial pressure is estimated from

$$p_i = p^* - \frac{70.65q_o\mu_o\beta_o}{kh} [p_{DMBHe}(t_{pDA})]_{\text{ordinate from lower curve in Figure 5-9}} \quad (6-14)$$

and the average pressure at the instant of shut-in is computed from

$$p_i = p^* - \frac{70.65q_o\mu_o\beta_o}{kh} [p_{DMBHe}(t_{pDA})]_{\text{ordinate from upper curve in Figure 5-9}} \quad (6-15)$$

where

$$t_{pDA} = \frac{0.000264kt_p}{\phi\mu_o c_t A} \quad (\text{hr}) \quad (6-16)$$

$$k = \frac{162.6q_o\mu_o\beta_o}{mh} \quad (\text{mD})$$

m = slope of the straight line from Horner plot, psi/cycle.

MDH Method

A normal plot of buildup pressure versus $\log \Delta t$ is made and the drainage boundary, p_i , and average pressure, \bar{p} , are then estimated by the following equations:

$$p_i = p_{ws}(\Delta t) + \frac{m}{1.1513} [p_{DMDM}(\Delta t_{DA})]_{\text{ordinate from dashed curve in Figure 5-12}} \quad (6-17)$$

or

$$\frac{kh}{141.2q_o\mu_o\beta_o} (p_i - p_{ws}(\Delta t)) = \text{ordinate from curve in Figure B-2 for square system}$$

The average pressure \bar{p} is estimated from

$$\frac{kh(\bar{p} - p_{ws}(\Delta t))}{141.2q_o\mu_o\beta_o} = \text{ordinate from curve in Figure B-1 for square system} \quad (6-18)$$

where Δt_{DA} is the time t_p read for \bar{p} or p_i for circular or square system with constant pressure boundaries and is given by

$$\Delta t_{DA} = \frac{0.000264k(\Delta t)}{\phi\mu_o c_t A} \quad (6-19)$$

A = area in acres $\times 43,560$, ft²

m = the slope of semilog straight line from MDH plot (p_{ws} versus $\log \Delta t$), psi/cycle

$$k = \frac{162.6q_o\mu_o\beta_o}{mh} \quad (\text{mD}) \quad (6-20)$$

$p_{ws(\Delta t)}$ = the shut-in pressure at any time, Δt , on the semilog straight line.

Dietz Method

Dietz method¹ requires the use of MDH data plot of buildup pressure versus $\log \Delta t$. The semilog straight-line portion of MDH plot (p_{ws} versus $\log \Delta t$) is extrapolated directly to read the value of p_i or \bar{p} . The time, Δt_{DA} , when \bar{p} may be read directly from the extrapolated semilog straight line, is given by

$$\Delta t_{DA} = \frac{t_p}{C_A t_{pDA}} = \frac{\phi\mu_o c_t A}{0.000264 C_A k} \quad (6-21)$$

where

C_A = the shape factor taken from Table B-2.

The Dietz method is quick and simple and usually is the preferred method for wells without a significant skin factor ($s > -3$ or $r_{wa} < -0.05r_e$) caused by acidizing or fracturing. This method applies only when $t_{pDA} > 0.25$ and $s > -3.0$.

Modified Muskat Method

Modified Muskat method⁴ requires plotting of $\log(\bar{p} - p_{ws})$ versus Δt ; a value of \bar{p} is assumed and $\log(\bar{p} - p_{ws})$ versus Δt is plotted. If the plot is a straight line, the correct value of \bar{p} has been found. If the plot is not a straight line, another value of \bar{p} is assumed and the process is repeated. The method also requires that Δt and its corresponding p_{ws} value should be chosen in the range given by the following relationship:

$$\frac{250\phi\mu_o c_t r_e^2}{k} \leq \Delta t \leq \frac{750\phi\mu_o c_t r_e^2}{k} \quad (6-22)$$

This method seems to be more applicable in water-drive reservoirs than in closed reservoirs.

Example 6-4 *Estimating Average Drainage Region Pressure and Analyzing Pressure Buildup Test in a Water-Drive Reservoir*

Rework Example 5-7; other data are: $t_p = 4320$ hours, $q = 350$ stb/day, $\mu_o = 0.8$ cP, $\beta_o = 1.136$ rb/stb, $c_t = 17.0 \times 10^{-6}$ psi⁻¹, $r_w = 0.29$ ft, $h = 49$ ft, $\phi = 0.23$, and $A = 7.72$ acres; well in center of a square with constant pressure boundaries, 580×580 ft² = 336,400 ft². Estimate \bar{p} and p_e using the following methods: (1) MBH method, (2) MDH method, (3) Dietz method, (4) modified Muskat method, and (5) Ramey and Cobb method.

Solution

(1) *MBH method*: $t_p = 4320$ hours (from Example 5-7) and $p^* = 4978$ psi (from Example 5-7).

Calculate dimensionless well-producing time before shut-in using Eq. 6-1:

$$t_{pDA} = \frac{0.000264kt_p}{\phi\mu_o c_t A} = \frac{0.000264(6.94)(4320)}{0.23(0.8)(17.0 \times 10^{-6})(7.72 \times 43,560)} = 7.54$$

$$t_{pss} = \frac{\phi\mu_o c_t A}{0.000264k} = \frac{0.23(0.8)(17.0 \times 10^{-6})(7.72 \times 43,560)}{0.000264 \times 6.94} = 57.4 \text{ hr}$$

Calculate the average reservoir pressure, \bar{p} , using upper curve in Figure 5-9

$$\frac{kh}{70.65q_o\mu_o\beta_o}(p^* - \bar{p}) = 4.75$$

or

$$\bar{p} = p^* - 4.75 \frac{70.65(350)(0.8)(1.136)}{6.94(49)} = 4978 - 314 = 4664 \text{ psi}$$

and calculate the initial reservoir pressure, p_i , using lower curve in Figure 5-9.

$$\frac{kh}{70.65q_o\mu_o\beta_o}(p^* - p_i) = 3.90$$

or

$$p_i = p^* - 3.90 \frac{70.65(350)(0.8)(1.136)}{6.94(49)} = 4978 - 258 = 4720 \text{ psi}$$

(2) *MDH method:*

Choose $\Delta t = 20$ hours on the straight-line section of the MDH buildup curve in Figure 5-15. From Eq. 6-1

$$\Delta t_{DA} = \frac{0.000264 \times 7.04 \times 20}{0.23 \times 0.8 \times 17.0 \times 10^{-6} \times 7.72 \times 43,560} = 0.0352$$

Calculate average reservoir pressure, \bar{p} , from upper curve in Figure 5-12; p_{DMDH} at $\Delta t_{DA} = 0.0352$ is 0.22. From Figure 5-15 p_{ws} at $\Delta t = 20$ hr is 4490 psi and $m = 150$ psi/cycle. Then, using Eq. 6-6

$$\begin{aligned} \bar{p} &= p_{ws} + \frac{mp_{DMDH}(\Delta t_{DA})_{\text{lower curve in Figure 6-3}}}{1.1513} \\ &= 4490 + \frac{150 \times 0.22}{1.1513} = 4490 + 29 = 4519 \text{ psi} \end{aligned}$$

This is a close check of the value of 4648 psi obtained by the Horner graph. Calculate initial reservoir pressure, p_i , from upper curve in Figure 6-3; p_{DMDH} at $(\Delta t_{DA}) = 0.0352$ is 0.68. Using Eq. 6-6a

$$\begin{aligned} p_i &= p_{ws} + mp_{DMDH}(\Delta t_{DA})_{\text{upper curve in Figure 6-3}} \\ &= 4490 + 150 \times 0.68/1.1513 = 4490 + 89 = 4579 \text{ psi} \end{aligned}$$

This value is also a close check of the value of 4720 psi obtained by the Horner graph.

(3) *Dietz method:*

This method² requires the use of the MDH plot given in Figure 5-15. From Example 5-7

$$m = 150 \text{ psi/cycle}, \quad k = 7.04 \text{ mD}, \quad p^* = 5055 \text{ psi}$$

Then, using Eq. 6-7

$$(\Delta t)_{\bar{p}} = \frac{0.23(0.8)(17.0 \times 10^{-6})(7.72 \times 43,560)}{0.000264(30.8828)(7.04)} = 18.33 \text{ hours}$$

The average reservoir pressure is now read from Figure 5-15 at $(\Delta t)_{\bar{p}} = 18.33$ hours, which is equal to $\bar{p} = 4430$ psi.

(4) *Modified Muskat method:*

This method⁴ requires plotting of $\log(\bar{p} - p_{ws})$ versus Δt . A value of \bar{p} is assumed. If the plot is a straight line, the correct value of \bar{p} has been found.

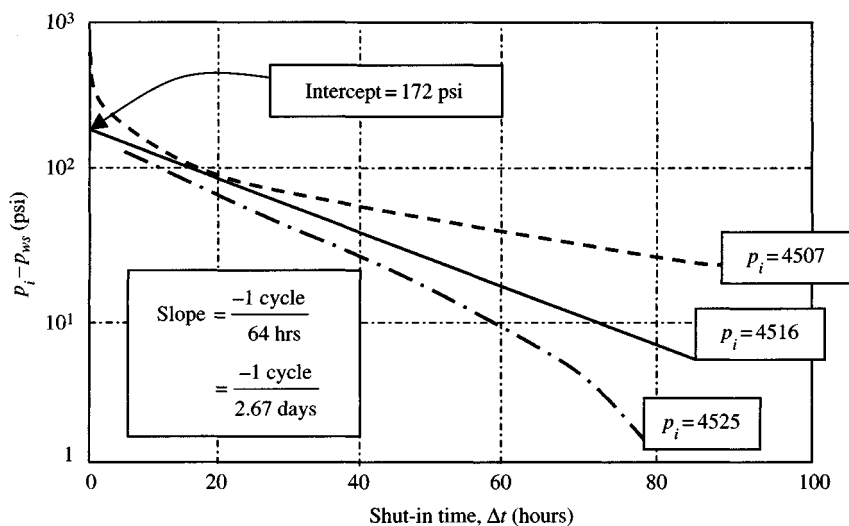


Figure 6-7. Muskat graph.

The Muskat graph is a plot of an assumed p_i less than the measured shut-in pressure versus shut-in time as shown in Figure 6-7. The pressure difference needed to make this graph is also given in Table 6-4. Three columns are given for assumed p_i of 4507, 4516, and 4525 psi. Inspection of Figure 6-7 shows that the 4507 psi case bends sharply downwards, indicating that the estimated p_i is too low. The line for 4516 psi appears straight after 15 hours. The line for 4525 psi bends upwards, although this fact is easier to see if a straight edge is placed along the line.

Table 6-4
Buildup Test Data for Muskat Plot

Shut-in time, Δt (hr)	Shut-in pressure, p_{ws} (psig)	$p_i = 4507$ (psig)	$p_i = 4516$ (psig)	$p_i = 4525$ (psig)
0	3561	946	955	964
10	4387	120	129	138
20	4432	75	84	93
30	4455	52	61	70
40	4473	34	43	52
50	4486	21	30	39
60	4495	12	21	30
70	4501	6	15	24
80	4506	1	10	19

From Figure 6-7 the following information is obtained:

$$\text{Intercept} = 172 \text{ psi, slope}(m_M) = -\frac{1}{64} \text{ hr}^{-1} = -0.015625 \text{ cycle/hr} = -\frac{1}{2.67} \text{ day}^{-1}$$

Using Eq. 5-42

$$t_{pDA} = \frac{0.0002637kt_p}{\phi\mu_o c_t r_w^2} = \frac{0.0002637(7.04)(4320)}{(0.23)(0.8)(17.0 \times 10^{-6})(7.72)(43,560)} = 7.52$$

References 3 and 6 have provided the values of dimensionless Muskat intercepts:

$$\text{For constant pressure boundary, } p_{DM \text{ int}} = 1.34 \quad [t_{pDA} > 0.25] \quad (6-23)$$

$$\text{For closed squared system, } p_{DM \text{ int}} = 0.67 \quad [t_{pDA} > 0.1] \quad (6-24)$$

Minimum and maximum range of Δt and its corresponding p_{ws} values are:

$$\frac{250\phi\mu_o c_t r_e^2}{k} \leq \Delta t \leq \frac{750\phi\mu_o c_t r_e^2}{k}$$

$$\frac{250 \times 0.23 \times 0.8 \times 17.0 \times 10^{-6} \times 327^2}{7.04} \leq \Delta t$$

$$\leq \frac{750 \times 0.023 \times 0.8 \times 17.0 \times 10^{-6} \times 327^2}{7.04}$$

$$12 \leq \Delta t \leq 36.0 \text{ hours}$$

Reservoir permeability, k , may be estimated from Eq. 6-23:

$$k = \frac{141.2q_o\mu_o\beta_o}{h(\bar{p} - p_{ws})_{int}} \times 1.34$$

$$k = \frac{141.2 \times 350 \times 1.136 \times 0.8}{49 \times 175} \times 1.34 = 7.03 \text{ mD}$$

This closely checks the Horner method value of 7.04 mD. Using Eq. 5-48, find

$$\phi c_t = -0.0559 \frac{k}{\mu A} \left(\frac{1}{\text{slope, cycle/day}} \right)$$

$$= -0.0559 \times \frac{7.03}{0.8 \times 7.72 \times 43,560} \frac{1}{(-2.67)} = 5.47 \times 10^{-6} \text{ psia}^{-1}$$

This checks the values given:

$$\phi c_t = 0.23 \times 17.0 \times 10^{-6} = 3.91 \times 10^{-6} \text{ psia}^{-1} \Rightarrow \text{approximately close}$$

(5) *Ramey and Cobb method*:

$$t_p = 4320 \text{ hours}, \quad t_{pss} = 57.4, \quad C_A = 30.8828 \quad (\text{shape factor})$$

$$t_p \geq \Delta t_{pss}$$

Therefore

$$\begin{aligned} \left(\frac{t_p + \Delta t}{\Delta t} \right)_{\bar{p}} &= C_A t_p D_A = \frac{0.000264 k t_p C_A}{\phi \mu c_t A} \\ &= \frac{0.000264(6.94)(4320)(30.8828)}{0.23(0.8)(17.0 \times 10^{-6})(7.72 \times 43,560)} = 232.5 \end{aligned}$$

From Horner graph, using Figure 5-14, the average reservoir pressure is

$$\bar{p} = 4420 \text{ psi}, \quad \left(\frac{t_p + \Delta t}{\Delta t} \right)_{\bar{p}} = 232.5$$

6.5 Summary

This chapter treats to estimate original and average reservoir pressures using various techniques such as the Horner, MBH, MDH, Dietz, Ramey, and Muskat and Arps methods. This chapter also includes determining constant pressure at aquifer in water-drive reservoir.

References and Additional Reading

1. Dietz, D. N., "Determination of Average Reservoir Pressure From Build-Up Surveys," *Trans. AIME* (1965).
2. Mathews, C. S., Brons, F., and Hazebrock, P., "A Method for Determination of Average Pressure in a Bounded Reservoir," *Trans. AIME* (1954).
3. Ramey, H. J., Jr., and Cobb, W. M., "A General Buildup Theory for a Well in a Closed Drainage Area," *J. Pet. Technol.* (Dec. 1971), 1493-1505; *Trans. AIME*, 251.
4. Muskat, M., *Physical Principles of Oil Production*, McGraw-Hill Book Co, Inc., NY, 1949, 378ff.

5. Arps, J. J., and Smith, A. E., "Practical Use of Bottom-Hole Pressure Buildup Curves," *Drill. and Prod. Pract. API* (1949), 155–165.
6. Kumar, A., and Ramey, H. J., Jr., "Well-Test Analysis for a Well in a Constant Pressure Square," paper SPE 4054, presented at the SPE-AIME 47th Annual Fall Meeting, San Antonio, TX, Oct. 8–11, 1972.
7. Miller, C. C., Dyes, A. B., and Hutchinson, C. A., Jr., "The Estimation of Permeability and Reservoir Pressure From Bottom Hole Pressure Buildup Characteristics," *Trans. AIME* (1950) 189, 91–104.

Chapter 7

Well Testing Methods for Naturally Fractured Reservoirs

7.1 Introduction

Naturally fractured reservoirs are different from conventional (unfractured) reservoirs. They are heterogeneous in type and consist of matrix blocks separated from one another by the fracture system as shown in Figure 7-1. The matrix blocks are made of the original rock that was present before fracturing took place. The matrix is characterized by its permeability k_m and porosity ϕ_m . The fracture system is characterized by its permeability k_f and porosity ϕ_f . It means a naturally fractured reservoir is a double-porosity and double-permeability reservoir. This chapter presents identification of fractures, main characteristics, and brief review of the most widely used well testing models.

7.2 Identification of Natural Fractures

It is essential to identify fractures during exploration and drilling. Well logs are useful tools in identifying these natural fractures. A program for fracture detection based on logging techniques consists of using different logs.

- Borehole televiewer logs can be used to identify induced and natural fractures.
- Acoustic, receptivity, and temperature logs can be used to obtain a realistic picture of fractures and their width and orientation in the vicinity of wellbore.
- Variable-density logs can define fracture intervals.

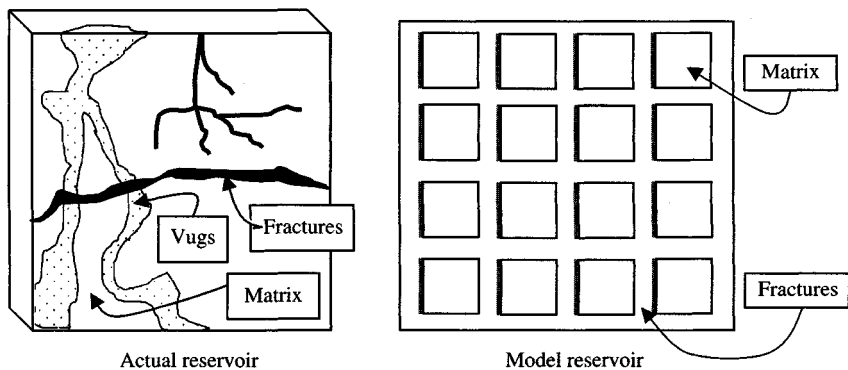


Figure 7-1. Idealization of a naturally fractured heterogeneous porous media.

Both core analysis and logging are valuable techniques for explored wells in detecting fracture porosity ϕ_f , permeability k_f , and nature of the matrix or intergranular porosity. However, there are many wells drilled where no core was taken and the logs do not show any evidence of fractures. Therefore, well test analysis is the only technique used for getting information about the fractured nature of formation, and can provide information on fractured reservoir parameters such as k_m , ϕ_m , ϕ_f , k_f , size and shape of the matrix blocks, and the nature and orientation of the fracture pattern, in addition to determining \bar{p} or p_i and skin factor s .

7.3 Characteristics of Naturally Fractured Reservoirs

These types of reservoirs are heterogeneous and have characteristics as shown in Figure 7-2.

7.4 Typical Pressure Drawdown Behavior Curve Shapes

Graph of pressure drawdown in individual wells can be divided into three areas:

- Transient radial flow through fracture (first parallel straight line).
- Transitional slowdown rate of decline in pressures.
- Late-transient radial flow (second parallel straight line).

These portions are illustrated for a pressure drawdown case in Figure 7-3. Characteristic curve of Figure 7-3 is obtained for $\omega > 0$ and $\lambda \cong 10^{-5}$.

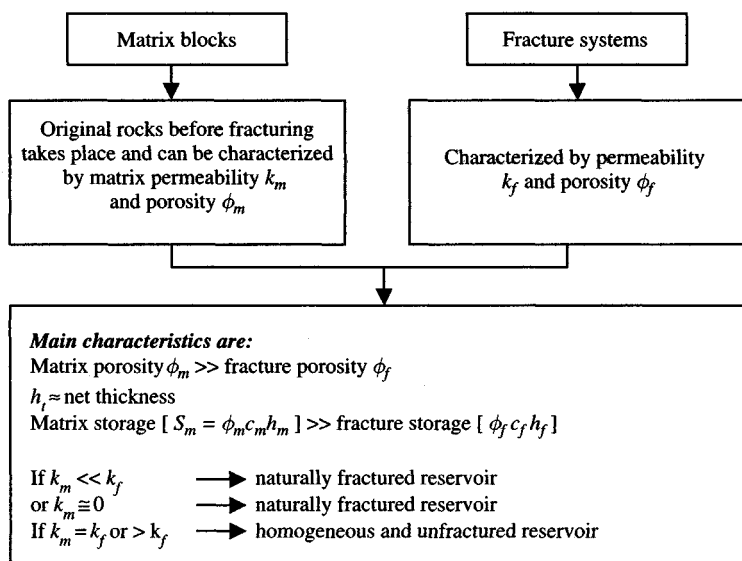


Figure 7-2. Main characteristics of matrix blocks and fracture systems.

7.5 Pressure Buildup Behavior Characteristics

Figure 7-4 shows pressure buildup well behavior from a naturally fractured reservoir at a constant rate.

Pressure Buildup Analysis Equations

Slopes m_1 and m_3 are equal, and slope m_2 is approximately equal to half of the first and final slopes. Fracture permeability is calculated using equation:

$$k_f = \frac{162.6q\mu\beta}{m_1 h} \quad (\text{mD}) \quad (7-1)$$

Time at the point of intersection of the final straight line and the transitional straight line of one-half slope is equal to

$$\Delta t_x = \frac{0.182L^2}{\eta_m} \quad (\text{hours}) \quad (7-2)$$

where

L = length of matrix block, ft

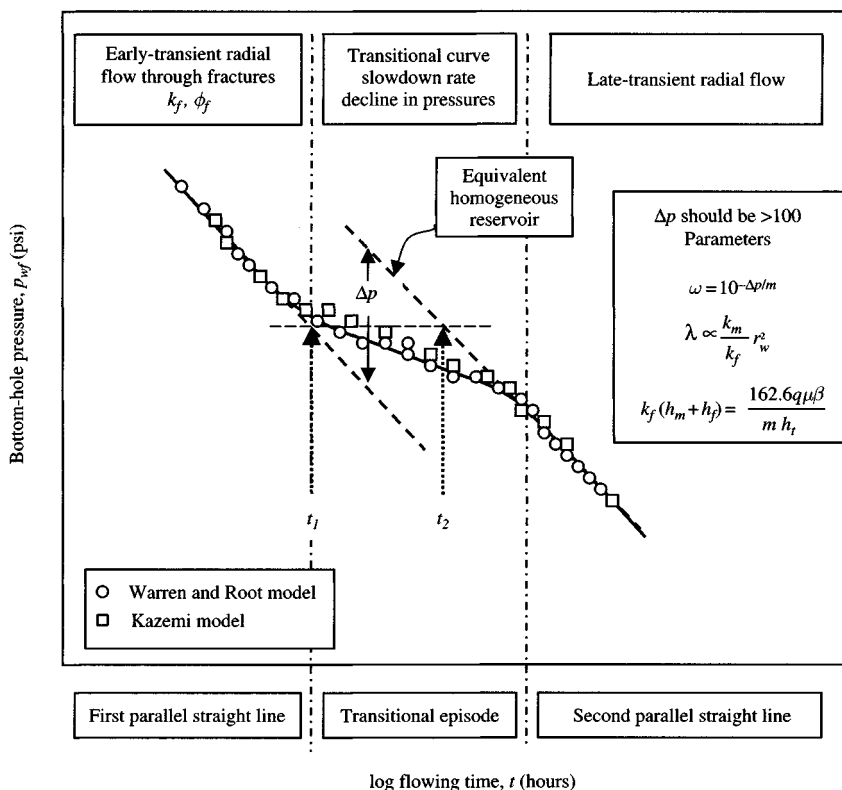


Figure 7-3. Typical pressure drawdown behavior curve shapes.¹

$$\eta_m = \frac{2.637 \times 10^{-4}}{\mu \phi_m c_m} \quad (\text{ft}^2/\text{hr}) \quad (7-3)$$

Note: The larger the matrix block dimension, L , the tighter the matrix.

$$\text{Ratio} = \frac{\text{Matrix storage capacity}}{\text{Fracture storage capacity}} = \frac{S_m}{S_f} = \left[\frac{\log t_1}{\log t_2} \right] \quad (7-4)$$

7.6 Well Test Interpretation Methods, Uses, and Limitations

The main purposes of well test analysis are to determine k_m , ϕ_m , k_f , ϕ_f , size and shape of the matrix blocks, and the nature and orientation of the fracture pattern, in addition to determining \bar{p} or p_i and the skin factor s . All these parameters cannot be determined by merely measuring pressure versus time.

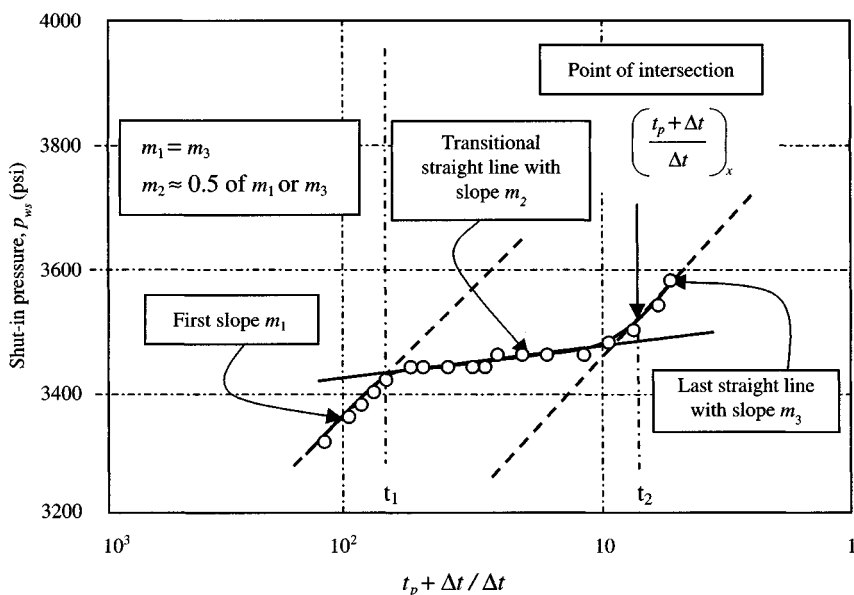


Figure 7-4. Pressure buildup curve in naturally fractured reservoir – semilog plot.²

Furthermore, interpretation of well test data depends on whether the assumptions made in formulating the interpretation model correspond to the reality of the reservoir on hand. Thus, a choice of the interpretation model is necessary. Most widely used well testing interpretation models are shown in Figure 7-5.

Figure 7-5a shows an overview of well test interpretation models.

Pseudo-Steady-State Model

Warren and Root¹ characterized the naturally fractured porous media by two parameters (ω and λ). The parameter ω is defined as the ratio of fracture storage to total storage. The interporosity flow parameter λ is proportional to the ratio of matrix permeability to fracture permeability. Thus,

$$\omega = \frac{S_f}{S_f + S_m} \quad (7-5)$$

where

$$S_f = \text{fracture storage} = \phi_f c_f h_f \quad (7-6)$$

$$S_m = \text{matrix storage} = \phi_m c_m h_m \quad (7-7)$$

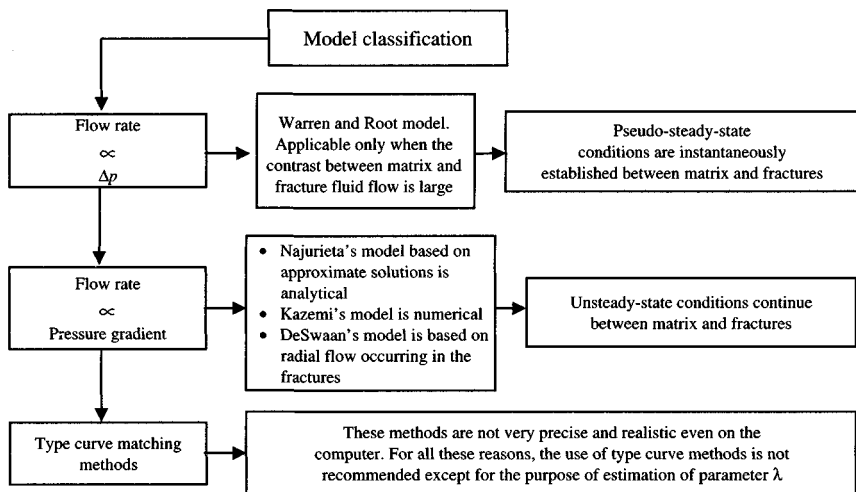


Figure 7-5. Most common interpretation methods.

and

$$\lambda \propto \frac{k_m}{k_f} \quad (7-8)$$

or

$$\lambda = \alpha \frac{r_w^2 k_m}{k_f} \quad (7-9)$$

where

λ = interporosity flow coefficient

α = geometric parameter, $1/L^2$

r_w = wellbore radius, ft

k_m = matrix permeability, mD

k_f = fracture permeability, mD.

If the value of ω in the neighborhood of 0.01 would indicate substantial fracture porosity caused by wide fracture, a value of λ in the neighborhood of 10^{-5} would indicate that the permeability of the matrix is in hundreds of millidarcies. From an infinite, naturally fractured reservoir, with the assumption that matrix to fracture flow occurs under pseudo-steady-state conditions for a well producing at a constant rate, Warren and Root derived drawdown and buildup equations. Useful forms of the equations for buildup and drawdown were presented by Kazemi.³

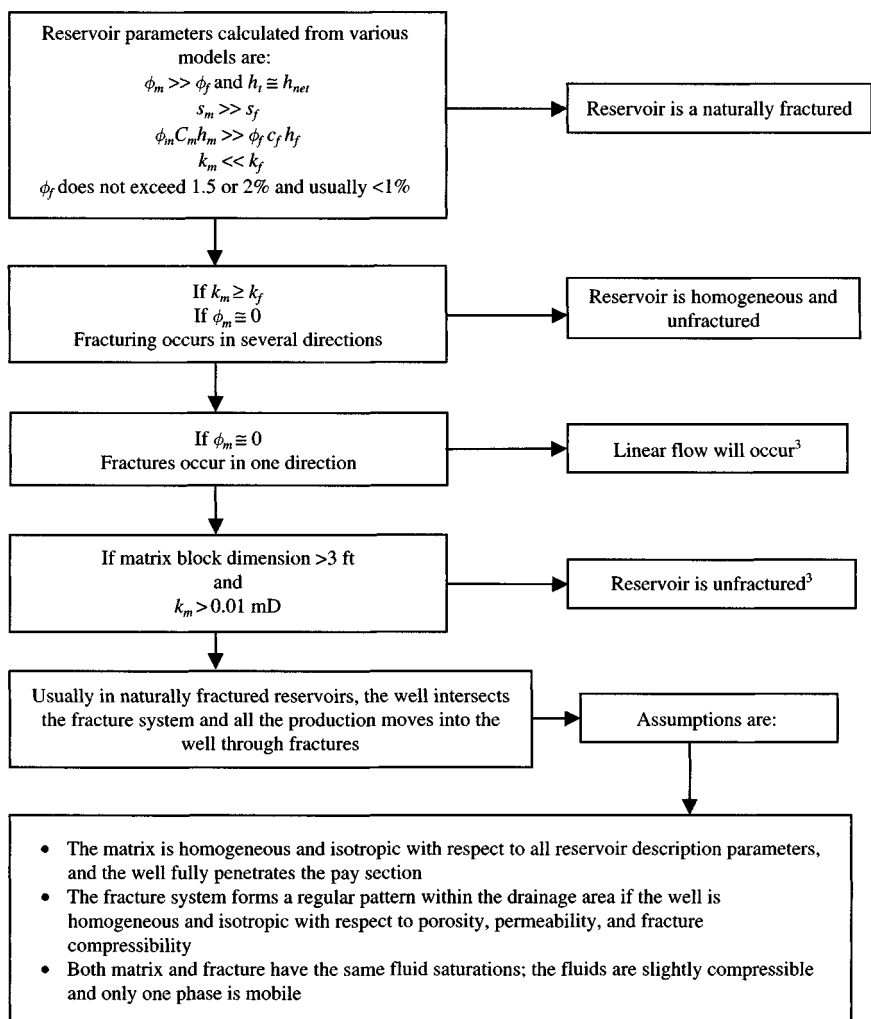


Figure 7-5a. Main characteristics and behavior of naturally fractured reservoirs.

For buildup:

$$p_i - p_{ws} = \frac{162.6q_o\beta_o\mu_o}{k_f(h_f + h_m)} \left\{ \log \frac{t_p + \Delta t}{\Delta t} = 0.435E_i[-\lambda\Delta t_D/\omega(1-\omega)] \right. \\ \left. + 0.435E_i[-\lambda\Delta t_D/(1-\omega)] \right\} \quad (7-10)$$

For drawdown:

$$p_i - p_{ws} = \frac{162.6q_o\beta_o\mu_o}{k_f(h_f + h_m)} \left\{ \log t + \log \frac{k}{(\phi_m c_m + \phi_f c_f)\mu_o r_w^2} - 3.23 + 0.435E_i \right. \\ \left. [-\lambda t_D/\omega(1 - \omega)] - 0.435E_i[-\lambda\Delta t_D/(1 - \omega)] + 0.87s \right\} \quad (7-11)$$

where

$$t_D = \frac{0.000264k_f t}{(\phi_f c_f + \phi_m c_m)\mu_o r_w^2} \quad (7-12)$$

$$\Delta t_D = \frac{0.000264k_f \Delta t}{(\phi_f c_f + \phi_m c_m)\mu_o r_w^2} \quad (7-13)$$

$$q_D = \frac{141.2\beta_o\mu_o q}{k_f h(p_i - p_f)} \quad (7-14)$$

and function is

$$E_i(-x) = \ln x + 0.5772 - x + \frac{x^2}{2 \times 2!} - \frac{x^3}{3 \times 3!} + \frac{x^4}{4 \times 4!} - \cdots + \frac{x^n}{n \times n} \quad (7-15)$$

Transient-State Model

Najurieta's Approach

This method¹⁴ is approximate and has limited applications.

Pressure Gradient Models

Streltsova⁴ and DeSwaan⁵ Techniques

Streltsova⁴ pointed out that Horner's plot will not exhibit the characteristic three-segment curve according to his theory unless the buildup is proceeded by a sufficiently long drawdown period such that the third straight line would develop over one log cycle before shut-in. According to Streltsova, if a well is produced from a naturally fractured reservoir at a constant rate, a plot of p_{wf} versus t on semilog graph paper (see Figure 7-5b) would initially be a straight line of slope m_1 given by

$$m_1 = \frac{162.6q_o\mu_o\beta_o}{k_f h_f} \quad (7-16)$$

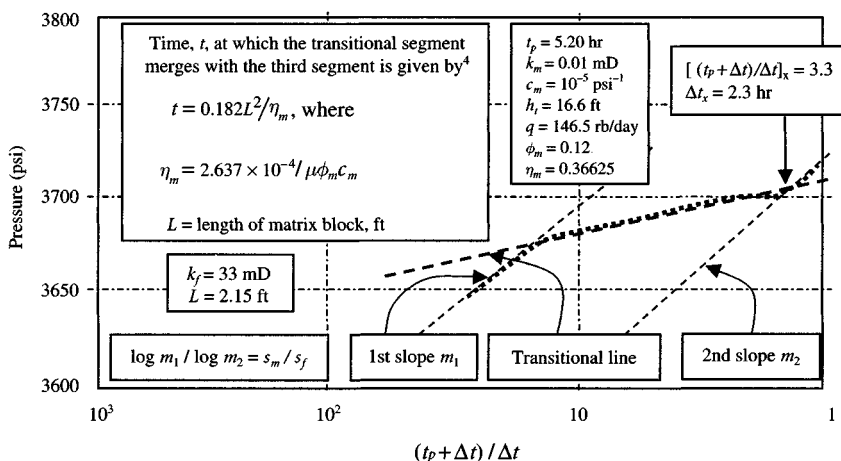


Figure 7-5b. Pressure buildup data plot – naturally fractured reservoir.⁴

Type Curve Matching Technique

Type curves are useful interpretation methods and have limited applications. If wellbore storage effects are present but the 45° line does not develop on the log-log plot, then the early part of the test cannot be interpreted, even with type curves. If a characteristic semilog plot develops, then one can calculate k_f , ω , and s from this plot, and it would then be possible to use type curves to estimate λ . Figure 7-6 shows wellbore storage and skin type curves, which can be used to match the early data with one of the type curves labeled $C_D e^{2s}$. The label of the matched curve is now referred to as $(C_D e^{2s})_f$. The permeability k_f is estimated from the pressure match, and C is calculated from the time match as follows:

$$k_f = \frac{141.2q\mu\beta}{h} \left(\frac{p_D}{\Delta p} \right)_{\text{match}} \quad (7-17)$$

$$C = \frac{kh}{3389\mu} \left(\frac{\Delta t}{(t_D/C_D)} \right)_{\text{match}} \quad (7-18)$$

The final segment is also matched to one of the curves labeled $C_D e^{2s}$, but this time the label is referred to as $(C_D e^{2s})_{f+m}$. The permeability, k_f , and C are estimated by Eqs. 7-17 and 7-18. If total reservoir storage

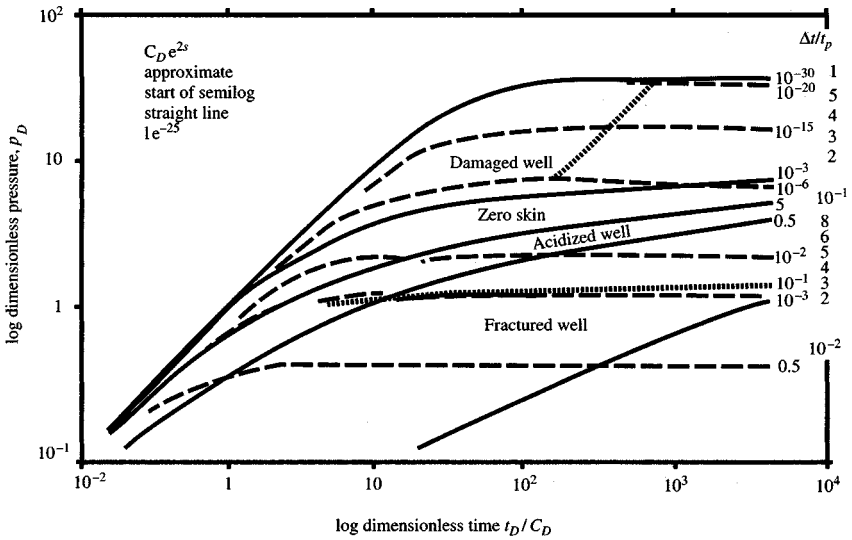


Figure 7-6. Wellbore storage and skin type curves in a double-porosity reservoir.⁶

$(S_f + S_m)$ is known from well logs, then parameter $(C_D)_{f+m}$ is determined as follows:

$$(C_D)_{f+m} = \frac{0.8936C}{(S_f + S_m)r_w^2} \quad (7-19)$$

$$s = 0.5 \ln \frac{(C_D e^{2s})_{f+m}}{(C_D)_{f+m}} \quad (7-20)$$

$$\omega = \frac{(C_D e^{2s})_{f+m}}{(C_D e^{2s})_f} \quad (7-21)$$

The intermediate segment is matched to one of the curves labeled λe^{-2s} , and λ is determined as follows:

$$\lambda = (\lambda e^{-2s})_{match} \times e^{2s} \quad (7-22)$$

Pressure Derivative Method^{6,7}

The pressure derivative type curves are used to match the derivative of pressure data to a derivative type curve and then read the matching

parameters on the original type curves shown in Figure 7-7. The following equations can be used to calculate reservoir parameters such as ω , kh , C , C_D , s , and λ for pressure buildup analysis.

Parameter ω is calculated from the equation

$$\omega = \frac{(C_D e^{2s})_{f+m}}{(C_D e^{2s})_f} \quad (7-23)$$

Product kh is calculated from the equation

$$kh = 141.2q\mu\beta \left(\frac{p_D}{\Delta p} \right)_{match} \quad (7-24)$$

Wellbore storage constant is calculated from the equation

$$C = \frac{0.000295kh}{\mu} \left(\frac{\Delta t}{C_D/t_D} \right)_{match} \quad (7-25)$$

$$(C_D)_{f+m} = \frac{0.8936C}{\phi c_t h r_w^2} \quad (7-26)$$

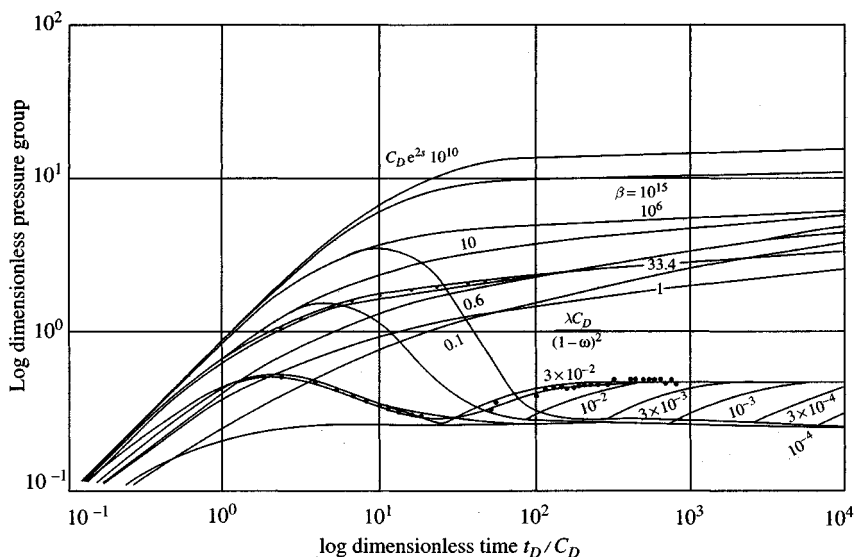


Figure 7-7. Pressure derivative type curves.⁶

From curve match points

$$s = 0.5 \ln \left[\frac{(C_D e^{2s})_{f+m}}{(C_D)_{f+m}} \right] \quad (7-27)$$

From transition curve match points

$$\lambda = \left(\frac{\lambda C_D}{(1 - \omega)^2} \right)_{match} \times \frac{(1 - \omega)^2}{(C_D)_{f+m}} \quad (7-28)$$

Example 7-1¹⁵ *Analyzing Pressure Buildup Test in Naturally Fractured Reservoir*

Pressure buildup test data for a naturally fractured well are given in Table 7-1. Other well and reservoir data are given below:

Rate at the beginning, stb/day	2952
Time of flow, hours	1.33
Closing time, hour	0.31
Open again rate, stb/day	960
Flowing time, hours	5.05
Close again, hour	0.39
Open again rate, stb/day	960
Flowing again, hours	31.13
Final shut-in and pressure-time data recorded	see Table 7-1

$q_o = 960$ stb/day, $\phi = 0.07$, $\mu_o = 1.0$ cP, $h = 36$ ft, $\beta_o = 1.280$ rb/stb, $c_t = 1.0 \times 10^{-5}$ psi⁻¹, and $r_w = 0.29$ ft. Calculate the following using Horner plot and type curve matching method:

- Total producing time.
- Reservoir properties such as ω , kh , C , s , and λ .

Solution

$$\text{Total oil produced} = \frac{2952}{24} [1.33 + 5.05] + \frac{960}{24} \times 31.13 = 2030 \text{ stb}$$

$$\therefore \text{Pseudo-producing time, } t_p = \frac{2030}{960/24} = 50.75 \text{ hours}$$

- Figure 7-8 is the log-log plot of Δp_{ws} versus Δt ; the 45° line is plotted in Figure 7-8 and it shows that this test was affected by wellbore storage.

Table 7-1
Pressure Buildup Data¹⁵

Shut-in time, Δt (hr)	Δp (psi)	$(t_p + \Delta t)/\Delta t$	Slope (psi/hr)	Pressure derivative term
0.0000	0.00	—	3180	—
0.0035	11.10	14,547.22	1727.63	8.56
0.0091	20.69	5612.17	847.26	11.65
0.0146	25.40	3477.03	486.90	9.74
0.0202	28.11	2518.92	337.14	8.31
0.0257	29.98	1974.86	257.22	7.64
0.0313	31.41	1624.14	196.56	7.10
0.0368	32.50	1379.24	159.66	6.56
0.0424	33.39	1198.56	127.80	6.10
0.0479	34.10	1059.76	107.28	5.64
0.0590	35.29	860.52	83.25	5.63
0.0702	36.21	724.39	69.48	5.36
0.0813	36.99	625.49	65.97	5.51
0.0924	37.72	550.38	55.07	5.60
0.1035	38.33	491.39	48.83	5.39
0.1257	39.42	404.71	43.65	5.83
0.1478	40.39	344.07	37.16	5.99
0.1702	41.21	299.25	34.38	6.11
0.1924	41.98	264.80	29.93	6.21
0.2146	42.64	237.49	28.85	6.33
0.2368	43.28	215.30	30.96	7.12
0.2590	43.97	196.92	25.78	7.39
0.2813	44.54	181.43	24.44	7.10
0.3035	45.09	168.22	25.79	7.67
0.3257	45.66	156.81	20.63	7.61
0.3813	46.80	134.11	18.58	7.53
0.4368	47.84	117.18	17.19	7.88
0.4924	48.79	104.07	16.36	8.34
0.5479	49.70	93.62	15.14	8.72
0.6035	50.54	85.09	12.50	8.44
0.6646	51.31	77.36	12.68	8.48
0.7146	51.94	72.02	11.70	8.83
0.7702	52.59	66.90	11.14	8.93
0.8257	53.21	62.46	10.58	9.11
0.8813	53.80	58.59	10.87	9.62
0.9368	54.40	55.17	8.53	9.26
0.9924	54.87	52.14	10.32	9.54
1.0479	55.45	49.43	7.70	9.64
1.1035	55.88	46.99	8.73	9.26
1.2146	56.85	42.78	7.57	10.14
1.3257	57.69	39.28	5.91	9.17

Table 7-1 (continued)

Shut-in time, Δt (hr)	Δp (psi)	$(t_p + \Delta t)/\Delta t$	Slope (psi/hr)	Pressure derivative term
1.4368	58.34	36.32	6.40	9.10
1.5479	59.05	33.79	6.05	9.93
1.6590	59.73	31.59	5.57	9.95
1.7702	60.35	29.67	5.44	10.08
1.8813	60.95	27.98	4.74	9.93
1.9924	61.48	26.47	4.67	9.75
2.1035	61.99	25.13	4.34	9.87
2.2146	62.48	23.92	3.99	9.62
2.4368	63.36	21.83	3.68 ^a	9.79
2.6924 ^a	64.30 ^a	19.85 ^a	3.06 ^a	9.55 ^a
2.9146 ^a	64.98 ^a	18.41	3.16	9.59
3.1368	65.69	17.18	2.44	9.34
3.3590	66.23	16.11	19.72	39.68

^a Pressure derivative term $\Delta t \Delta p'_{ws} \frac{t_p + \Delta t}{\Delta t}$, for $t_p = 51.75$ hours, is estimated as follows:

- $(64.98 - 64.30)/(2.9146 - 2.6924) = 3.06$.
- $[(3.68 + 3.06)/2] \times 19.85 \times 2.6924^2/50.75 = 9.55$.

- Figure 7-9 is Horner's plot. Buildup curve can be interpreted in terms of the models by Warren and Root, Streltsova, and Najurieta. Figure 7-9 also shows that vertical separation Δp is less than 100 psi; therefore, parameter ω cannot be determined accurately by the Warren and Root method.
- Figure 7-10 is a plot of the pressure derivative versus Δt on log-log graph.
- Figure 7-11 shows the data of Figures 7-8 and 7-10 matched to Bourdet's type curves. Matching procedure is as follows:
 - Copy the curve of Figure 7-11 on Figure 7-10.
 - Match the derivative curve of Figure 7-10 with one of the derivative type curves of Figure 7-11.
 - Choose any point and read its coordinates on both figures: $[\Delta p]_{match}$, $[\Delta t]_{match}$, $[p_D]_{match}$, and $[t_D/C_D]_{match}$.
 - Also, read the match derivative curve label $\lambda C_D/(1 - \omega)^2$, where C_D is $(C_D)_{f+m}$.
 - Read the values of the curves labeled $C_D e^{2s}$, which match the initial and final points of the data curve $(C_D e^{2s})_f$ and $(C_D e^{2s})_{f+m}$, respectively.
 - Calculate the reservoir parameters as follows:

From Eq. 7-23

$$\omega = \frac{(C_D e^{2s})_{f+m}}{(C_D e^{2s})_f} = \frac{0.6}{33.4} = 0.018$$

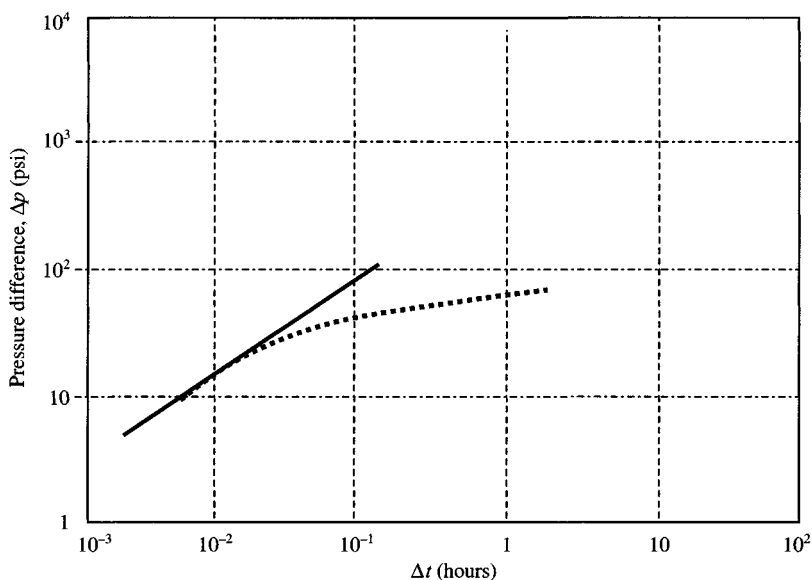


Figure 7-8. log-log pressure buildup data plot.

From Eq. 7-24

$$kh = 141.2q\mu\beta\left(\frac{p_D}{\Delta p}\right)_{match} = 141.2 \times 960 \times 1 \times 1.28 \times 0.053$$

$$= 9196 \text{ mD ft}$$

From Eq. 7-25

$$C = \frac{0.000295kh}{\mu} \left(\frac{\Delta t}{t_D/C_D}\right)_{match} = \frac{0.000295 \times 9196}{1.0 \times 270} = 0.01 \text{ bbl/psi}$$

From Eq. 7-26

$$(C_D)_{f+m} = \frac{0.8936C}{\phi c_t h r_w^2} = \frac{0.8936 \times 0.01}{0.07 \times 1 \times 10^{-5} \times 36 \times 0.29^2} = 4216$$

From Eq. 7-27

$$s = 0.5 \ln \left[\frac{(C_D e^{2s})_{f+m}}{(C_D)_{f+m}} \right] = 0.5 \ln [0.6/4216] = -4.4$$

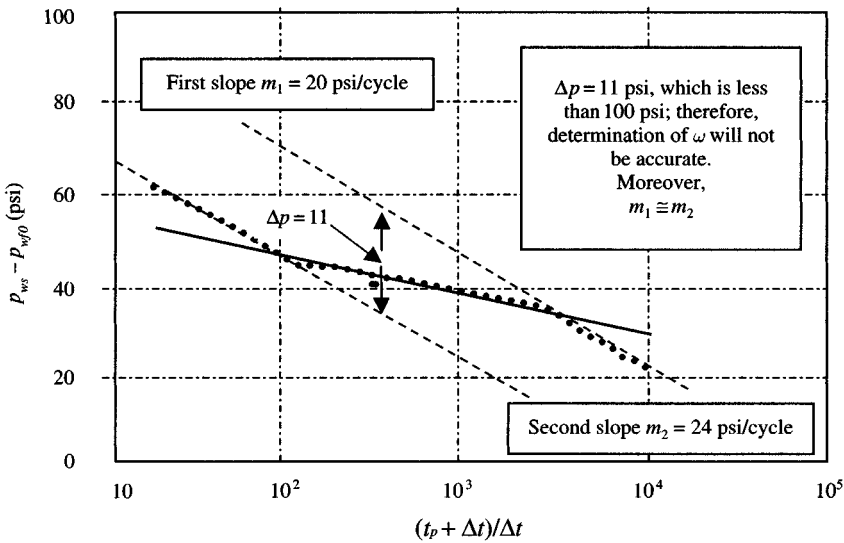


Figure 7-9. Horner's plot.

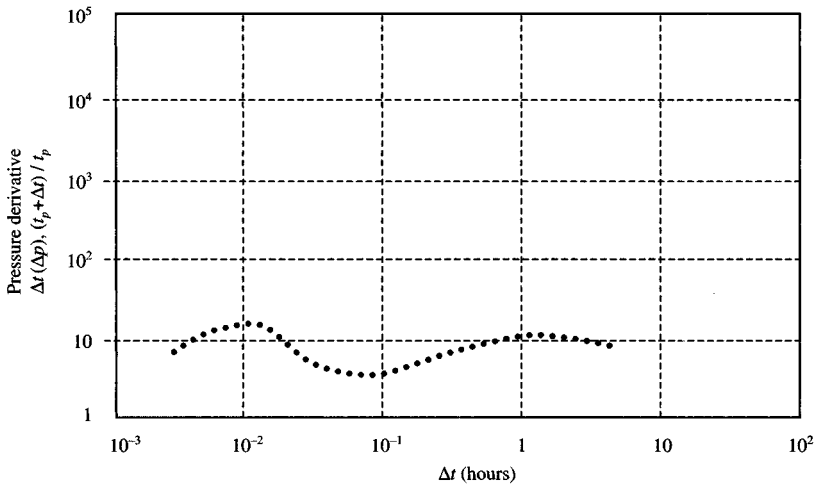


Figure 7-10. Buildup test data plot.

From Eq. 7-28

$$\lambda = \left(\frac{\lambda C_D}{(1 - \omega)^2} \right)_{match} \times \frac{(1 - \omega)^2}{(C_D)_{f+m}} = \frac{[3 \times 10^{-2}]_{curve}}{4216} \times (1 - 0.018)^2$$

$$= 6.86 \times 10^{-6}$$

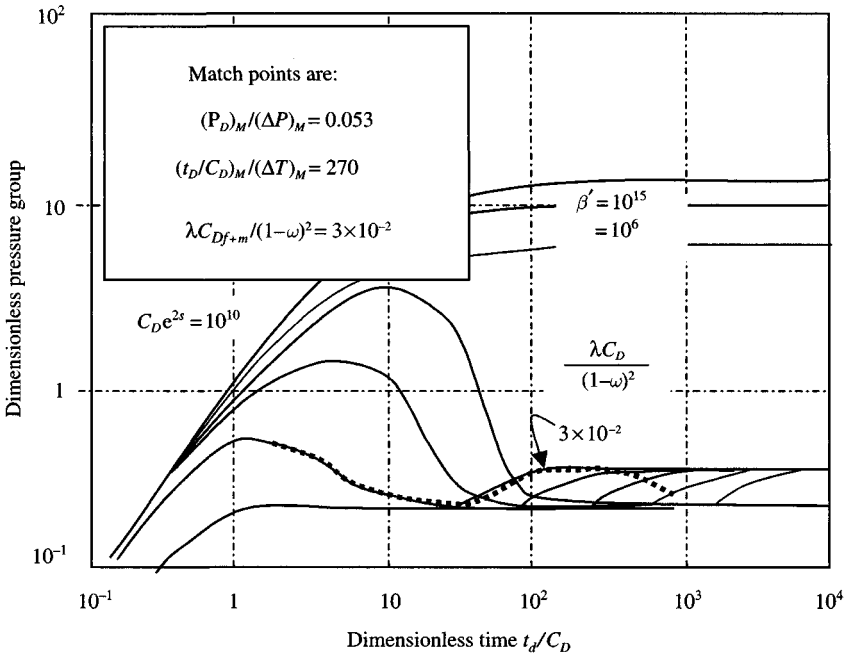


Figure 7-11. Type curve matching plot.¹⁵

7.7 Buildup Analysis Techniques for Tight Reservoir Matrix

In this section we will discuss the buildup test analysis of a naturally fractured reservoir. If the natural fractures are fed by tight reservoir matrix, then the method presented in the next section will be more appropriate.

The Horner plot of a buildup test conducted on a well completed in a naturally fractured reservoir will show two straight lines parallel to each other. The first straight line represents homogeneous semilog radial flow and the most permeable medium acting alone, whereas the second straight line corresponds to semilog radial flow in the total reservoir. The two straight lines are separated by a transient period during which pressure tends to stabilize. The slope of this portion is found to be one-half of the other straight line. Storage effects may obscure the initial semilog straight line. If the test is conducted for a long enough period of time so that semilog straight lines develop, the slope, p_{1hr} , and the extrapolated pressure, p^* , of the second straight line are used to calculate reservoir properties in exactly the same way as in the regular buildup test.

Several types of heterogeneous systems, such as reservoirs with non-communicating layers, may exhibit similar transient response curves.

The pseudo-steady-state behavior for a naturally fractured reservoir begins at a dimensionless time given by the following equation:

$$(t_{DA})_{pss} = \frac{0.000264(kh)_f t_{pss}}{[(\phi c_t)_f + (\phi c_t)_m] h \mu_o A} \approx 0.013 \quad (7-29)$$

In Eq. 7-29 the subscript f indicates fracture property while m indicates matrix property. Reference 3 presented a model composed of rectangular parallel pipes where the blocks represent the matrix and the space in between them the fractures. They concluded that two parameters were enough to characterize the behavior of the double-porosity system. One parameter, ω , represented a measure of the fluid capacitance, and the other parameter, λ , was related to the degree of heterogeneity of the system.

The ratio of porosity-compressibility product in the fracture to that for the total system is given by

$$\omega = 10^{-\Delta p/m} = \text{antilog}\left(\frac{\Delta p}{m}\right) \quad (7-30)$$

$$= \frac{(h\phi c_t)_f}{(h_m - h_f)(\phi c_t)_m + (h\phi c_t)_f} \quad (7-31)$$

$$= \frac{(\phi c_t)_f}{(\phi c_t)_m + (\phi c_t)_f} \quad (7-32)$$

where Δp is the vertical distance between the two straight lines, also referred to as the dimensionless matrix storability. Average total porosity is given by the following equation:

$$\phi = \frac{(\phi h)_f + (h_m - h_f)\phi_m}{h_m} \quad (7-33)$$

and the fracture porosity is given by

$$\phi_f = \frac{\omega(h_m - h_f)(\phi c_t)_m}{(h c_t)_f(1 - \omega)} \quad (7-34)$$

The fracture porosity attached to bulk-fracture properties is calculated from

$$\phi = \frac{(h\phi)_f}{h_m} \quad (7-35)$$

Compressibilities c_m and c_f in most cases are assumed to be equal, while h_f and h_m could be obtained from a combination of well logs and core

analyses. The average permeability of the double-porosity system is given by the following equation:

$$k_{Av} = \frac{k_f h_f + k_m (h_m - h_f)}{h_m} \quad (7-36)$$

The skin factor can be determined from the transitional pressure segment with slope $m' = m/2$ by using the following equation:

$$s = 0.5756 \left[\frac{p_{1hr} - p_{wf}}{m'} - \log \frac{\Delta t_x t_p}{t_p + \Delta t_x} - 2 \log \frac{k}{\phi_m \mu_o c_{tm} r_w^2} + 6.455 \right] \quad (7-37)$$

where Δt_x is read at the intersection of the two straight lines of slopes m and m' . If the matrix block size, H (ft), can be estimated, the matrix permeability can be determined using the following equation:

$$k_m = \frac{2765.15 H^2 \phi_m c_m \mu_o}{\Delta t_x} \quad (7-38)$$

The parameter λ is

$$\lambda = \frac{\alpha k_m r_w^2}{\bar{k}} \quad (7-39)$$

where α is the shape factor controlling the flow between two systems and \bar{k} the effective permeability of fractures.

Example 7-2¹⁴ Analyzing Pressure Buildup Test in Naturally Fractured Reservoir

Pressure buildup test data for a naturally fractured well are given in Table 7-2. Other well and reservoir data are as follows: $q = 2554$ stb/day, $\phi = 0.21$, $\mu = 1.0$ cP, $\beta = 2.3$ rb/stb, p_{fws} at $\Delta t=0 = 6352$ psi, $r_w = 0.375$ ft, $t_p = 8661$, $\phi_m = 0.21$, $k_m = 0.1$ mD, $h_m = 17.0$ ft, and $c_t = 18.7 \times 10^{-6}$ psi⁻¹. From well logs and core analyses find matrix storage, S_m , and η_m , and from pressure buildup (using Najurieta model) find the following:

- Formation fracture permeability, k_f .
- Fissured parameter, ω .
- Fracture storage, S_f , and parameter, η_{co} .
- Skin factor, s .

Solution From Figure 7-12, find the following:

First straight-line slope, $m_1 = 32.0$ psi/cycle

Table 7-2
Pressure Buildup Data for the Well¹⁴

Shut-in time, Δt (hr)	Shut-in pressure, p_{ws} (psia)	$\frac{t_p + \Delta t}{\Delta t}$
0.00	6352	—
0.003	6617	8611
0.017	6632	143.52
0.030	6643	71.76
0.07	6650	35.88
0.13	6654	17.94
0.27	6661	8.97
0.53	6666	4.49
1.07	6669	2.24
2.13	6678	1.12
4.26	6685	0.56
8.53	6696	0.28
17.07	6705	0.14
34.13	6712	0.07

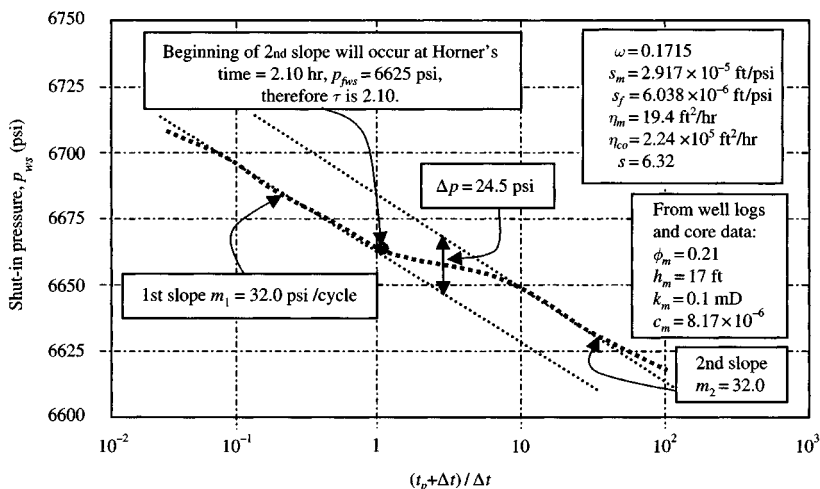


Figure 7-12. Semilog graph of buildup test.

$$\Delta p = 24.25 \text{ psia}$$

At the beginning of the second slope line, $\Delta t = 2.10$ hr and $p_{fws} = 6660$ psi. From Eq. 7-30, the ratio ω is

$$\omega = 10^{-\Delta p/m} = 10^{-24.5/32} = 0.1715$$

Calculate matrix storage S_m from well logs and core data:

$$S_m = \phi_m h_m c_m = 0.21 \times 17 \times 8.17 \times 10^{-6} = 2.917 \times 10^{-5} \text{ ft/psi}$$

Because the reservoir is stratified

$$S_f = \frac{\omega S_m}{(1 - \omega)} = \frac{0.1715 \times 2.917 \times 10^{-5}}{(1 - 0.1715)} = 6.038 \times 10^{-6} \text{ ft/psi} \quad (7-39a)$$

$$\eta_m = \frac{0.140 h_m^2}{\tau} = \frac{0.140 \times 17^2}{2.11} = 19.4 \text{ ft}^2/\text{hr} \quad (7-39b)$$

Parameter η_m from core analysis is

$$\frac{2.637 \times 10^{-4} k_m}{\mu \phi_m c_f} = \frac{2.637 \times 10^{-4} \times 0.1}{1 \times 0.21 \times 8.17 \times 10^{-6}} = 15.4 \text{ ft}^2/\text{hr}$$

Estimate T_f from equation

$$T_f = \frac{162.6 q \beta}{m} = \frac{162.6 \times 2554 \times 2.3}{32.0} = 29,848 \text{ mD ft/cP} \quad (7-39c)$$

Calculate parameter η_{co} from equation:

$$\begin{aligned} \eta_{co} &= \frac{2.64 \times 10^{-4} \times T_f}{S_m + S_f} = \frac{2.64 \times 10^{-4} \times 29,848}{2.917 \times 10^{-5} + 6.038 \times 10^{-6}} \\ &= 2.24 \times 10^5 \text{ ft}^2/\text{hr} \end{aligned} \quad (7-39d)$$

Estimate skin factor, s , such that

$$\begin{aligned} s &= 1.151 \left[\frac{P_{f,ws} - P_{f,wf_{\Delta t=0}}}{m} - \log \frac{\eta_{co} (\Delta t) \Delta t}{r_w^2} \right] \\ &= 1.151 \left[\frac{6660 - 6352}{32.0} - \log \frac{2.24 \times 10^5 \times 0.00861}{(0.375)^2} \right] = 6.32 \end{aligned} \quad (7-39e)$$

Important notes: If the shape of the matrix is cubic, use the following equations:

$$S_f = \frac{\omega S_m}{3(1 - \omega)} \quad (7-39f)$$

$$\tau_{co} = \frac{2.64 \times 10^{-4} \times 3T_f}{3S_f + S_m} \quad (7-39g)$$

- If $t = \tau$, final straight line on semilog plot begins approximately at $t = \tau$.
- If $t > \tau$, naturally fractured reservoirs behave as a homogeneous non-fractured reservoir.
- If $t < \tau$, then $\eta_m = \eta_{co}$ (it is not possible to detect natural fractures by well testing).

7.8 Interpretation of Interference Tests in Matrix and Fractured Reservoirs

Interference tests in fractured formation can provide very important information related to the zone surrounding the well from which the production comes.

Uses of Interference Tests

Figure 7–13 illustrates the uses of interference tests in matrix and fractured reservoirs.

Dimensionless Fracture Pressure Solution

Figure 7–14 shows the solution for dimensionless fracture pressure, p_{fD} , versus t_D/r_D^2 for several values of ω and θ , where parameter θ is equal λr_D^2

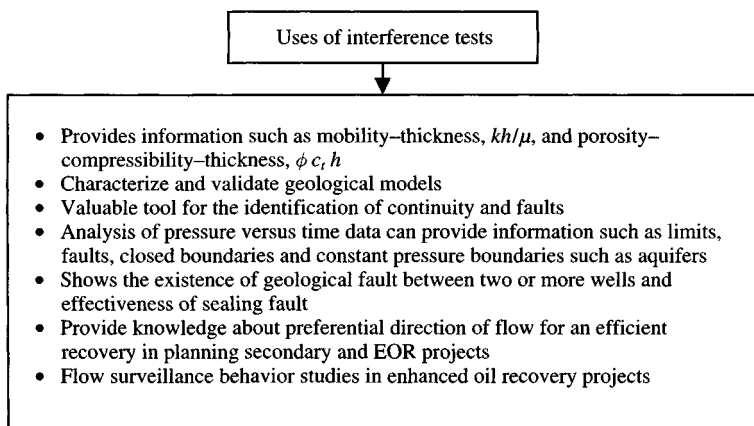


Figure 7–13. Uses of interference tests in fissured and matrix formations.

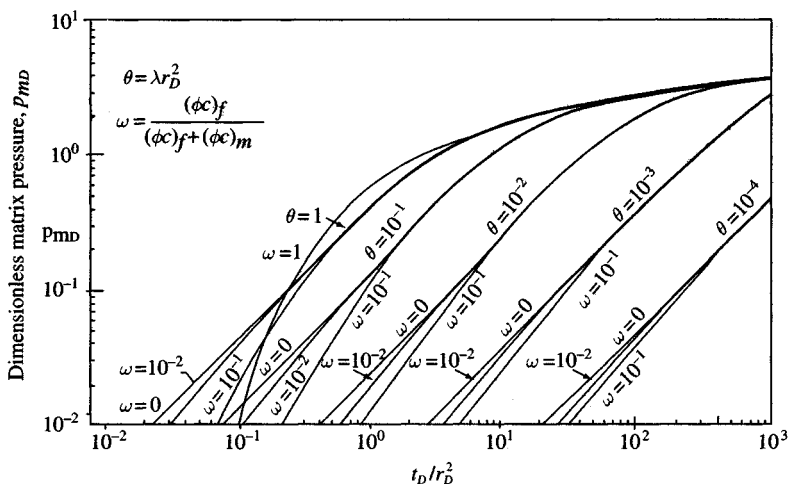


Figure 7-15. Dimensionless matrix pressure solution for several values of ω and θ .¹⁰

Interference Test Analysis Using Type Curve Match Equations

For a given match, ω and λ can be obtained directly using the type curves of Figure 7-14. The following type curve match equations¹⁰ can be used to estimate other fracture parameters such as

$$[\theta]_{curve} = \lambda r_D^2 \quad (7-42)$$

$$[\omega]_{curve} = \frac{(\phi c)_f}{(\phi c)_f + (\phi c)_m} \quad (7-43)$$

From pressure match points, fracture permeability can be found using equation

$$k_f = \frac{141.2q\mu_f\beta}{h} \left[\frac{p_{iD}}{\Delta p} \right]_M \quad (7-44)$$

From time match points

$$[(\phi c)_f + (\phi c)_m] = \frac{0.000264k_f}{r_2} \left[\frac{t}{t_D/r_D^2} \right]_M \quad (7-45)$$

Using Eqs. 7-43 and 7-45, find

$$(\phi c)_f = [(\phi c)_f + (\phi c)_m] \omega \quad (7-46)$$

Product αk_m can be calculated from equation¹⁰

$$\alpha k_m = \frac{\theta k_f}{r^2} = \frac{\lambda r_D^2}{r^2} \quad (7-47)$$

7.9 Horizontal Well Pressure Behavior Curve Shapes

Figure 7-16 shows curves during various flow periods.

Identification of Various Flow Periods

Figure 7-17 shows various flow periods and their identification.

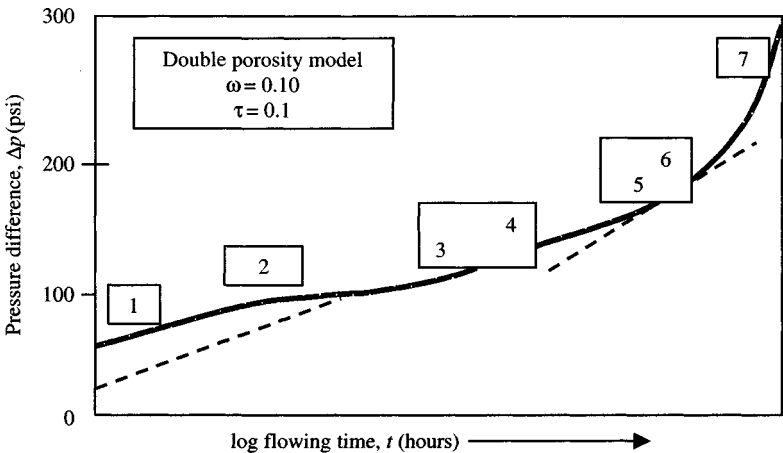


Figure 7-16. Drawdown flow periods in a horizontal well with dual-porosity flow.⁹

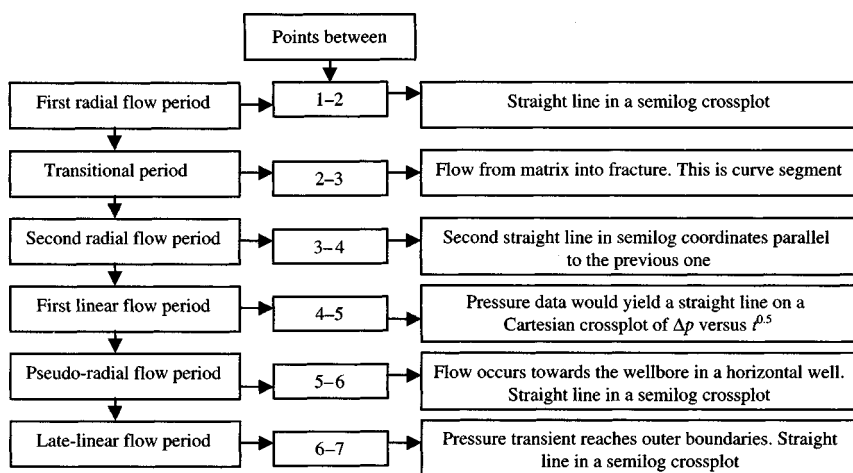


Figure 7-17. Various flow periods and their identification.

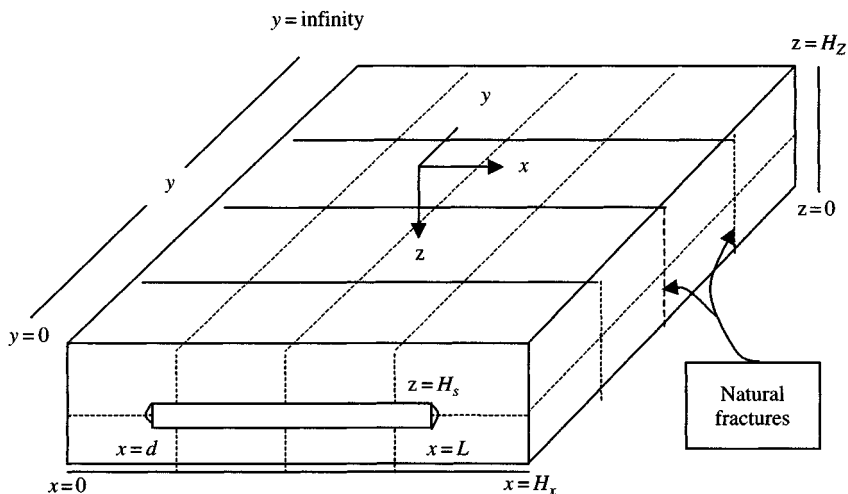


Figure 7-18. Horizontal well model in a naturally fractured reservoir.⁹

Well Test Analysis Equations and Solutions

Figure 7-18 shows a horizontal well model in a naturally fractured reservoir.

Pressure Drawdown Analysis Equations for Dual-Porosity Systems

Average permeability of all fractures intercepting the wellbore in the z - y direction is given by

$$[k_z k_y]^{0.5} = 162.6 \frac{q\mu\beta}{m_{1r}(L-d)} \quad (7-48)$$

where m_{1r} is the slope of semilog straight line in the first or third radial flow period. (The two lines are parallel.)

From the first linear flow period, the permeability k_y is estimated using the equation

$$k_y = \left[\frac{8.128q\beta}{H_z(L-d)m_{1L}} \sqrt{\frac{\mu}{\phi c}} \right]^{2.0} \quad (7-49)$$

where m_{1L} is the slope of semilog straight line in the first or third radial flow period. (The two lines are parallel.)

Average permeability $(k_x k_y)^{0.5}$ is estimated from

$$(k_x k_y)^{0.5} = 162.6 \frac{q\mu\beta}{m_{3r} k_z} \quad (7-50)$$

Skin effect can be estimated from first, second, third, and fourth flow periods using the equations given below.

First Flow Period

$$s_m = 1.151 \left[\frac{p_i - p_{1hr}}{m_{1r}} - \log \left(\frac{(k_z k_y)^{0.5}}{\phi_f \mu c_f r_w^2} \right) + 3.23 \right] \quad (7-51)$$

where fracture porosity is calculated using the following equation:

$$\phi_f = \frac{\omega \phi_m c_m}{c_f (1 - \omega)} \quad (7-52)$$

Fraction of the total storage within the fracture is calculated from

$$\omega = \frac{t_1}{t_2} \quad (7-53)$$

Second Flow Period

This flow occurs in very rare occasions.

Third Flow Period

Skin is calculated from Eq. 7-51 using total porosity and total compressibility.

Fourth Flow Period

$$s_m = \frac{0.058}{H_z} \sqrt{\frac{k_z}{\pi \mu c}} \left[\frac{p_i - p_{1hr}}{m_{1L}} \right] - s_z \quad (7-54)$$

where s_z is a pseudo-skin due to partial penetration in the z -direction and is calculated from the equation¹³

$$s_z = 0.07958 \frac{H_z}{r'_w} [F_1 + F_2 - F_3 - F_4] \quad (7-55)$$

The values of F_1 , F_2 , F_3 , and F_4 are given by

$$F_1 = 0.52 \left(\frac{\pi}{H_z} \right) r'_w \quad (7-56)$$

$$F_2 = 0.52 (2H_z + 3.48r'_w) \quad (7-57)$$

$$F_3 = -3.48 \left(\frac{\pi}{H_z} r'_w \right) \quad (7-58)$$

$$F_4 = \left(\frac{\pi}{H_z} \right) (2H_s - 0.52r'_w) \quad (7-59)$$

Fifth Flow Period

$$s_m = 1.151 \left[\frac{L-d}{H_z} \right] \left[\frac{k_z}{k_x} \right]^{0.5} \times \left[\frac{p_i - p_{1hr}}{m_{3r}} - \log \left(\frac{k_x}{\phi_f \mu c_f (L-d)^2} \right) + 2.02 \right] - s_z \quad (7-60)$$

where

$$s_z = 0.07958 \frac{H_z}{r'_w} [F_5 + F_6 - F_7 - F_8] \quad (7-61)$$

and

$$F_5 = 0.00203 \text{ radians}$$

$$F_6 = 3.14780 \text{ radians}$$

$$F_7 = -0.0176 \text{ radians}$$

$$F_8 = 3.13900 \text{ radians.}$$

Sixth Flow Period

$$s_m = \frac{0.058(L-d)}{H_x H_z} \sqrt{\frac{k_y}{\phi_f \mu c_f} \left[\frac{p_i - p_{1hr}}{m_{2L}} \right]} - s_z - s_x \quad (7-62)$$

where s_x is pseudo-skin due to partial penetration in the x -direction and is calculated from¹³

$$s_x = 0.3183 \frac{H_x}{(k_z/k_x)^{0.5}} [F_9 + F_{10} - F_{11} - F_{12}] \quad (7-63)$$

and

$$F_9 = 0.13(\pi/H_x)(L-d)$$

$$F_{10} = (\pi/H_x)(1.87L + 0.13d)$$

$$F_{11} = -0.87(\pi/H_x)(L-d)$$

$$F_{12} = (\pi/H_x)(0.87L + 1.13d).$$

The slope m_{2L} is obtained from the straight line in the Cartesian crossplot of pressure differential versus square root of time.

Pressure Buildup Analysis Equations for Dual-Porosity Systems

Average permeability is estimated from the semilog straight line in the first or third flow period:

$$[k_z k_y]^{0.5} = 162.6 \frac{q \mu \beta}{m_{1r}(L-d)} \quad (7-64)$$

Permeability k_y is calculated based on a crossplot of $(p_{ws} - p_{wf})$ versus $\Delta t^{0.5}$ or $(p_{ws} - p_{wf})$ versus $(t_p + \Delta t)^{0.5} - (\Delta t)^{0.5}$ using the following equation:

$$k_y = \left[\frac{8.128 q \beta}{H_z(L-d)m_{iL}} \sqrt{\frac{\mu}{\phi c}} \right]^{2.0} \quad (7-65)$$

Permeability product $(k_x k_y)^{0.5}$ is calculated based on the last radial flow period from

$$(k_x k_y)^{0.5} = 162.6 \frac{q \mu \beta}{m_3 r k_z} \quad (7-66)$$

Storage capacity coefficient is calculated from

$$\omega = \frac{[(t_p + \Delta t) / \Delta t]_1}{[(t_p + \Delta t) / \Delta t]_2} \quad (7-67)$$

where

$[(t_p + \Delta t) / \Delta t]_1$ = Horner time at first semilog straight line (first flow period)

$[(t_p + \Delta t) / \Delta t]_2$ = Horner time at third semilog straight line (third flow period).

Dimensionless matrix to fracture permeability ratio, λ , is estimated from

$$\lambda = \frac{4n(n+2)k_m}{k_f h_m^2} r_w^2 \quad (7-68)$$

where

k_m = matrix permeability, mD

k_f = fracture permeability, mD

r_w = wellbore radius, ft

$n = 1$ for a stratum model.

Skin factor during first flow period is estimated from

$$s_m = 1.151 \left[\frac{p_{1hr} - p_{wf}}{m_{1r}} - \log \left(\frac{(k_z k_y)^{0.5}}{\phi_f \mu c_f r_w^2} \right) + 3.23 \right] \quad (7-69)$$

Skin factor during third flow period is estimated from

$$s_m = \frac{0.058}{H_z} \sqrt{\frac{k_z}{\pi \mu c}} \left[\frac{p_{0h} - p_{wf}}{m_{1L}} \right] - s_z \quad (7-70)$$

Fracture porosity can be calculated from

$$\phi_f = \frac{\omega \phi_m c_m}{[c_f (1 - \omega)]} \quad (7-71)$$

Initial pressure or the value of p^* is calculated from Horner plot using the fifth flow period (last radial) or from a crossplot of $(t_p + \Delta t)^{0.5} - (\Delta t)^{0.5}$ using data from the sixth flow period (last linear).

7.10 Horizontal Well Production Forecasting – Dual-Porosity Reservoir

References 10–12 presented the following solution to the dual-porosity diffusivity equation.

For early times:

$$q = \frac{1}{\ln r_{eD} - 0.75} \exp\left(\frac{-2}{r_{eD}^2 (\ln r_{eD} - 0.75) \omega} t_{Df}\right) \quad (7-72)$$

For late times:

$$q_D = \left(\frac{r_{eD}^2 - 1}{2}\right) \lambda \exp\left(\frac{-\lambda}{1 - \omega} t_{Df}\right) \quad (7-73)$$

where

$$q_D = \frac{141.3q\mu\beta}{kh\Delta p} \quad (7-74)$$

$$t_{Df} = \frac{0.000264kt}{\phi_t \mu c_t r_{we}} \quad (7-75)$$

$$r_{eD} = \frac{r_e}{r_{we}} \quad (7-76)$$

$$r_{we} = \frac{r_{eh}(L/2)}{a \left\{ 1 + \left[1 - (L/2a)^2 \right]^{0.5} \right\} (h/2r_w)^{\beta h/L}} \quad (7-77)$$

where

r_{eh} = horizontal drainage radius, ft

L = length of horizontal well, ft

h = reservoir height, ft

$\beta = (k_h/k_v)^{0.5}$

k_h = horizontal permeability, mD

k_v = vertical permeability, mD

$$a = \left(\frac{L}{2}\right) \left[0.5 + \sqrt{0.25 + \left(\frac{2r_{eh}}{L}\right)^4} \right]^{0.5} \quad (7-78)$$

$$r_{we} = r_w e^{-s} \quad (7-79)$$

The above equations can be used for production forecast in dual-porosity reservoirs.

7.11 Summary

- Semilog plot of the data obtained from wells producing from naturally fractured reservoirs would exhibit the characteristic curve predicted by References 1, 5, 8, and 14.
- Pressure derivative type curve matching method is theoretical and very useful.
- Semilog analysis is more than adequate.
- If there is a linear boundary in a homogeneous reservoir, the derivative method will indicate a naturally fractured reservoir.
- Interference testing is a valuable tool for the identification of continuity and faults. It can also provide information such as limits, faults, closed boundaries, and constant pressure boundaries such as aquifers. Investigation about flow behavior and flow surveillance studied can be performed for secondary and EOR projects.

References and Additional Readings

1. Warren, J. E., and Root, P. J., "The Behavior of Naturally Fractured Reservoirs," *Soc. Pet. Eng. J.* (Sept. 1963), 245–255.
2. Streltsova, T. D., *Well Testing in Heterogeneous Formations*, John Wiley & Sons, New York, 1988, p. 377.
3. Kazemi, H., "Pressure Transient Analysis of Naturally Fractured Reservoirs with Uniform Fracture Distribution," *Soc. Pet. Eng. J.* (Dec. 1960), 451–462.
4. Streltsova, T. D., "Well Pressure Behavior of a Naturally Fractured Reservoir," *Soc. Pet. Eng. J.* (Oct. 1983), 769–780.
5. DeSwaan, A., "Analytic Solutions for Determining Naturally Fractured Reservoir Properties by Well Testing," *Soc. Pet. Eng. J.* (June 1976), 117–122; *Trans. AIME*, 261.
6. Bourdet, D., and Gringarten, A. C., "Determination of Fissure Volume and Block Size in Fractured Reservoirs by Type-Curve Matching," paper SPE 9293, presented at the Annual Technical Conference and Exhibition, Dallas, Sept. 21–24, 1980.
7. Bourdet, D., et al., "New Type-Curve Aid Analysis of Fissured Zone Well Tests," *World Oil* (April 1984), 111–120.
8. Odeh, A. S., "Unsteady-State Behavior of Naturally Fractured Reservoirs," *Soc. Pet. Eng. J.* (March 1965), 60–64; *Trans. AIME*, 234.
9. Aguilera, R., and Ng, M. C., "Transient Pressure Analysis of Horizontal Wells in Anisotropic Naturally Fractured Reservoirs," *SPEFE* (March 1991).
10. Da Prat, G., et al., "Decline Curve Analysis Using Type Curves for Two-Porosity Systems," *SPE J.* (June 1981), 354–362.

11. Sageev, A., et al., "Decline Curve Analysis for Double-Porosity Systems," paper SPE 13630, presented at the California Regional Meeting, Bakersfield, CA, March 27–29, 1985.
12. Joshi, S. D., "Horizontal Well Production Forecasting Methods and a Comparison of Horizontal Wells and Stimulated Vertical Wells," paper presented at the NPD Seminar on Thin Oil Zone Development, Stavanger, Norway, April 21–22, 1988.
13. Goode, P. A., and Thambynayagam, R. K. M., "Pressure Drawdown and Buildup Analysis of Horizontal Wells in Anisotropic Media," *SPEFE* (Dec. 1987), 683–697; *Trans. AIME*, 283.
14. Najurieta, H. L., "A Theory for Pressure Transient Analysis in Naturally Fractured Reservoirs," *J. Pet. Technol.* (July 1980), 1241–1250.
15. Bourdet, D., et al., "New Type Curves Aid Analysis of Fissured Zone Well Tests," *World Oil* (April 1984), 111–126.

Chapter 8

Fundamentals of Type Curve Matching Methods for Oil Wells

8.1 Introduction

This chapter discusses the quantitative use of type curves in oil well test analysis. Methods of using type curves are presented to enable the engineer to use, understand, and apply newer type curves as they appear in the literature. Some of the curves are used to help identify the MTR, while other type curves are used to estimate the permeability, skin factor, fracture length, etc. The type curves are used to properly analyze a test or to double-check the results obtained with conventional methods with those obtained with type curve matching. Fundamentally, a type curve is a pre-plotted family of pressure drawdown curves generated by obtaining solutions to the flow equations with specified initial and boundary conditions. Some of these solutions are analytical; others are based on finite-difference approximations generated by computer reservoir simulators. Some of the specific type curves are presented in the following section.

8.2 Application to Conventional Tests

Type curves are advantageous because they may allow test interpretation even when wellbore storage distorts most or all of the test data; in that case, conventional methods fail.

Ramey's Type Curves

Ramey's type curves are plots of dimensionless pressure change p_D versus dimensionless time change t_D . These curves can be distinguished from one

another by two parameters: the skin factor s and the dimensionless wellbore storage constant C_{SD} . For an infinite-acting reservoir, specification of C_{SD} and s uniquely determines the value of p_D at a given value of t_D . The curves were generated from analytical solutions to the diffusivity equation, with boundary conditions. The skin factor s is used to characterize the wellbore damage or stimulation; as we have seen, this causes an additional pressure drop Δp_s across the altered zone in terms of the skin factor s :

$$\Delta p_s = 141.2 \frac{q\beta_o\mu_o}{kh} s \quad (8-1)$$

In terms of the slope m of the MTR

$$\Delta p_s = 0.869ms \quad (8-2)$$

Figure 8-1 is a log-log plot of p_D versus t_D with parameters s and C_{SD} :

$$p_D = \frac{kh \Delta p}{141.2q\beta_o\mu_o} \quad (8-3)$$

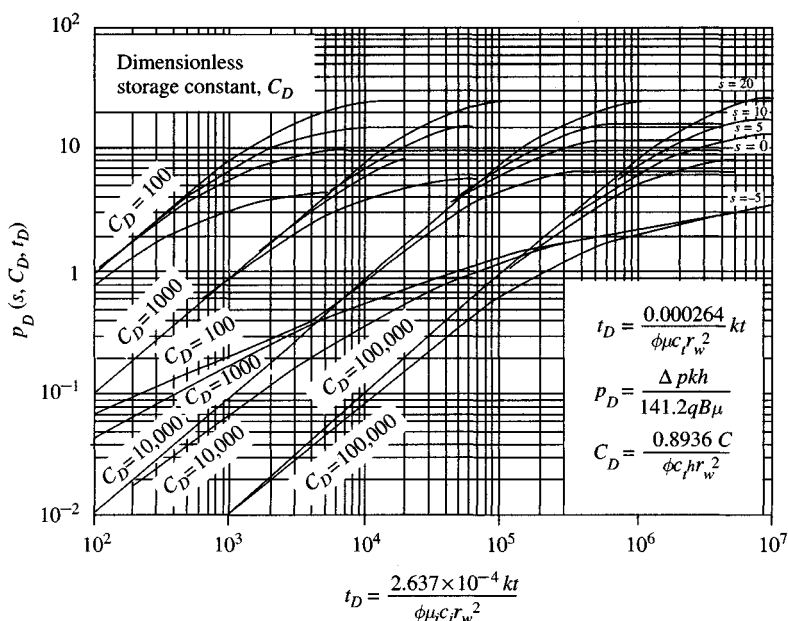


Figure 8-1. Dimensionless pressures for a single well in an infinite system; wellbore storage and skin included (copyright ©, 1970, SPE from Trans. AIME, 1970).¹

and

$$t_D = \frac{0.000264kt}{\phi\mu_o c_t r_w^2} \quad (8-4)$$

where

$$\Delta p = p_i - p_{wf} \quad (\text{drawdown test})$$

$$\Delta p = p_{ws} - p_{wf} \quad (\text{buildup test})$$

$$C_{SD} = \frac{0.894C_S}{\phi c_t h r_w^2} \quad (8-5)$$

where C_S is the wellbore storage constant and can be determined from the following relation:

$$C_S = \frac{q\beta_o}{24} \left(\frac{\Delta t}{\Delta p} \right)_{\text{unit-slope line}} \quad (\text{bbl/psi}) \quad (8-6)$$

If there is liquid/gas interface in the wellbore

$$C_S = \frac{25.65A_{wb}}{\rho} \quad (\text{bbl/psi}) \quad (8-7)$$

If a wellbore is filled with a single-phase liquid or gas

$$C_S = C_{wb} V_{wb} \quad (\text{bbl/psi}) \quad (8-8)$$

Successful application of Ramey's type curves depends significantly on our ability to establish the correct value of C_{SD} to be used for curve matching.

Pressure Drawdown or Buildup Analysis

Ramey's type curves (Figure 8-1) involves the following steps:

1. Plot Δp versus time on log-log paper, the same size as Ramey's type curve.
2. If the test has a uniform-slope region (45° line at earliest times), choose any point t , $(p_i - p_{wf})$ or $[\Delta t, (p_{ws} - p_{wf})]$ on the unit-slope line and calculate the wellbore storage constant C_S as

$$C_S = \frac{q\beta_o}{24} \left(\frac{\Delta t}{\Delta p} \right)_{\text{unit-slope line}} \quad (8-6)$$

3. Calculate the dimensionless wellbore storage constant

$$C_{SD} = \frac{0.894C_S}{\phi c_t h r_w^2} \quad (8-5)$$

4. If a unit-slope line is not present, C_S and C_{SD} must be calculated from the wellbore properties.
5. Using type curves with C_{SD} as calculated in steps (2) and (3), find the curve that best fits all the plotted data.
6. Note the values of the match point $(p_D)_M$, $(\Delta p)_M$, $(t_D)_M$, $(t \text{ or } \Delta t)_M$ and value of s .
7. Calculate the permeability k from pressure match point:

$$k = \frac{141.2q\beta_o\mu_o}{h} \frac{(p_D)_M}{(\Delta p)_M} \quad (8-9)$$

8. Calculate ϕc_t from the time match point:

$$\phi c_t = \frac{0.000264k}{\mu_o r_w^2} \frac{(t \text{ or } \Delta t)_M}{(t_D)_M} \quad (8-10)$$

9. Compare the value of ϕc_t with values used to determine C_{SD} from C_S :

$$\phi c_t = \frac{0.894C_S}{hr_w^2 C_{SD}} \quad (8-11)$$

Note: One of the main features of these type curves is that they permit detection of the correct straight line in the conventional semilog plot.

Tables 8-1 through 8-5 present the values of dimensionless pressure Δp_D versus t_D with dimensionless storage constant, C_D , as parameters and skin effects of zero, +5, +10, +20, and -5, respectively.

Example 8-1⁸ Analyzing Drawdown Test Using Ramey's Type Curves

Pressure time data of a drawdown test are given in Table 8-6. Additional pertinent data are given: reservoir datum = 4500 ft; $t = 200^\circ\text{F}$; $q_o = 500$ stb/day; $p_i = 3000$ psi; $p_{sc} = 14.65$ psia; $\text{API}^\circ = 18^\circ$; $h = 56$ ft; $\phi = 0.2$; $\mu_o = 0.8$ cP; $\beta_o = 1.2$ rb/stb; $r_w = 0.3$ ft; tubing size = 2.25 inch; and $c_t = 1.000 \times 10^{-5}$ psi⁻¹.

Solution Using Ramey's type curve Figure 8-2 is a plot of Table 8-6 on log-log graph paper of the same scale of the type curves of Figure 8-1. From the unit-slope line on which the data lie for $t \leq 0.1$ hr using Eq. 8-6:

$$\begin{aligned} C_S &= \frac{q\beta_o}{24} \left[\frac{t}{p_i - p_{wf}} \right]_{\text{point on unit slope}} \\ &= \frac{500 \times 1.2 \times 0.1}{24 \times 215} = 0.0116 \text{ rb/psi} \end{aligned}$$

Table 8-1
Values of $\Delta p_D (s, C_D, t_D)$ versus t_D including Wellbore Storage and Skin Effects¹ [$s = 0$]

Dimensionless time, t_D	Dimensionless storage constant			
	$C_D (\times 10^2)$	$C_D (\times 10^3)$	$C_D (\times 10^4)$	$C_D (\times 10^5)$
100	0.7975	0.09763	0.00998	0.00100
200	1.3724	0.1919	0.01992	0.00200
500	2.4357	0.4585	0.04956	0.00500
1000	3.2681	0.8585	0.0984	0.00999
2000	3.9274	1.5298	0.1944	0.01995
5000	4.5585	2.8832	0.4697	0.0497
10,000	4.9567	4.0328	0.8925	0.0989
20,000	5.3288	4.9350	1.6275	0.1958
50,000	5.8027	5.6762	3.2109	0.4765
100,000	6.1548	6.0940	4.6773	0.9141
200,000	6.5043	6.4736	5.8871	1.6931
500,000	6.9643	6.9515	6.7895	3.4571
1,000,000	7.3116	7.3049	7.2309	5.2164
2,000,000	7.6585	7.6550	7.6185	6.7731
5,000,000	8.1168	8.1154	8.1004	7.8983
10,000,000	8.4635	8.4627	8.4550	8.3701
20,000,000	8.8101	8.8097	8.8057	8.7663
50,000,000	9.2683	9.2681	9.2664	9.2523
100,000,000	9.6149	9.6148	9.6139	9.6082

Table 8-2
Values of $\Delta p_D (s, C_D, t_D)$ versus t_D including Wellbore Storage and Skin Effects¹ [$s = +5$]

Dimensionless time, t_D	Dimensionless storage constant			
	$C_D (\times 10^2)$	$C_D (\times 10^3)$	$C_D (\times 10^4)$	$C_D (\times 10^5)$
100	0.9319	0.09929	0.009993	0.00100
200	1.7512	0.1973	0.01997	0.00200
500	3.6982	0.4843	0.04984	0.00500
1000	5.7984	0.9410	0.0994	0.00999
2000	7.8403	1.7820	0.1977	0.01998
5000	9.3823	3.8349	0.4863	0.0499
10,000	9.8913	6.1533	0.9480	0.0995
20,000	10.300	8.5524	1.8062	0.1979
50,000	10.792	10.436	3.9463	0.4878
100,000	11.150	11.025	6.4558	0.9536
200,000	11.693	11.445	9.1982	1.8256
500,000	12.311	11.941	11.488	4.0388
1,000,000	12.311	12.300	12.156	6.7163
2,000,000	12.658	12.652	12.859	9.7845
5,000,000	13.117	13.114	13.090	12.517
10,000,000	13.463	13.462	13.450	13.286
20,000,000	13.810	13.809	13.803	13.734
50,000,000	14.268	14.268	14.265	14.239
100,000,000	14.613	14.615	14.613	14.601

Table 8-3
Values of $\Delta p_D (s, C_D, t_D)$ versus t_D including Wellbore Storage and Skin Effects¹ [$s = +10$]

Dimensionless time, t_D	$C_D (\times 10^2)$	Dimensionless storage constant		
		$C_D (\times 10^3)$	$C_D (\times 10^4)$	$C_D (\times 10^5)$
100	0.9594	0.09958	0.01000	0.001000
200	1.8463	0.1984	0.01998	0.002000
500	4.1401	0.4904	0.04990	0.005000
1000	7.0124	0.9629	0.0996	0.0100
2000	10.487	1.8587	0.1985	0.0200
5000	13.852	4.2027	0.4911	0.0499
10,000	14.797	7.2010	0.9658	0.0997
20,000	15.269	10.995	1.8693	0.1986
50,000	15.781	14.811	4.2568	0.4918
100,000	16.144	15.917	7.3677	0.9683
200,000	16.499	16.413	11.382	1.8785
500,000	16.962	16.930	15.737	4.3043
1,000,000	17.311	17.295	17.031	7.5162
2,000,000	17.658	17.650	17.556	11.773
5,000,000	18.117	18.113	18.079	16.631
10,000,000	18.463	18.462	18.445	18.138
20,000,000	18.810	18.809	18.801	18.699
50,000,000	19.268	19.268	19.264	19.227
100,000,000	19.615	19.165	19.613	19.595

Table 8-4
Values of $\Delta p_D (s, C_D, t_D)$ versus t_D including Wellbore Storage and Skin Effects¹ [$s = +20$]

Dimensionless time, t_D	$C_D (\times 10^2)$	Dimensionless storage constant		
		$C_D (\times 10^3)$	$C_D (\times 10^4)$	$C_D (\times 10^5)$
100	0.9776	0.09977	0.01000	0.00100
200	1.9130	0.1991	0.02000	0.00200
500	4.4896	0.4946	0.0499	0.00500
1000	8.1212	0.9787	0.0998	0.0100
2000	13.478	1.9172	0.1992	0.0200
5000	21.101	4.5125	0.4948	0.0500
10,000	24.241	8.1986	0.9797	0.0998
20,000	25.186	13.709	1.9209	0.1993
50,000	25.758	21.786	4.5333	0.4953
100,000	26.134	25.271	8.2698	0.9810
200,000	26.494	26.324	13.925	1.9252
500,000	26.960	26.907	22.443	4.5545
1,000,000	27.310	27.284	26.268	8.3394
2,000,000	27.657	27.645	27.460	14.133
5,000,000	28.116	28.112	28.055	23.085
10,000,000	28.463	28.461	28.434	27.297
20,000,000	28.810	28.809	28.795	28.606
50,000,000	29.268	29.268	29.262	29.216
100,000,000	29.615	29.615	29.612	29.596

Table 8-5
Values of Δp_D (s, C_D, t_D) versus t_D including Wellbore Storage and Skin Effects¹ [$s = -5$]

Dimensionless time, t_D	Dimensionless storage constant			
	$C_D (\times 10^2)$	$C_D (\times 10^3)$	$C_D (\times 10^4)$	$C_D (\times 10^5)$
100	0.0697	0.0447	0.00896	0.00099
200	0.0992	0.0715	0.0172	0.00197
500	0.1557	0.1263	0.0394	0.00487
1000	0.2164	0.1872	0.0718	0.00963
2000	0.2977	0.2697	0.1267	0.01896
5000	0.4446	0.4199	0.2518	0.0458
10,000	0.5913	0.5701	0.3990	0.0879
20,000	0.7722	0.7548	0.5972	0.1655
50,000	1.0646	1.0523	0.9313	0.3622
100,000	1.3232	1.3145	1.2254	0.6219
200,000	1.6086	1.6028	1.5422	0.9926
500,000	2.0170	2.0139	1.9806	1.6088
1,000,000	2.3420	2.3401	2.3201	2.0895
2,000,000	2.6757	2.6747	2.6630	2.5324
5,000,000	3.1248	3.1243	3.1197	3.0598
10,000,000	3.4677	3.4675	3.4644	3.4323
20,000,000	3.8124	3.8123	3.8107	3.7932
50,000,000	4.2693	4.2693	4.2685	4.2608
100,000,000	4.6154	4.6154	4.6150	4.6108

Then from Eq. 8-5,

$$C_{SD} = \frac{0.894C_S}{\phi c_t h r_w^2} = \frac{0.894 \times 0.0116}{(0.2)(10^{-5})(56)(0.3)^2} = 1.03 \times 10^3 \cong 10^3$$

For $C_{SD} = 10^3$, the best-fitting type curve is for $s = 5$. It is now evident that we should match the field data with one of the type curves labeled $C_{SD} = 10^3$ for $s = 5$. From the pressure match point, find the value of k by using Eq. 8-9:

$$k = \frac{141.2q\beta_o\mu_o (p_D)_M}{h (\Delta p)_M} = \frac{141.2 \times 500 \times 1.2 \times 0.8}{56} \frac{0.85}{100} = 10.3 \text{ mD}$$

From the time match point, find the product ϕc_t by using Eq. 8-10:

$$\phi c_t = \frac{0.000264k}{\mu_o r_w^2} \left(\frac{t}{t_D} \right)_M = \frac{0.000264 \times 10.3}{0.8 \times 0.3^2} \left(\frac{1}{19,300} \right) = 1.957 \times 10^{-6} \text{ psi}^{-1}$$

Table 8-6
Pressure Drawdown Test Data

Time, t (hr)	Pressure, p_{wf} (psig)	$(p_i - p_{wf})$ (psig)	$\frac{(p_i - p_{wf})}{t}$ (psi/hr)
0.0109	2976	24	2.20E + 03
0.0164	2964	36	2.20E + 03
0.0218	2953	47	2.16E + 03
0.0328	2930	70	2.13E + 03
0.0382	2919	81	2.12E + 03
0.0437	2908	92	2.11E + 03
0.0491	2897	103	2.10E + 03
0.0546	2886	114	2.09E + 03
0.1090	2785	215	1.97E + 03
0.1640	2693	307	1.87E + 03
0.2180	2611	389	1.78E + 03
0.2730	2536	464	1.70E + 03
0.3280	2469	531	1.62E + 03
0.3820	2408	592	1.55E + 03
0.4370	2352	648	1.48E + 03
0.4910	2302	698	1.42E + 03
0.5460	2256	744	1.36E + 03
1.0900	1952	1048	9.61E + 02
1.6400	1828	1172	7.15E + 02
2.1800	1768	1232	5.65E + 03
2.7300	1734	1266	4.64E + 02
3.2800	1712	1288	3.93E + 02
3.8200	1696	1304	3.41E + 02
4.3700	1684	1316	3.01E + 02
4.9100	1674	1326	2.70E + 02
5.4600	1665	1335	2.45E + 02
6.5500	1651	1349	2.06E + 02
8.7400	1630	1370	1.57E + 02
10.9000	1614	1386	1.27E + 02
16.4000	1587	1413	8.62E + 01

Comparing those with the values used to determine C_{SD} from C_S , we obtain

$$\phi c_t = (0.2)(10^{-5}) = 2 \times 10^{-6} \text{ [Value in = Value out]}$$

From Ramey's type curve, $s = 5.0$.

Using Conventional Method

From Figure 8-3, using slope m and p_{1h} , estimate the values of k and s using Eqs. 4-8 and 4-10:

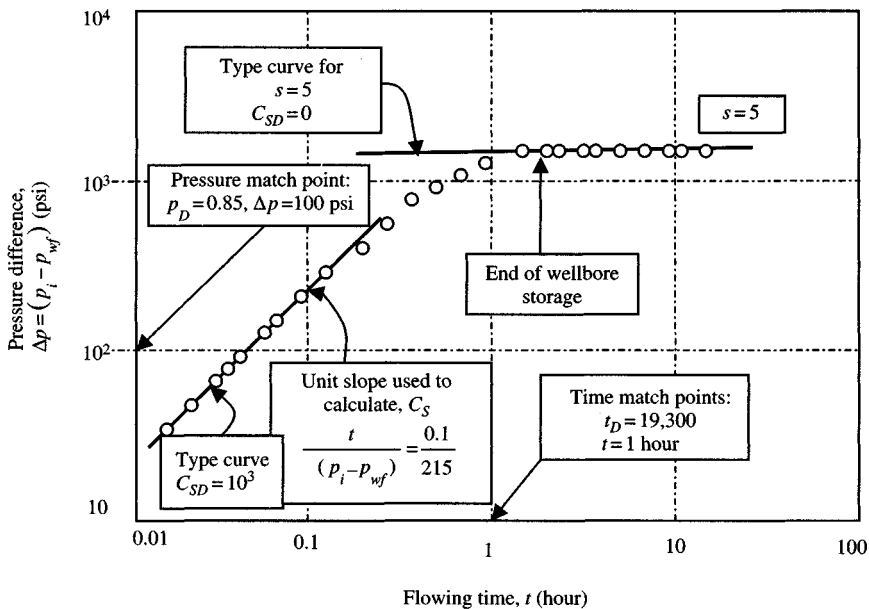


Figure 8-2. Pressure drawdown test analysis using Ramey type curves.

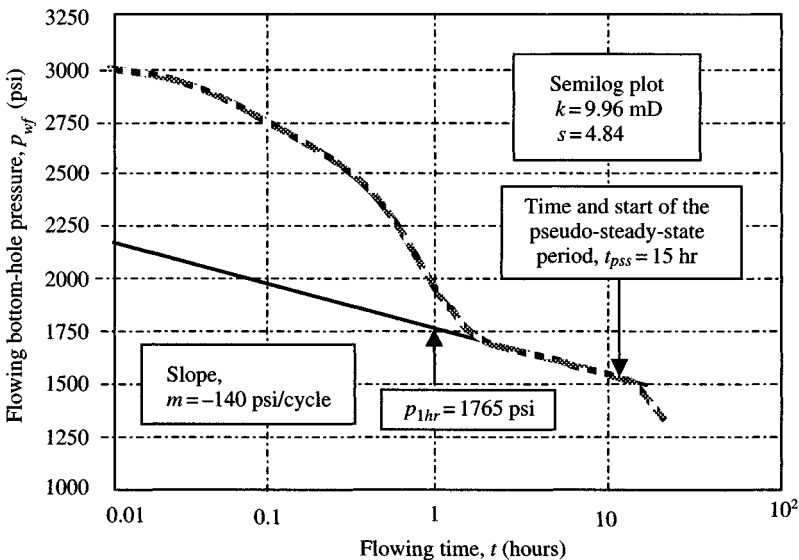


Figure 8-3. Pressure drawdown data – semilog plot.

$$k = \frac{-162.6q\mu\beta}{hm} = \frac{-162.6 \times 500 \times 0.8 \times 1.200}{56 \times (-140.0)} = 9.96 \text{ mD}$$

and

$$s = 1.151 \left[\frac{[p_i - p_{1hr}]}{m} - \log \left(\frac{k}{\phi\mu c_r r_w^2} \right) \right]$$

$$= 1.151 \left[\frac{(3000 - 1765)}{140} \right] - \log \left(\frac{9.96}{0.2 \times 0.8 \times 10 \times 10^{-6} \times (0.3)^2} \right) = 4.84$$

Example 8-2⁸ Analyzing Buildup Test Using Ramey Type Curves

Figure 8-4 shows a linear plot of pressure drawdown test data. Pressure buildup data tests are given in Table 8-7. Additional pertinent data are given: reservoir datum = 4500 ft, reservoir temperature = 200°F, $\phi = 0.039$, $\mu_o = 0.8$ cP, $\beta_o = 1.136$ rb/stb, $A_{wb} = 0.0218$ ft², $\rho = 51.50$ lb/ft³, last production rate = 250 stb/day, API° = 40°, cumulative production at shut-in time = 141.979 mstb, and pressure prior to shut-in $p_{wfo} = 3534$ psia.

Solution Figure 8-5 is a plot of Table 8-7 on log-log graph paper of the same scale of the type curves of Figure 8-1. From the unit-slope line on which the data lie for $t \leq 0.8$ hours, using Eq. 8-6:

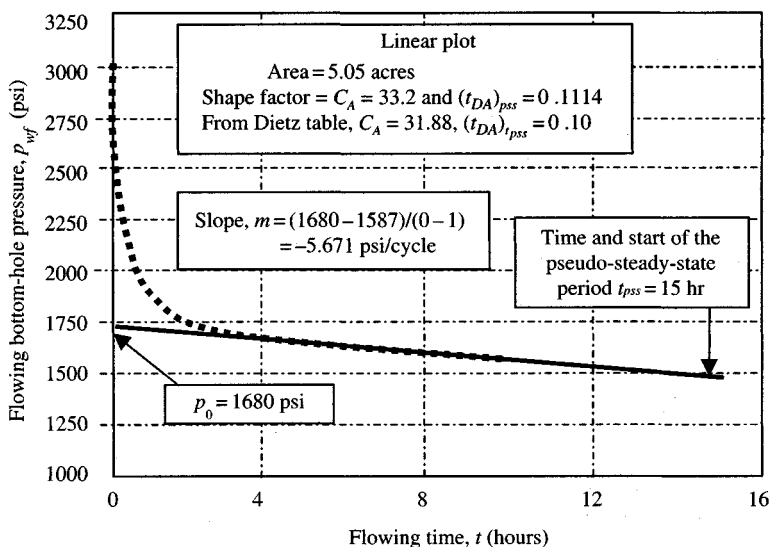


Figure 8-4. Pressure drawdown data – linear plot.

Table 8-7
Pressure Buildup Test Data

Time, Δt (hr)	$\frac{(t_p + \Delta t)}{\Delta t}$	$\frac{\Delta t}{(1 + \Delta t/t_p)}$	p_{ws} (psig)	$p_{ws} - p_{wf}$ (psig)	p_{ws} (psia)	$p_{ws} - p_{wf}$ (psia)	$\frac{(p_{ws} - p_{wf})}{\Delta t}$ (psi/hr)
0.00	—	—	3519	0	3534	0	—
0.15	90,867.56	0.15	3665	146	3680	146	9.73E + 02
0.20	68,150.93	0.20	3708	189	3723	189	9.45E + 02
0.30	45,434.28	0.30	3785	266	3800	266	8.87E + 02
0.40	34,075.96	0.40	3851	332	3866	332	8.30E + 02
0.50	27,260.97	0.50	3905	386	3920	386	7.72E + 02
1.00	13,630.99	1.00	4088	569	4103	569	5.69E + 02
2.00	6815.99	2.00	4235	716	4250	716	3.58E + 02
4.00	3408.50	4.00	4305	786	4320	786	1.97E + 02
6.00	2272.66	6.00	4325	806	4340	806	1.34E + 02
7.00	1948.14	7.00	4329	810	4344	810	1.16E + 02
8.00	1704.75	8.00	4335	816	4350	816	1.02E + 02
12.00	1136.83	11.99	4349	830	4364	830	6.92E + 01
16.00	852.87	15.98	4358	839	4373	839	5.24E + 01
20.00	682.50	19.97	4364	845	4379	845	4.23E + 01
24.00	568.92	23.96	4369	850	4384	850	3.54E + 01
30.00	455.33	29.93	4378	859	4393	859	2.86E + 01
40.00	341.75	39.88	4383	864	4398	864	2.16E + 01
50.00	273.60	49.82	4387	868	4402	868	1.74E + 01
60.00	228.17	59.74	4390	871	4405	871	1.45E + 01
72.00	190.31	71.62	4392	873	4407	873	1.21E + 01

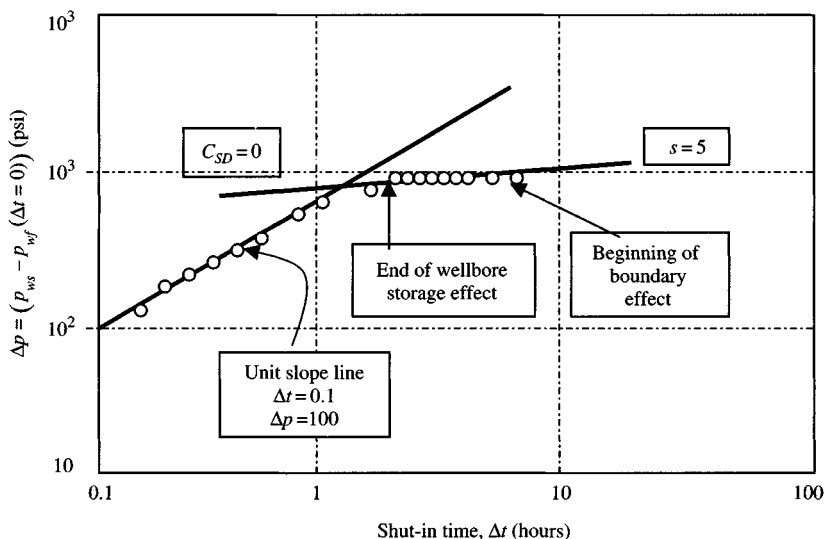


Figure 8-5. log-log data plot.

$$C_S = \frac{q\beta_o}{24} \left[\frac{t}{p_{ws} - p_{wf}} \right]_{\text{point on unit slope}}$$

$$= \frac{250 \times 1.136 \times 0.1}{24 \times 100} = 0.01183 \text{ bbl/psi}$$

Then, using Eq. 8-5, dimensionless wellbore storage is

$$C_{SD} = \frac{0.894 C_S}{\phi c_t h r_w^2} = \frac{0.894 \times 0.01183}{0.039 \times 1.7 \times 10^{-5} \times 69(0.198)^2} = 5.90 \times 10^3$$

Using wellbore properties, the wellbore storage constant from Eq. 8-7 is

$$C_S = \frac{25.65 \times A_{wb}}{\rho} = \frac{25.65 \times 0.0218}{51.50} = 0.01086 \text{ bbl/psi}$$

and

$$C_{SD} = \frac{0.894 \times C_S}{\phi c_t h r_w^2} = \frac{0.894 \times 0.01086}{0.039 \times 1.7 \times 10^{-5} \times 69(0.198)^2} = 5.42 \times 10^3$$

The value is close with the value calculated from unit-slope line. Therefore, for $C_{SD} = 5.9 \times 10^3$, the best-fitting type curve is for $s = 5.00$. It is now evident that we should match the field data with one of the type curves

labeled $C_{SD} = 10^3$ for $s = 5$. From the pressure match point, find the value of k using Eq. 8-9:

$$k = \frac{141.2q\beta_o\mu_o}{h} \frac{(p_D)_M}{(\Delta p)_M} = \frac{141.2 \times 250 \times 0.8 \times 1.136}{69} \times \frac{14}{850} = 7.67 \text{ mD}$$

From Ramey's type curve, $s = 5.0$.

Earlougher and Kersch Type Curves²

These type curves (Figure 8-6) involve the following steps:

1. Keep the two grids parallel, slide the tracing paper data plot horizontally until the best match is obtained with one of the curves in Figure 8-6.
2. Trace the matched curve onto the data plot and read the value of $C_D e^{2s}$ for the matched curve of Figure 8-6.
3. Pick a convenient match point with coordinates of $(\Delta p/\Delta t)_M$, $(\Delta t)_M$ from the tracing paper data plot; read the coordinate values lying directly under this point from Figure 8-6:

$$\left(\frac{\Delta p}{\Delta t} \times \frac{24C}{q\beta_o} \right)_{\text{Figure 8-6, } M} \quad \text{and} \quad \left(\frac{kh \Delta t}{\mu_o C} \right)_{\text{Figure 8-6, } M}$$

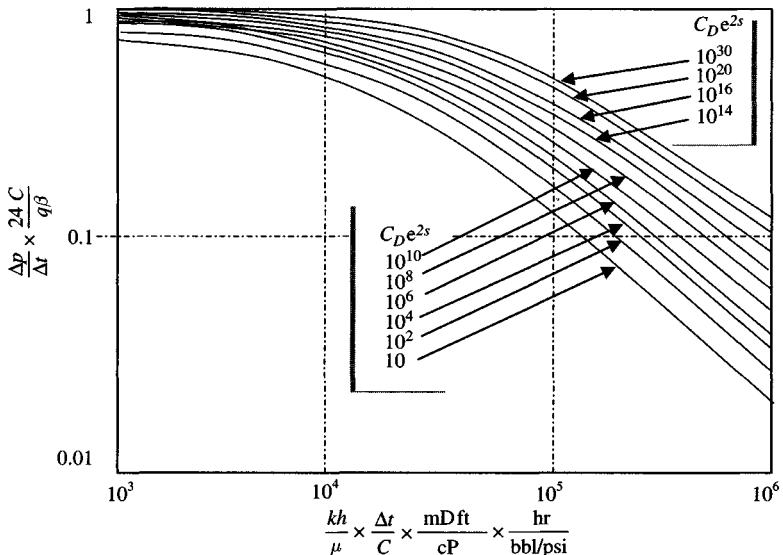


Figure 8-6. Type curve in an infinite system; wellbore storage and skin effect (after Earlougher and Kersch).²

4. Recomplete the wellbore storage coefficient using the following equation:

$$C = \frac{q\beta_o \left(\frac{\Delta p}{\Delta t} \frac{24C}{q\beta_o} \right)_{\text{Figure 8-6, } M}}{24 \left(\frac{\Delta p}{\Delta t} \right)_M} \quad (8-12)$$

This value of the wellbore storage coefficient should be essentially the same as the value estimated from the following equation or from completion details:

$$C = V_w C_w \text{ for a wellbore without a gas-liquid interface} \quad (8-12a)$$

or

$$C = \frac{V_u}{\left(\frac{\rho}{144 g_c} \right)} \text{ for a wellbore with changing liquid level} \quad (8-12b)$$

5. Estimate the permeability k from the abscissa in Figure 8-6:

$$k = \frac{C\mu_o \left(\frac{kh}{\mu} \cdot \frac{\Delta t}{C} \right)_{\text{Figure 8-6, } M}}{h(\Delta t)_M} \quad (8-13)$$

6. Estimate the skin factor from the parameter on the matched curve

$$s = 0.5 \ln \left[\frac{\phi c_t h r_w^2 (C_D e^{2S})_{\text{Figure 8-6, } M}}{0.89359C} \right] \quad (8-14)$$

Example 8-3⁸ Rework Example 8-2 using Earlougher and Kersch type curves.

Solution Plot $\Delta p = (p_i - p_{wf})$ versus t as log-log scale on tracing paper laid over the Figure 8-6 grids. Figure 8-7 shows the resulting data plot. We slide the tracing paper data plot on Figure 8-7 until a good match results. Figure 8-7 shows the data plot matched to Figure 8-6. Match point data are given in Figure 8-8. Estimate the wellbore storage coefficient using Eq. 8-9 and the match data from Figure 8-12:

$$\begin{aligned} C &= \frac{q\beta_o \left(\frac{\Delta p}{\Delta t} \frac{24C}{q\beta_o} \right)_{\text{Figure 8-7, } M}}{24 \left(\frac{\Delta p}{\Delta t} \right)_M} \\ &= \frac{500 \times 1.2}{24} \times \left(\frac{0.05}{100} \right) = 0.0125 \text{ bbl/psi} \end{aligned}$$

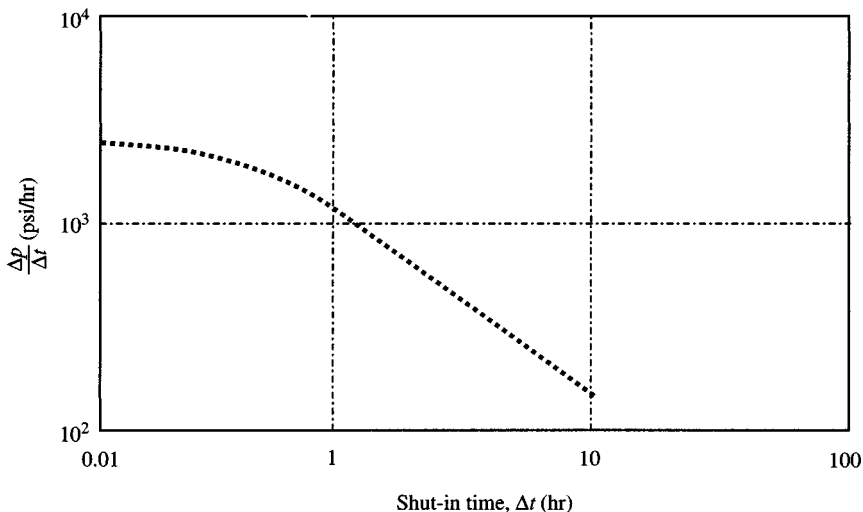


Figure 8-7. log-log data plot.

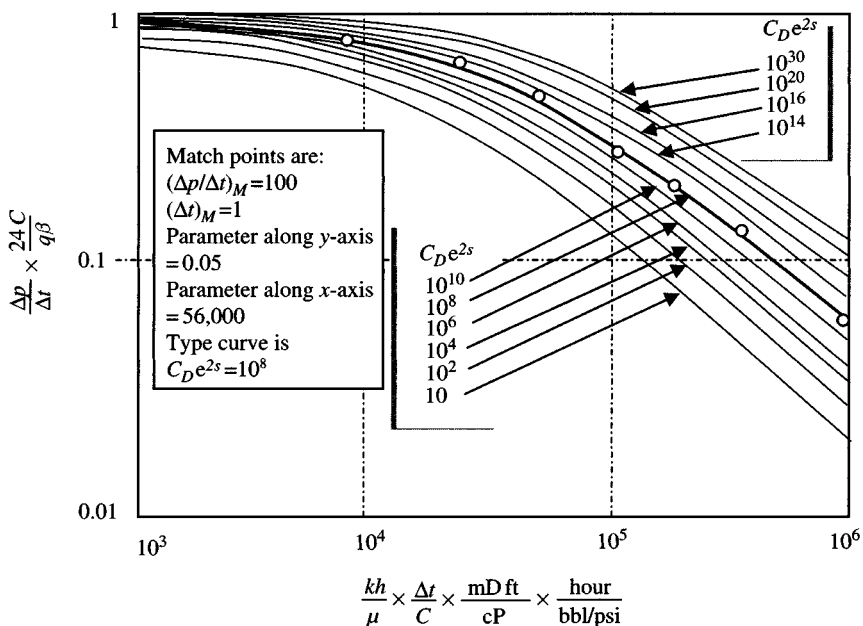


Figure 8-8. Type curve in an infinite system; wellbore storage and skin effect (after Earlougher and Kersch).²

Calculate C from wellbore properties or using conventional method (Eq. 8-12a):

$$C = V_w C_w = \frac{500 \times 1.2}{24} \times \left| \frac{0.1}{215} \right|_{\text{point on unit slope}}$$

$$= 0.0116 \text{ bbl/psi}$$

Estimate the permeability k from Eq. 8-13:

$$k = \frac{C \mu_o}{h} \frac{\left(\frac{kh \Delta t}{\mu C} \right)_{\text{Figure 8-8, } M}}{\Delta t}$$

$$= \frac{0.0125 \times 0.8}{56} \frac{5.6 \times 10^4}{1} = 10.0 \text{ mD}$$

Estimate the skin factor from Eq. 8-14:

$$s = 0.5 \ln \left[\frac{\phi c_t h r_w^2 (C_D e^{2s})_{\text{Figure 8-8, } M}}{0.89359 C} \right]$$

$$= 0.5 \ln \left[\frac{0.2 \times 1.000 \times 10^{-5} \times 56 \times (0.3)^2 \times 10^8}{0.89359 \times 0.0125} \right] = 5.71$$

$$C = \frac{q \beta_o \left(\frac{\Delta p}{\Delta t} \frac{24 C}{q \beta_o} \right)_{\text{Figure 8-8, } M}}{24 \left(\frac{\Delta p}{\Delta t} \right)_M}$$

$$= \frac{250 \times 1.136}{24} \times \left(\frac{0.1}{100} \right) = 0.0118 \text{ bbl/psi}$$

Check with the value of C calculated using wellbore properties, i.e.,

$$C = \frac{25.65 \times A_{wb}}{\rho} = \frac{25.65 \times 0.0218}{51.50} = 0.01086 \text{ bbl/psi}$$

McKinley's Type Curves

McKinley³ proposed type curves which can be used to characterize damage or stimulation in a drawdown or buildup test in which wellbore storage

distorts most or all of the data. A set of McKinley type curves is included in Figure 8–10. These curves were computed by numerical simulation of the complete afterflow process by forming a dynamic balance between the capacities of the wellbore to store fluid and the resistance of the wellbore to the flow of fluid from the reservoir. Shut-in time, Δt (min), has been plotted as a function of pressure buildup group $[5.6146\Delta p C_S/q\beta_o]$ on log-log paper for several values of parameter $(kh/\mu)/5.6146C_S$. These variables are in field units. Note that the skin factor s does not appear as a parameter, because these curves were computed assuming no mechanical skin factor. If a well is damaged, this fact is evident since the pressure buildup plot will deviate from the McKinley type curve; while the analysis does not determine the skin factor, it does allow a comparison to be made between the kh values in the damaged and undamaged parts of the reservoir.

Pressure Drawdown or Buildup Analysis

The steps for using McKinley's type curves are as follows:

1. Plot time (minutes) as ordinate versus Δp as abscissa on 3×5 cycle log-log paper, the same size as McKinley's type curves where

$$\begin{aligned} \text{Time} &= t \rightarrow \text{drawdown test} \\ &= \Delta t \rightarrow \text{buildup test} \\ \Delta p &= p_i - p_{wf} \rightarrow \text{drawdown test} \\ &= p_{ws} - p_{wf} \rightarrow \text{buildup test} \end{aligned}$$

2. Match the time axis of the test data plot with one of McKinley's type curves.
Move the data along the plot horizontal (no vertical shifting allowed) until the earliest data fall along one of the type curves.
3. Record the parameter value $(kh/\mu)/5.6145C_S$ for the correct type curve.
4. Choose a data match point (any Δp from the test graph paper and the corresponding value of $5.615\Delta p C_S/q\beta_o$ from the type curve).
5. Determine the wellbore storage constant C_S from pressure match point:

$$C_S = \frac{q\beta_o}{5.615} \left(\frac{5.615\Delta p C_S}{q\beta_o} \right)_M \quad (8-15)$$

6. Calculate the near-well transmissibility, $(kh/\mu)_{wb}$, from the value $|(kh/\mu)/5.615C_S|_M$ and C_S :

$$\left(\frac{kh}{\mu}\right)_{wb} = 5.615C_S \left(\frac{kh/\mu}{5.615C_S}\right)_{wb} \quad (8-16)$$

7. If the data trend away from the type curve, shift the data plot horizontally to find another type curve that better fits the later data. A shift to a higher value of $(kh/\mu)/5.615C_S$ indicates damage; a shift to a lower value indicates stimulation.
8. Calculate the formation transmissibility

$$\left(\frac{kh}{\mu}\right)_f = \frac{|(kh/\mu) \times 5.615C_S|_f}{|(kh/\mu \times 5.615C_S)_{wb}} \times \left(\frac{kh}{\mu}\right)_{wb} \quad (8-17)$$

and the formation permeability, k_f :

$$k_f = \left(\frac{kh}{\mu}\right)_f \times \frac{\mu}{h} \quad (8-18)$$

9. Estimate the flow efficiency, FE as

$$FE \approx \frac{\Delta p^* - \Delta p_s}{\Delta p^*} \quad (8-19)$$

The quantities Δp^* and Δp_s can be estimated from McKinley's type curves in the following manner:

1. Δp^* is the vertical asymptote approached by Δp in McKinley's plot?
2. Δp_s can be calculated from Δp_D , the time at which the actual test data depart from the earliest fitting type curve.
3. McKinley³ states that Δp_s and Δp_D are related by

$$\Delta p_s = \left(1 - \frac{k_{wb}}{k_f}\right) \Delta p_D \quad (8-20)$$

4. Thus, F can be calculated:

$$F \approx \frac{\Delta p^* - \Delta p_s}{\Delta p^*} \quad (8-21)$$

The following examples will clarify the use of McKinley's type curves.

Example 8-4⁸ Analyzing Drawdown Test Using McKinley's Type Curves

Determine the near-well formation permeability and flow efficiency from the data below and in Table 8-8, which were obtained in a pressure drawdown test on an oil well.

Table 8-8
Pressure Drawdown Test Data

Time, t (hr)	Time, t (min)	Pressure, p_{wf} (psig)	$\Delta p = (p_i - p_{wf})$ (psig)	Pressure buildup group $5.6146 \times \Delta p \times \frac{C_S}{(q \times \beta_o)(ft^2 \text{ day/rbbl})}$
0.02	1.31	2953	47	4.39E-03
0.03	1.97	2930	70	6.54E-03
0.04	2.29	2919	81	7.57E-03
0.04	2.62	2908	92	8.60E-03
0.05	2.95	2897	103	9.63E-03
0.05	3.28	2886	114	1.07E-02
0.11	6.54	2785	215	2.01E-02
0.16	9.84	2693	307	2.87E-02
0.22	13.10	2611	389	3.64E-02
0.27	16.40	2536	464	4.34E-02
0.33	19.70	2469	531	4.96E-02
0.38	22.90	2408	592	5.53E-02
0.44	26.20	2352	648	6.06E-02
0.49	29.50	2302	698	6.52E-02
0.55	32.80	2256	744	6.95E-02
1.09	65.40	1952	1048	9.79E-02
1.64	98.40	1828	1172	1.10E-01
2.18	131.00	1768	1232	1.15E-01
2.73	164.00	1734	1266	1.18E-01
3.28	197.00	1712	1288	1.20E-01
3.82	229.00	1696	1304	1.22E-01
4.37	262.00	1684	1316	1.23E-01
4.92	295.00	1674	1326	1.24E-01
5.47	328.00	1665	1335	1.25E-01
6.55	393.00	1651	1349	1.26E-01
8.73	524.00	1630	1370	1.28E-01
10.90	654.00	1614	1386	1.30E-01
16.40	984.00	1587	1413	1.32E-01

$T = 200^\circ\text{F}$; depth = 4500 ft; $q_o = 500$ stb/day; $\text{API}^\circ = 32^\circ$ tubing ID = 2 inch; $\beta_o = 1.2000$ rb/stb; $\mu_o = 0.8$ cP; $\phi = 0.20$; $h = 56$ ft; $c_t = 10.0 \times 10^{-6}$ psi $^{-1}$; $r_w = 0.3$ ft.

Solution Prepare the data for plotting as t (min) versus $\Delta p = p_i - p_{wf}$ (Table 8-8). The data plot (Figure 8-9) and the match with the best-fitting McKinley's type curves in the early data are shown in Figures 8-10 and 8-11, respectively. Match points for the early fit data are:

$$(\Delta p)_M = 107 \text{ psi} \quad \text{and} \quad \left(\frac{5.615 \Delta p C_S}{q \beta} \right)_M = 0.010$$

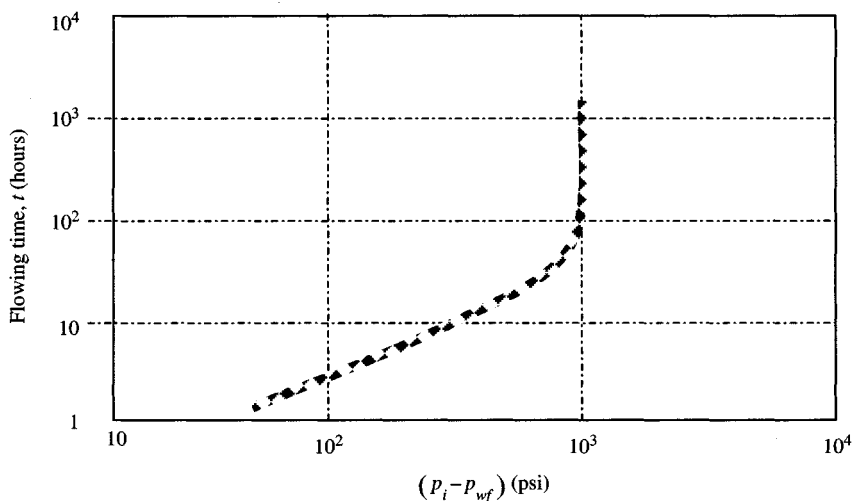


Figure 8-9. log-log data plot.

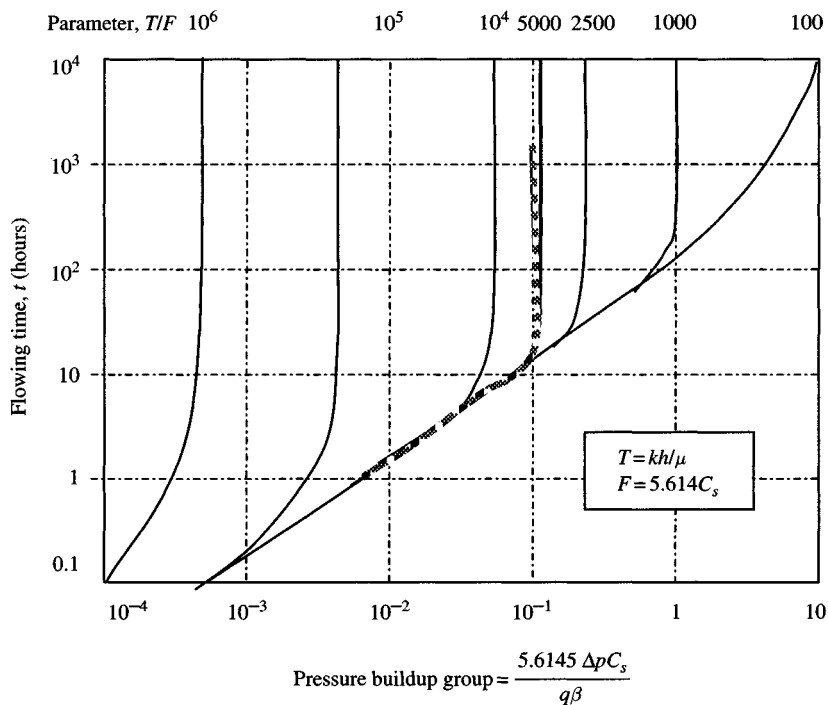


Figure 8-10. log-log type curve - McKinley type curves.

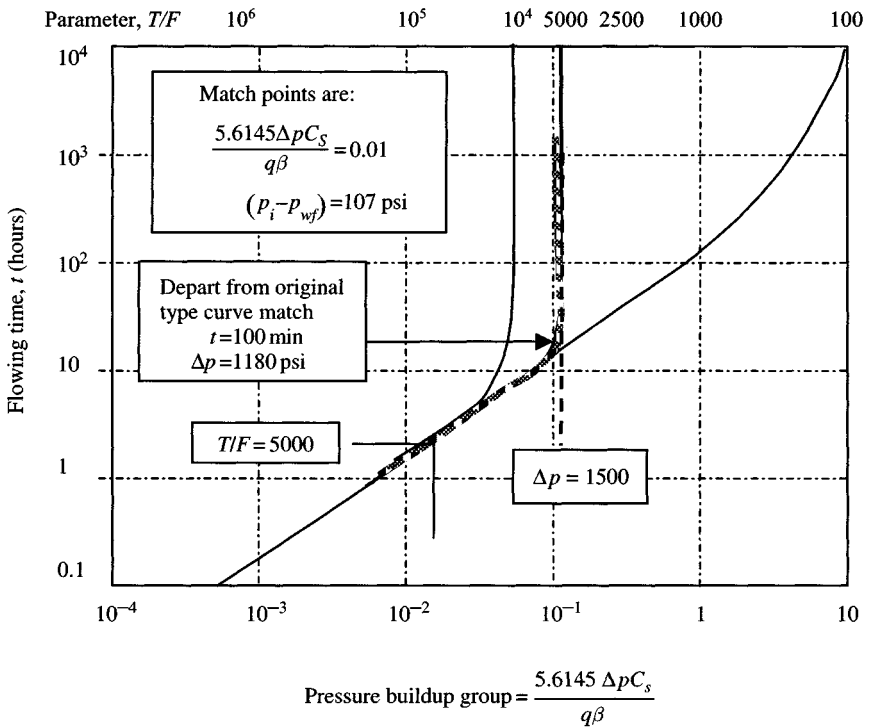


Figure 8-11. log-log type curve – McKinley type curves.

Calculate the wellbore storage constant C_S using Eq. 8-15:

$$C_S = \frac{\left(\frac{5.615 \Delta p C_S}{q\beta}\right)_M}{(\Delta p)_M} \times \frac{q\beta}{5.615} = \frac{0.010}{107} \times \frac{500 \times 1.2}{5.615} = 0.01 \text{ rb/psi}$$

Estimate the near-well transmissibility and apparent permeability from Eq. 8-16:

$$\left(\frac{kh}{\mu}\right)_{wb} = 5.615 C_S \left(\frac{kh/\mu}{5.615 C_S}\right)_{wb} = 5.615 \times 0.01(5000) = 281 \text{ mD ft/cP}$$

Then,

$$k_{wb} = \frac{281(0.8)}{56} = 4.01 \text{ mD}$$

Calculate the formation transmissibility and permeability from Eq. 8-17:

$$\begin{aligned} \left(\frac{kh}{\mu}\right)_f &= \frac{[kh/\mu \times 5.615C_s]_f}{[kh/\mu \times 5.615C_s]_{wb}} \times \left(\frac{kh}{\mu}\right)_{wb} \\ &= \frac{10,000}{5000} (281) = 562 \text{ mD ft/cP} \end{aligned}$$

and from Eq. 8-18:

$$k_f = \left(\frac{kh}{\mu}\right)_f \times \frac{\mu}{h} = 562 \left(\frac{0.8}{56}\right) = 8.03 \text{ mD}$$

Determine the flow efficiency as follows:

$$\Delta p^* = 1500 \text{ psia} \quad (\text{Figure 8-11})$$

From Eq. 8-20:

$$\Delta p_s = \left(1 - \frac{k_{wb}}{k_f}\right) \Delta p_D = \left(1 - \frac{4.01}{8.03}\right) \times 1180 = 590 \text{ psi}$$

From Eq. 8-21:

$$\begin{aligned} F &\approx \frac{\Delta p^* - \Delta p_s}{\Delta p^*} \\ &\approx \frac{1500 - 590}{1500} \times 100 = 60.7\% \end{aligned}$$

Example 8-5⁸ *Analyzing Pressure Buildup Test Using McKinley's Type Curves*

Determine the near-well formation permeability and flow efficiency from the data below and in Table 8-9, which were obtained in a pressure buildup test on an oil well.

$q_o = 231$ stb/day; $t_p = 3184.935$ minutes; $T = 200^\circ\text{F}$; well depth = 4500 ft; $h = 10$ ft; $\beta_o = 1.30$ rb/stb; $\mu_o = 0.6$ cP; $\text{API}^\circ = 40$; $\phi = 0.20$; $c_t = 20.0 \times 10^{-6}$ psi⁻¹; $r_w = 0.30$ ft; tubing ID = 2 inch; $p_{wf}(\Delta t=0) = 1615$ psia; cumulative production = 30,655 stb; and pressure prior to shut-in = 1600 psia.

Solution Prepare the data for plotting as t (min) versus $\Delta p = p_{ws} - p_{wf}$ (Table 8-9). The data plot (Figure 8-12) and the match with the best-fitting

Table 8-9
Pressure Buildup Test Data

Time, Δt (min)	$\frac{(t_p + t)}{\Delta t}$	$\frac{\Delta t}{(1 + \Delta t/t_p)}$	Pressure, p_{ws} (psig)	$(p_{ws} - p_{wf}) = \Delta p$ (psig)	$(p_{ws} - p_{wf}) = \Delta p$ (psia)	Pressure BU group $\frac{5.6146 \times \Delta p \times C_S}{qB_o}$ (ft ³ day/rbbl)
0.00	—	—	1600	0	15	—
20.00	160.25	19.88	1920	320	335	5.42E-03
40.00	80.62	39.50	2160	560	575	6.54E-03
60.00	54.08	58.89	2350	750	765	7.57E-03
90.00	36.39	87.53	2525	925	940	8.60E-03
120.00	27.54	115.64	2650	1050	1065	9.63E-03
150.00	22.23	143.25	2726	1126	1141	1.07E-02
180.00	18.69	170.37	2779	1179	1194	2.01E-02
210.00	16.17	197.01	2822	1222	1237	2.87E-02
240.00	14.27	223.18	2852	1252	1267	3.64E-02
270.00	12.80	248.90	2879	1279	1294	4.34E-02
300.00	11.62	274.37	2900	1300	1315	4.96E-02
360.00	9.85	323.44	2935	1335	1340	5.53E-02
420.00	8.58	371.07	2960	1360	1375	6.06E-02
480.00	7.64	417.13	2980	1380	1395	6.52E-02
540.00	6.90	461.72	2998	1398	1413	6.95E-02
600.00	6.31	504.89	3011	1411	1417	9.79E-02
660.00	5.83	546.71	3022	1422	1437	1.10E-01
720.00	5.42	587.24	3035	1435	1450	1.15E-01

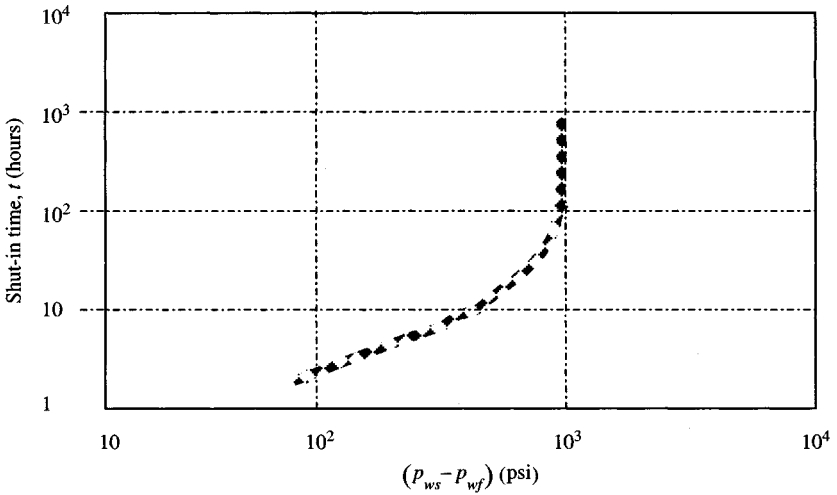
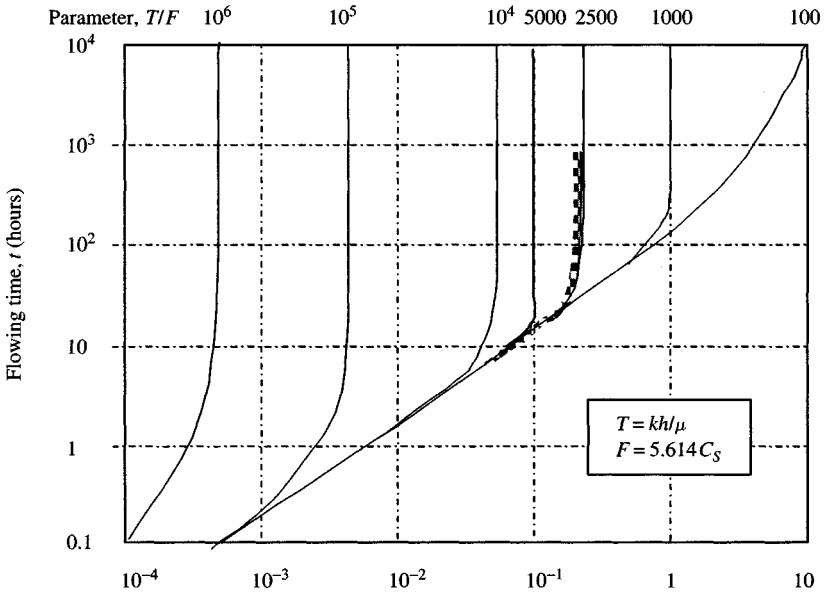


Figure 8-12. log-log data plot.



$$\text{Pressure buildup group} = \frac{5.6145 \Delta p C_S}{q\beta}$$

Figure 8-13. log-log type curve - McKinley type curves.

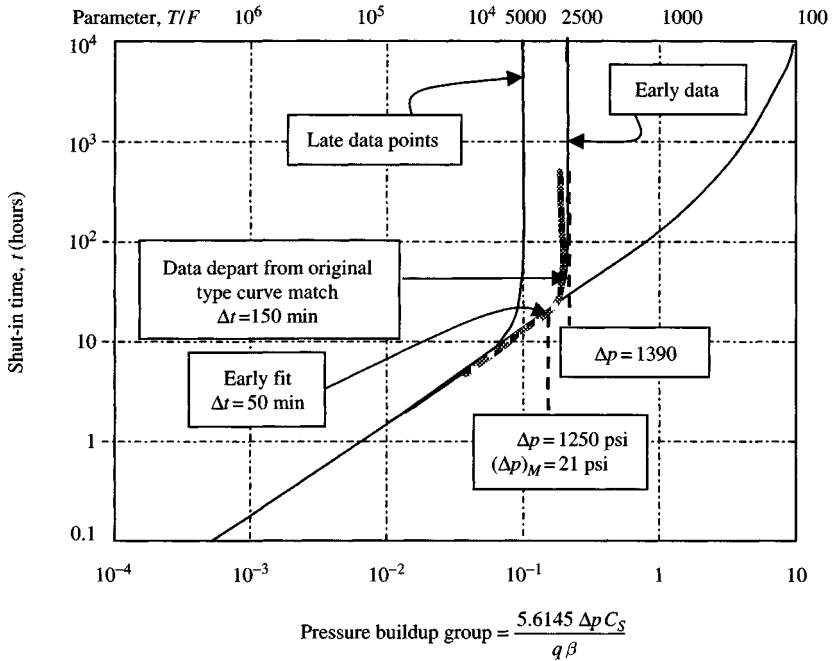


Figure 8-14. log-log type curve – McKinley type curves.

McKinley's type curves in the early data are shown in Figures 8-13 and 8-14, respectively. Match points for the early fit data are:

$$(\Delta p)_M = 760 \text{ psi} \quad \text{and} \quad \left(\frac{5.615 \Delta p C_S}{q \beta} \right)_M = 0.14$$

Calculate the wellbore storage constant C_S using Eq. 8-15:

$$\begin{aligned} C_S &= \frac{\left(\frac{5.615 \Delta p C_S}{q \beta} \right)_M}{(\Delta p)_M} \times \frac{q \beta}{5.615} \\ &= \frac{0.14}{760} \times \frac{231 \times 1.3}{5.615} = 0.009853 \text{ rb/psi} \end{aligned}$$

Estimate the near-well transmissibility and apparent permeability from Eq. 8-16:

$$\begin{aligned} \left(\frac{kh}{\mu} \right)_{wb} &= 5.615 C_S \left(\frac{kh/\mu}{5.615 C_S} \right)_{wb} \\ &= 5.615 \times 0.009853 (2500) = 138.31 \text{ mD ft/cP} \end{aligned}$$

Then

$$k_{wb} = \frac{138.31(0.6)}{10} = 8.30 \text{ mD}$$

$$\text{Early data parameter} = \frac{T}{F} = \left(\frac{kh/\mu}{5.615C_S} \right)_{wb} = 2500$$

$$\text{Late data parameter} = \frac{T}{F} = \left(\frac{kh/\mu}{5.615C_S} \right)_f = 5000$$

Using the values of early and late data parameters, calculate the formation transmissibility from Eq. 8-17:

$$\begin{aligned} \left(\frac{kh}{\mu} \right)_f &= \frac{[kh/\mu \times 5.615C_S]_f}{[kh/\mu \times 5.615C_S]_{wb}} \times \left(\frac{kh}{\mu} \right)_{wb} \\ &= \frac{5000}{2500} (138.31) = 276.62 \text{ mD ft/cP} \end{aligned}$$

and from Eq. 8-18:

$$k_f = \left(\frac{kh}{\mu} \right)_f \times \frac{\mu}{h} = 276.62 \left(\frac{0.6}{10} \right) = 16.60 \text{ mD}$$

Determine the flow efficiency as follows:

$$\Delta p^* = 1390 \text{ psia} \quad (\text{Figure 8-15})$$

From Eq. 8-20,

$$\Delta p_s = \left(1 - \frac{k_{wb}}{k_f} \right) \Delta p_D = \left(1 - \frac{8.30}{16.60} \right) \times 1250 = 625 \text{ psi}$$

From Eq. 8-21,

$$\begin{aligned} F &\approx \frac{\Delta p^* - \Delta p_s}{\Delta p^*} \\ &\approx \frac{1390 - 625}{1390} \times 100 = 55.03\% \end{aligned}$$

8.3 Fracture Type Curve Matching Techniques

It is believed that hydraulic fracturing results in the formation of vertical fractures. At depths shallower than 3000, the likelihood is that horizontal fractures will be induced. In this section, the methods of analysis of well test data in the presence of both vertical and horizontal hydraulic fractures have been discussed. However, in most cases only vertical fractures are encountered. Vertical fractures are further divided into two types, uniform-flux fracture and infinite-conductivity fracture. In uniform-flux fracture, fluid enters the fracture at a uniform rate per unit cross-sectional area at all points along the fracture. On the other hand, an infinite-conductivity fracture has infinite permeability and therefore uniform pressure throughout.

The following theoretical guidelines are helpful in analysis tests in these wells; however, it has been found that in practice the linear flow lasts much longer in massive hydraulically fractured tight formation than what the guidelines suggest.

For values of $x_e/x_f > 1$, the linear flow period ends at

$$t_{Dxf} \cong 0.016 \quad (\text{infinite-conductivity fracture})$$

$$t_{Dxf} \cong 0.16 \quad (\text{uniform-flux fracture})$$

The pseudo-radial flow period begins at

$$t_{Dxf} \cong 3 \quad (\text{for infinite-conductivity fracture})$$

$$t_{Dxf} \cong 2 \quad (\text{uniform-flux fracture})$$

In the pseudo-radial flow period, the conventional buildup analysis techniques apply. In order to choose the correct linear or radial flow, the following condition should be satisfied:

$$\Delta p_{bsi} \geq 2\Delta p_{el} \quad (8-22)$$

where Δp_{bsi} is the pressure change at the beginning of the pseudo-radial semilog straight line (Horner method applies) and Δp_{el} the pressure change at the end of the linear flow line. Δp_{el} is the last point on the $\sqrt{\Delta t}$ plot after which the pressure starts to deviate from the straight line. The linear flow period is characterized by a half-unit slope on a log-log plot of Δp versus Δt , or a straight line on a plot of Δp versus $\sqrt{\Delta t}$. The slope of the line Δp versus $\sqrt{\Delta t}$ plot, symbol m_{vf} , is used to calculate the fracture length of x_f as follows:

$$x_f = \frac{4.064q_o\beta_o}{hm_{vf}} \left(\frac{\mu}{\phi c_t k} \right)^{0.5} \quad (8-23)$$

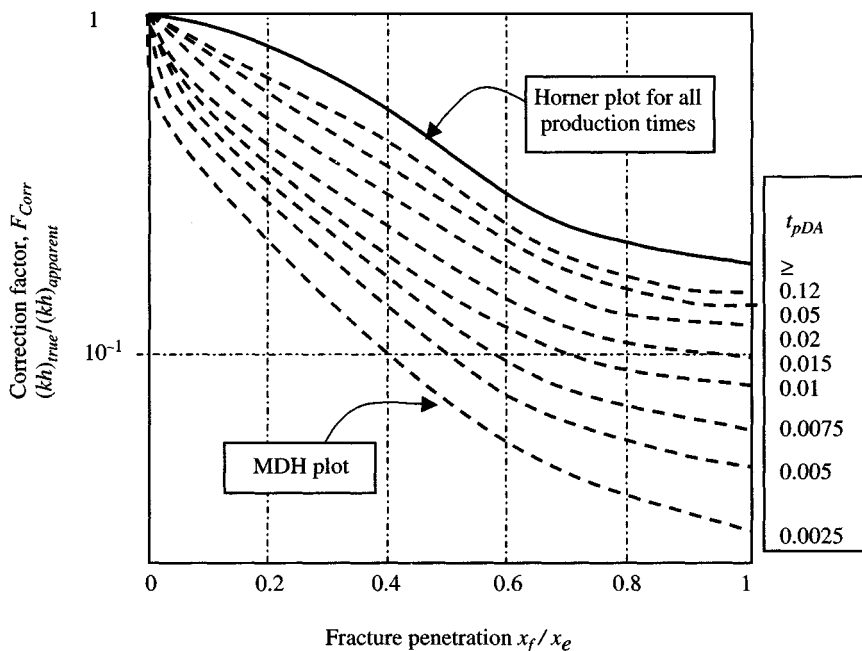


Figure 8–15. Correction factor for kh estimated from pressure buildup tests in vertical fractured wells.⁴

If the buildup test is run for a sufficient duration of time that a semilog straight line is developed, then the Horner method is applicable. However, the slope of this line and thus the calculated permeability is affected by the fracture length. This means that the permeability calculated using this slope has to be corrected. To correct the permeability estimated from a Horner or MDH plot, the following equation and Figure 8–15 will be used:

$$k = k_{cal} F_{corrected} \quad (8-24)$$

where k_{cal} is the permeability calculated using the following equation:

$$k = \frac{162.6q\mu_o\beta_o}{mh}$$

and

$$F_{corrected} = \left[\frac{(kh)_{true}}{(kh)_{apparent}} \right] \quad (\text{obtained from Figure 8-15})$$

The fracture length is estimated using the following equation, where m is the slope of the Horner or MDH straight line:

$$x_f = \frac{0.3187}{m_{vf}} \left(\frac{mq\beta_o}{\phi c_t h F_{corrected}} \right)^{0.5} \quad (8-25)$$

A type curve matching approach introduced by Gringarten et al. is a recommended method for analyzing pressure buildups in hydraulically fractured reservoirs.⁵ Curve matching is performed using Figures 8-16 through 8-18.

The linear flow in tight (low-permeability) wells may last several hundred hours or days and months. In this case, the test data will deviate from the half-unit slope line of the log Δp versus Δt plot, or the straight-line plot of Δp versus $\sqrt{\Delta t}$. In such cases, only the upper limit of the permeability value and the lower limit of the fracture length could be calculated using the last Δp and Δt on the half-unit slope line, using the following equations.

For infinite-conductivity fractures and $x_e/x_f \gg 1$:

$$k \leq \frac{(0.215)(141.2)q\mu_o\beta_o}{h \Delta p} \quad (8-26)$$

$$x_f \geq \frac{0.000264kt}{0.016\phi\mu c_t} \quad (8-27)$$

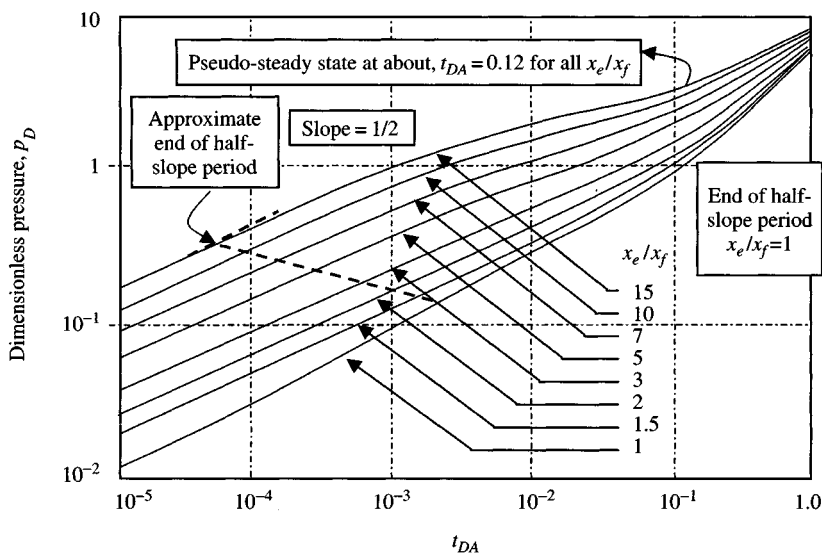


Figure 8-16. Dimensionless pressure versus dimensionless time – vertical fracture no wellbore storage, infinite-conductivity fracture.⁵

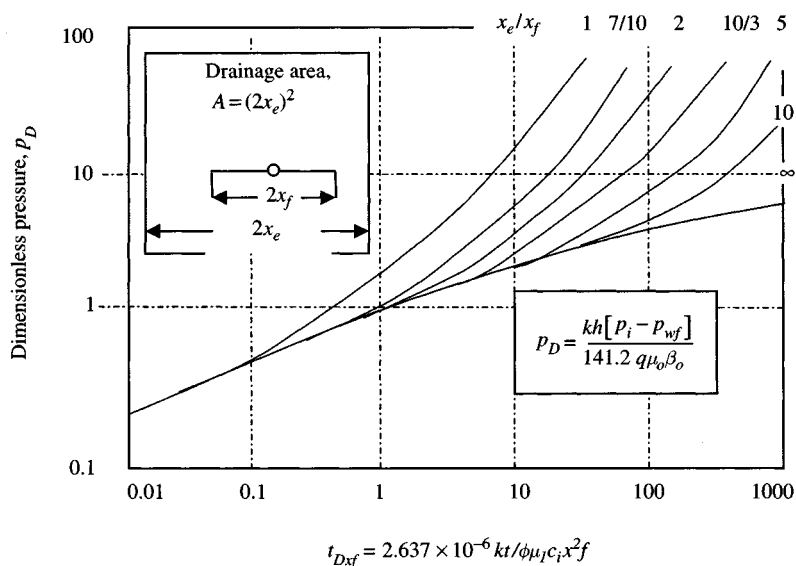


Figure 8-17. Type curve matching for vertical fractured well – infinite fracture conductivity.^{5,6}

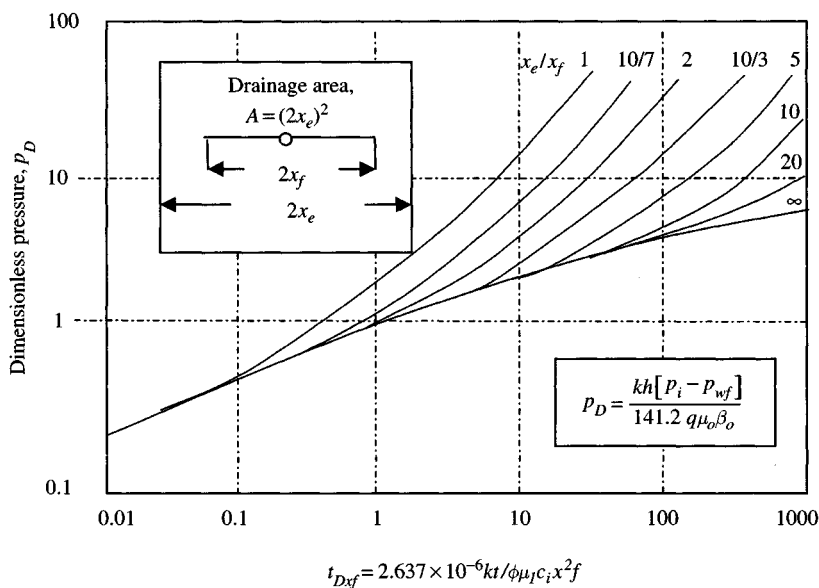


Figure 8-18. Type curve matching for vertical fractured well – infinite fracture conductivity.^{5,6}

For uniform-flux fractures:

$$k \leq \frac{(0.76)(141.2)q\mu_o\beta_o}{h \Delta p} \quad (8-28a)$$

$$x_f \geq \frac{0.000264kt}{0.16\phi\mu c_t} \quad (8-28b)$$

Type Curves for Vertical Fractured Oil Wells

Gringarten et al.^{5,6} developed type curves for hydraulically fractured wells in which vertical fracture with two equal wings as created. The type curves (Figure 8-16) are developed for a constant-rate drawdown test for a slightly compressible fluid; however, they can also be used for buildup tests for $\Delta t_{max} \leq 0.1t_p$. Wellbore storage effects are ignored. Gringarten et al. type curves are presented in Figures 8-17 and 8-18, which are log-log plot of p_D versus t_{Dxf} with parameter x_e/x_f :

$$p_D = \frac{kh(p_i - p_{wf})}{141.2q\beta_o\mu_o} \quad (\text{drawdown test}) \quad (8-29)$$

and

$$t_{Dxf} = \frac{0.000264kt}{\phi\mu c_t x_f^2} \quad (8-30)$$

$$t_{Dxf} = \frac{t_D r_w^2}{x_f^2} \quad (8-31)$$

For a linear flow, $t_{Dxf} \cong 0.16$ for $x_e/x_f > 1$ and for a radial flow, $t_{Dxf} \cong 2$ for $x_e/x_f > 5$.

Pressure Drawdown Analysis

The type curve (Figures 8-16 through 8-18) involves the following steps:

1. Plot $(p_i - p_{wf})$ versus t on a 3×5 cycle log-log paper.
2. Select the best match by sliding the actual test data plot both horizontally and vertically.
3. Estimate the formation permeability from the pressure match point:

$$k = 141.2 \frac{q\beta_o\mu_o}{h} \frac{(p_D)_M}{(p_i - p_{wf})_M} \quad (8-32)$$

4. Estimate the fracture length from the time match point:

$$x_f = \sqrt{\frac{0.000264k(t)_M}{\phi\mu c_t(t_{Dxf})_M}} \quad (8-33)$$

5. If a half-slope (linear flow) region appears on the test data plot, re-plot data from the region as p_{wf} versus \sqrt{t} from the slope m_L and linear flow theory:

$$x_f\sqrt{k} = \frac{4.064q\beta_o}{hm_L} \sqrt{\frac{\mu_o}{\phi c_t}} \quad (8-34)$$

6. If a radial flow region appears before the data deviate from the $x_e/x_f = \text{infinity}$ curve, a plot of p_{wf} versus $\log t$ should show that $k = 162.6q\beta_o\mu_o/mh$, which is in agreement with type curve analysis.
7. If a well proves to be in a finite (bounded) reservoir, it may be possible to estimate from the matching parameter, x_e/x_f , to compare with the known value of x_e to check the quality of the match.
8. Estimate the skin factor from

$$s = -\ln\left(\frac{r_{wa}}{r_w}\right) \quad (8-35)$$

where $r_{wa} = x_f/2$.

Example 8-6⁸ Analyzing Pressure Drawdown Test for Vertical Fractured Well Using Conventional and Gringarten et al.'s Type Curves

A drawdown test was run in a vertically fractured oil well; the results are given in Table 8-10. Using conventional method and Gringarten et al. type curves, estimate the formation permeability, fracture length, and skin factor. Identify linear flow and radial flow regions and verify the type curve analysis with conventional analysis of the radial flow regions. As part of the conventional analysis of the radial flow region, estimate the time at the beginning and end of the MTR. The test data were as follows: $q = 200$ stb/day (constant); $h = 12$ ft; $c_t = 20 \times 10^{-6}$ psi⁻¹; $\beta_o = 1.288$ rb/stb; $\phi = 0.10$; and $\mu_o = 0.5$ cP.

Solution Conventional Analysis

Figure 8-19 shows a straight line with a slope of one-half, thus indicating a linear flow that lasted less than 0.45 hr and no wellbore storage effects. From the slope of the straight line of Figure 8-20, $m_{vf} = 60.0$ psi/hr^{0.5} and $\Delta p_{el} = 35$ psi, we get $\Delta p_{bsi} = 2 \times 35 = 70$ psi. Figure 8-21 fits the semilog

Table 8–10
Pressure Drawdown Test Data for Vertical Fractured Oil Well

Time, t (hr)	Time \sqrt{t} (hr) ^{0.5}	Pressure, p_{wf} (psig)	$(p_i - p_{wf})$ (psig)	$(p_i - p_{wf})$ (psia)	$\frac{(p_i - p_{wf})}{t}$ (psi/hr)
0.0000	0	4000	0	15	0.00E + 00
0.1500	0.39	3982	18	33	1.20E + 02
0.2000	0.45	3978	22	37	1.10E + 02
0.3000	0.55	3975	25	40	8.33E + 01
0.4000	0.63	3969	31	46	7.75E + 01
0.5000	0.71	3965	35	50	7.00E + 01
0.6000	0.77	3960	40	55	6.67E + 01
0.8000	0.89	3957	43	58	5.38E + 01
1.0000	1.00	3950	50	65	5.00E + 01
1.5000	1.22	3932	68	83	4.53E + 01
2.0000	1.41	3922	78	93	3.90E + 01
3.0000	1.73	3907	93	108	3.10E + 01
4.0000	2.00	3896	104	119	2.60E + 01
5.0000	2.24	3886	114	129	2.28E + 01
6.0000	2.45	3879	121	136	2.02E + 01
8.0000	2.83	3866	134	149	1.68E + 01
10.0000	3.16	3856	144	159	1.44E + 01
15.0000	3.87	3837	163	178	1.09E + 01
20.0000	4.47	3823	177	192	8.85E + 00
30.0000	5.48	3803	197	212	6.57E + 00
40.0000	6.32	3789	211	226	5.28E + 00
50.0000	7.07	3778	222	237	4.44E + 00
60.0000	7.75	3768	232	247	3.87E + 00
80.0000	8.94	3755	245	260	3.06E + 00
100.0000	10.0	3744	256	271	2.56E + 00

straight line as shown. The slope of the semilog straight line is found to be 107 psi/cycle. Thus using Eq. 4–8:

$$k = \frac{162.6q\mu_o\mu_o}{mh} = \frac{162.6 \times 200 \times 0.50 \times 1.288}{107(12)} = 16.31 \text{ mD}$$

From Eq. 8–34:

$$\begin{aligned} x_f^2 &= \left(\frac{4.064q\beta_o}{hm_{vf}} \right)^2 \frac{\mu_o}{\phi c_t k} \\ &= \left(\frac{4.064 \times 200 \times 1.288}{12 \times 107} \right)^2 \frac{0.50}{0.10 \times 20 \times 10^{-6} \times 16.33} = 10,185.12 \end{aligned}$$

Therefore $x_f = 100.9$ ft.

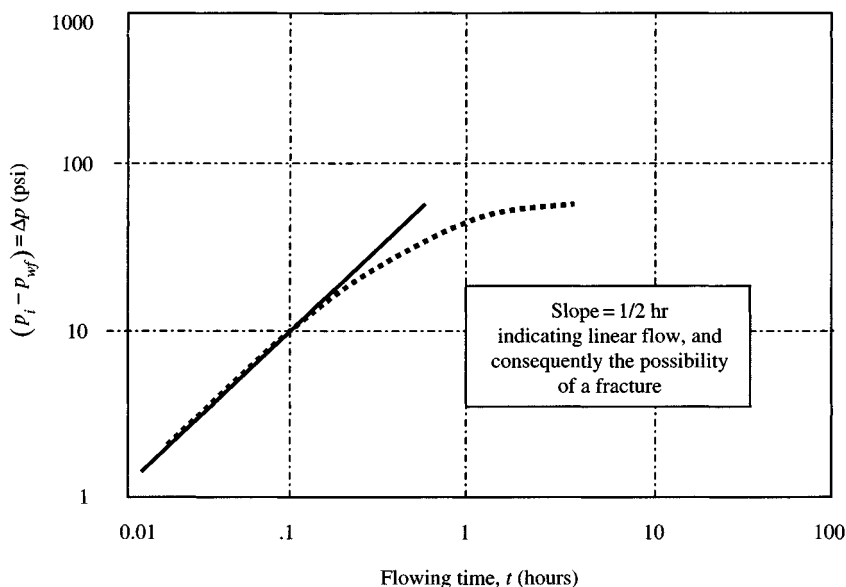


Figure 8-19. log-log data plot.

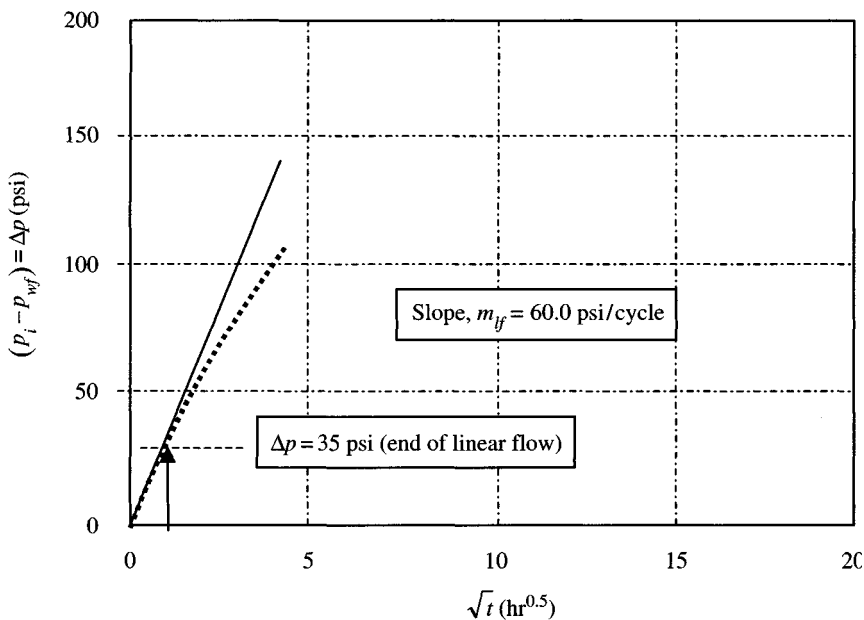


Figure 8-20. Linear data plot.

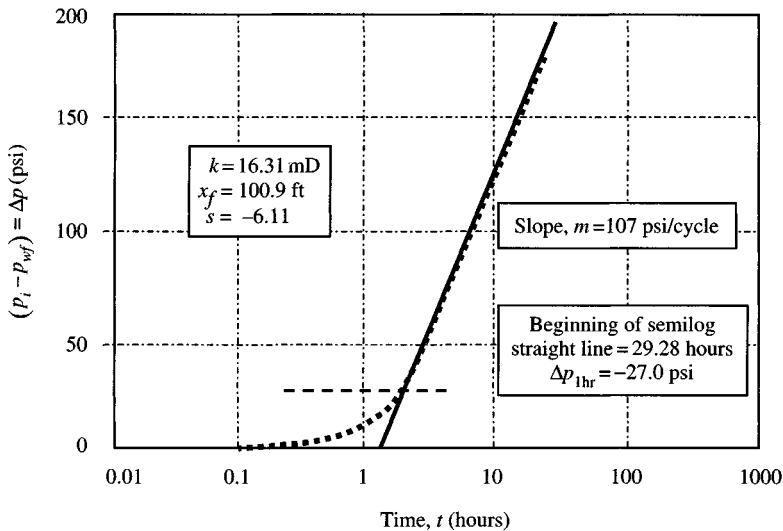


Figure 8-21. Linear data plot.

Note: However, the estimation of x_f is very sensitive to the reservoir parameters. For example, if β_o is taken equal to 1 instead of 1.288, x_f would be equal to 78 ft instead of 100.9 ft. Thus, one has to keep in mind that x_f is correct only if all the reservoir and fluid parameters are correct. In the absence of wellbore storage, it was found that the semilog straight line which indicates radial flow, develops at $t_{Dxf} = 3$, where

$$t_{Dxf} = \frac{0.000264kt}{\phi\mu c_t x_f^2} \quad (8-36)$$

Having calculated h and x_f , we substitute in the above equation, and thus at

$$t = \frac{11,376.6\phi\mu c_t x_f^2}{k} \quad (8-37)$$

$$t = \frac{11,376.6 \times 0.1 \times 0.5 \times 20 \times 10^{-6}}{16.33} = 29.28 \text{ hours} \quad (8-38)$$

where t is the time of the beginning of the semilog straight line, which is 38.06 h. Therefore, the beginning of the semilog straight line must meet the following criteria:

$$\Delta p \geq 70 \text{ psi}, \quad t = 29.28 \text{ hours}$$

Since the straight line in Figure 8-21 satisfies these two criteria, it must be concluded that it is the correct line. To estimate the skin factor s , we determine Δp_{1hr} on the semilog straight line, not from the data table. This is done by

$$\frac{125.0 - 18.0}{\log 10 - \log 1} = 107.0, \quad \Delta p_{1hr} = -27.0 \text{ psi}, \quad p_i - p_{1hr} = \Delta p_{1hr}$$

By substituting in Eq. 4-10, we found that

$$\begin{aligned} s &= 1.151 \left[\frac{p_i - p_{1hr}}{m_{vf}} - \log \left(\frac{k}{\phi \mu c_i r_w^2} \right) + 3.23 \right] \\ &= 1.151 \left[\frac{-27.0}{107.0} - \log \left(\frac{16.31}{0.1(0.5)(20 \times 10^{-6})(0.29)^2} \right) + 3.23 \right] = -6.11 \end{aligned}$$

Note that the analytical procedure, which we followed to determine k and x_f , is based on the assumption that the well was producing in the infinite-acting state. In the event that the semi-steady state has been reached or even approached, the analytical procedure cannot be applied and one must resort to solution presented in the form of type curves.

Type Curve Method of Analysis

Figure 8-17 shows a type curve for an infinite-conductivity vertical fracture with storage. Note that there is an initial unit slope (storage) and then a long transitional period toward the one-half slope fracture line. The matching procedure of actual pressure data and type curves can be carried out as follows:

1. Plot the log of drawdown time versus log of $\Delta p = (p_i - p_{wf})$ on the tracing paper with the same dimensions of the type curves.
2. Check if the initial data form a straight line with a one-half slope. This would indicate a fractured reservoir, since the one-half slope is typical of linear flow.
3. Place the "data curve" over the type curves for fractured reservoirs until the "data curve" matches one type curve. The match determines the approximate start of the semilog straight line and makes an estimate of the formation capacity, half-fracture length, and possible distance to the outer boundary using the following equation:

$$t_{Dxf} = \frac{0.000264kt}{\phi \mu c_i x_f^2} = \frac{0.000264kt}{\phi \mu c_i L^2}$$

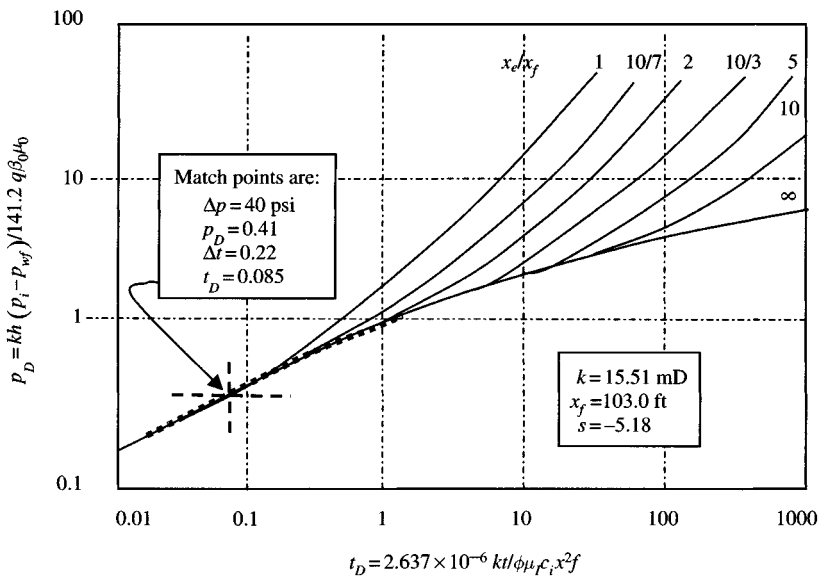


Figure 8–22. Type curve matching for vertical fractured well – infinite fracture conductivity.^{5,6}

Figure 8–19 shows the actual drawdown data plot. The initial data formed a straight line with a half-unit slope. This gave an indication of linear flow and consequently the possible presence of a fracture.

The data curve was placed over the type curve for infinite-conductivity vertical fracture (Figure 8–17 or 8–18) and was displaced until a match was obtained as shown in Figure 8–22.

Estimate the effective reservoir permeability and fracture half-length as follows:

1. Match points are obtained from Figure 8–22. For example, $p_D = 0.41$ at $\Delta p = 40$ psi and $t_D = 0.045$ at $t = 0.44$ hour.
2. Calculate the effective reservoir permeability from Eq. 8–32:

$$k = 141.2 \frac{q\beta_o\mu_o}{h} \left[\frac{p_D}{\Delta p} \right]_M = \frac{141.2(200)(1.288)(0.5)}{12} \times \frac{0.41}{40} = 15.51 \text{ mD}$$

3. Calculate the fracture half-length (or distance that the vertical fracture extends from the center of the well) from Eq. 8–33 as

$$x_f^2 = \sqrt{\frac{0.000264k}{\phi\mu c_i} \times \left(\frac{t}{t_D} \right)_M} = \sqrt{\frac{0.000264(15.51)}{0.1(0.5)(20 \times 10^{-6})} \times \frac{0.22}{0.085}}$$

$$= 10,593 \text{ ft}^2$$

or $x_f = 103$ ft.

Notice that if the match had gone as far as reaching any particular value of x_e/x_f , the distance at the outer reservoir boundary could have been calculated.

4. Estimate the skin factor from Eq. 8-35:

$$s = -\ln\left(\frac{r_e}{r_w}\right)$$

where $r_{wa} = x_f/2 = 103/2 = 51.5$ ft and $s = -\ln(51.5/0.29) = -5.18$.

Pressure Buildup Analysis

The type curve (Figure 8-17 or 8-18) involves the following steps:

1. Plot $(p_{ws} - p_{wf})$ versus Δt_e on a 3×5 cycle log-log paper.
2. Select the best match by sliding the actual test data plot both horizontally and vertically.
3. Note the values of the match points.

$$(p_D)_M, \quad (p_{ws} - p_{wf})_M, \quad \text{and} \quad (t_{DLf})_M(\Delta t)_M$$

4. Estimate the formation permeability from the pressure match point:

$$k = 141.2 \frac{q\mu\beta}{h} \frac{(p_D)_M}{(p_{ws} - p_{wf})_M} \quad (8-39)$$

5. Estimate the fracture length from time match point:

$$x_f = \sqrt{\frac{0.000264k}{\phi\mu c_t} \frac{(t)_M}{(t_{DLx})_M}} \quad (8-40)$$

6. If a half-slope (linear flow) region appears on the test data plot, re-plot data from the region as p_{ws} versus $\sqrt{\Delta t}$; from the slope m_L and linear flow theory,

$$x_f\sqrt{k} = \frac{4.064q\beta}{hm_L} \sqrt{\frac{\mu}{\phi c_t}} \quad (8-41)$$

which should agree with the result from the type curve analysis.

7. If a radial flow region appears before the data deviate from the $x_e/x_f = \text{infinity}$ curve, a plot of p_{ws} versus $\log \Delta t$ or $\log((t_p + \Delta t)/\Delta t)$

should show that $k = 162.6q\mu\beta/mh$, in agreement with type curve analysis.

- If a well proves to be in bounded (finite) acting reservoir, it may be possible to estimate x_e from a matching parameter, x_e/x_f , to compare with known value of x_e to check the quality of the match.

Example 8-7⁸ *Analyzing Pressure Buildup Test for Vertical Fractured Well Using Conventional and Gringarten et al.'s Type Curve Matching Techniques*

Table 8-11 lists the pressure buildup test data for a well believed to be fractured vertically. From the data presented below, estimate the formation

Table 8-11
Pressure Buildup Test Data for Vertical Fracture Oil Well

Time, Δt (hr)	$\frac{(t_p + \Delta t)}{\Delta t}$	Time ^{0.5} (hr ^{0.5})	Pressure, p_{ws} (psig)	$(p_{ws} - p_{ws}(\Delta t=0))$ (psig)	$\frac{p_{ws} - p_{ws}(\Delta t=0)}{\Delta t}$ (psig/hr)	Time, $\sqrt{\Delta t}$ (hr ^{0.5})
0.00	—	—	3420	0	—	—
0.08	93,638.46	0.289	3431	11	1.20E + 02	0.283
0.17	46,707.59	0.409	3435	15	1.10E + 02	0.412
0.25	31,201.00	0.500	3438	18	8.33E + 01	0.500
0.50	15,601.00	0.707	3445	25	7.75E + 01	0.707
0.75	10,401.00	0.866	3449	29	7.00E + 01	0.866
1.00	7801.00	1.000	3452	32	6.67E + 01	1.000
2.00	3901.00	1.414	3463	43	5.38E + 01	1.414
3.00	2601.00	1.732	3471	51	5.00E + 01	1.732
4.00	1951.00	2.000	3477	57	4.53E + 01	2.000
5.00	1561.00	2.236	3482	62	3.90E + 01	2.236
6.00	1301.00	2.449	3486	66	3.10E + 01	2.450
7.00	1115.29	2.646	3490	70	2.60E + 01	2.646
8.00	976.00	2.828	3495	75	2.28E + 01	2.828
9.00	867.67	3.000	3498	78	2.02E + 01	3.000
10.00	781.00	3.162	3500	80	1.68E + 01	3.162
12.00	651.00	3.464	3506	86	1.44E + 01	3.464
24.00	326.00	4.899	3528	108	1.09E + 01	4.900
36.00	217.67	6.000	3544	124	8.85E + 00	6.000
48.00	163.50	6.928	3555	135	6.57E + 00	6.928
60.00	131.00	7.746	3563	143	5.28E + 00	7.746
72.00	109.33	8.485	3570	150	4.44E + 00	8.485
96.00	82.25	9.798	3582	162	3.87E + 00	9.798
120.00	66.00	10.954	3590	170	3.06E + 00	10.955
144.00	55.17	12.000	3600	180	2.56E + 00	12.000
192.00	41.63	13.856	3610	190	0.00E + 00	13.856
240.00	33.50	15.492	3620	200	0.00E + 00	15.492

permeability, fracture length, and skin factor. Producing time t_p was significantly greater than the maximum shut-in time. Well depth = 9500 ft; $q = 419$ stb/day; $h = 82$ ft; $r_w = 0.28$ ft; $\phi = 0.12$ fraction; $\mu = 0.65$ cP; $\beta = 1.260$ rb/stb; $c_t = 21.0 \times 10^{-6}$ psi $^{-1}$; cumulative production at shut-in time = 136,175 stb; and pressure prior to shut-in = 3435 psia.

Solution

$$t_p = \frac{24N_p}{q} = \frac{24 \times 136,175}{419} = 7800 \text{ hours}$$

Figure 8-23 shows the matching procedure and the coordinate of the match point. From the definition of t_d and p_D , which are given in Figure 8-17, and from the coordinates of the match point, it is clear from Figure 8-23 that the well remained in the transient state throughout the 7800 h of production. Estimate the formation permeability k from the pressure match point, using Eq. 8-43:

$$k = \frac{141.2q\beta\mu (p_D)_M}{h (\Delta p)_M} = \frac{141.2(419)(1.260)(0.65) 1.22}{82 \cdot 100} = 7.21 \text{ mD}$$

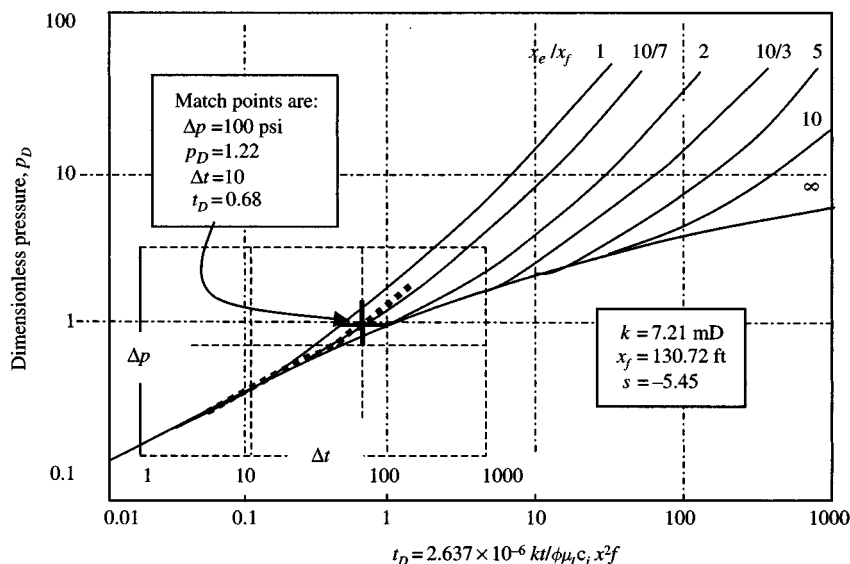


Figure 8-23. Type curve matching for vertical fractured well – infinite fracture conductivity.^{5,6}

Calculate the fracture length from the time match point using Eq. 8-40:

$$x_f = \sqrt{\frac{0.000264k}{\phi\mu c_t} \left[\frac{(\Delta t)_M}{(t_{DLf})_M} \right]} = \sqrt{\frac{0.000264(7.21)}{0.12(0.65)(21.0 \times 10^{-6})} \frac{10}{0.68}} = 130.72 \text{ ft}$$

Apparent radius, $r_{wa} = x_f/2 = 130.72/2 = 65.36$ ft. Estimate the skin factor from Eq. 8-32:

$$s = -\ln\left(\frac{r_{wa}}{r_w}\right) = -\ln\left(\frac{65.36}{0.28}\right) = -5.45$$

Example 8-8^s

Rework Example 8-7 using a plot of Δp versus $\sqrt{\Delta t}$.

Solution The log-log plot is shown in Figure 8-24 and has no unit slope, but has a slope of 1/2 from 5 to 45 min. Thus, we suspect a fractured well. For a formation at a depth of 9500 ft, the fracture should be vertical.⁸ Figure 8-25 is a plot of Δp versus $\sqrt{\Delta t}$, as suggested by Eq. 8-41. The graph has a

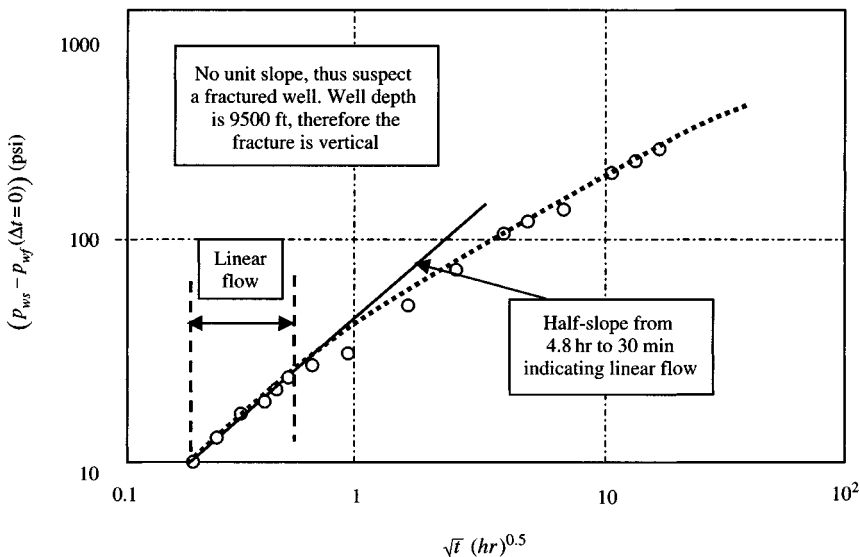


Figure 8-24. log-log data plot to detect fracture.

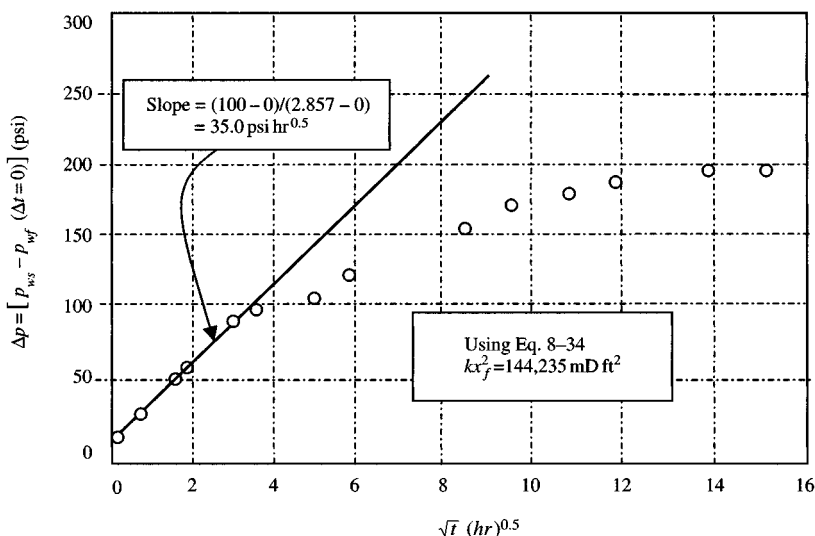


Figure 8-25. Square root data plot.

straight line with $m_{vf} = 31.60 \text{ psi hr}^{0.5}$ up to at least $\Delta p = 55 \text{ psi}$, and Eq. 8-41 can be used to estimate

$$kx_f^2 = \left(\frac{4.064q\beta}{hm_{vf}} \right)^2 \frac{\mu}{\phi c_t} = \left(\frac{4.064(419)(1.260)}{82(35)} \right) \frac{0.65}{0.12(21 \times 10^{-6})} = 144,235 \text{ mD ft}^2$$

According to Eq. 8-40, Δp at the beginning of the semilog straight line should be at least $2 \times 55 = 110 \text{ psi}$. Since the test ended before that Δp , the semilog plot will not be helpful. Thus, we must use type curve matching for further analysis of the test. In Example 8-7, permeability and fracture length by curve matching are:

$$k = 7.21 \text{ mD} \quad \text{and} \quad x_f = 130.72 \text{ ft}$$

Therefore

$$kx_f^2 = (7.21)(130.72)^2 = 123,202 \text{ mD ft}^2$$

compares with $144,235 \text{ mD ft}^2$ computed from Eq. 8-41, that is about 15% difference. If k is assumed to be correct, then

$$131 < x_f < 142 \text{ ft}$$

or if x_f is assumed to be correct, then

$$7.21 < k < 8.5$$

This discrepancy provides an estimate of the accuracy of the type curve matching method.

8.4 Type Curves – Horizontal Fractured Oil Wells

Gringarten and Ramey⁷ developed type curves for a single horizontal fracture located at the center of the productive interval in an infinite-acting system, and they are given in Figure 8–26. No fracture storage or wellbore is included in that figure. Figure 8–26 is a log-log plot of p_D/h_D versus t_{Drf} with parameter h_D . The value of h_D is from 0.05 to 100. The low values of h_D ($h_D < 1$) indicate vertical fractures and high values of h_D ($h_D > 3$) indicate horizontal fractures. Figure 8–26 shows the log-log type curve based on that

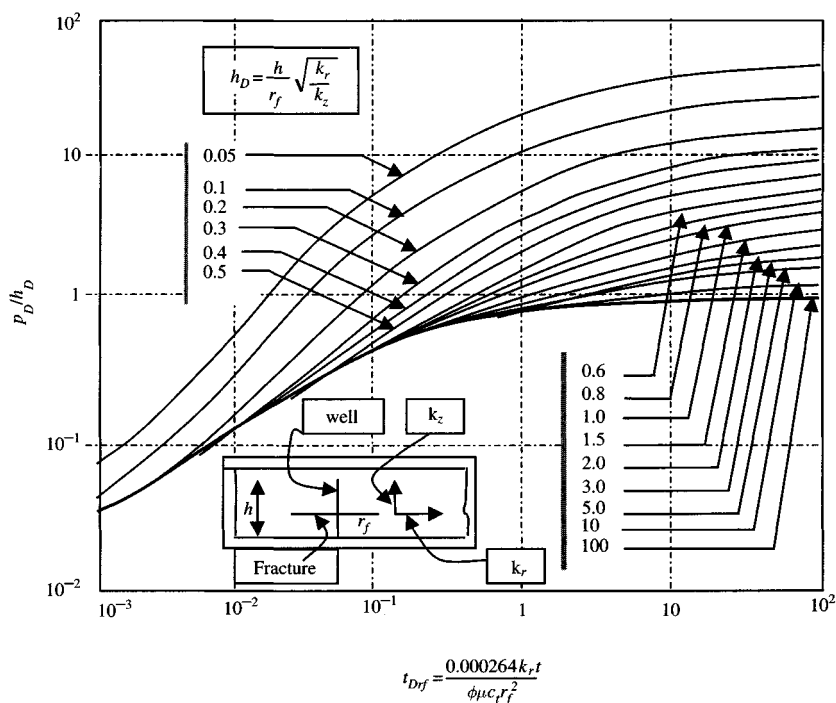


Figure 8–26. Dimensionless pressure versus dimensionless time horizontal fracture (uniform flux).⁷

solution. In this case, the dimensionless pressure p_D is defined as a function of real pressures by the relationship

$$\frac{p_D}{h_D} = \frac{(k_r k_z)^{0.5} r_f \Delta p}{141.2 q \mu \beta} \quad (8-42)$$

and the dimensionless time is defined by

$$t_{Drf} = \frac{0.000 k_f t}{\phi \mu c_i r_f^2} \quad (8-43)$$

where

$$h_D = \frac{h}{r_f} \left(\frac{k_r^{0.5}}{k_z} \right) = \text{dimensionless reservoir thickness} \quad (8-44)$$

k_r = radial formation permeability, mD

r_f = horizontal fracture radius, ft

k_z = vertical formation permeability, mD

q = total withdrawal rate from fracture, stb/day.

At short flow times, there is a period of linear vertical flow from the formation to the horizontal fracture. During those times, the dimensionless pressure is given by⁷

$$p_D = 2 h_D \sqrt{\frac{t_{Drf}}{\pi}} \quad (8-45)$$

where

$$h_D = \frac{h}{r_f} \sqrt{\frac{k_r}{k_z}} \quad (8-46)$$

and

$$t_{Drf} = \frac{0.000 k_r t}{\phi \mu c_i r_f^2} \quad (8-47)$$

During the linear flow period

$$p_{wf} = p_i + m_{Hf} \sqrt{t} \quad (8-48)$$

Eq. 8-43 indicates that a plot of flowing bottom-hole pressure p_{wf} versus \sqrt{t} should have an early-time straight line with intercept p_i and slope

$$m_{Hf} = -\frac{2.587q\beta}{r_f^2} \sqrt{\frac{\mu}{k_z\phi c_t}} \quad (8-49)$$

Eq. 8-42 may be used with superposition to devise a technique for pressure buildup plotting for the linear flow period. If h_D is large, very long flowing or shut-in times would be required to reach the start of the proper straight line (semilog analysis), and the dimensionless pressure is given by

$$p_D = 0.5 \left(\ln t_{Drf} + 1.80907 + \frac{h_D^2}{6} \right) \quad (8-50)$$

Using Pressure Drawdown Data

Eq. 8-46 is used for the drawdown period as well as the shut-in period. Gringarten et al. also indicate how type matching may be used to estimate k_r , k_z , and r_f for a horizontal fractures well. The type curve (Figure 8-26) involves the following steps:

1. Sufficient pressure drawdown or injection data must be available as one of the h_D curves is clearly matched.
2. Estimate $\sqrt{k_r k_z r_f}$ from pressure match point:

$$\sqrt{k_r k_z r_f} = 141.2q\beta\mu \frac{(p_D/h_D)_M}{(\Delta p)_M} \quad (8-51)$$

3. Estimate k_r/r_f^2 from time scale match point:

$$\frac{k_r}{r_f^2} = \frac{\phi\mu c_t}{0.000264} \frac{(t_D)_M}{(t)_M} \quad (8-52)$$

4. Compute the vertical permeability k_z by

$$k_z = \frac{k_r}{r_f^2} \left[\frac{h}{(h_D)_M} \right]^2 \quad (8-53)$$

5. Compute fracture radius by

$$r_f = \left(\frac{-2.587q\beta}{m_{Hf}} \sqrt{\frac{\mu}{k_z\phi c_t}} \right)^{0.5} \quad (8-54)$$

6. Estimate the radial directional permeability by

$$k_r = \left(r_f^2 \right) \frac{\phi \mu c_t}{0.000264} \frac{(t_D)_M}{(t)_M} \quad (8-55)$$

Example 8-9⁸ Analyzing Pressure Drawdown Test for Horizontal Fractured Well Using Gringarten et al.'s Type Curves

Drawdown data are presented in Table 8-12 and fluid properties are: $q = 275$ stb/day; $\mu_o = 0.23$ cP; $\beta_o = 1.760$ rb/stb; $h = 12$ ft; $\phi = 0.30$; and $c_t = 30.0 \times 10^{-6}$ psi⁻¹. Calculate the radial and vertical permeabilities and fracture radius.

Solution A log-log cross plot of $\Delta p = (p_i - p_{wf})$ versus $\log t$ is shown in Figure 8-27. The initial data formed a straight line with a half-unit slope, which indicated a fracture reservoir. The data curve was placed over the type curve for a constant-flux horizontal fracture at the center of interval and was

Table 8-12
Pressure Drawdown Test Data for Horizontal Fractured Oil Well

Time, t (min)	Pressure, p_{wf} (psig)	$(p_i - p_{wf})$ (psig)	$\frac{(p_i - p_{wf})}{t}$ (psig/min)	Time (hr)	\sqrt{t} (hr ^{0.5})
0.0000	4000	0	0.00	—	—
1.0000	3963	37	37.00	0.0167	0.129
5.0000	3918	82	16.40	0.0833	0.289
10.0000	3886	114	11.40	0.1670	0.409
15.0000	3860	140	9.33	0.250	0.500
20.0000	3839	161	8.05	0.333	0.577
25.0000	3819	181	7.24	0.417	0.646
30.0000	3805	195	6.50	0.500	0.707
35.0000	3789	211	6.03	0.583	0.764
40.0000	3778	222	5.55	0.667	0.817
45.0000	3765	235	5.22	0.750	0.866
50.0000	3759	241	4.82	0.833	0.913
60.0000	3740	260	4.33	1.000	1.000
75.0000	3704	295	3.93	1.750	1.118
120.0000	3645	355	2.96	2.000	1.414
150.0000	3610	390	2.60	2.500	1.581
240.0000	3540	460	1.92	4.00	2.000
285.0000	3520	480	1.68	4.75	2.179
480.0000	3440	560	1.17	8.00	2.828
720.0000	3370	630	0.88	12.00	3.464

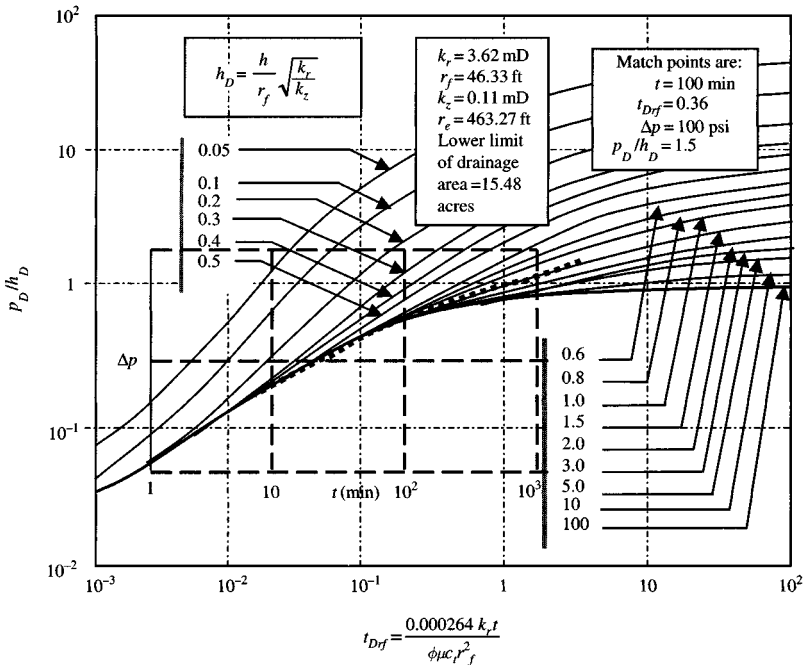


Figure 8-27. Dimensionless pressure versus dimensionless time horizontal fracture (uniform flux).⁷

placed until a match was obtained (Figure 8-28). Estimation of radial and vertical permeabilities and fracture radius can be obtained as follows:

1. Match points are obtained from Figure 8-27: $t_M = 100$ min, $(t_D)_M = 0.36$, $(\Delta p)_M = 100$ psi, and $(p_D/h_D)_M = 0.185$ with $h_D = 1.58$.
2. Estimate $\sqrt{k_r k_z r_f}$ from pressure match point using Eq. 8-51:

$$\begin{aligned} \sqrt{k_r k_z r_f} &= 141.2 q \beta \mu \frac{(p_D/h_D)_M}{(\Delta p)_M} \\ &= 141.2(275)(1.76)(0.23) \times \left(\frac{0.185}{100} \right) = 29.08 \text{ mD ft} \end{aligned}$$

3. Determine k_r/r_f^2 from time match point using Eq. 8-47:

$$\begin{aligned} \frac{k_r}{r_f^2} &= \frac{\phi \mu c_t (t_D)_M}{0.000264 (t)_M} \\ &= \frac{0.30(0.23)(30 \times 10^{-6})}{0.000264} \left(\frac{0.36}{100/60} \right)_M = 0.001693 \end{aligned}$$

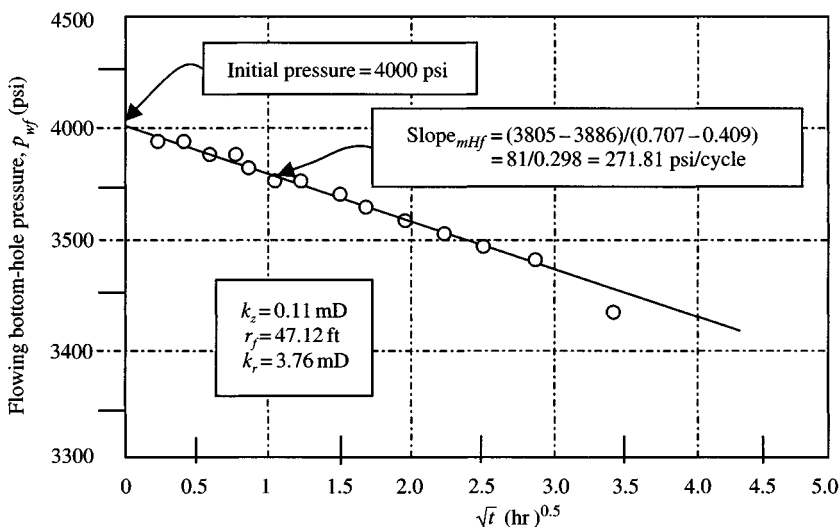


Figure 8-28. Linear plot drawdown test data.

Therefore

$$\frac{\sqrt{k_r}}{r_f} = \sqrt{.001693} = 0.0412 \quad (8-56)$$

4. Eqs. 8-51 and 8-56 provide two relationships for three unknowns. The third relation is provided by the parameter h_D , which is read from the match:

$$h_D = \frac{h}{r_f} \sqrt{\frac{k_r}{k_z}} = 1.5$$

that is

$$\frac{1}{r_f} \sqrt{\frac{k_r}{k_z}} = \frac{h_D}{h} = \frac{1.5}{12} = 0.125 \text{ ft}^{-1} \quad (8-57)$$

5. Calculate the radial permeability k_r by combining Eqs. 8-47 and 8-48 as follows:

$$\sqrt{k_r k_z} r_f \left(\frac{1}{r_f} \sqrt{\frac{k_r}{k_z}} \right) = k_r = (29.08)(0.125) = 3.65 \text{ mD} \quad (8-58)$$

6. Estimate the fracture radius, r_f , by combining Eqs. 8-56 and 8-58 as follows:

$$\frac{\sqrt{k_r}}{r_f} = 0.0412, \quad \text{therefore} \quad r_f = \frac{\sqrt{k_r}}{0.0412} = \frac{\sqrt{3.65}}{0.0412} \quad (8-59)$$

$$= 46.37 \text{ ft}$$

7. Calculate the vertical permeability, k_z , by combining Eqs. 8-46, 8-51, and 8-59 as follows:

$$\sqrt{k_z} = \frac{(\sqrt{k_r k_z} r_f)}{(\sqrt{k_r} r_f)} = \frac{29.08}{\sqrt{3.65}(46.7)} = 0.3273$$

Hence

$$k_z = \sqrt{0.3273} = 0.11 \text{ mD}$$

Interrelated Data Using Gringarten et al. Type Curves

Dimensionless pressure from type curve, $p_D/h_D = 0.185$;

Pressure change from test data, $\Delta p = 100$ psig;

Time match point (dimensionless time), $t_D = 0.36$;

Time match point from test data, $\Delta t = 100$.

Calculated Parameters

$(k_r k_z)^{0.5} r_f = 29.08 \text{ mD ft}$, $k_r^{0.5}/r_f = 0.04 \text{ mD}^{0.5}/\text{ft}$;

$1/r_f (k_r/k_z)^{0.5} = 0.13 \text{ ft}^{-1}$;

Effective horizontal permeability, $k_r = 3.63 \text{ mD}$;

Fracture radius, $r_f = 46.33 \text{ ft}$;

Effective vertical permeability, $k_z = 0.11 \text{ mD}$;

Lower limit of drainage radius, $r_e = 463.27 \text{ ft}$;

Lower limit of drainage area, $A = 15.48 \text{ acres}$.

Example 8-10⁸ Rework Example 8-9 by plotting flowing bottom-hole pressure p_{wf} versus \sqrt{t} .

Solution From Example 8-10, the match points (see Figure 8-28) are: $t_M = 100 \text{ min}$, $(t_D)_M = 0.36$, $(\Delta p)_M = 100 \text{ psi}$, and $(p_D/h_D)_M = 0.185$ with $h_D = 1.5$.

Figure 8-28 is a plot of p_{wf} versus \sqrt{t} on Cartesian coordinates, and the early time data give a straight line with slope equal to 271.81 psi/cycle. Calculate k_z , r_f , and k_r as follows:

- Estimate $\sqrt{k_r k_z} r_f = 141.2 q \mu \beta \frac{[p_D/h_D]_M}{[\Delta p]_M}$ from pressure match point:

$$\sqrt{k_r k_z} r_f = 141.2 \times 225 \times 1.76 \times 0.23 \times \frac{0.185}{100} = 29.08 \text{ mD ft}$$

- Calculate k_r/r_f from time match points:

$$\frac{k_r}{r_f^2} = \frac{\phi \mu c_l}{0.000264} \times \frac{[t_{Drf}]_M}{[t]_M}$$

$$\frac{k_r}{r_f^2} = \frac{0.30 \times 0.23 \times 30 \times 10^{-6}}{0.000264} \times \frac{[0.36]_M}{[100/60]_M} = 0.001694$$

- Compute the vertical permeability k_z by the following equation:

$$k_z = \frac{k_r}{r_f^2} \times \left[\frac{h}{(h_D)_M} \right]^2 = 0.001694 \times \left[\frac{12}{1.5} \right]^2 = 0.11 \text{ mD}$$

- Calculate the fracture radius r_f from Eq. 8-49:

$$\begin{aligned} r_f &= \left(\frac{-2.587 q \beta}{m_{Hf}} \times \sqrt{\frac{\mu}{k_z \phi c_l}} \right)^{0.5} \\ &= \left(\frac{2.587 \times 275 \times 1.76}{271.81} \times \sqrt{\frac{0.23}{0.11 \times 0.30 \times 30 \times 10^{-6}}} \right)^{0.5} \\ &= (4.607 \times 481.999)^{0.5} = 47.12 \text{ ft} \end{aligned}$$

- Determine the radial directional permeability k_r from Eq. 8-52:

$$\begin{aligned} k_r &= r_f^2 \frac{\phi \mu c_l}{0.000264} \frac{(t_{Drf})_M}{(t)_M} \\ &= (47.12)^2 \left(\frac{0.30 \times 0.23 \times 30 \times 10^{-6}}{0.000264} \right) \left(\frac{0.36}{100/60} \right) \\ &= (2220.29)(0.001694) = 3.76 \text{ mD} \end{aligned}$$

Estimation of Upper Limit of Permeability Thickness Product

Last point on the half-slope line may be used to estimate an upper limit of permeability–thickness product. Using this value of permeability,

a corresponding fracture length may be calculated. The appropriate equations⁷ to be used are:

$$\frac{kh\Delta p}{141.2q\beta\mu} = \frac{p_D}{h_D} \leq 0.215 \quad (8-60)$$

and

$$\frac{0.000264kt}{\phi\mu c_t x_f^2} = t_D \leq 0.016 \quad (8-61)$$

where Δp and t are, respectively, the pressure change and time corresponding to the last available point on the half-slope line. Eqs. 8-60 and 8-61 can be used if data beyond the half-slope line are available but are not sufficiently long to perform a type curve match or to use the semilog graph. If the natural fractures are analyzed in this fashion, then the right-hand sides of Eqs. 8-60 and 8-61 should be

$$\frac{kh\Delta p}{141.2q\beta\mu} = \frac{p_D}{h_D} \leq 0.76 \quad (8-62)$$

and

$$\frac{0.000264kt}{\phi\mu c_t x_f^2} = t_D \leq 0.16 \quad (8-63)$$

8.5 Summary

Based on the material presented in this chapter, the following remarks are pertinent:

- A new technique is presented to analyze data in the bilinear flow period. It is shown that, during this flow period, a graph of (p_{wf}) versus $t^{1/4}$ yields a straight line when the slope is inversely proportional to $h_f(k_f b_f)^{1/2}$.
- New type curves are now available for pressure analysis of fractured oil wells and the problem in the analysis is reduced considerably with the use of these type curves.
- Pre-fracture information about the reservoir is necessary to estimate the fracture parameters.
- The type curve analysis method must be used simultaneously with the specific analysis methods (p_{wf}) versus $t^{1/4}$, (p_{wf}) versus $t^{1/2}$, and (p_{wf}) versus $\log t$ to produce reliable results.

References and Additional Reading

1. Agarwal, R. G., Al-Hussainy, R., and Ramey, H.J., Jr., "An Investigation of Wellbore Storage and Skin Effect in Unsteady Liquid Flow. I. Analytical Treatment," *Soc. Pet. Eng. J.* (1970) 10, 279–290.
2. Earlougher, R. C., Jr., and Kersch, K. M., "Analysis of Short-Time Transient Test Data by Type-Curve Matching," *J. Pet. Tech.* (1974) 26, 793–800.
3. McKinley, R. M., "Wellbore Transmissibility from Afterflow-Dominated Pressure Buildup Data," paper SPE 2416, 45th Fall Meeting of AIME, Houston, TX.
4. Raghavan, R., Cady, G. V., and Ramey, H. J., Jr., "Well Test Analysis for Vertically Fractured Wells," *J. Pet. Tech.* (Aug. 1972) 1014–1020; *Trans. AIME*, 246.
5. Gringarten, A. C., Ramey, H. J., Jr., and Raghavan, R., "Pressure Analysis for Fractured Wells," paper SPE 4051 presented at the SPE-AIME 47th Annual Fall Meeting, San Antonio, TX, Oct. 8–11, 1972.
6. Gringarten, A. C., Ramey, H., Jr., and Raghavan, R., "Unsteady-State Pressure Distribution Created by a Well with a Single Infinite-Conductivity Vertical Fracture," *Soc. Pet. Eng. J.* (Aug. 1974) 347–360; *Trans. AIME*, 257.
7. Gringarten, A. C., and Ramey, H., Jr., "Unsteady-State Pressure Distribution Created by a Well with a Single Horizontal Fracture," *Soc. Pet. Eng. J.* (Aug. 1974) 413–426; *Trans. AIME*, 257.
8. Amanat U. C., *Pressure Transient Test Analysis User's Handbook*, Advanced TWPSOM Systems Inc., Houston, TX, Vol. 8, Oct. 1995.

Chapter 9

Flow Regime Identification and Analysis Using Special Methods

9.1 Introduction

Transient behavior of oil well with a finite-conductivity vertical fracture has been simulated by Cinco et al. Usually it is assumed that fractures have an infinite conductivity; however, this assumption is weak in the case of large fractures or very low-capacity fractures. Finite-conductivity vertical fracture in an infinite slab is shown in Figure 9-1. Transient behavior of a well with a finite-conductivity vertical fracture includes several flow periods. Initially, there is a fracture linear flow characterized by a half-slope straight line; after a transition flow period, the system may not exhibit a bilinear flow period, indicated by a one-fourth-slope straight line. As time increases, a formation linear flow period might develop.

Eventually, in all cases, the system reaches a pseudo-radial flow period. Pressure data for each flow period should be analyzed using a specific interpretation method such as

$\Delta\psi$ versus $(t)^{1/4}$ for bilinear flow

$\Delta\psi$ versus $(t)^{1/2}$ for linear flow

and

$\Delta\psi$ versus $\log t$ for pseudo-radial flow

9.2 Fracture Linear Flow Period^{1,4,8}

During this flow period, most of the fluid entering the wellbore comes from the expansion of the system within the fracture and the flow is

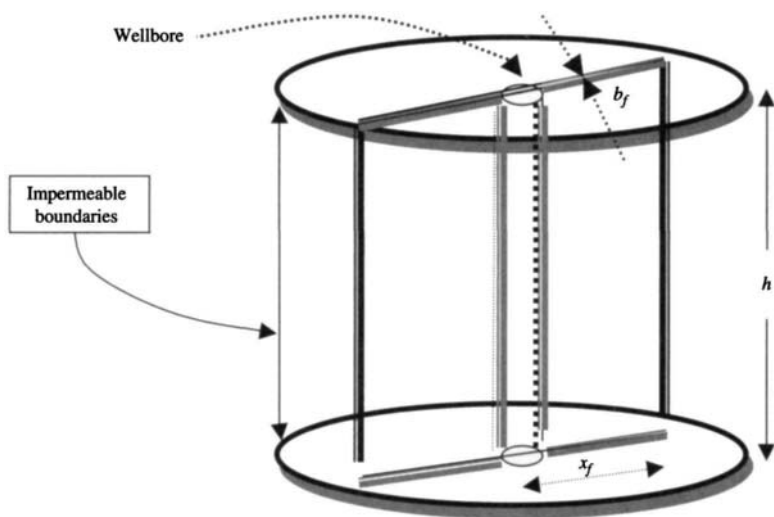


Figure 9-1. Finite-conductivity vertical fracture in an infinite slab reservoir (after Cinco and Samaniego, 1978).²

essentially linear, as shown in Figure 9-2. Pressure response at the wellbore is given by

$$p_{WD} = \frac{3.546}{(k_f b_f)_D} \left[\frac{k_f \phi c_t}{k \phi_f c_{ft}} t_{Dx_f} \right]^{0.5} \quad (9-1)$$

$$p_i - p_{wf} = \frac{0.3918 q \beta}{b_f h} \left(\frac{\mu t}{k_f \phi_f c_{ft}} \right)^{0.5} \quad (9-2)$$

Eq. 9-2 indicates that a log-log graph of pressure difference against the time yields a straight line whose slope is equal to one-half. A graph of pressure versus the square root of time also gives a straight line whose slope depends on the fracture characteristics excluding the fracture half-length, x_f .

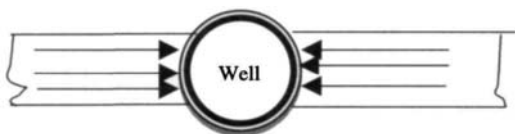


Figure 9-2. Fracture linear flow.¹

The fracture linear flow ends when

$$t_{Dx_f} = \frac{0.01(k_f b_f)_D^2}{\left(\frac{k_f \phi c_t}{k \phi c_{fi}}\right)^2} \quad (9-3)$$

This flow period occurs at a time too early to be of practical use.

9.3 Bilinear Flow^{1,4,8}

It is a new type of flow behavior called bilinear flow because two linear flows occur simultaneously. One flow is linear within the fracture and the other is in the formation, as shown in Figure 9-3. The dimensionless wellbore pressure for the bilinear flow period is given by

$$p_{WD} = \frac{2.45}{[(k_f b_f)_D]^{0.5}} (t_{Dx_f})^{1/4} \quad (9-4)$$

This equation indicates that a graph of p_{WD} versus $(t_{Dx_f})^{1/4}$ produces a straight line whose slope is $2.45/[(k_f b_f)_D]^{0.5}$, intercepting the origin. Figure 9-4 presents that type of graph for different values of $(k_f b_f)_D$. The existence of bilinear flow can be identified from a log-log plot of Δp versus Δt from which the pressure behavior for bilinear flow will exhibit a straight line whose slope is equal to one-fourth to the linear flow period in which the slope is one-half. The duration of this period depends on both dimensionless fracture conductivity, $(k_f b_f)_D$, and wellbore storage coefficients (dimensionless storage capacity), C_{fDf} . For buildup analysis of bilinear flow period, the pressure drop may be expressed as

$$\Delta p = \frac{44.1q\beta\mu}{h(k_f b_f)^{0.5}(\phi\mu c_t k)^{0.25}} (t)^{0.25} \quad (9-5)$$

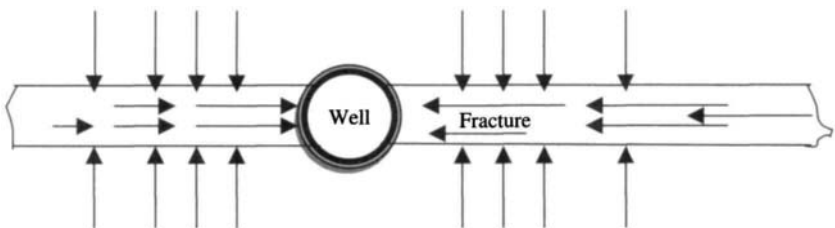


Figure 9-3. Bilinear flow.²

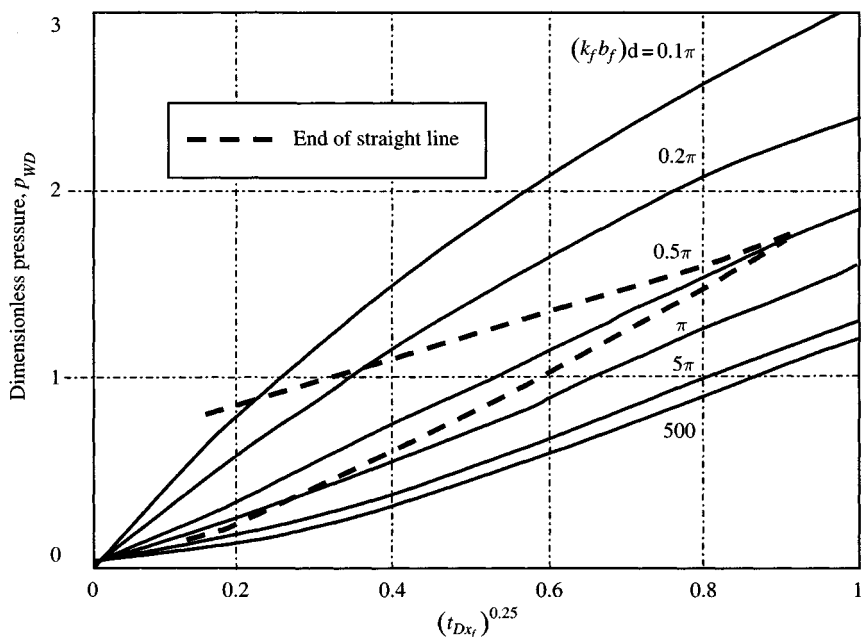


Figure 9-4. p_{WD} versus $[t_{Dx_f}]^{0.25}$ for a well with a finite-conductivity vertical fracture (after Cinco and Samaniego, 1978).²

where Δp is the pressure change for a given test. Eq. 9-5 indicates that a graph of Δp versus $t^{1/4}$ produces a straight line passing through the origin whose slope, m_{bf} , is given by

$$m_{bf} = \frac{44.1q\mu\beta}{h(k_f b_f)^{0.5}(\phi\mu_g c_i k)^{0.25}} \quad (9-6)$$

Hence, the product $h(k_f b_f)^{0.5}$ can be estimated by using the following equation:

$$h(k_f b_f)^{0.5} = \frac{44.1q\mu\beta}{m_{bf}(\phi\mu_g c_i k)^{0.25}} \quad (9-7)$$

Figure 9-5 shows a graph for analysis of pressure data of bilinear flow, while Figure 9-6 is a log-log graph of pressure data for bilinear flow. Figure 9-6 can be used as a diagnostic tool. The above equations indicate that the values of reservoir properties must be known to estimate the group $h(k_f b_f)^{0.5}$. The dimensionless time at the end of bilinear flow period is given by the following equation:

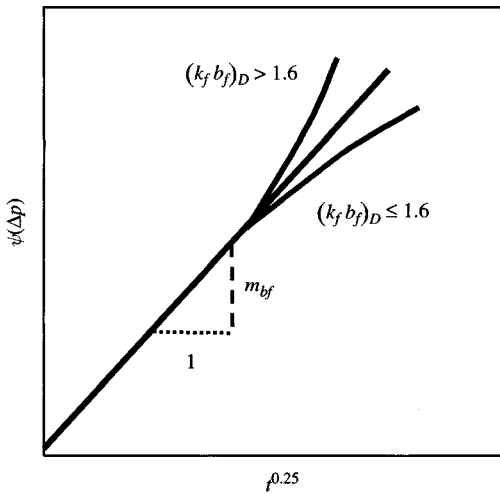


Figure 9-5. Graph for analysis of pressure data of bilinear flow (after Cinco and Samaniego, 1978).²

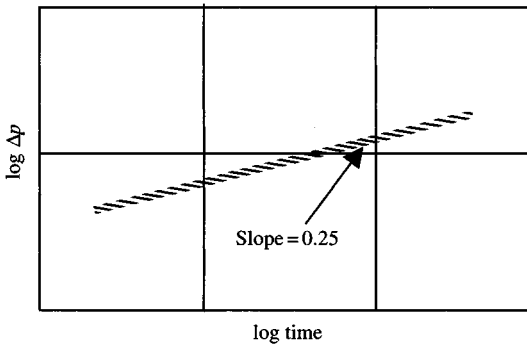


Figure 9-6. log-log graph of pressure data for bilinear flow analysis (after Cinco and Samaniego, 1978).²

For $(k_f b_f)_D \leq 1.6$

$$t_{Defl} = \left[\frac{4.55}{(k_f b_f)^{0.5}} - 2.5 \right]^{-4} \quad (9-8)$$

For $(k_f b_f)_D \geq 3$

$$t_{Defl} \approx \frac{0.10}{(k_f b_f)_D^2} \quad (9-9)$$

For $1.6 \leq (k_f b_f)_D \leq 3$

$$t_{Defb} \approx 0.0205[(k_f b_f)_D - 1.5]^{-1.53} \quad (9-10)$$

Figure 9-7 shows a graphical representation of these equations. From Eqs. 9-5 and 9-8 through 9-10, if $(k_f b_f)_D \geq 3$, the dimensionless pressure drop at the end of the bilinear flow period is given by

$$(p_{WD})_{ebf} = \frac{1.38}{(k_f b_f)_D} \quad (9-11)$$

Hence, the dimensionless fracture conductivity can be estimated using the following equation:

$$(k_f b_f)_D \approx \frac{1.38}{(p_{WD})_{ebf}} \quad (9-12)$$

$(p_{WD})_{ebf}$ can be calculated using the following equation:

$$(p_{WD})_{ebf} \approx \frac{kh(\Delta p)}{141.2q\mu\beta} \quad (9-13)$$

where Δp is obtained from the bilinear flow graph. From Eq. 9-5, a graph of $\log \Delta p$ versus $\log t$ (see Figure 9-6) yields a quarter-slope straight line that can be used as a diagnostic tool for bilinear flow detection.

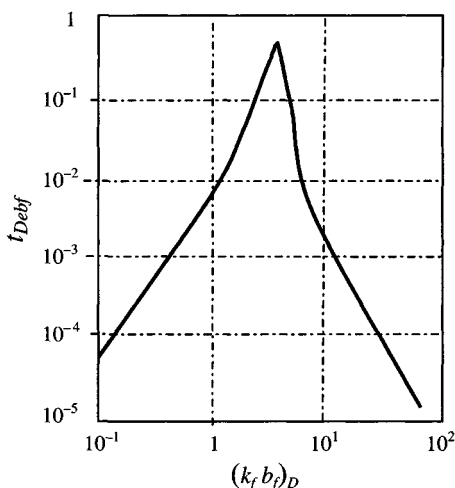


Figure 9-7. Dimensionless time for the end of the bilinear flow period versus dimensionless fracture conductivity.²

9.4 Formation Linear Flow^{1,4,8}

Figure 9–8 represents formation linear flow. Figure 9–9 shows a graph of $\log [p_{wD}(k_f b_f)_D]$ versus $\log [t_{Dxf}(k_f b_f)_D^2]$. For all values of $(k_f b_f)_D$ the behavior of both bilinear flow (quarter-slope) and the formation linear flow (half-slope) is given by a single curve. Note that there is a transition period between bilinear and linear flows. Bilinear flow ends when fracture tip effects are felt at the wellbore.

The beginning of the formation linear flow occurs at $(k_f b_f)_D^2 \approx 10^2$, that is

$$t_{Dbf} = \frac{100}{(k_f b_f)_D^2} \quad (9-14)$$

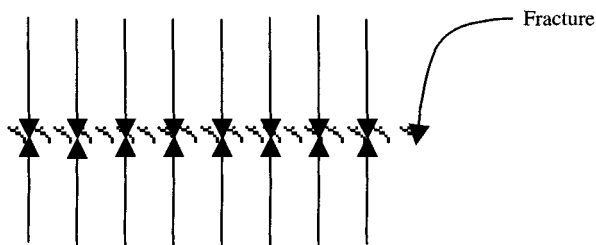


Figure 9–8. Formation linear flow.²

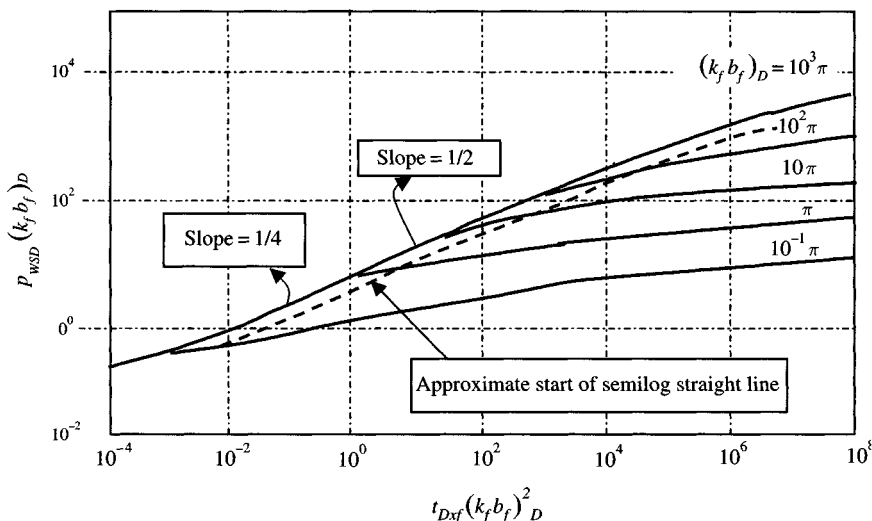


Figure 9–9. Type curve for vertically fractured oil wells (after Cinco and Samaniego, 1978).²

The end of this flow period is given by^{1,8}

$$t_{Delf} \approx 0.016$$

Hence, the fracture conductivity may be estimated as follows:

$$(k_f b_f)_D \approx \frac{10}{(t_{Dblf})^{0.5}} \quad (9-15)$$

or

$$(k_f b_f)_D \approx 1.25 \times 10^{-2} \left(\frac{t_{elf}}{t_{blf}} \right)^{0.5} \quad (9-16)$$

These equations apply when $(k_f b_f)_D \geq 100$.

9.5 Pseudo-Radial Flow^{1,4,8}

Figure 9-10 illustrates pseudo-radial flow. The dashed line in Figure 9-9 indicates the approximate start of the pseudo-radial flow period (semilog straight line).

9.6 Type Curve Matching Methods^{1,7,8}

Figure 9-9 can be used as a type curve to analyze pressure data for a fractured well. Pressure data on a graph of $\log \Delta p$ versus $\log t$ are matched on a type curve to determine

$$[\psi(\Delta p)]_M, \quad [p_{WD}(k_f b_f)_D]_M$$

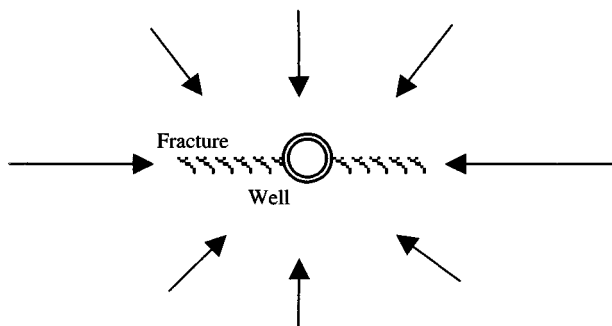


Figure 9-10. Pseudo-radial flow.²

$$(t)_M, \quad [t_{Dx_f}(k_f b_f)_D^2]_M$$

$$[t_{bif}]_M, \quad [t_{bst}]_M$$

Dimensionless fracture conductivity:

$$[(k_f b_f)_D]_M$$

Formation permeability for oil:

$$k = \frac{141.2q\mu\beta [p_{WD}(k_f b_f)_D]_M}{h[(\Delta p)]_M [(k_f b_f)_D]_M} \quad (9-17)$$

Fracture half-length:

$$x_f = \frac{0.000264k(t)_M [(k_{fbf})_D^2]_M}{\phi\mu g c_i [(k_{fbf})_D]_M} \quad (9-18)$$

Fracture conductivity:

$$k_f b_f = k x_f [(k_f b_f)_D]_M \quad (9-19)$$

End of bilinear flow:

$$[t_{ibf}]_M$$

Beginning of formation linear flow:

$$[t_{bif}]_M$$

Beginning of pseudo-radial flow:

$$[t_{bst}]_M$$

Pressure Data Analysis

If large span pressure data are available, the reliable results can be obtained using the specific analysis graphs. Now we will discuss various cases where all the pressure data fall on a very small portion of the type curve and a complete set of information may not be obtained.

Field Case Studies

Case 1: Bilinear Flow Type of Analysis⁴

Pressure data exhibit one-fourth-slope on a log-log graph; and when a log-log graph of pressure data indicates that the entire test data are dominated by bilinear flow (quarter-slope), the minimum value of fracture half-length x_f can be estimated at the end of bilinear flow, i.e., for $(k_f b_f)_D \geq 3$, using the following equation^{1,8}:

$$x_f \geq \left(\frac{0.0002637(k_f b_f)^2 t_{ebf}}{\phi \mu c_i k} \right)^{0.25} \quad (9-20)$$

By definition, the dimensionless fracture conductivity is

$$(k_f b_f)_D = \frac{k_f b_f}{k x_f} \quad (9-21)$$

where $k_f b_f$ is calculated using Eq. 9-25 and slope m_{bf} can be found from bilinear flow graph which is a rectangular graph of pressure difference against the quarter root of time. This graph will form a straight line passing through the origin. Deviations occur after some time depending on the fracture conductivity. The slope of this graph, m_{bf} , is used for the calculation of the fracture permeability-fracture width product $(k_f b_f)$. The dimensionless fracture conductivity is correlated to the dimensionless effective wellbore radius, r'_w/r_f , as shown in Table 9-1. Then, the skin can be calculated from the following relationship:

$$s = -\ln \left(\frac{r_w}{r'_w} \right) \quad (9-22)$$

Generally, wellbore storage affects a test at early time. Thus it is expected to have pressure data distorted by this effect, causing deviation from the one-fourth-slope characteristic of this flow period. It is important to note that pressure behavior in Figure 9-11 for both wellbore storage-dominated and bilinear flow portions is given by a single curve that completely eliminates the uniqueness matching problem. Figure 9-11 is a new type curve and is used when pressure data exhibit one-fourth-slope on a log-log graph. The end of wellbore storage effects occurs when $F_2(t_{Dx_f}) = 2 \times 10^2$, yielding

$$t_{eWS} = 65,415.24 \left[\frac{C^4}{(k_f b_f)^2 h^4 \phi c_i k} \right]^{1/3} \quad (9-23)$$

Table 9-1
The Values of Effective
Wellbore Radius as a Function
of Dimensionless Fracture
Conductivity for a Vertical
Fractured Well²

Dimensionless fracture conductivity, $(k_f b_f)_D$	$\frac{r'_w}{x_f}$
0.1	0.026
0.2	0.050
0.3	0.071
0.4	0.092
0.5	0.115
0.6	0.140
0.7	0.150
0.8	0.165
0.9	0.175
1.0	0.190
2.0	0.290
3.0	0.340
4.0	0.360
5.0	0.380
6.0	0.400
7.0	0.410
8.0	0.420
9.0	0.430
10.0	0.440
20.0	0.450
30.0	0.455
40.0	0.460
50.0	0.465
100.0	0.480
200.0	0.490
300.0	0.500

If Figure 9-11 is used as a type curve, the following information may be obtained:

$$[F_1(p_{WD})]_M, \quad [F_2(t_{Dx_f})]_M, \quad (\Delta p)_M, \quad (t)_M$$

Hence, we can estimate the following:

Wellbore storage constant for oil:

$$C = \frac{0.234q\mu\beta(t)_M [F_1(p_{WD})]_M}{(\Delta p)_M [F_2(t_{Dx_f})]_M} \quad (9-24)$$

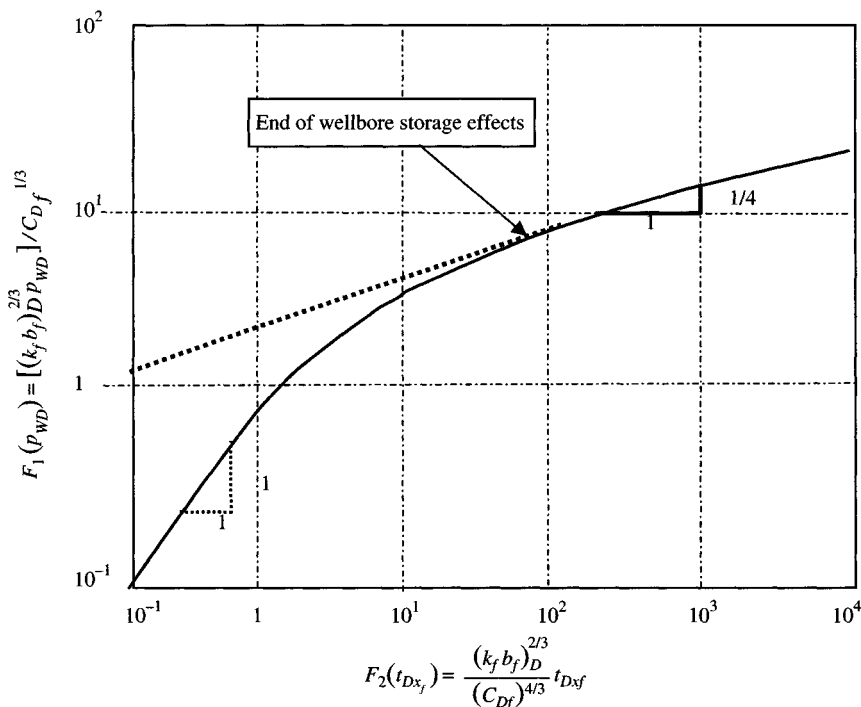


Figure 9-11. Type curve for wellbore storage under bilinear flow conditions (after Cinco and Samaniego, 1978).²

Fracture conductivity for oil:

$$k_f b_f = \frac{0.4}{h^2} \sqrt{\frac{C}{\phi c_i k} \left\{ \frac{141.2 q \mu \beta [F_1(p_{WD})_M]}{(\Delta p)_M} \right\}^3} \quad (9-25)$$

Case 2: Pressure Data Partially Match Curve for the Transition Period Between Bilinear and Linear Flows

Cinco and Samaniego² (1978) have presented a new set of type curves that are given in Figure 9-9. Figure 9-9 shows a graph of $\log [p_{WD}(k_f b_f)_D]$ versus $\log [t_{Dx_f}(k_f b_f)_D^2]$. The main feature of this graph is that for all values of $(k_f b_f)_D$ the behavior of both bilinear flow (quarter-slope) and the formation linear flow (half-slope) is given by a single curve. The type curve match is unique because the transition period has a characteristic

shape. This comment is valid for dimensionless fracture conductivity, $(k_f b_f)_D \geq 5\pi$. From the type curve match of pressure data for this case in Figure 9-9, we obtain

$$[p_{WD}(k_f b_f)_D]_M, \quad [t_{Dx_f}(k_f b_f)_D^2]_M, \quad (\Delta t)_M, \quad \psi(\Delta p)_M, \quad [(k_f b_f)_D]_M$$

Hence, for oil

$$\left(\frac{k_f b_f}{x_f}\right) = \frac{141.2q\mu\beta [p_{WD}(k_f b_f)_D]_M}{h (\Delta p)_M} \quad (9-26)$$

Fracture half-length and fracture conductivity for oil are given by

$$x_f = \left(\frac{k_f b_f}{x_f}\right) \left[\frac{0.0002637 (t)_M}{\phi\mu c_i k [t_{Dx_f}(k_f b_f)_D^2]_M} \right]^{0.5} \quad (9-27)$$

and

$$k_f b_f = (x_f) \left[\frac{k_f b_f}{x_f} \right] \quad (9-28)$$

Since the formation permeability is generally known from prefracture tests, the dimensionless fracture conductivity can be estimated by using the following equation:

$$(k_f b_f)_D = \frac{k_f b_f}{x_f} \frac{1}{k}$$

Then using Table 9-1, find the value of r'_w/x_f ; since x_f is known r'_w can be calculated. Estimate skin factor from Eq. 9-22.

If all pressure data fall on the transition period of the curve, type curve matching (Figure 9-9) is the only analysis method available.

Case 3: Pressure Data Exhibit a Half-Slope Line on a log-log Graph (See Figure 9-12)

There is no unique match with Figure 9-9; however, the linear flow analysis presented by Clark⁴ can be applied to obtain fracture half-length if formation permeability is known. In addition, a minimum value for the dimensionless fracture conductivity, $(k_f b_f)_D$, can be estimated using Eq. 9-29. If the wellbore storage effects are present at early times in a test

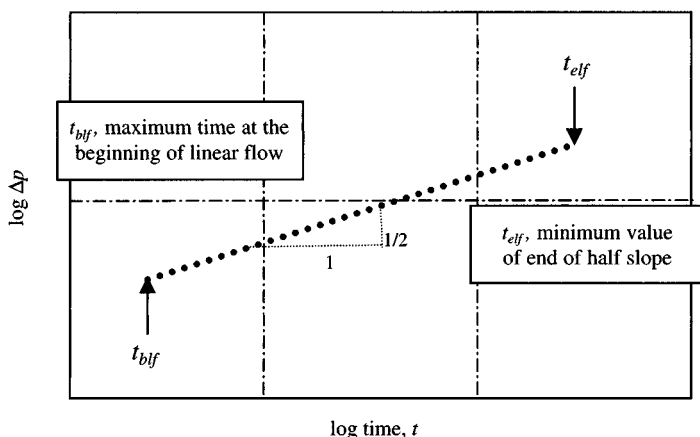


Figure 9-12. Pressure data for a half-slope straight line in a log-log graph (after Cinco and Samaniego, 1978).²

for this case, the analysis can be made using the type curve presented by Ramey and Gringarten.³

$$(k_f b_f)_D = 1.25 \times 10^{-2} \left(\frac{t_{elf}}{t_{blf}} \right)^{0.5} \quad (9-29)$$

Using Table 9-1, find r'_w/x_f ; then using Eq. 9-22, estimate skin factor, s .

Case 4: Pressure Data Partially Falling in the Pseudo-Radial Flow Period⁵

Figure 9-13 is a graph of p_{WD} versus $t_{Dr'_w}$ which is the dimensionless time defined by using r'_w instead of x_f . This curve provides an excellent tool for type curve analysis of pressure data partially falling in the pseudo-radial flow period because the remaining data must follow one of the curves for different fracture conductivities. Table 9-1 must be used to determine $(k_f b_f)_D$ when using Figure 9-13. The type curve in Figure 9-13 involves the following steps:

1. Plot a log-log graph of the pressure data; neither a one-fourth-slope nor a half-slope is exhibited by the data.
2. Apply Figure 9-13 to match pressure data.
3. Estimate reservoir permeability from pressure match point

$$k = \frac{141.2 q \mu \beta (p_{WD})_M}{h (\Delta p)_M} \quad (9-30)$$

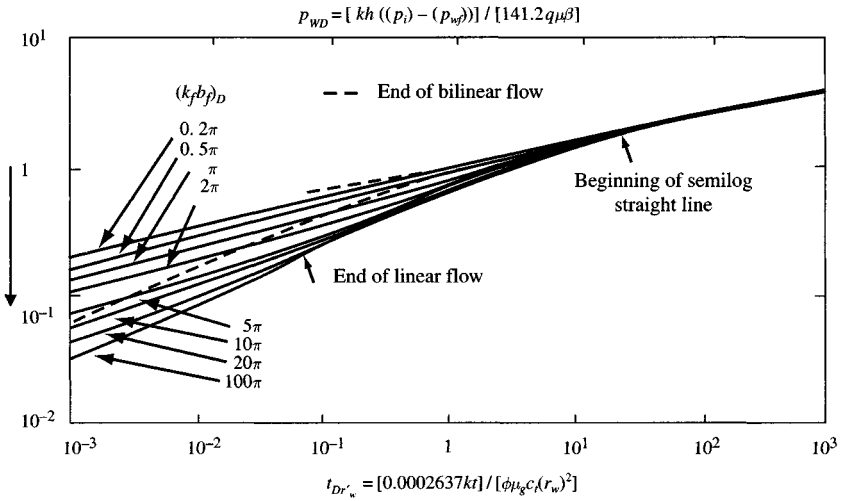


Figure 9-13. Type curve for a finite-conductivity vertical fracture (after Cinco and Samaniego, 1978).²

- Using information from time match estimate effective wellbore radius

$$r'_w = \left[\frac{0.0002637k (\Delta t)_M}{\phi \mu_g c_t (t_{Dr'_w})_M} \right]^{0.5} \quad (9-31)$$

- By using $[(k_f b_f)_D]_M$ in Figure 9-13, obtain $(r'_w/x_f)_{\text{Table 9-1}}$; hence

$$x_f = \frac{r'_w}{\left[\frac{r'_w}{x_f} \right]_{\text{Table 9-1}}} \quad (9-32)$$

- Estimate the skin factor as follows:

$$s = \ln \left(\frac{r_w}{r'_w} \right) \quad (9-33)$$

- Calculate fracture conductivity as follows:

$$k_f b_f = (k_f b_f)_D k x_f \quad (9-34)$$

- The pressure data falling in the pseudo-radial flow period also must be analyzed using semilog methods to estimate k , r'_w , and s .

The following three field examples illustrate the application of several of the methods and theory previously discussed.

Example 9-1⁶ Pressure Data Analysis for Pseudo-Radial Flow

A buildup test was run on this fractured oil well after a flowing time of 1890 hours. Reservoir and test data are as follows: $q_o = 220$ stb/day; $h = 49$ ft; $c_t = 0.000175$ psi⁻¹; $r_w = 0.25$ ft; $p_{wf} = 1704$ psi; $\phi = 0.15$ (fraction); $\mu_o = 0.8$ cP; $c_t = 17.6 \times 10^{-6}$ psi⁻¹. Identify type of flow period and determine the following using type curve matching and semilog analysis techniques, and estimate reservoir parameters.

Solution Figure 9-14 shows a log-log graph of the pressure data; from this graph we can see that neither a one-fourth-slope nor a half-slope is exhibited by the data. Figure 9-14 shows that the pressure data match the curve for $(k_f b_f)_D = 2\pi$ given in Figure 9-13 and the last 14 points fall on the semilog straight line. Match points from Figure 9-14 are given below.

Pressure match points: $(\Delta p)_M = 100$ psi, $(p_{WD})_M = 0.34$

Time match points: $(\Delta t)_M = 1$ hour, $(t_{D'w})_M = 0.19$

$$(p_{WD})_M = 0.45, \quad [t_{D'w}]_M = 1.95$$

From the pressure match using Eq. 9-30, estimate reservoir permeability:

$$k = \frac{141.2 q \mu \beta (p_{WD})_M}{h (\Delta p)_M}$$

$$= \frac{141.2 \times 220 \times 0.8 \times 1.2 \times 0.34}{49 \times 100} = 2.07 \text{ mD}$$

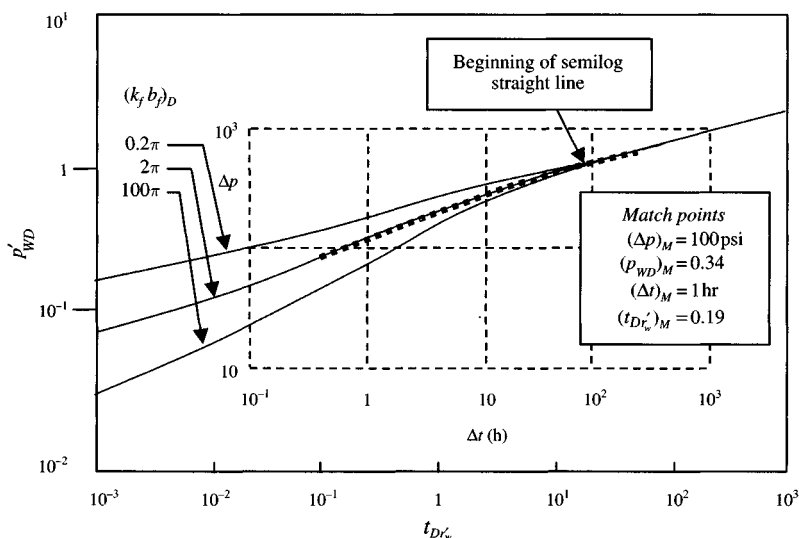


Figure 9-14. Type curve matching for Example 11-2.

Using the information from time match in Eq. 9-31

$$r'_w = \left[\frac{0.0002637k}{\phi\mu_g c_l} \frac{(\Delta t)_M}{(t_{Dr'_w})_M} \right]^{0.5}$$

$$= \left[\frac{0.0002637 \times 2.07}{0.15 \times 0.8 \times 17.6 \times 10^{-6}} \frac{1}{0.19} \right]^{0.5} = 36.9 \text{ ft}$$

From Table 9-1, $r'_w/x_f = 0.403$; hence, $x_f = 36.9/0.403 = 88.9$ ft. The skin factor is estimated by using Eq. 9-33:

$$s_f = \ln \left(\frac{r_w}{r'_w} \right) = \ln \left(\frac{0.25}{36.9} \right) = -4.99$$

From Eq. 9-34, the fracture conductivity is

$$k_f b_f = (k_f b_f)_D k x_f$$

$$= 2\pi \times (2.07)(88.9) = 1156.2 \text{ mD ft}$$

Semilog analysis:

Figure 9-15 is a semilog graph for this example. The correct semilog straight line has a slope $m = 307$ psi/cycle and $(\Delta p)_{1hr} = -47$ psi. The formation permeability can be calculated from Eq. 5-2:

$$k = \frac{162.6q\mu\beta}{mh}$$

$$= \frac{162.6 \times 220 \times 0.8 \times 1.2}{307 \times 49} = 2.28 \text{ mD}$$

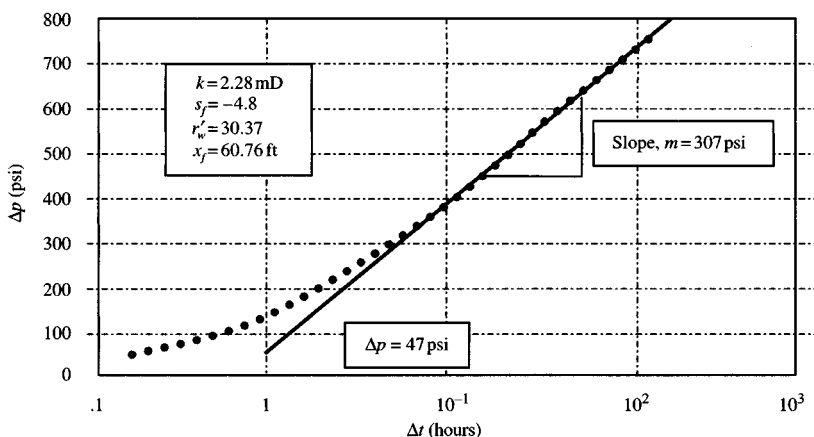


Figure 9-15. Semilog plot.

Table 9-2
Summary of Analysis Results

Analysis results	Type curve matching solution	Semilog solution
Permeability (mD)	2.07	2.28
Fracture skin factor, s_f	-4.99	-4.8
Effective wellbore radius, r'_w (ft)	36.89	30.37
Fracture half-length, x_f (ft)	88.7	60.76
Fracture conductivity (mD ft)	1156	-
$(k_f b_f)_D$	2π	-

Using Eq. 5-3, the fracture skin factor is

$$\begin{aligned}
 s_f &= 1.151 \left[\frac{(\Delta p)_{1hr}}{m} - \log \frac{k}{\phi \mu_o c_t r_w^2} + 3.23 \right] \\
 &= 1.151 \left[\frac{-47}{307} - \log \frac{2.28}{0.15 \times 0.8 \times 17.6 \times 10^{-6} \times 0.25^2} + 3.23 \right] \\
 &= 1.151[-0.227 - 6.92 + 3.23] = -4.8
 \end{aligned}$$

Find the effective wellbore radius by re-arranging Eq. 9-32:

$$r'_w = r_w e^{-s_f} = 0.25 e^{-(-4.8)} = 30.37 \text{ ft}$$

Finally, the fracture half-length is calculated as:

$$\ln(x_f) = \ln(2r_w) - s_f = \ln(2 \times 0.25) - (-4.8) = -0.6931 + 4.8 = 4.11$$

Hence

$$x_f = e^{\ln(x_f)} = e^{4.11} = 60.76 \text{ ft}$$

Summary of analysis results is given in Table 9-2. The results provided by both the type curve analysis and semilog analysis methods are reasonable.

From these examples it is demonstrated that type curve matching analysis, when applied properly, provides an excellent diagnostic tool and a technique to estimate both reservoir and fracture parameters.

9.7 Summary

- Prefracture information about the reservoir is necessary to estimate fracture parameters.
- The type curve analysis methods must be used simultaneously with the specific analysis methods to produce reliable results.

(p_{wf}) versus $t^{1/4}$,
 (p_{wf}) versus $t^{1/2}$, and
 (p_{wf}) versus $\log t$

- It provides new techniques for analyzing pressure transient data for wells intercepted by a finite-conductivity vertical fracture. This method is based on the bilinear flow theory which considers transient linear flow in both fracture and formation. These new type curves overcome the uniqueness problem exhibited by other type curves.

References

1. Cinco, H., Samaniego, F., and Dominguez, N., "Transient Pressure Behavior for a Well with a Finite-Conductivity Vertical Fracture," *Soc. Pet. Eng. J.* (Aug. 1981), 253–264.
2. Cinco, H., and Samaniego, F., "Effect of Wellbore Storage and Damage on the Transient Pressure Behavior for a Well with a Finite-Conductivity Vertical Fracture," *Soc. Pet. Eng. J.* (Aug. 1978), 253–264.
3. Ramey, H. J., Jr., and Gringarten, A. C., "Effect of High-Volume Vertical Fractures in Geothermal Steam Well Behavior," Proc. Second United Nations Symposium on the Use and Development of Geothermal Energy, San Francisco, May 20–29, 1975.
4. Clark, K. K., "Transient Pressure Testing of Fractured Water Injection Wells," *J. Pet. Technol.* (June 1968), 639–643; *Trans. AIME*, 243.
5. Agarwal, R. G., Carter, R. D., and Pollock, C. B., "Evaluation and Prediction of Performance of Low Permeability Gas Wells Stimulated by Massive Hydraulic Fracturing," *J. Pet. Technol.* (March 1979), 362–372.
6. Raghavan, R., and Hadinoto, N., "Analysis of Pressure Data for Fractured Wells: The Constant-Pressure Outer Boundary," *Soc. Pet. Eng. J.* (April 1978), 139–150; *Trans. AIME*, 265.
7. Barker, B. J., and Ramey, H. J., Jr., "Transient Flow to Finite-Conductivity Vertical Fractures," Ph.D. Dissertation, Stanford University, Palo Alto, CA, 1977.
8. Gringarten, A. C., Ramey, H. J. Jr., and Raghavan, R., "Applied Pressure Analysis for Fractured Wells," *J. Pet. Technol.* (July 1975), 887–892; *Trans. AIME*, 259.

Additional Reading

1. Raghavan, R., Cady, G. V., and Ramey, H. J., Jr., "Well Test Analysis for Vertically Fractured Wells," *J. Pet. Technol.* (1972) 24, 1014–1020.

2. Raghavan, R., "Pressure Behavior of Wells Intercepting Fractures," Proc. Invitational Well-Testing Symposium, Berkeley, CA, Oct. 19–21, 1977.
3. Wattenbarger, R. A., and Ramey, H. J., Jr., "*Well Test Interpretations of Vertically Fractured Gas Wells*," *J. Pet. Technol.* (May 1969), 625–632; *Trans. AIME*, 246.

Chapter 10

Application of Pressure Derivative in Oil Well Test Analysis

10.1 Introduction

The pressure derivative application in oil well test analysis involves the combined use of existing type curves in both the conventional dimensionless pressure form (p_D) and the new dimensionless pressure derivative grouping ($p'_D \times t_D/C_D$). Thus, this new approach has combined the most powerful aspects of the two previously distinct methods into a single-stage interpretive plot. Use of the pressure derivative with pressure behavior type curves reduces the uniqueness problem in type curve matching and gives greater confidence in the results. Features that are hardly visible on the Horner plot or that are hard to distinguish because of similarities between a reservoir system and another are easier to recognize on the pressure derivative plot.

10.2 Pressure Derivative Applications in Well Test Analysis

Figure 10–1 illustrates the application of pressure derivative to homogeneous reservoirs, naturally fractured reservoirs, and vertically fractured reservoirs.

10.3 Pressure Derivative Analysis Methods

Bourdet et al.³ developed a new set of type curves (see Figure 10–2) based on the pressure and pressure derivative. In Figure 10–2, at early time, the curves follow a unit-slope log–log straight line. When infinite-acting radial

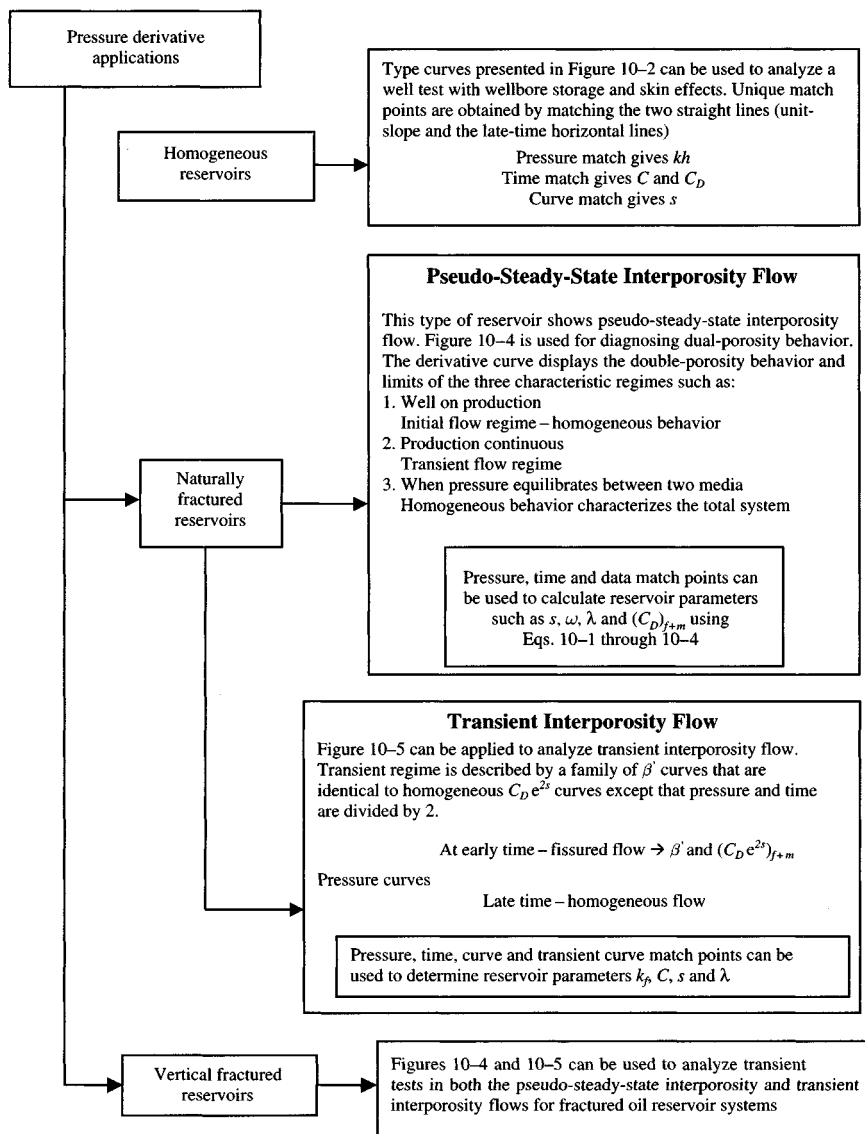


Figure 10-1. Well with wellbore storage and skin in a homogeneous reservoir (© SPE, [J. Pet. Technol. Oct. 1988]).¹

flow is reached at late time, the curves become horizontal at a value of $p'_D(t_D/C_D) = 0.5$. Between these two asymptotes, at intermediate times, each $C_D e^{2s}$ curve produces a specific shape and is different for varying values of

Dimensionless groups are:

$$p'_D = \frac{kh}{141.2q\mu\beta} \Delta p \quad \text{and} \quad \frac{t_D}{C_D} p'_D = \frac{kh}{141.2q\mu\beta} \Delta t \Delta p$$

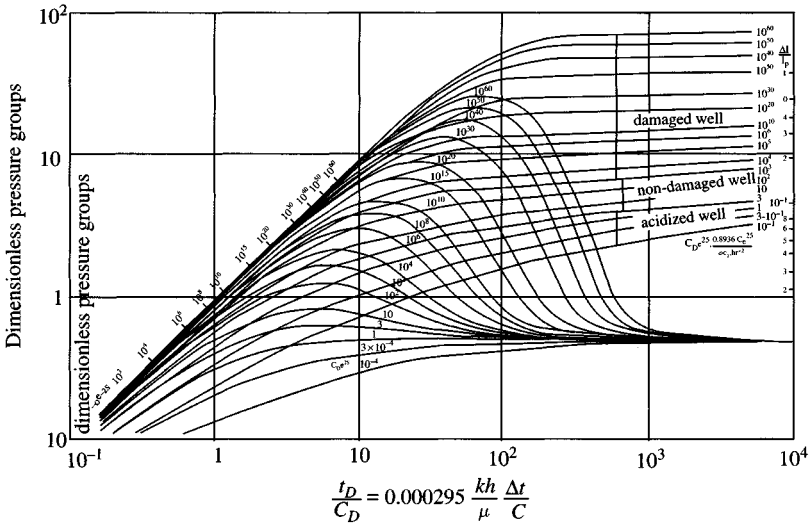


Figure 10-2. Derivative and pressure type curves for a well with wellbore storage and skin in infinite-acting homogeneous reservoir.³

$C_D e^{2s}$. Thus, it is easy and simple to identify the correct $C_D e^{2s}$ curve corresponding to the data. By matching the two straight lines (unit-slope and the late-time horizontal lines) a unique match point is provided. The double plot provides as a check, as the two data set must match on their respective curves. The matching procedures for pressure buildup and draw-down tests are as follows.

Pressure Buildup Test Data Matching Procedure

- Plot Δp versus Δt on 3×5 -cycle log-log paper.
- Calculate the pressure derivative of the field data.
- Plot $\Delta t'(\Delta p')$ versus Δt on same 3×5 -cycle log-log paper.
- Select the best match by sliding the actual test data plot both horizontally and vertically.
- Note the values of the match points:

$$(p_D)_M, \quad (\Delta p)_M, \quad \left(\frac{\Delta t}{t_D/C_D} \right)_M, \quad (C_D e^{2s})_M$$

- Determine the formation permeability, k , from pressure match points:

$$k = \frac{141.2q\mu\beta (p_D)_M}{h (\Delta p)_M} \quad (10-1)$$

- Estimate the wellbore storage, C , from time match point:

$$C = 0.000295 \frac{kh}{\mu} \left(\frac{\Delta t}{t_D/V_D} \right)_M \quad (10-2)$$

- Calculate the dimensionless wellbore storage, C_D , from

$$C_D = 0.8936 \frac{C}{\phi h c_i r_w^2} \quad (10-3)$$

- Estimate the skin factor, s , from curve match point:

$$s = 0.5 \ln \left[\frac{(C_D e^{2s})_M}{C_D} \right] \quad (10-4)$$

Pressure Drawdown Test Data Matching Procedure

- Plot $\Delta p = (p_i - p_{wf})$ versus t on 3×5 -cycle log-log paper.
- Calculate the pressure derivative of the field data.
- Plot $t'(\Delta p')$ versus t on same 3×5 -cycle log-log paper.
- Select the best match by sliding the actual test data plot both horizontally and vertically.
- Note the values of the match points:

$$(p_D)_M, \quad (\Delta p)_M, \quad \left(\frac{t}{t_D/C_D} \right)_M, \quad (C_D e^{2s})_M$$

- Determine the formation permeability, k , from pressure match points:

$$k = \frac{141.2q\mu\beta (p_D)_M}{h (\Delta p)_M} \quad (10-5)$$

- Estimate the wellbore storage, C , from time match point:

$$C = 0.000295 \frac{kh}{\mu} \left(\frac{t}{t_D/V_D} \right)_M \quad (10-6)$$

- Calculate the dimensionless wellbore storage, C_D , from

$$C_D = 0.8936 \frac{C}{\phi h c_t r_w^2} \quad (10-7)$$

- Estimate the skin factor, s , from curve match point:

$$s = 0.5 \ln \left[\frac{(C_D e^{2s})_M}{C_D} \right] \quad (10-8)$$

Example 10-1 *Analyzing Single-Rate Buildup Test Using Pressure Derivative Curves*

A single-rate pressure buildup test was run in an oil well. Table 10-1 shows the pressure-time data. The reservoir and well data are: oil rate, $q_o = 550$ stb/s; $h = 100$ ft; $\mu = 0.95$ cP; $\beta_o = 1.05$ rb/day; $\phi = 0.16$; $c_t = 1.95 \times 10^{-5}$ psi⁻¹; $r_w = 0.29$ ft. Find the reservoir permeability and skin factor. Table 10-1 shows single-rate pressure buildup data.

Solution The points are plotted on tracing paper superimposed on the “homogeneous reservoir” set of curves. Figure 10-3 shows the matching curve. The match points are:

Table 10-1

Δt (hr)	Δp (psi)
0.19	70
0.28	98
0.58	145
0.82	171
1.12	188
2.20	219
4.01	248
6.75	277
10.71	290
14.92	301
20.70	310
29.82	315
40.45	325
60.00	330

Dimensionless groups are:

$$p_D' = \frac{kh}{141.2q\mu\beta} \Delta p \quad \text{and} \quad \frac{t_D}{C_D} p_D' = \frac{kh}{141.2q\mu\beta} \Delta t \Delta p$$

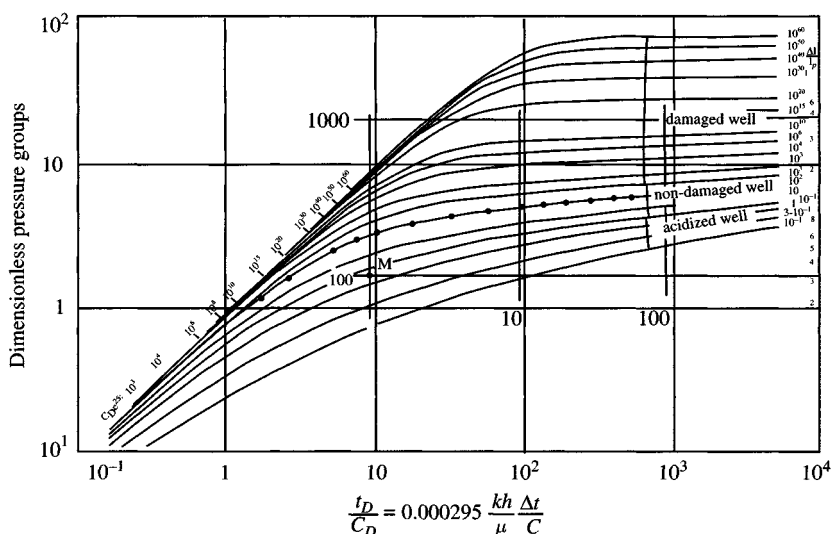


Figure 10-3. Buildup data plotted and matched to pressure derivative type curve of Figure 10-2.

$$(\Delta t)_{MP} = 1.0 \text{ hour}, \quad \left(\frac{t_D}{C_D}\right)_{MP} = 9.5, \quad (\Delta p)_{MP} = 100 \text{ psi}, \quad (p_D)_{MP} = 1.75$$

For the same point, the following are read on the type curve set:

$$\left[\frac{t_D}{C_D}\right] = 8$$

and the designation of the superimposed type curve is noted as

$$C_D e^{2s} = 10^2$$

From the pressure match points, calculate k using Eq. 10-5:

$$k = \frac{141.2q\mu\beta (p_D)_{MP}}{h (\Delta p)_{MP}} = \frac{141.2 \times 550 \times 0.95 \times 1.05}{100} \times \frac{1.75}{100} = 13.56 \text{ mD}$$

From the time match points, find the wellbore storage constant, C , using Eq. 10-6:

$$C = 0.000295 \frac{kh}{\mu} \left(\frac{\Delta t}{t_D/C_D} \right)_{MP} = 0.000295 \times \frac{13.56 \times 100}{0.95} \left[\frac{1.0}{8} \right] \\ = 0.0526 \text{ bbl/psi}$$

Find the dimensionless wellbore constant, C_D , using Eq. 10-7:

$$C_D = 0.8936 \frac{C}{\phi h c_f r_w^2} = 0.8936 \times \frac{0.0526}{0.16 \times 100 \times 1.95 \times 10^{-5} \times (0.29)^2} = 1791$$

Find the skin factor, s , from Eq. 10-8:

$$s = 0.5 \ln \left[\frac{C_D e^{2s}}{C_D} \right] = 0.5 \ln \left[\frac{10^2}{1791} \right] = 0.5(-2.89) = -1.44$$

The above values indicate that the well has been improved.

10.4 Fractured Reservoir Systems

New type curves suitable for practical applications, based on the model by Warren and Root, were introduced by Bourdet et al.^{2,3} These curves are primarily used for diagnosing dual-porosity behavior and for ensuring that an optimum, conclusive test is obtained. The idea behind these curves is that the log-log plot consists of three typical flow regimes as follows:

1. The first flow regime represents radial flow in a homogeneous reservoir with wellbore storage, skin, permeability, k_f , and reservoir storage, S_f .
2. The second flow represents a transient period.
3. The third flow represents radial flow in a homogeneous system with wellbore storage, skin, permeability, k_f , and reservoir storage ($S_f + S_m$).

Pseudo-State Interporosity Flow

Bourdet et al. type curves, as shown in Figure 10-4, can be used for the analysis of fractured reservoirs with pseudo-steady-state interporosity flow. Only two parameters (ω and λ) characterize the reservoir heterogeneity. The parameter ω is defined as the ratio of fracture storage to total storage.

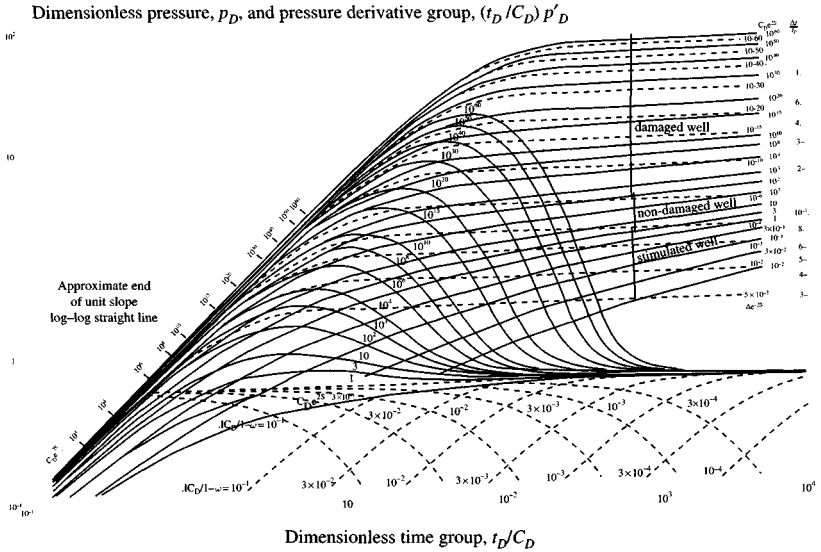


Figure 10-4. Type curve showing the behavior of both the pressure and its derivative (after Bourdet et al., 1984).³ It can be used to analyze test data from fractured reservoirs. The behavior of the pressure derivative is reasonably resolvable for the identification of the transition period.

The interporosity flow parameter λ is proportional to the ratio of matrix permeability to fracture permeability. Thus,

$$\omega = \frac{S_f}{S_f + S_m} \tag{10-9}$$

where

$$S_f = \text{fracture storage} = \phi_f c_f h_f$$

$$S_m = \text{matrix storage} = \phi_m c_m h_m$$

and

$$\lambda \propto \frac{k_m}{k_f}$$

or

$$\lambda = \frac{\alpha r_w^2 k_m}{k_f} \tag{10-10}$$

where α is a shape factor, which is defined as

$$\alpha = \frac{4n(n+2)}{L}$$

n = number of normal set of fractures

L = length of matrix, ft.

In Figure 10-4, the dimensionless pressure (p_D versus t_D/C_D) curves show two families of component curves such as the $C_D e^{2s}$ curves that correspond to homogeneous behavior and the λe^{2s} curves that show pressure behavior during transition. The pressure derivative curve response follows this sequence:

- Initially, due to wellbore storage effects, the derivative curve follows $(C_D e^{2s})_f = 1$ type curve.
- When the infinite-acting radial flow occurs in the fissured system, the pressure derivative group will follow the 0.5 horizontal straight lines.
- During the transition period, when pressure stabilizes, the derivative with respect to natural logarithm of time drops and follows the $\lambda C_D / \omega(1 - \omega)$ type curve until it reaches a minimum and then bounces back up along the $\lambda C_D / (1 - \omega)^2$ curve before returning to the 0.5 straight line. The 0.5 horizontal lines correspond to the infinite-acting radial flow in the total system $(C_D e^{2s})_{f+m}$.

To use the type curve in Figure 10-4, one has to match the early data with one of the type curves labeled $C_D e^{2s}$. The label of the matched curve is now referred to as $(C_D e^{2s})_f$. The permeability, k_f , is calculated from the pressure match and C is calculated from the time match. The matching procedure is as follows:

- Plot pressure derivative versus Δt on log-log graph paper.
- Plot Δp_{ws} versus Δt on log-log paper.
- Match the derivative curve with one of the derivative type curves of Figure 10-4.
- Choose any point and read its coordinates on both figures. Thus,

$$(\Delta p)_M, \quad (\Delta t)_M, \quad (p_D)_M, \quad \left(\frac{t_D}{C_D} \right)_M$$

would become known. Also, read the matched derivative curve labeled $\lambda C_D / (1 - \omega)^2$; here C_D is $C_{D_{f+m}}$.

- Now, with the match still maintained, change your focus from the derivative curve to the data curve. Read the values of the curves labeled $C_D e^{2s}$, which match initial and final segments of the data curves, $(C_D e^{2s})_f$ and $(C_D e^{2s})_{f+m}$, respectively.

- Calculate the different parameters as follows:

$$\omega = \frac{(C_D e^{2s})_{f+m}}{(C_D e^{2s})_f} \quad (10-11)$$

$$k_f = \frac{50,300 q_g TP_{sc}}{h T_{sc}} \frac{(p_D)_M}{\psi(\Delta p)_M} \quad (\text{mD ft}) \quad (10-12)$$

$$C = \frac{0.000295 kh (\Delta t)_M}{\mu_g \left(\frac{t_D}{C_D} \right)_M} \quad (10-13)$$

$$C_{D_{f+m}} = \frac{0.8936 C}{\phi c_i h r_w^2} \quad (10-14)$$

Assuming that the total reservoir storage ($S_f + S_m$) is known from well logs,

$$s = 0.5 \ln \left[\frac{(C_D e^{2s})_{f+m}}{C_{D_{f+m}}} \right] \quad (10-15)$$

and λ can be calculated from the label of the matched derivative curve $\lambda C_{D_{f+m}} / (1 - \omega)^2$:

$$\lambda = \frac{(1 - \omega)^2}{C_{D_{f+m}}} \left[\frac{\lambda C_{D_{f+m}}}{(1 - \omega)^2} \right]_M \quad (10-16)$$

Transient Interporosity Flow

Bourdet et al. type curves, as shown in Figure 10-5, can be used for the analysis of fractured reservoir with transient interporosity flow.³ The transient period is described by a family of β' curves that are identical to homogeneous $C_D e^{2s}$ curves except that pressure and time are divided by 2. In the transient interporosity flow period, the double-porosity responses do not flatten out but tend to develop a semilog straight line, the slope of which is half of the true radial flow slope. The dimensionless interporosity transient flow parameter β' is defined by the following equation:

$$\beta' = \frac{\delta' (C_D e^{2s})_{f+m}}{\lambda e^{-2s}} \quad (10-17)$$

the curve match and Eq. 10-18. The parameter λ is calculated from the transition curve match and the following equation:

$$\lambda = \delta' \frac{(C_D e^{2s})_{f+m}}{\beta'} \frac{1}{e^{2s}} \quad (10-18)$$

10.5 Pressure Derivative Trends for Other Common Flow Regimes

Figure 10-6 shows pressure derivative trends for common flow regimes.

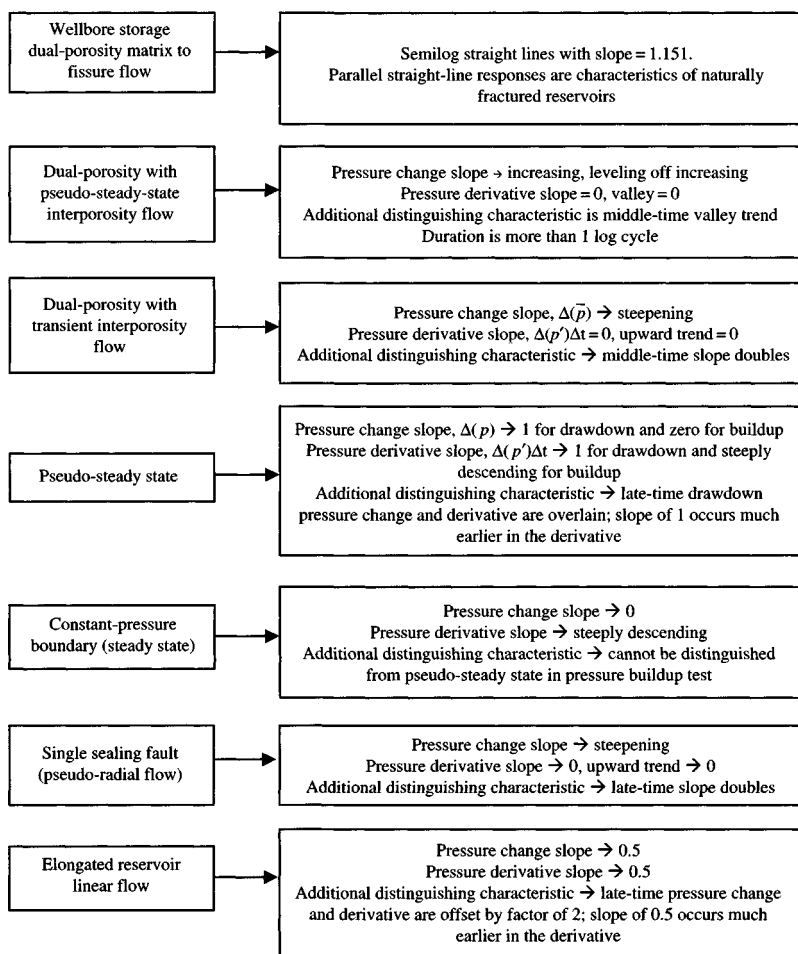


Figure 10-6. Illustration of pressure derivative trends for other common flow regimes.

10.6 Summary

- A new technique is presented to analyze data in the bilinear flow period. It is shown that, during this flow period, a graph of p_{wf} versus $t^{1/4}$ yields a straight line when slope is inversely proportional to $h_f(k_f b_f)^{1/2}$.
- New type curves are now available for pressure analysis of fractured oil wells, and the problem in the analysis is reduced considerably with the use of these type curves.
- Prefracture information about the reservoir is necessary to estimate fracture parameters.
- The type curve analysis method must be used simultaneously with the specific analysis methods p_{wf} versus $t^{1/4}$, p_{wf} versus $t^{1/2}$, and p_{wf} versus $\log t$ to produce reliable results.

References

1. Economides, C. E., "Use of the Pressure Derivative for Diagnosing Pressure-Transient Behavior," *J. Pet. Technol.* (Oct. 1988), 1280–1282.
2. Bourdet, D., Whittle, T. M., Douglas, A. A., and Pirard, Y. M., "A New Set of Type Curves Simplifies Well Test Analysis," *World Oil* (May 1983).
3. Bourdet, D., Alagoa, A., Ayoub, J. A., and Pirard, Y. M., "New Type Curves Aid Analysis of Fissured Zone Well Tests," *World Oil* (April 1984).

Additional Reading

1. Bourdet, D., Ayoub, J. A., Whittle, T. M., Pirard, Y. M., and Kniazeff, Y., "Interpreting Well Tests in Fractured Reservoirs," *World Oil* (Oct. 1983).

Chapter 11

Massive Hydraulic-Fractured Oil Well Behavior Analysis

11.1 Introduction

Agarwall et al.¹ and Cinco-Ley and Samaniego² presented a new set of type curves. These type curves were specifically needed for massive hydraulic-fractured (MHF) wells to handle production under constant pressure and constant rate. A fracture is said to have an infinite flow capacity when there is little or no pressure drop along the axis of the fracture. The fracture is said to have a finite flow capacity when there is a significant pressure drop along its axis. Since the distinction between the definitions of fracture flow capacity and formation flow capacity is often confusing, it may be worthwhile to restate the definition of the formation flow capacity.

$$\text{Formation flow capacity} = kh \quad (\text{mD-ft}) \quad (11-1)$$

$$\text{Fracture flow capacity} = k_f w \quad (\text{mD-ft}) \quad (11-2)$$

11.2 Methods of Evaluating MHF Oil Wells

Figure 11-1 illustrates the methods of analyzing MHF wells.

11.3 Analyzing Infinite Flow Capacity Fractures

In a fractured well, where fracture flow capacity is high and wellbore storage and damage effects are minimum, early-time flow should be linear, and early-time pressure data plotted as a function of $\sqrt{\text{time}}$ should fall on a

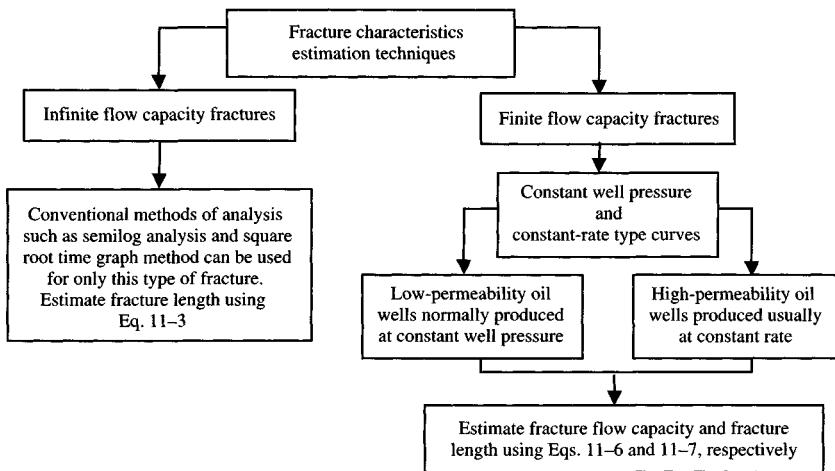


Figure 11-1. Methods of evaluating MHF oil wells.

straight line. The slope of this straight line can be used to determine the fracture length by the following equation:^{6,7}

$$x_f = \frac{4.064q\beta}{m_f h} \sqrt{\frac{\mu}{k\phi c_t}} \quad (11-3)$$

When using the fracture length equation, the formation permeability k can be estimated from a semilog plot of late-time post-fracturing buildup data. The type curve analysis methods described in Chapter 8 can also be used for infinite flow capacity fractures.

11.4 Analyzing Finite Flow Capacity Fractures

Constant Wellbore Pressure Case

Figure 11-2 presents the constant wellbore pressure type curves for finite flow capacity fractures. These type curves are especially useful when analyzing performance data (production rate versus time) for MHF oil wells that generally are produced at a constant wellbore pressure rather than a constant rate. The reciprocal of the dimensionless rate, $1/q_D$, was plotted as a function of dimensionless time, t_{Dxf} , on log-log paper with dimensionless fracture flow capacity, F_{CD} , as a parameter. Definitions of $1/q_D$, t_{Dxf} , and F_{CD} are defined as follows.

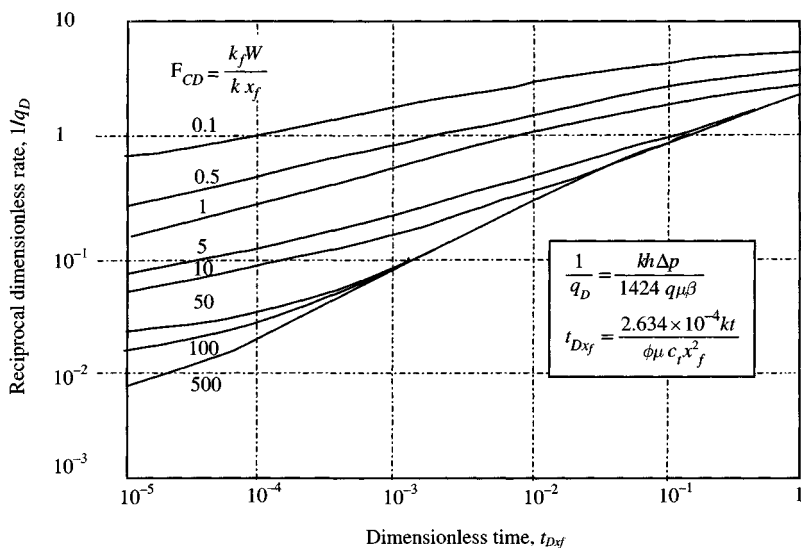


Figure 11-2. Constant-pressure log-log type curves for finite-capacity vertical fractures (after Agarwall et al., Jan. 1979).¹

Dimensionless rate, $1/q_D$:

$$\frac{1}{q_D} = \frac{kh[p_i - p_{wf}]kh}{141.2q\mu\beta} \quad (11-4)$$

Dimensionless time, t_{Dxf} :

$$t_{Dxf} = \frac{0.0002637kt}{\phi\mu_i c_i x_f^2} \quad (11-5)$$

Dimensionless flow capacity, F_{CD} :

$$F_{CD} = \frac{k_f w}{k x_f} \quad (11-6)$$

Fracture half length, x_f :

$$x_f = \sqrt{\frac{0.0002637k(t)_M}{\phi\mu_i c_i (t_{DXF})_M}} \quad (11-7)$$

Fracture skin, s_f :

$$s_f = \left[s_f + \ln\left(\frac{x_f}{r_w}\right) \right]_{\text{Table 11-1}} - \ln\left(\frac{x_f}{r_w}\right) \quad (11-8)$$

Constant-Rate Case

Figure 11-3 presents the constant-rate type curves for finite flow capacity fractures. Dimensionless pressure drop p_{wD} has been plotted as a function of dimensionless time t_{Dxf} on log-log paper with the dimensionless fracture flow capacity F_{CD} as a parameter. Dimensionless variables shown in Figure 11-3 are defined as follows.

Dimensionless pressure, p_{wD} :

$$p_{wD} = \frac{kh[p_i - p_{wf}]}{141.2q\mu\beta} \quad (11-9)$$

Dimensionless time, t_{Dxf} :

$$t_{Dxf} = \frac{0.0002637kt}{\phi\mu_i c_i x_f^2} \quad (11-10)$$

Dimensionless flow capacity, F_{CD} , here is defined as

$$F_{CD} = \frac{k_f w}{k x_f} \quad (11-11)$$

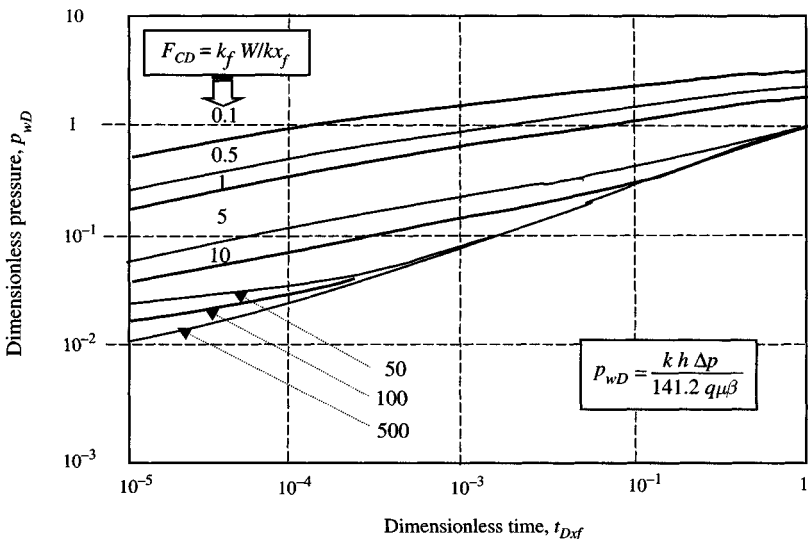


Figure 11-3. log-log type curve for finite-capacity vertical fractures (constant well rate) (after Cinco-Ley and Samaniego, 1981).⁴

This definition of the dimensionless fracture flow capacity is slightly different from that used by earlier investigators, but appears more convenient.

Definition in terms of Prats et al. (1962):

$$\alpha = \frac{\pi}{2F_{CD}} \quad (11-12)$$

Definition in terms of Gringarten et al.⁵

$$c_r = \frac{F_{CD}}{\pi} \quad (11-13)$$

Fracture conductivity:

$$k_f W = F_{CD}(k x_f) \quad (11-14)$$

Fracture half-length, x_f :

$$x_f = \sqrt{\frac{0.0002637k(t)_M}{\phi\mu_i c_i(t_{Dxf})_M}} \quad (11-15)$$

Fracture skin, s_f :

$$s_f = \ln\left(\frac{x_f}{r_w}\right) \quad (11-16)$$

The value of fracture skin s_f may be calculated using Eq. 11-17 or from Table 11-1:

$$s_f = \left[s_f + \ln\left(\frac{x_f}{r_w}\right) \right]_{\text{Table 11-1}} - \ln\left(\frac{x_f}{r_w}\right) \quad (11-17)$$

The dimensionless fracture flow capacity F_{CD} ranges from 0.2 to 100 (Figure 11-3). Note that the higher values of F_{CD} normally correspond to higher fracture flow capacity. However, higher values of F_{CD} may also be caused by lower formation permeability or short fracture length. The infinite flow capacity fracture solution is shown by the dotted line in Figure 11-3. A curve for F_{CD} values of 100 or greater should represent an infinite flow capacity fracture approximately. This accounts for the utility of the infinite flow capacity type curves of Gringarten et al. for the analysis of wells stimulated with conventional fractures. For greater values of t_{Dxf} , Cinco-Ley et al. type curves may be used. For t_{Dxf} values smaller than 10^{-5} , type curves are influenced by porosity and compressibility in the fracture.

Table 11-1
Pseudo-Skin Factor for a Well with a
Finite-Conductivity Vertical Fracture²

$k_{fD}W_{fD} = \frac{k_f W}{k x_f}$	$S_f \ln(x_f/r_w)$
0.1	3.00
0.2	2.10
0.3	2.40
0.4	2.20
0.5	2.00
0.6	1.90
0.7	1.85
0.8	1.75
0.9	1.73
1.0	1.60
2	1.20
3	1.10
4	1.00
5	0.94
6	0.90
7	0.85
8	0.88
9	0.84
10	0.82
20	0.800
30	0.790
40	0.770
50	0.785
60	0.778
70	0.777
80	0.776
90	0.775
100	0.774
200	0.772
300	0.772
400	0.772
500	0.772
600	0.772
700	0.772
800	0.772
900	0.772
1000	0.772

11.5 Estimating Formation Characteristics of Finite Conductivity Fractures

Agarwall et al.¹ and Cinco-Ley and Samaniego⁴ have provided log-log type curve to analyze finite conductivity vertical fracture, which is a plot of dimensionless pressure p_D versus dimensionless time t_D with c_r as a parameter (Figure 11-4). An interesting finding was that for a well with a low- or an intermediate-conductivity fracture, the slope at early times did not exhibit the typical one-half slope straight line. The following key assumptions were used in developing these curves:

- A homogeneous isotropic horizontal infinite reservoir of constant thickness, h , permeability, k , and porosity, ϕ , which are independent of pressure.
- Viscosity and compressibility are constant. Production comes from a vertical fractured well intersected by a fully penetrating finite-conductivity fracture of width, w , half-fracture length, r_f , and permeability, k_f .

Quantitative reservoir evaluation is carried out with the use of p_D and t_D as mentioned earlier, and a new parameter called dimensionless fractured conductivity c_r is introduced as

$$c_r = \frac{wk_f}{\pi x_x k} \quad (11-18)$$

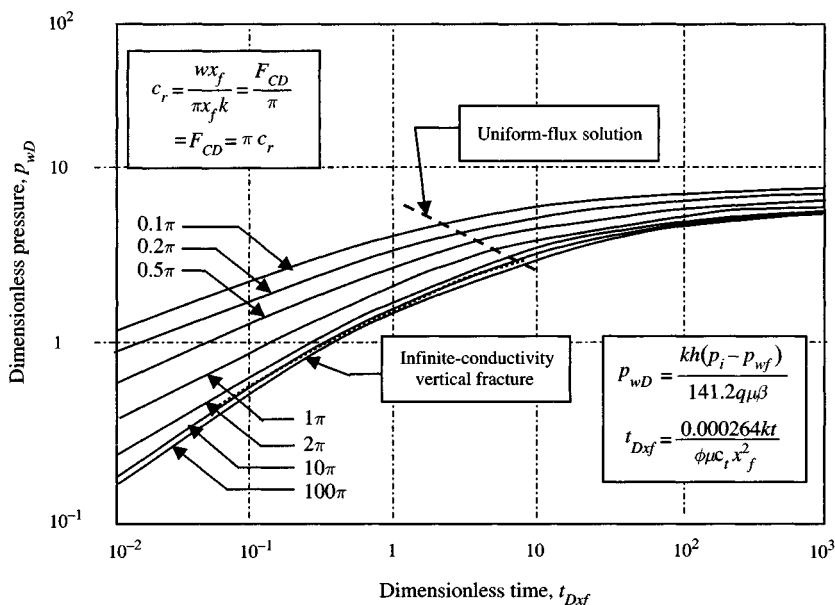


Figure 11-4. Constant-rate type curves for finite flow capacity vertical fracture.^{1,2}

or

$$c_r = C_{fD}\eta_{fD} \quad (11-19)$$

where

C_{fD} = dimensionless fracture storage capacity

η_{fD} = dimensionless fracture hydraulic diffusivity

The product of the following two dimensionless variables can also express the dimensionless fracture flow conductivity:

$$k_{fD} = \frac{k_f}{k} \quad (11-20)$$

$$w_{fD} = \frac{w}{x_f} \quad (11-21)$$

where

k_{fD} = dimensionless fracture permeability

w_{fD} = dimensionless fracture width

Combining Eqs. 11-19 through 11-21 leads to the relationship

$$k_{fD}w_{fD} = C_{fD}\eta_{fD}\pi = \frac{k_f w}{k x_f} \quad (11-22)$$

Eq. 11-22 can be useful to analyze the pressure behavior in wells with a finite-conductivity vertical fracture. Table 11-1 can be used to correlate the fracture skin factor (or pseudo-skin effect) from which it is possible to evaluate s_f as a function of $w_{fD}k_{fD}$ and x_x/r_w .

Curve Matching Procedures

- Prepare a log-log plot of Δp versus time on a sheet of tracing paper, where Δp is the incremental pressure (psi) that is equal to $p_i - p_{wf}$ (for drawdown test) and $p_{ws} - p_{wf}$ (for buildup test), and time = t in a drawdown test and time = Δt in buildup test.
- Note the slope for early-time data.
- Place the data curve over the type curve for a finite-conductivity vertical fracture and displace until a match was obtained.
- Record the values of match point $(p_D)_M$, $(\Delta p)_M$, $(t_{fD})_M$, $(t)_M$, and value of parameter c_r .
- Estimate the formation permeability k from pressure match point:

$$k = \frac{141.2q\mu\beta}{h} \left(\frac{p_D}{\Delta p} \right)_M \quad (\text{mD}) \quad (11-23)$$

- Calculate the half-fracture length from time match point:

$$x_f = \sqrt{\frac{0.000264k}{\phi\mu c_t} \left(\frac{t}{t_{Df}}\right)_M} \quad (\text{ft}) \quad (11-24)$$

- Calculate the fracture conductivity:

$$k_f w = k x_f [k_{fD} w_{fD}]_{\text{Figure 11-4}} \quad (\text{mD-ft}) \quad (11-25)$$

- Determine the fracture skin factor with the use of Table 11-1:

$$s_f = \left[s_f + \ln\left(\frac{x_f}{r_w}\right) \right]_{\text{Table 11-1}} - \ln\left(\frac{x_f}{r_w}\right) \quad (11-26)$$

Example 11-1 *Analyzing Pressure Drawdown Test Using Cinco et al. Type Curves for Finite-Conductivity Vertical Fracture*

The reservoir and drawdown data are given below and are presented in Table 11-2.

$\phi = 0.25$; $h = 25$ ft; $r_w = 0.29$ ft; $q = 275$ stb/day; $c_t = 19.5 \times 10^{-6}$ psi⁻¹; $p_i = 2850$ psi; $\mu = 0.75$ cP; and $\beta = 1.550$ rb/stb. Estimate k , x_f , $k_f w$, and s_f .

Table 11-2
Pressure Drawdown Test Data

Time, t (hr)	Pressure, p_{wf} (psi)	$\Delta p = (p_i - p_{wf})$ (psi)
0.30	2791	59
0.55	2780	70
1.05	2768	80
2.55	2742	108
5.50	2728	136
10.0	2714	170
20.0	2680	215
30.0	2635	240
40	2610	265
50	2585	282
60	2568	300
70	2550	315
80	2545	330
90	2520	337
100	2518	350
155	2558	392

Solution To analyze this test, follow these steps: A log-log cross-plot of $(p_i - p_{wf})$ versus time was prepared on a sheet of tracing paper (Figure 11-5). Notice that at early times the slope is smaller than 0.5. The data curve was placed over the type curve for a finite-conductivity vertical fracture (Figure 11-6).

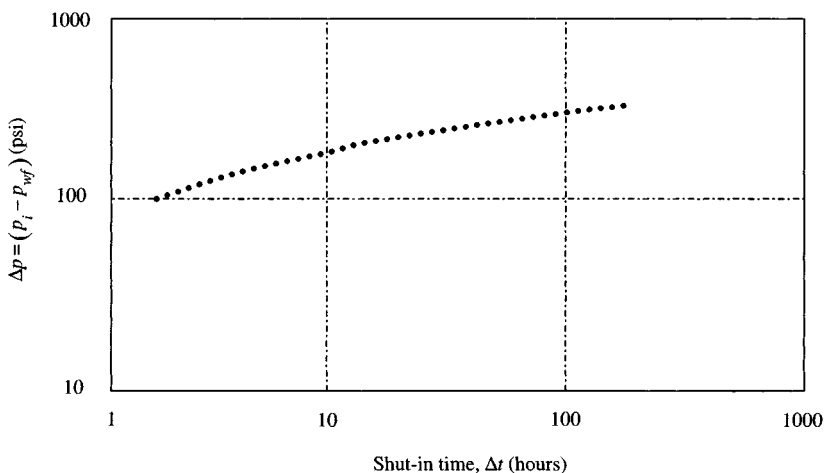


Figure 11-5. log-log data plot.

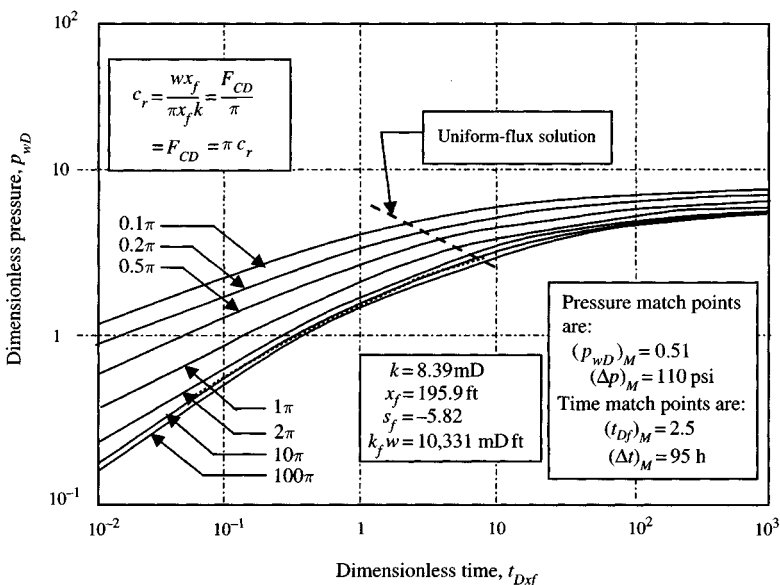


Figure 11-6. Constant-rate type curves for finite flow capacity vertical fracture.²

This match was obtained, and the pressure and time match points are
 $(p_{wD})_M = 0.51$ psi, $(\Delta p)_M = 110$ psi, $(t_{Df})_M = 2.5$ hours, $(\Delta t)_M = 95$ hours

Estimate the formation permeability k from Eq. 11-23:

$$k = \frac{141.2q\mu\beta (p_{wD})_M}{h (\Delta p)_M} = \frac{141.2(275)(0.75)(1.55)}{25} \times \frac{0.51}{110} = 8.39 \text{ mD}$$

Determine the half-fracture length x_f from Eq. 11-24:

$$x_f = \sqrt{\frac{0.000264k}{\phi\mu c_i} \left(\frac{t}{t_{Df}}\right)_M} = \sqrt{\frac{0.000264(8.39)}{0.25(0.75)(19.5 \times 10^{-6})} \times \frac{95}{1.5}} = 195.9 \text{ ft}$$

Calculate the fracture conductivity using Eq. 11-25:

$$[k_{fD}w_{fD}]_{\text{Figure 11-4}} = \frac{k_f w}{k x_f}$$

$$\begin{aligned} k_f w &= k x_f [k_{fD}w_{fD}]_{\text{Figure 11-4}} \\ &= 8.39 \times 295.9 \times 2\pi = 8432.67 \text{ mD ft} \end{aligned}$$

Estimate the fracture skin factor using Eq. 11-26:

$$\begin{aligned} s_f &= \left[s_f + \ln\left(\frac{x_f}{r_w}\right) \right]_{\text{Table 11-1}} - \ln\left(\frac{x_f}{r_w}\right) \\ &= 0.89 - \ln\left(\frac{195.9}{0.29}\right) = -5.63 \end{aligned}$$

This skin factor indicates that the fracture is large enough to provide an improvement in well productivity in spite of the fact that the dimensionless fracture conductivity has an intermediate value.

Conventional Method of Analysis

Pressure drawdown test is long enough to reach and pass the dashed line representing the approximate start of the semilog straight line. This compares very favorably with the semilog graph in Figure 11-7, which shows a straight line through the last points with a slope $m = 285$ psi/cycle.

- Calculate the conventional formation permeability k from Eq. 11-28:

$$k = \frac{162.6q\mu\beta}{mh} = \frac{162.6(275)(0.75)(1.55)}{255(25)} = 8.15 \text{ mD}$$

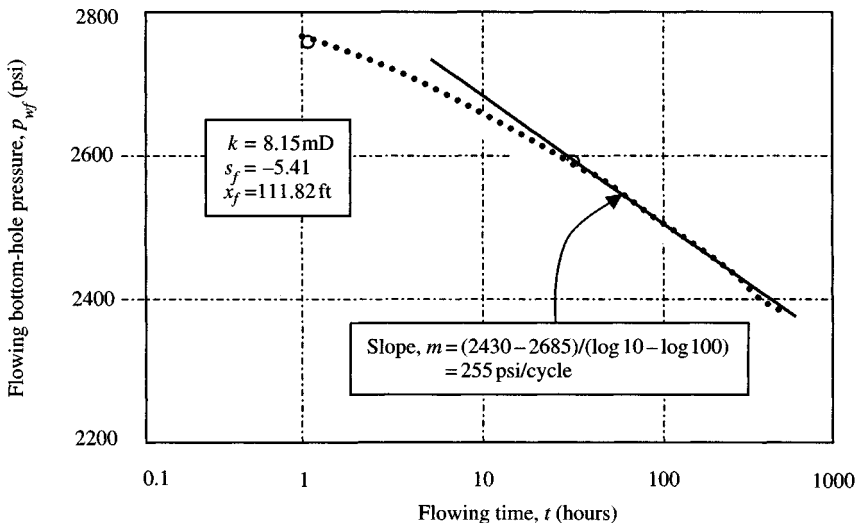


Figure 11-7. Semilog data plot.

which compares with 8.39 mD calculated by type curve matching technique.

- Calculate the skin fracture from Eq. 11-29:

$$\begin{aligned}
 s_f &= 1.151 \left[\frac{p_{1hr} - p_i}{m} - \log \left(\frac{k}{\phi \mu c_t r_w^2} \right) + 3.23 \right] \\
 &= 1.151 \left[\frac{2810 - 2850}{255} - \log \left(\frac{8.15}{0.15(0.75)(19.5 \times 10^{-6})(0.25)^2} \right) + 3.23 \right] \\
 &= -5.41
 \end{aligned}$$

which compares with 6.63 calculated by type curve matching technique. This skin factor indicates that the fracture is large enough to provide an improvement in well productivity in spite of the fact that the dimensionless fracture conductivity has an intermediate value.

- Estimate the fracture half-length x_f from the following equation:

$$x_f = 2r_w e^{-S_f} = 2 \times 0.25 e^{-(-5.41)} = 111.82 \text{ ft} \quad (11-27)$$

The $x_f = 2r_w e^{-S_f}$ can rarely be used in practice. Because this equation applies only for infinite-conductivity fractures, the fracture half-length can be underestimated from finite-conductivity fractures using this approach.

11.6 Pretreatment Testing of Hydraulically Fractured Candidate

This section presents the theoretical and practical aspects of methods used to determine the formation permeability, fracture length, and fracture conductivity in low-permeability, hydraulically fractured oil reservoirs.

Horner Analysis

Plot buildup test data on a conventional Horner graph, determine the slope m , and thus estimate the formation permeability k from equation

$$k = \frac{162.6q_o\beta_o\mu_o}{mh} \quad (\text{mD}) \quad (11-28)$$

and fracture skin factor s_f from equation

$$s_f = 1.151 \left[\frac{(p)_{1h} - (p_{wf})}{m} - \log \left(\frac{k}{\phi\mu_g c_t r_w^2} \right) + 3.23 \right] \quad (11-29)$$

Calculate the fracture half-length from equation

$$x_f = 2r_w e^{-s_f} \quad (11-30)$$

Linear Flow Analysis – High-Conductivity Fractures

When linear flow into a fracture dominates (at earliest times), a plot of Δp versus a square-root-of-time function will result in a straight line with slope m_{lf} related to the fracture half-length and formation permeability:

$$x_f = \frac{4.064q_o\beta_o}{m_{lf}h} \left(\frac{\mu_o}{k\phi c_t} \right)^{0.5} \quad (11-31)$$

or

$$kx_f^2 = \left(\frac{4.064q_o\beta_o}{m_{lf}h} \right)^2 \left(\frac{\mu_o}{\phi c_t} \right) \quad (11-32)$$

Calculate the fracture skin factor, s_f ,

$$s_f = \ln \left(\frac{2r_w}{x_f} \right) \quad (11-33)$$

Eq. 11–33 limits its applicability in many cases. These limiting assumptions include the following:

- Formation permeability k must be available, if we wish to estimate x_f .
- High fracture conductivity (but not infinite) and F_{CD} are greater than 100.
- Earliest time data is dominated by linear flow and no wellbore storage distortion.

Type Curve Analysis

Several type curves^{4–6,8} have potential application to analysis of transient tests in low-permeability fracture oil reservoirs. Particularly important are Cinco et al.'s^{2–4} curves and Agarwal et al.'s¹ curves for finite-conductivity fracture. These type curves have been discussed in Chapter 8.

Bilinear Flow Analysis – Low-Conductivity Fractures

In the case of the bilinear flow regime, a Cartesian graph of Δp versus $t^{1/4}$ would yield a straight line. From the slope, the fracture permeability width $k_f w$ product may then be calculated using

$$k_f w = \left(\frac{44.1 q_o \beta_o \mu_o}{m_{bl} h} \right)^2 \left(\frac{1}{k \phi \mu_o c_t} \right)^{0.5} \quad (11-34)$$

or

$$k (k_f w)^2 = \left(\frac{44.1 q_o \beta_o \mu_o}{m_{bl} h} \right)^4 \left(\frac{1}{\phi \mu_o c_t} \right) \quad (11-35)$$

Note that the reservoir permeability k is calculated from semilogarithmic graph.

11.7 Summary

Based on the material presented in this chapter, the following remarks are pertinent:

- New type curves are now available for pressure analysis of MHF oil wells and the problem in the analysis is reduced considerably with the use of these type curves.
- Prefracture information about the reservoir is necessary to estimate the fracture parameters.
- The type curve analysis method must be used simultaneously with the specific analysis methods to produce reliable results.

- This chapter also reviews the advances in oil well stimulation techniques such as MHF. It is a proven technique for developing commercial wells in low-permeability or “tight” oil formations. Limitations of conventional analysis methods and alternative techniques for determining fracture length and fracture flow capacity on MHF wells are presented. This chapter also discusses how to analyze past performance and forecast future performance of tight oil wells stimulated by MHF using finite fracture flow capacity type curves. The limitations of conventional pressure transient analysis and other methods of evaluating MHF treatment are discussed. A set of constant well rate and wellbore pressure type curves are also presented.

References

1. Agarwall, R. G., Carter, R. D., and Pollock, C. B., “Evaluation and Prediction of Performance of Low-Permeability Gas Wells Stimulated by Massive Hydraulic Fracturing,” *J. Pet. Tech.* (March 1979), 362–372; *Trans. AIME*, 267.
2. Cinco-Ley, H., and Samaniego, F., “Transient Pressure Analysis for Finite Conductivity Fracture Case versus Damage Fracture Case,” SPE Paper 10179, 1981b.
3. Cinco, H., and Samaniego, F., “Effect of Wellbore Storage and Damage on the Transient Pressure Behavior for a Well with a Finite-Conductivity Vertical Fracture,” *Soc. Pet. Eng. J.* (Aug. 1978), 253–264.
4. Cinco-Ley, H., and Samaniego, F., “Transient Pressure Analysis for Fractured Wells,” *JPT*, (Sept. 1981a), pp. 1749–1766.
5. Gringarten, A. C., Ramey, H. J., Jr., and Raghavan, R., “Applied Pressure Analysis for Fractured Wells,” *J. Pet. Tech.*, (1975) 17, 887–892.
6. Prats, M., Hazebrock, P., and Strickler, W. R., “Effect of Vertical Fractures on Reservoir Behavior – Incompressible Fluid Case,” *Soc. pet. J.* (June 1962), 87–94.
7. Earlougher, R. C., Jr., *Advances in Well Test Analysis*, Monograph Series No. 5, Society of Petroleum Engineers of AIME, Dallas, TX, 1977, p. 151.
8. Russell, D. G., and Truitt, N. E., “Transient Pressure Behavior in Vertically Fractured Reservoirs,” *Soc. Pet. Eng.*, August 1964.

Additional Reading

1. Economides, M. J., “Observations and Recommendations in the Evaluation of Tests of Hydraulically Fractured Wells,” SPE Paper 16396, 1987.
2. Aguilera, R., “Well Test Analysis of Naturally Fractured Reservoirs,” *SPEFEJ* (Sept. 1987), pp. 239–252.
3. Russell, D. G., and Truitt, N. E., “Transient Pressure Behavior in Vertically Fractured Reservoirs,” *Soc. Pet. Eng.*, August 1964.

Chapter 12

Drill-Stem Testing Methods

12.1 Introduction

Drill-stem testing provides a method of temporarily completing a well to determine the productive characteristics of a specific zone. As originally conceived, a drill-stem test provided primarily an indication of formation content. The pressure chart was available, but served mainly to evaluate tool operation. Currently, analysis of pressure data in a properly planned and executed DST can provide, at reasonable cost, good data to help evaluate the productivity of the zone, the completion practices, the extent of formation damage and perhaps the need for stimulation. A drill-stem test provides an estimate of formation properties and wellbore damage. These data may be used to determine the well's flow potential with a regular completion that uses stimulation techniques to remove damage and increase effective wellbore size.

Reservoir characteristics that may be estimated from DST analysis include:

- *Average effective permeability*: This may be better than core permeability since much greater volume is averaged. Also, effective permeability rather than absolute permeability is obtained.
- *Reservoir pressure*: Measured, if shut-in time is sufficient, or calculated, if not.
- *Wellbore damage*: Damage ratio method permits the estimation of what the well should make without damage.
- *Barriers, permeability changes, and fluid contacts*: These reservoir anomalies affect the slope of the pressure buildup plot. They usually require substantiating data to differentiate one from the other.
- *Radius of investigation*: An estimate of how far away from the wellbore the DST can "see".
- *Depletion*: Can be detected if the reservoir is small and the test is properly run.

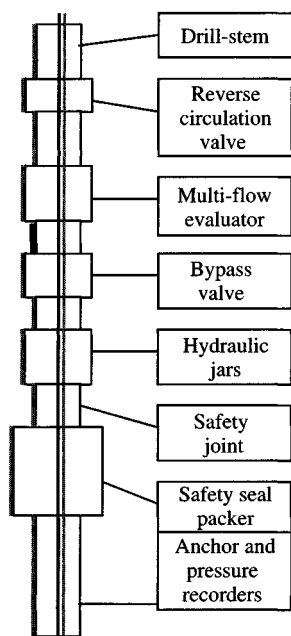
12.2 DST Equipment and Operational Procedures

The DST tool is an arrangement of packers and valves placed at the end of the drill pipe. The packers help in isolating the zone of interest from drilling mud in the hole and to let it produce into the test chamber, drill collar, and drill pipe. The packers also help in reducing wellbore storage effects. Figure 12-1 shows a diagram of operational DST tool and sequence of operations for MFE tool.

DST Pressure Behavior

Figure 12-2 shows a pressure record from a drill-stem test. Sequences of pressure recording are:

- A. Increase in hydrostatic mud pressure as the tool is lowered into the hole.
- B. Setting of the packers causes compression of the mud in the annulus in the test interval, and a corresponding increase in pressure is noted.
- C. When the tool is opened and inflow from the formation occurs, the pressure behavior is as shown in this section.



Basics of DST Operations

The drill-stem test often uses two bombs and one or more flow, and shut-in sequences are recorded. Some important factors of the DST chart are:

1. Going into hole
2. Initial flow period
3. Initial shut-in period
4. Final flow period
5. Final shut-in period
6. Going out of hole

In summary, the DST, if properly applied, has become a very useful tool for the Well Completion Engineer

Figure 12-1. Operational DST tool.

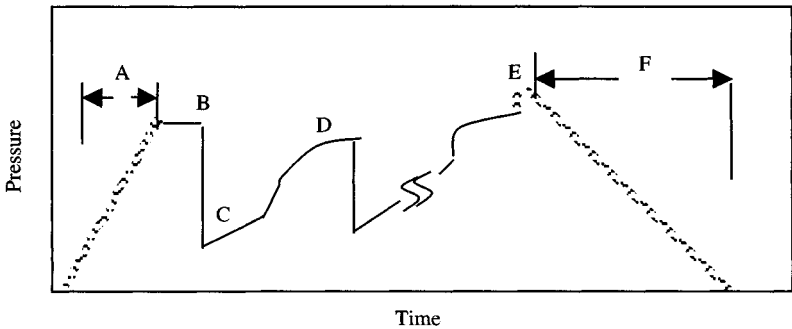


Figure 12-2. DST pressure record.

- D. After the test tool is closed, a period of pressure buildup results.
- E. Finally, the test is ended and the packers are pulled loose, causing a return to hydrostatic mud pressure.
- F. Tool is pulled. Fluid recovery from the test may be determined from the contents of the drill pipe or from the amount recovered at the surface if a flowing DST is obtained.

12.3 Recommended Flow and Shut-In Time for Drill-Stem Tests

The key to DST evaluation is obtaining and recording good data. The DST must be planned to fit the specific situation. Past experience in the area should be studied in planning subsequent tests. The first flow is very short and is designed (usually 5–15 min) to remove any excess pressure, which may have resulted from setting the packers. The first buildup is rather long (usually 30–60 min) since reliable value for the initial reservoir pressure is desired. The second flow is somewhat longer and is designed (usually 60 min) to evaluate the formation for some distance from the well. The second shut-in is usually 30 min to several hours to calculate the transmissibility and other characteristics of the reservoir. If the second extrapolated pressure is less than the pressure of the first shut-in, depletion of the small reservoir should be suspended. If extrapolated pressure p^* is equal to p_i from the two shut-in periods, then depletion results. Figure 12-3 shows the DST pressure chart for a two-cycle test. The first cycle in Figure 12-3 includes the initial flow and buildup periods, while the second cycle includes the second flow and final buildup periods. Figure 12-4 shows tests with more than two cycles are possible. In this figure, the pressure increases upward.

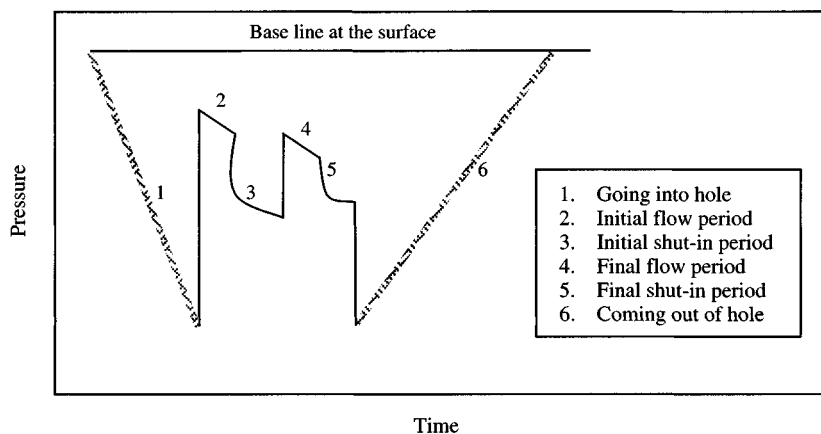


Figure 12-3. DST pressure chart for a two-cycle test.

12.4 Troubleshooting DST Pressure Charts

It is important to carefully examine the DST charts and decide if the test was mechanically and operationally successful. A good DST chart has the following characteristics:

- The pressure base line is straight and clear;
- Recorded initial and final hydrostatic mud pressures are the same and are consistent with depth and mud weight;
- Flow and buildup pressures are recorded as smooth curves.

The DST pressure chart will also indicate bad hole conditions and tool malfunctions, and other difficulties can be identified from the DST charts. The actual DST charts on the following pages show examples of DST problems that restrict the calculation possibilities. Included also are sample situations which can be reasonably interpreted by “eyeball” methods.

DST Charts for Barrier Detection

To recognize a poor DST, one must be familiar with DST chart characteristics. Murphy¹² and Timmerman and Van Poolen³ provide such information. A good DST chart has the following characteristics: (a) the pressure base line is straight and clear; (b) recorded initial and final hydrostatic mud pressures are the same and are consistent with depth and mud weight; and (c) flow and buildup pressures are recorded as smooth curves.

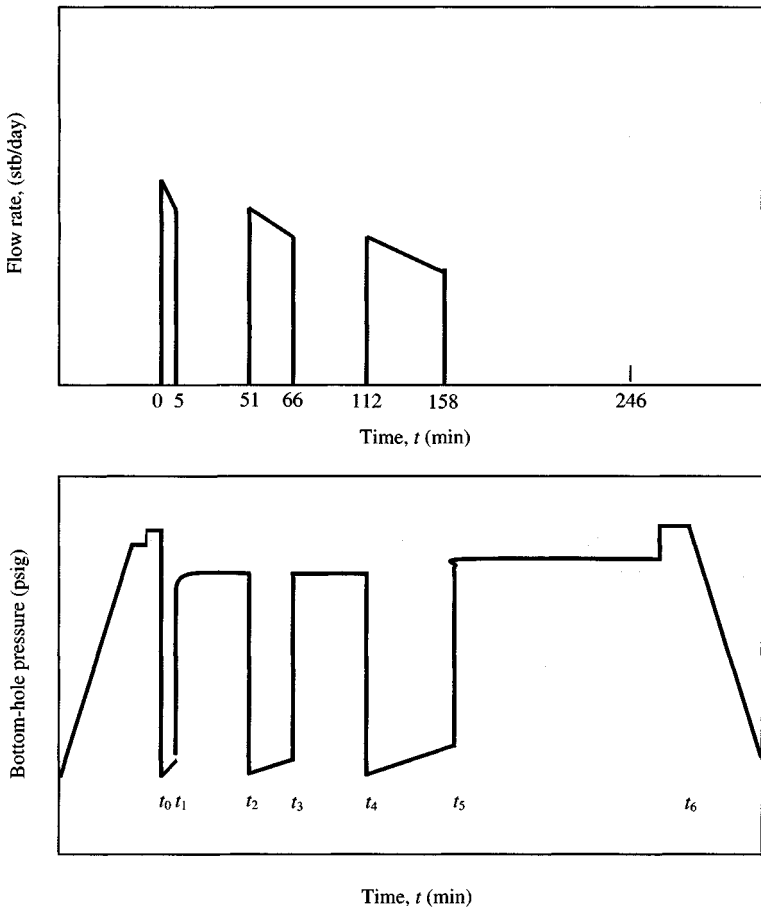


Figure 12-4. Three-cycle drill-stem test.

Figures 12-5 through 12-8 illustrate the pressure chart interpretation for various testing conditions.^{3,12,13} The captions of each figure explain its characteristics.

12.5 Checking Validity and Consistency of Reporting DST Data

To check the recorded (DST) data, follow these steps:

- Calculate the hydrostatic mud pressure and check against the recorded initial and final hydrostatic mud pressures by using the following equations:

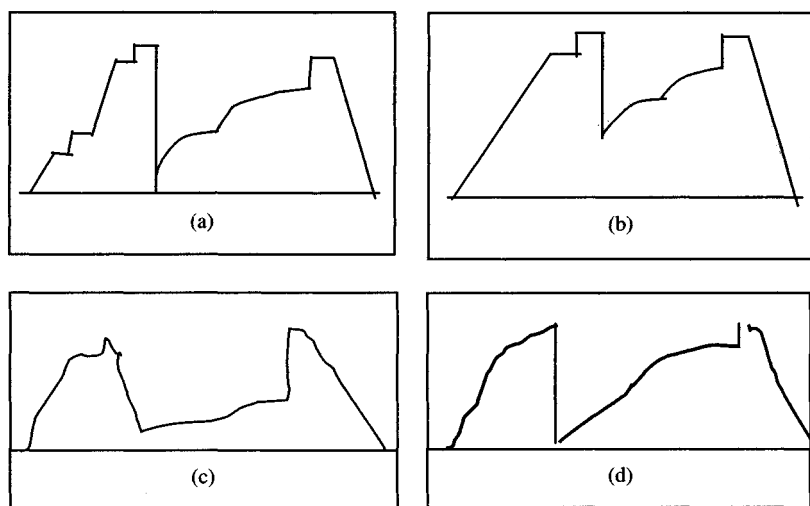


Figure 12-5. (a) Fluid loss before packer. (b) Leak in drill pipe. (c) Leak in drill pipe. (d) Effect of rough sea.

$$\text{Mud gradient} = \frac{0.433}{8.33} \times \text{mud weight in lb/gal} \quad (\text{ft/psi}) \quad (12-1)$$

$$\text{Hydraulic pressure} = \text{Well depth in feet} \times \text{mud gradient} \quad (\text{psi}) \quad (12-2)$$

$$\text{Mud weight} = \text{Hydrostatic pressure} \times \text{well depth}$$

$$\times \frac{8.33}{0.433} \quad (\text{lb/gal}) \quad (12-3)$$

- Check with the reported mud weight;
- Check accuracy of p_i [estimated from extrapolated MTR line of the second shut-in to $(t_p + \Delta t)/\Delta t = 1$].

12.6 Estimation of Average Flow Rate

To calculate the initial flow rate (DST), follow these steps:

- Calculate mud gradient, MGR , as

$$MGR = (\text{mud density, lb/gal}) \left(\frac{0.433}{8.33} \right) \quad (\text{psi/ft}) \quad (12-4)$$

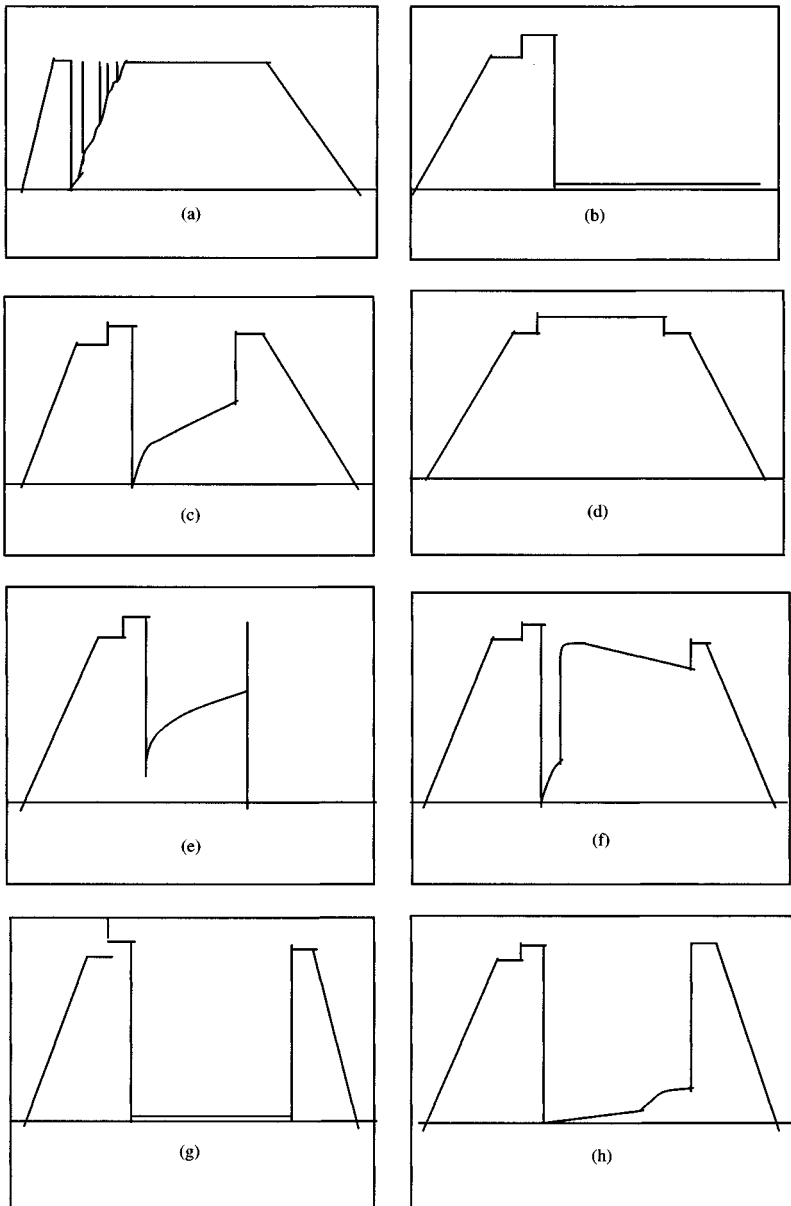


Figure 12-6. (a) Packer failed and could not be set. (b) Runaway clock. Clock spring released. (c) Tool failed to close. No buildup is obtained. (d) Tool failed to open. (e) Clock stopped at shut-in drill-stem normal. (f) Effect of large superpressure. Pressure buildup during flow and buildup period. (g) No formation permeability small amount of mud may be recovered. (h) Low-permeability formation.

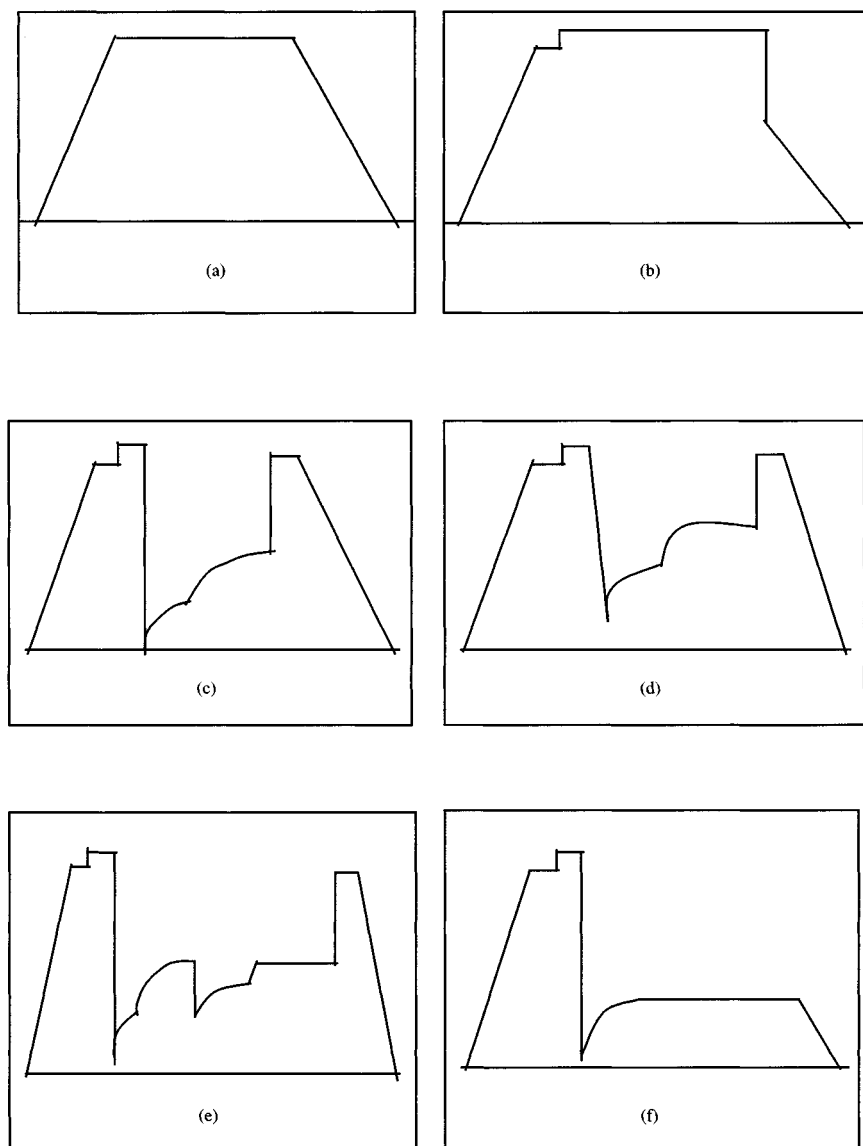


Figure 12-7. (a) Gauge plugged with tool on bottom before packer was set. (b) Gauge plugged after packer was set but before tool was opened. (c) Two-layer effects. Caused by two producing zones. (d) Well interference. The DST is usually too short to notice interference with today's well spacing. (e) Two tests with the same gauge. Second buildup-extrapolated pressure is lower than that of first. (f) Gauge gradually plugged during flow period.

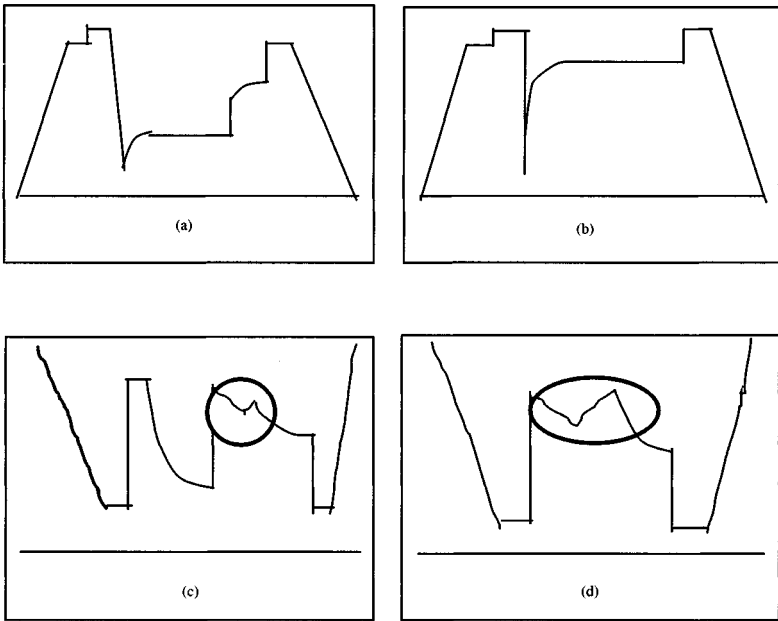


Figure 12-8. (a) Gauge plugged during flow and unplugged late in buildup. (b) Single test with two gauges. Suggests highly permeable formation with little or no skin. (c) This behavior typically occurs in gas reservoirs when flow occurs at the surface. (d) The rippled appearance in the flow curve indicates that gas has broken through the liquid in the drill string and the well flowing by heads.

- Estimate feet of mud, FOM , as

$$FOM = \frac{\text{(initial shut-in pressure at the end of first flow period)}}{MGR}$$

- Calculate capacity of the drill collar, CDR , as

$$CDR = C_S \frac{\rho}{144} \quad (\text{bbl/ft}) \quad (12-5)$$

where

$$C_S = 25.65 \times \frac{A_{wb} \text{ (ft}^2\text{)}}{\rho \text{ (lb}_m\text{/ft}^3\text{)}} = \text{wellbore storage coefficient}$$

$$A_{wb} = \pi r_p^2 \text{ (ft}^2\text{)}$$

$$\rho = \text{fluid density (lb}_m\text{/ft}^3\text{)} = \frac{141.5}{131.5 + API^\circ}$$

$$r_p = \text{ID drill collar (ft)}$$

$$API = \text{fluid gravity}$$

- Estimate fluid produced from formation, FPF , as

$$FPF = CDR \times FOM \quad (\text{ft}) \quad (12-6)$$

- Calculate initial flow rate

$$q_i = \frac{FPF}{\text{Flow time (1440 min/day)}} \quad (\text{stb/day})$$

12.7 DST Analysis Methods, Uses, and Limitations

Analysis of DST provides a practical and economical means for estimating important formation parameters prior to well completion. A proper run and interpreted DST yield more valuable information. DST pressure buildup data are analyzed much like any other pressure buildup data; the techniques of Chapter 5 apply. Figure 12-9 shows various DST analysis methods, uses, and their limitations.

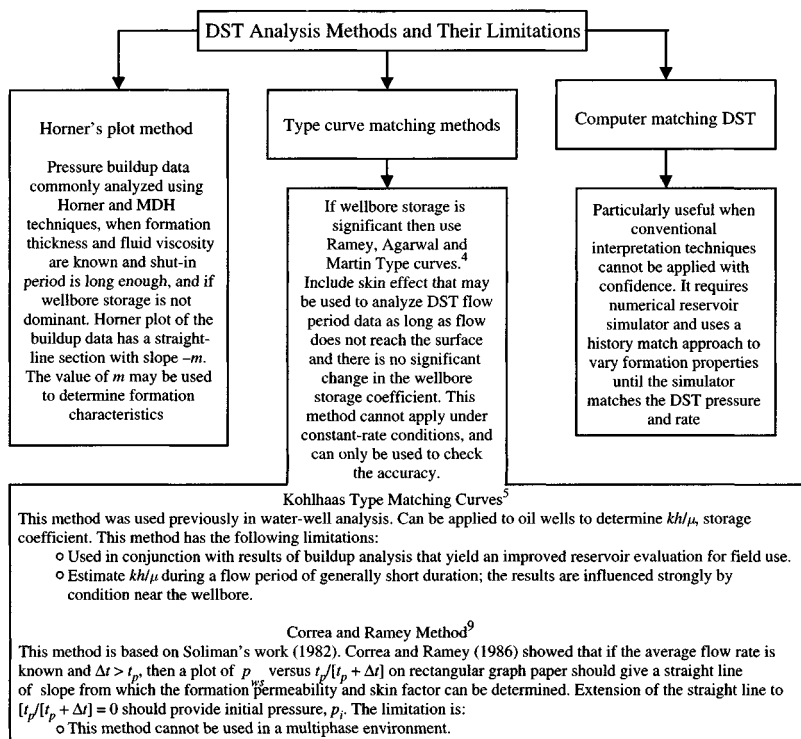


Figure 12-9. Most common methods to analyze DST data and their limitations.

Horner's Plot Method

DST pressure buildup data are analyzed much like any other pressure buildup data. In a DST, the flow period is about the same duration as the shut-in period, and so pressure buildup data must be analyzed with the Horner plot, p_{ws} versus $\log[(t_p + \Delta t)/\Delta t]$. The value used for t_p is usually the length of the preceding flow period. However, if initial flow period is very long, it is more accurate to use the sum of the flow period length for t_p for the final buildup. If the shut-in period is long enough, and if wellbore storage is not dominant, a Horner plot of buildup should have a straight-line section with slope $-m$, the value of m may be used to estimate the formation permeability k from the following equation:

$$k = \frac{162.6q_o\beta_o\mu_o}{mh} \quad (12-7)$$

Formation thickness h must be the net thickness of productive zone, which should be determined from log analysis. If net thickness h is not available, kh or formation capacity is determined:

$$kh = \frac{162.6q_o\beta_o\mu_o}{m} \quad (12-8)$$

If all the reservoir parameters are unknown, transmissibility $kh/\mu_o\beta_o$ is estimated:

$$\frac{kh}{\mu_o\beta_o} = \frac{162.6q_o}{m} \quad (12-9)$$

If μ_o and h are not known, kh/μ_o may be estimated by rearranging Eq. 12-9. The flow rate normally used is the average over t_p . Many times DST results are affected by formation damage. Thus, to be meaningful, the effect of flow restriction caused by the damaged zone must be accounted for in analyzing a specified DST. The skin factor is estimated from the following empirical equation for a dimensionless value s denoting "skin factor."

$$s = 1.151 \left[\frac{P_{1hr} - P_{wf}(\Delta t=0)}{m} - \log \left(\frac{k}{\phi\mu_o c_t r_w^2} \right) + \log \left(\frac{t_p + 1}{t_p} \right) + 3.23 \right] \quad (12-10)$$

The term $\log[(t_p + 1)/t_p]$ is normally neglected when $t_p \gg 1$ or when the skin factor is high.

The skin factor is useful in comparing damage between wells; however, it cannot be readily applied to a specified formation to show what that zone should make if damage was removed. Zak and Phil Griffin⁸ carried

Eq. 12-10 one step further introducing the concept of damage ratio (DR), which compares flow rate observed on a DST (q_o) to the theoretical flow rate without damage (q_t).

$$DR = \frac{q_t}{q_o} \quad (12-11)$$

An equation for calculation of DR based on the skin factor is related to the equation¹⁴

$$DR = \frac{p_i - p_{wf}}{m \left(\log \left(\frac{kt_p}{\phi \mu_o c_t r_w^2} \right) - 2.85 \right)} \quad (12-12)$$

DR substantially greater than 1.0 indicates damage. Eq. 12-12 can be simplified by assigning average values to the formation parameters k , ϕ , c_t , μ_o , and r_w . This produced an equation for estimated damage ratio (EDR):

$$EDR = \frac{p_i - p_{wf}}{m(\log t_p + 2.65)} \quad (12-13)$$

An equation for calculation of DR based on the skin factor relation is reported as

$$\frac{J_{ideal}}{J_{actual}} = \frac{\bar{p} - p_{wf}}{\bar{p} - p_{wf} - (\Delta p)_{skin}} \quad (12-14)$$

where pressure drop across the skin is computed as

$$(\Delta p)_{skin} = \frac{141.2 q_o \mu_o \beta_o}{kh} s = 0.869 ms \quad (12-15)$$

A more dependable means of evaluating the necessity of well remedial treatment for skin effect or for production stimulation is by calculating the flow efficiency of the well:

$$\text{Flow efficiency} = \frac{p_i - p_f - (\Delta p)_{skin}}{p_i - p_f} \quad (12-15a)$$

Initial or average pressure \bar{p} is estimated by extrapolating the Horner straight line to infinite shut-in time $(t_p + \Delta t)/\Delta t = 1$. Both the first buildup plot and the second buildup plot extrapolate to the same static or initial pressure. A second DST is sometimes required to define the depletion. If the second buildup static pressure is lower than the first, then depletion of the reservoir is possible.

If the rate varies during the flow period, then the multiple analysis technique is used. Odeh and Selig² proposed a simplified analysis technique that is useful for large rate variation when t_p is less than shut-in time. The rate and t_p are modified by

$$q^* = \frac{1}{t_p^*} \sum_{j=1}^N q_j(t_j - t_{j-1}) \quad (12-16)$$

and

$$t_p^* = 2 \left[t_p - \frac{\sum_{j=1}^N q_j(t_j^2 - t_{j-1}^2)}{2 \sum_{j=1}^N q_j(t_j - t_{j-1})} \right] \quad (12-17)$$

The modified values, t_p^* and q^* are used in the Horner plot. For practical purpose, the radius of investigation during DST is equivalent to the radius of drainage given by

$$r_i = \sqrt{\frac{k \Delta t_{max}}{948 \phi \mu_o c_t}} \quad (\text{ft}) \quad (12-18)$$

The following equation from Van Poollen¹ may be used to estimate the radius of investigation of a particular DST in an infinite radial flow system:

$$r_i = \sqrt{\frac{k t_p}{5.76 \times 10^4 \phi \mu_o c_t}} \quad (12-19)$$

Type Curve Matching Methods^{4,5}

Using Ramey, Agarwal, and Martin Type Matching Curves⁴

These type curves shown in Figure 12-10 include skin effect that may be used to analyze DST flow period data. In this figure, the dimensionless pressure ratio is defined as

$$p_{Dr} = \frac{p_D}{p_{Do}} = \frac{p_i - p_{wf}(t)}{p_i - p_o} \quad (12-20)$$

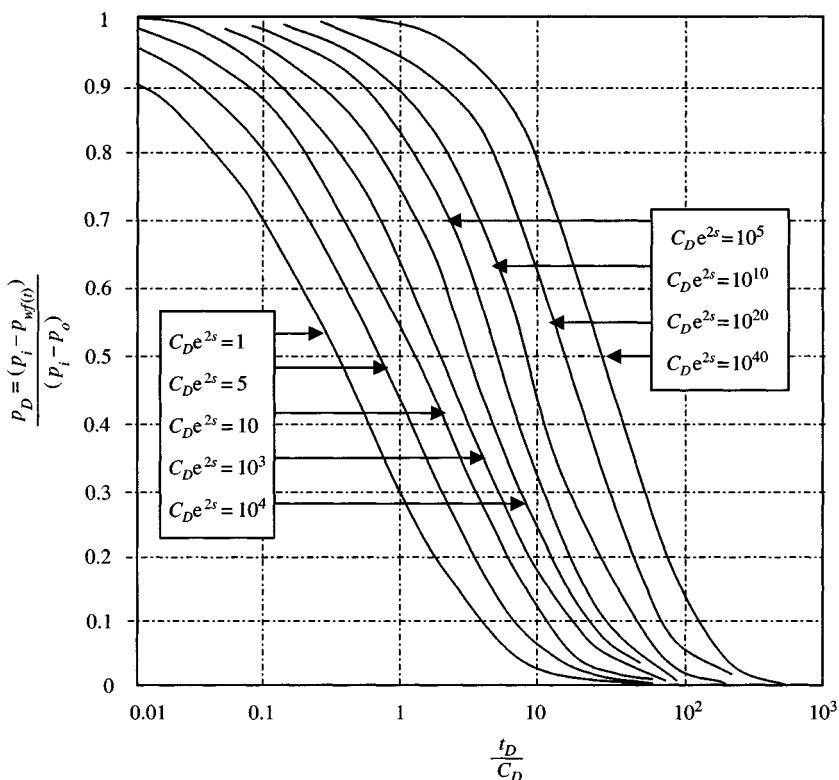


Figure 12-10. Semilog type curves for DST flow period for early- and late-time data (after Ramey et al.).⁴

where p_o is the pressure in the drill string immediately before the flow period begins or for the final flow period p_o would be the pressure at the end of first flow period.

The dimensionless time t_D is defined by

$$t_D = \frac{0.0002637kt}{\phi\mu_o c_t r_w^2} \quad (12-21)$$

and the dimensionless wellbore storage coefficient is defined by

$$C_D = \frac{6.615C}{2\pi\phi c_t h r_w^2} \quad (12-22)$$

For a DTS flow period, the wellbore storage coefficient usually results from a rising liquid level in the drill pipe. Thus,

$$C = \frac{V_u}{\left(\frac{\rho}{144} \frac{g}{g_c}\right)} \quad (12-23)$$

where V_u is the volume per unit length of the drill pipe in barrels per foot. The following steps are used to analyze DST test using Ramey et al. type curves:

- The matching technique is similar to the method described in Chapter 8. The pressure ratio always goes from zero to one and is independent of flow rate and formation properties.
- Plot pressure ratio versus log time, minutes on semilog tracing paper (same scale as type curve).
- Laid over the grid of Figure 12-10, the pressure scale is fixed. When tracing paper data plot is slid to match one of the type curves, only horizontal section is used.
- Once the field data have been matched to one of the type curves, data from both the overlay and the underlying type curves are read at a convenient match point.
- Three data items are required
 - Parameter on curve match $(C_D e^{2s})_M$;
 - The time scale match point t_M ;
 - And the corresponding point from the type curve, $(t_D/C_D)_M$.

Permeability may be estimated from the time scale match point by using the following equation:

$$k = 3389 \frac{\mu_o C}{h t_M} \left(\frac{t_D}{C_D} \right)_M \quad (12-24)$$

Skin factor is estimated from the parameter on the curve matched

$$s = 0.5 \ln \left[\frac{\phi c_t h r_w^2 (C_D e^{2s})_M}{0.89359 C} \right] \quad (12-25)$$

DST analyses commonly report damage ratio, DR

$$DR = \frac{J_{ideal}}{J_{actual}} = \frac{\bar{p} - p_{wf}}{\bar{p} - p_{wf} - (\Delta p)_{skin}} \quad (12-26)$$

where the pressure drop across the skin is computed:

$$(\Delta p)_{skin} = \frac{141.2 q_o \mu_o \beta_o}{kh} s \quad (12-27)$$

Using Kohlhaas et al. Method^{5,6} Type Matching Curves

This method can be used in conjunction with data from buildup analysis, the reservoir evaluation of reservoir conditions through verifying or contrasting of results. These type curves are shown in Figure 12-11.

Method of Analysis

- Record pressure during the flow period between initial and final shut-in pressure.
- Calculate $(p_w - p_i)/(p_o - p_i)$ versus time and plot on graph paper of the same type and size where p_o is the pressure at the beginning.
- Obtain match point; curve match $C r_s^2/r_p^2$ with $[Tt/r_p^2]_M$; find $[t]_M$ in minutes corresponding to match points where T is equal to kh/μ .
- Calculate permeability from the time scale match points:

$$k = 3647 \frac{\mu r_p^2}{\rho h [t]_M} \left[\frac{Tt}{r_p^2} \right]_M \quad (12-28)$$

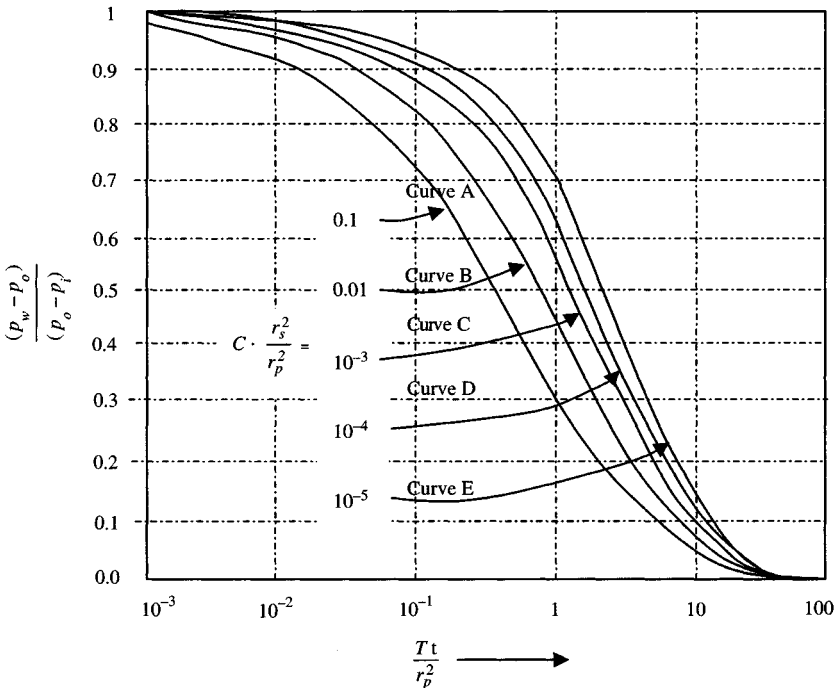


Figure 12-11. Type curves for flow period analysis.⁵

- From value of curve and with r_s and r_p , calculate wellbore storage coefficient, C

$$C = \left[\frac{r_s^2}{r_p^2} \right] \times \text{value of curve} \quad (12-29)$$

where r_s and r_p are radii of hole size and drill pipe, respectively.

- Porosity is estimated as

$$\phi = 2.31 \frac{C}{\rho_w h c_t} \quad (12-30)$$

Correa and Ramey's Method^{9,10}

Correa and Ramey showed that if the average flow rate, q_{avg} , is known and $\Delta t > t_p$ then a plot of p_{ws} versus $t_p/[t_p + \Delta t]$ on rectangular graph paper should give a straight line of slope m_c , from which formation permeability and skin factor can be estimated using the equations given below:

$$k = \frac{70.6 q_{avg} \mu \beta}{m_c h} \quad (12-31)$$

Estimate skin factor from equation

$$s = \frac{p_i - p_{wfo}}{2m_c} \frac{q_{avg}}{q(t_p)} - \frac{1}{2} \ln \left(\frac{kt_p}{\phi \mu c_t r_w^2} \right) + 3.72 \quad (12-32)$$

where

$$t_p = \frac{q_t}{q_1}$$

and

$$q_{avg} = \frac{q_t}{t_p}$$

q_1 , q_{avg} , and q_t = flow rate before shut-in, average flow rate during the test, and total liquid recovered, respectively.

Extension of the straight line to $t_p/[t_p + \Delta t] = 0$ will provide initial pressure, p_i .

Initial pressure can be estimated using equation

$$p_i = p_{ws} + m_c \left(\frac{t_p}{t_p + \Delta t} \right) \quad (12-33)$$

Drill-Stem Buildup Test Analysis with Limited Data

If the pressure data available are incomplete, the analysis procedure explained previously cannot be used. A few key data points are read at the well site just after the test. These include:

- Initial hydrostatic mud pressure;
- Initial shut-in pressure, p_{isi} ;
- Pressure at the end of first flow period;
- Pressure at the end of second flow period;
- Final shut-in pressure, p_{fsi} .

The flow and shut-in period duration are usually also reported. Such limited data may be used to estimate reservoir properties, using the following equations:

- The initial reservoir pressure is taken as

$$p_i \approx \bar{p} \approx p_{isi} \quad (12-34)$$

- The value of m for the semilog straight line is approximately given by

$$m = \frac{p_{ist} - p_{isi}}{\log \left[\frac{t_p + \Delta t}{\Delta t} \right]} \quad (12-35)$$

where Δt is the total shut-in time (time when p_{isi} was read)

- Permeability may be estimated as

$$k = \frac{162.6q_o\mu_o\beta_o}{mh} \quad (12-36)$$

Note: This practical method will not be useable, if the initial and final shut-in pressures are the same, m estimated from Eq. 12-35 will be zero.

Estimate damage ratio using the following equations:

$$\frac{J_{ideal}}{J_{Actual}} = \frac{0.183(p_{isi} - p_{fsi})}{m} \quad \text{or} \quad \frac{J_{ideal}}{J_{Actual}} = \frac{(p_{isi} - p_{fsi})}{m(4.42 + \log t_p)} \quad (12-37)$$

The following examples will clarify DST analysis by various methods.

Example 12-1¹⁶ *Analyzing DST Using Horner Plot*

A DST was conducted on an oil well. The following information was reported by the DST Company. The pressure buildup data are given in Tables 12-1 and 12-2. Well/reservoir and pressure buildup data are given in Tables 12-1 and 12-2.

Determine the following:

- Check validity and consistency of reported DST data
- Formation permeability, k
- Skin factor and pressure drop due to skin
- Initial reservoir pressure
- Flow efficiency
- Damage ratio
- Apparent wellbore radius
- Radius of investigation

Table 12-1¹⁶

Test type = open hole
Hole size = 7.88 in.
Pipe length = 240 ft
Diameter of collar = 45 in.
Reservoir pressure @ gauge depth = 2560 psi
Pressure at the end of first flow = 371 psi
Final shut-in pressure = 1005 psi
Pressure at the end of second flow period = 643 psi
Final shut-in pressure = 1969 psi
API° = 36.87 API
$c_t = 8.0 \times 10^{-6}$ psi ⁻¹
Initial shut-in pressure = 2660 psi
$\beta_o = 1.215$ rb/stb
$V_u = 0.0197$ bbl/ft and $\rho = 52.78$ lb/ft ³
Total well depth = 6550 ft
Mud density = 7.5 lb/gal
Collar length = 240 ft
Gauge depth = 6549 ft
First flow period = 6 min
First shut-in period = 30 min
Second flow period = 60 min
Second shut-in period = 120 min
$\phi = 16\%$
$\mu_o = 1.0$ cP
$h = 17$ ft
$r_w = 0.33$ ft
$t_{p1} = 6$ min, $t_{p2} = 120$ min

Table 12-2
Pressure Buildup Test Data¹⁵

(1) Time, Δt (min)	Time, Δt (hr)	Dimensionless time $\frac{(t_p + \Delta t)}{\Delta t}$	Pressure, p_{ws} (psig)
First flow period			
0	0.000	—	371
3	0.050	3.00	665
6	0.100	2.00	672
9	0.150	1.67	692
12	0.200	1.50	737
15	0.250	1.40	786
18	0.300	1.33	832
21	0.350	1.29	874
24	0.400	1.25	919
27	0.450	1.22	962
30	0.500	1.20	1005
Second flow period			
3	0.050	41.00	665
6	0.100	21.00	672
9	0.150	14.33	692
12	0.200	11.00	737
15	0.250	9.00	786
18	0.300	7.67	832
21	0.350	6.71	874
24	0.400	6.00	919
27	0.450	5.44	962
30	0.500	5.00	1005
33	0.550	4.64	1046
36	0.600	4.33	1085
39	0.650	4.08	1128
42	0.700	3.86	1170
45	0.750	3.67	1208
48	0.800	3.50	1248
51	0.850	3.35	1289
54	0.900	3.22	1318
57	0.950	3.11	1361
60	1.000	3.00	1395
63	1.050	2.90	1430
66	1.100	2.82	1467
69	1.150	2.74	1499
72	1.200	2.67	1536
75	1.250	2.60	1570
78	1.300	2.54	1602
81	1.350	2.48	1628
84	1.400	2.43	1655
87	1.450	2.38	1683

Table 12-2 (continued)

(1) Time, Δt (min)	Time, Δt (hr)	Dimensionless time $\frac{(t_p + \Delta t)}{\Delta t}$	Pressure, p_{ws} (psig)
90	1.500	2.33	1713
93	1.550	2.29	1737
96	1.600	2.25	1767
99	1.650	2.21	1794
102	1.700	2.18	1819
105	1.750	2.14	1845
108	1.800	2.11	1869
111	1.850	2.08	1894
114	1.900	2.05	1917
117	1.950	2.03	1948
120	2.000	2.00	1969

Solution To analyze pressure buildup test, follow these steps:

- Identify the MTR and find the slope of MTR, p_{1hr} , and p^* of the Horner plot of the second shut-in period (Figure 12-12).
- Prepare Horner plot of the first and second shut-in buildup pressures on the same graph paper as shown in Figure 12-13.
- Check validity and consistency of reported DST data.

$$\text{Mud gradient} = \frac{7.5 \times 0.433}{8.33} = 0.390 \text{ ft/psi} \quad (\text{Eq. 12-1})$$

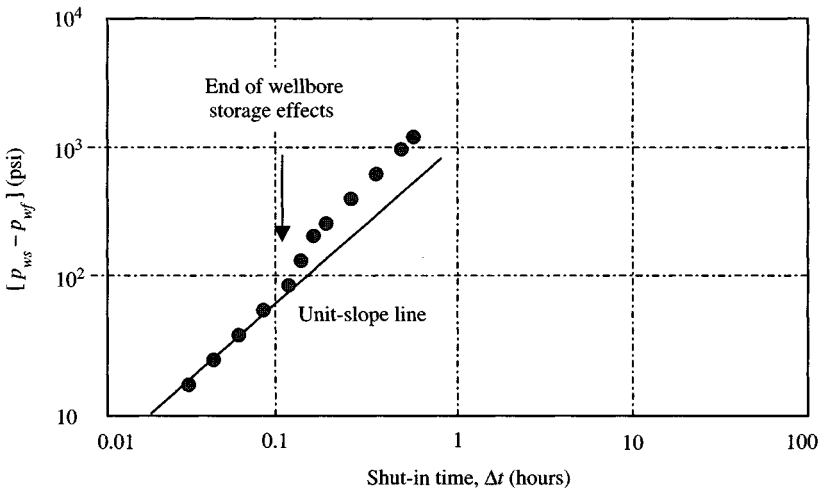


Figure 12-12. log-log data plot.

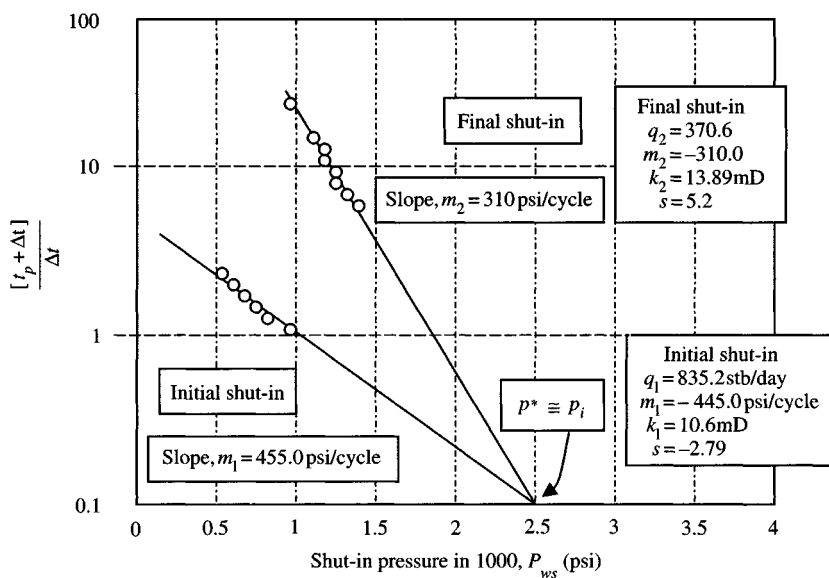


Figure 12-13. Semilog Horner plot for data.

$$\text{Hydrostatic pressure} = 6549 \times 0.390 = 2554 \text{ psi} \quad (\text{Eq. 12-2})$$

The reported initial reservoir pressure at gauge depth is 2560 psi, which is in good agreement with $p_i = p^* = 2554$ psi (extrapolated pressure from the first shut-in straight line). The mud weight should be

$$\text{Mud weight} = \frac{(8.33)(2554)(6540)}{0.433} = 7.52 \text{ lb/gal} \quad (\text{Eq. 12-3})$$

Thus the reported mud weight is correct.

- Formation permeability, k .

From the extrapolated MTR, line of the second shut-in to $(t_p + \Delta t)/\Delta t = 1$

$$p_i = p^* = 2550 \text{ psi}$$

Using Eq. 12-7

$$k = \frac{162.6q_o\mu_o\beta_o}{m_2h} = \frac{162.6(835.2)(1.0)(1.215)}{(445.0)(17)} = 21.81 \text{ mD} \quad (\text{from initial slope})$$

$$k = \frac{162.6q_o\mu_o\beta_o}{m_2h} = \frac{162.6(370.6)(1.0)(1.215)}{(310.0)(17)} = 13.89 \text{ mD} \quad (\text{from final slope})$$

In general k as determined from the initial shut-in could be different from that determined from the final shut-in. This is because of the differences in the radii of investigation.

- Skin factor and pressure drop due to skin from Eqs. 12-10 and 12-15:

$$\begin{aligned}
 s &= 1.151 \left[\frac{p_{1hr} - p_{wf}(\Delta t=0)}{m} - \log \left(\frac{k}{\phi \mu_o c_t r_w^2} \right) + \log \left(\frac{t_p + 1}{t_p} \right) + 3.23 \right] \\
 &= 1.151 \left[\frac{1395 - 371}{445} - \log \left(\frac{10.6}{(0.16 \times 1 \times 8.00 \times 10^{-6} \times (0.33)^2)} \right) \right. \\
 &\quad \left. + \log \left(\frac{3}{2} \right) + 3.23 \right] \\
 &= 1.151 [1.6900 - 7.8884 + 0.1761 + 3.23] = -2.79 \\
 (\Delta p)_{skin} &= 0.869 ms = 0.869(445)(-2.79) = -1079 \text{ psi}
 \end{aligned}$$

- Initial reservoir pressure

$$p_i \cong p^* = 2550 \text{ psi}$$

- Flow efficiency

$$\begin{aligned}
 \text{Flow efficiency} = FE &= \frac{p_i - p_{wf} - (\Delta p)_{skin}}{\bar{p} - p_{wf}} \quad (\text{Eq. 12-15a}) \\
 &= \frac{2550 - 371 - (-1079)}{2550 - 371} = 1.50
 \end{aligned}$$

- Damage ratio

$$\text{Damage ratio} = DR = \frac{1}{FE} = \frac{1}{1.5} = 0.67 \quad (\text{Eq. 12-12})$$

- Apparent wellbore radius

$$r_{wa} = r_w e^{-s} = 0.33 e^{-(-2.79)} = 5.37 \text{ ft}$$

- Radius of investigation

$$\begin{aligned}
 r_i &= \sqrt{\frac{k \Delta t_{max}}{948 \phi \mu_o c_t}} = \sqrt{\frac{10.6 \times 120/60}{948 \times 0.16 \times 1 \times 8.0 \times 10^{-6}}} \quad (\text{Eq. 12-18}) \\
 &= 132 \text{ ft}
 \end{aligned}$$

Example 12-2¹⁶ *Reworking Example 12-1 Using Type Curve Matching Techniques*

- Ramey, Agarwal, and Martin Method
- Kohlhaas Method

Solution *Using Ramey, Agarwal, and Martin Method*

Table 12-3 shows the test data and computation results. Figure 12-14 shows the data plot of Table 12-3 matched to Figure 12-10.

First calculate wellbore storage coefficient C :

$$C = \frac{0.0197}{\frac{52.78}{144}(32.17)} = 0.0517 \text{ bbl/psi} \quad (\text{Eq. 12-23})$$

$$C_D = \frac{5.615 \times 0.0517}{2 \times 3.142 \times 0.16 \times 17 \times 8.0 \times 10^{-6} (0.328)^2} = 2.973 \times 10^4 \quad (\text{Eq. 12-22})$$

Find formation permeability and skin factor using semilog type curves – early- and late-time data

$$k = 3389 \times \frac{1}{17} \left(\frac{0.0517}{\log 108} \right) \times (7.057) = 35.77 \text{ mD} \quad (\text{Eq. 12-24})$$

$$s = 0.5 \ln \left[\frac{0.16 \times 8.0 \times 10^{-6} (0.33)^2 \times 10^{10}}{0.89359 \times 0.0517} \right] = 5.15 \quad (\text{Eq. 12-25})$$

Using Kohlhaas Method: Numerical values of type curves are presented in Table 12-4 and graphical form (see Figure 12-15) for various values of the skin factor.

Calculate permeability from the time scale match points using Eq. 12-28:

$$k = 3647 \frac{\mu r_p^2}{\rho h [t]_M} \left[\frac{Tt}{r_p^2} \right] = 3647 \times \frac{1.0 \times (1.9)^2 \times 1}{0.82 \times 17 \times 66} = 14.3 \text{ mD}$$

Porosity is estimated using Eq. 12-30:

$$\phi = 2.31 \times \frac{C}{\rho_w h c_t} = 2.31 \times \frac{18.82 \times 10^{-7} \times 0.0517}{0.82 \times 17 \times 8.0 \times 10^{-6}} = 0.20$$

Example 12-3¹⁶ *Analyzing DST Using Correa and Ramey's Techniques*

The following initial shut-in pressure data were taken from Ref. 16: Flow rate before shut-in = 175 stb/day, average flow rate during initial

Table 12-3
Drill-Stem Data for Flow Period Analysis⁴

Time (min)	Pressure (psig)	$(p_i - p_{wft})(3475 - \text{pressure})$ (psig)	$(p_i - p_o)$ (3475 - 643) (psig)	Dimensionless pressure ratio	Ratio of dimensionless time and wellbore storage t_D/C_D read from type curve after matching
				$\frac{(p_i - p_o)(3475 - 643)}{(p_i - p_{wft})(3475 - \text{pressure})}$	
0.0	643	2832	2832	1.0000	—
3.0	665	2810	2832	0.9922	0.196
6.0	672	2803	2832	0.9898	0.392
9.0	692	2783	2832	0.9827	0.588
12.0	737	2738	2832	0.9668	0.784
15.0	786	2689	2832	0.9495	0.980
18.0	832	2643	2832	0.9333	1.176
21.0	874	2601	2823	0.9184	1.372
24.0	919	2556	2823	0.9025	1.568
27.0	962	2513	2823	0.8874	1.764
30.0	1005	2470	2823	0.8722	1.960
33.0	1046	2429	2823	0.8577	2.156
36.0	1085	2390	2823	0.8439	2.352
39.0	1128	2347	2823	0.8287	2.548
42.0	1170	2305	2823	0.8139	2.744
45.0	1208	2267	2823	0.8005	2.940
48.0	1248	2227	2823	0.7864	3.317
51.0	1289	2186	2823	0.7719	3.333
54.0	1318	2157	2823	0.7617	3.529
57.0	1361	2114	2823	0.7465	3.725
60.0	1395	2080	2823	0.7345	3.921

Table 12-3 (continued)

Time (min)	Pressure (psig)	$(p_i - p_{wft})(3475 - \text{pressure})$ (psig)	$(p_i - p_o)$ (3475 - 643) (psig)	Dimensionless pressure ratio	Ratio of dimensionless time and wellbore storage t_D/C_D read from type curve after matching
				$\frac{(p_i - p_o)(3475 - 643)}{(p_i - p_{wft})(3475 - \text{pressure})}$	
63.0	1430	2045	2823	0.7221	4.117
66.0	1467	2008	2823	0.7090	4.313
69.0	1499	1976	2823	0.6977	4.509
72.0	1536	1939	2823	0.6847	4.705
75.0	1570	1905	2823	0.6727	4.901
78.0	1602	1873	2823	0.6614	5.097
81.0	1628	1847	2823	0.6522	5.293
84.0	1655	1820	2823	0.6427	5.489
87.0	1683	1792	2823	0.6328	5.685
90.0	1713	1762	2823	0.6222	5.881
93.0	1737	1738	2823	0.6137	6.077
96.0	1767	1708	2823	0.6031	6.273
99.0	1794	1681	2823	0.5936	6.469
102.0	1819	1656	2823	0.5847	6.665
105.0	1845	1630	2823	0.5756	6.861
108.0	1869	1606	2823	0.5671	7.057
111.0	1894	1581	2823	0.5583	7.253
114.0	1917	1558	2823	0.5501	7.449
117.0	1948	1527	2823	0.5392	7.645
120.0	1969	1506	2823	0.5318	7.841

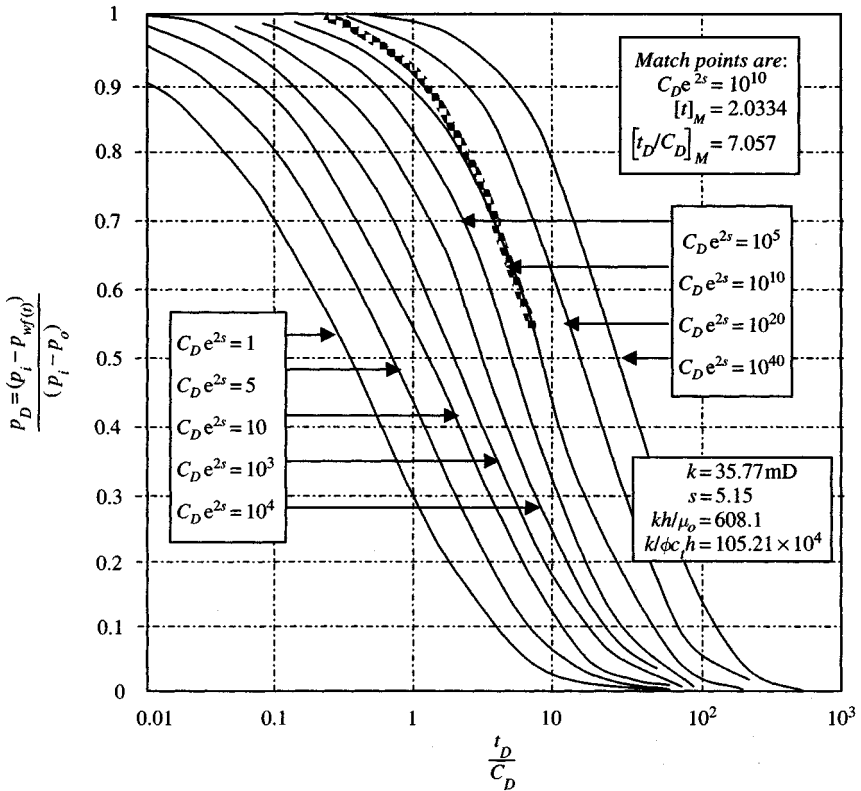


Figure 12-14. Semilog type curve match for DST flow period – early- and late-time data (after Ramey et al.).⁴

flow = 395 stb/day; t_p (initial flow) = 21 min; $\mu_o = 0.85$ cP; $\beta_o = 1.021$ rb/stb; $h = 35$ ft; total fluid recovered = 32.5 stb; $r_w = 0.29$ ft; $c_t = 4.75 \times 10^{-5}$ psi⁻¹; and $\phi = 0.12$ fraction. Estimate formation permeability and skin factor.

Solution Figure 12-16 is a plot of the initial shut-in data of Table 12-5 according to Correa and Ramey's method. From this figure the following information can be obtained. Slope of the straight line = 488 psi/cycle. Estimate formation permeability and skin factor using Eqs. 12-31 and 12-32.

$$k = \frac{70.6 q_{avg} \mu \beta}{m_c h} = \frac{70.6 \times 395 \times 0.85 \times 1.021}{488 \times 35} = 1.415 \text{ mD}$$

$$s = \frac{p_i - p_{wfo}}{2m_c} \frac{q_{avg}}{q(t_p)} - \frac{1}{2} \ln \left(\frac{kt_p}{\phi \mu c_t r_w^2} \right) + 3.72$$

Table 12-4
To Construct Type Curves (For Instantaneous Charge in a Well of Finite Diameter³; Cooper et al.⁶)

$\frac{kh\Delta t}{\mu_o r_p^2}$	10^{-1} Curve A	10^{-2} Curve B	10^{-3} Curve C	10^{-4} Curve D	10^{-5} Curve E
1.00E-03	0.977100	0.992000	0.996900	0.998500	0.999200
2.15E-03	0.965800	0.987600	0.994900	0.997400	0.998500
4.64E-03	0.965800	0.980700	0.991400	0.995400	0.997000
1.00E-02	0.923800	0.969300	0.985300	0.991500	0.994200
2.15E-02	0.886000	0.950500	0.974400	0.984100	0.988800
4.64E-02	0.829300	0.918700	0.954500	0.970100	0.978100
1.00E-01	0.746000	0.865500	0.918300	0.943400	0.957200
2.15E-01	0.628900	0.778200	0.853800	0.893500	0.916700
4.64E-01	0.478200	0.643600	0.743600	0.803100	0.841000
1.00E+00	0.311700	0.459800	0.572900	0.652000	0.708000
2.15E+00	0.166500	0.259700	0.354300	0.436400	0.503800
4.64E+00	0.074150	0.108900	0.155400	0.208200	0.262000
7.00E+00	0.046250	0.062040	0.085190	0.116100	0.152100
1.00E+01	0.030650	0.037800	0.048210	0.063550	0.083780
1.40E+01	0.020920	0.024140	0.028440	0.034920	0.044260
2.15E+01	0.012970	0.014140	0.015450	0.017230	0.019990
3.00E+01	0.009070	0.009615	0.010160	0.010830	0.011690
4.64E+01	0.005711	0.005919	0.006111	0.006319	0.006554
7.00E+01	0.003722	0.003809	0.003884	0.003962	0.004046
1.00E+02	0.002577	0.002618	0.002653	0.002688	0.002725
2.15E+02	0.001179	0.001187	0.001194	0.001210	0.001208

$$\begin{aligned}
 &= \frac{2220 - 0}{2 \times 488} \times \frac{395}{175} - \frac{1}{2} \ln \left(\frac{1.415 \times 21/60}{0.12 \times 0.85 \times 4.75 \times 10^{-6} \times 0.29^2} \right) + 3.72 \\
 &= 2.2887 \times 2.2571 - 0.5(16.3132) + 3.72 = 0.73
 \end{aligned}$$

12.8 Wireline Formation Test Data Evaluation

The wireline formation tester was introduced by Schlumberger Well Surveying Corporation in 1955 and is now available as a service from most of the well logging companies. In principle, the fluid sample (tester) provides a means for tapping formation fluids and filling a sample container varying in size from one gallon to 5½ gallons with the efflux from the tapped reservoir. Sampling may be done in open-hole or in cased-hole.

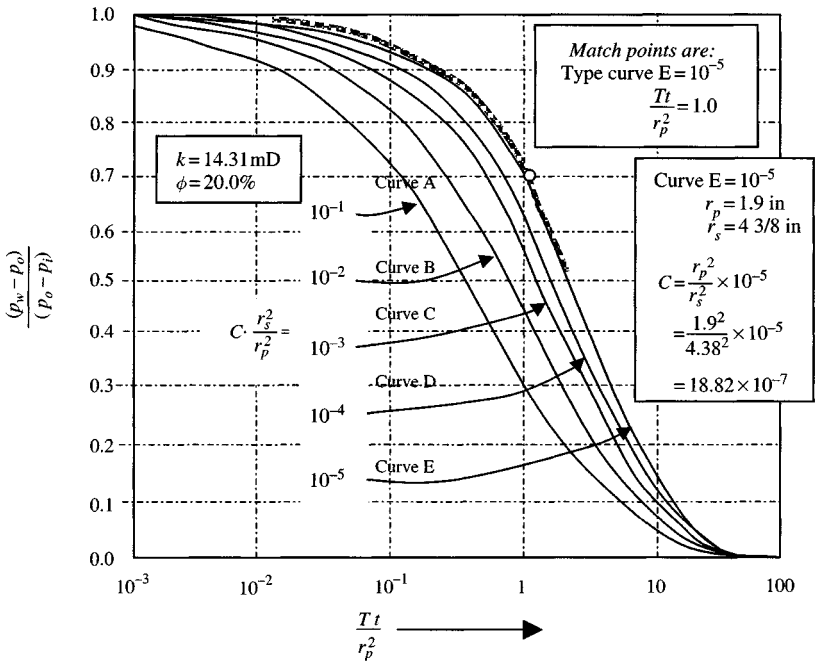


Figure 12-15. Type curves for flow period analysis.⁵

Open-Hole Formation Test

The formation tester is connected to the logging cable and lowered into the hole until it is opposite the formation to be tested. It is then expanded, forcing a pad tightly against the wall of the hole to form a seal between the mud column and the formation. Two bullets, or shaped charges are fired through the pad and into the formation. Through these perforations and connecting tubes, the formation fluids flow into a chamber in the tool. When the chamber is filled, the fluid sample valve is closed and the fluid sample is sealed in at maximum pressure. The pad and back up shoe are then retreated and the tool is brought to the surface where the sample is removed for detailed study.

Throughout the entire test, electrical circuits permit a complete recording at the surface of the progress of the whole operation. The data recorded include mechanical action, sample shots, pressure buildup, formation shut-in pressure, and finally hydrostatic mud pressure. Figure 8-23 gives such a record as a function of time together with other pertinent information about the test. Open-hole formation tester data recorded include:

- Mechanical action;
- Sample shots;

- Pressure buildup;
- Formation shut-in pressure; and
- Hydrostatic mud pressure.

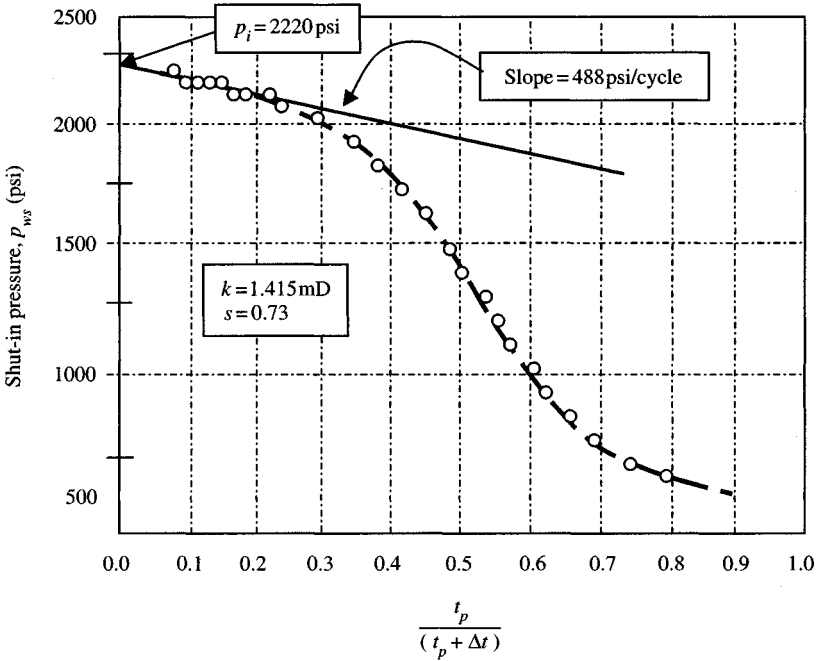


Figure 12-16. Analysis of initial shut-in data by Correa and Ramey's method.

Table 12-5
DST data

Time (min)	p_{ws} (psig)	$\frac{t_p}{[t_p + \Delta t]}$
0	543	1.0000
3	565	0.9756
6	572	0.9756
9	562	0.9302
12	569	0.9091
15	575	0.8889
18	580	0.8696
21	584	0.8511

Table 12-5 (continued)

Time (min)	p_{ws} (psig)	$\frac{t_p}{[t_p + \Delta t]}$
24	588	9.8333
27	590	0.8163
30	610	0.8000
33	635	0.7843
36	668	0.7692
39	675	0.7547
42	690	0.7407
45	735	0.7273
48	745	0.7143
51	760	0.7018
54	785	0.6897
57	808	0.6778
60	847	0.6667
63	865	0.6557
66	920	0.6452
69	942	0.6349
72	975	0.6250
75	987	0.6154
78	1004	0.6061
81	1020	0.5970
84	1045	0.5882
87	1077	0.5797
90	1109	0.5714
93	1120	0.5634
96	1210	0.5556
99	1250	0.5480
102	1254	0.5405
105	1296	0.5333
108	1345	0.5263
111	1360	0.5195
114	1375	0.5128
117	1675	0.4512
121	1717	0.4275
125	1760	0.4080
128	1885	0.3507
131	2010	0.3010
133	2012	0.2505
137	2125	0.2000
141	2158	0.1404
145	2190	0.0800

Empirical Interpretation from Sampler for High- and Low-Permeability Formations

High-permeability formations are highly porous and are also known as soft rock. Gas recovered at the surface is entered on the chart, together with oil recovered, and this fixes a point on the log-log plot (see Figure 12-17):

- If this point lies above the curve's line corresponding to the shut-in pressure recorded on the tester log, hydrocarbons will be produced;
- If the point lies below the corresponding pressure line, water production may be expected;
- Parallel lines, at 45°, show the GOR;
- If the point plots above the recorded shut-in pressure value, dry gas well is indicated.

Low-permeability formations, which are consolidated sandstones, yield formation tester recoveries and liquids, which differ considerably from those in high-permeability formations. Effecting porosity range from 6 to 25% and permeability ranging from 0.1 to 100 mD.

- When there is only a small show of oil in the fluids recovery from low-permeability formation and a large amount of gas, the formation tester log may be an indication of either oil or gas production. One may interpret the following cases:

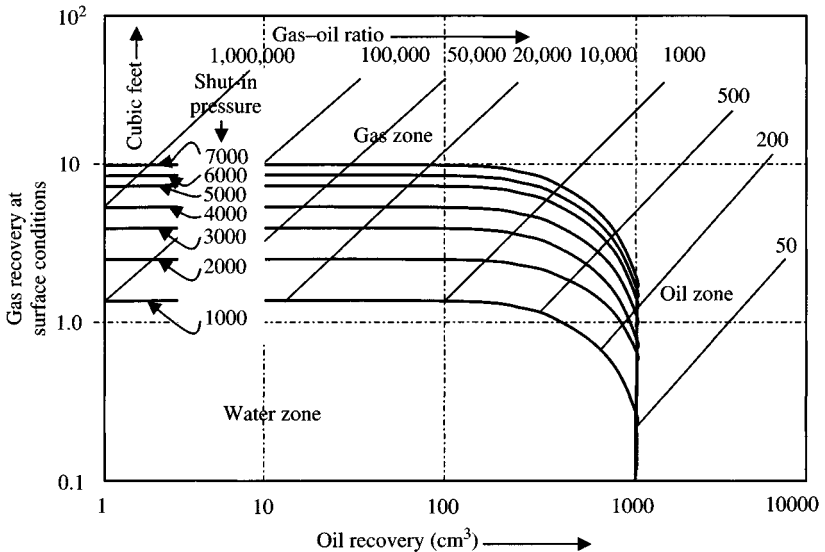


Figure 12-17. Empirical interpretation charts for full chamber fluid recovery.¹¹

Case 1	Case 2	Case 3	Case 4
Oil, water, and gas are recovered	Slight show of oil and small amount of filtrate with a large amount of gas	More than 5 ft ³ of gas and some water is recovered	Less than 5 ft ³ gas is recovered with some water
Water mud filtrate recovered → well will produce clean oil	If well will produce oil it will require stimulation by acidizing or fracturing to make a commercial well	The zone will produce gas only	Gas bearing horizon will be indicated. The chart of Figure 12-18 can be used to forecast whether the well will produce gas or water
Water recovered containing more than 10% formation water as determined by resistive measurement or chemical analysis → well will produce water cut	If more than 1000 cm ³ of filtrate is required, the well on completion will also produce water	If more than 10% formation water is present in the recovered water → water will be produced with gas	

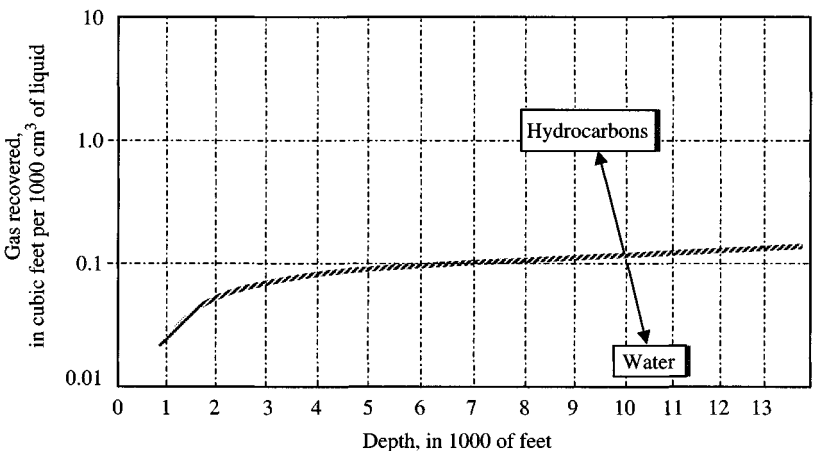


Figure 12-18. Interpretation chart for formation tester results for partial fluid recovery.¹¹

Closed-Hole Formation Test

Testing in closed holes offers many advantages as it can be carried out more safely than open and highly desired holes. It is successful and can be performed without mud in the casing, which avoids the possibility of mudding the perforation. In interpreting the fluid recovery data from the formation tester, one may consider two type of formations: high and low permeabilities.

- In high-permeability formations, which are soft rock, highly porous formations, there is no difficulty in obtaining a full chamber of formation fluids. For such cases an empirical interpretation chart can be used. Knowing how much oil (cm^3) and gas (ft^3) recovered, the solution GOR value can be approximated corresponding to the shut-in pressure recorded on the tester log. If this point lies above the curved corresponding pressure line, then the well will produce hydrocarbons. If the point lies below the corresponding pressure line, then water production may be expected.
- Low-permeability formations, such as consolidated sandstones, have effective porosities that range from about 6 to 25%, and permeabilities ranging from 0.1 to a few hundred. Invasion in such formations may be quite deep; hence it results in damage to the formation. When there is a small amount of oil in the fluids recovered from low permeability formation and a large amount of gas, the formation tester log may be indicative of either oil or gas production. One may distinguish the following cases:
 - Oil, water, and gas are recovered. If only water is recovered in mud filtrate, the well will produce oil. If the water recovered contains more than 10% formation water as determined by resistivity measurement or chemical analysis, the well will produce with water cut.
 - Only a slight show of oil and a small amount of filtrate are recovered with a large amount of gas. The well on test will produce oil but it will require stimulation by acidizing or fracturing to make a commercial well provided the effective pay thickness is sufficient. If more than 1000 cm^3 of filtrate is removed, experience shows that the well on completion will also produce water.
 - More than 5 ft^3 of gas and some water is recovered. The zone will produce gas only. If more than 10% formation water is present in the recovered water, experience shows that some water will be produced with the gas.
 - Less than 5 ft^3 of gas is recorded with some water. Great care must be taken in interpreting the results.

Closed-Hole Formation Tester Advantages over Open-Hole Formation Tester

- More safe and carried out in open and highly deviated holes.
- Percentage of success is much greater than in open-hole testing, because it can be performed with mud.
- Formation testing permits the recording of bottom-hole shut-in pressure both before and after the fluid sample. The evaluation of such records permits the determination of static bottom-hole pressure.
- Petrochemical interpretation of formation tester records helps to evaluate heterogeneity of the reservoir rock's porosity system whether it is coarse or fine pore systems. Pollard-type plot [$\log(p_s - p)$ versus time] will help to identify the type of prevailing porosity.

Empirical Interpretation Charts for Formation Tester Results

Empirical interpretation chart has been shown in Figure 12–18, which pertains to the recovery of a full $2\frac{3}{4}$ gallons sample chamber. However, if the $5\frac{1}{2}$ gal or the 1 gal tester is run, then their reservoirs may, to a first approximation, be divided by two or multiplied by $2\frac{3}{4}$, respectively, before entering the chart. In any case, the sample chamber must be full.

Gas recovered in ft^3 at surface conditions is entered in the chart, together with the cm^3 of oil recovered, and this fixes a point on the log–log grid. If this point lies above the curved line corresponding to the shut-in pressure recorded on the tester log, then the well will produce hydrocarbons. If the point lies below the corresponding pressure line, the water production may be expected.

The parallel lines, at 45° , show the solution gas–oil ratios as obtained from the ft^3 of gas per cm^3 of oil recovered, converted to ft^3 per bbl of oil. The solution GOR should be approximately that obtained on a production test.

If the gas is recorded without any oil, the point may be plotted on the ordinate corresponding to 1 cm^3 of oil, since the pressure lines are practically horizontal at this value. If the point plots above the recorded shut-in pressure value, a dry gas well is indicated.

It happens sometimes that the presence of a small amount of light oil or distillate in the recovered fluid cannot be detected visually. Under these circumstances, if the liquid recovered is centrifuged, an appreciable quantity of oil or distillate may be obtained. Such a procedure improves the interpretation and the value of the solution GOR obtained from the chart of Figure 12–18.

In very rare cases the seal valve may leak, and practically in every such case, some gas, but generally no liquid, will escape. This condition of a leaky

seal valve is easily recognized by the fact that the pressure reading at the surface of the undrained sample chamber is less by a few hundred psi than the shut-in pressure recorded on the formation test log.

Reservoir Rock's Porosity Distribution System Analysis

Evaluation of heterogeneity of the reservoir rock's porosity systems can be made using a wireline formation tester. It is a sample chamber of up to several gallons capacity combined with pressure gauges. The test chambers are forced against the borehole wall in a sealing pad, and firing a shaped charge perforates the formation. The signal to fire the charge is transmitted on logging cable. Fluid is collected during sampling, and pressure is recorded. Following sample collection, shut-in pressures are recorded as they build up with time.

The pressure versus time records from the formation tester permit the evaluation of the heterogeneity of the reservoir rock's porosity system, whether it may be considered as a uniform and homogeneous porosity development or as a multiple porosity system made up of matrix porosity and of course porosity (vugs, fracture, fissures, joints, etc.). By a Pollard-type plot (1959)⁷ [$\log(p_s - p)$ versus time], it is possible to identify the type of prevailing porosity and the respective fraction of each; these data are of importance in the interpretation of fractured rocks. It has been shown by Pirson and Pirson⁷ that the respective volumes of the coarse and fine pore system may be evaluated by plotting the successive pressure differences versus time on semilog paper. Figure 12-19 is a representation of porosity

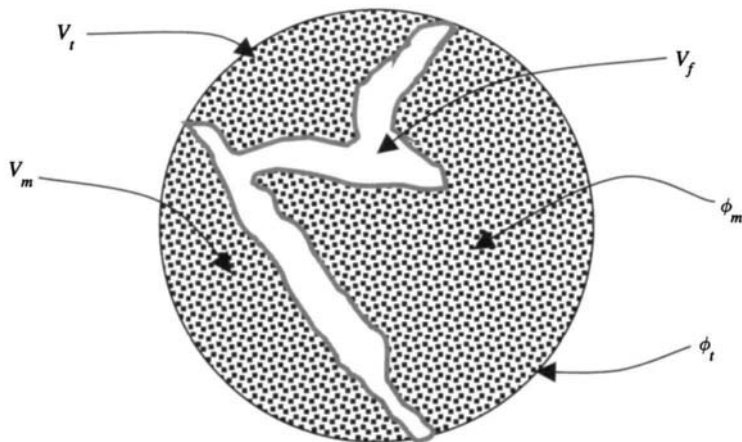


Figure 12-19. Porosity partition in heterogeneous porous rock.

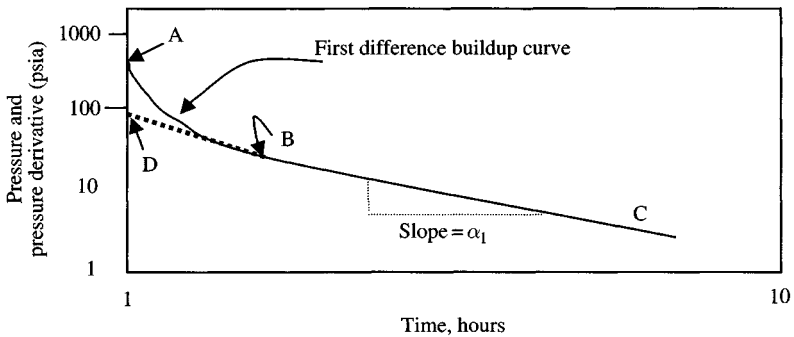


Figure 12-20. $\log(p_s - p_w)$ versus time – first difference curve.

partition in heterogeneous porous rock and shows how to develop the equation of partitioning coefficient. Notice that this approach interrelates buildup analysis with log interpretation. Figure 12-20 is a $\log(p_s - p_w)$ versus time plot. The straight-line portion (BC) indicates the matrix porosity re-pressuring the fracture porosity, when Δp within the fractures and Δp between the coarse fissures and the wellbore has become negligible. Figure 12-21 is a log of pressure differential (average fracture pressure – well pressure) across “skin” near the wall of the well. This is represented by the difference plot (AB – DB) versus time. When the pressure drop due to skin becomes negligible, a straight line (FG) results. Pollard concluded that such plots of the log of pressure differential associated with any of the regions

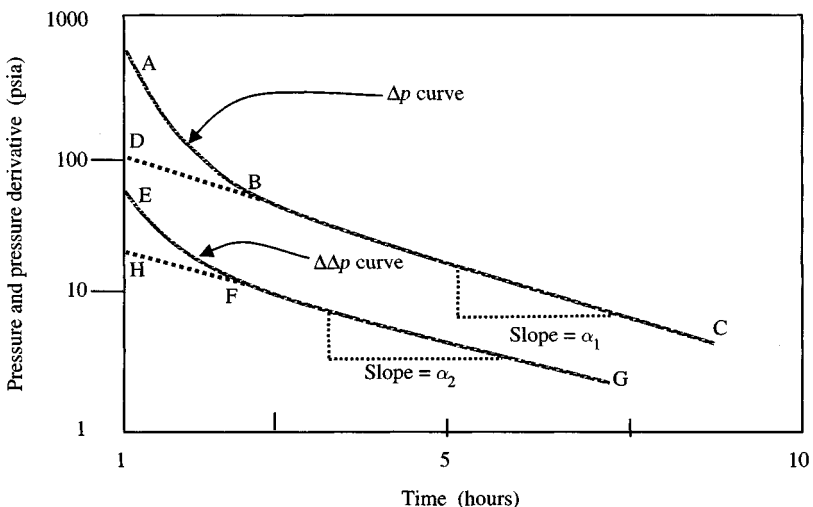


Figure 12-21. $\log(p_s - p_w)$ versus time – first and second difference curves.

against time would result in a straight line from which it would be possible to determine properties such as volume of the fracture pore space system and well skin effect.

Matrix Pore Volume Calculation

With plots of Figures 12-20 and 12-21, it is possible to calculate the matrix pore volume V_m from the following relationship as proposed by Pirson and Pirson:⁷

$$V_m = \frac{q}{\alpha_1 \phi_m (D + H) c_f} \quad (12-38)$$

where

- q = flow rate at moment of shut-in, cm^3/s
- α_1 = slope of straight line (BC) of first differences, s/cycle
- ϕ_m = matrix porosity, fraction
- D = intercept of first difference at time zero, psi
- H = intercept of second difference at time zero, psi
- C_f = compressibility of fluid in the fracture, psi .

Fracture Pore Volume Calculation

From Figures 12-20 and 12-21, we can also evaluate the pore volume of the fracture V_f from the relationship

$$V_f = \frac{q}{\alpha_2 H c_f} \quad (12-39)$$

where α_2 is the slope of the straight line (FG) of second difference (s/cycle).

Partitioning Coefficient Estimation

Partitioning coefficient concept, introduced by Pirson, has proven an important tool for the evaluation of fracture media. It is porosity breakdown between coarse (fracture) and fine (fracture) pore space. The partitioning coefficient v can be estimated from the following relationship. Figure 12-19 shows how to develop the equation of partitioning coefficient.

$$V_o = V_f + V_m \quad (12-40)$$

$$V_t = V_f + V_m\phi_m = \text{total volume of a heterogeneous porous rock} \quad (12-41)$$

$$v = \frac{V_f}{V_t} = \frac{V_f}{V_f + V_M\phi_m} \quad (12-42)$$

$$= \frac{\phi_t - \phi_m}{(1 - \phi_m)\phi_t}$$

where

$$\phi_t = \frac{V_f + V_m \times \phi_m}{V_f + V_M} = \frac{V_t}{V_o} \quad (12-43)$$

Also

$$v = \frac{1}{1 + \frac{\alpha_2 H}{\alpha_1 (D + H)}} \quad (12-44)$$

Well Skin Effects

Figure 12-21 indicates that the extrapolated E value is approximately the difference between the pressure in the fractures close to the wellbore and the average coarse fissure flowing pressure at shut-in. The pressure differential due to skin Δp is

$$\Delta p_s = (p_s - D - E) \quad (\text{psi}) \quad (12-45)$$

A sample problem will illustrate the technique.

Example 12-4¹⁶ Analyzing Reservoir Rock's Porosity Distribution System

The pressure record of a formation tester is read as follows as a function of time in seconds in an oil well. The results are recorded in Table 12-6. Estimate partitioning coefficient and well skin effect.

Solution The static pressure (p_s) recorded is 925 psi. A first difference (Δp) is made by subtracting the observed pressure from p_s . The values of Δp so obtained are plotted on a semilogarithmic plot (Figure 12-22). A series of straight lines are obtained. The reciprocal slope α_1 is read yielding 1032 sec/cycle and the intercept $C = 112$ psi. The value of the second difference ($\Delta\Delta p$) is obtained by reading the difference between the Δp curve and the extended straight line of slope α_1 . These points are plotted on the $\Delta\Delta p$ curve and give

Table 12-6
Pressure Record of Formation Tester for Oil Well ($p_{static} = 2000$)

Shut-in time (min)	Shut-in time (sec)	Pressure (psi)	$\Delta p = p_{static} - p_w$ (psi)	$\Delta\Delta p$ (psi)
0.6667	40	400	-	-
1.1667	70	500	1500	1105
1.5000	90	600	1400	1010
1.6667	100	700	1300	907
1.7500	105	800	1200	820
2.0000	120	950	1050	672
2.5000	150	1300	700	335
3.0000	180	1500	500	145
3.5000	210	1600	400	55
3.8333	230	1650	350	12
4.6667	280	1675	325	0
5.5000	330	1715	285	
7.1667	430	1725	275	
7.6667	460	1740	260	
9.5000	570	1755	245	

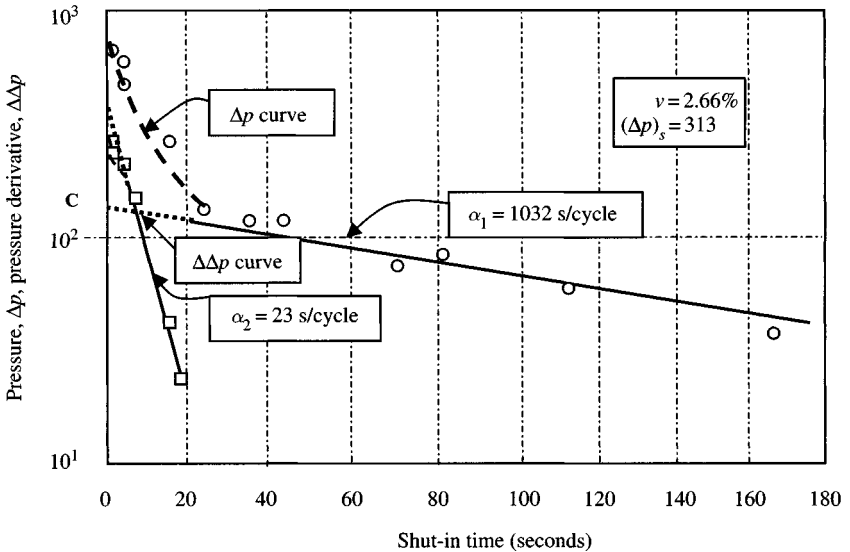


Figure 12-22. Formation test pressure difference plot.

a reciprocal slope $\alpha_2 = 23$ sec/cycle and an intercept $D = 500$ psi. The porosity partitioning coefficient or porosity breakthrough is determined using Eq. 12-44:

$$\begin{aligned} v &= \frac{1}{1 + (\alpha_2/\alpha_1) \left(\frac{D}{(D+C)} \right)} \\ &= \frac{1}{1 + \frac{1032}{23} \left(\frac{500}{(500+112)} \right)} \\ &= 2.66\% \end{aligned}$$

which represents the fraction of large pore space (vugs, fracture, fissures, joints) in the total porosity, which controls the fluid flow at the wellbore. The skin effect in this well can be calculated using Eq. 12-45:

$$\Delta p_s = p_s - D - C = 925 - 500 - 112 = 313 \text{ psi}$$

or about one-third of the total pressure drawdown during sampling.

12.9 Summary

This chapter discusses DST equipment and operational procedures, recommended flow, and shut-in time for DST. It presents trouble-shooting DST pressure charts for barrier detection, checking validity and consistency of reported DST data, DST analysis methods such as Horner's plot, type curve matching techniques, DST buildup test analysis with limited data. These methods are discussed in detail for their uses and limitations including wireline formation test data evaluation.

References and Additional Reading

1. Van Poollen, H. K., "Status of Drill-Stem Testing Techniques and Analysis," *J. Pet. Tech.* (April 1961) 333-339. Also Reprint Series, No. 9 - Pressure Analysis Methods, Society of Petroleum Engineers of AIME, Dallas, TX, 1967, pp. 104-110.
2. Odeh, A. S., and Selig, F., "Pressure Buildup Analysis - Variable Rate Case," *J. Pet. Tech.* (July 1963) 228, 790-794; *Trans. AIME*, 228. Also Reprint Series, No. 9 - Pressure Analysis Methods, Society of Petroleum Engineers of AIME, Dallas, TX, 1967, pp. 131-135.

3. Timmerman, E. H., and Van Poolen, H. K., "Practical Use of Drill-Stem Test," *J. Can. Pet. Tech.* (April–June 1972) 31–41.
4. Ramey, H. J., Agarwal, R. G., and Martin, I., "Analysis of Slug Test or DST Flow Period Data," *J. Can. Pet. Tech.* (July–Sept. 1975) 37–42.
5. Kohlhaas, C. A., "A Method for Analyzing Pressures Measured During Drill-Stem Test Flow Periods," SPE-AIME, Oct. 11, 1971.
6. Cooper, H. H., Jr., Bredehoeft, J. D., and Papadopoulos, "Instantaneous Charge of Water," *Water Resources Res.* (1967) 3, No. 1, 263–269.
7. Pirson, R. S., and Pirson, S. J., "An Extension of the Pollard Analysis Method of Well Pressure Build-Up and Drawdown Tests," paper SPE 101 presented at the SPE-AIME 36th Annual Fall Meeting, Dallas, Oct. 8–11, 1961.
8. Zak, a. J, Jr., and Phil Griffin, III, "Evaluation of DST Data," *Oil Gas J.* April, p. 122, April 29, p. 136, May 13, p. 136, May 27, p. 125, 1957.
9. Correa, A. C., and Ramey, H. J., Jr., "A Method for Pressure Buildup Analysis of Drillstem Tests," SPE paper 16802 presented at the 1987 Annual Technical Conference and Exhibition, Dallas, Sept. 27–30.
10. Soliman, M. Y., "Analysis of Pressure Buildup Tests with Short Production Time," paper presented at the SPE-AIME 57th Annual Fall Technical Conference and Exhibition, New Orleans, LA, Sept. 26–29, 1982. Also SPEFE, Aug. 1986, pp. 363–371.
11. Schlumberger Educational Services, repeat Formation Tester, SMP-9070, Houston, TX, 1986.
12. Murphy, W. C., "The Interpretation and Calculation of Formation Characteristics from Formation Test Data," Pamphlet T-101, Halliburton Co., Duncan, OK, 1970.
13. Black, W. M., "A Review of Drill-Stem Testing Techniques and Analysis," *J. Pet. Tech.* (June 1956) 21–30.
14. Van Everdingen, A. F., "The Skin Effect and Its Influence on the Productive Capacity of a Well," *Trans. AIME* (1953) 198, 171–176.
15. Amman, C. B., "Case Histories of Analyses of Characteristics of Reservoir Rock from Drill-Stem Tests," *J. Pet. Tech.* (May 1960) 27–36.
16. Amanat, U. C., "Pressure Transient Test Analysis: User's Handbook," Vol. 8, Advanced TWPSOM Petroleum Systems Inc., Houston, TX, 1995.

Chapter 13

Interference and Pulse Test Analysis Methods

13.1 Introduction

Both interference and pulse tests, also known as multiple-well testing, involve more than one well. These types of tests can be used to obtain an adequate reservoir description for homogeneous (both isotropic and anisotropic) and heterogeneous systems. Numerical solutions must be used to analyze pressure transient data from heterogeneous systems. At the same time, it is one of the most important and useful tests to understand the well behavior in a water flood and enhanced oil recovery projects. Figure 13-1 shows field application of interference and pulse tests.

13.2 Interference Test Analysis Techniques

Interference testing is one form of multiple-well testing. These tests are used to determine whether two or more wells are in pressure communication in the same reservoir and, when communication exists, to provide estimates of vertical formation permeability k and porosity/compressibility product ϕc_i , in the vicinity of the tested wells. In the homogeneous isotropic system, the porosity and thickness are the same everywhere in the reservoir. Permeability k is also the same everywhere and in all direction. Interference is conducted by producing from or injecting into one of these wells (active well) and the pressure response is observed in the other well (observation well) (see Figure 13-2). The active well starts producing at uniform pressure at time zero and the other pressure response in the observation well at a distance r from active well begins after some time lag.

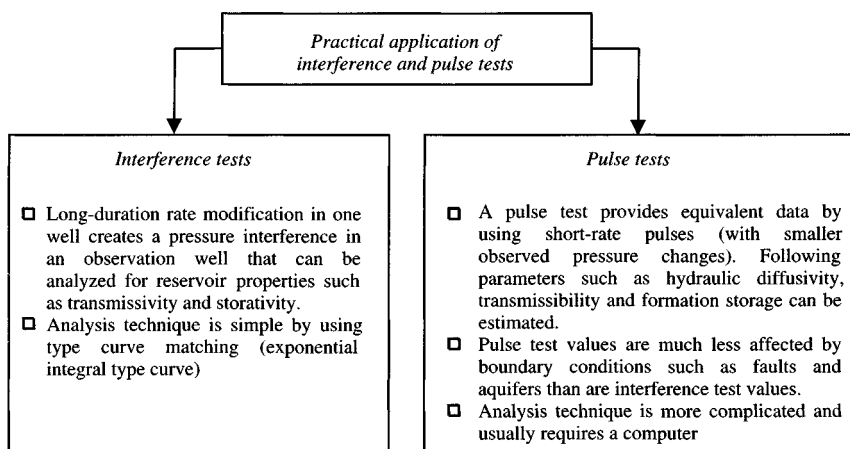


Figure 13-1. Field application of interference and pulse tests.

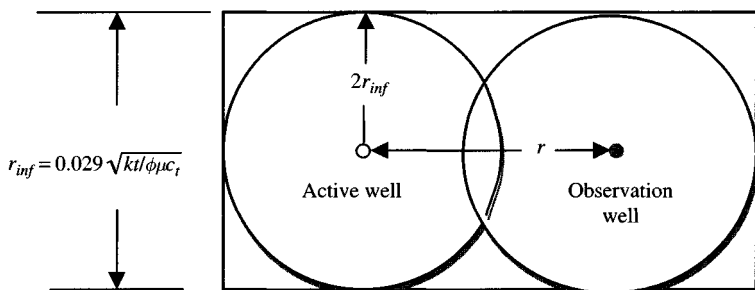


Figure 13-2. Influence region for interference or pulse testing.

Interference Test Analysis by Type Curve Matching

Type curve matching technique is applied to interference test analysis. Type curve matching is simpler for interference testing than for single-well testing because there is only one type curve (Figure 13-3). To consider for infinite-acting system, the following steps are used to analyze an interference test:

- Plot pressure drawdown data in an observation well, $\Delta p = p_i - p_{wf}(t)$, versus time, t , on tracing paper using the grid of Figure 13-3.
- Slide the plotted test data over the type curve (horizontal or vertical) until a match is found.
- The match point data are used to estimate formation properties. In Figure 13-3, the ordinate of the type curve is dimensionless pressure,

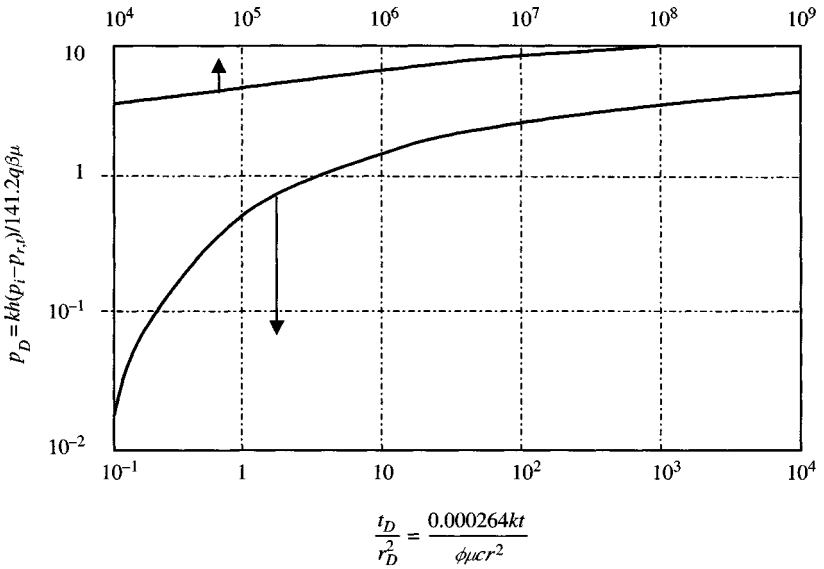


Figure 13-3. Exponential integral solution type curve.³

which is estimated using the pressure match points and the following equation:

$$p_D = \frac{(p_i - p_{wf}(t))kh}{141.2q_w\mu_w\beta_w} \quad (13-1)$$

- By substituting match point values and rearranging Eq. 13-1, we estimate permeability in the test region using the pressure match points and the following equation:

$$k = 141.2 \frac{q_w\mu_w\beta_w (p_D)_{MP}}{h (\Delta p)_{MP}} \quad (13-2)$$

- Similarly, use the definition on the abscissa of the type curve in Figure 13-3, to estimate the dimensionless time and dimensionless radius.

$$t_D = \frac{0.00026372kt}{\phi\mu_w c_t r_w^2}$$

$$r_d = \frac{r}{r_w} \quad (13-3)$$

With the time scale match point data and the permeability just determined, estimate the product ϕc_t , using the following equation:

$$\phi c_t = \left[\frac{0.0002637k}{\mu_w r^2} \right] \frac{(\Delta t)_{MP}}{(t_D/r_D^2)_{MP}} \quad (13-4)$$

where r is the distance between the two wells. The type curve analysis method is simple, fast, and accurate when the exponential integral (see Figure 13-3) applies; that is, when $r_D = r/r_w > 20$ and $t_D/r_D^2 > 0.5$.

Knowing ϕ , we can calculate total system compressibility, c_t , and hence estimate liquid saturation from the following equation.²

$$s_o = \frac{c_t - c_w - c_f}{c_o - c_w} \quad (13-5)$$

Example 13-1 Analyzing Interference Test Using Type Curve Matching Technique

An interference test was conducted in an oil well. Water was injected into well 1 for 48 hr. The pressure response in well 2 (65 ft away) was observed for 148 hr. The observed pressure data are given in Table 13-1, and the known well/reservoir properties are given. Determine permeability and porosity of the formation between the two tested wells.

$p_i = 0$ psig, $t_1 = 48$ hr, $q_w = -185$ stb/day, $\beta_w = 1.00$ rb/stb, $\mu_w = 1.00$ cP, $r = 80$ ft, $c_t = 13.82 \times 10^{-6}$ psi⁻¹, $h = 55$ ft.

Table 13-1
Interference Test Data for Observation Well

t (hr)	p_w (psig)	$\Delta p = p_i - p_w$ (psig)	$\Delta t = t_1 - 48$ (hr)	Δp_{west} (psig)	$\Delta p_{\Delta t} = \Delta p_{west} - \Delta p_w$ (psig)
0	$0 = p_i$	-	-	-	-
4.5	23	-23	-	-	-
21.86	83	-83	-	-	-
30.01	96	-96	-	-	-
46.00	121	-121	-	-	-
48.00	Injection		Ends		
52.00	110	-110	4	126	16
70.00	56	-56	21	140	84
72.00	48	-48	24	142	94
92.00	33	-33	44	156	123
144.00	17	-17	93	182	165
148.00	16	-16	100	183	167

Solution Figure 13-4 shows data match points with the type curve in Figure 13-3.

The match points are:

$$(p_D)_{MP} = 0.975, \quad t_{MP} = 100 \text{ hr}, \quad (\Delta p)_{MP} = 100 \text{ psig},$$

$$(t_D/r_D^2)_{MP} = 120$$

Calculate formation permeability k and porosity from Eqs. 13-2 and 13-4:

$$k = 141.2 \frac{q_w \mu_w \beta_w (p_D)_{MP}}{h (\Delta p)_{MP}} = 141.2 \frac{185(1)(1)}{55} \times \frac{0.975}{100} = 4.63 \text{ mD}$$

$$\phi c_i = \left[\frac{0.0002637k}{\mu_w r^2} \right] \frac{(\Delta t)_{MP}}{(t_D/r_D^2)_{MP}} = \left[\frac{0.000264 \times 4.63}{65^2} \right] \times \frac{100}{120} = 2.41 \times 10^{-7} \text{ psi}^{-1}$$

$$\phi = \frac{\phi c_i}{c_i} = \frac{2.41 \times 10^{-7}}{13.82 \times 10^{-7}} = 17.44\%$$

To check the accuracy of the above method of analysis, plot $(p_{w\text{extended}} - p_w)$ versus Δt points as shown in Figure 13-4. Since the $(p_{w\text{extended}} - p_w)$ versus Δt data fall on the curve, the analyses are correct.

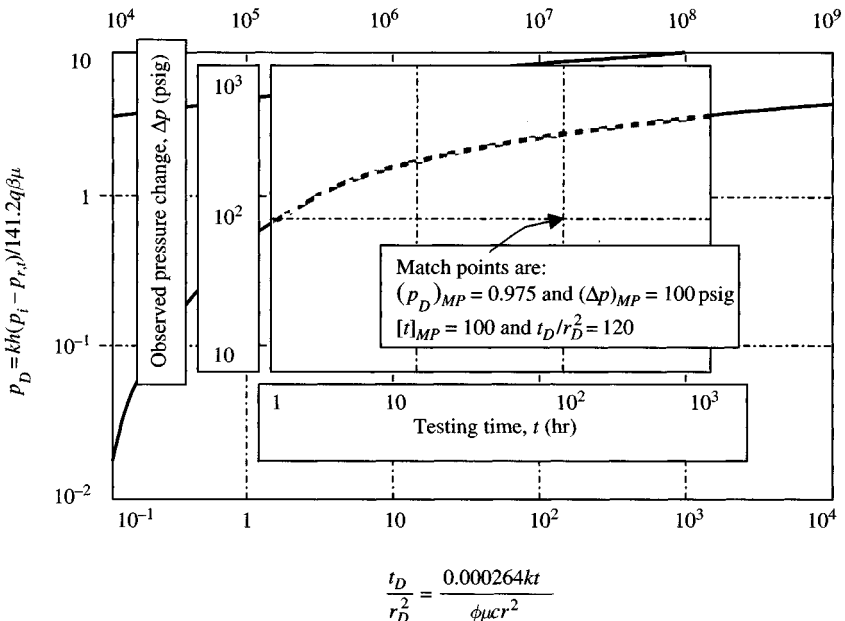


Figure 13-4. Type curve matching for an interference test.

13.3 Analysis of Pulse Test Pressure Response

Pulse tests have the same objective as conventional interference tests to determine whether well pairs are in pressure communication and to determine reservoir permeability, k , and product of ϕc_l in the area of tested wells. The tests are conducted by sending a coded signal or pulse sequence from an active well to a shut-in observation well. The pulse sequence is created by producing from (or injecting into) the active well, then shutting it in, and repeating that sequence in a regular pattern. An example is indicated in Figures 13-5 and 13-6. Highly sensitive pressure gauges usually are required to detect these small coded pulses, which may have magnitudes of less than 0.1 psi.

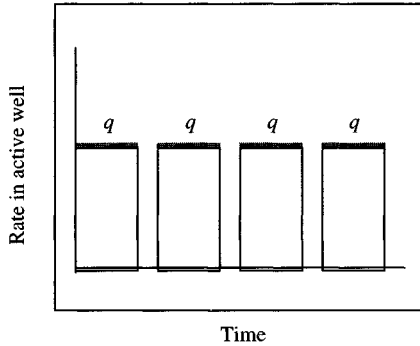


Figure 13-5. Typical rate schedules in pulse test.

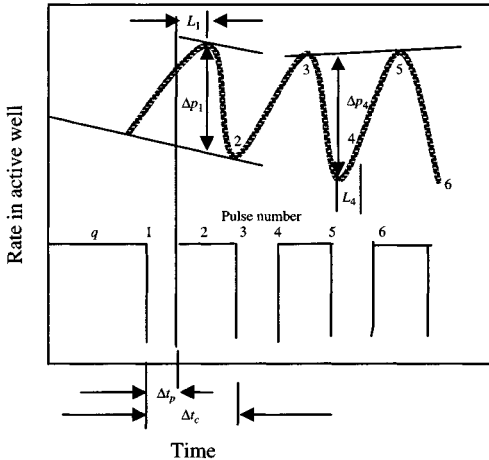


Figure 13-6. Pressure response in pulse test.

Analysis techniques for pulse tests usually are based on simulating the pressure response in an observation well with the familiar E_i -function solution to the diffusivity equation, using superposition to model the rate changes in the pulsing sequence. From the simulations of pulse tests, Kamal and Brigham¹ have developed charts relating key characteristics of the tests to reservoir properties. Before we discuss these charts (Figures 13–8 through 13–15) and their application, it will be useful to introduce nomenclature used in pulse test analysis, using the system of Earlougher³ and his schematic pulse test rate and pressure response history. Pulses can be analyzed for k and ϕc_t . It is a good idea to analyze several pulses and compare the results.

Characteristics of Pressure Response

For each pulse the pressure response (very small) at the observation well is recorded with a very sensitive pressure gauge. The pressure response in the pulse test is schematically illustrated in Figure 13–6. In pulse tests the pulses 1 and 2 have characteristics that differ from all subsequent pulses. Following these pulses, all odd pulses have similar characteristics and all even pulses also have similar characteristics. Any one of the pulses can be analyzed for k and ϕc_t . It is a good idea to analyze several pulses and compare the results.

Pulse Test Responses with Flow and Shut-In Time

Figure 13–7 shows pulse testing for a two-well system. The lower portion of the figure illustrates the pressure behavior at the observation well and correlates the pressure pulses with the rate pulses. The upper portion of the curve shows the constant production rate before the test and the rate pulses' flow time and shut-in time are equal as shown in Figure 13–7. Pulse testing can be done with unequal flow and shut-in times.

Pulse Test Analysis Method – Two-Well System

The following equations are used to calculate permeability and the porosity–compressibility product (ϕc_t):

$$k = \frac{141.2q\beta\mu}{h\Delta p} \left(\frac{\Delta p_D \left(\frac{t_L}{\Delta t_c} \right)^2}{\left(\frac{t_L}{\Delta t_c} \right)^2} \right) \quad (13-6)$$

Figures 13–8 to 13–15

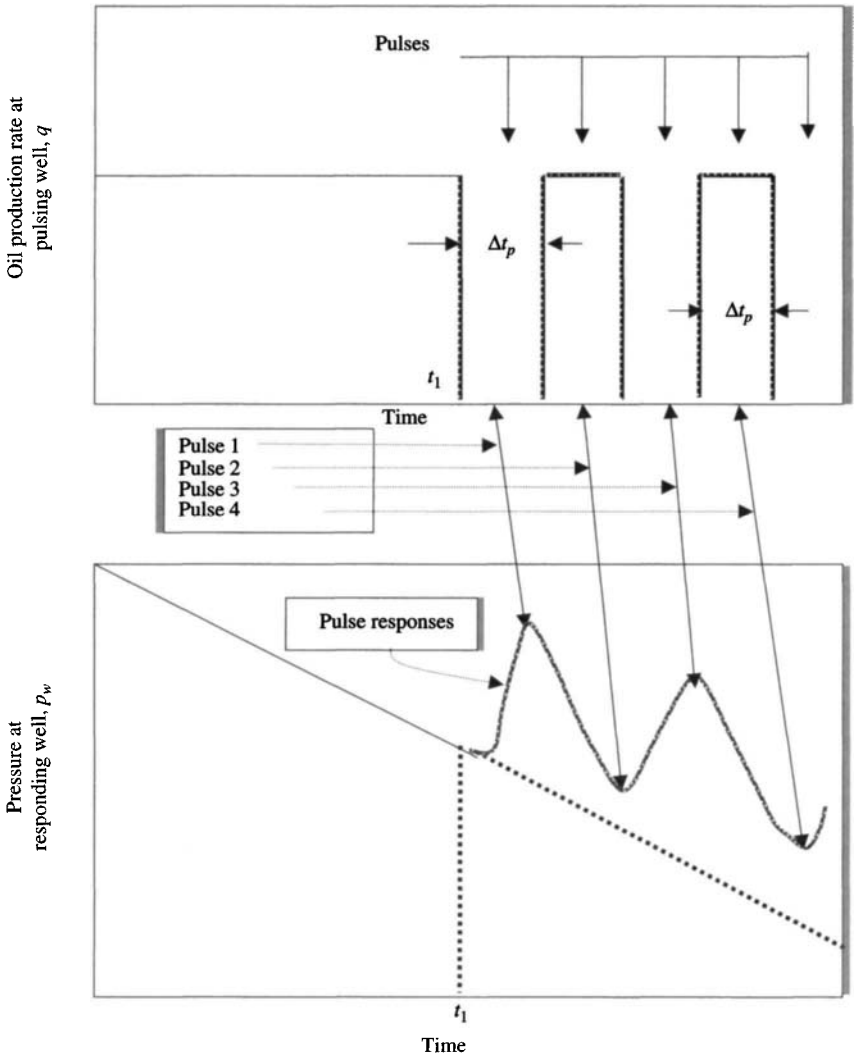


Figure 13-7. Rate history and pressure response for a pulse test (after Johnson et al., *J. Pet. Technol.*, Dec. 1966).²

$$\phi c_t = \frac{0.000264ktL}{\mu_g r^2 \left[\frac{(t_L)_D}{r_D^2} \right]} \quad (13-7)$$

Figures 13-8 to 13-15

where

Δp = amplitude of a pulse

$\Delta p = \Delta t_c$ = total cycle length (including both shut-in and flow periods)

t_L = time lag (time elapsed between the end of a pulse and the pressure peak caused by the pulse)

Δp_D = dimensionless pressure response amplitude and is equal to

$$\Delta p_D = \frac{kh\Delta p}{141.2q\mu B}$$

$(t_L)_D$ = dimensionless time lag and is given by

$$(t_L)_D = \frac{0.0002637kt_L}{\phi\mu_g c_i r_w^2}$$

$r_D = r/r_w$ = dimensionless distance between the tested wells (r_w is for observation well). The values of the terms $\Delta p_D(t_L/\Delta t_c)^2$ and $[(t_L)_D/r_D^2]$ are obtained from Figures 13–8 through 13–15. These figures use $t_L/\Delta t_c$ and $F' = \Delta t_p/\Delta t_c$, where Δt_p is the length of the pulse period. Example 13–2 illustrates how these figures are applied.

Horizontal Pulse Test Analysis Techniques

Kamal and Brigham¹ have presented a technique to analyze horizontal pulse tests, once pulse test data are available and plotted and time lags and pressure responses are measured. They provided the equations and

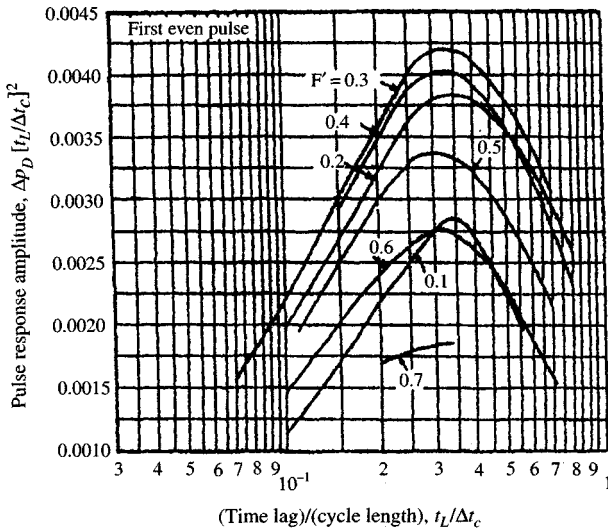


Figure 13–8. Time lag and response amplitude relationship for first odd pulse.¹

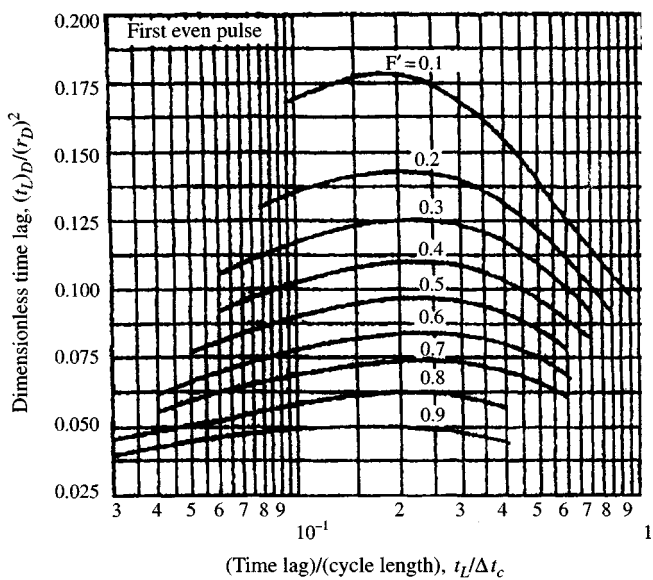


Figure 13-9. Time lag and cycle length relationship for first odd pulse.¹

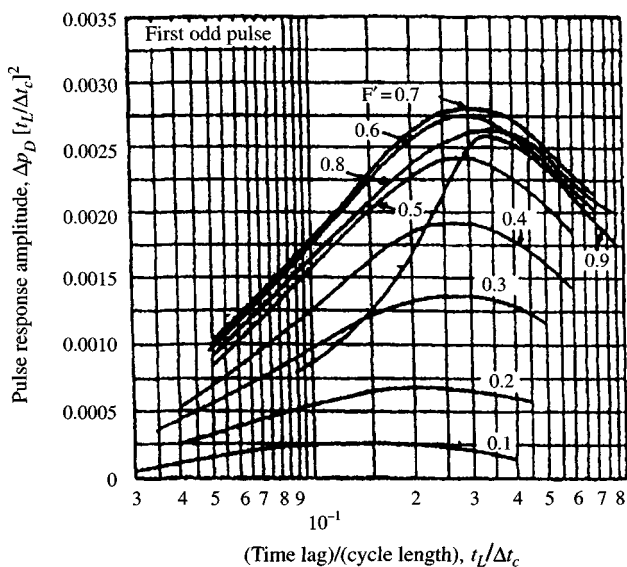


Figure 13-10. Time lag and response amplitude relationship for first even pulse.¹

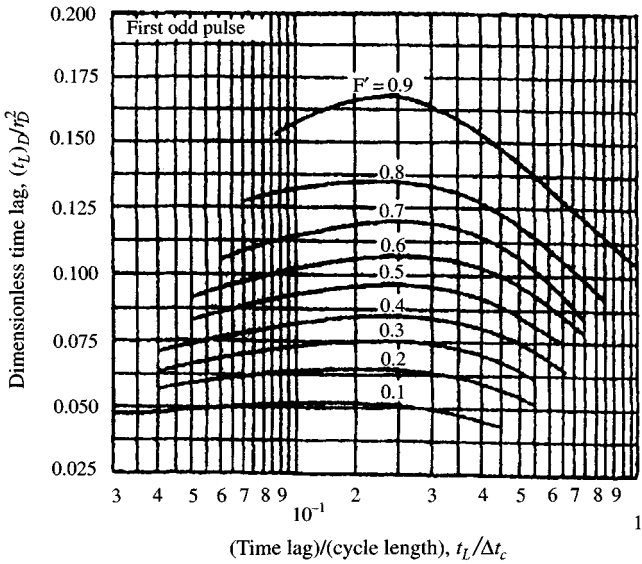


Figure 13-11. Time lag and cycle length relationship for first even pulse.¹

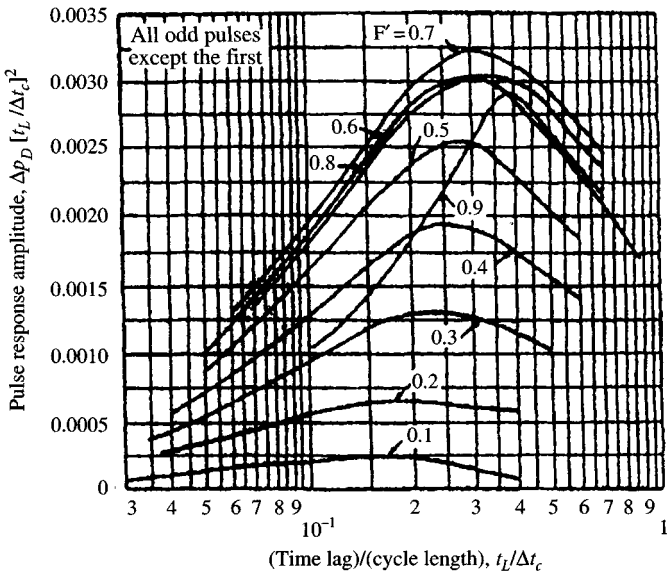


Figure 13-12. Time lag and response amplitude relationship for all odd pulses after the first.¹

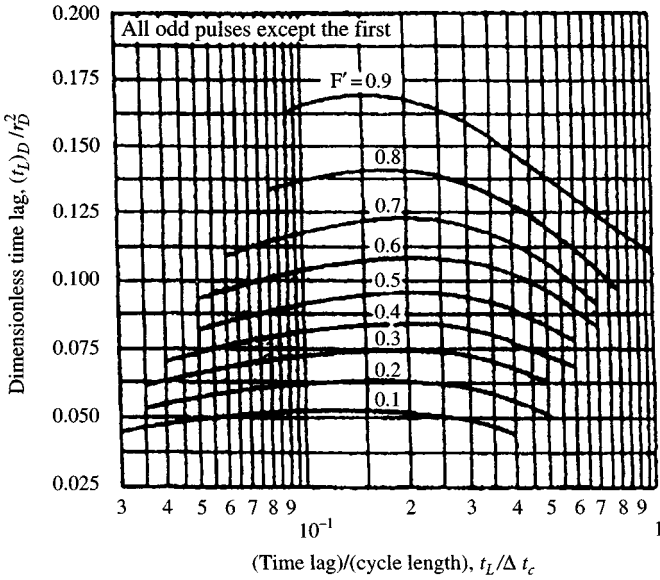


Figure 13-13. Time lag and cycle length relationship for all odd pulses after the first.¹

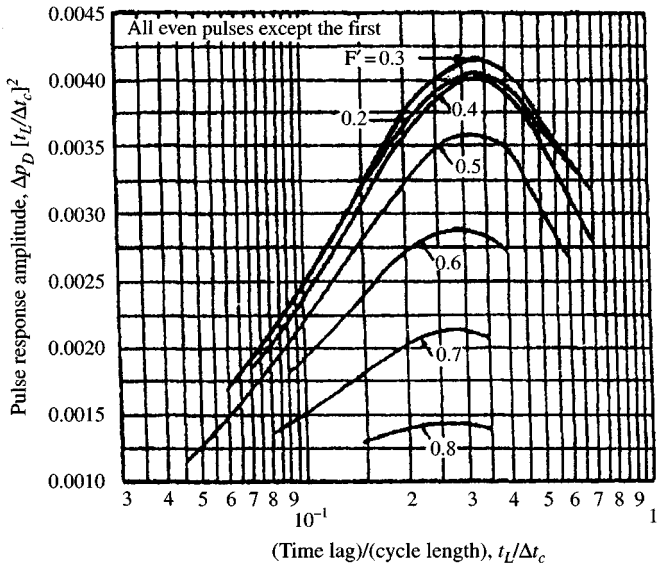


Figure 13-14. Time lag and response amplitude relationship for all even pulses after the first.¹

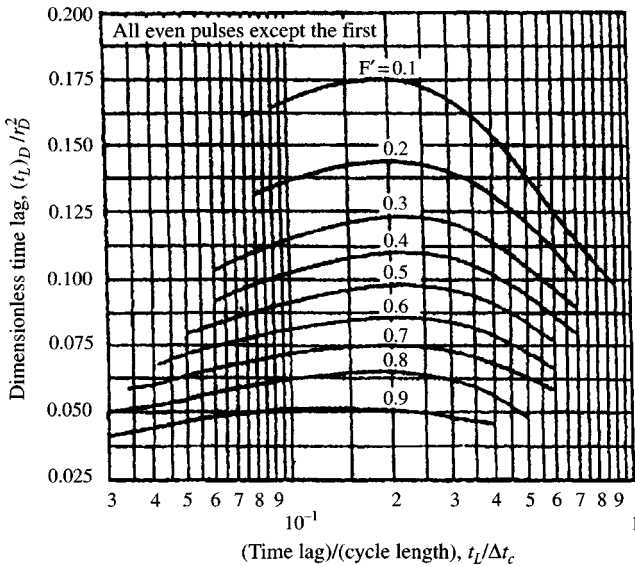


Figure 13-15. Time lag and cycle length relationship for all even pulses after the first.¹

Figures 13-8 through 13-15 to analyze pulse test rapidly. Figure 13-6 is a schematic pulse test rate and pressure history showing definition of time lag (t_L) and pulse response amplitude (Δp). This technique is rapid to analyze pulse test to get an idea of the reliability of the results.

Ratio of pulse length to the total cycle length is

$$F' = \frac{\Delta t_p}{\Delta t_c} = \frac{\text{pulse period}}{\text{pulse period} + \text{shut-in period}} \quad (13-8)$$

$$\frac{t_L}{\Delta t_c} = \frac{\text{time lag}}{\text{total cycle length}} \quad (13-9)$$

Dimensionless time lag

$$(t_L)_D = \frac{0.0002637kt_L}{\phi\mu c_r r_w^2} \quad (13-10)$$

Dimensionless distance between the active and observation wells

$$r_D = \frac{r}{r_w} \quad (13-11)$$

Dimensionless pressure response amplitude

$$\Delta p_D = \frac{kh\Delta p}{141.2q\mu\beta} \quad (13-12)$$

where q is the rate at active well.

Permeability is estimated from

$$k = \frac{141.2q\mu\beta \left\{ \Delta p_D \left[\frac{t_L}{\Delta t_c} \right] \right\}_{\text{Figures 13-8 through 13-11}}}{h\Delta p \left(\frac{t_L}{\Delta t_c} \right)^2} \quad (13-13)$$

where Δp and t_L are from the observation well response for the pulse being analyzed.

Porosity-compressibility product is estimated from

$$\phi c_t = \frac{0.0002637kt_L}{\mu r^2 \left[\left(\frac{(t_L)_D}{r_D^2} \right) \right]_{\text{Figures 13-12 through 13-15}}} \quad (13-14)$$

Formation storage is determined from

$$S = \phi c_t h \quad (13-15)$$

Hydraulic diffusivity is estimated from

$$\eta = \frac{k}{\phi c_t \mu} \quad (13-16)$$

Example 13-2 Analyzing Horizontal Pulse Test

Figures 13-16 and 13-17 show pulse test data. Two producing wells, 1 and 2, were tested by pulsing, $\Delta t_p = 1$ hr; $q = 300$ stb/day; and the response at well 2 was observed. At some other time, well 2 was tested by pulsing ($\Delta t_p = 1$ hr), $q = 310$ stb/day and response at well 1 was observed. Analyzing second peak (third pulse response) of Figures 13-16 and 13-17 for illustrations. Table 13-2 shows the pulse test data. The well/reservoir data are $q_o = 300$ stb/day; $\phi = 0.12$; $\mu_o = 1.15$ cP; $h = 62$ ft; $\beta_o = 1.252$ rb/stb; $r = 660$ ft. Estimate kh/μ and $\phi c_t h$.

Solution Find the following pulse test parameters from Figures 13-16 and 13-17:

$$\frac{\Delta p}{q} = 12.40 \times 10^{-4} \text{ psi/(stb/day)}$$

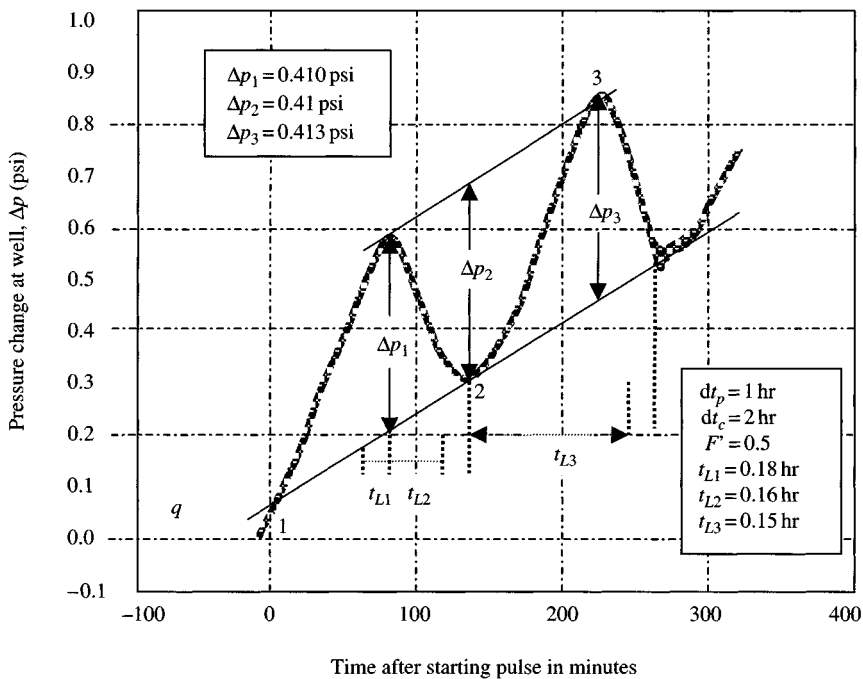


Figure 13-16. Pressure response in pulse test.

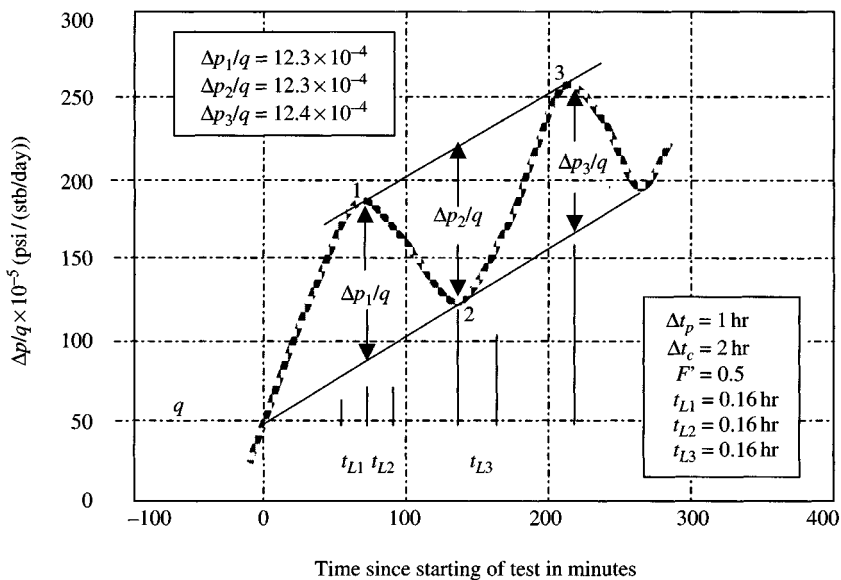


Figure 13-17. Pressure response in pulse test.

Table 13-2
Horizontal Pulse Test data

Time (min)	p_{wf} (psig)	Δp (psig)	$\Delta p/q$ (psi/(stb/day))
0.0	365.000	0.000	—
15.0	365.055	0.055	18.33×10^{-5}
19.8	365.205	0.150	50.00×10^{-5}
30.0	365.425	0.220	73.33×10^{-5}
35.0	365.725	0.300	10.00×10^{-4}
45.0	366.110	0.385	12.83×10^{-4}
50.0	366.560	0.450	15.00×10^{-4}
60.0	367.083	0.523	17.40×10^{-4}
65.0	367.683	0.600	20.00×10^{-4}
75.0	368.273	0.588	19.60×10^{-4}
90.0	368.796	0.525	17.50×10^{-4}
100.0	369.268	0.472	15.73×10^{-4}
102.0	369.668	0.400	13.33×10^{-4}
105.0	370.026	0.358	11.93×10^{-4}
120.0	370.328	0.307	10.07×10^{-4}
135.0	370.673	0.345	11.50×10^{-4}
140.0	371.183	0.430	14.33×10^{-4}
150.0	371.626	0.523	17.43×10^{-4}
155.0	372.226	0.600	20.00×10^{-4}
165.0	377.897	0.671	22.37×10^{-4}
175.0	373.647	0.750	25.00×10^{-4}
180.0	374.444	0.797	26.57×10^{-4}
195.0	375.392	0.858	28.60×10^{-4}
210.0	376.099	0.797	26.57×10^{-4}
215.0	376.819	0.720	24.00×10^{-4}
225.0	377.479	0.660	22.00×10^{-4}
230.0	378.089	-0.610	20.33×10^{-4}
240.0	378.639	0.550	18.33×10^{-4}
250.0	379.239	0.600	20.00×10^{-4}
255.0	379.828	0.589	19.63×10^{-4}
270.0	380.515	0.687	22.90×10^{-4}

and $t_L = 0.16$ hr; for these tests, $\Delta t_c = 2$ hr and $\Delta t_p = 1$ hr; thus

$$\frac{t_L}{\Delta t_c} = \frac{0.16}{2.00} = 0.08$$

Find F' from Eq. 13-8

$$F' = \frac{\Delta t_p}{\Delta t_c} = \frac{1}{2} = 0.5$$

Knowing F' and $t_L/\Delta t_c$, read $\Delta p_D[t_L/\Delta t_c]^2$ from Figure 13-9 (all even pulses except the first), which is equal to 0.00185. Then, calculate kh/μ by rearranging Eq. 13-13:

$$\frac{kh}{\mu} = \frac{141.2 \times 1.252}{12.40 \times 10^{-4}} \times \frac{0.00185}{(0.08)^2} = 41,211 \text{ mD ft/cP}$$

From Figure 13-10 (all odd pulses except the first), find $(t_L)_D/r_D^2 = 0.078$. Estimate $\phi c_i h$ using rearranged Eq. 13-14:

$$\begin{aligned} \phi c_i h &= \frac{0.0002637k}{\mu r^2} \frac{t_L}{\left| (t_L)_D / r_D^2 \right|_{\text{Figure 13-10}}} \\ &= \frac{0.0002637 \times 764.39}{1.15 \times 660^2} \times \frac{0.16}{0.078} = 8.254 \times 10^{-7} \text{ ft/psi} \end{aligned}$$

13.4 Vertical Pulse Test Design and Analysis Methods

Falade and Brigham^{4,5} have described testing and analyzing techniques based on the arrival time of the first peak. They considered the situation with perforations at the upper and lower reservoir boundaries. The next section will describe brief procedure and methods of designing and analyzing vertical pulse tests.

Vertical Pulse Test Design Calculations

Once the test well is selected, it is important to design the pulse length and magnitude to be compatible with formation characteristics and the pressure instrument resolution. The pulse duration must be long enough so that the pressure instrument detects the pulses, but short enough so that the pulses are easily identified. Table 13-3 is a test design table for vertical pulse testing.

To design a pulse test follow these steps:

- From Table 13-3, choose any reasonable value of

$$[\Delta t_{PDV}]_{\text{Table 13-3}} \text{ from column 1}$$

Find

$$\left[\frac{(t_L)_\infty}{\Delta t_p} \right]_{\text{Table 13-3}} \text{ from column 2}$$

Table 13-3
Vertical Pulse Testing Design Table⁵

Dimensionless pulse length, Δt_{PDV}	Infinite-system time lag pulse length, $\frac{(t_L)_\infty}{\Delta t_p}$	$(\Delta p_{DV})_\infty \left[\frac{(t_L)_\infty}{\Delta t_p} \right]$
0.1450	0.1000	0.0145
0.1250	0.1500	0.0155
0.1000	0.1750	0.0188
0.0900	0.1890	0.0190
0.0800	0.2200	0.0192
0.0700	0.2700	0.0193
0.0600	0.3000	0.0920
0.0500	0.3700	0.0175
0.0400	0.4800	0.0159
0.0300	0.6300	0.0137
0.0200	0.9000	0.0087
0.0100	1.6500	0.0004

and

$$(\Delta p_{DV})_\infty \left[\frac{(t_L)_\infty}{\Delta t_p} \right]_{Table\ 13-3} \quad \text{from column 3}$$

- Estimate pulse length from the following equation:

$$\Delta t_p = \frac{\phi \mu_o c_t \Delta z_R^2 (\Delta t_{PDV})_{Table\ 13-3}}{0.0002637 k_z} \quad (13-17)$$

where

Δt_p = pulse length, hour

Δz_R = distance between upper and lower of perforations, ft

k_z = vertical permeability, mD

$$= \frac{141.2 q_o \beta_o \mu_o}{\Delta z_R \Delta p} \left[(\Delta p_{PD})_\infty \right]_{Table\ 13-3} \quad (13-18)$$

- Estimate expected time lag given by

$$t_L = \left[\frac{(t_L)_\infty}{\Delta t_p} \right]_{Table\ 13-3} \quad (13-19)$$

- Calculate response amplitude by

$$\Delta p = \frac{141.2 q_o \mu_o \beta_o \left[(\Delta p_{PDV})_\infty \left[\frac{(t_L)_\infty}{\Delta t_p} \right] \right]_{Table\ 13-3}}{k_r \Delta z_R \left[\frac{(t_L)_\infty}{\Delta t_p} \right]_{Table\ 13-3}} \quad (13-20)$$

where

Δp = pressure gauge should be chosen appropriately, psi
 k_r = horizontal permeability, mD

$$= \frac{141.2q_o\mu_o\beta_o}{\Delta z_r\Delta p} [(\Delta p_{PDV})_\infty]_{Table\ 13-3} \quad (13-21)$$

- Calculate geometric factor such as

$$G_p = \frac{\Delta z_p}{\Delta z_r} \quad (13-22)$$

and

$$G_R = \left(\frac{h}{\Delta z_r} - G_p - 1 \right) \quad (13-23)$$

where

G_p = primal geometric factor
 G_R = reciprocal geometric factor
 Δz_R = vertical distance from upper formation boundary to center of upper perforations, ft.

Figure 13-18 shows vertical interference and pulse test nomenclature.

Example 13-3 Designing Vertical Pulse Test

Given data are: $k_z \approx 1.0$ mD; $k_r = 10$ mD; $\phi = 0.15$; $\mu = 1.85$ cP; $c_t = 1.2 \times 10^{-5}$ psi⁻¹; $\Delta z_R = 45$ ft; $\beta = 1.0$ rb/stb. Design a pulse test using Table 13-6.

Solution From Table 13-3, choose a reasonable value such as 0.04 from column 1 and find the other values of parameters from columns 3 and 2:

$$(\Delta t_{PDV})_{Table\ 13-3} = 0.04 \text{ (column 1)}$$

$$(\Delta p_{PDV})_\infty \left[\frac{(t_L)_\infty}{\Delta t_p} \right]_{Table\ 13-3} = 0.0159 \text{ (column 3)}$$

$$\left[\frac{(t_L)_\infty}{\Delta t_p} \right]_{Table\ 13-3} = 0.48 \text{ (column 2)}$$

From Eq. 13-17, find

$$\Delta t_p = \frac{\phi\mu c_t\Delta z_R^2(\Delta t_{PDV})_{Table\ 13-3}}{0.0002637k_z} \approx 1.03 \text{ hr}$$

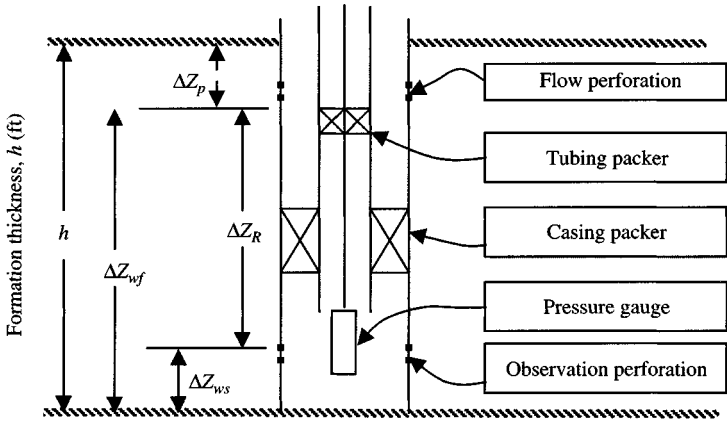


Figure 13-18. Vertical interference and pulse test nomenclature.^{4,5}

Calculate time lag from Eq. 13-19:

$$t_L = \left[\frac{(t_L)_\infty}{\Delta t_p} \right] \Delta t_p = 0.48 \times 1.03 \approx 0.49 \text{ hr}$$

Estimate response amplitude from Eq. 13-20:

$$\Delta p = \frac{141.2q\mu\beta}{k_r\Delta Z_R} \left[\frac{\text{column 3}}{\text{column 2}} \right]_{\text{Table 13-3}} = \frac{141.2 \times 1.85 \times 1.0}{10 \times 45} \times \frac{0.0159}{0.48} q \approx 0.0192q \text{ psi}$$

Thus, for an injection (or production) rate of 450 stb/day, we would expect a pressure change of about:

$$\Delta p = (0.0192)(450) = 8.64 \text{ psi}$$

Hence the pressure gauge should be chosen appropriately.

13.5 Design and Analysis of Unequal Pulses

Kamal and Brigham¹ and Johnson et al.² have presented new methods to analyze pulse tests with unequal pulse and shut-in periods. These methods allow the engineer to design and analyze pulse tests simply and accurately. These methods will enable the use of pulse tests without limitations on the

length of the different periods. Thus, the optimum ratio between the pulse and shut-in periods that gives the maximum pulse test response can be used. Figure 13-19 shows the pulse test terminology. To design and analyze any well test is simply to relate the test parameters to the reservoir and well properties. In the case of pulse testing, the test parameters are:

- pulse period,
- the shut-in period,
- the time lags, and
- the response amplitude.

The reservoir properties are:

- formation permeability,
- porosity and thickness,
- fluid viscosity,
- the total compressibility, and
- the distance between the pulsing and responding wells.

The reservoir properties and the test parameters can be used to design the following dimensionless groups.

Pulse ratio:

$$R' = \frac{\Delta t}{\Delta t + R\Delta t} = \frac{\Delta t}{\Delta t_{cyc}} \quad (13-24)$$

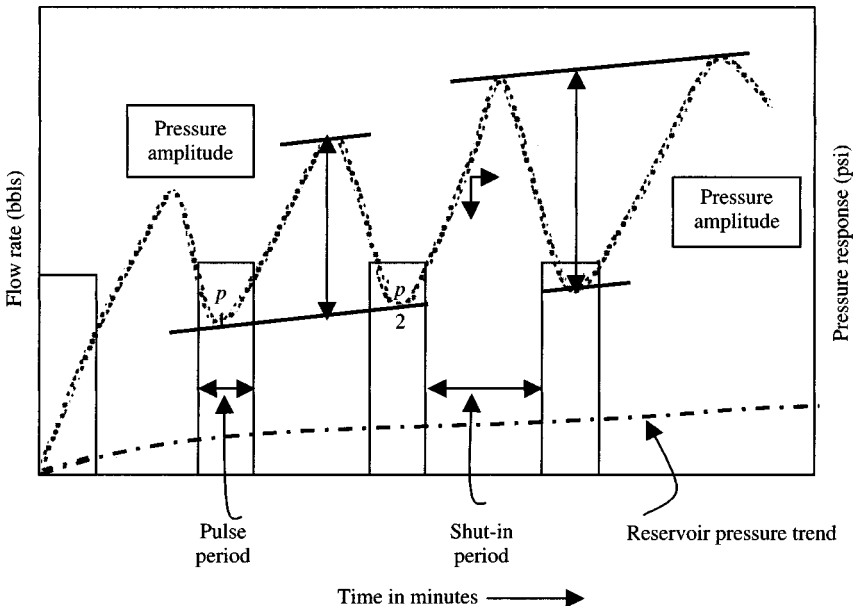


Figure 13-19. Pulse test terminology.

Dimensionless cycle period:

$$\Delta t_{cycD} = \frac{k\Delta t_{cyc}}{56,900\phi\mu_o c_t r_{pr}^2} \quad (13-25)$$

Dimensionless time lag:

$$t_{LD} = \frac{t_L}{\Delta t_{cyc}} = \frac{t_L}{\Delta t(1+R)} \quad (13-26)$$

Dimensionless response amplitude:

$$\Delta p_D = \frac{kh\Delta p}{70.6\mu_o\beta_o q_o} \quad (13-27)$$

where

R' = pulse ratio

Δt = pulse period

$R'R\Delta t$ = shut-in period

R = ratio between pulse period and shut-in period

Δt_{cycD} = dimensionless cycle period

Δt_{cyc} = cycle period = $\Delta t(1 - R)$, min

r_{pr} = distance between the pulsing and the responding wells, ft

t_{LD} = dimensionless time lag

t_L = time lag, min

μ_o = oil viscosity, cP

ϕ = porosity, fraction

Δp_D = dimensionless response amplitude

Δp = response amplitude, psi

h = formation thickness, ft

k = permeability, mD.

The above equations relating to the time lag, using the unsteady-state flow model of the line source for an infinite-acting, homogeneous reservoir containing a single-phase slightly compressible fluid developed the cycle period and the response amplitude for any pulse ratio. The equation relating the dimensionless cycle period to the dimensionless time lag is

$$\Delta t_{cycD} = Ct_{LD}^A + D \quad (13-28)$$

where

$D = -0.325$ for odd pulses and

$D = -0.675$ for even pulses.

A and C are functions of the pulse ratio. The values of these functions are given in Tables 13-4 and 13-5. The equation relating the dimensionless time lag and the dimensionless response amplitude is

Table 13-4
Values of Parameter A as a Function of the Pulse Ratio¹

Pulse ratio, R'	1st even pulse	All other even pulses	1st odd pulse	All other odd pulses
0.20	-0.795	-0.805	-0.825	-0.812
0.25	-0.779	-0.779	-0.828	-0.815
0.30	-0.763	-0.752	-0.830	-0.818
0.35	-0.747	-0.745	-0.835	-0.826
0.40	-0.730	-0.738	-0.839	-0.833
0.45	-0.708	-0.727	-0.847	-0.841
0.50	-0.691	-0.715	-0.854	-0.849
0.55	-0.683	-0.708	-0.858	-0.861
0.60	-0.675	-0.700	-0.864	-0.873
0.65	-0.665	-0.698	-0.874	-0.884
0.70	-0.655	-0.695	-0.885	-0.895
0.75	-0.650	-0.689	-0.858	-0.915
0.80	-0.645	-0.682	-0.930	-0.935

Table 13-5
Values of Parameter C as a Function of the Pulse Ratio¹

Pulse ratio, R'	1st even pulse	All other even pulses	1st odd pulse	All other odd pulses
0.20	0.955	0.950	0.432	0.432
0.25	0.942	0.936	0.452	0.453
0.30	0.928	0.921	0.471	0.473
0.35	0.905	0.898	0.493	0.496
0.40	0.882	0.875	0.515	0.518
0.45	0.864	0.850	0.539	0.542
0.50	0.845	0.825	0.562	0.565
0.55	0.824	0.803	0.581	0.587
0.60	0.802	0.781	0.600	0.609
0.65	0.776	0.753	0.618	0.628
0.70	0.750	0.725	0.635	0.647
0.75	0.725	0.695	0.643	0.657
0.80	0.700	0.665	0.650	0.667

$$\frac{\Delta p_D}{\Delta t_{\text{cyc}D}} = H[F \exp(Et_{LD}) + 0.01] \quad (13-29)$$

where

$H = -1$ for odd pulses and

$H = 1$ for even pulses.

E and F are functions of the pulse ratio. The values of these functions are given in Tables 13-6 and 13-7.

where

$$R' = \text{pulse ratio} = \frac{\Delta t}{\Delta t_{cyc}}$$

Δt = pulse period and Δt_{cyc} = cycle period.

Table 13-6
Values of Parameter E as a Function of the Pulse Ratio¹

Pulse ratio, R'	1st even pulse	All other even pulses	1st odd pulse	All other odd pulses
0.20	-3.100	-3.259	-8.000	-8.221
0.25	-3.125	-3.258	-6.250	-6.505
0.30	-3.150	-3.265	-5.000	-5.482
0.35	-3.186	-3.330	-4.751	-5.005
0.40	-3.221	-3.395	-4.502	-4.250
0.45	-3.348	-3.448	-4.354	-4.486
0.50	-3.425	-3.500	-4.205	-4.221
0.55	-3.540	-3.628	-4.080	-4.058
0.60	-3.604	-3.755	-3.953	-3.895
0.65	-3.878	-3.984	-3.902	-3.826
0.70	-4.152	-4.213	-3.850	-3.756
0.75	-4.380	-4.359	-3.829	-3.711
0.80	-4.607	-4.504	-3.807	-3.665

Table 13-7
Values of Parameter F as a Function of the Pulse Ratio¹

Pulse ratio, R'	1st even pulse	All other even pulses	1st odd pulse	All other odd pulses
0.20	0.0925	0.0867	0.0749	0.0775
0.25	0.1050	0.0975	0.0884	0.0975
0.30	0.1195	0.1075	0.0975	0.1000
0.35	0.1288	0.1150	0.1040	0.1105
0.40	0.1320	0.1220	0.1100	0.1162
0.45	0.1346	0.1245	0.1139	0.1201
0.50	0.1350	0.1248	0.1164	0.1225
0.55	0.1325	0.1225	0.1150	0.1223
0.60	0.1300	0.1175	0.1126	0.1202
0.65	0.1225	0.1085	0.1072	0.1172
0.70	0.1140	0.0975	0.0995	0.1090
0.75	0.0950	0.0804	0.0886	0.0950
0.80	0.0600	0.0643	0.0775	0.0845

Pulse Test Designing Methods

Pulse tests can be designed graphically and analytically.

Designing Pulse Test Graphically¹

The following steps are used in designing pulse test graphically:

- Select the pulse ratio. If a specific pulse ratio¹, R' , is more convenient for oilfield operation, this ratio should be used; otherwise a pulse ratio near 0.7 (odd) or 0.3 (even) is recommended, depending on whether the odd pulse or the even pulse will be used to analyze the results of the test. The pulse ratio should not be below 0.2 or above 0.8.
- Calculate the dimensionless time lag, t_{LD} , using equation

$$t_{LD} = 0.09 + 0.3R' \quad (\text{odd pulses}) \quad (13-30)$$

$$\text{or } t_{LD} = 0.09 \times 0.3(1 - R') \quad (\text{even pulses}) \quad (13-31)$$

- Determine the dimensionless cycle period, Δt_{cycD} , using the dimensionless time lag and the appropriate curve in Figure 13-9, 13-11, 13-13, or 13-15.
- Determine the dimensionless amplitude, Δp_D , using the appropriate curve in Figure 13-8, 13-10, 13-12, or 13-14.
- Calculate the cycle period using the equation

$$\Delta t_{cyc} = \frac{56,900\phi\mu_o c_t r_{pr}^2 \Delta t_{cycD}}{k} \quad (\text{min}) \quad (13-32)$$

- Calculate the pulse period as

$$\Delta t = R' \Delta t_{cyc} \quad (\text{min}) \quad (13-33)$$

- Calculate the shut-in period, $R\Delta t$, as

$$R\Delta t = (\Delta t_{cyc} - R' \Delta t_{cyc}) \quad (\text{min}) \quad (13-34)$$

- Calculate response amplitude, Δp , by rearranging Eq. 13-27

$$\Delta p = \frac{70.6q_o\mu_o\beta_o\Delta p_D}{kh} \quad (13-35)$$

The following examples will illustrate the design and analysis techniques for pulse tests.

Example 13-4 *Designing Pulse Test Using Graphical Method*

The reservoir has the following properties:

$$h = 50 \text{ ft}, \quad k = 250 \text{ mD}, \quad \phi = 0.18,$$

$$r_{pr} = 660 \text{ ft}, \quad \mu_o = 1.750 \text{ cP},$$

$$\beta_o = 1.126 \text{ rb/stb}, \quad c_t = 2.5 \times 10^{-5} \text{ psi}^{-1}$$

Production rate = 200 bbl/day. Assume most convenient pulse ratio, R' , to be 0.65.

Solution Since the optimum pulse ratio is 0.65, the odd pulse should be used rather than the even pulse. Follow these steps:

- Calculate the dimensionless time lag from Eq. 13-30:

$$t_{LD} = 0.09 + 0.3R' = 0.90 + 0.3(0.65) = 0.285$$

- Determine the dimensionless cycle period, Δt_{cycD} , such as using first odd pulse at $R' = 0.65$ and $t_{LD} = 0.285$:

$$\Delta t_{cycD} \times t_{LD} = 0.45, \quad \Delta t_{cycD} = \frac{0.45}{0.285} = 1.579$$

- Determine the dimensionless response amplitude, Δp_D , at $R' = 0.65$ and $t_{LD} = 0.285 \Rightarrow \Delta p_D \times t_{LD}^2 = -0.0057$; then

$$\Delta p_D = \frac{-0.0057}{0.285^2} = -0.0702$$

- Calculate the cycle period, Δt_{cycD} , from Eq. 13-32:

$$\begin{aligned} \Delta t_{cyc} &= \frac{56,900 \phi \mu_o c_t r_{pr}^2 \Delta t_{cycD}}{k} \\ &= \frac{56,900(0.18)(2.5 \times 10^{-5})(1.75)(660)^2}{250} = 781 \text{ min} \end{aligned}$$

- Calculate the pulse period using Eq. 13-33:

$$\Delta t = R' \Delta t_{cyc} = 0.65 \times 781 = 508 \text{ min}$$

- Estimate the shut-in period using Eq. 13-34:

$$R \Delta t = \Delta t_{cyc} - \Delta t = 781 - 508 = 200 \text{ min}$$

- Calculate the response amplitude Δp from Eq. 13–35:

$$\begin{aligned}\Delta p &= \frac{70.6q_o\mu_o\beta_o\Delta p_D}{kh} \\ &= \frac{70.6(1.126)(1.75)(200)}{250(50)} \times (-0.0702) = -0.156 \text{ psi}\end{aligned}$$

Designing Pulse Tests Analytically

Follow these steps:

- Select the pulse ratio as in the graphical method.
- Calculate the dimensionless time lag using Eq. 13–30 or 13–31.
- Find the values of parameters A and C using Tables 13–4 and 13–5.
- Find the values of parameters E and F using Tables 13–6 and 13–7.
- Calculate the dimensionless cycle period using Eq. 13–28.
- Calculate the dimensionless response amplitude using Eq. 13–29.
- Calculate the cycle period and response amplitude using Eqs. 13–25 and 13–27.

Example 13–5 *Designing Pulse Test Using Analytical Method*

Rework Example 13–4 using analytical method.

Solution Since the optimum pulse ratio is 0.65, the odd pulse should be used rather than the even pulse. Follow these steps:

- Calculate the dimensionless time lag from Eq. 13–30:

$$t_{LD} = 0.09 + 0.3R' = 0.90 + 0.3(0.65) = 0.285$$

- Calculate the dimensionless cycle period using Eq. 13–28:

$$\Delta t_{cycD} = Ct_{LD}^A + D \quad (\text{for odd pulses})$$

$$D = -0.325$$

$$C = 0.628 \quad (\text{from Table 13–5})$$

$$A = -0.884 \quad (\text{from Table 13–4})$$

Substituting these values in Eq. 13–28, we get

$$\Delta t_{cycD} = 0.628(0.285)^{-0.884} + (-3.25) = 1.580$$

- Calculate the dimensionless response amplitude, Δp_D , from Eq. 13–29:

$$\frac{\Delta p_D}{\Delta t_{cycD}} = H[F \exp(Et_{LD}) + 0.01]$$

For odd pulses

$$H = -1$$

$$F = 0.1172 \quad (\text{from Table 13-7})$$

$$E = -3.826 \quad (\text{from Table 13-6})$$

Substituting these values in Eq. 13–29, we get

$$\frac{\Delta p_D}{\Delta t_{cycD}} = -1[0.1172 \exp(-3.826 \times 0.285) + 0.01] = -0.0494$$

Therefore, $\Delta p_D = -0.0494 \times 1.580 = -0.078$.

- Calculate the cycle period, Δt_{cycD} , from Eq. 13–32:

$$\Delta t_{cycD} = \frac{k\Delta t_{cyc}}{56,900\phi c_i\mu r^2} \quad \text{After rearranging, we get}$$

$$\begin{aligned} \Delta t_{cyc} &= \frac{56,900\phi c_i\mu r^2}{k} \Delta t_{cycD} = \frac{56,900 \times 0.18 \times 2.5 \times 10^{-5} \times 1.75 \times 660^2}{250} \\ &= 781 \text{ min} \cong 800 \text{ min} \end{aligned}$$

- Calculate the pulse period using Eq. 13–33:

$$\Delta t = R'\Delta t_{cyc} = 0.65 \times 800 = 520 \text{ min}$$

The shut-in period = $800 - 520 = 280$ min

- Calculate the shut-in period using Eq. 13–34:

$$R\Delta t = \Delta t_{cyc} - \Delta t = 800 - 520 = 280 \text{ min}$$

- Calculate the dimensionless response amplitude, Δp_D , from Eq. 13–35:

$$\Delta p_D = \frac{kh\Delta p}{70.6\mu\beta q}$$

where

$$\Delta p_D = \frac{(t_{LD})}{(t_{LD})^2} = \frac{-0.0056}{(0.285)^2} = -0.0689$$

Therefore

$$\begin{aligned} \Delta p &= \frac{70.6q_o\mu_o\beta_o\Delta p_D}{kh} \\ &= \frac{70.6(200)(1.75)(1.126)}{250(50)} \times (-0.0689) = -0.1534 \text{ psi} \end{aligned}$$

This is in good agreement with the graphical method.

Note: The difference between the two values of Δp calculated using graphical and analytical methods is less than 1.7%.

Pulse Test Analysis Methods

Analyzing Pulse Test Using Graphical Method

After running the test, drawing the slopes, and measuring the time lags and the response amplitudes, the following method may be used to determine the values of kh/μ and $\phi c_i h$.

- Calculate the dimensionless time lag using Eq. 13–26:

$$t_{LD} = \frac{t_L}{\Delta t_{cyc}}$$

- Determine the dimensionless cycle period using the dimensionless time lag and the appropriate curve in Figures 13–9, 13–11, 13–13, and 13–15.
- Determine the dimensionless response amplitude using the dimensionless time lag and the appropriate curve in Figures 13–8, 13–10, 13–12, and 13–14.
- Calculate the value of kh/μ from Eq. 13–27:

$$\frac{kh}{\mu} = \frac{70.6\beta q\Delta p_D}{\Delta p} \quad (\text{mD ft/cP})$$

- Calculate the value of $\phi c_i h$ using Eq. 13–32:

$$\phi c_i h = \frac{kh}{56,900\mu r^2} \frac{\Delta t_{cyc}}{\Delta t_{cycD}} \quad (\text{ft/psi})$$

Example 13-6 *Analyzing Pulse Test Using Graphical Method*

Rework Example 13-4. The following information is obtained from pulse test: $\Delta p = -0.30$, $t_L = 210$, and $\Delta t_{cyc} = 700$ min.

Solution Optimum pulse ratio, $R' = 0.65$.

- Calculate the dimensionless time lag from Eq. 13-26:

$$t_{LD} = \frac{t_L}{\Delta t_{cyc}} = \frac{210}{700} = 0.30$$

- Knowing R' and t_{LD} , find the value of $\Delta t_{cycD} \times t_{LD} = 0.45$; then, determine the dimensionless response cycle period, $\Delta t_{cycD} = 0.45/0.3 = 1.5$.
- Estimate the dimensionless response amplitude:

$$\Delta p_D = \frac{(-0.0063)}{0.3^2} = -0.070$$

- Calculate the value of kh/μ using Eq. 13-27:

$$\begin{aligned} \frac{kh}{\mu} &= \frac{70.6\beta q \Delta p_D}{\Delta p} = \frac{70.6(1.126)(200)(-0.070)}{-0.25} \\ &= 4451.75 \text{ mD ft/cP} \end{aligned}$$

- Calculate the value of $\phi c_i h$ after rearranging Eq. 13-25:

$$\begin{aligned} \phi c_i h &= \frac{kh}{56,900\mu r^2} \frac{\Delta t_{cyc}}{\Delta t_{cycD}} = \frac{4451.75}{56,900 \times 660^2} \times \frac{700}{1.5} \\ &= 8.38 \times 10^{-6} \text{ ft/psi} \end{aligned}$$

Analyzing Pulse Test Using Analytical Method

The following steps are used to analyze pulse test analytically:

- Calculate the dimensionless time lag using Eq. 13-26:

$$t_{LD} = \frac{t_L}{\Delta t_{cyc}}$$

- Calculate the dimensionless cycle period using Eq. 13-28:

$$\Delta t_{cycD} = Ct_{LD}^A + D$$

- Determine the dimensionless response amplitude using Eq. 13–29:

$$\frac{\Delta p_D}{\Delta t_{cycD}} = H[F \exp(Et_{LD}) + 0.01]$$

- Calculate the value of kh/μ from Eq. 13–27:

$$\frac{kh}{\mu} = \frac{70.6\beta q \Delta p_D}{\Delta p} \quad (\text{mD-ft/cP})$$

- Calculate the value of $\phi c_i h$ using Eq. 13–25:

$$\phi c_i h = \frac{kh}{56,900\mu r^2} \frac{\Delta t_{cyc}}{\Delta t_{cycD}} \quad (\text{ft/psi})$$

Example 13–7 Analyzing Pulse Test Using Analytical Method

Rework Example 13–4. Optimum pulse ratio, R' , is 0.65 and pulse test shows the following information: $\Delta p = -0.25$, $t_L = 210$ min, and $\Delta t_{cyc} = 700$ min.

Solution

- Calculate the dimensionless time lag using Eq. 13–26:

$$t_{LD} = \frac{t_L}{\Delta t_{cyc}} = \frac{210}{700} = 0.3$$

- Calculate the dimensionless cycle period using Eq. 13–28:

$$\Delta t_{cycD} = Ct_{LD}^A + D$$

where

$$D = -0.325$$

$$C = 0.628 \quad (\text{from Table 13–5})$$

$$A = -0.884 \quad (\text{from Table 13–4}).$$

Substituting the values of D , C , and A in Eq. 13–28, we get

$$\Delta t_{cycD} = 0.628(0.3)^{-0.884} + (-0.325) = 1.4955$$

- Determine the dimensionless response amplitude using Eq. 13–29:

$$\frac{\Delta p_D}{\Delta t_{cycD}} = H[F \exp(Et_{LD}) + 0.01]$$

where

$$H = -1$$

$$F = -0.1172 \text{ (from Table 13-7)}$$

$$E = -3.826 \text{ (from Table 13-6).}$$

Substituting the values of H , F , and E in Eq. 13-29, we get

$$\frac{\Delta p_D}{\Delta t_{cycD}} = -1[0.1172 \exp(-3.826 \times 0.3) + 0.01] = -0.0472$$

Therefore, $\Delta p_D = 1.4955(-0.0472) = -0.071$.

- Calculate the value of kh/μ from Eq. 13-27:

$$\begin{aligned} \frac{kh}{\mu} &= \frac{70.6(1.26)(200)(-0.071)}{(-0.25)} \\ &= 5052.7 \text{ mD-ft/cP} \end{aligned}$$

- Calculate the value of $\phi c_i h$ using Eq. 13-25:

$$\begin{aligned} \phi c_i h &= \frac{kh}{56,900\mu r^2} \frac{\Delta t_{cyc}}{\Delta t_{cycD}} \\ &= \frac{5052.7}{56,900(660)^2} \times \frac{700}{1.4955} = 9.54 \times 10^{-5} \text{ ft/psi} \end{aligned}$$

Note: The difference between the two values of kh/μ calculated using graphical and analytical methods is less than 0.90%. For the value of $\phi c_i h$, the difference is 0.88%.

Example 13-8 Analyzing Pulse Test from Field Data

The pulse test was run in an oilfield, the distance from the pulsing well 1 to the responding well 4 is 660 ft. The reservoir properties are: $\phi = 0.19$; $h = 110$ ft; $\mu = 1.350$ cP; $\beta = 1.257$ rb/stb; $c_t = 1.915 \times 10^{-6}$ psi⁻¹. Test parameters are:

$$\Delta q = 750 \text{ stb/day}$$

$$\Delta t = \Delta t_1 = 180 \text{ hours (pulse period)}$$

$$\Delta t_{cyc} = \Delta t_2 = 950 \text{ hours (cycle period)}$$

$$t_L = 360 \text{ hours (time lag)}$$

$$\Delta p = -2.5 \text{ psi (response amplitude)}$$

Estimate kh/μ and the product $\phi c_i h$

Solution From Eq. 13-24, the pulse ratio is

$$R' = \frac{\Delta t}{\Delta t + R\Delta t} = \frac{\Delta t}{\Delta t_{cyc}} = \frac{180}{950} \cong 0.19$$

The value of R' is outside the range of analytical method. Therefore, graphical method can be used. Time lag, $t_L = 360$ hours; then using Eq. 13-26

$$t_{LD} = \frac{t_L}{\Delta t_{cyc}} = \frac{360}{950} = 0.379$$

From Figure 13-19 (use first even pulse), find $\Delta t_{cyc} t_{LD}$ at $t_{LD} = 0.379$ and $R' = 0.19$:

$$\Delta t_{cyc} t_{LD} = 0.530$$

Then

$$\Delta t_{cycD} = \frac{0.530}{t_{LD}} = \frac{0.530}{0.379} = 1.398$$

Find $\Delta p_D t_{LD}^2$:

$$\Delta p_D t_{LD}^2 = 0.0075 \quad (\text{at } t_{LD} = 0.379 \text{ and } R' = 0.19)$$

Then

$$\Delta p_D = \frac{0.0075}{t_{LD}^2} = \frac{0.0075}{(0.379)^2} = 0.0522$$

Calculate kh/μ from Eq. 13-27:

$$\frac{kh}{\mu} = 70.6q\beta \frac{\Delta p_D}{\Delta p} = 70.6(750)(1.257) \frac{0.0522}{-2.5} = 1389.73 \text{ mD ft/cP}$$

$$kh = \frac{kh}{\mu} \mu = 1389.73 \times 1.35 = 1876.14 \text{ mD ft,}$$

$$k = \frac{kh}{h} = \frac{1876.14}{110} = 17.1 \text{ mD}$$

Estimate $\phi c_t h$ from Eq. 13-25:

$$\begin{aligned} \phi c_t h &= \frac{kh}{\mu} \frac{1}{56,900} \frac{\Delta t_{cyc}}{\Delta t_{cycD}} = 1389.73 \frac{1}{56,900 \times 660^2} \times \frac{950}{1.398} \\ &= 3.81 \times 10^{-5} \text{ ft/psi} \end{aligned}$$

Check the results:

$$c_t \cong \frac{\phi c_i h}{\phi h} \cong \frac{3.81 \times 10^{-5}}{0.19 \times 110} = 1.823 \times 10^{-6} \text{ psi}^{-1} \quad (\text{close enough})$$

13.6 Summary

This chapter reviews interference and pulse tests, also known as multiple-well testing. These types of tests can be used to obtain an adequate reservoir description for homogeneous (both isotropic and anisotropic) and heterogeneous systems. Numerical solutions must be used to analyze pressure transient data from heterogeneous reservoir systems. At the same time, it is one of the most important and useful tests to understand the well behavior in a water flood and EOR projects.

References

1. Kamal, M., and Brigham, W. E., "Pulse Testing Response for Unequal Pulse and Shut-In Periods," *Soc. Pet. Eng. J.* (Oct. 1975), 399–410; *Trans. AIME* 259.
2. Johnson, C. R., Greenhorn, R. A., and Woods, E. G., "Pulse Testing: A New Method for Describing Reservoir Flow Properties Between Wells," *J. Pet. Technol.* (Dec. 1966), 1599–1604, *Trans. AIME* 237.
3. Earlougher, R. C., Jr., *Advances in Well Test Analysis*, Society of Petroleum Engineers, Dallas, TX, 1977.
4. Falade, G. K., and Brigham, W. E., "The Dynamics of Vertical Pulse Testing in a Slab reservoir," paper SPE 5055A presented at the SPE-AIME 49th Annual Fall Meeting, Houston, Oct. 6–9, 1974.
5. Falade, G. K., and Brigham, W. E., "The Analysis of Single-Well Pulse Tests in a Finite-Acting Slab Reservoir," paper SPE 5055B presented at the SPE-AIME 49th Annual Fall Meeting, Houston, Oct. 6–9, 1974.

Additional Reading

1. Mueller, T. D., and Witherspoon, P. A., "Pressure Interference Effects Within Reservoirs and Aquifers," *J. Pet. Technol.* (April 1965), 471–474; *Trans. AIME* 234.
2. Wattenbarger, R. A., and Ramey, H. J., "Well Test Interpretation of Vertical Fractured Gas Wells," *J. Pet. Technol.* (May 1969), 625–632.

Chapter 14

Injection Well Transient Testing and Analysis

14.1 Introduction

This chapter presents pressure analysis techniques in injection wells. The injectivity test and the fall-off tests are used to estimate the reservoir properties of injection wells in waterflood and tertiary recovery projects. The knowledge of reservoir properties and near wellbore conditions in injection wells is as important as in the producing wells. Injection well transient testing and analysis are simple as long as the mobility ratio between the injected and in-situ fluids is about unity and the radius of investigation is not beyond the water (injected fluid) bank. Figure 14-1 shows types of tests, limitations, and their uses.

14.2 Injectivity Test Analysis Methods

Figure 14-2 shows rate schedule and pressure response for injectivity testing.

Under Steady-State Conditions

Reservoirs with injection wells can reach true steady-state condition when total injection rate is equal to total production rate. Hall¹ has provided a method to analyze injection wells that assumes a series of steady-state injection conditions (Figure 14-3). Figure 14-6 shows that a plot of integral

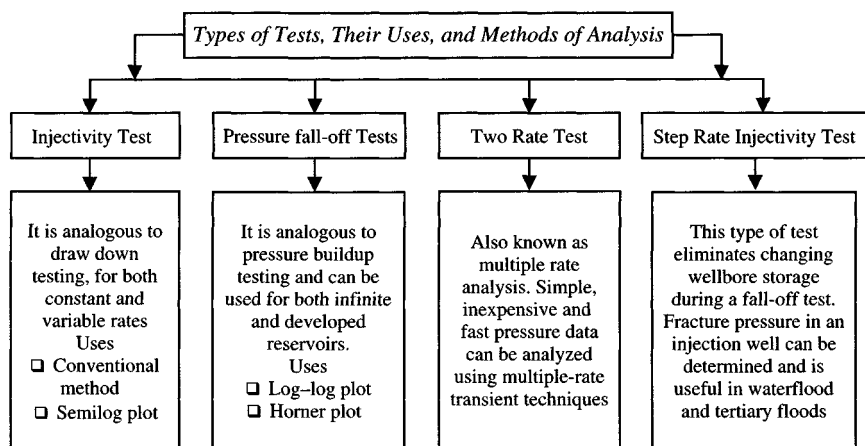


Figure 14-1. Types of tests, their uses, and methods of analysis.

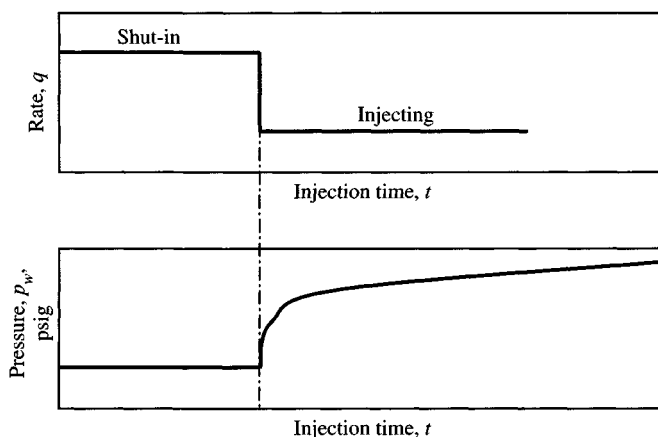


Figure 14-2. Rate schedule and pressure response in injectivity test.

or its approximation versus cumulative water injection should give a straight-line with slope:

$$m_H = \frac{141.2\mu(p_D + s_1)}{kh} \quad \text{psi (b/day)} \quad (14-1)$$

Methods of Analysis – Hall Plot¹

- If P_D and s_1 are known, then k/μ can be estimated.
- If P_D and k/μ are known, we can estimate s_1 .

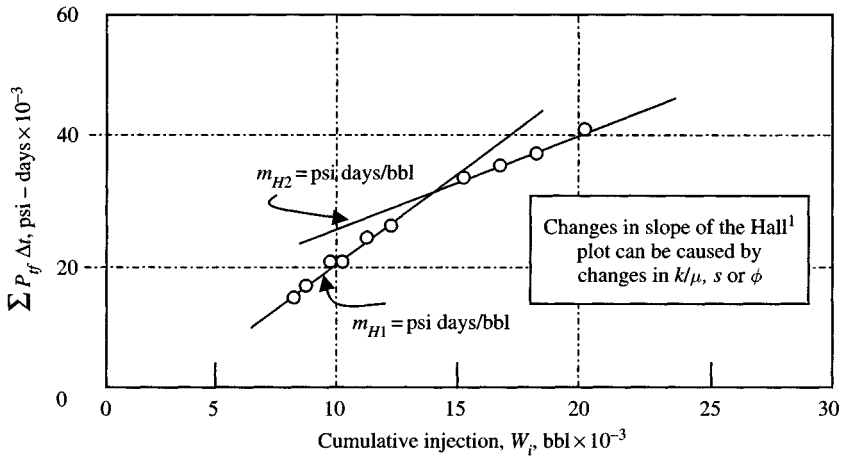


Figure 14-3. Water injection well showing stimulation effects under steady-state condition – Hall¹.

- If we obtain k/μ or s_1 from the transient test, then we must be able to determine p_D

$$s_2 = s_1 + \frac{kh}{141.2\mu}(m_{H2} - m_{H1}) \quad (14-2)$$

- Ratio of new flow efficiency is

$$\frac{(\text{Flow Efficiency})_2}{(\text{Flow Efficiency})_1} = \frac{m_{H1}}{m_{H2}} \quad (14-3)$$

Waterflood Reservoir with $M.R = 1.0$

An example calculation for waterflood reservoir with mobility ratio equal to one is given below.

Example 14-1⁶ Analyzing Injection Well Test Data (Waterflood Reservoir $M.R = 1.0$)

Table 14-1 shows the pressure fall-off test data; other well/water-flood reservoir data are: pressure prior to test, $p_{wf}(\Delta t=0) = 175$ psi, injection rate at time of test = -100 stb/day, injection time = 1.5 years; area within 5-spot pattern, $A = 40$ acres and s_w , a time of test = 0.4 fraction; well depth = 5002 ft; $h = 16$ ft; $\phi = 0.15$; $\mu_w = 1.0$ cP; $\beta_w = 1.0$ rb/stb; $c_t = 6.17 \times 10^{-5}$ psi⁻¹; $r_w = 0.25$ ft; $r_e = 744.6$ ft; $\rho_w = 66.45$ lb_m/ft³; water saturation at beginning of test $s_w = 0.42$ fraction.

Table 14-1
Injectivity Test Data^a

Time, t (hr)	Pressure response, p_{wf} (psig)	Injection rate q_w (stb/day)	Pressure drop, $\Delta p = (p_{wf} - p_i)$ (psig)	Radius of drainage, r_d (ft)
0.050	249.0	-100	55.0	21.2
0.175	284.0	-100	90.0	39.7
0.250	324.0	-100	130.0	47.4
0.350	360.0	-100	166.0	56.1
0.375	368.0	-100	174.0	58.1
0.400	372.0	-100	178.0	60.0
0.420	374.0	-100	180.0	61.5
0.500	384.0	-100	190.0	67.1
0.570	424.0	-100	230.0	71.6
0.700	454.0	-100	260.0	79.3
0.820	594.0	-100	400.0	85.9
1.000	709.0	-100	515.0	94.8
1.200	774.0	-100	580.0	103.9
1.250	784.0	-100	590.0	106.0
1.500	789.0	-100	595.0	116.1
1.750	792.0	-100	598.0	125.4
2.000	793.0	-100	599.0	134.1
3.000	798.0	-100	604.0	164.2
4.000	799.0	-100	605.0	189.7
5.000	800.0	-100	606.0	212.0
6.000	803.0	-100	609.0	232.3
7.000	804.0	-100	610.0	250.9

^a Drainage radius = 744.6 ft; time required to reach the boundaries of a tested reservoir = 61.7 ft.

- Estimate the wellbore storage coefficient, C ;
- Estimate the permeability, k , and skin factor, s ;
- Check to justify using the unit mobility ratio analysis.

Solution Cumulative water injected at time of test,

$$W_i = [q_i \times \beta_w \times \text{number of years} \times 365/\text{year}] \text{ bbl}$$

$$= 100 \times 1.00 \times 1.5 \times 365 = 54,750 \text{ bbls}$$

Method of Analysis

- Plot column 4 versus column 1 (Figure 14-4);
- Plot column 2 versus column 2 (Figure 14-5);
- Plot column 5 versus column 1 (Figure 14-6).

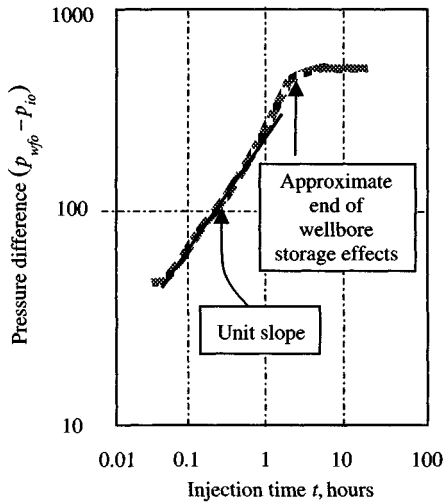


Figure 14-4. Log-log data plot.

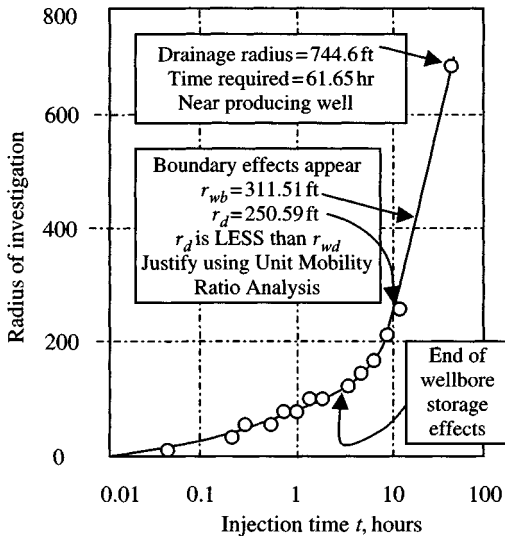


Figure 14-5. Unit mobility ratio analysis.

From these graphs, find the following using log-log type curve matching techniques.

1. Injection time t where wellbore storage effects end. (Time at the beginning of middle transient region MTR1.) Lower limits of usable straight line should be checked by plotting $\log(p_{wf} - p_i)$ versus \log

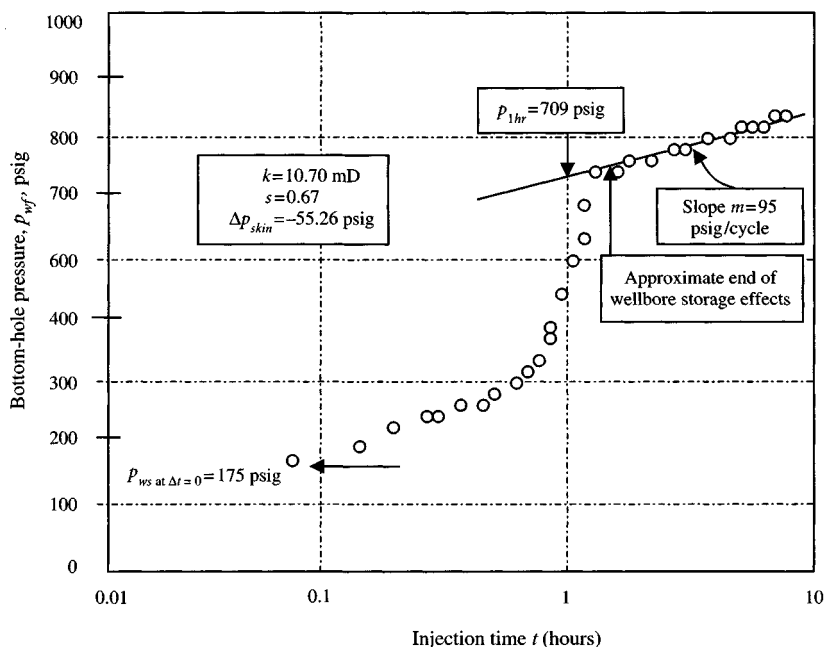


Figure 14-6. Semilog data plot.

time. The beginning of the straight line can be estimated by one of the two methods:

- (i) By the one and one half log cycle rule;
 - (ii) By the type curve overlay.
2. Injection time t where boundary effects appear. (Time at the end of middle transient region, MTR2, where data begin to deviate from the semilog straight line.)

Time (hr)	Radius of investigation r_d (ft)	Equation used	Remarks
2.25	142.2	(Eq. 14-12)	Wellbore storage effects end
6.00	232.3	(Eq. 14-12)	Boundary effects appear
61.65	744.6	(Eq. 14-12)	Near producing well drainage radius

Interpreted data

Pressure response at 1 hr = 709 psig

Tubing pressure before injection = 175 psig

Slope, m , from Figure 14-6 = 95 psig/cycle

Calculated parameters

Figures 14-4 and 14-6 are log-log and semilog plots for the test data shown in Table 14-1. Figure 14-5 is a semilog data plot to justify using unit mobility ratio concept. Total producing time, t_p , is 7.0 hr. Using $\Delta p = 100$ psi and $\Delta t = 0.2$ hr (from the unit slope line), estimate wellbore storage coefficient, C :

$$C = \frac{q_w \beta_w \Delta t}{24 \Delta p} = \frac{100(1.0)}{24} \times \frac{0.2}{100} = 0.0083 \text{ rb/psi} \quad (\text{from Eq. 8-6})$$

The value of C must be positive. Calculate wellbore volume corresponding to $C = 0.0083$ bbl/psi.

$$V_w = \frac{C}{c_w} = \frac{0.0083}{3.0 \times 10^{-6}} = 2767 \text{ bbls} \quad (\text{from Eq. 8-8})$$

At the depth of 5002 ft, a casing radius is 0.95 ft, which is too large for a hole of radius 0.25 ft. This clearly indicates the need for a check of the well completion equipment and surface connecting lines. The current straight lines in Figures 14-4 and 14-5 indicate $m = 95$ psi/cycle and $p_{1 \text{ hr}} = 709$ psi. Estimate the following parameters.

$$k = \frac{162.2 q_w \mu_w \beta_w}{mh} = \frac{162.2(100)(1.0)(1.0)}{95(16)} = 10.70 \text{ mD} \quad (\text{from Eq. 14-9})$$

$$\begin{aligned} s &= 1.151 \left[\frac{p_{1 \text{ hr}} - p_{ws@ \Delta t=0}}{m} - \log \left(\frac{k}{\phi \mu c_r r_w^2} \right) + 3.23 \right] \\ &= 1.151 \left[\frac{709 - 175}{95} - \log \left(\frac{10.70}{0.16(1.0)(6.17 \times 10^{-6})(0.25)^2} \right) + 3.23 \right] \\ &= 0.67 \quad (\text{from Eq. 14-10}) \end{aligned}$$

Pressure drop across skin using Eq. 14-13 is

$$\Delta p_{skin} = \frac{141.2(-q_w)\beta_w\mu_w}{kh} s = \frac{141.2(100)(1)(1)}{10.70 \times 16} (0.67) = -55.26 \text{ psig}$$

Radius of investigation

Radius of drainage, $r_d = 250.9$ ft (Table 14-1)

Distance to water bank, $r_{wb} = 311.51$ ft (Eq. 14-11)

Since r_d is less than r_{wb} , it is justified to use unit-mobility ratio analysis.

Liquid Filled Unit Mobility Ratio Reservoirs

Method of Analysis

The pressure will decline at a production well during drawdown, while pressure at an injection well will increase during injection. That difference is accounted for in the analysis method by using $q < 0$ for injection and $q > 0$ for production. The bottom-hole injection pressure for the constant rate injectivity test is given by:

$$p_{wf} = p_{1hr} + m \log t \quad (14-4)$$

Equation 14-4 indicates that a plot of bottom-hole injection pressure, p_{wf} , versus the logarithm of injection time should have a straight line section, the slope of which is given by:

$$m = -\frac{162.6q_o\mu_o\beta_o}{kh} \quad (14-5)$$

The intercept, p_{1hr} , is given by

$$p_{1hr} = p_i + m \left[\log \left(\frac{k}{\phi\mu_o c_i r_w^2} \right) - 3.2275 + 0.869s \right] \quad (14-6)$$

To estimate the duration of wellbore storage effects, a plot of $\log(p_{wf} - p_i)$ versus $\log t$ may be used. The beginning of the semilog straight line can be estimated by the following equation:

$$t > \frac{(200,200 + 12,000s)C}{kh/\beta\mu_o} \quad (14-7)$$

where

$$C = \text{wellbore storage coefficient} = \frac{q_o\beta_o\Delta t}{\Delta p} \quad (14-8)$$

The values of Δt and Δp can be found from the unit-slope portion of log-log plot. Once the semilog straight line is determined, reservoir permeability, k , and skin factor are estimated using Eqs. 14-9 and 14-10:

$$k = -\frac{162.6q_o\mu_o\beta_o}{mh} \quad (14-9)$$

$$s = 1.151 \left[\frac{p_{1hr} - p_i}{m} - \log \left(\frac{k}{\phi_o c_i r_w^2} \right) + 3.227 \right] \quad (14-10)$$

Distance to water bank is calculated from the following equation:⁵

$$r_{wb} = \sqrt{\frac{5.615W_i}{\pi h \phi \Delta s_w}} \quad (14-11)$$

where

r_{wb} = drainage radius (distance to water bank), ft

W_i = volume injected, res bbl

= $q_{inj} \times \beta_w \times$ injection time

β_w = water formation volume factor, rb/stk

The estimated permeability is used to determine a radius of drainage from:²

$$r_d \approx \sqrt{\frac{0.000841kt}{\phi \mu_o c_t}}, \quad r_d < r_{wb} \text{ (condition to justify unit mobility ratio analysis)} \quad (14-12)$$

The calculated value of r_d should be less than r_{wb} to justify using the unit-mobility ratio analysis. Pressure drop across the skin may be estimated from:

$$\Delta p_{skin} = \frac{141.2(-q_w)\beta_w \mu_w}{kh} s \quad (14-13)$$

Flow efficiency is given by

$$FE = \frac{p_i - p_{wf} - \Delta p_{skin}}{p_i - p_{wf}} \quad (14-14)$$

Equations 14-4 through 14-14 can be applied to injectivity testing in an infinite-acting reservoir. Example 14-2 illustrates how to analyze this type of test.

Example 14-2⁶ Analyzing Injectivity Test in Liquid Filled Unit Mobility Ratio Reservoir

Pressure response data for an injectivity test in a water-flooded reservoir are given in Table 14-2. Before the test, all the wells in the reservoir had been shut-in for several weeks and pressure had stabilized. Other known reservoir data are: depth = 1250 ft; $r_w = 0.25$ ft; $h = 20$ ft; $q_w = -120$ stb/day; $p_i = 225$ psig; $c_t = 6.5 \times 10^{-6}$ psi⁻¹; $\phi = 16\%$; $\mu_w = 1.0$ cP; $\rho_w = 62.5$ lb_m/cuft; $\beta_w = 1.027$ rb/stb; and tubing size = 2 in.

Table 14-2
Pressure Response Data in an Injectivity Test

Injection time, t (min)	Injection time, t (hr)	Bottom-hole pressure, p_{wf} (psig)	Pressure difference ($p_{wf} - p_i$) (psig)	Radius of drainage, r_d (Eq. 14-12) (ft)
6	0.11	279	54	31.44
9	0.15	281	56	36.71
12	0.20	297	72	42.39
24	0.40	330	105	59.95
30	0.50	360	135	67.02
39	0.65	387	162	76.42
45	0.75	535	310	82.08
51	0.85	625	400	87.38
60	1.00	755	530	94.78
66	1.10	807	582	99.41
72	1.20	814	589	103.83
96	1.60	815	591	119.89
108	1.80	817	593	127.16
132	2.20	819	595	140.58
150	2.50	825	600	149.86
192	3.20	826	601	169.55
222	3.70	827	602	182.32
240	4.00	826	601	189.56
330	5.50	828	603	222.28
402	6.70	827	602	245.34
450	7.50	828	603	259.57

Solution

Method of Analysis

Plot the following figures using data from Table 14-2. Figure 14-7 is a log-log data plot showing wellbore storage effects, which are important from 2 to 3 hr. Figures 14-8 and 14-9 show radius of drainage performance and semilog straight line through the data after 3 hours of injection. Interpreted data from Figure 14-9 are:

Pressure response at 1 hr, $p_{1 \text{ hr}} = 725$ psi

Tubing pressure before injection = 185.0 psi

Slope = 80 psig/cycle.

Calculated parameters

Permeability is calculated using Eq. 14-9:

$$k = -\frac{162.6q_o\beta_o}{mh} = \frac{162.6(-120)(1.027)}{80(20)} = 12.52 \text{ mD}$$

Estimate distance to water bank from Eq. 14-11:

$$r_{wb} = \sqrt{\frac{5.615W_i}{\pi h\phi\Delta s_w}} = \sqrt{\frac{5.615(120)(1.00)(2.0 \text{ years})(365 \text{ day/year})}{22/7(0.15)(20)(0.35)}} = 380.1 \text{ ft}$$

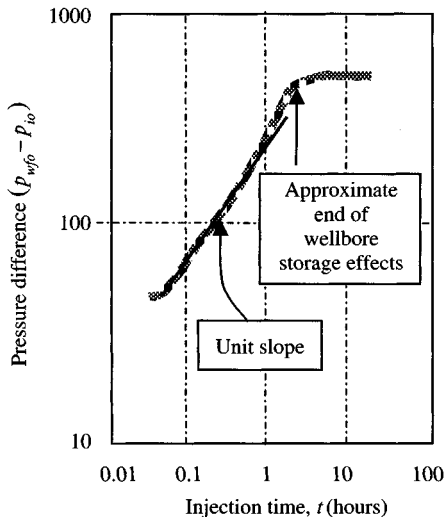


Figure 14-7. Log-log data plot.

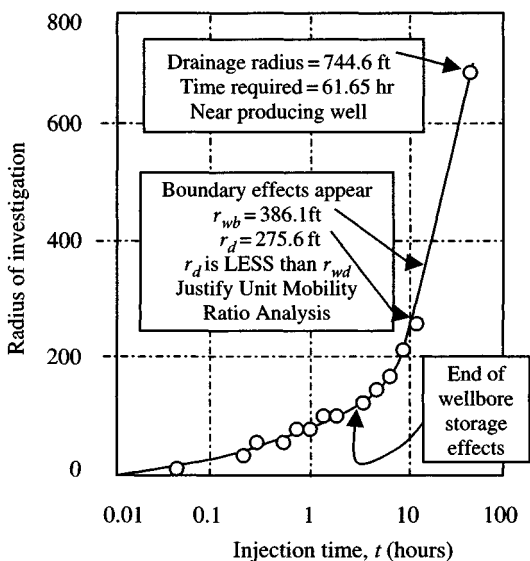


Figure 14-8. Unit mobility ratio analysis.

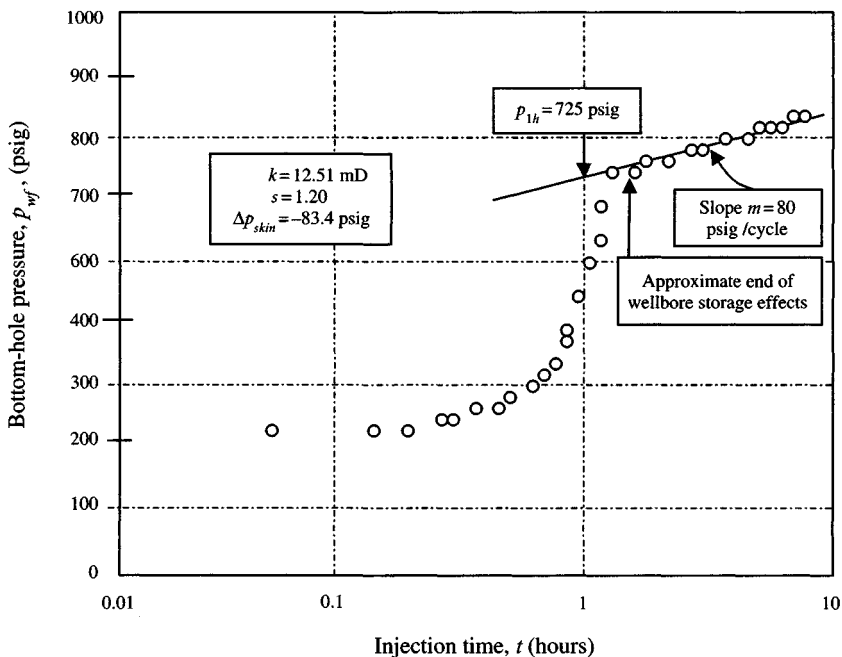


Figure 14-9. Semilog data plot.

Calculate radius of investigation from Eq. 14-12:

$$r_d \approx \sqrt{\frac{0.000841kt}{\phi\mu_o c_t}} = \sqrt{\frac{0.000841 \times 12.52 \times 7.5}{0.16(1.00)(6.5 \times 10^{-6})}} = 275.6 \text{ ft}$$

Since $r_d < r_{wb}$, using unit mobility ratio analysis is justified and Eq. 14-10 can be used to estimate skin factor:

$$\begin{aligned} s &= 1.151 \left[\frac{p_{1hr} - p_i}{m} - \log \left(\frac{k}{\phi_o c_t r_w^2} \right) + 3.227 \right] \\ &= 1.151 \left[\frac{725 - 225}{80} - \log \left(\frac{12.51}{0.16(6.5 \times 10^{-6})(0.25)^2} \right) + 3.227 \right] = 1.20 \end{aligned}$$

Estimate pressure drop across the skin from Eq. 14-13:

$$\Delta p_{skin} = \frac{141.2(-q_w)\beta_w\mu_w}{kh} s = \frac{141.2(-120)(1.0)(1.027)}{12.51(20)} (1.20) = -83.4 \text{ psi}$$

14.3 Pressure Fall-Off Test Analysis Methods

Pressure fall-off tests are performed on injection wells. Injection is analogous to production (but the rate, q , used in Eqs. 14-17 and 14-19 is negative for injection while it is positive for production). Shutting in an injection well results in a pressure fall-off that is analogous to a pressure buildup. Therefore the equations for production well testing apply to injection well testing as long as sign conversions are observed. In this section we will discuss pressure fall-off testing and injectivity tests for unit mobility and non-unit mobility ratio cases including two-rate and step injectivity tests, utilizing test data that may be used to determine well and reservoir parameters, along with examples illustrating the analysis procedures. Figure 14-10 shows rate schedule and pressure response for fall-off testing.

Liquid-Filled Unit Mobility Ratio Reservoirs

Eq. 14-15 can express the pressure fall-off behavior for both infinite-acting and developed reservoirs:

$$p_{ws} = p^* - m \log \left(\frac{t_p + \Delta t}{\Delta t} \right) \quad (14-15)$$

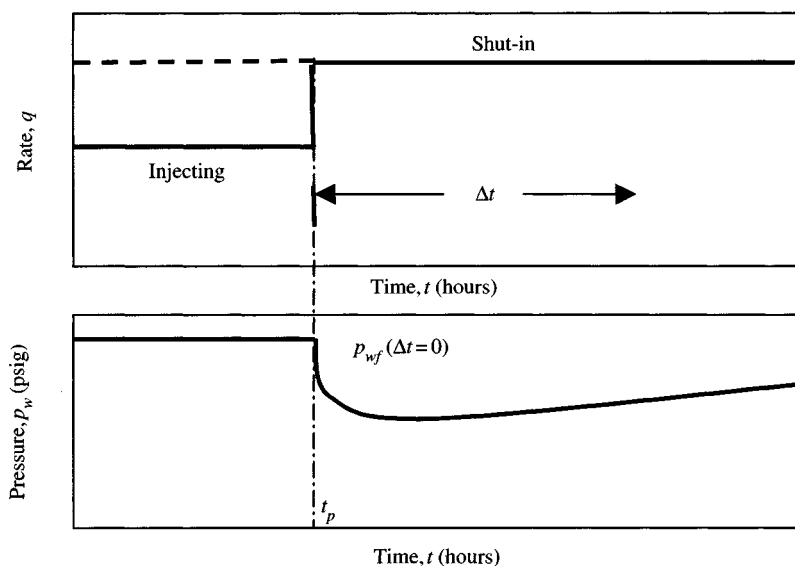


Figure 14-10. Rate schedule and pressure response for fall-off testing.

where t_p is the equivalent injection time and may be approximated by:

$$t_p = \frac{24V_p}{q_w} \quad (14-16)$$

If $t_p > 2t_{pss}$, then the time to reach pseudo-steady state (or steady state, which for a five-spot system occurs at $t_{DA} = 0.25$ with $A =$ area per well) should be used in place of t_p . V_p is the cumulative volume injected since the last pressure equalization and q_w is the water injection rate just before shut-in. Equation 14-15 indicates that a plot of p_{ws} versus $\log[(t_p + \Delta t)/\Delta t]$ should have a straight line portion with intercept p^* at $(t_p + \Delta t)/\Delta t = 1$ and with slope $-m$ where m is given by:

$$m = -\frac{162.2q_w\mu_w\beta_w}{kh} \quad (14-17)$$

The log-log data plot should also be made so that the end of wellbore storage effects may be estimated and a proper semilog straight line can be chosen. Equation 14-18 may be used to estimate the beginning of the semilog straight line for fall-off testing:

$$t = \frac{170,000Ce^{0.14s}}{(kh/\mu_w)} \quad (\text{hour}) \quad (14-18)$$

but the log-log plot is preferred. Reservoir permeability and the skin factor are determined from Eqs. 14-19 and 14-20 as

$$k = \frac{162.6q_w\mu_o\beta_w}{mh} \quad (14-19)$$

and

$$s = 1.151 \left[\frac{p_{wf}(\Delta t=0) - p_{1hr}}{m} - \log \left(\frac{k}{\phi_o c_t r_w^2} \right) + 3.227 \right] \quad (14-20)$$

Calculation of pressure loss due to skin Δp_{skin} (psi):

$$\Delta p_{skin} = 0.869ms \quad (14-21)$$

Calculation of injectivity index (b/day/psi) and flow efficiency

$$I_{ACTUAL} = \frac{i}{p_w - \bar{p}}, \quad I_{ideal} = \frac{i}{(p_w - \bar{p}) - \Delta p_{skin}} \quad (14-22)$$

$$\text{Flow efficiency} = \frac{I_{actual}}{I_{ideal}} \quad (14-23)$$

If injection time t_p is short, we can safely assume that $p^* = \bar{p}$. Otherwise determine the average pressure, \bar{p} , using the following procedure.

Find the slope of the fall-off curve and find k ; using k and other given data, calculate dimensionless flowing time:

$$t_{DA} = \frac{0.000264kt_p}{\phi\mu_o c_t A} \quad (14-24)$$

where A is the injection area and from Table 14-3, find the dimensionless pressure function, p_{MBH} :

$$p_{MBH} = \frac{\bar{p} - p^*}{(70.6i\mu/kh)} \quad (14-24a)$$

Since $70.6i\mu/kh = m/2.303$, $\bar{p} - p^* = p_{MBH}(m/2.303)$ (psi) or

$$\bar{p} = p_{MBH}(m/2.303) + p^* \text{ (psi)} \quad (14-25)$$

Example 14-3⁵ Analyzing Single Rate Pressure Fall-Off Test Data (Liquid-Filled Case-Unit Mobility Ratio)

Pressure response data for an injectivity test in a water-flooded reservoir are given in Table 14-4. Before the test, all the wells in the reservoir had been shut-in

Table 14-3
Function for Computing Average Waterflood Pressure³

Dimensionless injection time $t_{DA} = 0.00064kt/\phi\mu c_t A$ (Eq. 14-24)	Dimensionless pressure function $(p_{MBH}) = (\bar{p} - p^*)/70.6i\mu/kh$ (Eq. 14-24a)
0.01	0.00
0.02	0.00
0.03	0.04
0.04	0.05
0.05	0.10
0.06	0.13
0.07	0.18
0.08	0.21
0.09	0.28
0.10	0.31
0.15	0.50
0.20	0.70
0.25	0.85
0.30	1.00
0.35	1.10
0.40	1.20
0.50	1.40
0.60	1.55
0.70	1.68
0.80	1.80
0.90	1.90
1.00	2.00
1.50	2.32
2.00	2.65
2.50	2.83
3.00	3.00
3.50	3.17
4.00	3.30
4.50	3.40
5.00	3.53
5.50	3.60
6.00	3.70
6.50	3.75
7.00	3.85
7.50	3.92
8.00	4.00
8.50	4.05
9.00	4.10
9.50	4.15
10.0	4.20

Table 14-3 (continued)

Dimensionless injection time $t_{DA} = 0.00064kt/\phi\mu c_t A$ (Eq. 14-24)	Dimensionless pressure function $(p_{MBH}) = (\bar{p} - p^*)/70.6i\mu/kh$ (Eq. 14-24a)
20.0	4.90
30.0	5.30
40.0	5.60
50.0	5.84
60.0	6.00
70.0	6.18
80.0	6.40
90.0	6.43
100	6.52
200	7.22
300	7.63
393	7.91
400	7.93
500	8.14
600	8.33
700	6.48
800	8.60
900	8.70
1000	8.84

Table 14-4
Pressure Response Data in an Injectivity Test

Time, Δt (hr)	$(t_p + \Delta t)/\Delta t$	Tubing pressure, p_{tf} (psig)	Pressure difference, $(p_{tfo} - p_{tf}) = 525 - p_{tf}$ (psig)
0.00	—	525	0
0.07	572,231.00	300	225
1.00	40,057.10	268	257
1.50	26,705.07	251	274
2.00	20,029.05	245	280
3.00	13,353.03	202	323
4.00	10,015.02	184	341
5.00	8012.22	173	352
6.00	6677.02	159	366
7.00	5723.30	153	372
8.00	5008.01	145	380
9.00	4451.68	139	386

for several weeks and pressure had stabilized. Other known reservoir data are: depth = 4819 ft; $r_w = 0.354$ ft; $h = 49$ ft; $q = 1426$ stb/d; $c_t = 6.5 \times 10^{-6}$ psi $^{-1}$; $\phi = 16\%$; $\mu = 1.0$ cP; $p_w = 62.5$ lb $_m$ /cuft; $\beta = 1.027$ rb/stb and tubing size = 2 in; injected area = 20 acres; cumulative volume injected before test = 2380 mbbls; injection pressure at $p_{w(\Delta t=0)} = 525$ psi; hole size = 8.50 in; $c_o = 3.0 \times 10^{-6}$ psi $^{-1}$; $c_w = 3.0 \times 10^{-6}$ psi $^{-1}$; $c_g = 1.00 \times 10^{-4}$ psi $^{-1}$; $c_f = 4.0 \times 10^{-6}$ psi $^{-1}$; $s_o = 0.20$, $s_g = 0$ and $s_w = 0.80$.

Solution Pseudo-producing time $t_p = 24 \times 2380 \times 1000/1426 = 40,056.10$ hours (Eq. 14-16). The log-log data, Figure 14-11, indicate that wellbore storage is important for about 0.01 to 0.07 hr. From semilog plot, Figure 14-12, find the following: $\rightarrow p_{1hr} = 268$ psi, $p^* = -335$ psi, slope $m = 130$ psi/cycle.

Calculate permeability to water using Eq. 14-19:

$$k_w = \frac{162.6(1426)(1.0)(0.6)}{130(49)} = 21.84 \text{ mD}$$

Using this k value and other data given in the example, we calculate dimensionless flowing time for a 40-acre pattern flood (injection area A of 20 acres). From Eq. 14-24,

$$t_{DA} = \frac{0.000264kt_p}{\phi\mu c_t A} = \frac{0.000264(21.8)(40,056.1)}{(0.16)(0.6)(7.0 \times 10^{-6})(20 \times 43,560)} = 394.5$$

From Table 14-3,

$$\frac{(\bar{p} - p^*)}{70.6i\mu/kh} = 7.97, \quad \text{since} \quad \frac{70.6i\mu}{kh} = m/2.303$$

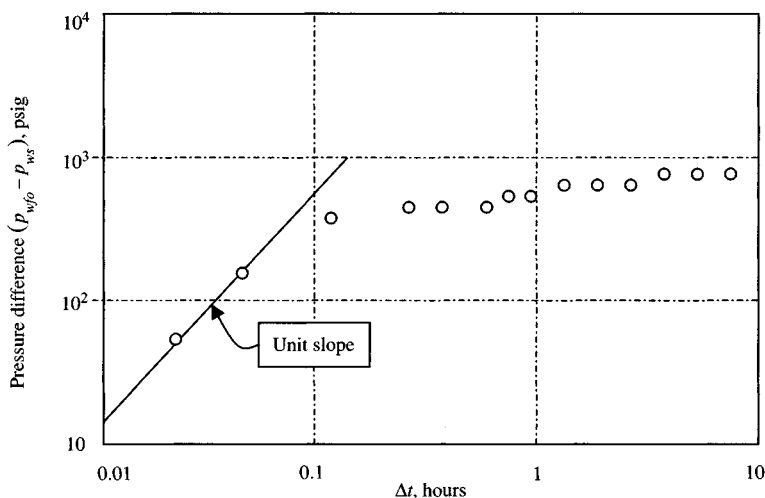


Figure 14-11. Log-log data plot – liquid-filled case (unit mobility ratio).

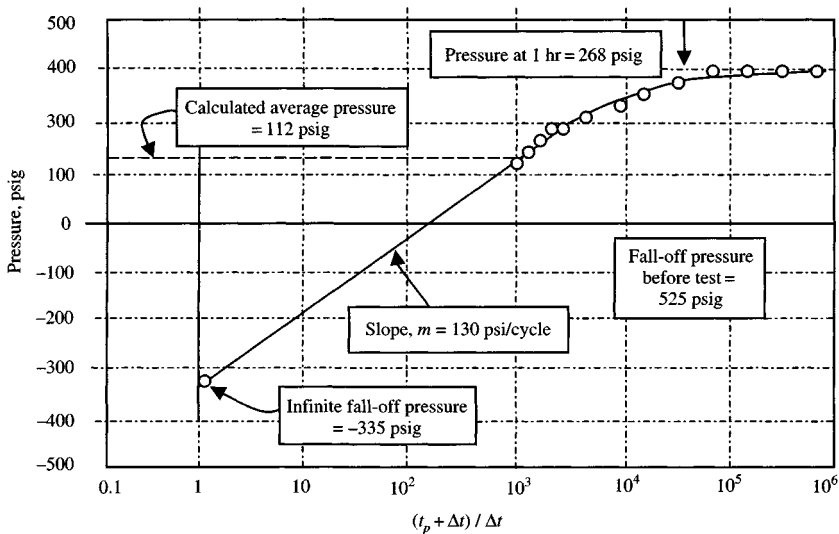


Figure 14-12. Pressure fall-off curve – liquid-filled case (unit mobility ratio).

Then, $\bar{p} - p^* = 7.96(m/2.303) = 7.96(130/2.303) = 449$ psig, and obtaining p^* from Figure 14-12 (semilog plot), we find, $\bar{p} = p_e = -335 + 449 = 115$ psi.

Calculate skin factor s and pressure loss due to skin, Δp_{skin} from Eqs. 14-20 and 14-21.

$$\begin{aligned}
 s &= 1.151 \left[\frac{p_w(\Delta t=0) - p_{1hr}}{m} - \log \left(\frac{k}{\phi \mu c_t r_w^2} \right) + 3.2275 \right] \\
 &= 1.151 \left[\frac{525 - 268}{130} - \log \left(\frac{21.84}{(0.16)(0.9)(7.0 \times 10^{-6})(0.354)^2} \right) + 3.2275 \right] \\
 &= 1.151 [1.977 - 8.238 + 3.2275] = -3.49
 \end{aligned}$$

$$\Delta p_{skin} = 0.869ms = 0.869(130)(-3.49) = -395 \text{ psi}$$

Calculate injectivity index and flow efficiency from Eqs. 14-22 and 14-23:

$$I_{actual} = \frac{i}{p_w - \bar{p}} = \frac{1426}{525 - 115} = 3.48 \text{ b/day/psi}$$

$$I_{ideal} = \frac{i}{(p_w - \bar{p}) - \Delta p_{skin}} = \frac{1426}{(525 - 115) - 394} = 1.77 \text{ b/day/psi}$$

$$FE = \frac{I_{actual}}{I_{ideal}} = \frac{3.48}{1.77} = 1.96$$

Estimate compressibility in the swept zone from the following equation:

$$c_t = c = s_o c_o + s_w c_w + c_f = 0.20(3.0 \times 10^{-6}) + 0.80(3.0 \times 10^{-6}) + 4.0 \times 10^{-4} = 7.0 \times 10^{-6} \text{ psi}^{-1}$$

Prior to Reservoir Fill-Up-Unit Mobility Ratio

Hazelbroek et al.³ have provided a solution for the pressure behavior in this type of reservoir.

Case 1: The surface pressure decreases slowly and the well stays filled up to the top for considerable closed-in time, because the reservoir pressure is high. After-flow into the formation is small since it results only from the expansion of fluid in the well as the pressure decreases.

Case 2: The surface pressure drops to zero a short time after closing in, after which the liquid level in the well starts to sink. The volume of inflow into the formation at any time is equal to the volume of the wellbore column between the top of the well and the liquid level.

For both conditions, the injection well closed-in pressure is given by³

$$p_{ws} - p_e = b_1 e^{-\beta_1 \Delta t} \quad (14-26)$$

where p_{ws} is the fall-off pressure in the well at closed-in time Δt , and p_e is the pressure at the outer radius of the oil bank. Equation 14-26 indicates that a plot of $\log(p_{ws} - p_e)$ versus Δt should be linear with slope $\beta_1/2.303$ and intercept b_1 at $\beta t = 0$. From the theoretical treatment in Reference 3, the intercept b_1 and the injection rate i is related to kh by

$$kh = \frac{i\mu}{b_1} \frac{1 - C_1 - C_2}{(1 - C_3)^2} f(\theta) \quad (14-27)$$

where i is the injection rate; b/d and the quantities C_1 , C_2 , and C_3 for case 1 are:

$$\begin{aligned} C_1 &= 0.0538 \times \frac{d_i^2 \beta_1 b_1 c_w (p_w - p_i)}{i\rho} \\ C_2 &= 0 \\ C_3 &= \frac{p_w - p_e}{b_1} \times C_1 \end{aligned} \quad (14-28)$$

For case 2 where the surface pressure drops to zero shortly after closing in,

$$\begin{aligned}
 C_1 &= 0.0538 \times \frac{d_i^2 \beta_1 b_1}{i\rho} \\
 C_2 &= \frac{p_t}{b_1} C_1 \\
 C_3 &= \frac{p_w - p_e}{b_1} \times C_1
 \end{aligned} \tag{14-29}$$

and for both case 1 and case 2

$$\theta = \frac{C_1(1 - C_3)}{2(1 - C_1 - C_2)} \tag{14-30}$$

where

d_i = diameter of tubing or casing, inches

ρ = density, gm/cc

c_w = water compressibility, psi^{-1}

p = pressure, psi

β_1 = slope in hr^{-1}

Knowing the value of parameter θ , we can find function $f(\theta)$ from Table 14-5 and then using Eq. 14-24, find permeability-thickness product, kh .

Skin factor s is calculated from the following equation:

$$s = \frac{0.00708(p_w - p_e)}{i\mu/kh} - \ln(r_e/r_w) \tag{14-31}$$

where

$$r_e = \sqrt{\frac{W_i(5.615)}{\pi\phi(s_g - s_{gr})h}} \tag{14-32}$$

The next example illustrates the use of these equations and method of analysis.

Example 14-4⁵ *Analyzing Single Rate Pressure Fall-Off Test Data (Prior to Reservoir Fill-Up) $M.R=1.0$*

Given data are: injection rate, $i = 1020$ bbl/day, wellhead injection pressure (tubing) = 0 psi; wellhead pressure (casing) = 598 psi; cumulative injected water, $W_i = 6.077$ mbbbls; $h = 45$ ft; $\phi = 0.3$; $\mu_w = 0.9$; $\beta_w = 1.0$ rb/stb; $\rho_w = 62.5 \text{ lb}_m/\text{ft}^3 = 1.0 \text{ gm/cc}$; $c_w = 3.0 \times 10^{-6}$; $c_f = 4.0 \times 10^{-6}$; $c_o = 3.0 \times 10^{-6}$; $c_g = 1.0 \times 10^{-4}$; $s_o = 0.56$; $s_w = 0.32$; $s_g = 0.12$; $s_{gr} = 0$; $r_w = 1.0$ ft; hole size = 6.366 in. Pressure fall-off test data are given in Table 14-6.

Table 14-5
Function $f(\theta)$ Versus θ for Calculating kh^3

Parameter θ calculated using Eq. 15-30	Function $f(\theta)$
0	181
0.0182	177
0.02	172
0.04	170
0.06	165
0.08	158
0.10	154
0.12	146
0.14	140
0.16	134
0.18	127
0.20	120
0.22	113
0.24	106
0.26	99
0.28	92
0.30	84
0.32	76
0.34	68
0.36	60
0.38	54
0.40	48
0.42	37
0.44	26
0.46	17
0.48	9
0.50	0

Solution The plot of $\log(p_{ws} - p_{av})$ versus injection time at various values of average pressures is shown in Figure 14-13; we find $p_e = p_{av} = 32$ psig, intercept at $\Delta t = 0$, $b_1 = 340$, and slope, $\beta_1 = 0.514 \text{ hr}^{-1}$. For the case where the pressure drops to zero shortly after closing-in, calculate the following parameters using Eq. 14-29.

$$C_1 = 0.0538 \times \frac{d_r^2 \beta_1 b_1}{i\rho} = 0.0538 \times \frac{(6.366)^2 (0.514)(34)}{(1020)(1.00)} = 0.0374$$

$$C_2 = 0, \text{ since } p_i = 0 \rightarrow C_3 = C_1 \times \frac{p_w - p_e}{b_1} = 0.0374 \times \frac{598 - 32}{340} = 0.0623$$

Table 14-6
Pressure Fall-Off Data

Injection time (hr)	Fall-off pressure, p_{ws} (psig)	Parameters at various values of average pressure ($p_{ws} - p_{Av}$) (psig)							
		10	20	32	50	75	100	125	150
0.000	598	588	578	566	548	523	498	473	448
0.250	597	587	577	565	547	522	497	472	447
0.500	552	542	532	520	502	477	452	427	402
0.800	530	520	510	498	480	455	430	405	380
1.000	515	505	495	483	465	440	415	390	365
1.450	482	472	462	450	432	407	382	357	332
2.000	442	432	422	410	392	367	342	317	292
3.000	382	372	362	350	332	307	282	257	232
4.000	352	342	332	320	302	277	252	227	202
5.000	324	314	304	292	274	249	224	199	174
6.000	304	294	284	272	254	229	204	179	154
7.000	289	279	269	257	239	214	189	164	139
8.000	262	252	242	230	212	187	162	137	112
9.000	257	247	237	225	207	182	157	132	107
10.000	245	235	225	213	195	170	145	120	95
11.000	232	222	212	200	182	157	132	107	82

Table 14-6 (continued)

Injection time (hr)	Fall-off pressure, p_{ws} (psig)	Parameters at various values of average pressure ($p_{ws} - p_{Av}$) (psig)							
		10	20	32	50	75	100	125	150
12.000	222	212	202	190	172	147	122	97	72
13.000	211	201	191	179	161	136	111	86	61
14.000	200	190	180	168	150	125	100	75	50
15.000	192	182	172	160	142	117	92	67	42
16.000	182	172	162	150	132	107	82	57	32
17.000	175	165	155	143	125	100	75	50	25
18.000	167	157	147	135	117	92	67	42	17
19.000	160	150	140	128	110	85	60	35	10

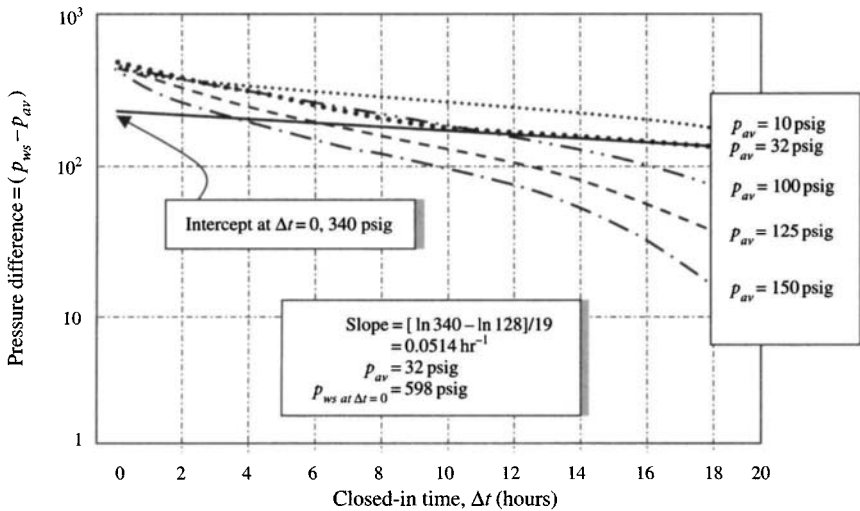


Figure 14-13. Pressure fall-off curves – prior to reservoir fill-up (unit mobility ratio case).

Then, from Eq. 14-30, we find

$$\theta = \frac{C_1(1 - C_3)}{2(1 - C_1 - C_2)} = \frac{0.0374(1 - 0.0623)}{2(1 - 0.0374 - 0)} = \frac{0.0351}{1.9252} = 0.0182$$

Knowing the value of θ , find function $f(\theta)$ from Table 14-5, which is equal to 177. Calculate permeability-thickness product, kh , from Eq. 14-27:

$$kh = \frac{i\mu(1 - C_1 - C_2)}{b_1(1 - C_3)^2} f(\theta) = \frac{1020(0.9)}{340} \times \frac{1 - 0.0374 - 0}{(1 - 0.0623)^2} (177.0) = 523.2 \text{ mDft}$$

and $k = 523.2/45 = 11.63 \text{ mD}$. Before finding skin factor s , first estimate distance to water bank from Eq. 14-32:

$$r_e = \sqrt{\frac{W_i(5.615)}{\pi\phi(s_g - s_{gr})h}} = \sqrt{\frac{(6.097 \times 1000)(5.615)}{22/7 \times 0.03(0.12 - 0)(45)}} = 82.0 \text{ ft}$$

Now calculate, skin factor, s from Eq. 14-31:

$$s = \frac{0.00708(p_w - p_e)}{i\mu/kh} - \ln(r_e/r_w) = 2.284 - 4.40 = -2.12$$

Prior to Reservoir Fill-Up – Non-Unit Mobility Ratio

Hazelbroek et al.³ have provided the following equations to analyze pressure fall-off single-rate test. Mobility ratio is given

$$M.R = \frac{k_w \mu_o}{k_o \mu_w} \quad (14-33)$$

Ratio of volume of oil bank to volume of water bank is

$$\text{Ratio} = \frac{V_o}{V_w} \quad (14-34)$$

Parameter γ and quantity r_{oD} are related to

$$\gamma = \frac{C_o}{C_w} \quad (14-35)$$

$$r_{oD} = \frac{1}{\sqrt{\frac{V_o}{V_w} + 1}} \quad (14-36)$$

Permeability-thickness product kh and skin factor s are estimated by using the following equations:

$$k_w h = \frac{i_w \mu_w}{b_1} \times 2F \quad (14-37)$$

$$s = \frac{0.00708(p_w - p_e)k_w h}{i_w \mu_w} - \left(\frac{M-1}{2} \right) \ln \left(\frac{V_o}{V_w} + 1 \right) - \ln \left(\frac{r_e}{r_w} \right) \quad (14-38)$$

where i_w is injection rate in b/d and function F can be determined from Figures B-9 through B-11. Figure 14-14 shows water and oil banks and Figure 14-15 illustrates fluid saturations.

The following example illustrates the application of Eqs. 14-33 through 14-38.

Example 14-5⁶ *Analyzing Single Rate Pressure Fall-Off Test Data (Non-Unit Mobility Ratio Case)*

For the data given in Example 14-4, for $\mu_o = 12$ cP, and for $k_o = 0.85$ mD, and $k_w = 0.255$ mD, $s_o = 0.56$, $s_{or} = 0.20$, $s_g = 0.12$, and $s_{gr} = 0.0$,

$$\text{Mobility ratio} = M.R = \frac{k_w \mu_o}{k_o \mu_w} = \frac{0.255 \times 12}{0.85 \times 0.9} = 4.0$$

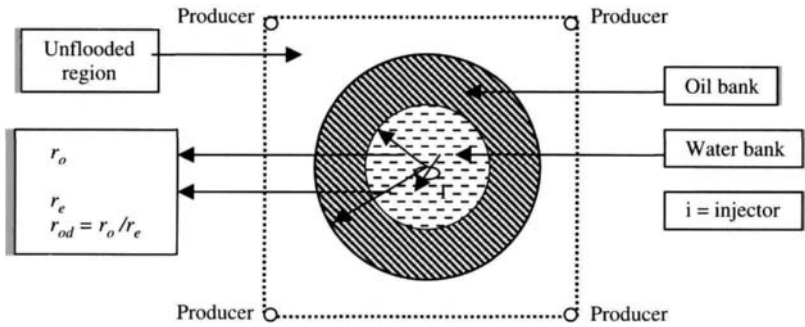


Figure 14-14. Showing water and oil banks.³

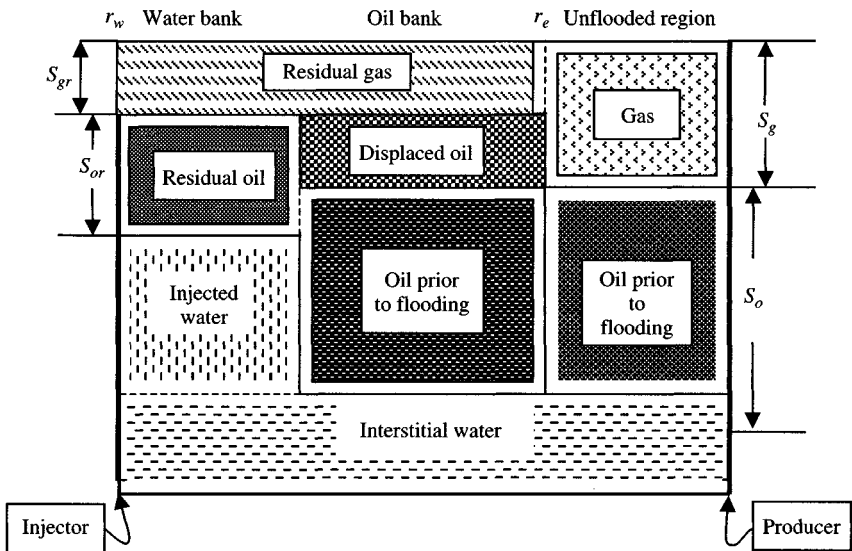


Figure 14-15. Oil, water, and gas saturations in the reservoir.³

Solution Pressure fall-off test data are given in Table 14-7. Figure 14-16 shows a semilog plot of $\log(p_w - p_{av})$ versus injection time; from this figure average reservoir pressure is:

$$p_{av} = p_e = 32 \text{ psi}$$

Volume of oil bank,

$$V_o = s_o - s_{or} = 0.56 - 0.20 = 0.36$$

Table 14-7
Pressure Fall-Off Test for Non-Unit Mobility

Injection time (hr)	Fall-off pressure p_{ws} (psig)	Parameter at various values of average pressure ($p_{ws} - p_{av}$), psig							
		10	20	32	50	75	90	100	120
0.000	598	588	578	566	548	523	508	498	478
0.250	597	587	577	565	547	522	507	497	477
0.500	552	542	532	520	502	477	462	452	432
0.800	530	520	510	498	480	455	440	430	410
1.000	515	505	495	483	465	440	425	415	395
1.450	482	472	462	450	432	407	392	382	362
2.000	442	432	422	410	392	367	352	342	322
3.000	382	372	362	350	332	307	292	282	262
4.000	352	342	332	320	302	277	262	252	232
5.000	324	314	304	292	274	249	234	224	204
6.000	304	294	284	272	254	229	214	204	184
7.000	289	279	269	257	239	214	199	189	169
8.000	262	252	242	230	212	187	172	162	142
9.000	257	247	237	225	207	182	167	157	137
10.000	245	235	225	213	195	170	155	145	125
11.000	232	222	212	200	182	157	142	132	112
12.000	222	212	202	190	172	147	132	122	102
13.000	211	201	191	179	161	136	121	111	91
14.000	200	190	180	168	150	125	110	100	80
15.000	192	182	172	160	142	117	102	92	72
16.000	182	172	162	150	132	107	92	82	62
17.000	175	165	155	143	125	100	85	75	55
18.000	167	157	147	135	117	92	77	67	47
19.000	160	150	140	128	110	85	70	60	40

Volume of water bank,

$$V_w = s_g - s_{gr} = 0.12 - 0.0 = 0.12$$

Therefore,

$$\frac{V_o}{V_w} = \frac{0.36}{0.12} = 3.0 \quad (\text{from Eq. 14-34})$$

Using Eqs. 14-35 and 14-36, find

$$\gamma = \frac{c_o}{c_w} = \frac{3.0 \times 10^{-6}}{3.0 \times 10^{-6}} = 1 \quad \text{and} \quad r_{oD} = \frac{1}{\sqrt{\frac{V_o}{V_w} + 1}} = \frac{1}{\sqrt{3 + 1}} = 0.5$$

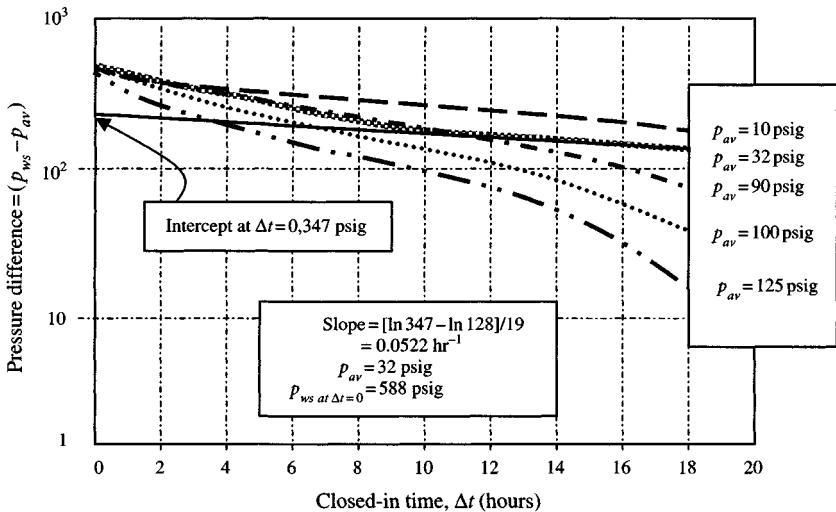


Figure 14-16. Pressure fall-off curves – prior to reservoir fill-up (non-unit mobility ratio case).

Further, $M.R = 4.0$ and $\gamma = 1$, since $c_o \cong c_w$ for this dead oil. Therefore, reading from Figures B-9 through B-11, we obtain, $F = 220$.

Calculate water formation permeability and thickness product, $k_w h$ from Eq. 14-37:

$$k_w h = \frac{i_w \mu_w}{b_1} \times 2F = \frac{1020(0.9)}{340} (2 \times 220) = 1188 \text{ mD ft}$$

This value of $k_w h$ is 2.27 times as large as that obtained for the single fluid case.

The skin factor is found from Eq. 14-38:

$$\begin{aligned} s &= \frac{0.00708(p_w - p_e)k_w h}{i_w \mu_w} - \left(\frac{M-1}{2}\right) \ln\left(\frac{V_o}{V_w} + 1\right) - \ln\left(\frac{r_e}{r_w}\right) \\ &= \frac{0.00708(598 - 32)(1188)}{1020(0.9)} - \left(\frac{4-1}{2}\right) \ln(3+1) - \ln\left(\frac{82}{1}\right) \\ &= 5.2272 - 2.0795 - 4.407 = -1.26 \end{aligned}$$

This value of s is less negative (indicating a smaller effective wellbore radius) than the value obtained in the single fluid case. Thus, use of the single fluid case has given too large a value for effective wellbore radius and, as noted above, too small a value for kh . This is the result one finds when the water mobility is greater than the oil mobility ($M > 1$). By obtaining too large an

effective wellbore radius from use of the single fluid case, the engineer may incorrectly decide that there is little possibility of injectivity improvement by well stimulation. Use of the proper mobility ratio would lead to a proper recommendation.

14.4 Two-Rate Injectivity Test Analysis

Using Conventional Methods

Pressure behavior of the well at time $\Delta t'$ after the change in injection rate is given by:³

$$\log\left(p_{iw} - \left\{\bar{p} + \frac{i_2}{i_1}[p_w - \bar{p}]\right\}\right) = \log\left(\frac{181.2(i_1 - i_2)\mu}{kh}\right) - 0.000664 \times \frac{k\Delta t'}{\phi\mu cr_e^2} \quad (14-39)$$

where

p_{iw} = injection well pressure after change in rate, b/day

p_w = injection well pressure at time of rate change, psi

\bar{p} = average pressure in area between injector and producer, psi

p_e = mid-point pressure between injector and producer, psi

Equation 14-39 indicates that a plot of $\log(p_{iw} - \{\bar{p} + (i_2/i_1)[p_w - \bar{p}]\})$ versus $\Delta t'$ should be linear; and from the intercept value of b at $\Delta t' = 0$, we find

$$kh = \frac{181.2(i_1 - i_2)\mu}{b} \quad (14-40)$$

Trial-and-error values of \bar{p} are used until the best straight-line is obtained. To determine the value of skin factor, s , at the time of rate change

$$p_w = \bar{p} + 141.2 \times \frac{i_1\mu}{kh} \left(\ln \frac{r_e}{r_w} + s\right) \quad (14-41)$$

Thus

$$s = \frac{p_w - \bar{p}}{141.2 \times \frac{i_1\mu}{kh}} - \ln\left(\frac{r_e}{r_w}\right) \quad (14-42)$$

where r_e can be determined from the slope of the plot of $\log(p_{iw} - [\bar{p} + (i_2/i_1)[p_w - \bar{p}]])$ versus $\Delta t'$

$$\beta = 0.000664 \times \frac{k}{\phi \mu c r_e^2} \quad (14-43)$$

Thus

$$r_e = \sqrt{\frac{0.000664k}{\beta \phi \mu c}} \quad (\text{ft}) \quad (14-44)$$

The average pressure must be determined by a trial-and-error procedure as noted above. The procedure is to try various values of \bar{p} until one is found that yields the best straight line on the plot of $\log(p_{iw} - [\bar{p} + (i_2/i_1)[p_w - \bar{p}]])$ versus $\Delta t'$.

An example application of this method is given below.

Example 14-6⁶ *Analyzing Two-Rate Injection Well Test in a Waterflood Reservoir before a Tertiary Recovery Test*

The well was stabilized at an injection rate of 2563 b/d. To obtain the transient pressure data the rate was reduced to 742 b/d and pressure response along with calculated data are shown in Table 14-8. Other data are as follows: injection well pressure is twice the rate change = 6777 psi and second injection rate = 742 b/d, well depth = 4819 ft, $h = 31 \text{ ft}_o = 3.0 \times 10^{-6} \text{ psi}^{-1}$, $c_f = 4.0 \times 10^{-6} \text{ psi}^{-1}$, $c_w = 3.0 \times 10^{-6} \text{ psi}^{-1}$, $c_g = 1.0 \times 10^{-4} \text{ psi}^{-1}$, $\phi = 0.244$, $\mu_w = 0.37 \text{ cP}$, $\beta_w = 1.0 \text{ rb/stb}$, $s_o = 0.20$, $s_w = 0.80$, $r_w = 0.30 \text{ ft}$, and $A = 95 \text{ acres}$. Estimate permeability, k , and skin factor, s , and compare your results with the conventional method of analysis.

Solution Table 14-8 shows the data for two-rate injectivity test. Find the average pressure in the region around the wellbore by trial and error procedure; as shown in Figure 14-17 the average pressure is found to be 3600 psi. Figure 14-18 is a two-rate injection test data plot using the Odeh and Jones method. From this plot, find the following parameters:

$$\text{Slope, } \beta = \frac{\log(740) - \log(460)}{50} = 0.00413 \text{ hr}^{-1}$$

$$\text{Intercept, } b = 740 \text{ psi}$$

Determine the value of k using Eq. 14-40:

$$kh = \frac{181.2(i_1 - i_2)\mu}{b} = \frac{181.2(2563 - 742)(0.37)}{740} = 165 \text{ mD ft}$$

$$k = 165/31 = 5.32 \text{ mD}$$

Table 14-8
Two-Rate Injectivity Test

Injection time, Δt (hr)	Fall-off pressure after rate change, p_{wi} (psig)	Function at various values of average pressure $p_{wi} - [p_{av} + q_2/q_1^*(p_w - p_{av})]$ (psig)							
		4500	4200	4000	3800	3600	3200	3000	2500
0.000	6777	1618	1831	1973	2115	2257	2541	2684	3039
0.100	6320	1161	1374	1516	1658	1800	2084	2227	2582
0.200	6120	961	1174	1316	1458	1600	1884	2027	2382
0.300	5920	761	974	1116	1258	1400	1684	1827	2182
0.400	5820	661	874	1016	1158	1300	1584	1727	2082
0.500	5720	561	774	916	1058	1200	1484	1627	1982
1.000	5620	461	674	816	958	1100	1384	1527	1882
2.000	5520	361	574	716	858	1000	1284	1427	1782
4.000	5380	221	434	576	718	860	1144	1287	1642
6.000	5320	161	374	516	658	800	1084	1227	1582
8.000	5300	141	354	496	638	780	1064	1207	1562
10.000	5250	91	304	446	588	730	1014	1157	1512
12.000	5200	41	254	396	538	680	964	1107	1462
14.000	5190	31	244	386	528	670	954	1097	1452
16.000	5170	11	224	366	508	650	934	1077	1432
18.000	5160	1	214	356	498	640	924	1067	1422
20.000	5125	-34	179	321	463	605	889	1032	1387
22.000	5115	-44	169	311	453	595	879	1022	1377
24.000	5110	-49	164	306	448	590	874	1017	1372
26.000	5105	-54	159	301	443	585	869	1012	1367
28.000	5102	-57	156	298	440	582	866	1009	1364
32.000	5090	-69	144	286	428	570	854	997	1352
36.000	5060	-99	114	256	398	540	824	967	1322
40.000	5030	-129	84	226	368	510	794	937	1292
44.000	5020	-139	74	216	358	500	784	927	1282
48.000	5000	-159	54	196	338	480	764	907	1262

Before using Eq. 14-41, first find the value of drainage radius, r_e , using Eq. 14-44, after rearranging this equation

$$r_e = \sqrt{\frac{0.000664k}{\beta\phi\mu c_t}} = \sqrt{\frac{0.000664(5.32)}{(0.00413)(0.244)(0.37)(7.0 \times 10^{-6})}} = 1164 \text{ ft}$$

Check:

$$r_e = \sqrt{\text{acres} \times 43,560 \times 22/7}$$

$$= \sqrt{95 \times 43,560 \times 22/7} = 1147 \text{ ft}$$

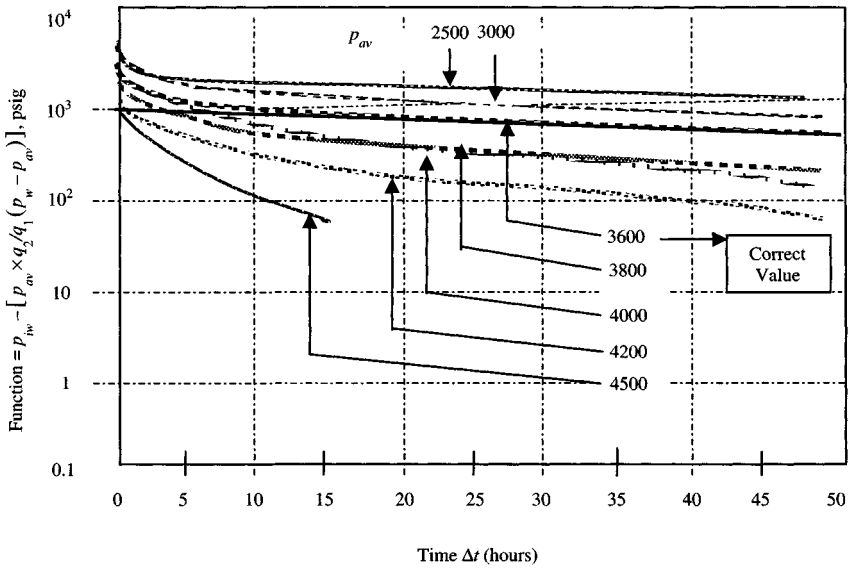


Figure 14-17. Two-rate injection tests – average pressure estimation.

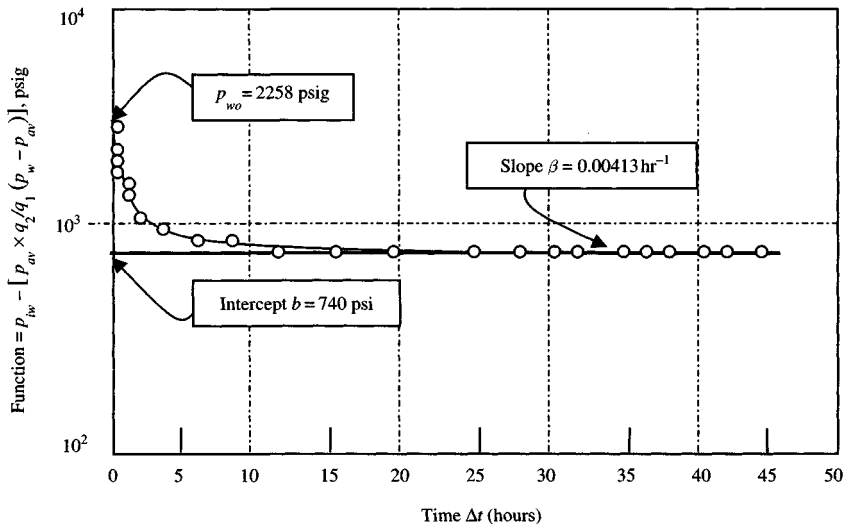


Figure 14-18. Two-rate injection test analysis using the Odeh and Jones method.

Substituting the values in Eq. 14-42,

$$s = \frac{p_w - \bar{p}}{141.2 \times \frac{i_1 \mu}{kh}} - \ln(r_e/r_w)$$

$$= \frac{6777 - 3600}{141.2 \times \frac{(2563)(0.37)}{5.32(31)}} - \ln(1164/0.3) = 3.9129 - 8.2636 = -4.35$$

Conventional Analysis

Two-rate injectivity test and pressure data are shown in Table 14-9. Figure 14-19 is a log-log plot; end of wellbore storage starts at about 0.05 h, and Figure 14-20 is a semilog plot; from this plot find the slope = 81 psi/cycle and $p_{1hr} = 621$ psig. These values agree quite well with the Hazelbroek et al. method.

14.5 Step-Rate Injectivity Testing Technique

Using Felsenthal et al. Method

Felsenthal⁴ presented a technique to estimate the fracture pressure in an injection well. Such information is important in water-flood and tertiary floods where it is important to avoid injecting expensive fluids through artificial fractures.

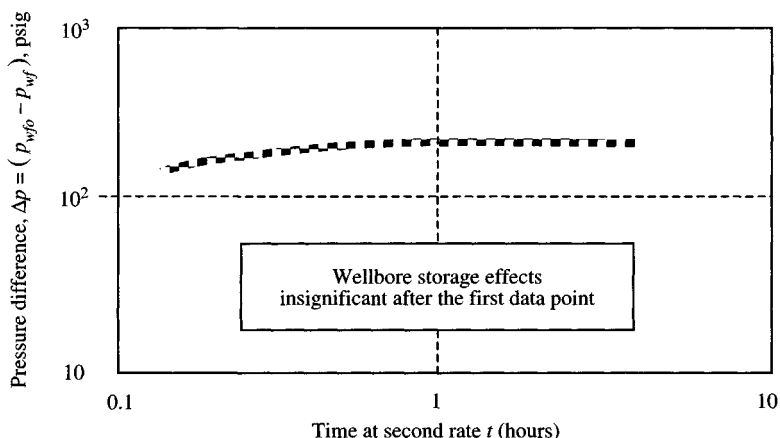


Figure 14-19. Log-log data plot for two-rate injection test.

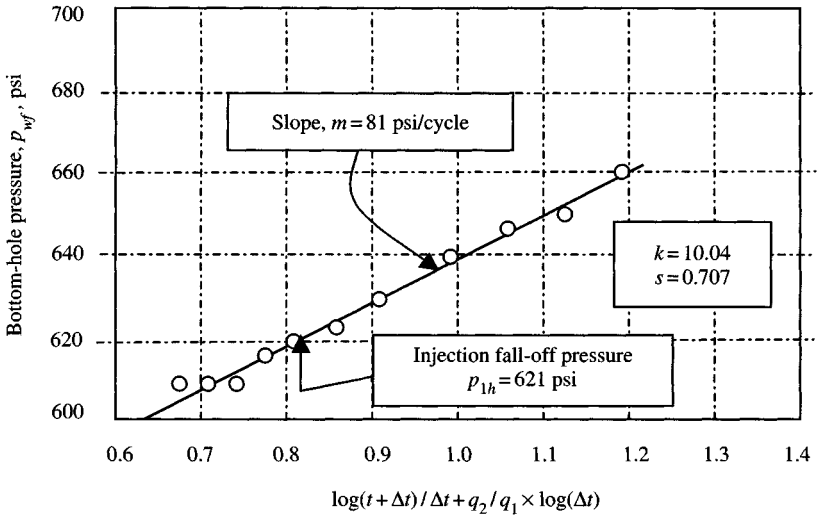


Figure 14-20. Coordinate plots – two-rate fall-off test.

A step rate injectivity test consists of injection fluid at a series of increasing rates. Each rate will last about 1 hour; 30 min injection times are adequate for formation with $k > 10$ mD. Normally four to eight rates are preferred.

Estimation of Formation Fracture Pressure

A plot of bottom-hole pressure or surface pressure versus injection rate should give two straight-line segments. The break in the time indicates formation fracture pressure, p_f . The fracture gradient is given by

$$\frac{[(G_{Rinj})(D) + p_f]}{D} \quad (14-45)$$

where

G_{Rinj} = injected fluid pressure gradient, psi/ft

D = depth, ft

p_f = formation fracture pressure, psi

Pressure data taken during each rate may be analyzed with multiple rate transient technique. Pressure behavior caused by a variable flow rate is given by:^{1,3}

$$\frac{P_i - P_{wf}}{q_N} = m' \sum_{j=1}^N \left[\frac{(q_j - q_{j-1})}{q_N} \times \log(t - t_{j-1}) \right] + b' \quad (14-46)$$

Table 14-9
Two-Rate Injectivity Test Data

Time, Δt (hr)	p_{wf} (psi)	Pressure difference ($p_{wfo} - p_{wf}$) (psi)	$\log(t_p + \Delta t)/\Delta t$	$\log \Delta t$	$\log(p_{wfo} - p_{wf}) + q_1/q_2 \log(t_p + \Delta t)/\Delta t$
0.000	832.0	—	—	—	—
0.167	661.3	170.7	1.5798	-0.7771	1.2029
0.333	642.0	190.0	1.2913	-0.4775	1.0597
0.500	639.0	193.0	1.1258	-0.3010	0.9798
0.667	628.0	204.0	1.0114	-0.1758	0.9261
0.833	623.1	208.9	0.9253	-0.0793	0.8868
1.000	621.0	211.0	0.8562	0.0000	0.8562
1.333	620.0	212.0	0.7510	0.1248	0.8116
1.667	611.7	220.3	0.6728	0.2219	0.7804
2.000	611.7	220.3	0.6118	0.3010	0.7577
3.000	611.7	220.3	0.4858	0.4770	0.7171
4.000	611.7	220.3	0.4057	0.6020	0.6977
5.000	611.7	220.3	0.3495	0.6988	0.6885

Eq. 14-46 is the equation of a straight line with slope

$$m' = \frac{162.6\beta\mu}{kh} \quad (14-47)$$

and intercept

$$b' = m' \left[\log \left(\frac{k}{\phi\mu c_t r_w^2} \right) - 3.23 + 0.869s \right] \quad (14-48)$$

A plot of $(p_i - p_{wf})/q_N$ versus $\sum_{j=1}^N [(q_i - q_{j-1})/q_N] \log(t - t_{j-1})$ should appear as a straight line. Once the data plot is made, straight-line slope and intercept are measured. Permeability and skin factor are estimated by using the following equations:

$$k = \frac{162.6\beta\mu}{m'h} \quad (14-49)$$

and

$$s = 1.1513 \left[\frac{b'}{m'} - \log \left(\frac{k}{\phi\mu c_t r_w^2} \right) + 3.23 \right] \quad (14-50)$$

In this multiple-rate analysis, a unit mobility ratio is assumed. The next example will illustrate the analysis of step-rate injectivity test.

Example 14-7 Analyzing Step-Rate Injectivity Test

Felsenthal⁴ provides the data in Table 14-10 for a step-rate test in a reservoir with the following properties: $h = 270$ ft; $c_t = 1.5 \times 10^{-5}$ psi⁻¹, $r_w = 0.25$ ft; $\phi = 0.186$ fraction; $\mu_w = 0.45$ cP; $\beta_w = 1.0$ rb/stb; well depth = 7260 ft and injected fluid pressure gradient = 0.433 psi/ft. Estimate formation permeability and skin factor.

Solution Figure 14-21 shows the normal step-rate data plot, p_{if} versus q . The break in the data indicates a surface fracture pressure of about 1000 psi. The fracture gradient is estimated by using Eq. 14-45.

$$[(0.433)(7260) + 1000]/7260 = 0.57 \text{ psi/ft}$$

The data in Table 14-10 also may be analyzed for formation properties by using the equation described in this section. Columns 4 and 5 in Table 14-10 contain the data to be plotted according to Eq. 14-46. Figure 14-22 shows

Table 14-10
Step-Rate Test Data

Time, t (hr)	Injection rate, q (stb/d)	Tubing pressure p_{tf} (psig)	$(p_i - p_{tf})/q$ psi/stb/d	$\sum [(q_i - q_{i-1})/q_n \times \log(t - t_{i-1})]$
0.00	0	642.0	—	—
0.50	-100	720.0	0.7800	-0.3000
1.00	-100	730.0	0.8800	0.0000
1.50	-250	856.0	0.8560	-0.1102
2.00	-250	874.0	0.9280	0.1204
2.25	-750	1143.0	0.6680	-0.3350
2.50	-750	1182.0	0.7200	-0.1124
3.00	-750	1216.0	0.7653	0.1238
4.00	-1150	1450.0	0.7026	0.2454

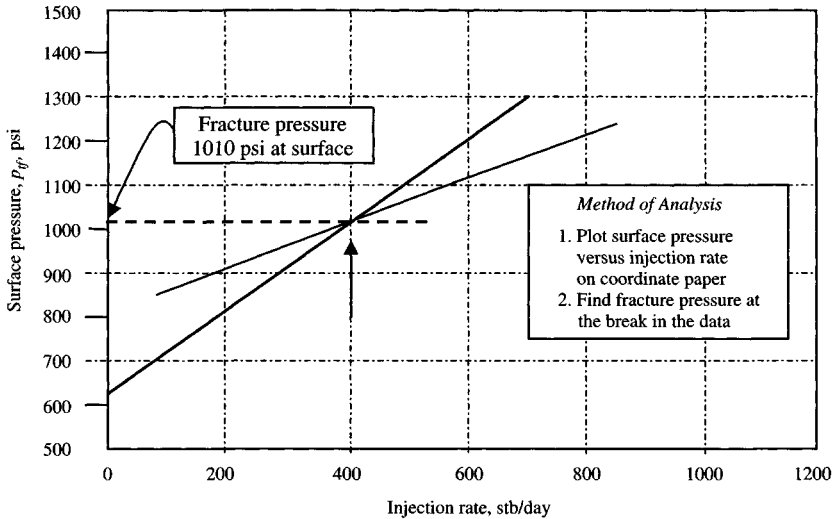


Figure 14-21. Fracture pressure calculation.

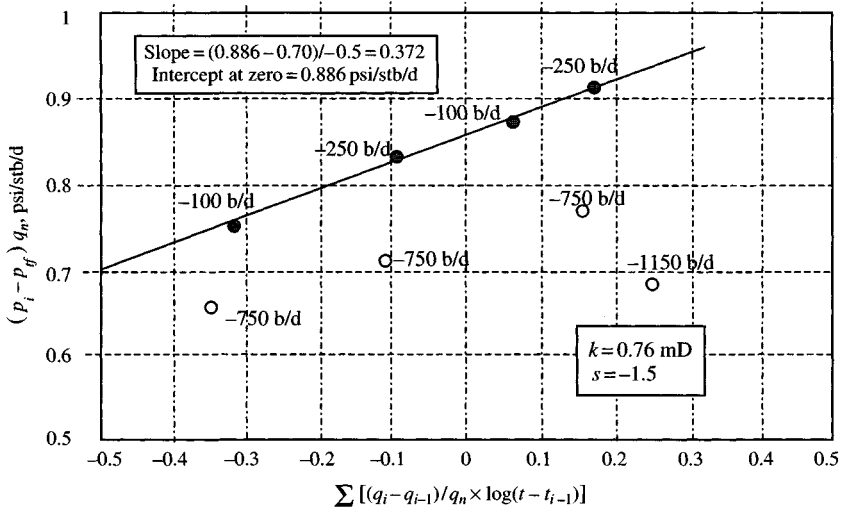


Figure 14-22. Step-rate injectivity test analysis for water flood reservoir.

the data plot. The first four points, for the rates before the fracture occurred, fall on the expected straight line. That line has the properties:

$$\text{Slope, } m' = 0.357[\text{psi/stb/day}]\text{cycle}$$

and

Intercept, $b' = 0.885[\text{psi}/(\text{stb}/\text{day})]$

Estimate formation permeability, k , from Eq. 14-49:

$$k = \frac{162.6\mu\beta}{m'h} = \frac{162.6(1.0)(0.45)}{(0.357)(270)} = 0.76 \text{ mD}$$

Determine skin factor, s , from Eq. 14-50:

$$s = 1.1513 \left[\frac{b'}{m'} - \log \left(\frac{k}{\phi\mu c_t r_w^2} \right) + 3.23 \right]$$

$$= 1.1513 \left[\frac{0.885}{0.357} - \log \left(\frac{0.76}{(0.186)(0.45)(1.5 \times 10^{-5})(0.25)^2} \right) + 3.23 \right] = -1.5$$

In Figure 14-22, the data points are for $q = -750$ and $q = -1150$ stb/d. It does not fall on the straight line. These points correspond to data taken after the formation fracture.

14.6 Summary

This chapter presents pressure analysis techniques in injection wells. The injectivity test and the fall-off tests are used to estimate the reservoir properties of injection wells in waterflood and EOR recovery projects. The knowledge of reservoir properties and near wellbore conditions in injection wells is as important as in the producing wells. Injection well transient testing and analysis are simple as long as the mobility ratio between the injected and in-situ fluids is about unity and the radius of investigation is not beyond the water (injected) fluid) bank.

References

1. Hall, H. N., "How to Analyze Waterflood Injection Well Performance," *World Oil* (Oct. 1963), 128-130.
2. Van Poolen, H. K., "Radius-of-Drainage and Stabilization Time Equation," *Oil Gas J.* (Sept. 14, 1964), 138-146.
3. Hazelbroek, P., Rainbow, H., and Matthews, C. S., "Pressure Fall-Off in Water Injection Wells," *Trans. AIME* (1958) 213, 250-260.
4. Felsenthal, M., "Step-Rate Tests Determine Safe Injection Pressures in Floods," *Oil Gas J.* (Oct. 28, 1974).

5. Matthews, C. S., and Russell, D. G., Pressure Build-up and Flow Tests in Wells. SPE of AIME Monograph. Vol. 1, Henry Doherty Series, 1967, pp. 78–80.
6. Amanat, U. C., “Pressure Transient Test Analysis, User’s Handbook,” Advanced TWPSOM Petroleum Systems Inc; Houston, Texas, Vol 8 (1995).

Additional Reading

1. Merrill, L. S., Jr., Kazemi, H., and Gogarty, W. B., “Pressure Falloff Analysis in Reservoirs With Fluid Banks,” *J. Pet. Technol.* (July 1974), 809–818; *Trans. AIME* 257.
2. Gogarty, W. B., Kinny, W. L., and Kirk, W. B., “Injection Well Stimulation With Micellar Solutions,” *J. Pet. Technol.* (Dec. 1970), 1577–1584.
3. Dowdle, W. L., “Discussion of Pressure Falloff Analysis in Reservoirs With Fluid Banks,” *J. Pet. Technol.* (July 1974), 818.
4. Kazemi, H., Merrill, L. S., and Jargon, J. R., “Problems in Interpretation of Pressure Fall-Off Tests in Reservoirs With and Without Fluid Banks,” *J. Pet. Technol.* (Sept. 1972), 1147–1156.
5. Earlougher, R. C., Jr., Kersch, K. M., and Ramey, H. J., Jr., “Wellbore Effects in Injection Well Testing,” *J. Pet. Technol.* (Nov. 1973), 1244–1250.

Chapter 15

Well Testing Methods in Multilayered Oil Reservoir Systems

15.1 Introduction

This chapter discusses various types and testing of layered oil reservoir systems including multilayered responses in fractured reservoirs. It also describes crossflow identification and the nature and degree of communication between layers. Performance equations for cases of constant flowing pressure and constant producing rate are presented and discussed. This chapter also reviews “layer effect” on pressure and/or production behavior including economic aspects of interlayer crossflow.

15.2 Identification of Layered Oil Reservoir Systems

Figure 15-1 shows the classification of layered oil reservoir systems.

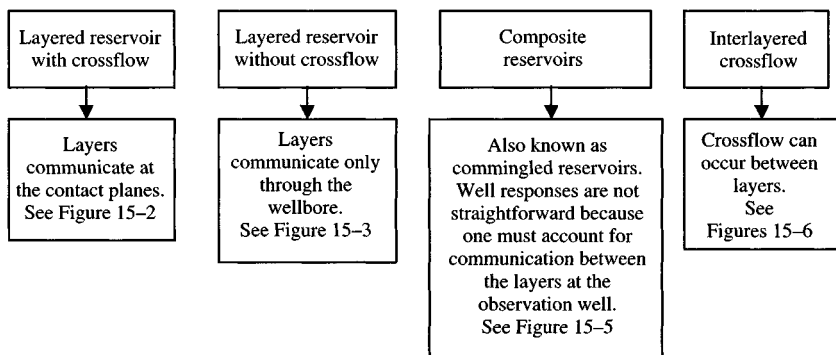


Figure 15-1. Classification of oil reservoir systems.

15.3 Analyzing Pressure Behavior in Multilayered Systems

Multilayered reservoirs can be classified into two categories: layered reservoirs with crossflow, in which layers are hydrodynamically communicating at the contact places and layered reservoirs without crossflow, in which layers communicate only through the wellbore. This type of system without crossflow is also called a “commingled system.”

Layered Reservoir with Crossflow

Figure 15–2 shows a four-layer oil reservoir with crossflow allowed between the layers. Pressure transient testing in such reservoirs is the same as the behavior of the homogeneous system. The following relationships can be applied for such systems.

Permeability–thickness product

$$(kh)_t = \sum_{j=1}^n (kh)_j \quad (15-1)$$

Porosity–compressibility product

$$(\phi c_t h)_t = \sum_{j=1}^n (\phi c_t h)_j \quad (15-2)$$

The total number of layers is n . The individual layer permeabilities may be approximated from

$$k_j = \left(\frac{q_j}{q} \right) \left[\frac{(kh)_t}{h_j} \right], \quad j = 1, 2, \dots, n \quad (15-3)$$

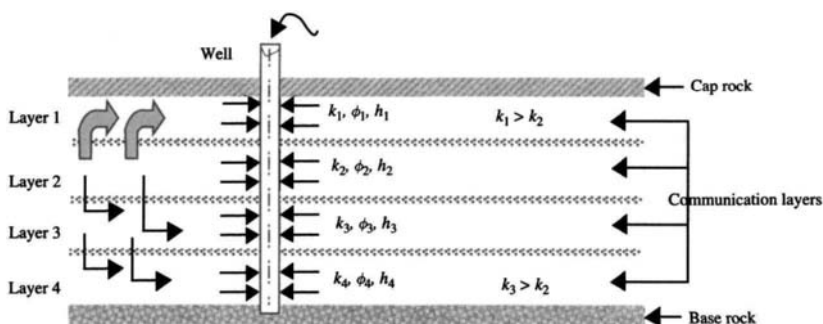


Figure 15–2. Four-layer crossflow reservoir.

Layered Reservoir without Crossflow

Figure 15-3 shows a four-layer reservoir with the layers separated by a shale barrier. Oil production is commingled at the well, so layers communicate only through the well. Early-time pressure drawdown behavior in such a system yields a straight line on the semilog plot as shown in Figure 15-4. Boundary effects cause the upward bending in Figure 15-4. After a long production time, pseudo-steady-state conditions exist and pressure behavior will be linear with time. Refs. 3, 5, and 7 have proposed methods for estimating both the location of the oil, water banks in Figure 14-14, and the permeability of the two fluid banks in a two-zone system. Pseudo-steady state begins approximately at:⁸

$$(t_{DA})_{pss} \cong 23.5 \left(\frac{k_1}{k_2} \right), \quad k_1 > k_2 \quad (15-4)$$

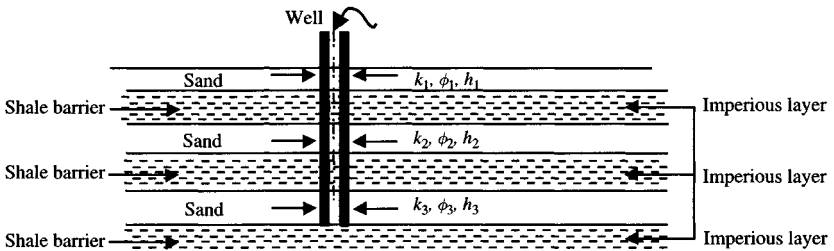


Figure 15-3. Three-layer without crossflow reservoir.

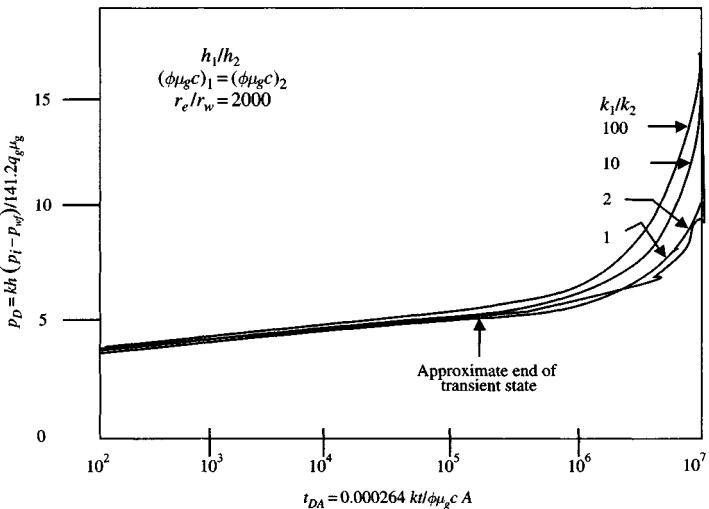


Figure 15-4. Muskat straight line intercepts for two-layer reservoirs without crossflow (after Ramey and Miller, JPT, Jan. 1972).⁴

Time at the beginning of pseudo-steady state also depends on

- relationship between ϕ , h , and compressibility in the various layers,
- reservoir shape,
- number of layers, and
- well location.

Figure 15-4 shows a graph of dimensionless pressure, p_D , versus dimensionless time, t_D , for a two-layer reservoir with permeability ratios k_1/k_2 of 1, 2, 10, and 100. All four curves are for r_e/r_w of 2000. The dimensionless terms are

$$t_D = \frac{0.000264\bar{k}t}{\phi\mu_g cr_w^2} \quad (15-5)$$

$$t_{DA} = \frac{0.000264\bar{k}t}{\phi\mu_g cA} \quad (15-6)$$

$$p_D = \frac{\bar{k}h(p_i - p_{wf})}{141.2q\mu_o\beta_o} \quad (15-7)$$

where

$$\bar{k} = \frac{k_1h_1 + k_2h_2}{h_1 + h_2} \quad (15-8)$$

$$\bar{h} = h_1 + h_2 \quad (15-9)$$

$$\bar{\phi} = \frac{\phi_1h_1 + \phi_2h_2}{h_1 + h_2} \quad (15-10)$$

Figure 15-4 indicates that during the early transient period, the slope of the straight line is 1.151 (2.303/2). The approximate semilogarithmic period ends at $t_D = 5 \times 10^5$ and behavior beyond the end of the semilogarithmic period is strongly influenced by permeability ratio.

Composite Reservoirs

This type of reservoir is also known as commingled reservoirs. Layers communicate only through the wellbore as shown in Figure 15-5. In recent years, investigators¹⁻³ have conducted studies on wells with commingled fluid production from two or more noncommunicating zones. In those cases, fluid is produced into the wellbore from two or more separate layers and is carried to the surface through a common wellbore.

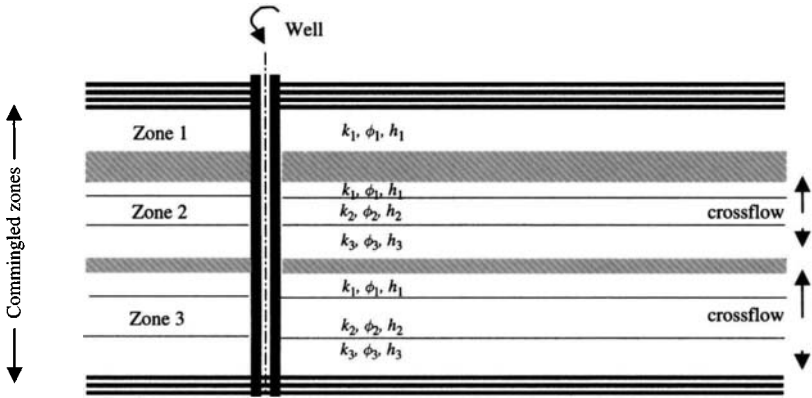


Figure 15-5. Reservoir consisting of commingled zones and crossflow layers.

Interlayer Crossflow Reservoir

Figure 15-6 shows that the crossflows between the layers can occur; the pressure and production behavior of a gas well can be interpreted by the use of homogeneous reservoir theory. An oil well in a layered reservoir with crossflow behaves as a well in a homogeneous, single-layer reservoir that possesses the same dimensions and pore volume as the crossflow system and

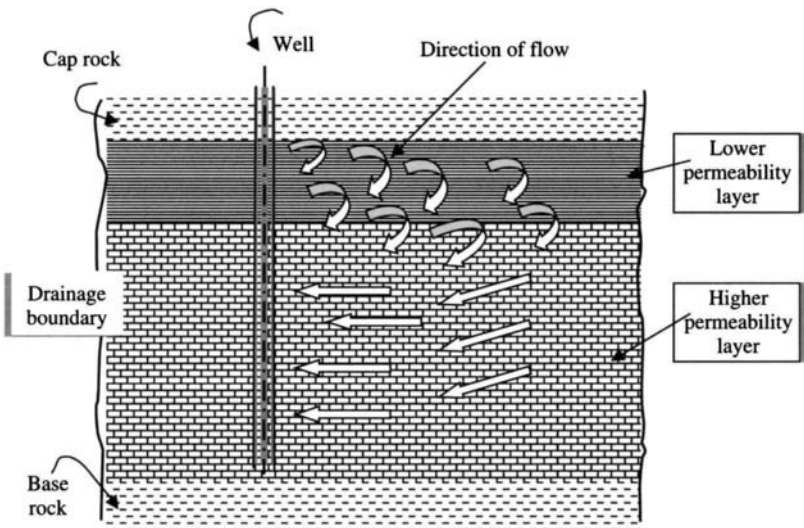


Figure 15-6. Schematic view of a portion of a two-layer reservoir with interlayer crossflow.

a permeability–thickness product (kh) equal to the total kh of the crossflow system. The occurrence of crossflow can be confirmed by the homogeneous-like appearance of the pressure and/or production behavior.

15.4 Concept of Reservoir Layer Fracture Conductivity

Raghavan et al.⁷ have introduced the concept of reservoir layer conductivity, C_{RDj} , given by

$$C_{RDj} = \frac{k_j h_j}{kh} \sqrt{\frac{\bar{\eta}}{\eta_j}} \quad (15-11)$$

where η_j = diffusivity of layer j , $\bar{\eta} = \bar{k}/(\bar{\phi}\bar{c}_t\mu_g)$, $C_{RD} = \sum_{j=1}^n C_{RDj}$, and an equivalent fracture length and equivalent fracture conductivity are defined, respectively, by

$$\bar{x}_f = \sum_{j=1}^n C_{RDj} x_{fj} \quad (15-12)$$

and

$$\bar{k}_f \bar{w} = \frac{\left(\sum_{j=1}^n \sqrt{k_{fj} w_j h_j C_{RDj}} \right)^2}{h_t} \quad (15-13)$$

The dimensionless fracture conductivity is then defined by

$$C_{fD} = \frac{\bar{k}_f \bar{w}}{\bar{k} \bar{x}_f} \quad (15-14)$$

Camacho et al.⁶ have studied the correlations of multilayer responses with the single-layer solutions for a number of cases. They assume that the fractures are not in communication. If fractures are in communication, the values of C_{fD} are somewhat higher and the ratio h_f/x_{fj} is an important factor in the performance of the fractured well. When layers are stimulated by fractures, then maximum productivity will be achieved if the fracture tip in each layer begins to affect the well response at approximately the same time. For a two-layer gas reservoir system, the criterion for maximum productivity is given by

$$\frac{\bar{C}_{fD2} h_2}{C_{fD1} h_1} = \frac{C_{RD2} x_{f2}}{C_{RD1} x_{f1}} \quad (15-15)$$

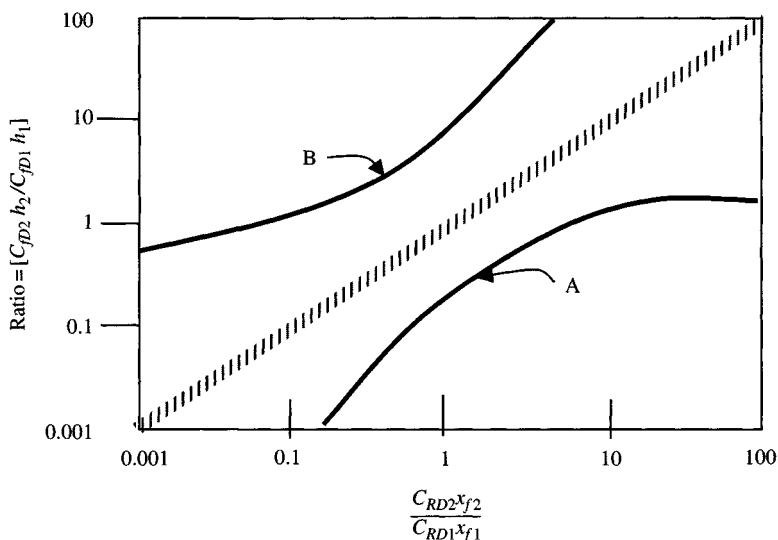


Figure 15-7. Criteria for maximum productivity (after Camacho et al., 1987).⁶

where

$$\bar{C}_f D_j = \frac{k_{fj} w_j}{\bar{k} x_{fj}}$$

The dashed lines in Figure 15-7 represent Eq. 15-15. These results are based on the assumption that boundary effects are negligible. The reservoir layer conductivity concept does not apply if boundary effects dominate the pressure response. During pseudo-steady-state flow the well response is given by (well in a circular reservoir)

15.5 Pressure Production Performance Response Equations

The pressure production performance relationships for the cases of constant producing pressure and constant producing rate are given below.^{4,10,14}

Constant Producing Pressure

For the case of constant bottom-hole producing pressure, the following formula for producing rate developed in Ref. 5 has also provided

the method to calculate cumulative production from multilayered reservoirs.

$$(kh)_t = k_1h_1 + k_2h_2, \quad (\phi h)_t = \phi_1h_1 + \phi_2h_2$$

$$q_o = \frac{(kh)_t(p_i - p_{wf})}{141.2\beta_o\mu_o \left(\ln \frac{r_e}{r_w} - 0.75 \right)} e^{-AB} \quad (15-16)$$

where

$$AB = \left[\frac{0.0127(kh)_t}{(\phi h)_t c \mu_o r_e^2 \left(\ln \frac{r_e}{r_w} - 0.75 \right)} \right]$$

Constant Producing Rate

Transient bottom-hole pressure performance of a well in a reservoir with crossflow is given by³

$$p_{wf} = p_i - \frac{162.6q_o\mu_o\beta_o}{(kh)_t T_{sc}} \left[\log \frac{(kh)_t t}{(\phi h)_t \mu_o c r_w^2} - 3.23 \right] \quad (15-17)$$

For semisteady state (larger times), the pressure behavior is described by

$$p_{wf} = p_i - \frac{141.2q_o\mu_o\beta_o}{(kh)_t} \left[\frac{0.000528(kh)_t t}{(\phi h)_t \mu_o c r_e^2} + \ln \left(\frac{r_e}{r_w} \right) - 0.75 \right] \quad (15-18)$$

where t = time in hours; $(kh)_t = k_1h_1 + k_2h_2$; $(\phi h)_t = (\phi_1h_1) + (\phi_2h_2)$; and $h_t = h_1 + h_2$.

The time at which semisteady state starts is given by

$$t \cong 1136.4 \frac{(\phi h)_t \mu_o c r_e^2}{(kh)_t} \quad (\text{hr}) \quad (15-19)$$

For semisteady-state flow, the slope of the plot of flowing bottom-hole pressure versus time is given by

$$\text{Slope} = 0.07455 \frac{q_o\beta_o}{(\phi h)_t c r_e^2} \quad (\text{psi/hr}) \quad (15-20)$$

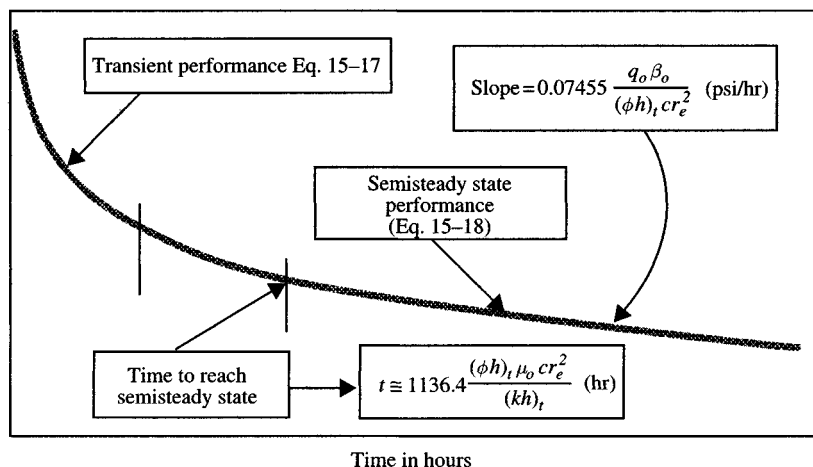


Figure 15-8. Idealized constant-rate pressure performance in two-layer reservoir with crossflow (after Russell and Prats, JPT, June 1962).⁸

Figure 15-8 shows an idealized constant-rate flowing bottom-hole pressure performance curve, and reservoirs of this type should possess the properties shown on this plot.

15.6 Investigating Degree of Communication and Type of Crossflow

Figure 15-9 presents the methods that can be used to identify the degree of communication between layers and type of crossflow.

15.7 Pressure Buildup Characteristics in Layered Reservoir Systems

Figure 15-10 shows pressure buildup behavior in single-well, multilayer reservoir systems. Lefkovits et al.¹ and Raghavan et al.⁷ have stated that, after the initial semilog straight line, the buildup curve flattens, then steepens, and finally flattens toward the average reservoir pressure as indicated in the figure. This is not always correct. The C-D portion in Figure 15-10 can be insignificant for some systems. This is particularly true for large contrasts in porosity or thickness, for more than two layers, or for nonsymmetrical systems. Classifications and pressure response characteristics including detailed analysis of multilayer reservoir systems are described in the previous sections.

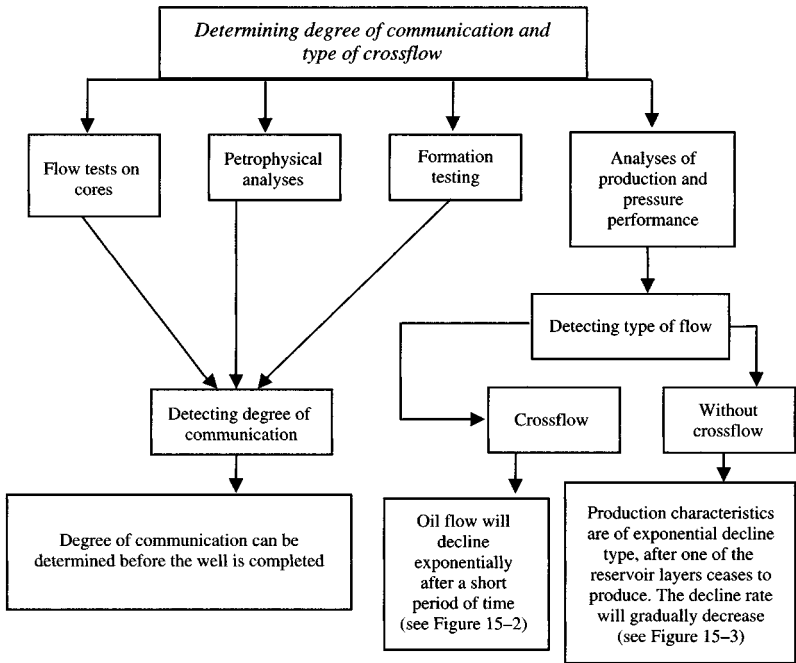


Figure 15-9. Systemic diagrams to determine degree of communication and type of crossflow.

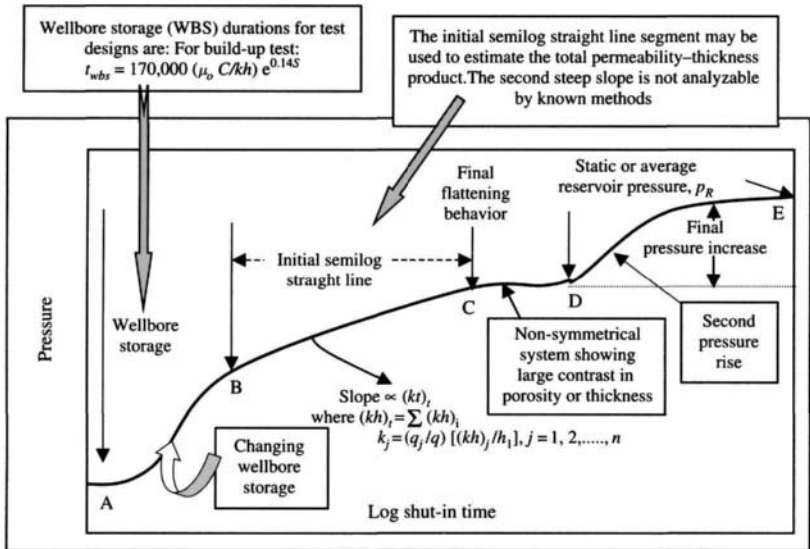


Figure 15-10. Schematic pressure buildup curve for layered reservoir system.⁵

15.8 Pressure Analysis Methods for Oil Wells Producing Commingled Zones

The following methods can be used to analyze multilayer reservoir systems.

Conventional Analysis Method (Horner Plot)

Early portion of the Horner buildup plot is linear with a slope of approximately 1.151. This early straight line provides a means of estimating $\bar{k}h$ directly. Under certain conditions buildup data can be extrapolated to static pressure. Late buildup is the result of additional buildup and is carried by fluids flowing from the lower kh to higher kh zone. This will be greater if permeability ratio and producing time are large. This method requires a plot of buildup pressure versus $\log(t_p + \Delta t)/\Delta t$. Buildup pressures would clearly be a linear function of $\log(t_p + \Delta t)/\Delta t$. Slope of such semilog plot would be 1.151. The average reservoir permeability can be estimated from the following equation:

$$\bar{k} = \frac{162.6q_o\mu_o\beta_o}{m\bar{h}} \quad (15-21)$$

where m is the slope of straight line of semilog plot. Figure 15-11 illustrates how to determine \bar{p} for a two-layer reservoir having permeability ratio

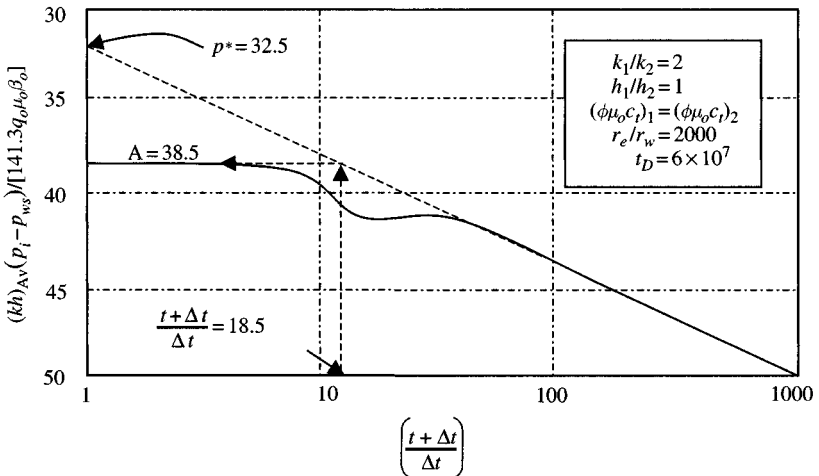


Figure 15-11. Extrapolation of initial Horner straight line to static pressure for a two-layer reservoir.

of 2. The entire pressure buildup can be computed by using the following equation:

$$\frac{\bar{k}h}{141.3q_o\mu_o\beta_o}(p_i - p_{ws}) = p_D(t + \Delta t)_D - p_D(\Delta t)_D \quad (15-22)$$

Extrapolation of the proper straight line to a time ratio of unity gives the false pressure, p^* . Thus we can determine graphically the MBH dimensionless function of $(p^* - \bar{p})$ as

$$\frac{\bar{k}h}{70.65q_o\mu_o\beta_o}(p^* - \bar{p}) = 2(A - p^*) = 2(38.5 - 32.5) = 12$$

$$\ln\left(\frac{t + \Delta t}{\Delta t}\right) = \ln(18.5) = 2.92$$

The value of A can be found from Horner plot as shown in Figure 15-11. Therefore \bar{p} is equal to

$$\bar{p} = p^* - \frac{141.3q_o\mu_o\beta_o(A - p^*)}{\bar{k}h}$$

Figure 15-11 shows that the proper straight line does indeed extrapolate to the fully static pressure at this value of time ratio. Fractional production rate from each layer during the early transient period is approximately equal to

$$\frac{q_1}{q} = \frac{k_1h_1}{k_1h_1 + k_2h_2}$$

and

$$\frac{q_2}{q} = 1 - \frac{q_1}{q} = \frac{k_2h_2}{k_1h_1 + k_2h_2}$$

At pseudo-steady state, the fractional production rate from such layer is equal to

$$\frac{q_1}{q} = \frac{h_1\phi_1}{h_1\phi_1 + h_2\phi_2}$$

and

$$\frac{q_2}{q} = 1 - \frac{q_1}{q} = \frac{h_2\phi_2}{h_1\phi_1 + h_2\phi_2}$$

MDH Method

This plot also provides a straight line for the case buildup and slope of 1.151 for a producing time of any length. $\bar{k}h$ can be estimated as well as static pressure. The following equation can be used to construct ideal MDH plots for any drainage shape for producing times of any length:

$$\frac{\bar{k}h}{141.3q_o\mu_o\beta_o}(\bar{p} - p_{ws}) = p_D(t_D) - p_D(\Delta t)_D - 2\pi t_{DA} \quad (15-23)$$

This plot should yield a straight line with a slope of approximately 1.151 on semilog graph paper. If the early straight line can be identified, the average reservoir permeability can be determined from

$$\bar{k} = \frac{162.6q_o\mu_o\beta_o}{m\bar{h}} \quad (15-24)$$

where m is the slope of the MDH straight line in psi/cycle. Estimation of static pressure depends greatly on the permeability ratio. Figure 15-12 can be used to reveal the essential character of pressure buildup for any specific flow system and determine fully static pressure. Figures 15-12 and 15-13 indicate that an initial straight line exists only to a shut-in time of about $\Delta t_{DA} = 0.01$. If values of Δt_{DA} greater than 0.01 are obtained, the choice of straight line should be suspect.

Extended Muskat Plot

Length of buildup to reach the proper straight line decreases as producing time increases. This method can be used to estimate flow capacity and static pressure and to determine reservoir pore volume. This method employs (\bar{p} assumed) the logarithm of $(\bar{p} - p_{ws})$ against Cartesian buildup time, Δt . The pressure \bar{p} is the fully static pressure desired for material balance study. The following equation provides a basis for making a dimensionless Muskat plot for a well located in any drainage region, shut-in after a producing time of any length:

$$\frac{\bar{k}h}{141.3q_o\mu_o\beta_o}(\bar{p} - p_{ws}) = p_D(t_D) - p_D(\Delta t)_D - 2\pi t_{DA} \quad (15-25)$$

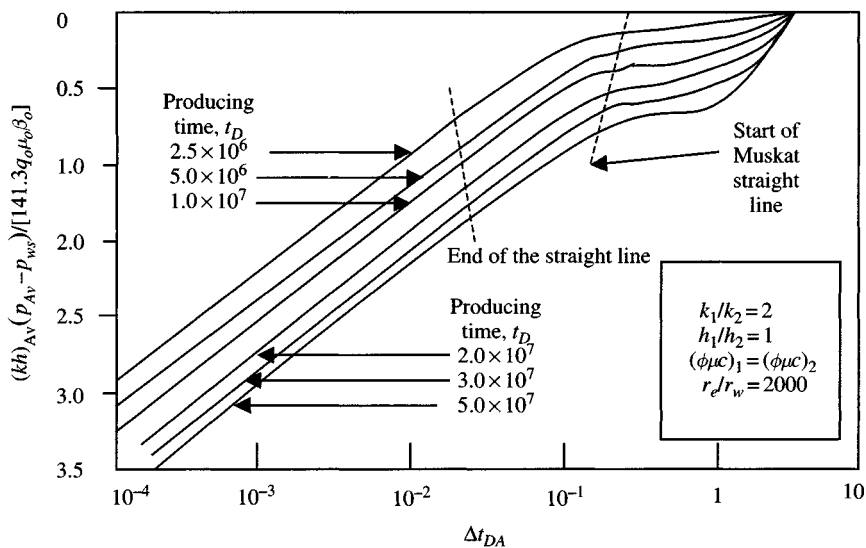


Figure 15-12. MDH buildup for a well in the center of a closed, two-layer reservoir with a permeability ratio of 2.4

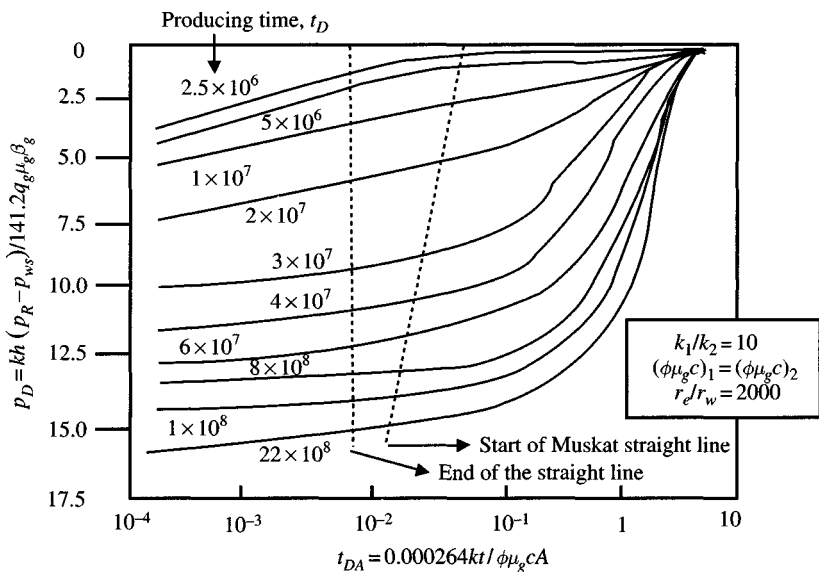


Figure 15-13. MDH buildup curves (after Raghavan et al., JPT, Sept. 1974).⁷

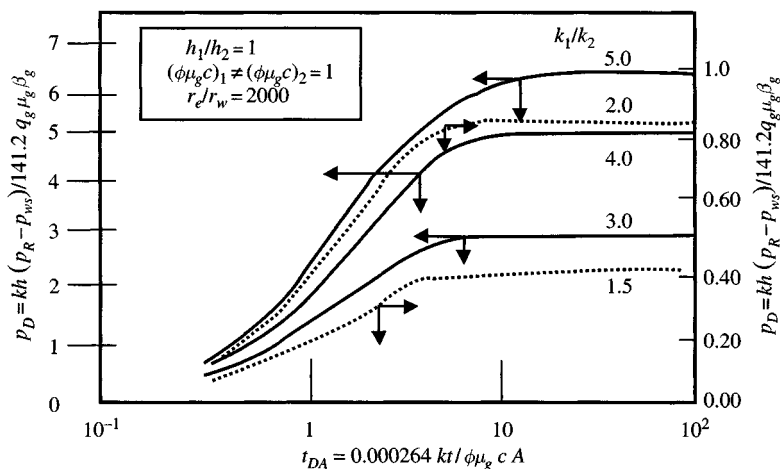


Figure 15-14. Muskat straight line intercepts for two-layer reservoirs (after Ramey and Miller, JPT, Jan. 1972).⁴

The Muskat method should be used with extreme care for determining static pressure. Figure 15-14 is a plot of Muskat straight-line intercepts versus the logarithm of producing time for selected permeability ratios. Thus, knowing the Muskat straight-line intercept at known permeability ratio, average reservoir permeability may be estimated by

$$\bar{k}h = \frac{141.3q_o\mu_o\beta_o (\text{intercept})_{\text{Muskat}}}{(\bar{p} - p_{ws})_{\Delta t=0}} \quad (15-26)$$

$$t_{DA} = 0.000264 \frac{\bar{k}t}{\phi\mu_o c_i A} \quad (15-27)$$

Interpretation equation for $A\phi c$ is

$$A\phi c = -(0.350)(0.000264) \frac{\bar{k}}{\mu_o} (m \log_{10} / \text{hr})^{-1} \quad (15-28)$$

where m is the slope of the Muskat plot straight line. For example, a two-layer reservoir with permeability contrast of 2. From Figure 15-14, the value is 0.87. The slope of all the straight lines for the reservoir with a permeability contrast of 2 is $-0.350 \log_{10}$.

Figure 15-15 presents a family of Muskat plots for a permeability ratio of 2, producing time, t_D being considered. The upper limiting curve represents the producing time required to reach pseudo-steady state before

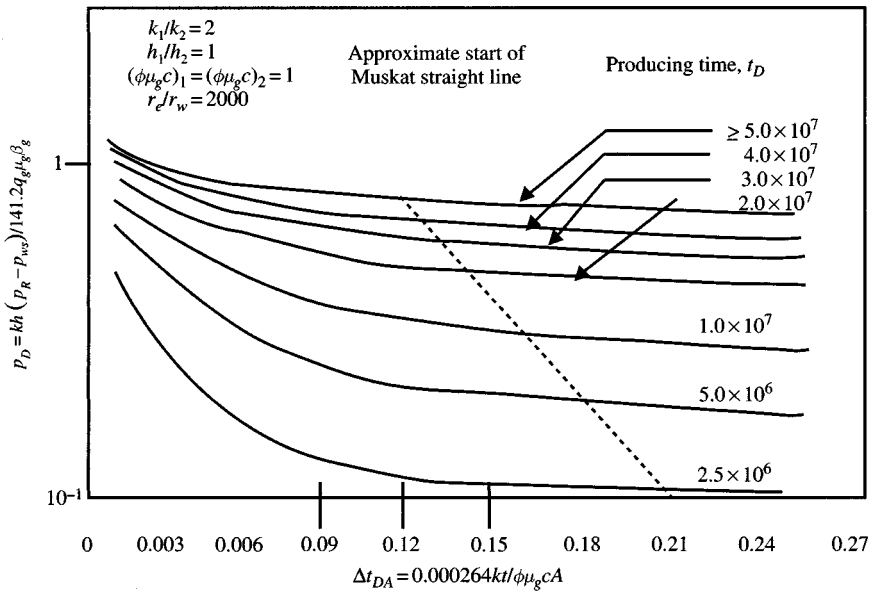


Figure 15-15. Muskat plot for four-layer reservoir with a permeability contract of 2. (after Ramey and Miller, Jan. 1972).⁴

shut-in. For producing times less than those shown, longer shut-in times should be expected.

Other Methods

Cobb et al.⁴ have provided techniques to determine average reservoir pressure in commingled systems. It requires some knowledge of the layer properties and correlations for specific systems. The following types of tests may be used to estimate individual zone properties for two-layer reservoir with communication only at the wellbore:

- single-well test,
- pulse tests, and
- flow meter surveys.

Apparent kh/μ_o is always equal to or greater than the actual total $(kh/\mu_o)_t$ for the reservoir. Apparent $\phi c_t h$ is always equal to or less than the total $(\phi c_t h)_t$ for the reservoir. Deviation of apparent values from actual total values depends on the pulse duration.

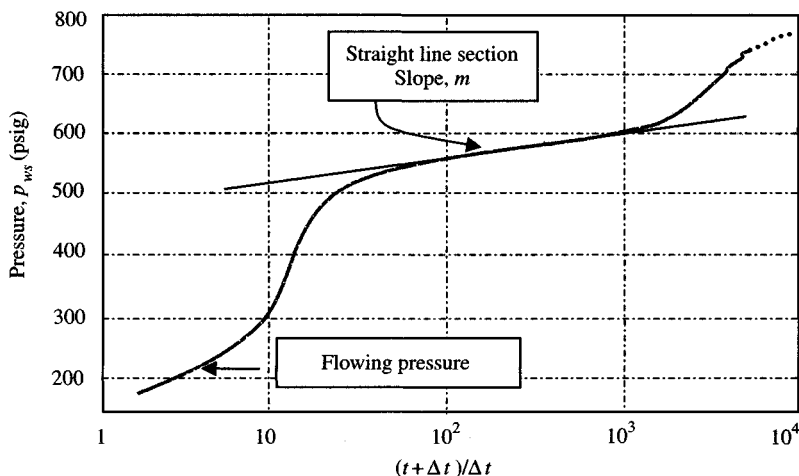


Figure 15-16. Pressure buildup behavior in two-layer oil reservoir.

The pressure builds up first in the more permeable layer, giving a straight-line section as shown in Figure 15-16. Then the less permeable layer, which is at a higher average pressure, begins to feed fluid into the more permeable layer. This causes the rise above the straight line. Finally, equalization will occur and the curve will flatten as indicated by the dotted line. Figure 15-16 shows pressure buildup behavior in two-layer oil reservoir including the effects of wellbore.

15.9 Factors Affecting Multilayered Reservoir Performance

The following factors can affect the performance of multilayered reservoir systems:

- *Relative permeability*: If both layers have the same relative permeability characteristics, average water saturation will be higher in the tighter layer than in the more permeable layer, because the average pressure is always higher in the less permeable layer.
- *Pore size*: If pore size in the tight layer is smaller than that in the more permeable layer, then it will tend to reduce crossflow. This effect can be estimated from capillary pressure curves.
- *Reservoir geometry*: Geometrical nature and extent of interlayer communication have some effect on observed field performance.
- *Permeability anisotropy*: In most petroleum reservoirs, vertical permeability is significantly less than horizontal permeability.

- *Reservoir n-layer system:* Analysis of performance can be handled to acceptable accuracy merely by the previously presented formulae $\sum_j^n k_j h_j$ and $\sum_j^n \phi_j h_j$ for $(kh)_i$ and $(\phi h)_i$, respectively.

15.10 Economic Aspects of Interlayer Crossflow

The absence or presence of crossflow between interlayer can control the economic success of oil production venture. Some of the advantages of interlayer crossflow are listed below:

- shorter operating life,
- higher ultimate oil production,
- reduced perforating and completion costs, and
- less engineering time for interpretation of routine tests.

Note: Without-crossflow reservoir can be converted into crossflow reservoir by fracturing. Thus a vertical fracture can help to establish vertically adjacent gas production strata which were not in communication prior to the fracture job except at the wellbore.

15.11 Summary

This chapter reviews various types and testing of layered oil reservoir systems including multilayered responses in fractured reservoirs. It also describes crossflow identification and the nature and degree of communication between layers. Performance equations for cases of constant flowing pressure and constant producing rate are presented and discussed. This chapter also reviews “layer effect” on pressure and/or production behavior including economic aspects of interlayer crossflow.

References and Additional Reading

1. Lefkovits, H. C., Hazebrock, P., Allen, E., and Matthews, C. S., “A Study of the Behavior of Bounded Reservoirs Composed of Stratified Layers,” *Soc. Petroleum Eng. J.* (March 1961), 43–58.
2. Cobb, W. M., “A Study of Transient Flow in Stratified Reservoirs with Commingled Fluid Production,” Ph.D. dissertation, Stanford University, Stanford, CA, 1970.
3. Russell, D. G., and Prats, M., “The Practical Aspects of Inter Layer Cross Flow,” *J. Petroleum Technol.* (June 1962), 589–594.

4. Cobb, W. M., Ramey, H. J., Jr., and Miller, F. G., "Well Test Analysis for Wells Producing Commingled Zones," *J. Petroleum Technol.* (Jan. 1972), 27-37; *Trans. AIME* 253.
5. Earlougher, R. C., Jr., Kersch, K. M., and Kunzman, W. J., "Some Characteristics of Pressure Buildup Behavior in Bounded Multiple Layer Reservoirs without Crossflow," *J. Petroleum Technol.* (Oct. 1974), 1178-1186; *Trans. AIME* 257.
6. Camacho, V., Raghavan, R., and Reynolds, A. C., "Response of Wells Producing Layered Reservoirs, Unequal Fracture Length," *SPE Formation Eval* (Feb. 1987), 9-28.
7. Raghavan, R., Topaloglu, H. N., Cobb, W. M., and Ramey, H. J., Jr., "Well Test Analysis for Wells Producing from Two Commingled Zones of Unequal Thickness," *J. Petroleum Technol.* (Sept. 1974), 1035-1043; *Trans. AIME* 257.
8. Russell, D. G., Goodrich, J. H., Perry, G. E., and Brushkoter, J. F., "Methods for Predicting Gas Well Performance," *J. Petroleum Technol.* (Jan. 1966), 99-108.

Chapter 16

Pressure Analysis Methods in Heterogeneous Oil Reservoir Systems

16.1 Introduction

This chapter discusses variations of heterogeneities in rock and fluid properties including causes and effect of pressure-dependent properties. It also presents how to analyze and interpret pressure behavior in heterogeneous reservoirs near fault or other barriers and lateral changes in the hydraulic diffusivity such as occur at fluid contacts. Pressure behavior analysis methods are presented in brief to obtain adequate reservoir description for isotropic, anisotropic, and heterogeneous systems. Numerical solutions must be used to analyze pressure transient data from heterogeneous systems.

16.2 Effect of Pressure on Rock Properties

It is well known from laboratory studies as well as from observed pressure behavior in some wells that both porosity and permeability decrease as reservoir pressure declines. For reservoir rocks, which are “normally” compacted, these effects are usually less than for those which have unusually high pore pressure, i.e., geopressed reservoirs. Carbonate rocks are more heterogeneous. Sandstone rocks are less complex than carbonate rocks. However, a quantitative evaluation of the porosity resulting from the interaction of the various factors is possible only by laboratory measurements. Sandstone and other classic rocks tend to be more elastic in their behavior than carbonate rocks. Limestone often is somewhat plastic in its behavior.

In general, it is expected to observe a decline in calculated permeability from successive transient pressure tests run throughout the life of a well in depleted reservoirs, declines of 10% or so may be observed, but because of variations of

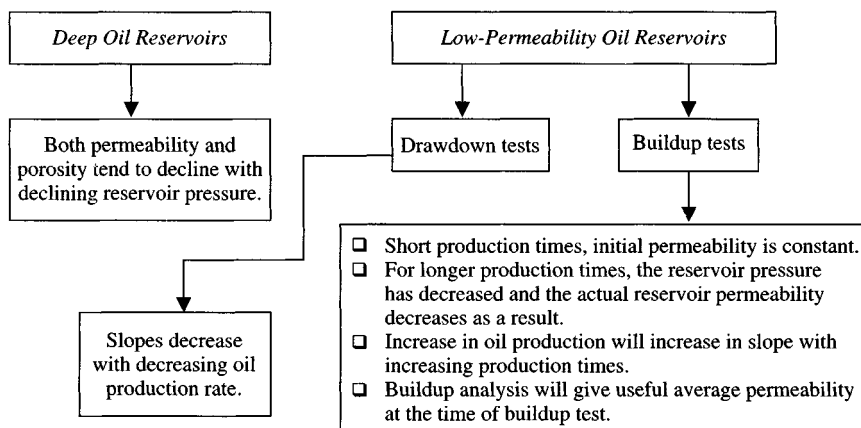


Figure 16–1. Effect of pressure-dependent permeability on drawdown and buildup tests.

other kinds such as two-phase flow effects, etc., quantitative evaluation becomes difficult. Therefore laboratory-determined curves of porosity and permeability versus pressure should be used to predict pressure behavior.

References 1 to 5 concluded that neither permeability nor skin factor should be estimated from drawdown or buildup tests using techniques like those given in Chapters 4 and 5 in formation with pressure-dependent permeability. Figure 16–1 illustrates their findings.

16.3 Major Causes of Heterogeneities

Heterogeneities may be caused because of:

- Post-depositional changes in reservoir lithology
- Folding and faulting
- Changes in fluid type or properties
- Variations in rock and fluid properties from one location to another
- Physical barriers, oil-water contacts, thickness changes, lithology changes
- Different properties in each layer, etc.
- Man-made heterogeneities include changes near the wellbore from hydraulic fracturing, acidizing, or water injection.

16.4 Pressure Responses Near No Flow Boundaries

Linear sealing faults and barriers have been an interesting topic in the transient-testing literature.^{6–8} Horner⁷ considers pressure buildup and

Russell¹¹ discusses two-rate flow testing in those systems. Regardless of test type, the linear flow barrier affects the test in about the same way. To obtain the effect of the linear fault, the following interpretation formulas, which are needed in this particular instance, are given. A computed example of a buildup test in a well located 225.0 ft from a fault is shown in Figure 17-6. The data assumed for this example are given in the figure. It can be seen that the buildup test plot possesses two distinct straight-line slopes. As in the case with a pressure buildup, the second or "late time" portion of the buildup test curve has a slope, which is exactly double that of the "early time" portion of the curve. The pressure response at a well near a sealing fault can be directly obtained from the following equation:

$$[\psi(p_{WD}(t_D))] = -0.5 \left[E_i \left(\frac{-1}{4t_D} \right) + E_i(-r_{dD}^2) + s \right] \quad (16-1)$$

Here $r_{dD} = 2L/r_w$, where L is the distance to this fault. If times are small enough, then the second term in Eq. 16-1 can be assumed to be negligible compared with the first, and the line source solution (Eq. 16-2) can be used to analyze responses in the conventional way.

$$[(p_D(r_D, t_D))] = 0.5 E_i \left(\frac{-r_D^2}{4t_D} \right) \quad (16-2)$$

If the logarithmic approximation to the exponential integral is used, then $[(p_D(r_D, t_D))]$ is given by:

$$[(p_D(r_D, t_D))] = 0.5 \left[\ln \left(\frac{4t_D}{r_D^2} \right) - 0.5772 \right] \quad (16-3)$$

If flow times are long enough such that both exponential integrals can be approximated by the logarithmic approximation, then we have

$$[(p_{WD})(t_D)] = \ln \left(\frac{4t_D}{e^{0.5772}} \right) - \ln(r_{dD}) + s \quad (16-4)$$

The above equation suggests that one should get a second straight line with a slope twice that of the first. In practice, the doubling of the slope on semi-logarithmic coordinates is normally taken to be indicative of a sealing fault. If a fault exists, then the first straight line should exist for a time period given by:

$$6 < t_D \leq 0.08r_{dD}^2 \quad (16-5)$$

The second straight line should begin at $3r_{dD}^2$. In the time range $0.08r_{dD}^2 < t_D < 3r_{dD}^2$ it can be used to analyze pressure measurements or predict pressure responses. The distance to the fault can be obtained if we equate the semilog approximation of the line source solution (Eq. 16-3), to the right-hand side of Eq. 16-4. If we denote this time by $0.8r_{dD}^2$, then $e^{0.5772}r_{dD}^2/4$; then the distance to the fault is given by:

$$L = d = \sqrt{e^{-0.5772} \left(\frac{0.0002637kt_x}{\phi c_t \mu_g} \right)} \quad (16-6)$$

where t_x is the intersection time in hours. This procedure assumes that both straight lines are evident.

Methods of Estimating Distance to a Linear Discontinuity

The effect of a sealing fault or barrier in an infinite-acting reservoir is to cause the buildup plot to start off as a straight line with the proper slope, gradually bend over, and eventually become another straight line with twice the slope of the first. The first straight line gives the proper value of kh . The second straight line gives the proper extrapolation to p_i . The distance between the well and the fault may be obtained by using the expression given by Davis and Hawkins⁹ for drawdown tests and seems to apply reasonably well to buildup tests. The approximation takes the final form:

$$L = \sqrt{\left(\frac{0.000148k\Delta t_x}{\phi\mu c} \right)} \quad (16-7)$$

where Δt_x = value at the intersection of the two lines.

The distance to a barrier can also be calculated by using the Eq. 16-8 developed by Van Poollen.¹⁰

$$L = \sqrt{\left(\frac{0.000933kt_p}{\phi\mu c \left(\frac{t_p + \Delta t_x}{\Delta t_x} \right)} \right)} \quad (16-8)$$

where $(t_p + \Delta t_x)/\Delta t_x$ is the value at the point of deviation from the first straight line. The following equation is applicable to both buildup and drawdown tests and is known as Gray's equation:⁸

$$\Delta p = \left(-\frac{70.6q\mu_o\beta_o}{kh} \right) \left[-E_i \left(-\frac{\phi\mu_o cL^2}{0.000264k\Delta t} \right) \right] \quad (16-9)$$

where q is oil rate in bbls/day. This equation is most accurate if Δt is large. This is a trial-and-error procedure by assuming various values of L until the RHS of Eq. 16-9 is equal to the LHS. Gray⁸ also suggested that distance to the nearest boundary can be estimated approximately by the following equation:

$$L \cong 0.01217 \sqrt{\frac{k\Delta t_x}{\phi\mu c}} \quad (16-10)$$

where Δt_x is the time at which the buildup curve becomes non-linear.

From pressure buildup testing, the intersection point of the two straight lines is related to the dimensionless pressure at the intersection line by:

$$\left\{ p_D \left[\frac{t_D}{\left(\frac{2L}{r_w} \right)^2} \right] \right\} = 0.5 \ln \left(\frac{t_p + \Delta t}{\Delta t} \right)_x \quad (16-11)$$

Calculate p_D from Eq. 16-11. Then from Table 16-1, with the value of p_D , determine $t_D/(2L/r_w)^2$. Finally use the following equation to estimate the distance to the fault.

$$L = \sqrt{\frac{0.0002637kt_p}{4\phi\mu c_t \left[\frac{t_D}{\left(\frac{2L}{r_w} \right)^2} \right]}} \quad (16-12)$$

Relationships between $p_D(t_D, r_D)$ and t_D/r_D^2 are given in Table 16-1. The detailed derivations of Eqs. 16-11 and 16-12 are given in Ref. 12.

Figures 16-2 and 16-3 show various situations of linear discontinuities for single and multiple boundary cases. Figure 16-4 shows various methods to estimate distance to linear discontinuity and their limitations.

Example 16-1²⁶ Estimating Distance to a No-Flow Boundary

A pressure buildup test was run in a newly drilled oil well. Geologists suspect a fault. Data from the test are given in Table 16-2. Total production before test is 14,206 stb; other reservoir and well data are: $\phi = 0.15$ (fraction); $\mu_o = 0.6$ cP, $h = 8$ ft; $r_w = 0.29$ ft; $c_t = 17.0 \times 10^{-6}$ psi⁻¹; $q_o = 1221$ stb/day.

$$\text{Pseudo-producing time, } t_p = \frac{14,206}{1221} \times 24 = 279.23 \text{ hr}$$

Calculate the distance to the linear fault using various methods.

Table 16-1
Dimensionless Pressure at Various
Values of Dimensionless Time⁷

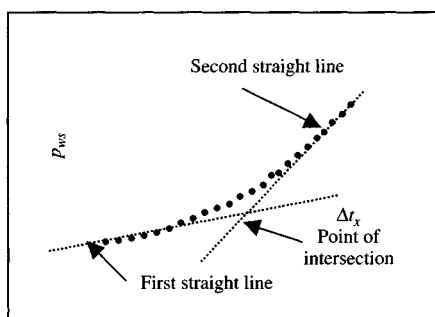
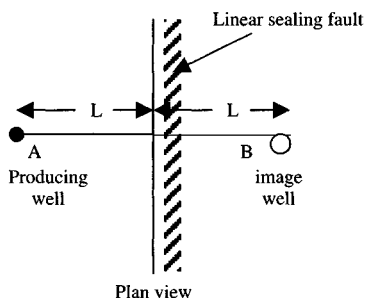
Dimensionless pressure, p_D	Dimensionless time, $t_D/(2L/r_w)^2$
0.01	0.00
0.02	0.00
0.03	0.00
0.04	0.15
0.05	0.16
0.06	0.18
0.07	0.19
0.08	0.20
0.09	0.22
0.10	0.24
0.20	0.38
0.30	0.52
0.40	0.70
0.50	0.94
0.60	1.20
0.70	1.65
0.80	2.00
0.90	2.50
1.0	3.00
1.1	4.00
1.2	4.80
1.3	6.00
1.4	8.00
1.5	8.50
1.6	9.0
1.7	12.0
1.8	17.0
1.9	20.0
2.0	25.0
2.1	27.5
2.2	30.0
2.3	45.0
2.4	60.0
2.5	70.0
2.6	80.0
2.7	90.0
2.8	110.0
2.9	140.0
3.0	170.0
3.1	220.0

Table 16-1 (continued)

Dimensionless pressure, p_D	Dimensionless time, $t_D/(2L/r_w)^2$
3.2	260.0
3.3	300.0
3.4	400.0
3.5	500.0
3.6	600.0
3.7	700.0
3.8	900.0
3.9	1200.0
4.0	1500
4.1	1750
4.2	2000
4.3	2500
4.4	3000
4.5	3500
4.6	4200
4.7	5000
4.8	7000
4.9	9000
5.0	1.0×10^4
5.5	3.0×10^4
6.0	7.0×10^4
6.5	1.75×10^5
7.0	5.0×10^5
7.5	2.0×10^6
8.0	5.0×10^6
8.5	1.5×10^7
9.0	3.0×10^7
9.5	1.5×10^8
10.0	2.0×10^8

Solution Pressure buildup data are shown in Figures 16-5 and 16-6. The log-log plot of Figure 16-5 indicates that wellbore storage effects are not important, so the increase in slope in Figure 16-6 is probably caused by reservoir heterogeneity. The ratio of the two slopes is 2.20. Since the absolute value of the slopes is increasing with shut-in time, and since the slope ratio is about 2, a linear fault is suspected. Formation permeability, k , is estimated from the first straight line using Eq. 5-16.

$$k = \frac{162.6q\mu\beta}{m} = \frac{162.6 \times 1221 \times 1.31 \times 0.6}{650 \times 8} = 30.0 \text{ mD}$$



$\text{Log}(t + \Delta t)/\Delta t$

Figure 16–2. Fault near single boundary.

Table 16–2
Analysis of Data from Well Near Boundary

Δt (hr)	$\frac{t_p + \Delta t}{\Delta t}$	p_{ws} (psia)	Δp (psia)	Distance to fault (ft)
6	47.54	3996	—	—
8	35.90	4085	16	252
10	28.92	4172	34	240
12	24.27	4240	52	225
14	20.95	4298	70	206
16	18.45	4353	88	189
20	14.96	4435	103	129
24	12.63	4520	135	71
30	10.31	4614	165	198
36	8.76	4700	204	285
42	7.65	4770	245	346
48	6.82	4827	275	400
54	6.17	4882	302	452
60	5.65	4931	330	498
66	5.23	4975	353	542

To estimate the distance to the fault, we determine $(t_p + \Delta t_x)/\Delta t_x = 17.0$ and $\Delta t_x = 17.23$.

1. Line source solution method

$$L = \sqrt{e^{-0.5772} \left(\frac{0.0002637 k t_x}{\phi \mu_g c_t} \right)}$$

$$= \sqrt{0.5615 \left(\frac{0.0002637 \times 30 \times 17.45}{0.15 \times 0.6 \times 17.0 \times 10^{-6}} \right)} = 225.0 \text{ ft} \quad (16-13)$$

2. David and Hawkin method⁹

$$L = \sqrt{\frac{0.000148 k \Delta t_x}{\phi \mu_g c_t}} = \sqrt{\frac{0.000148 \times 30 \times 17.45}{0.15 \times 0.6 \times 17.0 \times 10^{-6}}}$$

$$= 225.0 \text{ ft} \quad (16-14)$$

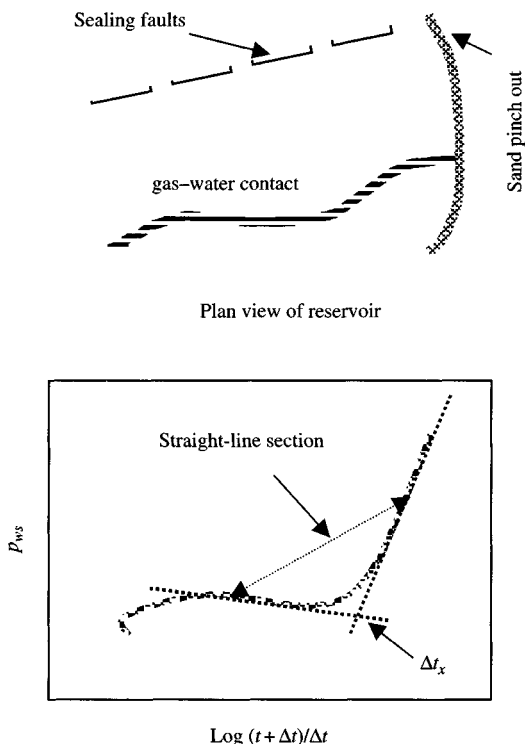


Figure 16-3. Fault nearby multiple boundaries.

3. Van Poollen method¹⁰

$$L = \sqrt{\frac{0.000933kt_p}{\phi\mu_g c \left(\frac{t_p + \Delta t_x}{\Delta t_x} \right)}} = \sqrt{\frac{0.00093(30)(279.23)}{0.15(0.6)(17.0 \times 10^{-6})(17)}}$$

$$= 548 \text{ ft} \quad (16-15)$$

4. Gray approximate method⁸

$$L = 0.01217 \sqrt{\frac{k\Delta t_x}{\phi\mu_g c_t}} = 0.01217 \sqrt{\frac{30 \times 17.47}{0.15 \times 0.6 \times 0.255 \times 17.0 \times 10^{-3}}}$$

$$= 225.25 \text{ ft} \quad (16-16)$$

5. Exponential integral solution method¹¹ (Eqs. 16-11 and 16-12)

$$\left\{ p_D \left[\frac{t_D}{\left(\frac{2L}{r_w} \right)^2} \right] \right\} = 0.5 \ln \left(\frac{t_p + \Delta t}{\Delta t} \right)_x = 0.5 \ln(17.0) = 1.4166$$

When $p_D > 10$, the values of $[t_D/(2L/r_w)^2]$ can be calculated from the following equation:

$$\left(\frac{t_D}{\left(\frac{2L}{r_w} \right)^2} \right) = 8.15 \text{ (from Table 16-1)}$$

$$L = \sqrt{\frac{0.0002637kt_p}{4\phi\mu_g c_t \left[\frac{t_D}{\left(\frac{2L}{r_w} \right)^2} \right]}} = \sqrt{\frac{0.0002637 \times 30 \times 279.23}{4 \times 0.15 \times 0.6 \times 17.0 \times 10^{-3} \times 8.15}} = 210.5 \text{ ft}$$

Table 16-3 shows that methods 1, 3, 4, and 5 give reasonably close linear fault values.

Discussion

Doubling of the slope in a transient test does not guarantee the existence of a linear fault boundary near the well. Pressure data taken during wellbore

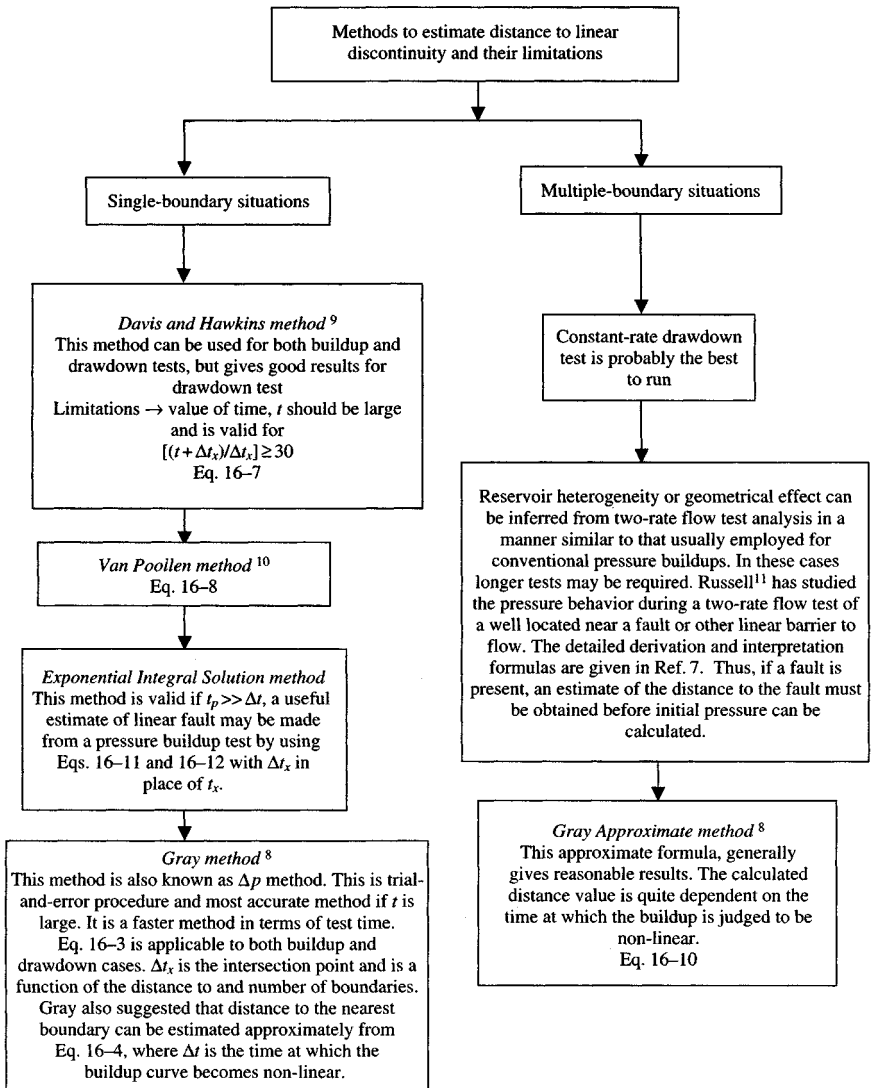


Figure 16-4. Various methods to determine distance to linear discontinuity.

storage domination can cause two apparent semilog straight lines with a slope increase (see Figure 16-6). In such cases, the apparent semilog straight lines are caused completely by wellbore effects and have nothing to do with reservoir characteristics. When slopes' increase is expected from a transient test, it is important to construct the log-log plot of transient test data to determine when wellbore storage effects are no longer important.

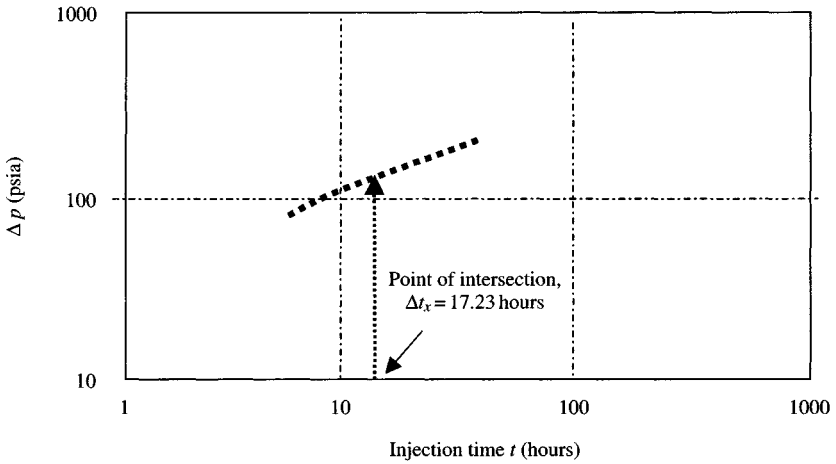


Figure 16-5. Δp versus Δt for buildup test (log-log plot).

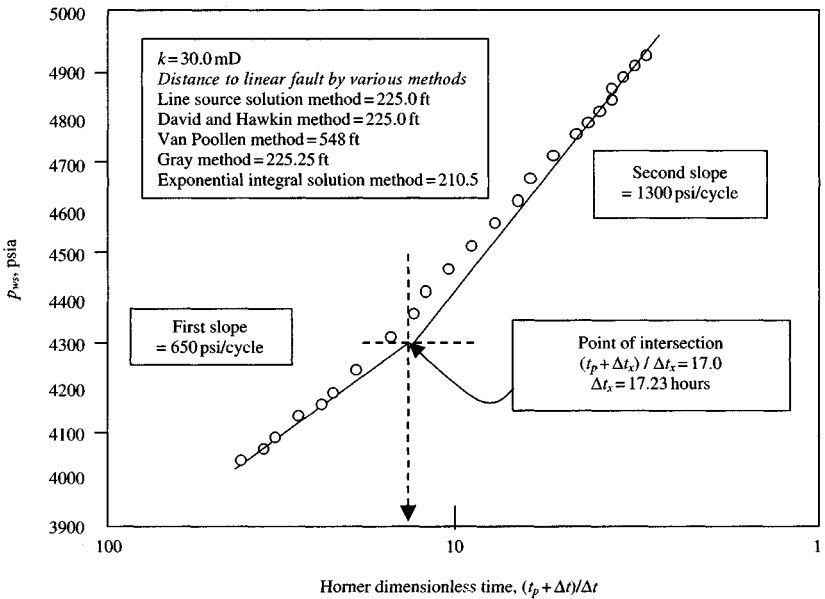


Figure 16-6. Estimating distance to a no-flow boundary.

16.5 Effect of Hydraulic Diffusivity on Reservoir Behavior

Figure 16-7 shows the idealized reservoir situation studies.^{10,21} Changes in the hydraulic diffusivity occur at the boundary between differing geological

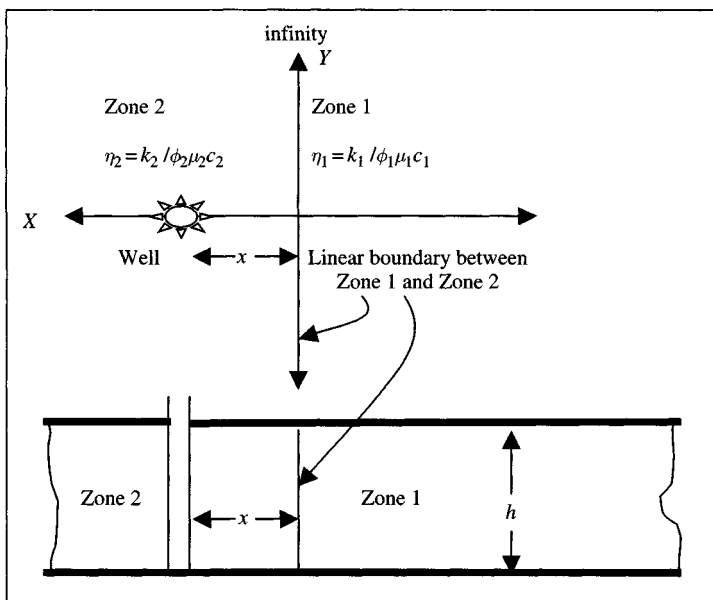


Figure 16-7. Schematic cross-section of some practical reservoir situation.

depositional units due to changes in porosity and permeability. Bixel et al.¹⁰ have investigated the effect of radial discontinuities in hydraulic diffusivity on pressure drawdown and buildup behavior. A brief summary in terms of the following parameters is given below:

$$\text{Zone 1: Hydraulic diffusivity, } \eta_1 = \frac{k_1}{\phi_1 \mu_1 c_1}$$

$$\text{Zone 2: Hydraulic diffusivity, } \eta_2 = \frac{k_2}{\phi_2 \mu_2 c_2}$$

$$\text{Ratio} = \frac{\eta_2}{\eta_1} = \frac{[(k_2 / \phi_2 \mu_2 c_2)]}{[(k_1 / \phi_1 \mu_1 c_1)]} = \frac{[k_2 \mu_1]}{[k_1 \mu_2]} \bigg/ \frac{[\phi_2 c_2]}{[\phi_1 c_1]} = \frac{M_k}{R_{pc}}$$

$$= \frac{\text{Permeability contrast}}{\text{Porosity contrast}}$$

The ratio of hydraulic diffusivities η_2/η_1 , is equal to M_k/R_{pc} . The greater the reduction in hydraulic diffusivity from the zone containing the well to the zone beyond the discontinuity, the closer the slope change will approach a factor of 2; as with faults, oil-water contacts may not be distinguishable from a fault in practical cases. Large increases in diffusivity across the discontinuity will cause the pressure drop to arrest and become essentially constant.

For diffusivity contrast ratio $M_k/R_{pc} = 1$, homogeneous reservoir behavior results. If the diffusivity contrast ratio $M_k/R_{pc} > 1$, the buildup curve slope will flatten. If the diffusivity contrast ratio $M_k/R_{pc} = 1$, the buildup curve slope increases after the effect of discontinuities.

16.6 Simple Procedures and Guidelines to Estimate Reservoir Heterogeneity Properties

Figure 16–8 shows the different mathematical techniques that can be utilized to determine reservoir heterogeneity properties.

16.7 General Approach to Estimate Fracture Trends or Heterogeneity

Kamal and Brigham¹³ have proposed the following equation to investigate the presence of an isotropic reservoir without fracture or discontinuities.

$$[\Delta p]_{Calculate} = \frac{70.6 \times 10^6 q_o \mu_o \beta_o}{kh} E_i \left(\frac{-56,900 \phi \mu_o c r^2}{kt} \right) \quad (16-17)$$

where r is the distance between producer and observation well in ft and t is the flowing time in minutes. Figures 16–9a, b, c, and d can be used to confirm communication through the reservoir between producer and observation well and to determine general trends or possibilities. Figure 16–10 shows a simple approach to determine fracture trends or heterogeneity.

16.8 Determination of Reservoir Parameters and Fracture Orientations

For more accurate determination of reservoir anisotropic parameters and fracture orientations the methods proposed by Elkins and Skov and by Ramey^{14,15} are recommended. The following formula will permit estimation of the reservoir parameters in various directions based upon pressure drops measured in observation wells for conditions of single-phase flow.

$$\Delta p = (p_i - p) = \frac{q_o \mu_o \beta_o}{4\pi \sqrt{k_x k_y} h (1.127)} E_i \left[\frac{\frac{(x - x_0)^2}{k_x} + \frac{(y - y_0)^2}{k_y}}{\frac{4t}{\phi c \mu_o} (6.32)} \right] \quad (16-18)$$

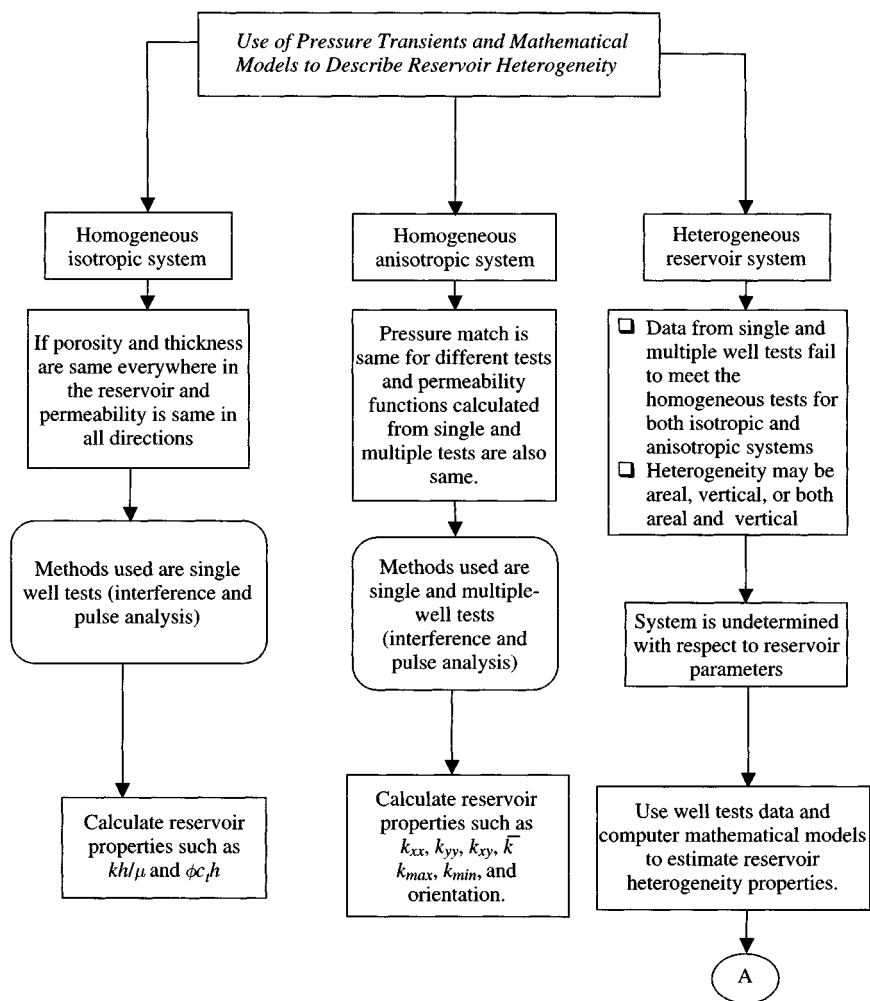


Figure 16-8. Systematic procedures and guidelines to describe reservoir heterogeneity.

where p_i = initial pressure, psi; p = pressure (psi) at x, y at time t in days; c = effective compressibility of oil, water, and rock, psi^{-1} ; k_x = effective permeability in x -direction, darcies; k_y = effective permeability in y -direction, darcies; $x - x_0$ = distance from producing to observation well in x -direction, ft; $y - y_0$ = distance from producing to observation well in y -direction, ft; q = oil rate, stb/day; β_o = oil formation volume factor; and E_i is exponential integral, $-E_i(-x)$. The pressure reductions at a point due to production

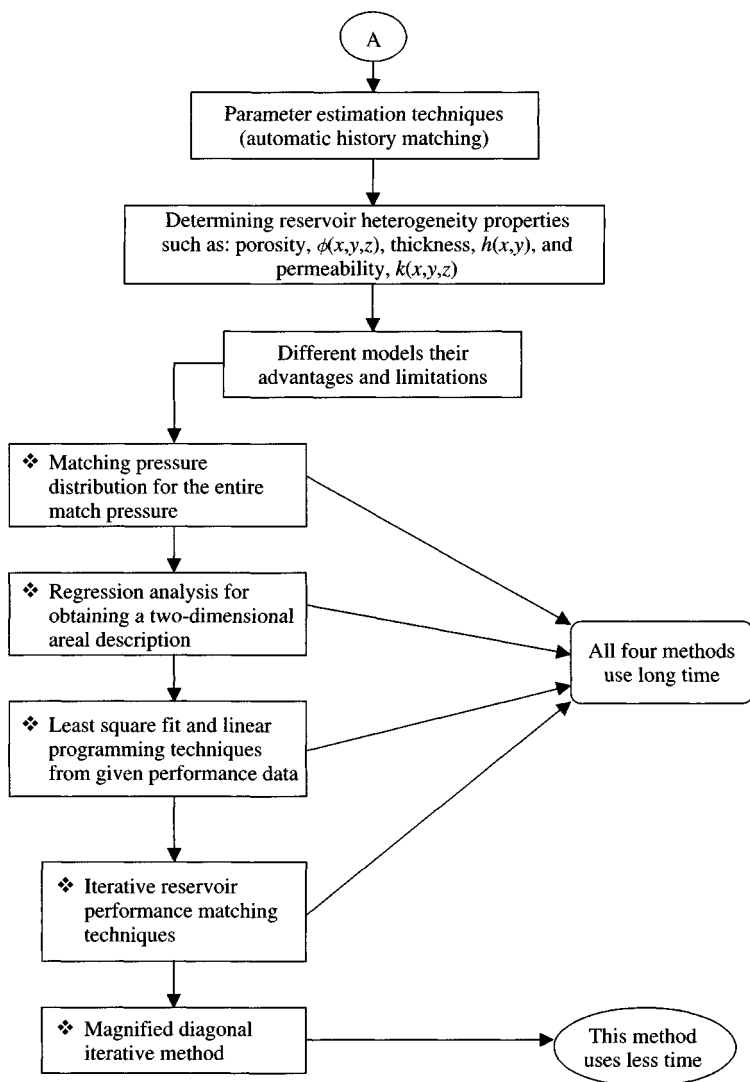


Figure 16–8. continued

of different wells are additive. For uniform permeability, Eq. 16–18 reduces to the simpler, well-known form involving r^2 and k . Reservoir parameters including effective compressibility and uniform or anisotropic permeability can be determined only by trial solutions until the set of values is found that gives the best match between calculated pressures and measured pressures. Fracture orientation, diffusivity parallel to the main fractures, and diffusivity

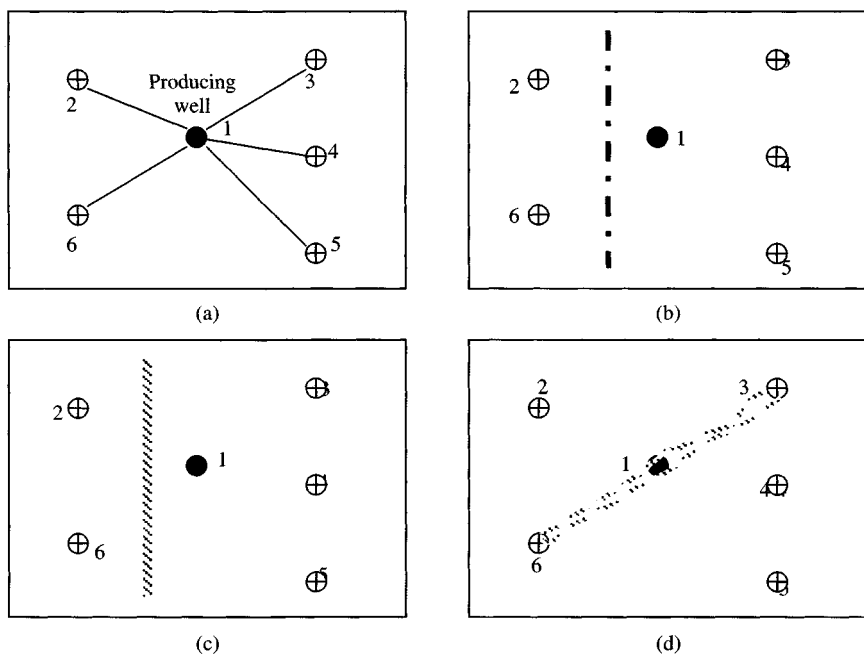


Figure 16-9 (a) Location and distance between wells. (b) Possible non-sealing faults. (c) Possible sealing fault. (d) Possible naturally fractured system.

perpendicular to the main fractures are related $\sqrt{k_x k_y}$ and p_i is explicit. The sequence to determine the best set of these factors is given in Figure 16-11 and requires a computer, while Figure 16-12a shows minimum and maximum variations.

16.9 Defining Reservoir Heterogeneity by Multiple-Well Tests

Pressure transient tests can be used to investigate and obtain adequate reservoir descriptions for homogeneous (both isotropic and anisotropic) and heterogeneous systems. Type curves have proven very useful for evaluating pressure buildup, interference, and pulse tests in oil reservoirs influenced by reservoir boundaries. Multiple-well tests (interference and pulse tests) are used to establish communication between wells and to determine the interwell properties.¹⁵

The basic equations describing the pressure responses as well as pressure drop at some distance from a producing well are presented along with

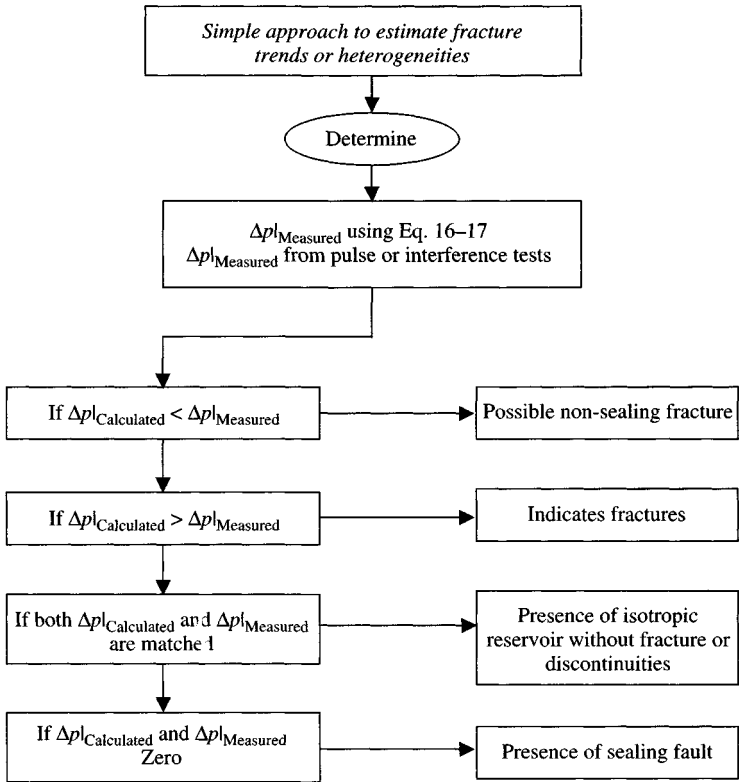


Figure 16–10. Systematic approaches to detect fracture trends and reservoir heterogeneity.

field examples in the next section to determine properties such as permeability $k(x, y, z)$, porosity $\phi(x, y, z)$, and thickness $h(x, y)$ in different systems.

Homogeneous Isotropic Reservoir Systems

In these types of systems, the permeability is the same everywhere and in all directions. Porosity and thickness are also the same everywhere in the reservoir. The following analysis techniques (interference and pulse tests) can be used to determine reservoir properties in homogeneous isotropic formations.

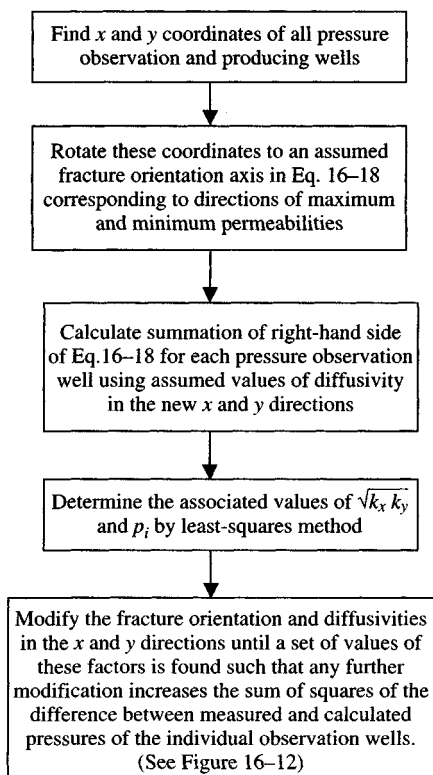


Figure 16-11. Systemic determination sequences of fracture orientations.

Interference Tests

Interference test can be analyzed by type curve matching method, because it is simple, fast, and accurate when the exponential integral p_D applies; that is, when $r_D = r/r_w > 20$ and $t_D/r_D^2 > 0.5$. The reservoir properties such as the mobility-thickness product kh/μ_g and the porosity-compressibility-thickness product $\phi c_i h$ can be calculated from the following relationships:

$$\frac{kh}{\mu_o} = 141.2 q_o \beta_o \frac{|p_D|_M}{|\Delta p|_M} \quad (16-19)$$

$$\phi c_i h = \frac{0.0002637}{r^2} \frac{kh}{\mu_o} \frac{|t|_M}{|t_D/r_D^2|_M} \quad (16-20)$$

Table 16-3
Comparison of Linear Discontinuities by Five Methods

Methods	Equations used	Distance to fault, <i>L</i> ft	Remarks
1. Line source solution	16-6	225.00	Good
2. David and Hawkin	16-7	225.00	Good
3. Van Poolen	16-8	548.00	High value
4. Gray equation	16-10	225.25	Good
5. Exponential integral solution	16-11 and 16-12	210.50	Fairly good

Pulse Tests

Pulse tests can be used to determine the same information as interference tests. Pulse tests are not affected by unknown linear trends in reservoir pressures. Therefore, conducting pulse tests rather than interference tests is preferable. Jahns²² has provided the relationships among dimensionless time lag, cycle period, and response amplitude in both graphical and analytical forms. The detailed discussion along with field examples can be found in Chapter 13. The following relationships can be applied to calculate the reservoir properties.

$$t_{tD} = \frac{t_l}{\Delta t_{cyc}} \quad (16-21)$$

$$\frac{kh}{\mu_g} = 70.6q_g\beta_g \frac{\Delta p_D}{\Delta p} \quad (16-22)$$

and

$$\phi c_l h = \frac{kh}{\mu_g} \frac{1}{56900r^2} \frac{\Delta t_{cyc}}{\Delta t_{cycD}} \quad (16-23)$$

General Remarks: If the reservoir is acting as a homogeneous isotropic system, reasonable identical values of kh/μ_g and $\phi c_l h$ can be calculated from several tests in the same areas. If there are big differences among the calculated values of kh/μ_g and those of $\phi c_l h$, then a homogeneous anisotropic system should be used.

Example 16-2²⁶ *Analyzing Interference Test in Homogeneous Isotropic Reservoir*

An interference test was conducted in oil well. Water was injected into well 1 for 48 hr. The pressure response in well 2 (80 ft away) was observed for

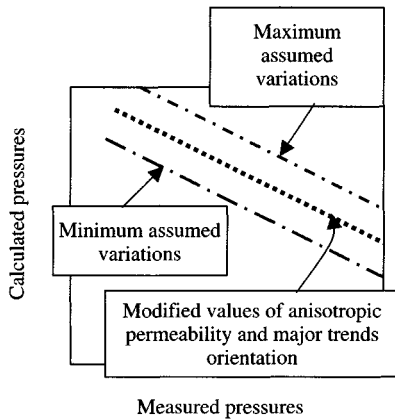


Figure 16-12a. Calculated versus measured pressures.

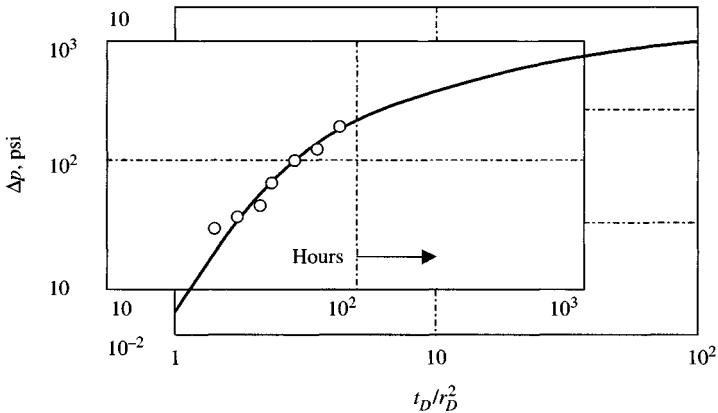


Figure 16-12b. Type curve data match.

148 h. The observed pressure data are given in Table 16-4, and the known well/reservoir properties are given. Determine permeability and porosity of the formation between the two tested wells.

Solution Figure 16-12b is a plot of Table 16-4 on log-log graph paper of the same scale of type curves of Figure 13-3.

The match points are:

$$(p_D)_{MP} = 0.975, \quad t_{MP} = 100 \text{ hours}$$

$$(\Delta p)_{MP} = 100 \text{ psig}, \quad (t_D/r_D^2)_{MP} = 8.95$$

Calculate formation permeability, k , and porosity from Eqs. 16-19 and 16-20.

$$k = 141.2 \frac{q_w \mu_w \beta_w (p_D)_{MP}}{h (\Delta p)_{MP}} = 141.2 \frac{185(1)(1)}{55} \times \frac{0.975}{100}$$

$$= 4.63 \text{ mD}$$

$$\phi c_t = \left[\frac{0.0002637k}{\mu_w r^2} \right] \frac{(\Delta p)_{MP}}{(t_D/r_D^2)_{MP}}$$

$$= \left[\frac{0.0002637 \times 4.63}{80^2} \right] \times \frac{100}{8.95} = 2.132 \times 10^{-6} \text{ psi}^{-1}$$

$$\phi = \frac{\phi c_t}{c_t} = \frac{2.132 \times 10^{-6}}{13.82 \times 10^{-6}} = 15.4\%$$

To check the accuracy of the above method of analysis, plot $(p_w|_{\text{extended}} - p_w)$ versus Δt points as shown in Figure 16-12a. Since the $(p_w|_{\text{extended}} - p_w)$ versus Δt data fall on the curve, the analyses are correct.

Table 16-4
Interference Test Data for Observation well

$p_i = 0$ psig, $t_1 = 48$ h, $q_w = -185$ stb/day, $\beta_w = 1.00$ rb/stb,
 $\mu_w = 1.00$ cP, $r = 80$ ft, $c_t = 13.82 \times 10^{-6} \text{ psi}^{-1}$, and $h = 55$ ft

t (hr)	p_w (psig)	$\Delta p = p_i - p_w$ (psig)	$\Delta t = t_1 - 48$ (hr)	Δp_{west} (psig)	$\Delta p_{\Delta t} = \Delta p_{west} - \Delta p_w$
0	$0 = p_i$				
4.5	23	-23			
21.86	83	-83			
30.01	96	-96			
46.00	121	-121			
48.00	Injection		Ends		
52.00	110	-110	4	126	16
70.00	56	-56	21	140	84
72.00	48	-48	24	142	94
92.00	33	-33	44	156	123
144.00	17	-17	93	182	165
148.00	16	-16	100	183	167

Anisotropic Reservoir Systems

Porosity and thickness are uniform throughout the reservoir. Permeability is the same everywhere, but varies with direction. Figure 16–13 shows the major and minor axes of the permeability and axes of well pattern. Many formations, such as channel sands, appear to exhibit simple k_y – k_x anisotropy. Directional permeability has an important effect on planning oil recovery by cycling. Ramey¹⁵ presents a method for estimating anisotropic reservoir properties from interference data. At least three observation wells are required for analysis. Figure 16–13 defines the necessary nomenclature. The active well is located at the origin of coordinate system and the observation wells are each located at coordinates indicated as (x, y) . The anisotropic analysis requires pressure data from at least three observation wells, assuming that the active well/observation well system is infinite-acting and homogeneous with the exception of having anisotropic permeability. Ramey¹⁵ shows that the pressure at an observation well is:

$$p(t, x, y) = p_i - \frac{141.2q_i\mu_w\beta_w}{\sqrt{k_{min}k_{max}}h} p_D \left(\left[\frac{t_D}{r_D^2} \right]_{direction} \right) \quad (16-24)$$

where

$$\left(\frac{t_D}{r_D^2} \right)_{direction} = \frac{0.0002637t}{\phi\mu_o c_i} \left[\frac{k_{min}k_{max}}{k_x y^2 + k_y x^2 - 2k_{xy}xy} \right] \quad (16-25)$$

In Eq. 16–25

- k_x = principal permeability in x -direction, mD
- k_y = principal permeability in y -direction, mD
- k_{xy} = principal permeability in xy -direction, mD
- k_{min} = minimum permeability in x -direction, mD
- k_{max} = maximum permeability in x -direction, mD
- θ = angle of orientation, degrees.

The following steps are used to analyze interference test:

- Observed pressure data from at least three wells are plotted and matched to the type curve of Figure 13–3. Each of the three data sets is matched, so the pressure match point $[\Delta p_{MP}, (p_D)_{MP}]$ is the same for all three observation well responses. The time match point $[t_{MP}, (t_D/r_D^2)_{MP}]$ will be different for each set of observation data.
- Rearranging Eq. 16–24 in the form of

$$\sqrt{k_{min}k_{max}} = \frac{141.2q_g\mu_w\beta_w}{h} \frac{(p_D)_{MP}}{(\Delta p)_{MP}} \quad (16-26)$$

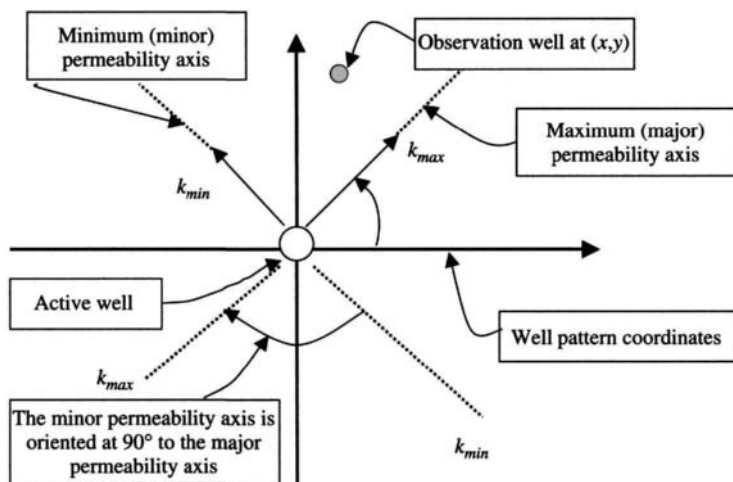


Figure 16-13. Nomenclatures for anisotropic permeability system.

$$k_{min}k_{max} = \left[\frac{141.2q_g\mu_w\beta_w}{h} \frac{(p_D)_{MP}}{(\Delta p)_{MP}} \right]^2 \quad (16-27)$$

$$k_{min}k_{max} = \text{Average system permeability, mD}$$

$$k_{min}k_{max} = \bar{k}^2 = [k_x k_y - k_{xy}^2] \quad (16-28)$$

$$\bar{k} = \sqrt{k_{min}k_{max}}, \text{ Average system permeability, mD} \quad (16-29)$$

Rearranging Eq. 16-25 in the form of

$$\frac{t_D}{r_D^2} = \left(\frac{0.0002637t}{\phi\mu_g c_t} \right) \left(\frac{k_{xx}k_{yy} - k_{xy}^2}{k_{xx}y^2 + k_{yy}x^2 - 2k_{xy}xy} \right) \quad (16-30)$$

or

$$\frac{t_D}{r_D^2} = \left(\frac{0.0002637t}{\phi\mu_g c_t} \right) \left(\frac{k_{max}k_{min}}{k_{xx}y^2 + k_{yy}x^2 - 2k_{xy}xy} \right) \quad (16-31)$$

Write the following equations for each observation well match;

$$\left[\frac{\left(\frac{t_D}{r_D^2} \right)_{MP}}{t_{MP}} \right]_{\text{Well 1}} = \frac{0.0002637}{\phi \mu_g c_t} \left(\frac{k_{max} k_{min}}{k_{xx} y^2 + k_{yy} x^2 - 2k_{xy} xy} \right) \quad (16-32)$$

$$\left[\frac{\left(\frac{t_D}{r_D^2} \right)_{MP}}{t_{MP}} \right]_{\text{Well 2}} = \frac{0.0002637}{\phi \mu_g c_t} \left(\frac{k_{max} k_{min}}{k_{xx} y^2 + k_{yy} x^2 - 2k_{xy} xy} \right) \quad (16-33)$$

$$\left[\frac{\left(\frac{t_D}{r_D^2} \right)_{MP}}{t_{MP}} \right]_{\text{Well 3}} = \frac{0.0002637}{\phi \mu_g c_t} \left(\frac{k_{max} k_{min}}{k_{xx} y^2 + k_{yy} x^2 - 2k_{xy} xy} \right) \quad (16-34)$$

where t_{MP} is the same for each well and $(t_D/r_D^2)_{MP}$ is different for each well. Estimate the average system permeability from Eq. 16-29. There are three Eqs. 16-32, 16-33, and 16-34 and four unknown, k_{xx} , k_{yy} , k_{xy} , and $\phi \mu_o c_t$. They may be solved simultaneously to obtain k_{xx} , k_{yy} , and k_{xy} , each in terms of the unknown $\phi \mu_g c_t$. Then k_x , k_y , and k_{xy} (in terms of $\phi \mu_g c_t$) are substituted into the following equation

$$k_x k_y - k_{xy}^2 = k_{min} k_{max} = \bar{k}^2 \quad (16-35)$$

Since the right side of the Eq. 16-28 is known from Eq. 16-26, it can be solved to estimate $\phi \mu_o c_t$. Then we estimate k_x , k_y , and k_{xy} from their relationship to $\phi \mu_o c_t$. Determine the minimum, maximum directional permeability and the angle of orientation by using the following equations:

$$k_{min} = k_{XX} = 0.5 \left[(k_x + k_y) - \sqrt{(k_x - k_y)^2 + 4k_{xy}^2} \right] \quad (16-36)$$

$$k_{max} = k_{YY} = 0.5 \left[(k_x + k_y) + \sqrt{(k_x - k_y)^2 + 4k_{xy}^2} \right] \quad (16-37)$$

$$\theta_{max} = \arctan \left(\frac{k_{max} - k_{XX}}{k_{xy}} \right) \quad (16-38)$$

$$\theta_{min} = \arctan \left(\frac{k_{max} - k_{YY}}{k_{xy}} \right) \quad (16-39)$$

where

β_g = gas formation volume factor, bbl/scf

c_t = total system effective compressibility, psi^{-1}

c_o = oil compressibility, psi^{-1}

c_w = water compressibility, psi^{-1}

c_f = pore space compressibility, psi^{-1}

h = net formation thickness, ft

\bar{k} = average system permeability, mD

k_{XX} = maximum (major) principal permeability, mD

k_{YY} = minimum (minor) principal permeability, mD

k_{xx} , k_{yy} , k_{xy} = components of the permeability tensor, mD

θ_{max} = direction of maximum permeability, K_{max}

θ_{min} = direction of minimum permeability, K_{min}

Total system compressibility can be related to the pore space saturation of the two phases.

$$c_t = s_g c_g + s_w c_w + c_f \quad (16-40)$$

$$s_o = \frac{c_t - c_w - c_f}{(c_o - c_w)} \quad (16-41)$$

Eq. 16-41 can be used to estimate in-place oil saturation using transient tests.

Important Note: Analysis of more than one interference test in the same area should, therefore, provide information on the feasibility of using homogeneous anisotropic technique. If the match of pressure is the same in different tests, the technique is applicable. If not, heterogeneous system analysis should be considered.

The following example will clarify the use of these equations to determine directional homogeneous anisotropic reservoir properties.

Example 16-3²⁶ Analyzing Interference Test in Homogeneous Anisotropic Reservoirs

An interference test was run in a 5-spot pattern. At the end of the injection period, before testing, all wells were shut-in. Test was run at injection rate of 120 stb/day and observing the fluid levels in the five of the shut-in production wells, during both the injection and the subsequent falloff period. The test information and reservoir properties are: $p_i = 265$ psi; $\mu_w = 1$ cP; $r_w = 0.550$ ft; $\beta_w = 1$ rbl/stb; $h = 30$ ft; injection rate = $q_i = 120$ stb/day; $\phi = 19\%$; $c_o = 7.5 \times 10^{-6} \text{psi}^{-1}$; $c_w = 3.3 \times 10^{-6} \text{psi}^{-1}$; $c_f = 3.7 \times 10^{-6} \text{psi}^{-1}$; API = 37°; $s_o = 0.25$; $s_w = 0.30$; well depth = 1200 ft. Figure 16-14 shows the well locations. Tables 16-5 and 16-6a and b give observation pressure data for wells 1, 2, and 3 during the water injection period. Figure 16-15 shows the well locations.

Estimate homogeneous anisotropic reservoir parameters

- Average system permeability, \bar{k}
- Product of $\phi\mu c_t$
- Maximum directional permeability, k_{max}
- Minimum directional permeability, k_{min}

- Directions of k_{max} and k_{min}
- In-place oil saturation

Solution Figure 16–15 shows well pattern, distances, and coordinates in ft, and Figure 16–14 is a net sand isopatch map. Figure 16–17a shows the match of the data in Tables 16–5 through 16–6c, to the type curve of Figure 13–3. The match was made, so the pressure match point $[(\Delta p)_{MP}, (p_D)_{MP}]$ is the same for all three responses, while the time match points vary.

	r (ft)	t_D/r_D^2
Well 1	480	25
Well 2	480	35
Well 3	702	45

- Calculate system permeability, \bar{k}

From the pressure match point for all wells, $(p_D)_{MP} = 0.29$ and $(\Delta p)_{MP} = 10$, rearranging Eqs. 16–26 and 16–29, we have:

$$\begin{aligned}
 k_{min}k_{max} &= \left[\frac{141.2q_i\mu_w\beta_w}{h} \frac{(p_D)_{MP}}{(\Delta p)_{MP}} \right]^2 \\
 &= \left[\frac{141.2 \times 120 \times 1.0 \times 1.0}{30} \times \frac{0.29}{10} \right]^2 = 268.3 \text{ mD}^2
 \end{aligned}$$

$$\bar{k} = \sqrt{k_{min}k_{max}} = \sqrt{268.3} = 16.38 \text{ mD}$$

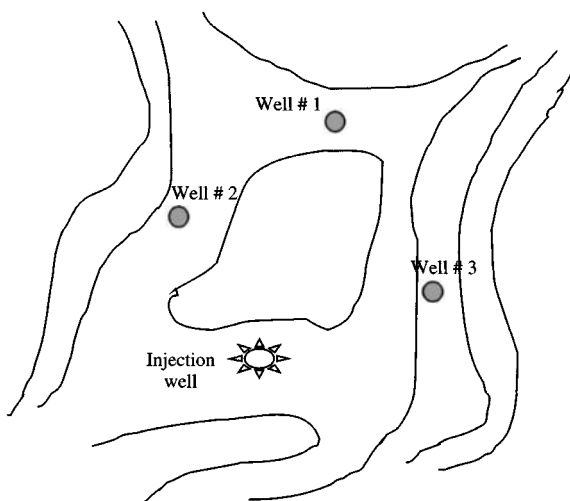


Figure 16–14. Net sand isopatch map.

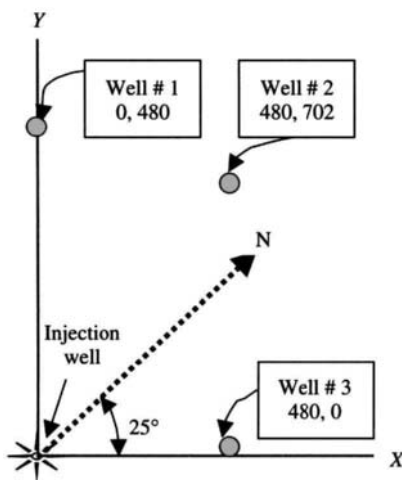


Figure 16-15. Well locations for Example 16-2.

$$\text{Also, } \bar{k} = \sqrt{(k_{xx}k_{yy} - k_{xy}^2)}$$

- Estimate product, $\phi\mu c_t$

Equations 16-32 through 16-34 now may be used with the time-match data to write three more equations. Match time was 10 hours and using the coordinate for each well from Figure 16-16 we have the following:

For Well 1

$$\left[\frac{(t_D/r_D^2)_{MP}}{t_{MP}} \right]_{\text{Well 1}} = \frac{0.0002637}{\phi\mu_o c_t} \left(\frac{k_{max}k_{min}}{k_{xx}y^2 + k_{yy}x^2 - 2k_{xy}xy} \right)$$

Table 16-5
Observation Pressure Data
for Well 1

t (hr)	$p_{x,y,t}$ (psi)	$\Delta p = p_i - p_{x,y,t}$ (psi)
34	272	
39	273	-8
50	279	-14
78	286	-21
98	291	-26
120	289	-24
188	280	-15

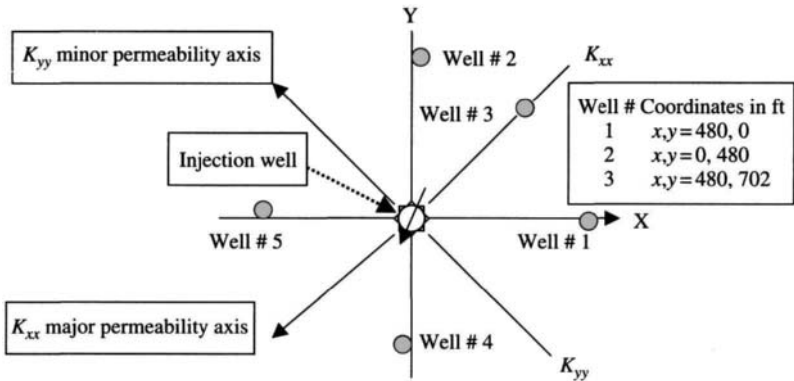


Figure 16-16. Coordinates for anisotropic permeability solution.

Table 16-6(a)
Observation Pressure Data for
Well 2

t (hr)	$p_{x,y,t}$ (psi)	$\Delta p = p_i - p_{x,y,t}$ (psi)
22	270	-5
49	277	-12
71	281	-16
93	286	-21
116	288	-23
124	291	-26
210	284	-19
289	281	-16

Table 16-6(b)
Observation Pressure Data for Well 3

t (hr)	$p_{x,y,t}$ (psi)	$\Delta p = p_i - p_{x,y,t}$ (psi)
28	269	-4
48	271	-6
70	275	-10
94	277	-12
117	282	-17
124	283	-18
190	276	-11
238	272	-7
297	271	-6

Table 16-6(c)

Well	Match points $(\Delta t)_{MP}$	t_D/r_D^2	t_{MP} (Figure 16-17)	r (ft)
1	10.0	25	30	480
2	10.0	35	38	480
3	10.0	45	70	702

Substituting the values, we get

$$\left[\frac{30}{25} \right]_{Well 1} = \frac{0.0002637}{\phi\mu c_t} \left[\frac{268.3}{480^2 k_x + (0)^2 k_y - 2(0)(480)k_{xy}} \right]$$

Simplifying and normalizing this equation becomes

$$k_x = \frac{3.685 \times 10^{-7}}{\phi\mu c_t} \quad (16-41a)$$

For Well 2

$$\left[\frac{30}{35} \right]_{Well 2} = \frac{0.0002637}{\phi\mu c_t} \left[\frac{268.3}{(0)^2 k_x + (480)^2 k_y - 2(0)(480)k_{xy}} \right]$$

Simplifying and normalizing this equation becomes:

$$k_y = \frac{3.334 \times 10^{-7}}{\phi\mu c_t} \quad (16-41b)$$

For Well 3

$$\left[\frac{70}{45} \right]_{Well 3} = \frac{0.0002637}{\phi\mu c_t} \left[\frac{268.3}{(530)^2 k_x + (480)^2 k_y - 2(480)(530)k_{xy}} \right]$$

Simplifying and normalizing this equation becomes

$$0.5521k_x + 0.4528k_y - k_{xy} = \frac{1.101 \times 10^{-6}}{\phi\mu c_t}$$

Combining Eqs. 16-41a and 16-41b gives

$$\begin{aligned} k_{xy} &= 0.5521 \frac{3.685 \times 10^{-7}}{\phi\mu c_t} + 0.4528 \frac{3.334 \times 10^{-7}}{\phi\mu c_t} - \frac{1.101 \times 10^{-6}}{\phi\mu c_t} \\ &= \frac{3.434 \times 10^{-8}}{\phi\mu c_t} \quad (16-41c) \end{aligned}$$

Using Eqs. 16–41a, b, and c in Eq. 16–35 results in:

$$k_x k_y - k_{xy}^2 = k_{min} k_{max} = \bar{k}^2$$

$$\frac{(3.685 \times 10^{-7})(3.334 \times 10^{-7})}{(\phi \mu c_t)(\phi \mu c_t)} - \left(\frac{3.434 \times 10^{-7}}{\phi \mu c_t} \right)^2 = 268.3$$

$$\frac{12.2858 \times 10^{-7}}{(\phi \mu c_t)^2} - \frac{22.7924 \times 10^{-7}}{(\phi \mu c_t)^2} = 268.3$$

Therefore

$$\phi \mu c_t = \sqrt{\frac{0.4934}{268.3}} = 3.24 \times 10^{-6} \text{ cP/psi}^{-1}$$

Now Eqs. 16–41a, b, and c are solved using the computed $\phi \mu c_t$

$$k_x = \frac{3.685 \times 10^{-7}}{3.24 \times 10^{-6}} = 11.373 \text{ mD}$$

$$k_y = \frac{3.334 \times 10^{-7}}{3.24 \times 10^{-6}} = 10.290 \text{ mD}$$

$$k_{xy} = \frac{3.434 \times 10^{-8}}{3.24 \times 10^{-6}} = 1.060 \text{ mD}$$

- Now we can estimate maximum permeability, k_{max} value using Eq. 16–37.
- Estimate minimum permeability, k_{min} value using Eq. 16–36.

$$k_{min} = k_{XX} = 0.5[21.663 - 2.3806] = 9.64 \text{ mD}$$

We know $\sqrt{k_{max} k_{min}} = 16.38$ and from Eq. 16–29, therefore we can check the computations:

$$k_{max} = k_{YY} = 0.5 \left[k_x + k_y + \sqrt{(k_{XX} - k_{YY})^2 + 4k_{xy}^2} \right]$$

$$= 0.5 \left[11.373 + 10.290 + \sqrt{(11.373 - 10.290)^2 + 4(1.06)^2} \right]$$

$$= 0.5[21.663 + 2.3806] = 12.02 \text{ mD}$$

$$\sqrt{k_{max} k_{min}} = \sqrt{(12.02)(9.64)} = 10.77 \rightarrow \text{Close enough}$$

- Determine the direction of maximum permeability, k_{max} , from Eq. 16–38.

$$\begin{aligned}\theta_{max} &= \arctan\left(\frac{k_{max} - k_{XX}}{k_{xy}}\right) = \arctan\left(\frac{12.02 - 11.373}{1.06}\right) = \arctan(0.6104) \\ &= \frac{0.5480(180)}{22/7} = 31.39^\circ \text{ from the } x\text{-axis}\end{aligned}$$

Correcting for the orientation of the axes, the maximum permeability direction is

$$31.39^\circ - 25^\circ = \text{N } 6.38 \text{ W}$$

Determine direction of minimum permeability, k_{min} , from Eq. 16-39.

$$\begin{aligned}\theta_{min} &= \arctan\left(\frac{k_{max} - k_{YY}}{k_{xy}}\right) = \arctan\left(\frac{12.02 - 10.29}{1.06}\right) = \arctan(0.6104) \\ &= \frac{1.021(180)}{22/7} = 58.48^\circ \text{ from the } x\text{-axis}\end{aligned}$$

Correcting for the orientation of the axes, the minimum permeability direction is

$$58.48^\circ - 25^\circ = \text{N } 33.48 \text{ W}$$

As shown in Figure 16-16, the x -axis was chosen as a line through wells 1, 2, and 3. True north lies along the line through wells 2 and 3.

Estimate water saturation using Eq. 16-41.

$$\begin{aligned}s_o &= \frac{c_t - c_w - c_f}{c_o - c_w} = \frac{7.85 \times 10^{-6} - 3.30 \times 10^{-6} - 3.70 \times 10^{-6}}{7.40 \times 10^{-6} - 3.30 \times 10^{-6}} \\ &= \frac{0.85 \times 10^{-6}}{4.1 \times 10^{-6}} = 0.21\end{aligned}$$

Hence water saturation is $s_w = 1 - s_o = 1 - 0.21 = 0.79$

Check these saturation values with electric log and core data, which agree good; hence it is possible for a rough estimate of in-place oil saturation using transient tests.

Summary: Eqs. 16-24 through 16-41, coupled with the log-log type curve procedure, are powerful tools for detecting reservoir anisotropy. The injection interference test described can be applied wildly to aid planning fluid injection programs.

Heterogeneous Reservoir Systems

If the data from multiwell tests fail to meet the homogeneous systems for both isotropic and anisotropic cases, numerical solutions must be used to analyze pressure transient data from heterogeneous systems. Chavent et al.¹⁷ and Chen et al.¹⁸ have suggested numerical solutions for performing the analysis by parameter estimation techniques to describe reservoir heterogeneities using pressure transient data. They consider the case of heterogeneous isotropic system using the following diffusion equation:

$$\nabla \left(\frac{kh}{\mu} \nabla p \right) = \phi c_t \frac{\partial p}{\partial t} + Q \dots \quad (16-42)$$

where Q is diffusion equation source term and p is pressure, psi. In order to estimate the values of $kh(x, y, z)$ and $\phi c_t h(x, y, z)$ that minimize E : Chavent et al.¹⁷

$$E = \sum_{s=1}^S \int_0^t (p_s^{obs} - p_s^{calc})^2 dT \quad (16-43)$$

Chen et al.¹⁸

$$E = \sum_{n=1}^{N_s} \sum_{s=1}^S (p_{n,s}^{obs} - p_{n,s}^{calc})^2 \quad (16-44)$$

where

E = Sum of the squares of the difference between observed and calculated pressure, psi

S = Number of observation wells

N = Number of observations at well

p_s^{obs} = Observed pressure at well, psi

p_s^{calc} = Calculated pressure at well, psi

$p_{n,s}^{obs}$ = Observed pressure at well and data point n , and

$p_{n,s}^{calc}$ = Calculated pressure at well and data point n .

16.10 Method for Calculating Fracture Orientation

Elkins and Skov¹⁴ have provided a method to estimate fracture orientation using pressure interference analysis technique. Elkins et al. assumed that pressure drawdown at a new well to constant single phase production of

another well in a horizontal reservoir of constant thickness with anisotropic permeability can be represented by the equation:

$$p_i - p_{x,y}@t = \frac{-q_o\mu_o\beta_o}{(1.127)4\pi\sqrt{k_x k_y}h} E_i \left[-\frac{\frac{(x-x_0)^2}{k_x} + \frac{(y-y_0)^2}{k_y}}{6.32 \frac{4t}{\phi\mu_o c}} \right] \quad (16-45)$$

where

p_i = initial pressure, psi

$p_{x,y}$ at t = pressure at x, y at time t , psi

$x - x_0$ = distance from producing well to pressure point in x -direction, ft

$y - y_0$ = distance from producing well to pressure point in y -direction, ft

k_x = effective permeability in x -direction, darcy

k_y = effective permeability in y -direction, darcy

Eq. 17-45 is solved on a trial-and-error basis by assuming effective compressibility of rock and fluids and permeabilities in the x and y directions, until a "good match" between calculated and measured pressure drop in the observed well is obtained. A more precise match can be obtained by the method of least squares using the sequence.¹⁴

16.11 Estimating Two-Dimensional Permeability with Vertical Interference Testing

Vertical interference testing technique can be used to estimate vertical and horizontal permeabilities in anisotropic reservoirs. Prats¹⁹ shows that if observed pressure, p_{ws} , is plotted versus $\log t$, a straight line should result with slope m and intercept at $t = 1$ hr of p_{1hr} . The horizontal permeability can be estimated from the slope using:

$$k_r = -\frac{162.6q_o\mu_o\beta_o}{mh} \quad (16-46)$$

The vertical permeability is estimated from the slope and intercept using

$$k_z = \frac{\phi\mu_o c_i h^2}{0.0002637} \text{antilog} \left(\frac{p_{1h} - p_i}{m} - \frac{G^* + h/(\Delta z_{mf} - \Delta z_{ws})}{2.3025} \right) \quad (16-47)$$

where

h = Reservoir thickness, ft

G^* = Geometric factor (geometrical function) can be found from Tables 16-7 through 16-12.

Δz_{mf} = Vertical distance from lower formation boundary to flow perforations, ft (see Figure 16–17b)

Δz_{ws} = Vertical distance from lower formation boundary to observation perforation, ft (see Figure 16–17b)

p_i = Initial pressure, psi at the time of test

This method requires the well to be thoroughly stabilized before testing.

Example 16–4²⁶ *Estimating Two-Dimensional Reservoir Permeability From Vertical Interference Test Data*

A vertical interference test was run. The active well is an injection well. The pressure response in observation well was measured as a function of time and is recorded in Table 16–12. Other data are: $q = -50$ stb/day, $h = 50$ ft, $\Delta Z_{wf} = 44$ ft, $\Delta Z_{ws} = 13$ ft, $c_i = 0.0000045$ psi⁻¹, $\phi = 10.5\%$, $\beta = 1.046$ rb/stb, $\mu = 1.15$ cP, and $p_i = 3000$ psi. Using the above data, estimate horizontal and vertical permeabilities.

Solution To analyze vertical interference test follow these steps:

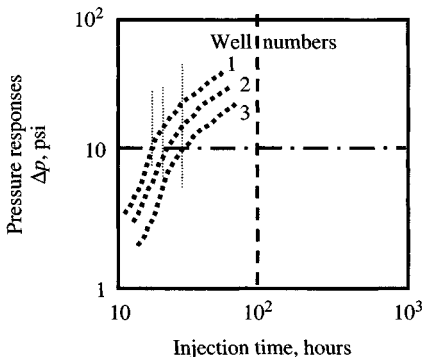
- Plot pressure response in an observation well, p_{ws} versus $\log t$.
- From Figure 16–18, find the following:

$$m = 21.5 \text{ psi/cycle and } p_{1hr} = 3022 \text{ psig}$$

- Estimate horizontal permeability, k_r , using Eq. 16–46

$$k_r = -\frac{162.6(-50)(1.046)(1.15)}{21.5(50)} = 9.10 \text{ mD}$$

$$\text{Transmissibility coefficient} = \frac{k_r h}{\mu} = \frac{9.10(50)}{1.15} = 395.65 \text{ mD ft/cP}$$



Match points		
The match was made so the pressure match point $[(\Delta p)_M, (p_D)_M]$ is the same for all three responses, while the time match points vary:		
Well #	r , ft	t_D/r_D^2
1	480	25
2	480	35
3	702	45

Figure 16–17a. Interference data matched to Figure 14–3. Pressure match is the same for all curves.

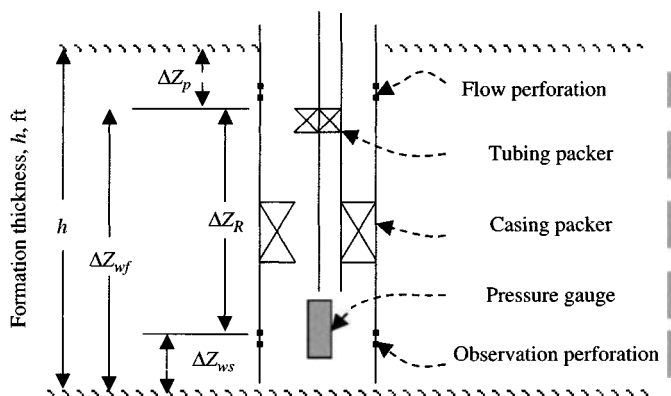


Figure 16-17b. Vertical interference and pulse test nomenclature.

$$\text{Formation storage} = \phi c_t h = 0.105 \times 0.0000245 \times 50 = 1.286 \times 10^{-5} \text{ psi}^{-1}$$

$$\begin{aligned} \text{Hydraulic diffusivity} &= \frac{k_r}{\phi c_t \mu} = \frac{9.10}{0.105(0.0000245)(1.15)} \\ &= 3.076 \times 10^6 \text{ mD psi}^{-1}/\text{cP} \end{aligned}$$

- Find such as, $\Delta Z_{wf}/h = 44/50 = 0.88$ and $\Delta Z_{ws}/h = 13/50 = 0.26$ from Tables 16-7 and 16-8, geometric factor, $G^* = 0.7565$
- Estimate vertical permeability, k_z using Eq. 16-47

$$\begin{aligned} k_z &= \frac{0.105(1.15)(2.45 \times 10^{-5})(50)^2}{0.0002637} \\ &\text{antilog}\left(\frac{3022 - 3015}{21.5} - \frac{0.7565 + 50/(44 - 13)}{2.3025}\right) \\ &= 28.047 \text{ antilog}(-0.7035) = 28.047 \times 0.1979 = 5.55 \text{ mD} \end{aligned}$$

$$\text{Transmissibility coefficient} = \frac{k_z h}{\mu} = \frac{5.55(50)}{1.15} = 241.34 \text{ mD ft/cP}$$

$$\begin{aligned} \text{Hydraulic diffusivity} &= \frac{k_z}{\phi c_t \mu} = \frac{5.55}{0.105(0.0000245)(1.15)} \\ &= 1.877 \times 10^6 \text{ mD psi}^{-1}/\text{cP} \end{aligned}$$

Table 16-7
Geometrical Function, G^* (Geometric Factor).¹⁹
For Various Values of $\Delta Z_{wf}/h$ With $\Delta Z_{ws}/h$ as a
Parameter [0.10 to 0.20]

$\Delta Z_{ws}/h = 0.10$		$\Delta Z_{ws}/h = 0.20$	
$\Delta Z_{wf}/h$	G^*	$\Delta Z_{wf}/h$	G^*
0.10	4.4361	0.10	2.5707
0.20	3.8879	0.12	2.3392
0.13	3.6459	0.13	2.2356
0.14	3.4251	0.14	2.1394
0.15	3.2232	0.15	2.0502
0.16	3.0389	0.16	1.9675
0.17	2.8708	0.17	1.8907
0.18	2.7177	0.18	1.8195
0.19	2.5785	0.19	1.7534
0.20	2.4520	0.20	1.6921
0.21	2.3373	0.21	1.6352
0.22	2.2332	0.22	1.5822
0.23	2.1389	0.23	1.5330
0.24	2.0535	0.24	1.4872
0.25	1.9762	0.25	1.4444
0.26	1.9060	0.26	1.4045
0.27	1.8424	0.27	1.3671
0.28	1.7846	0.28	1.3320
0.29	1.7320	0.29	1.2990
0.30	1.6840	0.30	1.2679
0.31	1.6400	0.31	1.2384
0.32	1.5995	0.32	1.2105
0.33	1.5621	0.33	1.1840
0.34	1.5272	0.34	1.1586
0.35	1.4946	0.35	1.1343
0.36	1.4638	0.36	1.1110
0.37	1.4346	0.37	1.0885
0.38	1.4066	0.38	1.0667
0.39	1.3796	0.39	1.0456
0.40	1.3533	0.40	1.0250
0.41	1.3276	0.41	1.0050
0.42	1.3023	0.42	0.9855
0.43	1.2773	0.43	0.9664
0.44	1.2524	0.44	0.9477
0.45	1.2276	0.45	0.9293
0.46	1.2028	0.46	0.9113
0.47	1.1779	0.47	0.8937
0.48	1.1529	0.48	0.8764

Table 16-7 (continued)

$\Delta Z_{ws}/h = 0.10$		$\Delta Z_{ws}/h = 0.20$	
$\Delta Z_{wf}/h$	G^*	$\Delta Z_{wf}/h$	G^*
0.49	1.1279	0.49	0.8594
0.50	1.1027	0.50	0.8428
0.51	1.0775	0.51	0.8265
0.52	1.0524	0.52	0.8107
0.53	1.0273	0.53	0.7952
0.54	1.0023	0.54	0.7802
0.55	0.9775	0.55	0.7657
0.56	0.9539	0.56	0.7517
0.57	0.9290	0.57	0.7383
0.58	0.9054	0.58	0.7255
0.59	0.8824	0.59	0.7133
0.60	0.8602	0.60	0.7018
0.61	0.8388	0.61	0.6911
0.62	0.8184	0.62	0.6811
0.63	0.7990	0.63	0.6719
0.64	0.7809	0.64	0.6636
0.65	0.7640	0.65	0.6562
0.66	0.7486	0.66	0.6498
0.67	0.7346	0.67	0.6443
0.68	0.7224	0.68	0.6399
0.69	0.7118	0.69	0.6365
0.70	0.7030	0.70	0.6342
0.71	0.6960	0.71	0.6330
0.72	0.6910	0.72	0.6329
0.73	0.6880	0.73	0.6339
0.74	0.6869	0.74	0.6361
0.75	0.6877	0.75	0.6394
0.76	0.6907	0.76	0.6439
0.77	0.6955	0.77	0.6495
0.78	0.7023	0.78	0.6561
0.79	0.7109	0.79	0.6638
0.80	0.7213	0.80	0.6726
0.81	0.7333	0.81	0.6823
0.82	0.7468	0.82	0.6929
0.83	0.7616	0.83	0.7044
0.84	0.7776	0.84	0.7166
0.85	0.7944	0.85	0.7295
0.86	0.8120	0.86	0.7430
0.87	0.8298	0.87	0.7569
0.88	0.8477	0.88	0.7711
0.89	0.8653	0.89	0.7855
0.90	0.8821	0.90	0.7999

Table 16-7 (continued)

$\Delta Z_{ws}/h = 0.10$		$\Delta Z_{ws}/h = 0.20$	
$\Delta Z_{wf}/h$	G^*	$\Delta Z_{wf}/h$	G^*
0.91	0.8977	0.91	0.8142
0.92	0.9118	0.92	0.8281
0.93	0.9236	0.93	0.8414
0.94	0.9327	0.94	0.8540
0.95	0.9385	0.95	0.8656
0.96	0.9404	0.96	0.8759
0.97	0.9375	0.97	0.8847
0.98	0.9292	0.98	0.8917
0.99	0.9148	0.99	0.8965
1.00	0.8933	1.00	0.8989

16.12 Application of Pulse Tests to Describe Reservoir Heterogeneity

The same analyses used to study the results of interference tests also apply to pulse test. Hirasaki²³ and Falade and Brigham^{24,25} have provided the relationships among dimensionless time lag, cycle period, and response amplitude in both graphical and analytical forms. A Cartesian plot of the

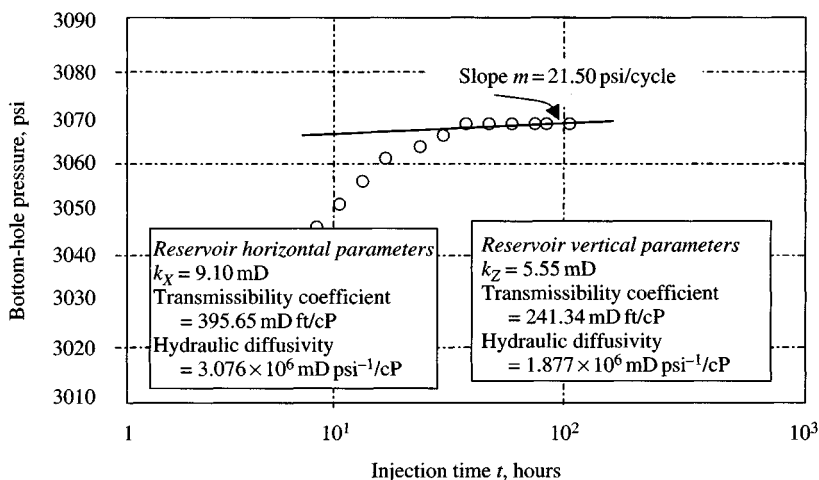


Figure 16-18. Semilog data plot.

Table 16-8
Geometrical Function, G^* (Geometric Factor).¹⁹ For
Various Values of $\Delta Z_{wf}/h$ With $\Delta Z_{ws}/h$ as a
Parameter [0.30 to 0.40]

Parameter $\Delta Z_{ws}/h = 0.3$		Parameter $\Delta Z_{ws}/h = 0.4$	
$\Delta Z_{wf}/h$	G^*	$\Delta Z_{wf}/h$	G^*
0.10	1.7562	0.10	1.3515
0.12	1.6443	0.12	1.2785
0.13	1.5921	0.13	1.2432
0.14	1.5423	0.14	1.2088
0.15	1.4947	0.15	1.1754
0.16	1.4493	0.16	1.1428
0.17	1.4059	0.17	1.1132
0.18	1.3645	0.18	1.0806
0.19	1.3249	0.19	1.0510
0.20	1.2871	0.20	1.0234
0.21	1.2511	0.21	0.9948
0.22	1.2366	0.22	0.9682
0.23	1.1837	0.23	0.9427
0.24	1.1523	0.24	0.9182
0.25	1.1223	0.25	0.8947
0.26	1.0936	0.26	0.8723
0.27	1.0662	0.27	0.8508
0.28	1.0400	0.28	0.8304
0.29	1.0150	0.29	0.8110
0.30	0.9910	0.30	0.7936
0.31	0.9682	0.31	0.7752
0.32	0.9464	0.32	0.7587
0.33	0.9256	0.33	0.7432
0.34	0.9055	0.34	0.7286
0.35	0.8864	0.35	0.7150
0.36	0.8682	0.36	0.7022
0.37	0.8508	0.37	0.6903
0.38	0.8341	0.38	0.6793
0.39	0.8182	0.39	0.6691
0.40	0.8030	0.40	0.6597
0.41	0.7885	0.41	0.6510
0.42	0.7747	0.42	0.6431
0.43	0.7616	0.43	0.6360
0.44	0.7490	0.44	0.6295
0.45	0.7371	0.45	0.6237
0.46	0.7259	0.46	0.6186
0.47	0.7151	0.47	0.6140
0.48	0.7049	0.48	0.6101

Table 16-8 (continued)

Parameter $\Delta Z_{ws}/h = 0.3$		Parameter $\Delta Z_{ws}/h = 0.4$	
$\Delta Z_{wf}/h$	G^*	$\Delta Z_{wf}/h$	G^*
0.49	0.6953	0.49	0.6067
0.50	0.6862	0.50	0.6038
0.51	0.6777	0.51	0.6014
0.52	0.6697	0.52	0.5996
0.53	0.6622	0.53	0.5981
0.54	0.6583	0.54	0.5971
0.55	0.6489	0.55	0.5965
0.56	0.6430	0.56	0.5962
0.57	0.6376	0.57	0.5963
0.58	0.6327	0.58	0.5968
0.59	0.6283	0.59	0.5975
0.60	0.6245	0.60	0.5985
0.61	0.6232	0.61	0.5998
0.62	0.6183	0.62	0.6014
0.63	0.6161	0.63	0.6032
0.64	0.6143	0.64	0.6052
0.65	0.6130	0.65	0.6074
0.66	0.6123	0.66	0.6098
0.67	0.6121	0.67	0.6124
0.68	0.6125	0.68	0.6151
0.69	0.6134	0.69	0.6181
0.70	0.6148	0.70	0.6212
0.71	0.6168	0.71	0.6245
0.72	0.6194	0.72	0.6280
0.73	0.6225	0.73	0.6317
0.74	0.6261	0.74	0.6355
0.75	0.6303	0.75	0.6396
0.76	0.6351	0.76	0.6439
0.77	0.6405	0.77	0.6484
0.78	0.6464	0.78	0.6532
0.79	0.6529	0.79	0.6582
0.80	0.6599	0.80	0.6636
0.81	0.6675	0.81	0.6692
0.82	0.6757	0.82	0.6753
0.83	0.6844	0.83	0.6818
0.84	0.6936	0.84	0.6887
0.85	0.7035	0.85	0.6961
0.86	0.7138	0.86	0.7040
0.87	0.7247	0.87	0.7126
0.88	0.7361	0.88	0.7218
0.89	0.7480	0.89	0.7327
0.90	0.7604	0.90	0.7424

Table 16-8 (continued)

Parameter $\Delta Z_{ws}/h = 0.3$		Parameter $\Delta Z_{ws}/h = 0.4$	
$\Delta Z_{wf}/h$	G^*	$\Delta Z_{wf}/h$	G^*
0.91	0.7732	0.91	0.7539
0.92	0.7867	0.92	0.7664
0.93	0.8005	0.93	0.7798
0.94	0.8148	0.94	0.7944
0.95	0.8294	0.95	0.8101
0.96	0.8445	0.96	0.8271
0.97	0.8599	0.97	0.8455
0.98	0.8756	0.98	0.8654
0.99	0.8916	0.99	0.8868
1.00	0.9079	1.00	0.9100

Table 16-9
 Geometrical Function, G^* (Geometric Factor).¹⁹ For
 Various Values of $\Delta Z_{wf}/h$ With $\Delta Z_{ws}/h$ as a
 Parameter [0.50 to 0.60]

Parameter $\Delta Z_{ws}/h = 0.5$		Parameter $\Delta Z_{ws}/h = 0.6$	
$\Delta Z_{wf}/h$	G^*	$\Delta Z_{wf}/h$	G^*
0.10	1.0055	0.10	0.8035
0.12	0.9546	0.12	0.7805
0.13	0.9311	0.13	0.7698
0.14	0.9087	0.14	0.7595
0.15	0.8875	0.15	0.7497
0.16	0.8674	0.16	0.7402
0.17	0.8484	0.17	0.7311
0.18	0.8303	0.18	0.7223
0.19	0.8132	0.19	0.7130
0.20	0.7971	0.20	0.7057
0.21	0.7819	0.21	0.6978
0.22	0.7675	0.22	0.6902
0.23	0.7540	0.23	0.6828
0.24	0.7412	0.24	0.6757
0.25	0.7292	0.25	0.6688
0.26	0.7179	0.26	0.6622
0.27	0.7073	0.27	0.6558
0.28	0.6974	0.28	0.6497
0.29	0.6881	0.29	0.6438
0.30	0.6794	0.30	0.6381

Table 16-9 (continued)

Parameter $\Delta Z_{ws}/h = 0.5$		Parameter $\Delta Z_{ws}/h = 0.6$	
$\Delta Z_{wf}/h$	G^*	$\Delta Z_{wf}/h$	G^*
0.31	0.6713	0.31	0.6327
0.32	0.6637	0.32	0.6276
0.33	0.6566	0.33	0.6227
0.34	0.6500	0.34	0.6181
0.35	0.6439	0.35	0.6138
0.36	0.6383	0.36	0.6097
0.37	0.6332	0.37	0.6060
0.38	0.6283	0.38	0.6026
0.39	0.6239	0.39	0.5996
0.40	0.6198	0.40	0.5969
0.41	0.6161	0.41	0.5946
0.42	0.6128	0.42	0.5927
0.43	0.6097	0.43	0.5912
0.44	0.6070	0.44	0.5901
0.45	0.6046	0.45	0.5895
0.46	0.6024	0.46	0.5894
0.47	0.6005	0.47	0.5898
0.48	0.5989	0.48	0.5908
0.49	0.5975	0.49	0.5922
0.50	0.5964	0.50	0.5943
0.51	0.5955	0.51	0.5969
0.52	0.5948	0.52	0.6002
0.53	0.5944	0.53	0.6041
0.54	0.5942	0.54	0.6086
0.55	0.5941	0.55	0.6139
0.56	0.5943	0.56	0.6199
0.57	0.5947	0.57	0.6266
0.58	0.5953	0.58	0.6340
0.59	0.5961	0.59	0.6423
0.60	0.5972	0.60	0.6513
0.61	0.5984	0.61	0.6611
0.62	0.5998	0.62	0.6718
0.63	0.6015	0.63	0.6834
0.64	0.6033	0.64	0.6958
0.65	0.6054	0.65	0.7091
0.66	0.6077	0.66	0.7233
0.67	0.6103	0.67	0.7385
0.68	0.6130	0.68	0.7546
0.69	0.6161	0.69	0.7716
0.70	0.6194	0.70	0.7896
0.71	0.6230	0.71	0.8086
0.72	0.6268	0.72	0.8285

Table 16-9 (continued)

Parameter $\Delta Z_{ws}/h = 0.5$		Parameter $\Delta Z_{ws}/h = 0.6$	
$\Delta Z_{wf}/h$	G^*	$\Delta Z_{wf}/h$	G^*
0.73	0.6309	0.73	0.8495
0.74	0.6354	0.74	0.8714
0.75	0.6402	0.75	0.8943
0.76	0.6453	0.76	0.9182
0.77	0.6507	0.77	0.9431
0.78	0.6565	0.78	0.9690
0.79	0.6627	0.79	0.9959
0.80	0.6693	0.80	1.0237
0.81	0.6762	0.81	1.0526
0.82	0.6837	0.82	1.0823
0.83	0.6915	0.83	1.1131
0.84	0.6999	0.84	1.1447
0.85	0.7087	0.85	1.1773
0.86	0.7181	0.86	1.2108
0.87	0.7280	0.87	1.2451
0.88	0.7384	0.88	1.2803
0.89	0.7495	0.89	1.3163
0.90	0.7611	0.90	1.3530
0.91	0.7734	0.91	1.3906
0.92	0.7863	0.92	1.4288
0.93	0.7999	0.93	1.4676
0.94	0.8143	0.94	1.5071
0.95	0.8294	0.95	1.5472
0.96	0.8452	0.96	1.5878
0.97	0.8619	0.97	1.6288
0.98	0.8793	0.98	1.6702
0.99	0.8977	0.99	1.7120
1.00	0.9169	1.00	1.7541

measured pressure response at the observation well versus time is used to estimate the time lag and the response amplitude (see Figure 16-19). The reservoir properties are then determined from the following relationships¹⁶:

$$t_{LD} = \frac{t_L}{\Delta t_{cyc}} \quad (16-48)$$

$$kh = 70.6q\beta \left(\frac{\Delta p_D}{\Delta p} \right) \quad (16-49)$$

and

$$\phi c_i h = \frac{kh}{\mu} \frac{1}{56,900 r_{bw}^2} \frac{\Delta t_{cyc}}{\Delta t_{cycD}} \quad (16-50)$$

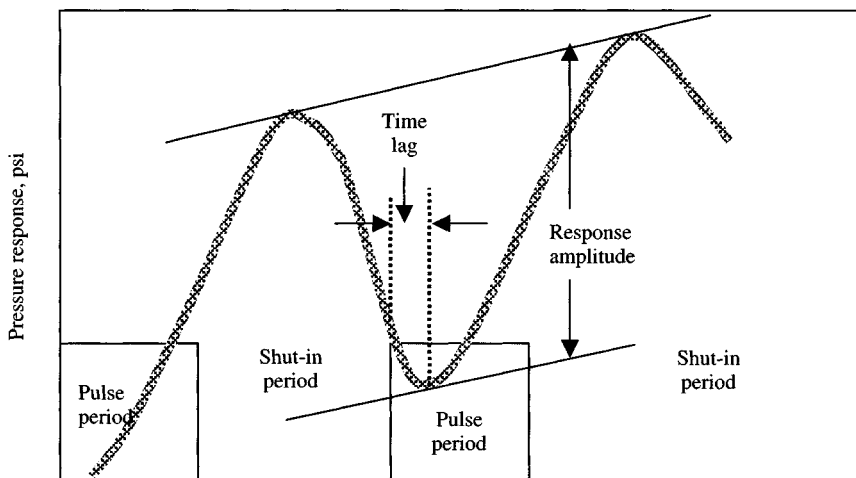


Figure 16-19. Pulse test terminology.

Table 16-10
Geometrical Function, G^* (Geometric Factor).¹⁹
For Various Values of $\Delta Z_{wf}/h$ With $\Delta Z_{ws}/h$ as
a Parameter [0.70 to 0.80]

Parameter $\Delta Z_{ws}/h = 0.7$		Parameter $\Delta Z_{ws}/h = 0.8$	
$\Delta Z_{wf}/h$	G^*	$\Delta Z_{wf}/h$	G^*
0.10	0.7987	0.10	0.8105
0.12	0.7745	0.12	0.7823
0.13	0.7633	0.13	0.7686
0.14	0.7522	0.14	0.7553
0.15	0.7418	0.15	0.7425
0.16	0.7319	0.16	0.7302
0.17	0.7224	0.17	0.7187
0.18	0.7135	0.18	0.7079
0.19	0.7051	0.19	0.6978
0.20	0.6971	0.20	0.6886
0.21	0.6897	0.21	0.6803
0.22	0.6828	0.22	0.6728
0.23	0.6763	0.23	0.6664
0.24	0.6704	0.24	0.6608
0.25	0.6649	0.25	0.6563
0.26	0.6600	0.26	0.6528
0.27	0.6555	0.27	0.6502
0.28	0.6516	0.28	0.6487

Table 16-10 (continued)

Parameter $\Delta Z_{ws}/h = 0.7$		Parameter $\Delta Z_{ws}/h = 0.8$	
$\Delta Z_{wf}/h$	G^*	$\Delta Z_{wf}/h$	G^*
0.29	0.6481	0.29	0.6482
0.30	0.6451	0.30	0.6486
0.31	0.6427	0.31	0.6500
0.32	0.6407	0.32	0.6524
0.33	0.6393	0.33	0.6557
0.34	0.6383	0.34	0.6600
0.35	0.6378	0.35	0.6651
0.36	0.6379	0.36	0.6711
0.37	0.6385	0.37	0.6780
0.38	0.6395	0.38	0.6857
0.39	0.6411	0.39	0.6941
0.40	0.6432	0.40	0.7034
0.41	0.6458	0.41	0.7133
0.42	0.6490	0.42	0.7240
0.43	0.6526	0.43	0.7353
0.44	0.6568	0.44	0.7473
0.45	0.6616	0.45	0.7599
0.46	0.6669	0.46	0.7731
0.47	0.6728	0.47	0.7869
0.48	0.6793	0.48	0.8013
0.49	0.6863	0.49	0.8162
0.50	0.6939	0.50	0.8316
0.51	0.7022	0.51	0.8475
0.52	0.7110	0.52	0.8640
0.53	0.7205	0.53	0.8809
0.54	0.7306	0.54	0.8984
0.55	0.7415	0.55	0.9164
0.56	0.7530	0.56	0.9350
0.57	0.7652	0.57	0.9541
0.58	0.7781	0.58	0.9738
0.59	0.7918	0.59	0.9941
0.60	0.8062	0.60	1.0151
0.61	0.8214	0.61	1.0368
0.62	0.8375	0.62	1.0593
0.63	0.8544	0.63	1.0826
0.64	0.8722	0.64	1.1068
0.65	0.8909	0.65	1.1320
0.66	0.9105	0.66	1.1582
0.67	0.9312	0.67	1.1856
0.68	0.9528	0.68	1.2144
0.69	0.9754	0.69	1.2445
0.70	0.9992	0.70	1.2762

Table 16-10 (continued)

Parameter $\Delta Z_{ws}/h = 0.7$		Parameter $\Delta Z_{ws}/h = 0.8$	
$\Delta Z_{wf}/h$	G^*	$\Delta Z_{wf}/h$	G^*
0.71	1.0241	0.71	1.3095
0.72	1.0501	0.72	1.3447
0.73	1.0774	0.73	1.3819
0.74	1.1059	0.74	1.4212
0.75	1.1358	0.75	1.4629
0.76	1.1670	0.76	1.5072
0.77	1.1936	0.77	1.5543
0.78	1.2336	0.78	1.6044
0.79	1.2692	0.79	1.6578
0.80	1.3064	0.80	1.7147
0.81	1.3452	0.81	1.7754
0.82	1.3857	0.82	1.8402
0.83	1.4280	0.83	1.9094
0.84	1.4722	0.84	1.9832
0.85	1.5182	0.85	2.0622
0.86	1.5662	0.86	2.1465
0.87	1.6163	0.87	2.2367
0.88	1.6685	0.88	2.3330
0.89	1.7229	0.89	2.4358
0.90	1.7796	0.90	2.5457
0.91	1.8387	0.91	2.6630
0.92	1.9093	0.92	2.7882
0.93	1.9644	0.93	2.9218
0.94	2.0312	0.94	3.0643
0.95	2.1007	0.95	3.2162
0.96	2.1731	0.96	3.3780
0.97	2.2484	0.97	3.5504
0.98	2.3268	0.98	3.7339
0.99	2.4083	0.99	3.9290
1.00	2.4932	1.00	4.1365

Homogeneous Isotropic Reservoir Systems

To analyze this type of reservoir by pulse test, Eqs. 16-49 and 16-50 should replace by Eqs. 16-51 and 16-52.

$$h\sqrt{\frac{k_{xx}k_{yy} - k_{xy}^2}{\mu}} = 70.6q\beta\left(\frac{\Delta p_D}{\Delta p}\right) \quad (16-51)$$

$$\phi c_i h = \left(\frac{k_{xx}k_{yy} - k_{xy}^2}{k_{xx}y^2 + k_{yy}x^2 - 2k_{xy}xy} \right) \cdot \frac{h}{\mu} \cdot \frac{1}{56,900} \cdot \frac{\Delta t_{cyc}}{\Delta t_{cycD}} \quad (16-52)$$

The values of k_{max} , k_{min} and θ are estimated using Eqs. 16-36 through 16-38. If calculated value of $\sqrt{k_{xx}k_{yy} - k_{xy}^2}$ from the pressure match is not the same for other tests, heterogeneous models should be used.

Anisotropic Reservoir Systems

In the case of homogeneous anisotropic reservoir systems, porosity is uniform throughout the reservoir, but permeability varies with direction. Figure 16-20 shows the major and minor axes of the permeability and the well pattern.

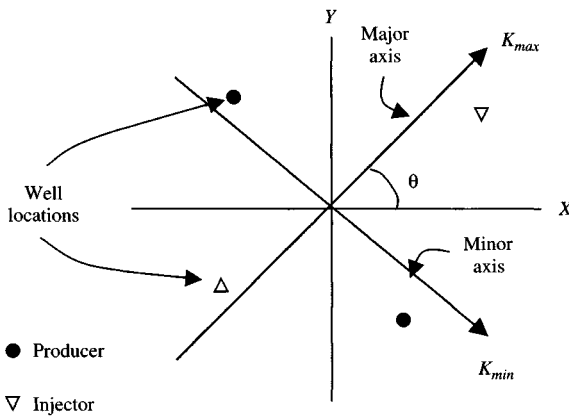


Figure 16-20. Anisotropic permeability and well axes.

Table 16-11
Geometrical Function, G^* (Geometric Factor)¹⁹
For Various Values of $\Delta Z_{wf}/h$ With $\Delta Z_{ws}/h$ as a
Parameter [0.90 to 1.0]

Parameter $\Delta Z_{ws}/h = 0.9$		Parameter $\Delta Z_{ws}/h = 1.0$	
$\Delta Z_{wf}/h$	G^*	$\Delta Z_{wf}/h$	G^*
0.10	0.8464	0.10	—
0.12	0.8072	0.12	—
0.13	0.7874	0.13	—
0.14	0.7681	0.14	—
0.15	0.7494	0.15	—
0.16	0.7317	0.16	—

Table 16-11 (continued)

Parameter $\Delta Z_{ws}/h = 0.9$		Parameter $\Delta Z_{ws}/h = 1.0$	
$\Delta Z_{wf}/h$	G^*	$\Delta Z_{wf}/h$	G^*
0.17	0.7153	0.17	—
0.18	0.7004	0.18	—
0.19	0.6871	0.19	—
0.20	0.6756	0.20	—
0.21	0.6660	0.21	—
0.22	0.6585	0.22	—
0.23	0.6532	0.23	—
0.24	0.6500	0.24	—
0.25	0.6490	0.25	—
0.26	0.6502	0.26	—
0.27	0.6536	0.27	—
0.28	0.6591	0.28	—
0.29	0.6660	0.29	—
0.30	0.6766	0.30	—
0.31	0.6884	0.31	—
0.32	0.7020	0.32	—
0.33	0.7175	0.33	—
0.34	0.7346	0.34	—
0.35	0.7533	0.35	—
0.36	0.7715	0.36	—
0.37	0.7950	0.37	—
0.38	0.8176	0.38	—
0.39	0.8413	0.39	—
0.40	0.8659	0.40	—
0.41	0.8913	0.41	—
0.42	0.9173	0.42	—
0.43	0.9438	0.43	—
0.44	0.9707	0.44	—
0.45	0.9978	0.45	—
0.46	1.0251	0.46	—
0.47	1.0524	0.47	—
0.48	1.0796	0.48	—
0.49	1.1066	0.49	—
0.50	1.1335	0.50	—
0.51	1.1600	0.51	—
0.52	1.1862	0.52	—
0.53	1.2121	0.53	—
0.54	1.2376	0.54	—
0.55	1.2628	0.55	—
0.56	1.2877	0.56	—
0.57	1.3123	0.57	—
0.58	1.3368	0.58	—

Table 16-11 (continued)

Parameter $\Delta Z_{ws}/h = 0.9$		Parameter $\Delta Z_{ws}/h = 1.0$	
$\Delta Z_{wf}/h$	G^*	$\Delta Z_{wf}/h$	G^*
0.59	1.3612	0.59	—
0.60	1.3857	0.60	—
0.61	1.4105	0.61	—
0.62	1.4357	0.62	—
0.63	1.4617	0.63	—
0.64	1.4885	0.64	—
0.65	1.5167	0.65	—
0.66	1.5463	0.66	—
0.67	1.5780	0.67	—
0.68	1.6120	0.68	—
0.69	1.6488	0.69	—
0.70	1.6889	0.70	—
0.71	1.7328	0.71	—
0.72	1.7811	0.72	—
0.73	1.8345	0.73	—
0.74	1.8936	0.74	—
0.75	1.9591	0.75	—
0.76	2.0318	0.76	—
0.77	2.1125	0.77	—
0.78	2.2021	0.78	—
0.79	2.3015	0.79	—
0.80	2.4118	0.80	—
0.81	2.5339	0.81	—
0.82	2.6690	0.82	—
0.83	2.8182	0.83	—
0.84	2.9827	0.84	—
0.85	3.1639	0.85	—
0.86	3.3631	0.86	—
0.87	3.5816	0.87	—
0.88	3.8211	0.88	—
0.89	4.0831	0.89	—
0.90	4.3691	0.90	—
0.91	4.6809	0.91	—
0.92	5.0202	0.92	—
0.93	5.3889	0.93	—
0.94	5.7890	0.94	—
0.95	6.2223	0.95	—
0.96	6.6911	0.96	—
0.97	7.1973	0.97	—
0.98	7.7434	0.98	—
0.99	8.3316	0.99	—
1.00	8.9443	1.00	—

Table 16-12
Pressure – Time Data From Vertical
Interference Test

Time t (hr)	Pressure response p_{ws} (psig)
1	3015
2	3020
3	3023
4	3030
5	3033
6	3038
7	3040
8	3043
10	3048
20	3050
30	3055
40	3060
50	3064
60	3066
70	3066
80	3067
90	3068
100	3070

The values of k_{max} , k_{min} and θ are determined using Eqs. 16-36 through 16-38. If the value of $\sqrt{k_{xx}k_{yy} - k_{xy}^2}$ calculated from the pressure match is not the same for different tests, then heterogeneous analysis technique should be used.

16.13 Validity of Various Models and Steps Used to Obtain Reservoir Description

<i>Analysis Models</i>	<i>Equations Used</i>	<i>Validity of Models</i>
A. Homogeneous isotropic model	Eqs. 16-19 to 16-23	Reservoir parameters are the same from different tests
B. Homogeneous anisotropic model	Eqs. 16-21 to 16-23 6-30, 16-36, 16-38 16-52-16-53	Pressure match is the same for different tests. Permeability from single tests is same from multiple-well tests
C. Heterogeneous 2D model	Eq. 16-44	Reasonable agreement between observed and calculated pressures
D. Heterogeneous 3D model	Eq. 16-44	Reasonable agreement between observed and calculated pressures

Figure 16-21. Most common models and criteria for their validity.

16.14 Summary

This chapter discusses variations of heterogeneities in rock and fluid properties including causes and effects of pressure-dependent properties. It also presents how to analyze and interpret pressure behavior in heterogeneous reservoirs near fault or other barriers and lateral changes in the hydraulic diffusivity such as occur at fluid contacts. Ref. 20 has presented a method for analyzing pressure build ups in fissured limestone reservoirs, which has proved to be quite useful. Pressure behavior analysis methods are discussed in brief to obtain adequate reservoir descriptions for isotropic, anisotropic, and heterogeneous systems including calculating fracture orientation and estimating two-dimensional permeability with vertical interference testing. Pressure transient tests can be used to obtain an adequate reservoir description for isotropic, anisotropic, and heterogeneous reservoir systems. Numerical solutions must be used to analyze pressure transient test data from heterogeneous reservoir systems. If a criterion for validity of model is not met, go to next stem. Figure 16-21 shows validity of proposed analysis models.

References and Additional Reading

1. Vairogs, J., Hearn, C. L., Dareing, D. W., and Rhoades, V. W., "Effect of Rock Stress on Gas Production from Low-Permeability Reservoirs," *J. Pet. Technol.* (Sept. 1971), 1161-1167; *Trans AIME* 251.
2. Thomas, R. D., and Ward, D. C., "Effect of Overburden Pressure and Water Saturation on the Gas Permeability of Tight Sandstone Cores," *J. Pet. Technol.* (Feb. 1972), 120-124.
3. Vairogs, J., and Rhoades, V. W., "Pressure Transient Tests in Formations Having Stress-Sensitive Permeability," *J. Pet. Technol.* (Aug. 1973), 965-970; *Trans. AIME* 255.
4. Raghavan, R., Scorer, J. D. T., and Miller, F. G., "An Investigation by Numerical Methods of the Effect of Pressure Dependent Rock and Fluid Properties on Well Flow Tests," *Soc. Pet. Eng. J.* (June 1972), 267-275; *Trans. AIME* 253.
5. Ramey, H. J., Jr., "Non-Darcy Flow and Wellbore Storage Effects in Pressure Buildup and Drawdown of Gas Wells," *J. Pet. Technol.* (Feb. 1965), 223-233; *Trans. AIME* 234. Also Reprint Series, No. 9 - Pressure Analysis Methods, Society of Petroleum Engineers of AIME, Dallas (1967) 233-243.
6. Matthews, C. S., and Russell, D. G., Pressure Buildup and Flow Tests in Wells. Monograph Series, Society of Petroleum Engineers of AIME, Dallas (1967).

7. Horner, D. R., "Pressure Build-up in Wells," Proc; Third World Pet. Cong; The Hague (1951) Sec II, 503–523. Also Reprint Series, No. 9 – Pressure Analysis Methods, Society of Petroleum Engineers of AIME, Dallas (1967) 25–43.
8. Gray, K. E., "Approximating Well-to-Fault Distance From Pressure Build-Up Tests," *J. Pet. Technol.* (July 1965), 761–767.
9. Davis, E. G., Jr., and Hawkins, M. F., Jr., "Linear Fluid-Barrier Detection by Well Pressure Measurements", *J. Pet. Technol.* (Oct. 1963), 1077–1079.
10. Bixel, H. C., Larkin, B. K., and Van Poolen, H. K., "Effect of Linear Discontinuities on Pressure Build-Up and Drawdown Behavior," *J. Pet. Technol.* (Aug. 1965), 885–895; *Trans. AIME* 228.
11. Russell, D. G., "Determination of Formation Characteristics From Two Rate Flow Tests," *J. Pet. Technol.* (Dec. 1963), 1347–1355; *Trans. AIME* 228. Also Reprint Series, No. 9 – Pressure Analysis Methods, Society of Petroleum Engineers of AIME, Dallas (1967) 136–144.
12. Pirson, R. S., and Pirson, S. J., "An Extension of the Pollard Analysis Method of Well Pressure Build-Up and Drawdown Tests," paper SPE 101 presented at the SPE-AIME 36th Annual Fall Meeting, Dallas, Oct. 8–11, 1961.
13. Kamal, M., and Brigham, W. E., "The Effect of Linear Pressure Trends on Interference Tests," *J. Pet. Technol.* (Nov. 1975), 1383–1384.
14. Elkins, L. F., and Skov, A. M., "Determination of Fracture Orientation From Pressure Interference," *Trans AIME* (1960) 219, 301–304. Also Reprint Series, No. 9 – Pressure Analysis Methods, Society of Petroleum Engineers of AIME, Dallas (1967) 97–100.
15. Ramey, H. J., Jr., "Interference Analysis for Anisotropic Formations – A Case History," *J. Pet. Technol.* (Oct. 1975), 1290–1298; *Trans. AIME* 259.
16. Brigham, W. E., "Planning and Analysis of Pulse Tests," *J. Pet. Technol.* (May 1970), 618–624; *Trans AIME* 249.
17. Chavent, C., Dupuy, M., and Lemonier, P., "History Matching by Use of Optimal Control Theory," *Soc. Pet. Eng. J.* (Feb. 1975), 74–86; *Trans. AIME* 259.
18. Chen, W. H., Gavalas, G. R., and Seinfelds, J. H., "A New Algorithm for Automatic History Matching," *Soc. Pet. Eng. J.* (Dec. 1974), 593–608; *Trans. AIME* 257.
19. Prats, M., "A Method for Determining the Net Vertical Permeability Near a Well From In-Situ-Measurements," *J. Pet. Technol.* (May 1970), 637–643; *Trans. AIME* 249.
20. Pollard, P. (1959) Evaluation of Acid Treatments from Pressure Build-up Analysis, *Trans. AIME* 216, 38–43.
21. Weller, W. H. C., and van Poolen, H. K., "Reservoir Performance During Two-Phase Flow," *J. Pet Technol.* (Feb. 1966), 240–247.

22. Jahns, H. O., "A Rapid Method for Obtaining a Two-Dimensional Reservoir Description From Well Pressure Response Data," *Soc. Pet. Eng. J.* (Dec. 1966), 315-327.
23. Hirasaki, G. J., "Pulse Tests and Other Early Transient Pressure Analyses for In-Situ Estimation of Vertical Permeability," *Soc. Pet. Eng. J.* (Feb. 1974), 75-90; *Trans. AIME* 257.
24. Falade, G. K., and Brigham, W. E., "The Dynamics of Vertical Pulse Testing in a Slab Reservoir," paper SPE 5055A presented at the SPE-AIME 49th Annual Fall Meeting, Houston, Oct. 6-9, 1974.
25. Falade, G. K., and Brigham, W. E., "The Analysis of Single-Well Pulse Tests in a Finite-Acting Slab Reservoir," paper SPE 5055B presented at the SPE-AIME 49th Annual Fall Meeting, Houston, Oct. 6-9, 1974.
26. Amanat, U. C., "Pressure Transient Test Analysis, User's Handbook," Advanced TWPSOM Petroleum Systems Inc; Houston, Texas, Vol 8 (1995).

Appendix A

Conversion Factors Between Unit Systems

Table A-1
Permeability Conversions

To convert from	To	Multiply by	Inverse
mD	Darcy	1.000000E-03	1.000000E+03
mD	meter ² (m ²)	9.86923E-16	1.01325E+15
mD	centimeter ² (cm ²)	9.86923E-12	1.01325E+11
mD	micrometer ² (μm ²)	9.86923E-04	1.01325E+03
mD	$\frac{(\text{cm}^3/\text{s})\text{cP}}{\text{cm}^2(\text{atm}/\text{cm})}$	1.00000E-03	1.00000E+03
mD	$\frac{(\text{cm}^3/\text{s})\text{cP}}{\text{cm}^2[(\text{dyne}/\text{cm}^2)/\text{cm}]}$	9.86923E-10	1.01325E+09
mD	$\frac{(\text{ft}^3/\text{s})\text{cP}}{\text{ft}^2(\text{psi}/\text{ft})}$	7.32441E-08	1.36530E+07
mD	$\frac{(\text{ft}^3/\text{s})\text{cP}}{\text{cm}^2[(\text{cm water})/\text{cm}]}$	3.41780E-11	2.92585E+10
mD	$\frac{(\text{B}/\text{D})\text{cP}}{\text{ft}^2(\text{psi}/\text{ft})}$	1.12712E-03	8.87217E+02
mD	$\frac{(\text{gal}/\text{min})\text{cP}}{\text{ft}^2[(\text{ft water})/\text{ft}]}$	1.42515E-05	7.01681E+04
mD	ft ²	1.06232E-14	9.41340E+13

Table A-2
Temperature Conversions

	°F	°C	°R	K
Degree Fahrenheit (°F)	1.000	(°F - 32)/1.8	°F + 459.67	(°F + 459.67)/1.8
Degree Celsius (°C)	1.8(°C) + 32	1.000	1.8(°C) + 491.67	°C + 273.15
Degree Rankine (°R)	°R - 459.67	(°R - 491.67)/1.8	1.000	°R/1.8
Kelvin (K)	1.8(K) - 459.67	K - 273.15	1.8(K)	1.000

Table A-3
Volume Conversion Multiplication Factors

	in^3	ft^3	cm^3	m^3
Cubic inches (in^3)	1.0	5.787035×10^{-4}	1.638706×10	1.638706×10^{-5}
Cubic feet (ft^3)	1.728×10^3	1.0	2.831685×10^4	2.831685×10^{-2}
Cubic centimeters (cm^3)	6.102376×10^{-2}	3.531466×10^{-5}	1.0	1.000×10^{-6}
Cubic meters (m^3)	6.102376×10^4	3.531466×10	1.000×10^6	1.0

Table A-4
Density Conversion Multiplication Factors

	gm/cm^3	lb/ft^3	kg/l	kg/m^3
gm/cm^3	1.0	6.242797×10	1.0	1.000×10^3
lb/ft^3	1.601846×10^{-2}	1.0	1.601846×10^{-2}	1.601846×10
kg/l	1.0	6.242797×10	1.0	1.000×10^3
kg/m^3	1.000×10^{-3}	6.242797×10^{-2}	1.0×10^{-3}	1.0

Table A-5
Rate of Flow Conversion Multiplication Factors

	ft^3/min	US gal/day	bbl/day	m^3/s
ft^3/min	1.0	1.077195×10^4	2.564749×10^2	4.719474×10^{-4}
US gal/day	9.283374×10^{-5}	1.0	2.380952×10^{-2}	4.381264×10^{-8}
bbl/day	3.899017×10^{-3}	42.0	1.0	1.840131×10^{-6}
m^3/s	2.11888×10^3	2.282477×10^7	5.434396×10^5	1.0

Table A-6
Mass Conversion Multiplication Factors

	Ounces (avoir) (oz)	Pounds (avoir) (lb)	Metric ton (t) (tonne)	Kilograms (kg)
Ounces	1.0	6.25×10^{-2}	2.834952×10^{-5}	2.834952×10^{-2}
Pounds	16.0	1.0	4.535924×10^{-4}	4.535924×10^{-1}
Metric ton	3.527397×10^4	2.204622×10^3	1.0	1.000×10^3
Kilograms	3.527397×10	2.204622	1.000×10^{-3}	1.0

Table A-7
Velocity Conversion Multiplication Factors

	ft/s	ft/min	ft/h	m/s
ft/s	1.0	60.0	3600.0	3.048000×10^{-1}
ft/min	1.666666×10^{-2}	1.0	60.0	5.080000×10^{-1}
ft/h	2.777777×10^{-4}	1.666666×10^{-2}	1.0	8.466667×10^{-5}
m/s	3.28084	1.968504×10^2	1.181102×10^4	1.0

Table A-8
Viscosity (Absolute) Conversion Multiplication Factors

	cP	poise g/(cm s)	lb(ft s)	Pascal second (Pa s)
Centipoise	1.0	1.00×10^{-2}	6.719689×10^{-4}	1.000000×10^{-3}
poise g/(cm s)	100.0	1.0	6.719689×10^{-2}	1.000×10^{-1}
lb/(ft s)	1.488164×10^3	1.488164×10	1.0	1.488164
Pascal second (Pa s)	1.000×10^3	10.0	6.719689×10^{-1}	1.0

Table A-9
Kinematic Viscosity: Absolute Viscosity in Mass Units Divided by Mass Density Conversion Factors

	gm/cm ³	lb/ft ³	kg/l	kg/m ³
gm/cm ³	1.0	6.242797×10	1.0	1.000×10^3
lb/ft ³	1.601846×10^{-2}	1.0	1.601846×10^{-2}	1.601846×10
kg/l	1.0	6.242797×10	1.0	1.000×10^3
kg/m ³	1.000×10^{-3}	6.242797×10^{-2}	1.0×10^{-3}	1.0

Table A-10
Land Measurement Conversion Multiplication Factors

	gm/cm ³	lb/ft ³	kg/l	kg/m ³
gm/cm ³	1.0	6.242797×10	1.0	1.000×10^3
lb/ft ³	1.601846×10^{-2}	1.0	1.601846×10^{-2}	1.601846×10
kg/l	1.0	6.242797×10	1.0	1.000×10^3
kg/m ³	1.000×10^{-3}	6.242797×10^{-2}	1.0×10^{-3}	1.0

1 League = 3 miles, 1 square mile = 640 acres, 1 township = 36 square miles, 1 section = 1 square mile, 1 rod = 16.5 feet.

Table A-11
Length Conversion Multiplication Factors

	Inches (in)	Feet (ft)	Yards (yd)	Miles (mi)	Centimeter (cm)	Meter (m)	Kilometer (km)
Inches (in)	1.0	8.333333×10^{-2}	2.777778×10^{-2}	1.578282×10^{-5}	2.540	2.540×10^{-2}	2.540×10^{-5}
Feet (ft)	12.0	1.0	3.333333×10^{-1}	1.893939×10^{-4}	30.480	3.048×10^{-1}	3.048×10^{-4}
Yards (yd)	36.0	3.0	1.0	5.681818×10^{-4}	91.44	9.144×10^{-1}	9.144×10^{-4}
Miles (mi)	6.336003×10^4	5.280×10^3	1.760×10^3	1.0	1.609344×10^5	1.609344×10^3	2.609344
Centimeter (cm)	3.937008×10^{-1}	3.28084×10^{-2}	1.093613×10^{-2}	6.213712×10^{-6}	1.0	1.000×10^{-2}	1.000×10^{-5}
Meter (m)	39.37008	3.28084	1.093613	6.213712×10^{-4}	100.0	1.0	1.000×10^{-3}
Kilometer (km)	39.37008×10^3	3.28084×10^3	1.093613×10^3	6.213712×10^{-1}	1.000×10^5	1.000×10^3	1.0

Table A-12
Area Conversion Multiplication Factors

	in²	ft²	mi²	cm²	m²	km²
Square inches (in ²)	1.0	6.944444×10^{-3}	2.490977×10^{-10}	6.451600	6.451600×10^{-4}	6.451600×10^{-10}
Square feet (ft ²)	1.440×10^2	1.0	3.587007×10^{-8}	9.290304×10^2	9.290304×10^{-2}	9.290304×10^{-8}
Square miles (mi ²)	4.014489×10^9	2.787840×10^7	1.0	2.589988×10^{10}	2.589988×10^6	2.589988
Square centimeters (cm ²)	1.550×10^{-1}	1.076391×10^{-3}	3.861022×10^{-11}	1.0	1.000×10^{-4}	1.000×10^{-10}
Square meters (m ²)	1.550×10^3	10.763910	3.861022×10^{-7}	1.000×10^4	1.0	1.000×10^{-6}
Square kilometers (km ²)	1.550×10^9	1.076391×10^7	3.861022×10^{-1}	1.000×10^{10}	1.000×10^6	1.0

1 Acre = 43,560 ft², 1 darcy = 1000 mD, 1 mD = 9.86×10^{-16} m² = 9.86×10^{-12} cm² = 1.127×10^{-3} (B/D)cP/ft²(psi/ft).

Table A-13
Liquid Volume Conversion Multiplication Factors

	gal	UK gal	bbl (oil)	ft ³	l	m ³
Gallons (US) (gal)	1.0	8.326739×10^{-1}	2.380952×10^{-2}	1.336805×10^{-1}	3.785412	3.785412×10^{-3}
Imperial gallons (UK gal)	1.200950	1.0	2.859406×10^{-2}	1.605437×10^{-1}	4.546092	4.546092×10^{-3}
Barrels (oil, 42 gal) (bbl)	42.0	3.497230×10	1.0	5.614583	1.589873×10^2	1.589873×10^{-1}
Cubic feet (ft ³)	7.48052	6.228833	1.781076×10^{-1}	1.0	2.831685×10	2.831685×10^{-2}
Liters (L)	2.641720×10^{-1}	2.199692×10^{-1}	6.289810×10^{-3}	3.531466×10^{-2}	1.0	1.000×10^{-3}
Cubic meters (m ³)	2.641720×10^2	2.199692×10^2	6.289810	3.531466×10	1.000×10^3	1.0

Table A-14
Pressure Conversion Multiplication Factors

	atm	bar	lbf/in²	kgf/cm²	inHg (32 °F)	mmHg (32 °F)	ftH₂O	Pa
atm (std)	1.0	1.013250	1.46960×10	1.033228	2.992133×10	7.600×10^2	3.389952×10	1.013250
bar	9.869233×10^{-1}	1.0	1.450377×10	1.019716	2.953006×10	7.500638×10^2	3.345623×10	1.000000
lbf/in ² (psi)	6.804573×10^{-2}	6.894757×10^{-2}	1.0	7.030695×10^{-2}	2.036026	5.171507×10	2.306730	6.894757
kgf/cm ²	9.678411×10^{-1}	9.806650×10^{-1}	1.422334×10	1.0	2.895909×10	7.355613×10^2	3.280935×10	9.806650
inHg (32 °F)	3.342097×10^{-2}	3.386380×10^{-2}	4.911529×10^{-1}	3.453147×10^{-2}	1.0	2.54×10^2	1.132955	3.386380
mmHg (32 °F)	1.315789×10^{-3}	1.333220×10^{-3}	1.933672×10^{-2}	1.359506×10^{-3}	3.93701×10^{-2}	1.0	4.460451×10^{-2}	1.333220
ft H ₂ O (39.2 °F)	2.949894×10^{-2}	2.988980×10^{-2}	4.335149×10^{-1}	3.047912×10^{-2}	8.826475×10^{-1}	2.241926×10	1.0	2.988980
Pa	9.869233×10^{-6}	1.000×10^{-5}	1.450377×10^{-4}	1.019716×10^{-5}	2.953006×10^{-4}	7.500638×10^{-3}	3.345623×10^{-4}	1.0

Table A-15
Conversion of Common Field Units to Metric (SI) Units (Base conditions:
Field 60 °F, 14.65 psia; Metric (SI) 15 °C, 101.325 kPa)

Field Unit	Multiplication Factor	Metric (SI) unit	Symbol
Acre	4.046856E+03	Square meter	m ²
Acre	4.046856E-01	Hectare	ha
Acre-foot	1.233482E+03	Cubic meter	m ³
Atmosphere	1.01325E+02	Kilopascal	kPa
Barrel (35 imp. gal.)	1.589873E-01	Cubic meter	m ³
Btu per standard cubic foot (60 °F, 14.65 psia)	8.799136E-01	Kilojoule per mole	kJ/mol
Centipoise	1.0E+00	Millipascal	mPa*s
Cubic foot	2.831685E-01	Cubic meter	m ³
Cubic foot gas per gallon (60 °F, 14.65 psia)	7.494773E+00	Mole per cubic meter	mol/m ³
Darcy	9.869233E-01	Square micrometer	μm ²
Degree Fahrenheit	(°F - 32)/9E+00	Degree Celsius	°C
Degree Rankine	5/9E+00	Kelvin	K
Gallon (Cdn)	4.54609E-03	Cubic meter	m ³
Gallon (US)	3.785412E-03	Cubic meter	m ³
Gas constant	8.31432E+00	Joule per mole kelvin	J/(mol*K)
Mcf (thousand cubic foot) (60 °F, 14.65 psia)	1.191574E+00 2.826231E+01	Kilomole cubic meter (API)	kmol m ³ API
Millidarcy	9.869233E-04	Square micrometer	μm ²
MMcf (million cubic foot) (60 °F, 14.65 psia)	1.191574E+00 2.826231E+01	Megamole cubic meter (API)	mmol m ³ API
Pound-force per square inch (psi)	6.894757E+00	Kilopascal	kPa
Pound-mass	4.535924E-01	Kilogram	kg
Psi per foot	2.262059E+01	Kilopascal per meter	KPa/m
Section (540 acres)	2.589988E+06	Square meter	m ²
Section (640 acres)	2.589988E+02	Hectare	ha
Standard cubic foot (60 °F, 14.65 psia - ideal gas)	1.191574E+00 2.826231E-02	Mole cubic meter (API)	mol m ³ API
Tcf (trillion cubic foot) (60 °F, 14.65 psia)	1.191574E+00 2.826231E-02	Teramole cubic meter (API)	Tmol m ³ API
Ton (US short - 2000 lb)	9.071847E-01	Tonne	t
Ton (UK long - 2240 lb)	1.016047E+00	Tonne	t

Appendix B

Correlation Tables and Dimensionless Functions

Table B-1

MBH Dimensionless Pressure Functions for Various Closed Shaped Reservoirs (after Earlougher et al., 1968)¹

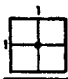
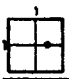
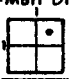
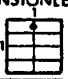
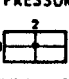
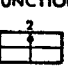




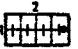

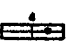



DIMENSIONLESS TIME t_{DA}	F = MBH DIMENSIONLESS PRESSURE FUNCTION							
								
0.0010	0.0126	0.0126	0.0126	0.0126	0.0126	0.0126	0.0126	0.0126
0.0015	0.0180	0.0180	0.0180	0.0180	0.0180	0.0180	0.0180	0.0180
0.0020	0.0231	0.0231	0.0231	0.0231	0.0231	0.0231	0.0231	0.0231
0.0025	0.0314	0.0314	0.0314	0.0314	0.0314	0.0314	0.0314	0.0314
0.0030	0.0377	0.0377	0.0377	0.0377	0.0377	0.0377	0.0377	0.0377
0.0040	0.0503	0.0503	0.0503	0.0503	0.0503	0.0503	0.0503	0.0503
0.0050	0.0620	0.0620	0.0620	0.0620	0.0620	0.0620	0.0620	0.0620
0.0060	0.0734	0.0734	0.0734	0.0734	0.0734	0.0734	0.0734	0.0734
0.0070	0.0800	0.0800	0.0800	0.0800	0.0800	0.0800	0.0800	0.0800
0.0080	0.1005	0.1005	0.1005	0.1005	0.1005	0.1005	0.1005	0.1005
0.0090	0.1131	0.1130	0.1128	0.1126	0.1131	0.1131	0.1131	0.1131
0.0100	0.1257	0.1234	0.1231	0.1231	0.1257	0.1257	0.1257	0.1257
0.0150	0.1805	0.1834	0.1823	-0.0162	0.1804	0.1804	0.1804	0.1804
0.0200	0.2513	0.2402	0.2387	-0.0700	0.2500	0.2500	0.2500	0.2500
0.0250	0.3161	0.2892	0.2830	-0.1181	0.3119	0.3119	0.3119	0.3119
0.0300	0.3769	0.3323	0.3044	-0.1584	0.3708	0.3708	0.3708	0.3708
0.0400	0.5036	0.4108	0.3087	-0.2166	0.4804	0.4804	0.4804	0.4804
0.0500	0.6237	0.4791	0.3099	-0.2532	0.6607	0.6607	0.6607	0.6607
0.0600	0.7415	0.5413	0.3002	-0.2694	0.7471	0.7471	0.7471	0.7471
0.0700	0.8537	0.5991	0.2826	-0.2766	0.8217	0.8217	0.8217	0.8217
0.0800	0.9597	0.6531	0.2700	-0.2765	0.8917	0.8917	0.8917	0.8917
0.0900	1.0592	0.7038	0.2553	-0.2716	0.9581	0.9581	0.9581	0.9581
0.1000	1.1524	0.7514	0.2427	-0.2633	1.0204	1.0204	1.0204	1.0204
0.1500	1.5364	0.9503	0.2226	-0.1931	1.2524	1.2524	1.2524	1.2524
0.2000	1.8312	1.1314	0.2037	-0.1027	1.4987	1.4987	1.4987	1.4987
0.2500	2.0639	1.2854	0.1812	0.0029	1.7064	1.7064	1.7064	1.7064
0.3000	2.2262	1.4257	0.4365	0.1129	1.8830	1.8830	1.8830	1.8830
0.4000	2.5139	1.6720	0.4440	0.3300	2.1678	2.1678	2.1678	2.1678
0.5000	2.7370	1.8797	0.8321	0.5368	2.3905	2.3905	2.3905	2.3905
0.6000	2.9193	2.0563	1.0028	0.6994	2.5728	2.5728	2.5728	2.5728
0.7000	3.0735	2.2003	1.1527	0.8499	2.7269	2.7269	2.7269	2.7269
0.8000	3.2070	2.3411	1.2847	0.9821	2.8605	2.8605	2.8605	2.8605
0.9000	3.3249	2.4586	1.4019	1.0994	3.0026	3.0026	3.0026	3.0026
1.0000	3.4302	2.5638	1.5070	1.2045	3.1782	3.1782	3.1782	3.1782
2.0000	4.1234	3.2549	2.2000	1.0776	3.7768	3.7768	3.7768	3.7768
4.0000	4.8164	3.9501	2.9933	2.5000	4.4701	4.4701	4.4701	4.4701
8.0000	5.5099	4.6435	3.5867	3.2842	5.1633	5.1633	5.1633	5.1633
10.0000	5.7391	4.8467	3.8096	3.5073	5.3965	5.3965	5.3965	5.3965

Table B-1 (continued)

DIMENSIONLESS TIME t_{DA}	F = MBH DIMENSIONLESS PRESSURE FUNCTION							
								
0.0010	0.0125	0.0126	0.0125	0.0126	0.0126	0.0126	0.0126	0.0126
0.0015	0.0179	0.0180	0.0179	0.0180	0.0180	0.0180	0.0180	0.0180
0.0020	0.0209	0.0211	0.0209	0.0211	0.0211	0.0211	0.0211	0.0211
0.0025	0.0203	0.0204	0.0203	0.0204	0.0204	0.0204	0.0204	0.0204
0.0030	0.0160	0.0161	0.0160	0.0161	0.0161	0.0161	0.0161	0.0161
0.0040	-0.0019	0.0502	-0.0027	0.0503	0.0460	0.0503	0.0460	0.0503
0.0050	-0.0284	0.0626	-0.0293	0.0628	0.0517	0.0628	0.0517	0.0628
0.0060	-0.0596	0.0745	-0.0612	0.0754	0.0537	0.0754	0.0537	0.0753
0.0070	-0.0932	0.0858	-0.0951	0.0879	0.0534	0.0879	0.0524	0.0878
0.0080	-0.1277	0.0962	-0.1298	0.1004	0.0483	0.1004	0.0483	0.1000
0.0090	-0.1620	0.1058	-0.1644	0.1129	0.0422	0.1129	0.0422	0.1119
0.0100	-0.1957	0.1144	-0.1983	0.1251	0.0345	0.1251	0.0345	0.1234
0.0150	-0.3468	0.1445	-0.3502	0.1823	-0.0162	0.1823	-0.0162	0.1713
0.0200	-0.4670	0.1589	-0.4718	0.2291	-0.0701	0.2291	-0.0701	0.2015
0.0250	-0.5615	0.1641	-0.5695	0.2643	-0.1186	0.2643	-0.1187	0.2163
0.0300	-0.6357	0.1633	-0.6507	0.2897	-0.1600	0.2897	-0.1600	0.2200
0.0400	-0.7795	0.1492	-0.7839	0.3197	-0.2231	0.3194	-0.2235	0.2075
0.0500	-0.8912	0.1274	-0.8945	0.3332	-0.2667	0.3315	-0.2682	0.1820
0.0600	-0.9399	0.0862	-0.9489	0.3385	-0.2957	0.3295	-0.3013	0.1516
0.0700	-0.8457	0.0437	-1.0949	0.3399	-0.3158	0.3290	-0.3278	0.1203
0.0800	-0.9422	-0.0028	-1.1859	0.3401	-0.3291	0.3199	-0.3510	0.0899
0.0900	-0.8272	-0.0512	-1.2723	0.3403	-0.3375	0.3072	-0.3727	0.0613
0.1000	-0.8038	-0.1004	-1.3542	0.3412	-0.3421	0.2915	-0.3942	0.0351
0.1500	-0.6223	-0.3522	-1.7021	0.3643	-0.3257	0.1826	-0.5128	-0.0580
0.2000	-0.4138	-0.5189	-1.9613	0.4269	-0.2661	0.0468	-0.6499	-0.0935
0.2500	-0.2194	-0.6580	-2.1508	0.5130	-0.1811	-0.0959	-0.7928	-0.0835
0.3000	-0.0479	-0.7555	-2.2854	0.6102	-0.0829	-0.2364	-0.9312	-0.0477
0.4000	0.2343	-0.8547	-2.4344	0.8152	0.1220	-0.4789	-1.1758	0.0723
0.5000	0.6567	-0.8671	-2.4768	1.0075	0.3143	-0.6712	-1.3681	0.2266
0.6000	0.6889	-0.8284	-2.4564	1.1782	0.6352	-0.8134	-1.5103	0.3753
0.7000	0.7931	-0.7630	-2.4011	1.3282	0.6331	-0.9129	-1.6098	0.5143
0.8000	0.9267	-0.6830	-2.3278	1.4682	0.7670	-0.9775	-1.6744	0.6409
0.9000	1.0444	-0.5969	-2.2468	1.5774	0.8843	-1.0143	-1.7114	0.7355
1.0000	1.1497	-0.5115	-2.1640	1.6825	0.9894	-1.0301	-1.7270	0.8395
2.0000	1.8439	0.1507	-1.3056	2.3755	1.6824	-0.7325	-1.4294	1.3516
4.0000	2.5363	0.8436	-0.8129	3.0688	2.3757	-0.0756	-0.7725	2.2448
6.0000	3.2295	1.5370	-0.8195	3.7623	3.0691	0.6173	-0.0796	2.9301
10.0000	3.4527	1.7601	0.1036	3.9834	3.2922	0.8406	0.1438	3.1615

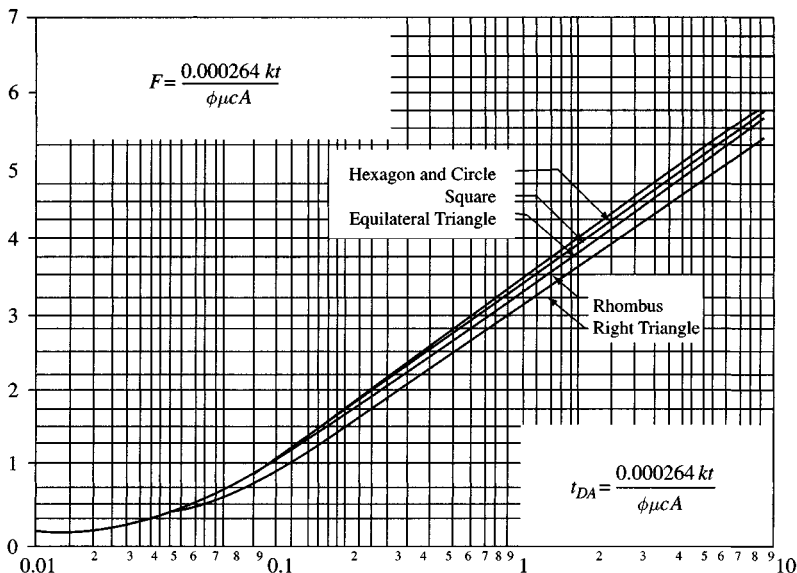


Figure B-1. MBH curves for a well at the center of a regular shaped drainage area (after Matthews et al.).³

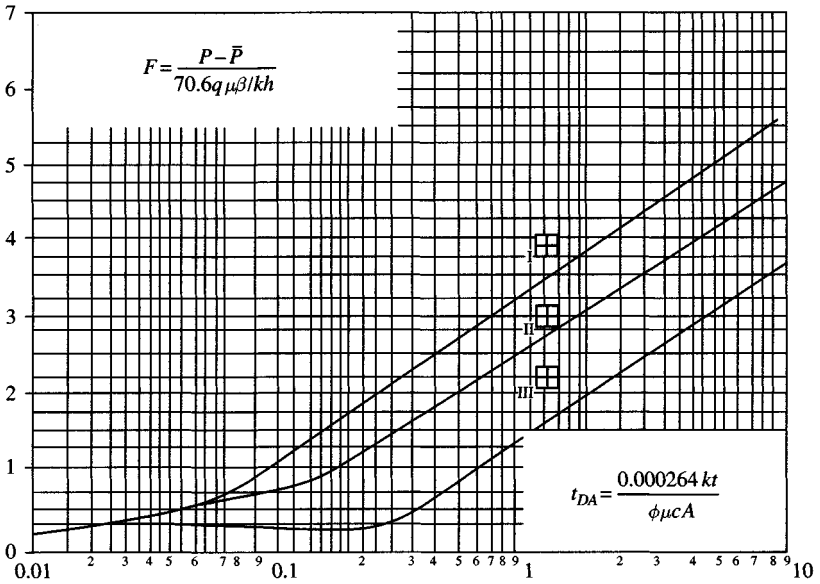


Figure B-2. MBH curves for a well situated within a square (after Matthews et al.).³

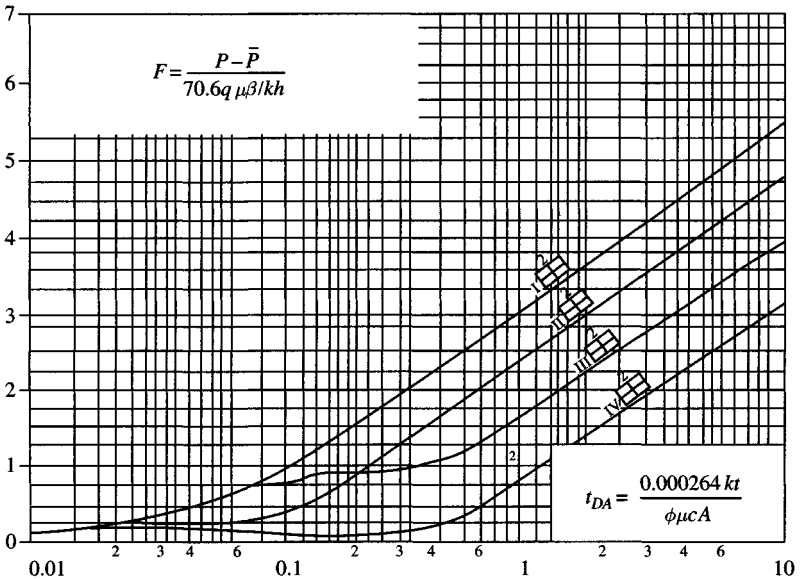


Figure B-3. MBH curves for a well situated within a 2:1 rectangle (after Matthews et al.).³

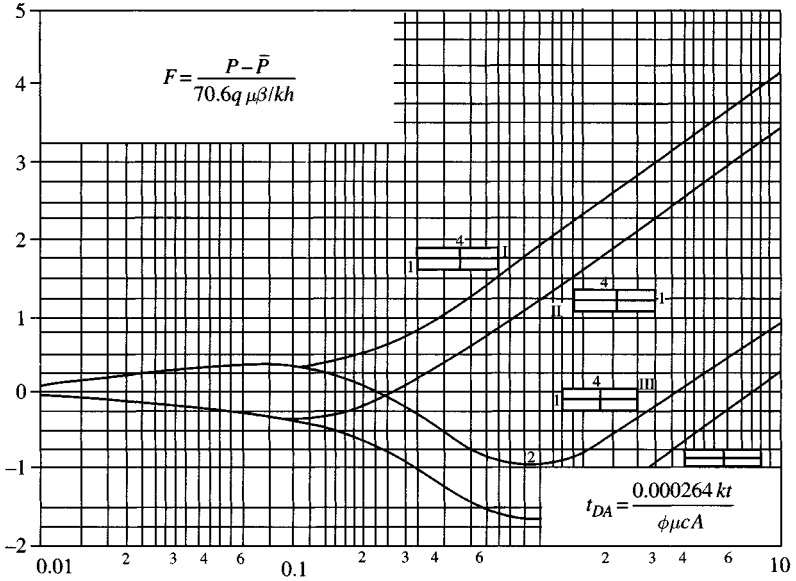


Figure B-4. MBH curves for a well situated within a 4:1 rectangle (after Matthews et al.).³

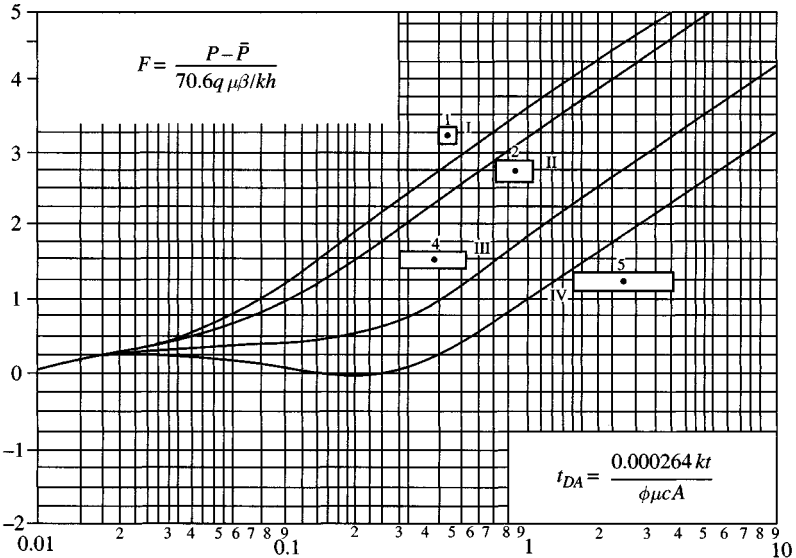


Figure B-5. MBH curves for a well situated in various rectangular geometries (after Matthews et al.).³

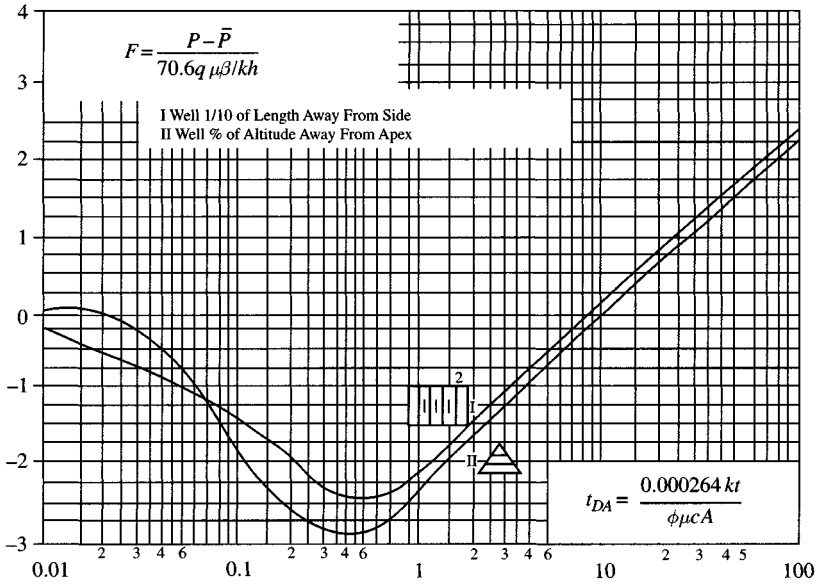


Figure B-6. MBH curves for a well situated within a square and in a 2:1 rectangle (after Matthews et al.).³

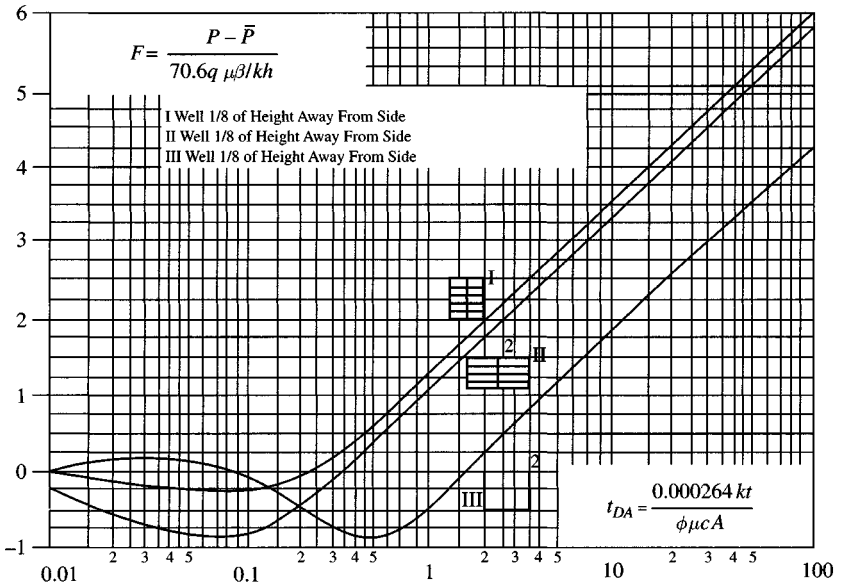


Figure B-7. MBH curves for a well situated in a 2:1 rectangle and in an equilateral triangle (after Matthews et al.).³

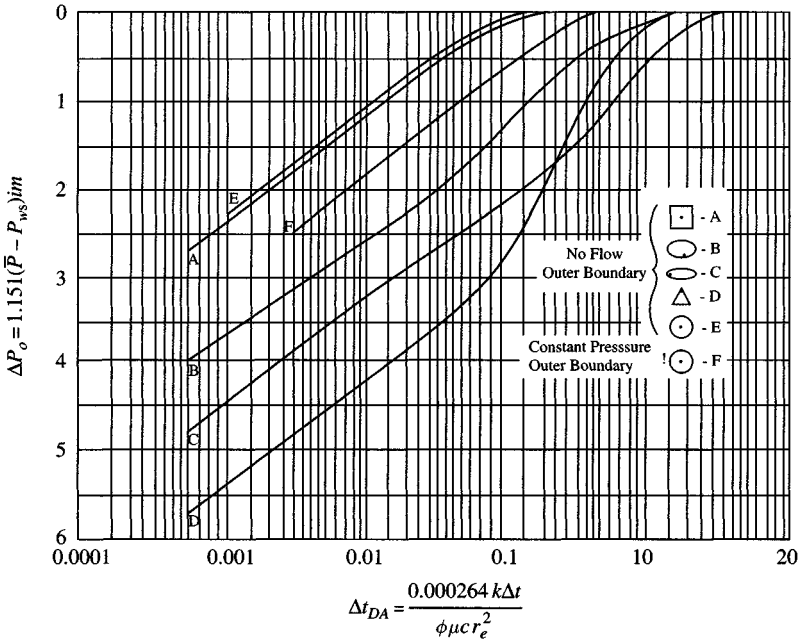


Figure B-8. MBH dimensionless pressures ABCDEF (after Pitzer, S. C. (1964)⁴).

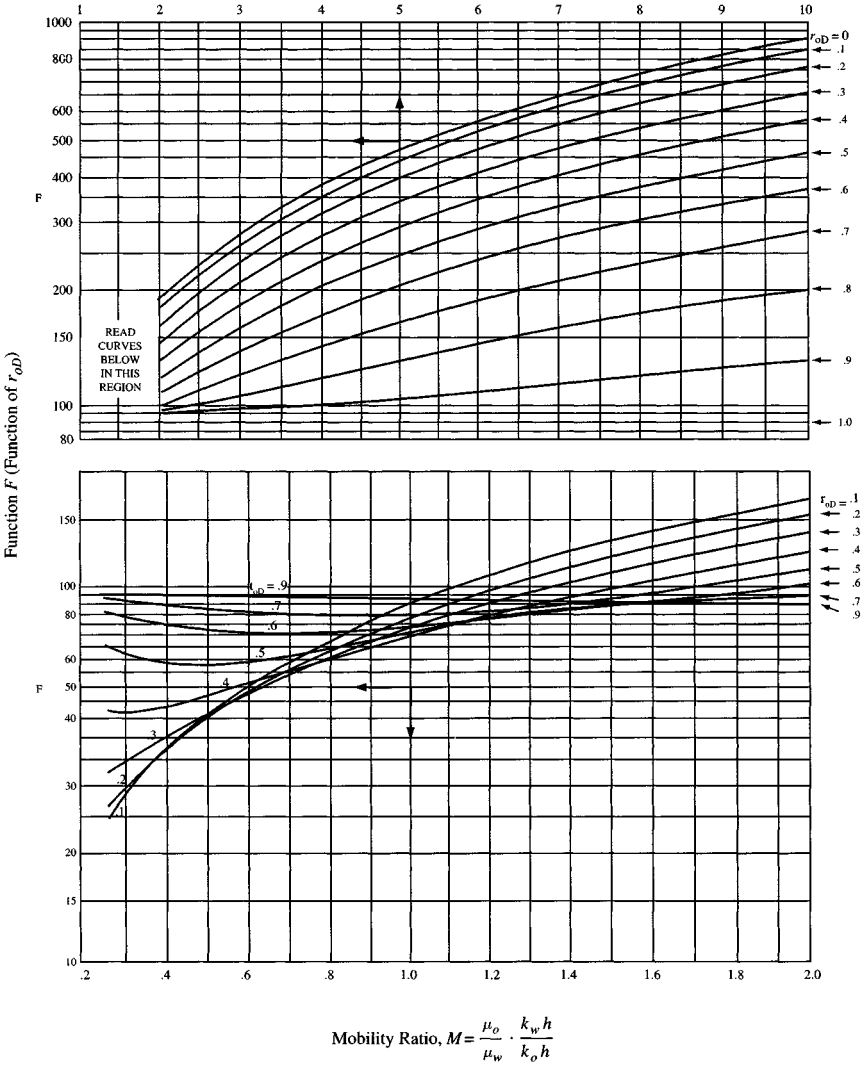


Figure B-9. Values of function F versus mobility ratio with various values of parameters.⁵

$$r_{oD} = \frac{1}{\sqrt{(V_o/V_w) + 1}} \text{ and } \gamma = \frac{c_o}{c_w} = 4$$

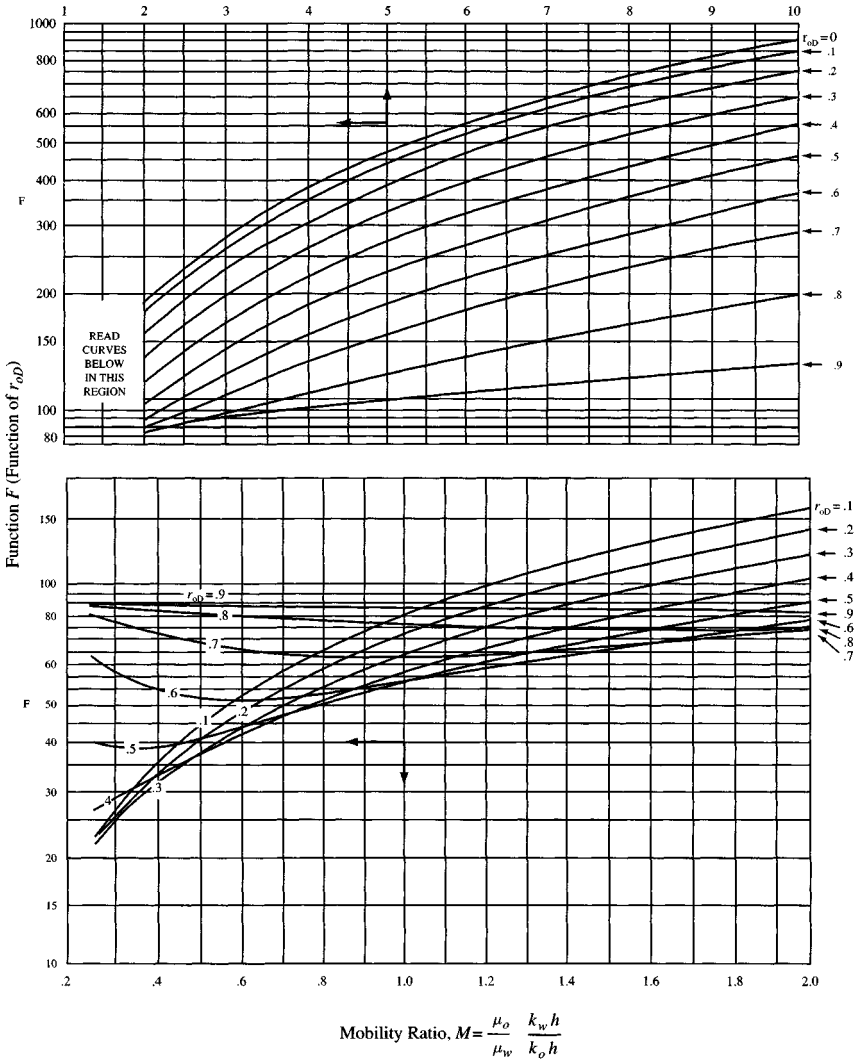


Figure B-10. Values of function F versus mobility ratio with various values of parameters.⁵

$$r_{oD} = \frac{1}{\sqrt{(V_o/V_w) + 1}} \text{ and } \gamma = \frac{c_o}{c_w} = 2$$

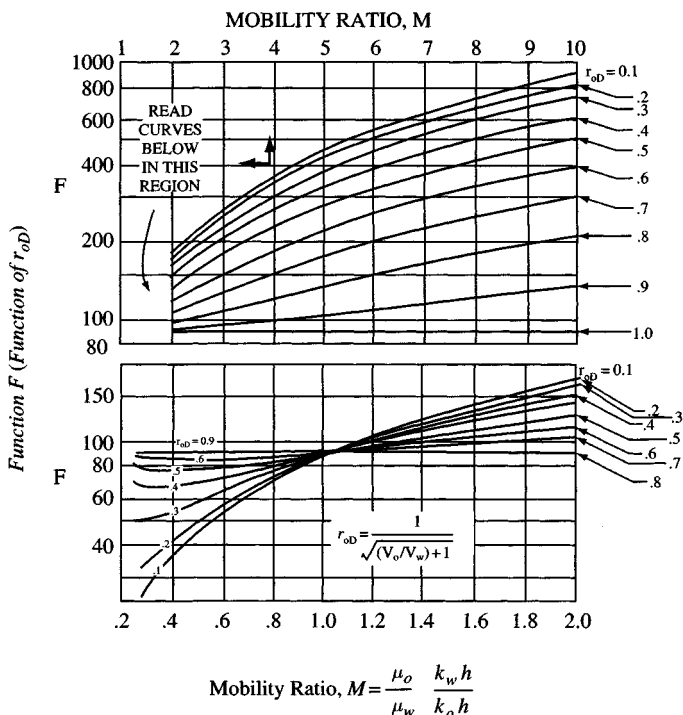


Figure B-11. Values of function F versus mobility ratio with various values of parameters.⁵

References and Additional Reading

1. Earlougher, R. C., Jr., Ramey, H. J., Jr., Miller, F. G., and Mueller, T. D., "Pressure Distributions in Rectangular Reservoirs," *J. Petroleum Technol.* (1968) 20, 199–208.
2. Dietz, D. N., "Determination of Average Reservoir Pressure From Build-up Surveys," *Trans. AIME* (1965) 234, 935–959.
3. Matthews, C. S., Brons, F., and Hazebroek, P. "A Method for Determination of Average Pressure in a Bounded Reservoir," *Trans. AIME* (1954) 209, 182–189.
4. Pitzer, S. C., "Evaluation of Acid Treatments from Pressure Buildup Analysis," *Trans. AIME* (1964) 216, 38–43.
5. Hazelbroek, P., Rainbow, H., and Matthews, C. S., "Pressure Fall-Off in Water Injection Wells," *Trans. AIME* (1958) 213, 250–260.

Appendix C

Pressure Drop through Vertical, Inclined, and Horizontal Oil Wells

Pressure should be recorded continuously during a transient test. Best results are obtained when the bottom-hole pressure is measured, although surface pressures often can be converted to bottom-hole values if adequate information is available about the wellbore system. It is usually beneficial to record bottom-hole, tubing-head, and casing-head pressures during a well test. This combination of data can provide information about wellbore effects, such as storage, and leaking packers or tubing. Such surface pressure data may be valuable in verifying correct operation of the down-hole pressure gauge. This appendix will describe two methods as shown below (see Figure C-1).

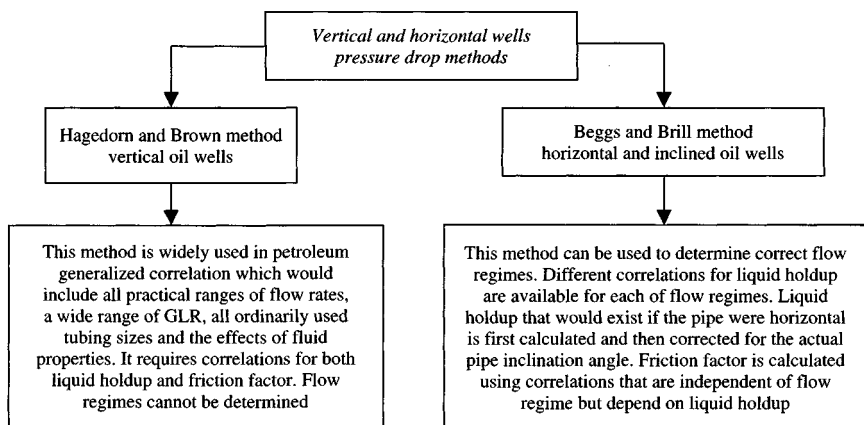


Figure C-1. Pressure drop calculation methods for vertical, inclined, and horizontal oil wells.

C.1 Hagedorn and Brown Method¹

This method is widely used and most accepted in the petroleum industry. The procedure for this method is

$$\Delta h = \frac{144(\Delta p) - \rho_m - \left[\frac{(V_{m1}^{22} - V_{m2}^2)}{2g_c} \right]}{\frac{[\bar{\rho}_m + fq_m^2]}{(2.9652 \times 10^{11} d_t^5 \bar{\rho}_m)}} \quad (\text{C-1})$$

A step-by-step procedure for using Eq. C-1 and calculating a vertical pressure traverse by this method is given below.

Pressure Traverse with Fixed Pressure Increment

1. Calculate average segment pressure and temperature.
2. Determine the total mass of oil, water, and gas associated with 1 barrel of stock tank liquid:

$$m_t = 350\gamma_o \left(\frac{1}{1 + \text{WOR}} + 350\gamma_w \right) \left(\frac{\text{WOR}}{1 + \text{WOR}} \right) + 0.0764\text{GLR}\gamma_g \quad (\text{C-2})$$

3. Find the flow rate at average segment point:

$$q_m = q_L m_t \quad (\text{lbm/day}) \quad (\text{C-3})$$

$$q_L = \text{total flow rate} \quad (\text{stb/day})$$

4. Determine physical properties R_s , β_o , \bar{Z} , $\bar{\mu}_o$, $\bar{\mu}_w$, σ_o , and σ_w from laboratory information or empirical correlations at average segment pressure and temperature.
5. Calculate the density of liquid phase:

$$\rho_L = \left[\frac{62.4\gamma_o + R_s\gamma_g/5.615}{\beta_o} \right] \left(\frac{1}{\text{WOR}} \right) + \left[62.4\gamma_w \left(\frac{\text{WOR}}{1 + \text{WOR}} \right) \right] \quad (\text{C-4})$$

6. Calculate the average gas density:

$$\bar{\rho}_g = 0.0764\gamma_g \left[\left(\frac{\bar{p}}{14.7} \right) \left(\frac{520}{T + 460} \right) \left(\frac{1}{z} \right) \right] \quad (\text{C-5})$$

7. Estimate viscosity of the liquid mixture:

$$\mu_L = \mu_o \left(\frac{1}{1 + \text{WOR}} \right) + \mu_w \left(\frac{\text{WOR}}{1 + \text{WOR}} \right) \quad (\text{C-6})$$

8. Estimate surface tension of liquid mixture:

$$\sigma_L = \sigma_o \left(\frac{1}{1 + \text{WOR}} \right) + \sigma_w \left(\frac{\text{WOR}}{1 + \text{WOR}} \right) \quad (\text{C-7})$$

9. Calculate liquid viscosity number:

$$N_L = 0.15726 \mu_L \left(\frac{1}{\sigma_L \sigma_L^3} \right)^{0.25} \quad (\text{C-8})$$

10. Find CN_L from Figure C-2.

11. Calculate the superficial liquid velocity:

$$V_{SL} = \frac{5.615 q_L}{86,400 A_t} \left[\beta_o \left(\frac{1}{1 + \text{WOR}} \right) + \beta_w \left(\frac{\text{WOR}}{1 + \text{WOR}} \right) \right] \quad (\text{C-9})$$

where A_t is cross-sectional area of tubing (ft^2).

12. Calculate the liquid velocity number:

$$N_{LV} = 1.938 V_{SL} \left(\frac{\rho_L}{\sigma_L} \right)^{0.25} \quad (\text{C-10})$$

13. Determine the superficial gas velocity V_{SG} (ft/s):

$$V_{SG} = \frac{q_L \left[GLR - R_s \left(\frac{1}{1 + \text{WOR}} \right) \right]}{86,400 A_t} \left(\frac{14.6}{\bar{p}} \right) \left(\frac{\bar{T} + 460}{520} \right)^z \quad (\text{C-11})$$

14. Find the gas velocity number:

$$N_{GV} = 1.938 V_{GV} \left(\frac{\rho_L}{\sigma_L} \right)^{0.25} \quad (\text{C-12})$$

15. Calculate the following parameters:

$$AA = 1.071 - \frac{0.2218 (V_{SL} + V_{SG})^2}{d_t} \quad (\text{C-13})$$

where d_t is the inside diameter of tubing (ft). If $AA \leq 0.13$, then use the calculated value, if it is less than 0.13, then use $AA = 0.13$.

$$BB = \frac{V_{SG}}{V_{SL} + V_{SG}} \quad (\text{C-14})$$

16. If $(BB - AA) \geq 0$, continue with the method. If $(BB - AA) < 0$, then use Griffith correlation for bubble flow (use Orkiszewski method).

17. Determine the pipe diameter number:

$$N_D = 120.872d_t \sqrt{\frac{\rho_L}{\sigma_L}} \quad (\text{C-15})$$

18. Calculate liquid holdup function:

$$\phi_{HL} = \left(\frac{N_{LV}}{N_{GV}^{0.575}} \right) \left(\frac{\bar{p}}{14.7} \right)^{0.10} \left(\frac{CN_L}{N_D} \right) \quad (\text{C-16})$$

19. Find H_L/ψ from Figure C-3.

20. Estimate the secondary correction factor:

$$\phi H_L = \frac{N_{GV} N_L^{0.380}}{N_D^{2.14}} \quad (\text{C-17})$$

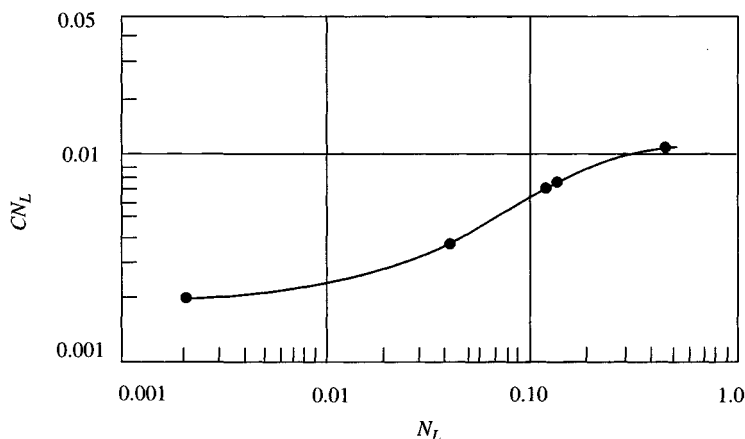


Figure C-2. Correlation for viscosity number coefficient C (© SPE, AIME, 1965).

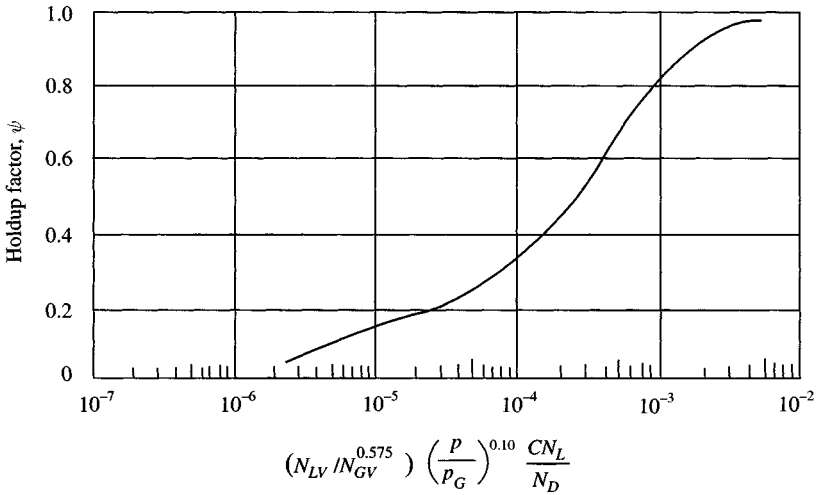


Figure C-3. Holdup factor correlation (© SPE, AIME, 1965).

21. Obtain ψ from Figure C-3; for low viscosity, $\psi = 1.0$.
22. Estimate two-phase Reynolds number:

$$(N_{RE})_{two-phase} = \frac{2.3 \times 10^{-2}}{d_t(\mu_L)^{HL}(\mu_g)^{1-HL}} \quad (C-18)$$

23. Find the friction factor from Figure C-4.
24. Calculate the average two-phase density of the mixture at average pressure by two methods and use the largest:

$$\bar{\rho}_m = \bar{\rho}_L H_L + \bar{\rho}_g (1 - H_L) \quad (C-19)$$

and map correlations

$$\rho_m = \frac{350\gamma_o + 0.0764\gamma_g R_s + 350\gamma_w(\text{WOR})}{5.615\beta_o + 5.615(\text{WOR}) + (V_{fg})(14.7/\bar{p}) + ((\bar{T} + 460)/520)\bar{Z}} \quad (C-20)$$

where V_{fg} = volume of free gas = $GOR - R_s$.

25. Calculate the two-phase mixture velocity at both p_1 and p_2 :

$$V_{m1} = V_{SL1} + V_{SG1} \quad (C-21)$$

$$V_{m2} = V_{SL2} + V_{SG2} \quad (C-22)$$

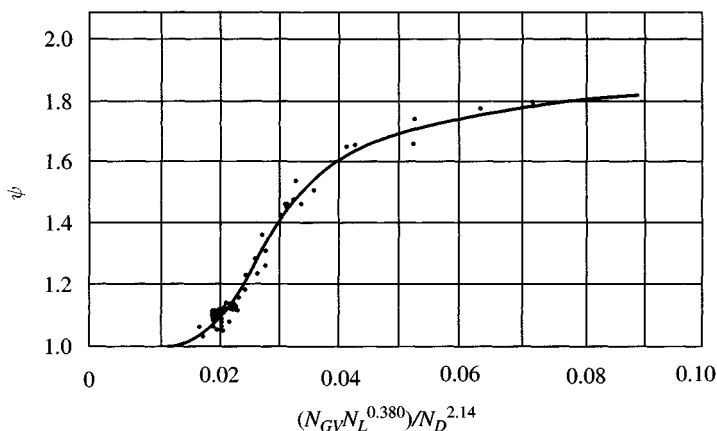


Figure C-4. Holdup factor correlation (© SPE, AIME, 1965).

26. Estimate the value for

$$\Delta(V_m^2) = V_{m1}^2 - V_{m2}^2 \quad (\text{C-23})$$

27. Calculate Δh (ft) corresponding to $\Delta p = p_1 - p_2$:

$$\Delta h = \frac{144\Delta p - \rho_m \Delta \left(\frac{V_m^2}{2g_c} \right)}{\frac{\bar{\rho}_m + f q_m^2}{2.9652 \times 10^{11} d_i^5 \bar{\rho}_m}} \quad (\text{C-24})$$

Find friction factor f from Figure C-4.

28. Repeat the pressure starting with p_2 and assume another point until reading the surface or the total depth, depending on whether the bottom or the top. Since the pressure traverse calculations are iterative, and the fluid properties and pressure gradient calculations are tedious, it is most convenient to write computer program.
29. For pressure traverse calculations, typical pressures developed by this method are in Table C-1 and Figure C-4.

Table C-1
Computed Flowing Pressure – Traverse – Hagedorn and Brown
Correlation

Pressure (psig)	Temperature (°F)	Depth (ft) at <i>GLR</i> (scf/bbl)						
		500	750	1000	1250	1500	2000	2500
500	135	0	0	0	0	0	0	0
800	135	1174	1283	1332	1363	1376	1384	1388
1000	135	1883	2049	2159	2222	2259	2270	2234
1200	135	2546	2777	2955	3037	3103	3155	3136
1400	135	3173	3466	3665	3817	3907	4007	4017
1600	135	3772	4121	4366	4582	4676	4827	4869
1800	135	4347	4749	5036	5246	5423	5605	5690
2000	135	4904	5355	5681	5924	6165	6357	6480
2200	135	5445	5942	6305	6579	6925	7084	7240
2400	135	5973	6513	6910	7213	7448	7794	7975
2600	135	6491	7070	7499	7830	8089	8497	8686
2800	135	6999	7615	8075	8432	8713	9204	9380
3000	135	7499	8151	8640	9021	9323	9926	10041
3500	135	8722	9456	10010	10447	10798	11316	11747

Example C-1 *Calculating the Flowing Bottom-Hole Pressure Using Hagedorn and Brown Method*

Input Data

Tubing size	2.000 in. ID
Producing rate	1000 bbl/day
Water cut	60%
Oil <i>API</i> gravity	22° <i>API</i>
Water specific gravity	1.074
Gas specific gravity	0.65
Wellhead temperature	120 °F
Bottom-hole temperature	150 °F
Tubing inclination angle	90°

Solution

Matching Parameters

Modification factor (roughness) to match field data	1
Modification factor (oil <i>API</i>) to match field data	1
Modification factor (<i>GOR</i>) to match field data	1.0025
Solution gas-oil ratio adjustment factor	1.0025
Oil viscosity adjustment factor	1.4167

(continued)

z-factor adjustment factor	1
Gas viscosity adjustment factor	1
Water <i>FVF</i> adjustment factor	1.0567
Water viscosity adjustment factor	1.048
Water surface tension adjustment factor	1.0526
Oil surface tension adjustment factor	0.8903

C.2 Beggs and Brill Method²

Procedure for Segmenting by Pressure Increments

Step 1: Starting with the known pressure, p_1 , at location L_1 , choose a length increment, ΔL , at least $\leq 10\%$ of total L .

Step 2: Estimate the incremental pressure change, Δp .

Step 3: Calculate incremental pressure and the average incremental temperature.

Step 4: Using map or empirical correlations, determine the necessary PVT properties at conditions of average pressure and temperature.

Step 5: Estimate the incremental pressure gradient, $\Delta p/\Delta L$, using tubing or pipe inclination adjustments.

Step 6: Determine the total incremental pressure change corresponding to the chosen length.

Step 7: Compare the estimated and calculated values of Δp found. If they are not within a close tolerance, use the calculated incremental pressure, Δp , for iteration of step 2 through step 7. Repeat steps 3 through 7 until the estimated and calculated values are within tolerance.

Step 8: Continue iteration until $L_1 + \sum \Delta L = L$ (total). At this point $p_1 + \sum \Delta p = p$ (total).

Figure C-5 shows computer flow diagram. Output results are presented in Table C-2.

Example C-2 *Calculating the Flowing Bottom-Hole Pressure Using Beggs and Brill Method*

Input Data

Base pressure	14.70 psia
Base temperature	60 °F
Tubing size	1.995 in. ID
Producing rate	1000 bbl/day
Solution gas-oil ratio	450 scf/stb
Water cut	60%
Oil <i>API</i> gravity	22° <i>API</i>
Water specific gravity	1.070

(continued)

Gas specific gravity	0.65
Wellhead pressure	500 psig
Wellhead temperature	120 °F
Bottom-hole temperature	152 °F
Gas-liquid ratio	500 scf/stb
Absolute roughness	0.00015

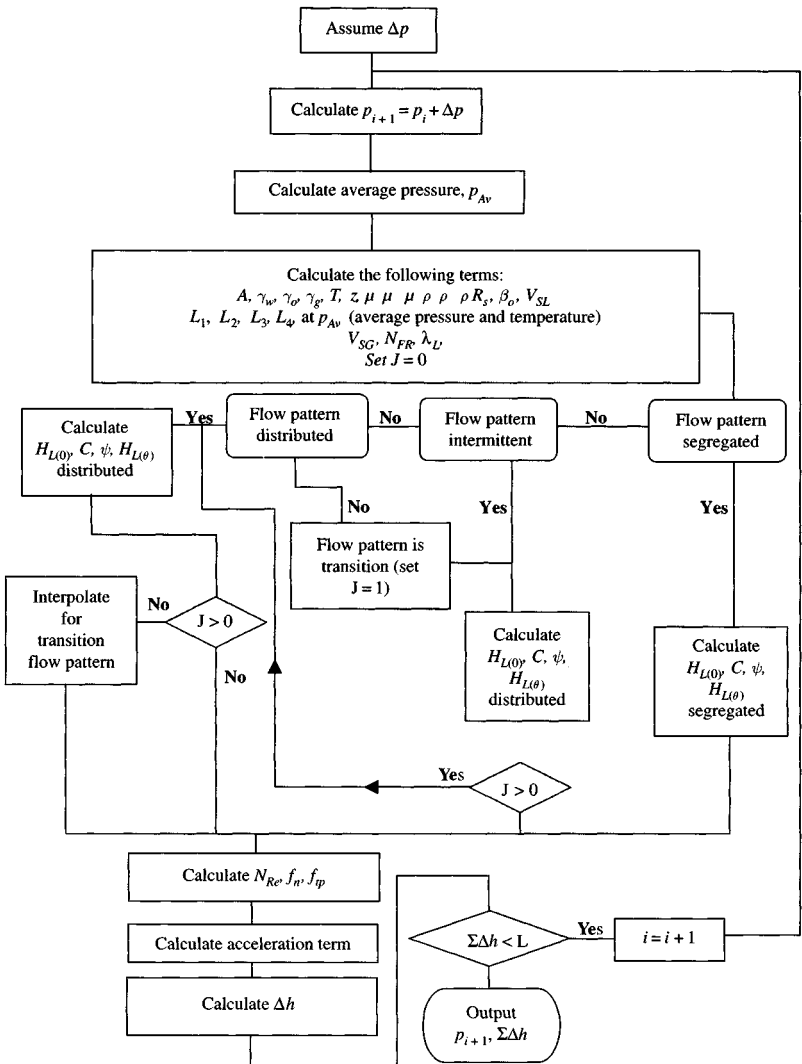


Figure C-5. Computer flow diagram for the Beggs and Brill method.

Table C-2
Computed Flowing Pressure – Traverse – Beggs and Brill Correlation

Assumed pressure (psig)	True depth (ft)	← Bottom hole pressures (psig) at inclination angles (°) →						
		0	10	20	30	40	50	60
500	500	610	567	582	573	562	549	535
800	1000	723	671	660	642	629	549	589
1000	2000	968	835	812	777	732	595	633
1250	3000	1236	1000	965	910	842	683	694
1500	4000	1532	1170	965	1043	950	768	753
2000	5000	1849	1345	1120	1119	1059	850	809
2200	6000	2181	1926	1280	1180	1059	932	865
2500	7000	2527	1714	1444	1533	1169	1013	920
2700	7500	2706	1810	1614	1533	1280	1135	940

Solution

Matching Parameters

Modification factor (roughness) to match field data	1
Modification factor (oil <i>API</i>) to match field data	1
Modification factor (<i>GOR</i>) to match field data	1.0025
Solution gas–oil ratio adjustment factor	1.000
Oil viscosity adjustment factor	7.552
<i>z</i> -factor adjustment factor	1
Gas viscosity adjustment factor	1
Water <i>FVF</i> adjustment factor	1
Water viscosity adjustment factor	1
Water surface tension adjustment factor	1
Oil surface tension adjustment factor	1

Figure C-6 shows effects of inclination, and Figure C-7 shows effects of *GLR*.

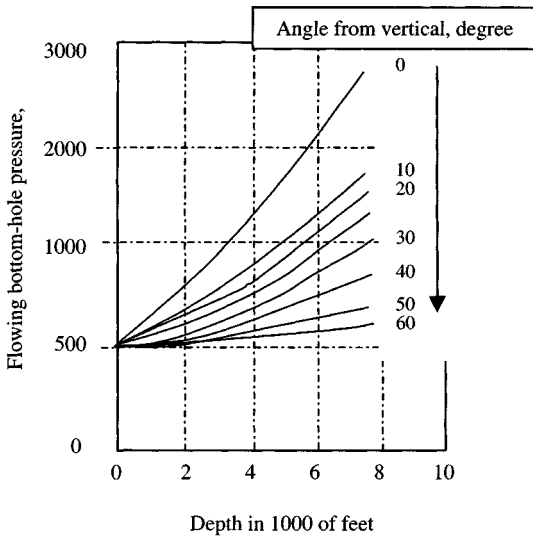


Figure C-6. Flowing pressure gradients showing effect of inclination – Hagedorn and Brown Method.

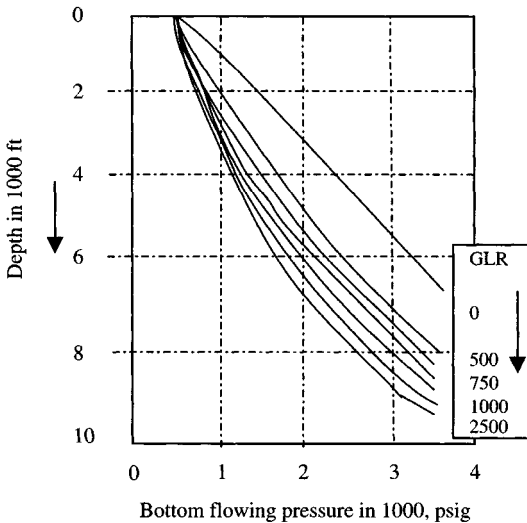


Figure C-7. Flowing pressure gradients showing effect of *GLR* – Beggs and Brill method.

References and Additional Reading

1. Hagedorn, A. R., and Brown, K. E., "Experimental Study of Pressure Gradients Occurring During Continuous Two-Phase Flow in Small Diameter Vertical Conduits," *J. Pet. Technol.* (April 1965) 475.
2. Beggs, H. D., and Brill, J. P., "A Study of Two-Phase Flow in Inclined Pipes," *J. Pet. Technol.* (May 1973) 1972.

Appendix D

Oil and Water PVT Properties and Correlation Equations

This appendix presents concepts and applications of fluid and rock properties usually required for solving reservoir engineering and transient well test analysis problems. The engineering equations and correlations presented in this appendix represent technical papers well known to the petroleum engineers. For most of these properties, laboratory analysis provides the most accurate answer; however, in many cases, laboratory results are not available, and the test analyst must use the following two approaches, which are adopted for computing or finding the various properties:

1. Equation approach and
2. Figure, chart, or table approach.

When laboratory results are not available, the test analyst must use empirical correlation of experimental data. This appendix provides a summary of correlations that have proved useful for test analysis. The appendix is divided into the following sections:

- Oil properties and correlations;
- Reservoir rock properties; and
- Reservoir PVT water property calculations.

For the properties where the equations require simple mathematical manipulations, both the equations and the charts are presented. You may use either the equations or the charts and tables. Each property computation and its use are illustrated by a solved example.

D.1 Oil PVT Properties and Correlations

Bubble-Point Pressure

The pressure at which the first bubble of gas evolves, as the oil pressure is reduced. This is also called saturation pressure. At this pressure, oil is saturated with gas.

Factors Affecting Bubble-Point Pressure

1. Reservoir temperature, T_R ;
2. Dissolved gas gravity, γ_{API} ;
3. Solution gas–oil ratio (GOR) at initial reservoir pressure, R_{sb} ;
4. Stock-tank oil gravity, γ_g .

Correlations for Bubble-Point Calculations

- Standing's correlation¹ (see Figure D-1)

$$p_b = 18 \times \left(\frac{R_{sb}}{\gamma_g} \right)^{0.83} \times 10^{\gamma_g} \quad (D-1)$$

$$\gamma_g = 0.00091(T_R) - 0.0125\gamma_{API} = \text{molefraction of gas} \quad (D-2)$$

R_{sb} = solution GOR at p_b , scf/stb

where p_b is the bubble-point pressure in psia, T_R the reservoir temperature in °F, and γ_{API} the API oil gravity.

- Lasater's correlation²

- (a) Using Figure D-2, find M_o , the effective molecular weight of the stock-tank oil from API gravity.
- (b) Calculate Y_g , the mole fraction of the gas in the system:

$$Y_g = \frac{R_{sb}/379.3}{R_{sb}/379.3 + 350\gamma_o/M_o} \quad (D-3)$$

- (c) Calculate bubble-point pressure factor $[p_b\gamma_g/T_R]$ using Figure D-3.
- (d) Calculate p_b as

$$p_b = \left(\frac{p_b\gamma_g}{T_R} \right) \frac{T_R}{\gamma_g} \quad (D-4)$$

EXAMPLE**REQUIRED:**

Bubble-point pressure at 200 °F of a liquid having a gas-oil ratio of 350 cfb, a gas gravity of 0.75, and a tank-oil gravity of 30° API.

PROCEDURE:

Starting at the left side of the chart, proceed horizontally along the 350 line to a gas gravity of 0.75. From this point drop vertically to the 30° API line. Proceed horizontally from the tank-oil gravity scale to the 200°F line. The required pressure is found to be 1930 psia.

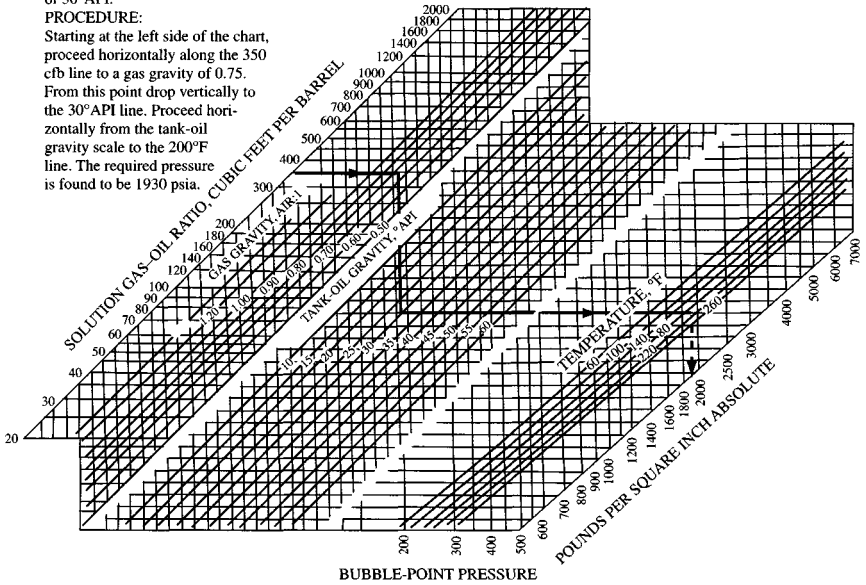


Figure D-1. Chart for calculating saturation pressure by Standing's correlation.¹

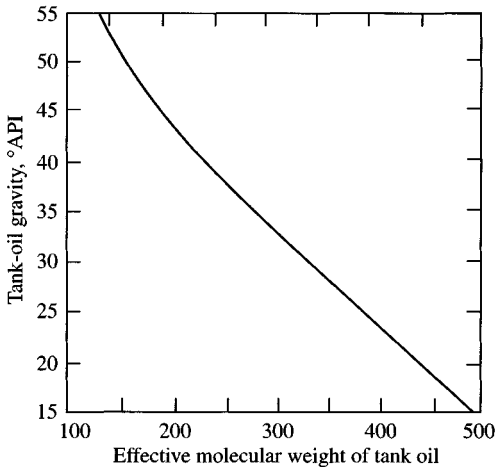


Figure D-2. Effective molecular weight related to stock-tank oil gravity.²

where

T_R = reservoir temperature, °R or (°F + 460),

p_b = bubble-point pressure, psia

γ_o = oil specific gravity = $\frac{141.5}{131.5 + \gamma_{API}}$

- Vasquez and Beggs' correlation³

$$p_b = \left[\frac{R_{sb}}{C_1 \gamma_g \exp[C_3 \gamma_{API} / (T_R + 460)]} \right]^{1/C_2} \quad (\text{D-5})$$

where

p_b = bubble-point pressure, psia

R_{sb} = solution GOR at p_b , scf/stb

γ_g = gas gravity

γ_{API} = oil gravity, °API, and

T_R = reservoir temperature, °F.

Additionally, C_1 , C_2 and C_3 are constants, which are listed in Table D-1.

Table D-1
Bubble-Point Equation Constants

	°API ≤ 30	°API ≥ 30
C_1	0.0362	0.0178
C_2	1.0937	1.1870
C_3	25.724	23.9310

Example D-1 Estimating Bubble-Point Pressure

For the following data, estimate bubble-point pressure, using Lasater's, and Vasquez and Beggs' correlations. $R_{sb} = 600$ scf/stb, $T_R = 250^\circ\text{F}$, $\gamma_g = 0.76$, $\gamma_{API} = 30^\circ$, and $\gamma_o = 0.876$.

Solution

$$T_R = 250^\circ\text{F} = 250 + 460 = 710^\circ\text{R}$$

Lasater's correlation²

- Calculate M_o , the effective molecular weight of stock-tank oil. From Figure D-2, $M_o = 330$.

(b) Calculate Y_g , the mole fraction of gas:

$$\begin{aligned}
 Y_g &= \frac{R_{sb}/379.3}{R_{sb}/379.3 + 350\gamma_o/M_o} \\
 &= \frac{600/379.3}{600/379.3 + 350 \times 0.876/330} \\
 &= 0.63
 \end{aligned}$$

(c) Calculate bubble-point pressure factor ($p_b\gamma_g/T_R$). From Figure D-3, $(p_b\gamma_g/T_R) = 3.6$.

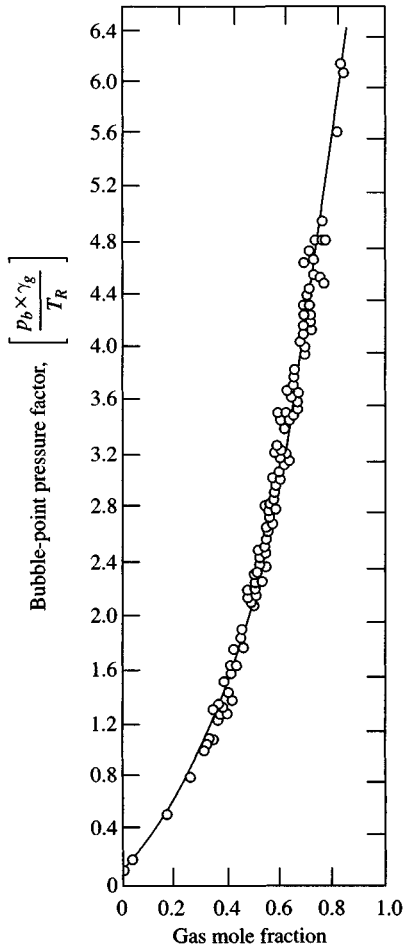


Figure D-3. Lasater's correlation of bubble-point pressure factor with gas mole fraction.²

(d) Calculate p_b as

$$p_b = \left(\frac{p_b \gamma_g}{T_R} \right) \times \frac{T_R}{\gamma_g} = 3.6 \times \frac{710}{0.76} = 3363 \text{ psia}$$

*Vasquez and Beggs' correlation*³

p_b is obtained from Eq. D-5 and using constants from Table D-1:

$$p_b = \left[\frac{600}{0.0362 \times 0.76 \exp \left[\frac{25.724(30)}{710} \right]} \right]^{1/1.0937} = 3430 \text{ psia}$$

Range of Validity of Different Correlations

Correlation	Date	No. of tests	Comments
Standing	1947	105	Based only on gas-crude systems from California
Lasater	1958	158	Developed from data on black oil systems produced in Canada, Western and mid-continent USA, and South America
Vasquez and Beggs	1976	5008	Based on more than 600 PVT analyses from fields all over the world

D.2 Solution Gas–Oil Ratio

R_s represents the amount of dissolved gas that will evolve from the oil as pressure is reduced from reservoir pressure to the atmospheric pressure.

Methods to Estimate Solution Gas–Oil Ratio

*Standing's correlation*¹

$$R_s = \gamma_g \left(\frac{p}{18 \times 10^{\gamma_g}} \right)^{1.204} \quad (\text{D-6})$$

where

$$\gamma_g = 0.00091T - 0.0125\gamma_{API}$$

R_s = solution GOR, scf/stb

p = pressure, psia

γ_g = gas gravity

γ_{API} = oil gravity, API

T = temperature, °F.

*Lasater's correlation*²

- (a) Using Figure D-2, find M_o , the effective molecular weight of the stock-tank oil, from the *API* gravity.
- (b) Calculate Y_g , the gas mole fraction. For $p\gamma_g/T < 3.29$:

$$Y_g = 0.359 \ln \left[\frac{1.473p\gamma_g}{T} + 0.476 \right] \quad (\text{D-7})$$

For $p\gamma_g/T > 3.29$:

$$Y_g = \left(\frac{0.121p\gamma_g}{T} - 0.236 \right)^{0.281} \quad (\text{D-8})$$

where T is in $^{\circ}\text{R}$ in Eqs. D-7 and D-8.

$$R_s = \frac{132,755\gamma_o Y_g}{M_o(1 - Y_g)} \quad (\text{D-9})$$

*Vasquez and Beggs' correlation*³

$$R_s = C_1 \gamma_g p^{C_2} \exp \left[\frac{C_3 \gamma_{API}}{T + 460} \right] \quad (\text{D-10})$$

where

R_s = gas in solution at p and T , scf/stb

γ_g = gas gravity

p = pressure, psia

γ_{API} = stock-tank oil gravity, $^{\circ}API$

T = temperature, $^{\circ}\text{R}$.

C_1 , C_2 , and C_3 are listed in Table D-1.

D.3 Oil Formation Volume Factor

B_o accounts for the shrinkage of oil due to evolution of gas as oil is brought from the reservoir (reservoir pressure and temperature) to stock-tank conditions (atmospheric pressure and temperature).

Correlations to Determine Oil Formation Volume Factor

Saturated Systems

- (a) *Standing correlation:*¹ Knowing R_s , T , p , γ_{API} , γ_g , use Figure D-4 to obtain B_o .

EXAMPLE

REQUIRED:

Formation volume at 200°F of a bubble-point liquid having a gas-oil ratio of 350 cfb, a gas gravity of 0.75, and a tank-oil gravity of 30° API.

PROCEDURE:

Starting at the left side of the chart, proceed horizontally along the 350 cfb line to a gas gravity of 0.75. From this point drop vertically to the 30° API line. Proceed horizontally from the tank-oil gravity scale to the 200°F line. The required formation volume is found to be 1.22 barrel per barrel of tank-oil.

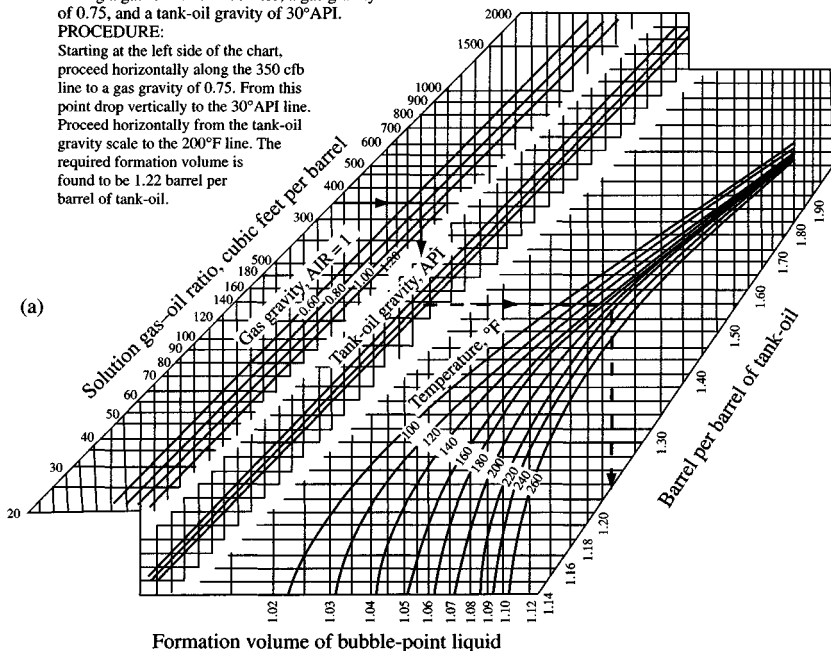


Figure D-4. Charts for calculating total formation volume factor for (a) bubble-point liquid and (b) gas plus liquid phases by Standing's correlation.¹

(b) *Vasquez and Beggs' correlation:*³

$$B_o = 1 + C_1 R_s + C_2 (T - 60) \left(\frac{\gamma_{API}}{\gamma_{gc}} \right) + C_3 R_s (T - 60) \left(\frac{\gamma_{API}}{\gamma_{gc}} \right) \quad (D-11)$$

where

B_o = oil FVF at p and T , rb/stb

R_s = solution GOR at p and T , scf/stb

T = temperature, °F

p = pressure, psia

γ_{API} = oil gravity, °API

γ_{gc} = gas gravity corrected (Air = 1) C_1 , C_2 , and C_3 are constants which are listed in Table D-2

γ_{gc} = corrected gas gravity which is given by

$$\gamma_{gc} = \gamma_g \left[1.0 + 5.912 \times 10^{-5} \gamma_{API} T_s \log \left(\frac{P_s}{14.7} \right) \right]$$

EXAMPLE

REQUIRED:

Formation volume of the gas + liquid phases of a 1500 cfb mixture, gas gravity = 0.80, tank-oil gravity = 40° API, at 200°F and 1000 psia.

PROCEDURE:

Starting at the left side of the chart, proceed horizontally along the 1500 cfb line to the gas gravity line. From this point drop vertically to 40° API line. Proceed horizontally to 200°F and from that point drop to the 1000 psia pressure line. The required formation volume is found to be 5.0 barrels per barrel of tank-oil.

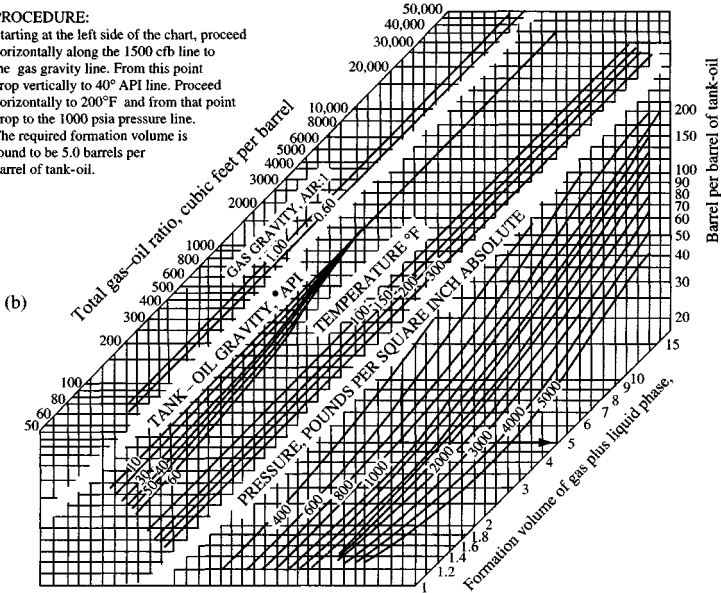


Figure D-4. Continued.

Table D-2
Constants for Oil FVF

	API ≤ 30	API > 30
C_1	4.677×10^{-4}	4.670×10^{-4}
C_2	1.751×10^{-5}	1.100×10^{-5}
C_3	1.811×10^{-8}	1.337×10^{-9}

where

T_s = separator temperature, °F

p_s = separator pressure, psia.

Undersaturated System (i.e., $p > p_b$)

The formation volume factor decreases with increase in pressure at $p > p_b$:

$$B_o = B_{ob} \exp[c_o(p_b - p)] \quad (\text{D-12})$$

and c_o is in psi^{-1} and p as well as p_b are in psia.

Example D-2 *Estimating Oil Formation Volume Factor*

Determine the oil formation volume factor FVF of oil with the following properties using Standing's, and Vasquez and Beggs' correlations: $p_b = 2700$ psia, $R_{sb} = 600$ scf/stb, $\gamma_g = 0.75$, $\gamma_{API} = 30^\circ API$, $T = 250^\circ F$, $p_s = 14.7$ psia, $T_s = 70^\circ F$.

Solution

1. *Standing's correlation:*¹ Find β_o from Figure D-4, which is equal to 1.380 bbl/stb.
2. *Vasquez and Beggs' correlation:*³ From Eq. D-11:

$$\gamma_{gc} = \gamma_g = 0.75$$

$$\begin{aligned} B_o &= 1 + 4.677 \times 10^{-4} \times 600 + 1.751 \times 10^{-5} \times (250 - 60) \\ &\quad \times (30/0.75) + (-1.811 \times 10^{-8}) \times 600 \times (250 - 60) \times (30/0.75) \\ &= 1.331 \text{ rb/stb} \end{aligned}$$

D.4 Total Formation Volume Factor

Total formation volume factor for oil, FVF , is the volume occupied by one stock-tank barrel of oil, its remaining solution gas, and the free gas ($R_{si} - R_s$) that has evolved from the oil. Knowing the values of GOR and gas and oil gravities, Figure D-4 can be used to determine β_t at a given pressure and temperature condition.

$$\beta_t = \beta_o + \beta_g(R_{si} - R_s) \quad (\text{D-13})$$

where

R_{si} = initial solution GOR , scf/stb

R_s = solution GOR , scf/stb

β_o = oil formation volume factor, rb/stb.

D.5 Oil Density

$$\text{Oil density} = \frac{\text{mass of oil}}{\text{oil volume}}$$

$$\rho_o = \frac{350\gamma_o + 0.0764\gamma_g R_s}{5.615B_o} \quad (\text{D-14})$$

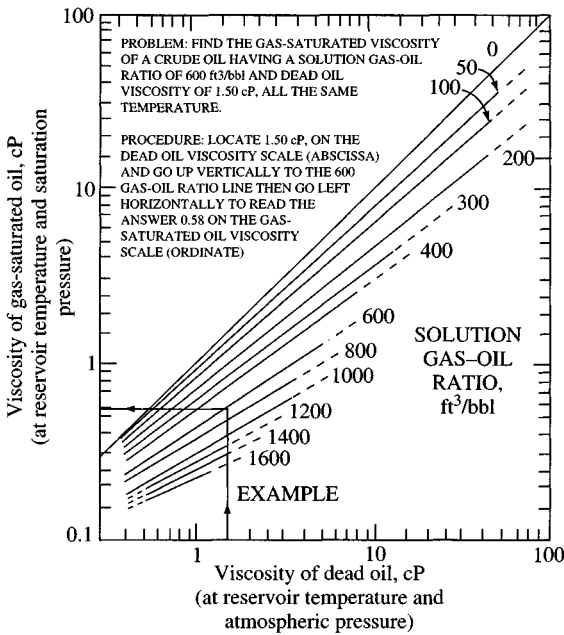


Figure D-5. Viscosity of gas-saturated crude at reservoir temperature and pressure, Chew and Connally's correlation.⁴

where

ρ_o = oil density, lbm/ft³

γ_o = oil specific gravity, dimensionless

γ_g = gas specific gravity, dimensionless

R_s = solution or dissolved gas, scf/stb

B_o = oil formation volume factor, rb/stb.

If $p > p_b$, the bubble-point pressure, then

$$\rho_o = \rho_{ob} \exp[c_o(p - p_b)] \quad (\text{D-15})$$

where

ρ_o = oil density at p , T , g/cm³

ρ_{ob} = oil density at p_b , T , g/cm³

p = pressure, psia

T = temperature of interest, °F

p_b = bubble-point pressure, psia

c_o = oil isothermal compressibility, psi⁻¹

c_o can be calculated using Eq. D-21, which is listed in the latter section.

D.6 Oil Viscosity

Viscosity is a measure of oil resistance to flow

$$\text{Kinematic viscosity} = \frac{\text{absolute viscosity}}{\text{density}}$$

Factors Affecting Oil Viscosity

1. *Composition*: μ increases with a decrease in *API* gravity.
2. *Temperature*: μ increases with a decrease in temperature.
3. *Dissolved gas*: Lightens the oil and thus decreases molecular weight and viscosity.
4. *Pressure*: An increase in pressure on undersaturated oil compresses the oil and causes the viscosity to increase.

Methods to Estimate Oil Viscosity

Figure D-7 can be used to calculate dead oil viscosity, which is based upon Beal's correlation.⁵

Saturated oil

Saturated oil is oil in equilibrium with gas at bubble-point pressure.

- (a) Chew and Connally's Correlation⁴ (see Figure D-5)
 - (i) Calculate gas-free or dead oil viscosity. Dead oil viscosity depends on *API* gravity of stock-tank oil and temperature of interest. Dead oil viscosity is calculated from Figure D-5, which is based upon Beal's correlation.⁵
 - (ii) Modify the dead oil viscosity to include effect of dissolved gas using Figure D-5 (Chew and Connally's correlation).
- (b) *Beggs and Robinson's correlation*.⁶ This correlation can be used for both dead and saturated oils
 - (i) Dead oil viscosity

$$\mu_{od} = 10^x - 1.0 \quad (\text{D-16})$$

where

$$x = T^{-1.163} \exp(6.9824 - 0.04658\gamma_{API}) \quad (\text{D-17})$$

where

μ_{od} = dead oil viscosity, cP

γ_{API} = stock-tank oil gravity, °*API*.

(ii) Saturated oil viscosity (μ_{os})

$$\mu_{os} = A(\mu_{od})^B \quad (\text{D-18})$$

where

 μ_{os} = saturated oil viscosity, cP μ_{od} = dead oil viscosity, cP

$$A = 10.715(R_s + 100)^{-0.515}$$

$$B = 5.440(R_s + 150)^{-0.338}$$

 R_s = solution GOR in scf/stb.

Undersaturated Oil System

Above the bubble-point pressure, only one phase exists in the reservoir, the liquid oil. This oil is called undersaturated oil and is capable of holding additional dissolved gas in solution. Increasing the pressure above p_s compresses the oil and increases the viscosity.

- (a) *Beal's Correlation*.⁵ Oil viscosity is calculated using Figure D-6, which can be used to calculate the rate of increase of viscosity above bubble-point pressure.

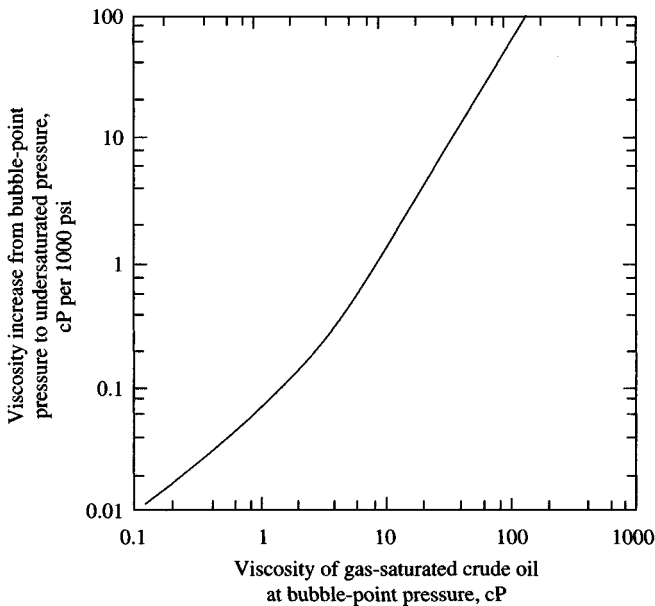


Figure D-6. Effect of pressure on viscosity of gas-saturated crude oils, Beal's correlation.⁵

(b) *Vasquez and Beggs' Correlation:*³

$$\mu_o = \mu_{ob} \left(\frac{p}{p_b} \right)^m \quad (\text{D-19})$$

where

 μ_o = viscosity at $p > p_b$, cP μ_{ob} = viscosity at p_b , cP p = pressure, psia p_b = bubble-point pressure, psia.The exponent m is pressure-dependent and is calculated from

$$m = C_1 p^{C_2} \exp(C_3 + C_4 p) \quad (\text{D-20})$$

where

 p = pressure, psia $C_1 = 2.6$ $C_2 = 1.187$ $C_3 = -11.513$ and $C_4 = -8.98 \times 10^{-5}$.**Example D-3** *Calculating Oil Viscosity*For the oil in Example D-1, calculate the oil viscosity at bubble-point pressure p_b of 2600 psia (given: reservoir temperature = 200°F).**Solution**Since μ_o is needed at p_b , one can use μ_o correlations for saturated oil.*Method 1*

1. Calculate dead oil viscosity, μ_{od} , using Beal's correlation. From Figure D-5, $\mu_{od} = 2.8$ cP.
2. Calculate saturated oil viscosity, μ_{os} , from Figure D-6, $\mu_{os} = 0.69$ cP.

Method 2

1. Calculate dead oil viscosity using Eqs. D-16 and D-17:

$$\begin{aligned} x &= T^{-1.163} \exp(6.9824 - 0.04658 \gamma_{API}) \\ &= T^{-1.163} \exp(6.9824 - 0.04658 \times 28) \\ &= 0.6164 \end{aligned}$$

$$\mu_{od} = 10^x - 1 = 10^{0.6164} - 1 = 3.13 \text{ cP}$$

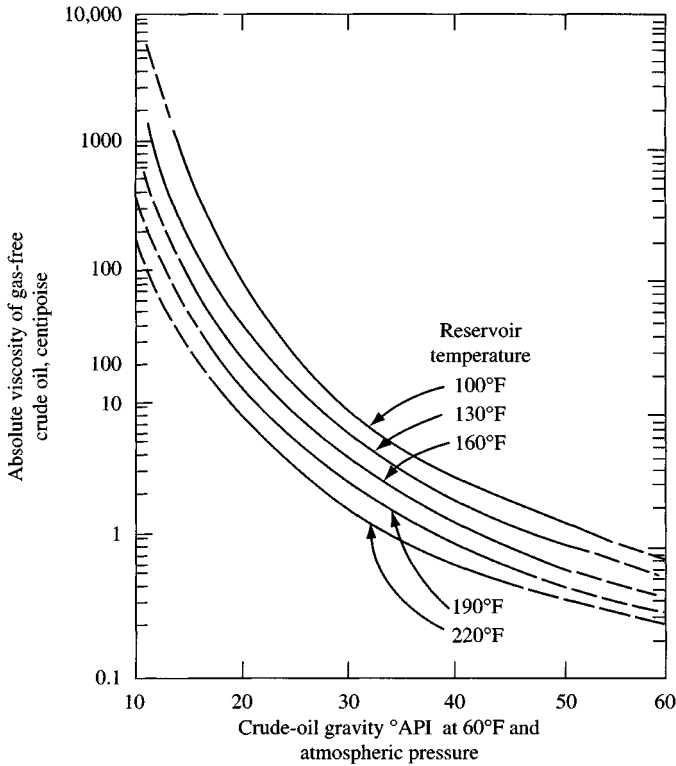


Figure D-7. Variation in viscosity of gas-free crude with stock-tank crude gravity.⁵

2. Calculate saturated oil viscosity, μ_{os} , using Eq. D-18:

$$\begin{aligned} A &= 10.715(R_s + 100)^{-0.515} \\ &= 10.715(600 + 100)^{-0.515} \\ &= 0.3670 \end{aligned}$$

$$\begin{aligned} B &= 5.44(R_s + 150)^{-0.338} \\ &= 5.44(600 + 150)^{-0.338} \\ &= 0.5805 \end{aligned}$$

$$\begin{aligned} \mu_{os} &= A(\mu_{os})^B = 0.367(3.13)^{0.5805} \\ &= 0.71 \text{ cP} \end{aligned}$$

Thus, Method 1, using charts, gives viscosity of 0.69 cP and Method 2, using correlations, shows viscosity of 0.71 cP.

D.7 Oil Compressibility

Oil compressibility is required to predict oil formation volume factors of undersaturated crude oils. Additionally, it is also needed to calculate oil density at different pressures and temperatures.

*Vasquez and Beggs' correlation*³

$$c_o = \left[\frac{5R_{sb} + 17.2T - 1180\gamma_g + 12.61\gamma_{API} - 1433}{p \times 10^5} \right] \quad (\text{D-21})$$

where T is in °F, p is in psi, and R_{sb} is the solution gas–oil ratio at bubble-point pressure in scf/stb.

Example D-4 Calculating Oil Compressibility

For the oil described in Example D-1, calculate the oil compressibility and hence the oil formation volume factor at 3000 psia. The following data are given: $p_b = 2700$ psia, $R_{sb} = 600$ scf/stb, $\gamma_g = 0.75$, $\gamma_{API} = 30^\circ\text{API}$, $T = 250^\circ\text{F}$, $B_o = 1.331$ rb/stb.

Solution The oil compressibility and formation volume factor are calculated using Eqs. D-21 and D-12, respectively.

$$c_o = \left[\frac{5 \times 600 + 17.2 \times 250 - 1180 \times 0.75 + 12.61 \times 30 - 1433}{3000 \times 10^5} \right]$$

$$= 1.787 \times 10^{-5} \text{ psi}^{-1}$$

$$B_o = 1.331 \exp[1.787 \times 10^{-5}(2700 - 3000)]$$

$$= 1.324 \text{ rb/stb} = \text{oil formation volume factor at } p_b, \text{ rb/stb}$$

Example D-5 Determining Oil Formation Volume Factor

Determine the oil formation volume factor, FVF , of oil with the following properties using Standing's, and Vasquez and Beggs' correlations: $p_b = 2700$ psia, $R_{sb} = 600$ scf/stb, $\gamma_g = 0.75$, $\gamma_{API} = 30^\circ\text{API}$, $T = 250^\circ\text{F}$, $p_s = 14.7$ psia, $T_s = 70^\circ\text{F}$.

Solution

1. *Standing's Correlation:*¹ From Figure D-4, $B_o = 1.380$ bbl/stb
2. *Vasquez and Beggs' Correlation:*³ $\gamma_{gc} = \gamma_g = 0.75$

$$B_o = 1 + 4.677 \times 10^{-4} \times 600 + 1.751 \times 10^{-5} \times (250 - 60) \times (30/0.75) +$$

$$(-1.811 \times 10^{-8}) \times 600 \times (250 - 60) \times (30/0.75)$$

$$= 1.331 \text{ rb/stb}$$

D.8 Reservoir Rock Properties

Naturally occurring reservoir rocks contain fluid, water, gas, or a combination of these fluids. The petroleum engineer is obviously concerned with the properties of reservoir rocks. These properties constitute a set of fundamental parameters by which the rock can be quantitatively described.

Formation Compressibility

Formation compressibility c_f in most cases is estimated from the correlation developed by Hall presented as Eq. D-22 and Table D-3 below:⁷

$$c_f = \frac{1.87}{10^6} \times \phi^{-0.415} \quad (\text{D-22})$$

where ϕ is the formation porosity in fraction and c_f the formation isothermal compressibility in psi^{-1} .

Total isothermal compressibility above dew point pressure:

$$c_t = c_g S_g + c_w S_w + c_f \quad (\text{D-23})$$

Table D-3
Formation Compressibility as
Function of Formation Porosity

Porosity (%)	$c_f \times 10^{-6} (\text{psi}^{-1})$
2	9.48
4	7.11
6	6.01
8	5.33
10	4.86
12	4.51
14	4.23
16	4.00
18	3.81
20	3.65
22	3.51
24	3.38

Total isothermal compressibility below dew point pressure:

$$c_t = c_o S_o + c_g S_g + c_w S_w + c_f \quad (\text{D-24})$$

Effective compressibility above dew point pressure:

$$c_e = c_g S_g + \frac{S_w}{1 - S_w} c_w + \frac{c_f}{1 - S_w} \quad (\text{D-25})$$

D.9 Reservoir PVT Water Properties

This section presents Tables D-4 through D-10 for computing reservoir formation PVT properties such as gas solubility and then compressibility, formation volume factor, density, and density gradient both for gas-free and gas-saturated conditions. Viscosity is calculated, which is gas-free. The author of this book using the data supplied by previous authors⁸⁻¹³ developed the graphical and empirical correlations.¹⁴ New tables showing water PVT properties as functions of pressure, temperature, and total dissolved solids are presented, which improve accuracy of prediction and save time.

Tables D-4 through D-10 show the following formation water PVT properties:

1. [C_w] Formation water compressibility – gas-free
2. Formation water compressibility – gas-saturated
3. [RSW] Gas solubility in brine
4. [FVF] Water formation volume factor – gas-free
5. Water formation volume factor – gas-saturated
6. Formation water density – gas-free
7. Formation water density – gas-saturated
8. Density gradient – gas-free
9. Density gradient – gas-saturated
10. Water viscosity – gas-free

Table D-4

Reservoir Formation Water PVT Properties¹⁴ (reservoir temperature, $T = 100^{\circ}\text{F}$ and total dissolved solids, $\text{TDS} = 0.10$; base pressure, $p_{sc} = 14.70$ psia; base temperature, $T_{sc} = 60^{\circ}\text{F}$; specific gravity, $\text{Sp. Gr.} = 1.721$; density of pure water at standard conditions = 62.42 lb/ft³; density of brine water at standard conditions = 66.92 lb/ft³)

Gas-free conditions

Pressure (psia)	Compressibility (psi ⁻¹)	FVF (bbl/bbl)	RSW (ft ³ /bbl)	Density (lb/ft ³)	Sp. Gr. (air = 1.000)	Gradient (psi/ft)	Viscosity (cP)
8000	0.210535E-05	0.9814	20.11	68.1923	1.0924	0.4736	0.9218
7000	0.220900E-05	0.9843	17.96	67.9884	1.0892	0.4722	0.9231
6000	0.227536E-05	0.9876	15.94	67.7648	1.0856	0.4706	0.9235
5500	0.230103E-05	0.9892	14.97	67.6495	1.0837	0.4698	0.9234
5000	0.232466E-05	0.9909	14.03	67.5334	1.0819	0.4690	0.9233
4500	0.234816E-05	0.9926	13.10	67.4177	1.0800	0.4682	0.9231
4000	0.237318E-05	0.9943	12.15	67.3030	1.0782	0.4674	0.9230
3500	0.240115E-05	0.9960	11.18	67.1900	1.0764	0.4666	0.9228
3000	0.243322E-05	0.9977	10.14	67.0792	1.0746	0.4658	0.9226
2500	0.247034E-05	0.9993	9.02	66.9708	1.0729	0.4651	0.9225
2000	0.251315E-05	1.0009	7.77	66.8648	1.0712	0.4644	0.9225
1500	0.256211E-05	1.0024	6.35	66.7612	1.0695	0.4636	0.9224
1000	0.261738E-05	1.0039	4.74	66.6597	1.0679	0.4629	0.9224
750	0.264737E-05	1.0047	3.84	66.6096	1.0671	0.4626	0.9224
500	0.267889E-05	1.0054	2.87	66.5599	1.0663	0.4622	0.9223
250	0.271191E-05	1.0062	1.82	66.5104	1.0655	0.4619	0.9223
15	0.274424E-05	1.0069	0.76	66.4641	1.0648	0.4616	0.9223

Table D-4 (continued)

Gas-saturated conditions							
Pressure (psia)	Compressibility (psi ⁻¹)	FVF (bbl/bbl)	RSW (ft ³ /bbl)	Density (lb/ft ³)	Sp. Gr. (air =1.000)	Gradient (psi/ft)	Viscosity (cP)
8000	0.253267E-05	0.9921	35.35	67.4558	1.0806	0.4685	
7000	0.255487E-05	0.9941	31.56	67.3182	1.0784	0.4675	
6000	0.257268E-05	0.9959	28.01	67.1968	1.0765	0.4667	
5500	0.258336E-05	0.9968	26.32	67.1383	1.0756	0.4663	
5000	0.259601E-05	0.9976	24.66	67.0800	1.0746	0.4658	
4500	0.21080E-05	0.9985	23.02	67.0209	1.0737	0.4654	
4000	0.262766E-05	0.9994	21.36	66.9606	1.0727	0.4650	
3500	0.264828E-05	1.0003	19.64	66.8989	1.0717	0.4646	
3000	0.266612E-05	1.0013	17.82	66.8358	1.0707	0.4642	
2500	0.268637E-05	1.0023	15.84	66.7714	1.0680	0.4637	
2000	0.270598E-05	1.0032	13.65	66.7064	1.0686	0.4633	
1500	0.272354E-05	1.0042	11.17	66.6415	1.0676	0.4628	
1000	0.273737E-05	1.0052	8.33	66.5777	1.0666	0.4624	
750	0.274227E-05	1.0056	6.74	66.5467	1.0661	0.4621	
500	0.274545E-05	1.0061	5.04	66.5163	1.0656	0.4619	
250	0.274562E-05	1.0065	3.20	66.4870	1.0651	0.4617	
15	0.274561E-05	1.0069	1.34	66.4605	1.0647	0.4615	

Table D-5

Reservoir Formation Water PVT Properties¹⁴ (reservoir temperature, $T = 100^{\circ}\text{F}$ and total dissolved solids, $\text{TDS} = 0.20$; base pressure, $p_{sc} = 14.70$ psia; base temperature, $T_{sc} = 60^{\circ}\text{F}$; specific gravity, $\text{Sp. Gr.} = 1.1311$; density of pure water at standard conditions = 62.42 lb/ft³; density of brine water at standard conditions = 70.61 lb/ft³)

Gas-free conditions

Pressure (psia)	Compressibility (psi⁻¹)	FVF (bbl/bbl)	RSW (ft³/bbl)	Density (lb/ft³)	Sp. Gr. (air =1.000)	Gradient (psi/ft)	Viscosity (cP)
8000	0.194705E-05	0.9886	12.43	71.4250	1.1442	0.4960	1.0574
7000	0.201171E-05	0.9912	11.09	71.2309	1.1411	0.4947	1.0600
6000	0.204519E-05	0.9940	9.85	71.0330	1.1379	0.4933	1.0607
5500	0.205627E-05	0.9954	9.25	70.9333	1.1363	0.4926	1.0606
5000	0.206628E-05	0.9968	8.67	70.8336	1.1348	0.4919	1.0604
4500	0.207698E-05	0.9982	8.09	70.7342	1.1332	0.4912	1.0601
4000	0.208983E-05	0.9996	7.51	70.6352	1.1316	0.4905	1.0597
3500	0.210608E-05	1.0010	6.90	70.5369	1.1300	0.4909	1.0594
3000	0.212672E-05	1.0024	6.26	70.4397	1.1284	0.4892	1.0591
2500	0.215249E-05	1.0038	5.57	70.3436	1.1269	0.4885	1.0589
2000	0.218389E-05	1.0051	4.80	70.2489	1.1254	0.4879	1.0587
1500	0.222116E-05	1.0064	3.93	70.1558	1.1239	0.4872	1.0586
1000	0.226432E-05	1.0071	2.93	70.0646	1.1224	0.4866	1.0585
750	0.228803E-05	1.0084	2.37	70.0197	1.1217	0.4863	1.0585
500	0.231310E-05	1.0090	1.77	69.9753	1.1210	0.4860	1.0585
250	0.233946E-05	1.0097	1.12	69.9315	1.1203	0.4856	1.0584
15	0.236534E-05	1.0130	0.47	69.8907	1.1196	0.4854	1.0583

Table D-5 (continued)

Gas-saturated conditions							
Pressure (psia)	Compressibility (psi ⁻¹)	FVF (bbl/bbl)	RSW (ft ³ /bbl)	Density (lb/ft ³)	Sp. Gr. (air =1.000)	Gradient (psi/ft)	Viscosity (cP)
8000	0.219652E-05	0.9952	35.35	70.9499	1.1366	0.4927	
7000	0.219763E-05	0.9973	31.56	70.7986	1.1342	0.4917	
6000	0.219689E-05	0.9992	28.01	70.6663	1.1321	0.4908	
5500	0.219866E-05	1.0001	26.32	70.6033	1.1311	0.4903	
5000	0.220264E-05	1.0009	24.66	70.5408	1.1301	0.4899	
4500	0.220914E-05	1.0018	23.02	70.4778	1.1291	0.4894	
4000	0.221830E-05	1.0027	21.36	70.4140	1.1280	0.4890	
3500	0.223008E-05	1.0037	19.64	70.3488	1.1270	0.4885	
3000	0.224427E-05	1.0046	17.82	70.2823	1.1259	0.4881	
2500	0.226042E-05	1.0056	15.84	70.2147	1.1248	0.4876	
2000	0.227790E-05	1.0066	13.65	70.1465	1.1237	0.4871	
1500	0.229580E-05	1.0076	11.17	70.0784	1.1227	0.4867	
1000	0.231300E-05	1.0085	8.33	70.0115	1.1216	0.4862	
750	0.232091E-05	1.0090	6.74	69.9789	1.1211	0.4860	
500	0.232810E-05	1.0094	5.04	69.9471	1.1206	0.4858	
250	0.233436E-05	1.0099	3.20	69.9163	1.1201	0.4855	
15	0.233920E-05	1.0103	1.34	69.8884	1.1196	0.4854	

Table D-6

Reservoir Formation Water PVT Properties¹⁴ (reservoir temperature, $T = 100^{\circ}\text{F}$ and total dissolved solids, $\text{TDS} = 0.30$; base pressure, $p_{sc} = 14.70$ psia; base temperature, $T_{sc} = 60^{\circ}\text{F}$; specific gravity, $\text{Sp. Gr.} = 1.1690$; density of pure water at standard conditions = 62.42 lb/ft³; density of brine water at standard conditions = 72.97 lb/ft³)

Gas-free conditions							
Pressure (psia)	Compressibility (psi ⁻¹)	FVF (bbl/bbl)	RSW (ft ³ /bbl)	Density (lb/ft ³)	Sp. Gr. (air = 1.000)	Gradient (psi/ft)	Viscosity (cP)
8000	0.161694	0.9902	7.06	73.6941	1.1806	0.5118	1.2172
7000	0.169788	0.9927	6.30	73.5047	1.1775	0.5105	1.2213
6000	0.174782	0.9952	5.59	73.3239	1.1746	0.5092	1.2224
5500	0.176674	0.9964	5.25	73.2351	1.1732	0.5086	1.2222
5000	0.178413	0.9976	4.92	73.1470	1.1718	0.5080	1.2219
4500	0.180151	0.9988	4.60	73.0592	1.1704	0.5074	1.2213
4000	0.182022	1.0000	4.26	72.9714	1.1690	0.5068	1.2208
3500	0.184130	1.0012	3.92	72.8838	1.1676	0.5062	1.2202
3000	0.186556	1.0024	3.56	72.7963	1.1662	0.5055	1.2198
2500	0.189357	1.0036	3.16	72.7092	1.1648	0.5049	1.2194
2000	0.192565	1.0048	2.72	72.6227	1.1634	0.5043	1.2192
1500	0.196187	1.0060	2.23	72.5372	1.1620	0.5037	1.2190
1000	0.200205	1.0071	1.66	72.4533	1.1607	0.5032	1.2189
750	0.202350	1.0077	1.35	72.4122	1.1600	0.5029	1.2189
500	0.204577	1.0083	1.01	72.3716	1.1594	0.5026	1.2188
250	0.206875	1.0088	0.64	72.3318	1.1588	0.5023	1.2187
15	0.209092	1.0093	0.27	72.2951	1.1582	0.5021	1.2186

Table D-6 (continued)

Gas-saturated conditions

Pressure (psia)	Compressibility (psi ⁻¹)	FVF (bbl/bbl)	RSW (ft ³ /bbl)	Density (lb/ft ³)	Sp. Gr. (air = 1.000)	Gradient (psi/ft)	Viscosity (cP)
8000	0.174606E-05	0.9939	35.35	73.4153	1.1761	0.5098	
7000	0.178667E-05	0.9961	31.56	73.2510	1.1735	0.5087	
6000	0.181628E-05	0.9981	28.01	73.1087	1.1712	0.5077	
5500	0.183038E-05	0.9990	26.32	73.0414	1.1701	0.5072	
5000	0.184514E-05	0.9999	24.66	72.9751	1.1691	0.5068	
4500	0.186110E-05	1.0008	23.02	72.9096	1.1680	0.5063	
4000	0.187865E-05	1.0017	21.36	72.8415	1.1669	0.5059	
3500	0.189794E-05	1.0027	19.64	72.7732	1.1658	0.5054	
3000	0.191899E-05	1.0036	17.82	72.7038	1.1647	0.5049	
2500	0.194158E-05	1.0046	15.84	72.6334	1.1636	0.5044	
2000	0.196533E-05	1.0056	13.65	72.5625	1.1624	0.5039	
1500	0.198963E-05	1.0066	11.17	72.4917	1.1613	0.5034	
1000	0.201368E-05	1.0076	8.33	72.4221	1.1602	0.5029	
750	0.202532E-05	1.0080	6.74	72.3882	1.1597	0.5027	
500	0.203651E-05	1.0086	5.04	72.3550	1.1591	0.5025	
250	0.204712E-05	1.0089	3.20	72.3229	1.1586	0.5023	
15	0.205642E-05	1.0093	1.34	72.2938	1.1581	0.5021	

Table D-7

Reservoir Formation Water PVT Properties¹⁴ (reservoir temperature, $T = 200^{\circ}\text{F}$ and total dissolved solids, $\text{TDS} = 0.10$; base pressure, $p_{sc} = 14.70$ psia; base temperature, $T_{sc} = 60^{\circ}\text{F}$; specific gravity, $\text{Sp. Gr.} = 1.0721$; density of pure water at standard conditions = 62.42 lb/ft³; density of brine water at standard conditions = 66.92 lb/ft³)

Gas-free conditions

Pressure (psia)	Compressibility (psi ⁻¹)	FVF (bbl/bbl)	RSW (ft ³ /bbl)	Density (lb/ft ³)	Sp. Gr. (air = 1.000)	Gradient (psi/ft)	Viscosity (cP)
8000	9.230275E-05	1.0099	40.59	66.2674	1.0616	0.4602	0.3695
7000	0.240640E-05	1.0133	33.47	66.0404	1.0580	0.4586	0.3599
6000	0.247276E-05	1.0168	27.13	65.8152	1.0544	0.4571	0.3699
5500	0.249844E-05	1.0186	24.27	65.7054	1.0526	0.4563	0.3698
5000	0.252207E-05	1.0202	21.59	65.5980	1.0509	0.4556	0.3697
4500	0.254556E-05	1.0218	19.10	65.4932	1.0492	0.4548	0.3695
4000	0.257058E-05	1.0234	16.77	65.3908	1.0476	0.4541	0.3694
3500	0.259855E-05	1.0250	14.59	65.2906	1.0460	0.4534	0.3693
3000	0.263063E-05	1.0286	12.52	65.1920	1.0444	0.4527	0.3692
2500	0.266774E-05	1.0281	10.54	66.0941	1.0428	0.4521	0.3691
2000	0.271056E-05	1.0296	8.61	64.9952	1.0412	0.4514	0.3690
1500	0.275951E-05	1.0312	6.69	64.8958	1.0396	0.4507	0.3690
1000	0.281478E-05	1.0328	4.73	64.7945	1.0380	0.4500	0.3690
750	0.284477E-05	1.0337	3.73	64.7418	1.0372	0.4496	0.3689
500	0.287629E-05	1.0346	2.69	64.6877	1.0363	0.5592	0.3689
250	0.290931E-05	1.0354	1.61	64.6321	1.0354	0.4488	0.3689
15	0.294164E-05	1.0363	0.57	64.5781	1.0345	0.4485	0.3689

Table D-7 (continued)

Gas-saturated conditions							
Pressure (psia)	Compressibility (psi ⁻¹)	FVF (bbl/bbl)	RSW (ft ³ /bbl)	Density (lb/ft ³)	Sp. Gr. (air = 1.000)	Gradient (psi/ft)	Viscosity (cP)
8000	0.268492E-05	1.0237	60.99	65.3742	1.0473	0.4540	
7000	0.273038E-05	1.0258	50.29	65.2393	1.0451	0.4531	
6000	0.276266E-05	1.0274	40.77	65.1363	1.0435	0.4523	
5500	0.277716E-05	1.0281	36.46	65.0916	1.0428	0.4520	
5000	0.279154E-05	1.0288	32.45	65.0492	1.0421	0.4517	
4500	0.280622E-05	1.0294	28.70	65.0079	1.0414	0.4515	
4000	0.282139E-05	1.0301	25.20	64.9664	1.0408	0.4512	
3500	0.283705E-05	1.0308	21.92	64.9239	1.0401	0.4509	
3000	0.285298E-05	1.0315	18.82	64.8798	1.0394	0.4506	
2500	0.286876E-05	1.0322	15.84	64.8337	1.0386	0.4502	
2000	0.288371E-05	1.0330	12.94	64.7855	1.0379	0.4499	
1500	0.289690E-05	1.0338	10.06	64.7353	1.0371	0.4496	
1000	0.290715E-05	1.0346	7.11	64.6835	1.0362	0.4492	
750	0.291074E-05	1.0350	5.60	64.6572	1.0358	0.4490	
500	0.291305E-05	1.0355	4.04	64.6306	1.0354	0.4488	
250	0.291386E-05	1.0359	2.43	64.6040	1.0350	0.4487	
15	0.291307E-05	1.0363	0.85	64.5791	1.0346	0.4485	

Table D-8

Reservoir Formation Water PVT Properties¹⁴ (reservoir temperature, $T = 200^{\circ}\text{F}$ and total dissolved solids, $\text{TDS} = 0.20$: base pressure, $p_{sc} = 14.70$ psia; base temperature, $T_{sc} = 60^{\circ}\text{F}$; specific gravity, $\text{Sp. Gr.} = 1.1311$; density of pure water at standard conditions = 62.42 lb/ft³; density of brine water at standard conditions = 70.61 lb/ft³)

Gas-free conditions							
Pressure (psia)	Compressibility (psi ⁻¹)	FVF (bbl/bbl)	RSW (ft ³ /bbl)	Density (lb/ft ³)	Sp. Gr. (air = 1.000)	Gradient (psi/ft)	Viscosity (cP)
8000	0.218482E-05	1.0165	27.38	69.4615	1.1128	0.4824	0.4275
7000	0.224948E-05	1.0196	22.57	69.2483	1.1094	0.4839	0.4281
6000	0.228296E-05	1.0226	18.30	69.495	1.1062	0.4795	0.4281
5500	0.229403E-05	1.0240	16.37	68.9550	1.1047	0.4789	0.4279
5000	0.230405E-05	1.0253	14.56	68.8634	1.1032	0.4782	0.4277
4500	0.231474E-05	1.0267	12.88	68.7743	1.1018	0.4776	0.4275
4000	0.232760E-05	1.0280	11.31	68.6871	1.1004	0.4770	0.4272
3500	0.234385E-05	1.0292	9.84	68.6012	1.0990	0.4764	0.4270
3000	0.236449E-05	1.0305	8.45	68.5161	1.0976	0.4758	0.4268
2500	0.239026E-05	1.0318	7.11	68.4311	1.0963	0.4752	0.4267
2000	0.242166E-05	1.0331	5.81	68.3452	1.0949	0.4746	0.4265
1500	0.245893E-05	1.0344	4.51	68.2577	1.0935	0.4740	0.4264
1000	0.250208E-05	1.0358	3.19	68.1676	1.0920	0.4734	0.4263
750	0.252580E-05	1.0365	2.51	68.1212	1.0913	0.4731	0.4263
500	0.255087E-05	1.0372	1.81	68.0738	1.0905	0.4727	0.4263
250	0.257723E-05	1.0380	1.09	68.0252	1.0898	0.4724	0.4262
15	0.260310E-05	1.0387	0.38	67.9784	1.0890	0.4721	0.4261

Table D-8 (continued)

Gas-saturated conditions

Pressure (psia)	Compressibility (psi ⁻¹)	FVF (bbl/bbl)	RSW (ft ³ /bbl)	Density (lb/ft ³)	Sp. Gr. (air = 1.000)	Gradient (psi/ft)	Viscosity (cP)
8000	0.238565E-05	1.0258	60.99	68.8313	1.1027	0.4780	
7000	0.240981E-05	1.0280	50.29	68.6830	1.1003	0.4770	
6000	0.242345E-05	1.0297	40.77	68.5701	1.0985	0.4762	
5500	0.242917E-05	1.0304	36.46	68.5216	1.0977	0.4750	
5000	0.243518E-05	1.0311	32.45	68.4758	1.0970	0.4755	
4500	0.244201E-05	1.0318	28.70	68.4314	1.0963	0.4752	
4000	0.245005E-05	1.0325	26.20	68.3871	1.0956	0.4749	
3500	0.245956E-05	1.0332	21.92	68.3420	1.0948	0.4746	
3000	0.247061E-05	1.0339	18.82	68.2954	1.0941	0.4743	
2500	0.248310E-05	1.0346	15.84	68.2468	1.0933	0.4740	
2000	0.249673E-05	1.0354	12.94	68.1962	1.0925	0.4736	
1500	0.251102E-05	1.0362	10.06	68.1434	1.0917	0.4732	
1000	0.252528E-05	1.0370	7.11	68.0890	1.0908	0.4729	
750	0.253214E-05	1.0374	5.60	68.0613	1.0903	0.4727	
500	0.253822E-05	1.0378	4.04	68.0334	1.0899	0.4725	
250	0.254470E-05	1.0363	2.43	68.0054	1.0894	0.4723	
15	0.254984E-05	1.0387	0.85	67.9791	1.0890	0.4721	

Table D-9

Reservoir Formation Water PVT Properties¹⁴ (reservoir temperature, $T = 200^{\circ}\text{F}$ and total dissolved solids, $\text{TDS} = 0.30$; base pressure $p_{sc} = 14.70$ psia; base temperature, $T_{sc} = 60^{\circ}\text{F}$; specific gravity, $\text{Sp. Gr.} = 1.721$; density of pure water at standard conditions = 62.42 lb/ft³; density of brine water at standard conditions = 72.97 lb/ft³)

Gas-free conditions

Pressure (psia)	Compressibility (psi ⁻¹)	FVF (bbl/bbl)	RSW (ft ³ /bbl)	Density (lb/ft ³)	Sp. Gr. (air = 1.000)	Gradient (psi/ft)	Viscosity (cP)
8000	0.186768E-05	1.0176	17.87	71.7131	1.1488	0.4980	0.5070
7000	0.194862E-05	1.0204	14.73	71.5082	1.1456	0.4966	0.5082
6000	0.199856E-05	1.0230	11.94	71.3282	1.1427	0.4953	0.5081
5500	0.201748E-05	1.0242	10.68	71.2449	1.1413	0.4949	0.5078
5000	0.203487E-05	1.0253	9.50	71.1650	1.1401	0.4942	0.5074
4500	0.205226E-05	1.0265	8.41	71.0876	1.1388	0.4937	0.5070
4000	0.207096E-05	1.0276	7.38	71.0117	1.1376	0.4932	0.5066
3500	0.209204E-05	1.0286	6.42	70.9367	1.1364	0.4926	0.5063
3000	0.211630E-05	1.0297	5.51	70.8619	1.1352	0.4921	0.5060
2500	0.214431E-05	1.0308	4.64	70.7864	1.1340	0.4916	0.5057
2000	0.217639E-05	1.0319	3.79	70.7098	1.1328	0.4911	0.5056
1500	0.221261E-05	1.0331	2.96	70.6313	1.1315	0.4905	0.5053
1000	0.225279E-05	1.0343	2.08	70.5503	1.1302	0.4899	0.5052
750	0.227424E-05	1.0349	1.64	70.5088	1.1295	0.4897	0.5051
500	0.229651E-05	1.0355	1.18	70.4665	1.1289	0.4894	0.5050
250	0.231949E-05	1.0361	0.71	70.4233	1.1282	0.4891	0.5049
15	0.234166E-05	1.0368	0.25	70.3819	1.1275	0.4888	0.5048

Table D-9 (continued)

Gas-saturated conditions

Pressure (psia)	Compressibility (psi ⁻¹)	FVF (bbl/bbl)	RSW (ft ³ /bbl)	Density (lb/ft ³)	Sp. Gr. (air = 1.000)	Gradient (psi/ft)	Viscosity (cP)
8000	0.194914E-05	1.0236	60.99	71.2876	1.1420	0.4951	
7000	0.200925E-05	1.0259	50.29	71.1265	1.1394	0.4939	
6000	0.205152E-05	1.0277	40.77	71.0044	1.1375	0.4931	
5500	0.206923E-05	1.0284	36.46	70.9521	1.1366	0.4927	
5000	0.208591E-05	1.0291	32.45	70.9031	1.1359	0.4924	
4500	0.210231E-05	1.0298	28.70	70.8558	1.1351	0.4921	
4000	0.211901E-05	1.0305	25.20	70.8089	1.1344	0.4917	
3500	0.213643E-05	1.0312	21.92	70.7614	1.1336	0.4914	
3000	0.215485E-05	1.0319	18.82	70.7126	1.1328	0.4911	
2500	0.217437E-05	1.0326	15.84	70.6518	1.1320	0.4907	
2000	0.219494E-05	1.0334	12.94	70.6089	1.1312	0.4904	
1500	0.221635E-05	1.0342	10.06	70.5540	1.1303	0.4900	
1000	0.223825E-05	1.0351	7.11	70.4972	1.1294	0.4896	
750	0.224923E-05	1.0356	5.60	70.4683	1.1289	0.4894	
500	0.226015E-05	1.0359	4.04	70.4391	1.1284	0.4892	
250	0.227094E-05	1.0363	2.43	70.4099	1.1280	0.4890	
15	0.228090E-05	1.0368	0.86	70.3842	1.1275	0.4888	

Table D-10

Reservoir Formation Water PVT Properties¹⁴ (reservoir temperature $T = 300^{\circ}\text{F}$ and total dissolved solids, TDS = 0.10; base pressure $p_{sc} = 14.70$ psia; base temperature, $T_{sc} = 60^{\circ}\text{F}$; specific gravity, Sp. Gr. = 1.721; density of pure water at standard conditions = 62.42 lb/ft³; density of brine water at standard conditions = 66.92 lb/ft³)

Gas-free conditions							
Pressure (psia)	Compressibility (psi ⁻¹)	FVF (bbl/bbl)	RSW (ft ³ /bbl)	Density (lb/ft ³)	Sp. Gr. (air = 1.000)	Gradient (psi/ft)	Viscosity (cP)
8000	0.278618E-05	1.0417	18.57	64.2415	1.0291	0.4461	0.2497
7000	0.288982E-05	1.0471	17.70	63.9103	1.0238	0.4438	0.2498
6000	0.295619E-05	1.0520	16.57	63.6167	1.0191	0.4418	0.2497
5500	0.298286E-05	1.0542	15.90	63.4833	1.0170	0.4409	0.2496
5000	0.300549E-05	1.0562	15.17	63.3580	1.0150	0.4400	0.2494
4500	0.302899E-05	1.0582	14.36	63.2400	1.0131	0.4392	0.2493
4000	0.305401E-05	1.0601	13.47	63.1282	1.0113	0.4384	0.2491
3500	0.308198E-05	1.0619	12.46	63.0212	1.0096	0.4377	0.2490
3000	0.311405E-05	1.0636	11.33	62.9175	1.0079	0.4369	0.2489
2500	0.315116E-05	1.0654	10.05	62.8155	1.0063	0.4362	0.2488
2000	0.319398E-05	1.0671	8.58	62.7131	1.0047	0.4355	0.2488
1500	0.324294E-05	1.0689	6.91	62.6083	1.0030	0.4348	0.2487
1000	0.329821E-05	1.0708	4.98	62.4986	1.0012	0.4340	0.2487
750	0.332820E-05	1.0718	3.91	62.4413	1.0003	0.4336	0.2486
500	0.335972E-05	1.0728	2.76	62.3817	0.9994	0.4332	0.2486
250	0.339273E-05	1.0738	1.53	62.3196	0.9984	0.4328	0.2486
15	0.342507E-05	1.0749	0.28	62.2587	0.9974	0.4324	0.2486

Table D-10 (continued)

Gas-saturated conditions

Pressure (psia)	Compressibility (psi ⁻¹)	FVF (bbl/bbl)	RSW (ft ³ /bbl)	Density (lb/ft ³)	Sp. Gr. (air = 1.000)	Gradient (psi/ft)	Viscosity (cP)
8000	0.340631	1.0619	99.02	63.0216	1.0096	0.4377	
7000	0.349258	1.0641	87.37	62.8899	1.0075	0.4367	
6000	0.354600	1.0657	68.19	62.7976	1.0060	0.4361	
5500	0.356373	1.0663	59.54	62.7600	1.0054	0.4358	
5000	0.357674	1.0669	51.52	62.7252	1.0049	0.4356	
4500	0.358576	1.0675	44.12	62.6915	1.0043	0.4354	
4000	0.359132	1.0681	37.31	62.6572	1.0038	0.4351	
3500	0.359375	1.0687	31.07	62.6209	1.0032	0.4349	
3000	0.359317	1.0694	25.38	62.5815	1.0026	0.4346	
2500	0.358949	1.0701	20.18	62.5381	1.0019	0.4343	
2000	0.358235	1.0709	15.43	62.4900	1.0011	0.4340	
1500	0.357121	1.0718	11.08	62.4367	1.0002	0.4336	
1000	0.355527	1.0728	7.06	62.3780	0.9993	0.4332	
750	0.354521	1.0734	5.15	62.3467	0.9988	0.4330	
500	0.353357	1.0739	3.30	62.3139	0.9983	0.4327	
250	0.352022	1.0745	1.50	62.2799	0.9977	0.4326	
15	0.350599	1.0751	0.16	62.2468	0.9972	0.4323	

References and Additional Reading

1. Standing, M. B., and Katz, D. L., "Density of Natural Gases," *Trans. AIME* (1942) 146, 140–149.
2. Lasater, J. A., "Bubble Point Pressure Correlation," *Trans. AIME* (1958), 379.
3. Vasquez, M., and Beggs, H. D., "Correlations for Fluid Physical Property Prediction," *J. Pet. Tech.* (June 1980) 32, 968–970.
4. Chew, J., and Connally, C. A., Jr., "A Viscosity Correlation for Gas-Saturated Crude Oils," *Trans. AIME* (1959) 216, 23–25.
5. Beal, C., "The Viscosity of Air, Water, Natural Gas, Crude Oil and Its Associated Gases at Oil Field Temperatures and Pressures," *Trans. AIME* (1946) 165, 94–115.
6. Beggs, H. D., and Robinson, J. R., "Estimating the Viscosity of Oil Systems," *J. Pet. Tech.* (September 1975), 1140–111.
7. Hall, H. N., "Compressibility of Reservoir Rocks," *Trans. AIME*, (1953) 198, 309–311.
8. Keenan, J. H., and Keyers, F. G., *Thermodynamic Properties of Steam*, Wiley New York, 1936.
9. Eichelberger, W. C., *Ind. Engr Chem.* (1955) 47, 223.
10. NcCain W. D., Jr., *The Properties of Petroleum Fluids*, Petroleum Publishing Co., Tulsa, OK, 1990.
11. Dodson, C. R., and Standing, M. B., "Pressure–Volume–Temperature and Solubility Relations for Natural Gas Water Mixtures," *Drill Prod. Prac. API* (1944), 173–179.
12. Frick, T. C., *Petroleum Production Handbook*, Vol. II, Millet the Printer, Inc., Dallas, TX, 1962.
13. Ulbertson, O. L., and Mcketta, J. J., "Solubility of Methane in Water at Pressures to 10,000 psia," *Trans. AIME* (1951) 192, 223–226.
14. Amanat U. C., "New Generalized Correlations for Predicting Reservoir Formation Water Properties as Functions of Pressure, Temperature and Total Dissolved Solids, Gives Best Accuracy, Computer Application, Chart or Table Use, Unpublished Development, June, 1998.

Index

<u>Index terms</u>	<u>Links</u>				
A					
Anisotropy	428	462	539	556	574
Anisotropic reservoir systems	523	545	570	574	
Nomenclatures for anisotropic permeability system	545	641			
Principal permeability in x-direction	545				
Principal permeability in y direction	545				
Principal permeability in xy direction	545				
Minimum permeability in x-direction	545				
Maximum permeability in x-direction	545				
Angle of orientation	545				
Average system permeability	546				
Average pressure	234				
Dietz method	238	247	249		
Matthews-Bron-Hazebrook method	236	245			
Miller-Dyes-Hutchinson method	237				
Muskat method	240	242	249		
Other methods	245				
Estimating constant pressure at aquifer in water drive reservoirs	244				
Ramey-Cobb method	238				
Afterflow	199				
Apparent wellbore radius	111	161	166	221	224
	409				
Afterflow rate normalizing graph	149				
Average porosity	507				

<u>Index terms</u>	<u>Links</u>				
Average thickness	507	516	518		
Average permeability	507	514	546		
Afterflow rate normalization log-log graph	149				
Afterflow rate normalized pressure-square root of time plot	229				
Application of type curves to estimate wellbore storage, permeability, and skin in homogeneous systems					
Using Ramey's type curves	287				
Using Earlougher and Kersch type curves	299				
Application of type curves to estimate wellbore storage, permeability, and skin in fractured formations					
Using McKinley's type curves	302				
Using vertical fracture type curves	313				
Using horizontal fracture type curves	329				
Using type curves for a finite conductivity vertical fracture	339				
Analyzing pulse test using graphical method	457				
Analyzing pulse test using analytical method	458				
Actual productivity index	162	212			
Afterflow analysis using Russell's technique	199				
 B					
Bottom-hole shut-in pressure	595				
Bilinear flow type analysis	339				
Estimating fracture conductivity	346	347	348	350	353
	356	357			
Estimating fracture half-length	353				
Estimating effective wellbore radius	355				
Estimating fracture skin factor	355	356			

Index terms**Links**

Brons-Miller method	237
Buildup testing and analysis	153
Infinite-acting reservoir	156
Single-rate test	162
Finite reservoir behavior	176
Average reservoir pressure	234
Horner and MBH method	236
Ramey and Cobb method	238
MDH method	237
Extended Muskat method	240
Dietz method	238
Arps and Smith method	241
Two-rate test	199
Variable rate test	206
Block diagram of various numerical simulation models	
One-dimensional horizontal model	29
One-dimensional dipping model	29
Two-dimensional horizontal model	30
Three-dimensional layered model	30
Two-dimensional coning model	31
Two-dimensional vertical model	31
Three-dimensional continuous model	32
Three-dimensional continuous (section) model	32
Bourdet's type curve matching plot	270
Bilinear flow analysis-low conductivity fractures	385
Beginning of formation linear flow	347
Beginning of pseudo radial flow	347

Index terms**Links****C**

Compressibility	623			
Formation (rock)	623			
Oil	622			
Total system	198	212	462	
Water	624			
Commingled reservoirs	507			
Constant pressure testing	111	180	182	218
Estimating permeability	117	122	123	125
	128	129	131	137
	141	143	144	154
	165	177	179	183
	187	191	200	204
	209	218	220	228
	246	251	272	290
	302	317	319	323
	352	354	357	362
	401	404	408	410
	431	435	461	499
Estimating porosity-compressibility product	442	544		
Conversion factors	577			
Comparison of linear discontinuities by six methods	526			
Correlation tables and charts for use in pressure buildup and flow test analysis	585			
Converting metric to English oil field units	577			
Constant pressure log type curves for finite capacity vertical fracture	374			
Constant well rate log-log type curves for finite capacity vertical fracture	375			
Cumulative water injected	461			

Index terms**Links****D**

Drill stem test	387				
DST pressure behavior	388				
Operational DST tool	388				
DST charts for barrier detection	390				
DST pressure charts	390				
Common method to analyze DST	396				
Horner's plot method	397				
Type curve matching method	399				
Ramey type curves	399				
Kohlhass matching curves	402				
Correa and Ramey's method	403				
DST buildup test analysis	404				
Wireline formation test	414				
Open hole formation test	415				
Empirical interpretation charts	418				
Closed hole formation test	420				
Reservoir rock's porosity distribution					
system analysis	422				
Porosity partition	423				
Partitioning coefficient	423	424			
Matrix pore volume calculation	424				
Fracture pore volume calculation	424				
Well skin effect	425				
Pollard type plot	422				
Determining reservoir permeability	117	122	123	125	126
	128	129	131	137	138
	141	143	144	154	159
	165	177	179	183	186
	187	191	200	204	207
	209	218	220	228	230

<u>Index terms</u>	<u>Links</u>				
Determining reservoir permeability (<i>Continued</i>)	246	251	272	290	300
	302	317	319	323	328
	352	354	357	362	397
	401	404	408	410	413
	431	435	461	499	
Determine skin factor	52	53	54	63	71
	97	99	100	101	107
	110	113	114	118	122
	124	126	128	129	132
	133	134	137	139	142
	143	144	148	149	154
	155	160	166	167	169
	172	179	184	186	187
	191	193	195	198	201
	294	205	207	209	211
	219	220	227	228	230
	263	265	296	300	318
	322	324	327	348	362
	365	368	397	401	403
	410	413	469	475	481
	483	498	492	496	499
Double porosity behavior	365				
Distance to the discontinuity	526				
Drawdown test analysis	107				
Single-rate test	112				
Two-rate drawdown test	121				
Multirate drawdown test	142				
Variable rate test	129				
Drawdown rate normalization	147				
Reservoir limit test	116				
Dimensionless storage constant	240	246	248	400	
Drawdown test analysis with type curve	289				

<u>Index terms</u>	<u>Links</u>				
Dimensionless pressure drop functions	365				
Diagrams to determine degree of communication and type of crossflow	513				
Determination sequences of fracture orientations	536				
Dimensionless interporosity transient flow parameter	368				
Dimensionless formation thickness	33				
Dimensionless fracture hydraulic diffusivity	535				
Dimensionless fracture flow conductivity	346	347	348	350	353
	357				
Designing transient pressure tests	523				
Interference test design	448				
Pulse test design	445				
Design of flow and buildup tests	390				
Differential equations: describing flow of fluid through porous media	21				
Dimensionless pressure drop	288				
Dimensionless time	62	147	284	321	341
	375	505			
Determine average reservoir pressure	244				
Drainage radius	112	114	116	121	146
	174	487	493		
Dimensionless fracture pressure solution for several values of ω and θ	276				
Dimensionless matrix pressure solution for several values of ω and θ	211				
Drawdown flow periods in a horizontal well with dual porosity flow	278				
Designing pulse test graphically	453				
Designing pulse tests analytically	455				

Index terms**Links**

Depletion or semi-steady state	17			
Damage ratio	166	398		
Dimensionless flow capacity	375			
Dimensionless fracture conductivity	378			
Distance to water bank	472			
Damage ratio	166	398	401	409
Dimensionless interporosity transient flow parameter	368			
Dimensionless flow capacity	374			
Dimensionless fracture permeability	379			
Dimensionless fracture width	374			
Dimensionless pressure functions	477			
Drainage areas of vertical and horizontal oil wells	62			
Horizontal and vertical well drainage areas	62			

E

Example calculation

Calculating improved permeability from steady state flow equation	16
Calculating flow rate and pressure drop due to skin from steady state flow equation in a water drive reservoir	16
Calculating porosity-thickness-permeability product from pseudo steady state equation	17
Determining the time to reach pseudo steady state	20
Calculating the time to reach pseudo steady state (20- and 60-Acres spacing)	20

Index terms**Links**Example calculation (*Continued*)

Calculating pseudo skin factor in a slanted well and evaluating actual well condition	35
Calculating steady state horizontal well productivity	
Using Joshi's method	47
Using Giger method	48
Using Borisov method	48
Calculating horizontal well productivity index including effect of reservoir anisotropy	49
Calculating effective wellbore radius for horizontal well	53
Calculating horizontal well productivity for anisotropic reservoir	56
Determining the effect of vertical well damage and reservoir anisotropy on horizontal well productivity ratio	57
Estimating drainage area of horizontal well	63
Calculating pseudo steady state horizontal oil well Productivity	78
Mutalik method	79
Kuchuk method	80
Odeh and Babu method	81
Estimating the time required to end early time radial flow	
Goode and Thambynaygam's equation	93
Odeh and Babu's equation	93
Ozkan <i>et al.</i> 's equation, equation	93
Calculating the time to start and time to end early time linear flow	94

Index terms**Links**Example calculation (*Continued*)

Calculating the time required to start a pseudo radial flow	94
Analyzing late transient drawdown test	113
Analyzing single rate, single phase pressure drawdown test	117
Analyzing two rate drawdown test when initial pressure is not known	123
Analyzing two rate drawdown test when initial pressure is known	126
Analyzing variable rate pressure drawdown test assuming transient flow	130
Analyzing variable rate drawdown test using Odeh and Jones method	134
Analyzing multi rate, single phase drawdown test	139
Analyzing multi rate, multi phase drawdown test	143
Normalizing drawdown test using after flow data	149
Analyzing ideal pressure buildup test	154
Analyzing single phase and single rate pressure buildup test	162
Analyzing incomplete perforated interval	169
Analyzing partially completed damage well	171
Estimating reservoir size from two pressure buildup tests	173
Analyzing pressure buildup test	
Using Homer Plot	179
Using MBH method	180
Using MDH method	181

Index terms**Links**Example calculation (*Continued*)

Analyzing single phase and single rate buildup test	185
Analyzing single phase and single rate pressure buildup test	188
Analyzing single phase and single rate buildup test using Δp plot in finite reservoir	192
Analyzing multiphase pressure buildup test	196
Analyzing afterflow pressure buildup test using Russell's technique	200
Analyzing two rate pressure buildup test	204
Analyzing variable rate pressure buildup test	207
Analyzing multiphase, multi rate pressure buildup test	213
Normalizing afterflow rate and analyzing pressure buildup test	221
Calculating average and initial reservoir pressure from pressure buildup data	239
Using MBH method	239
Using MDH method	240
Dietz method	240
Calculating average and initial reservoir pressure in square drainage area (closed reservoir)	242
Calculating average reservoir pressure using Muskat and Arps and Smith methods	242
Estimating average drainage region pressure and from pressure buildup test	248
Analyzing pressure buildup test in naturally fractured reservoir	265

Index terms**Links**Example calculation (*Continued*)

Analyzing pressure buildup test in naturally fractured Reservoir	272
Analyzing drawdown test	
Using Ramey's type	290
Using Earlougher and Kersch type curves	300
Analyzing drawdown test using McKinley's type curves	304
Analyzing Pressure Buildup test using McKinley's type curves	308
Analyzing pressure drawdown test for vertical fractured well	318
Using Conventional method	319
Using Gringarten <i>et al.</i> 's type curves	322
Analyzing pressure buildup test for vertical fractured well	
Using Conventional method	326
Using Gringarten <i>et al.</i> 's type curve	327
Using a plot of Δp versus $\sqrt{\Delta t}$	327
Analyzing pressure drawdown rest for horizontal fractured well	332
Analyzing pressure drawdown rest for horizontal fractured well using a plot of p_{wf} versus $\sqrt{\Delta t}$	332
Pressure data analysis for pseudo radial flow	453
Analyzing single rate buildup test using pressure derivative curves	363
Analyzing Pressure drawdown test using Cinco <i>et al.</i> type curves	380
Analyzing DST test using Homer plot	405
Using Ramey, Agarwal and Martin method	410

Index terms**Links**Example calculation (*Continued*)

Using Kohlhass method	410
Analyzing DST test using Correa and Ramey's type curves	410
Analyzing reservoir rock's porosity distribution system	425
Analyzing interference test using type curve matching technique	432
Analyzing horizontal pulse test	442
Designing vertical pulse test	447
Designing pulse test using graphical method	454
Designing pulse test using analytical method	455
Analyzing pulse test using graphical method	458
Analyzing pulse test using analytical method	459
Analyzing pulse test from field data	460
Analyzing injection well test data	
Waterflood reservoir M.R. = 1.0	465
Liquid filled unit mobility ratio reservoir	471
Analyzing single pressure fall-off test data	
Liquid filled case-unit mobility ratio	477
Prior to reservoir fill-up M.R. = 1.0	483
Prior to reservoir fill-up non-mobility ratio case	488
Analyzing two-rate injectivity well test	493
Analyzing step rate injectivity test	499
Estimating distance to a no flow boundary	527
Line Source method	531
Using David and Hawkin method	531
Using Van Poollen Equation	532
Using Gray approximate method	532
Exponential integral solution method	532

Index terms**Links**Example calculation (*Continued*)

Analyzing interference test in homogeneous isotropic reservoir	542	
Analyzing interference test in homogeneous anisotropic reservoir	548	
Estimating two-dimensional reservoir permeability from vertical interference test data	557	
Calculating flowing bottom hole pressure		
Using Hagedorn and Brown method	601	
Using Beggs and Brill Method	604	
Estimating saturation (bubble point) pressure	610	
Estimating oil formation volume factor	616	
Calculating oil viscosity	620	
Calculating oil compressibility	622	
Determining oil formation volume factor	622	
Effective wellbore radius for horizontal wells	51	54
Joshi techniques	51	
Van Der Vlis <i>et al.</i> method	52	
Effect of formation damage on horizontal well productivity	54	
Estimating productivity index	55	

F

Flow regime identification	339
Fracture linear flow	339
Bilinear flow	509
Formation linear flow	341
Pseudoradial flow	346
Bilinear flow type of analysis	341

<u>Index terms</u>	<u>Links</u>				
Flow regime identification (<i>Continued</i>)					
Bilinear flow graph	350				
Bilinear flow analysis	348				
Four-layer crossflow reservoir	505				
Fault near single boundary	530				
Fault near multiple boundaries	531				
Fracture permeability					
Estimating from pressure derivative curves	362	364			
Estimating using bilinear flow theory	342	344	346	347	352
	355				
Fracture skin factor	79	355	356	357	373
	374	382	383	384	
Fracture half-length	148	315	317	319	323
	327	376	380	383	
Flow efficiency	114	118	122	130	132
	130	161	162	166	210
	212	288	304	308	312
Estimating from drawdown testing	114	118	122	130	132
	139				
Estimating from buildup testing	161	162	166	210	212
Estimating from type curve matching	288	304	308	312	
Formation flow capacity	372				
Fracture conductivity	346	347	350		
False reservoir pressure	122	124	126	128	177
	178	184	187	239	
Formation compressibility	623				
Fracture penetration ratio	72				
Flow history of an oil well	211				
Finite flow capacity vertical fracture					
Agarwall type curves-Constant pressure	374				
Cinco-Ley type curves-constant well rate	375				

Index terms**Links**

Fracture storage	274		
Fracture porosity	271	283	
Formation flow capacity	372	380	382
Formation flow capacity	372		
Fracture gradient	497		

G

Geometric parameter	447		
Gas permeability	195	198	

H

Horizontal well	84	123	
Steady state flow equations and solution	44		
Joshi's method	45		
Goger method	45		
Borisol method	45		
Renard and Dupay method	45		
Solution of unsteady state flow equations	49		
Effective wellbore radius	51		
Effect of formation damage	54		
Solution of pseudosteady state equation	60		
Shape related skin factor for vertical wells	64		
Shape factor for horizontal wells	64		
Shape factor dependent skin factor	68		
Values of dimensionless function to estimate well productivity	67		
Skin factor	64		
Calculating pseudo-steady state productivity	73		
Mutalik method	73		
Kuchuk method	75		
Odeh and Babu method	75		

Index terms**Links**

Horizontal well (<i>Continued</i>)		
Horizontal well performance	84	95
Transient flow regimes	86	
Early time radial flow	86	
Intermediate time linear flow	86	
Late time radial flow	81	
Late time linear flow	82	
Solution of flow time equation	88	
Goode equation	88	
Odeh and Babu equation	90	
Ozakan equation	92	
Pressure response equation	95	
Under pressure drawdown test	95	
Under pressure buildup test	100	
Well response and normalized pressure derivative	103	
Effect of wellbore storage	104	
Calculating effective wellbore radius		
Joshi technique	51	
Van Der Vlis <i>et al.</i> method	52	
Effect of formation damage on well productivity	54	
Investigating effect of s_v and P on well productivity ratio	59	
Influence of reservoir anisotropy on horizontal well	52	
Quadratic equation to calculate turbulence factor	69	
Hydraulic diffusivity	558	
Uniform flux	85	
Infinite-conductivity solution	85	

Index terms**Links**Hydraulic diffusivity (*Continued*)

Uniform flux solutions with wellbore			
pressure averaging	85		
Horizontal well productivity	121		
Turbulence flow	124		
Turbulence identification	125		
Skin factor for horizontal well	90	92	93
IPR calculation for horizontal well	125		
Common flow regimes	86		
Flow time equations and solutions	88		
Solution under Pressure drawdown tests	95		
Solution under Pressure buildup tests	100		
Hall correlation for formation compressibility	623		
Heterogeneous reservoir systems	523	574	
Causes of heterogeneities	524		
Linear sealing faults and barriers	524		
Estimating distance to the linear			
discontinuity	527		
Line source solution equation	531		
Davis and Hawkins's method	531		
Van pollen equation	532		
Gray's approximate equation	532		
Gray Δp equation	532		
Exponential solution	532		
Effect of lateral changes on pressure			
behavior	523		
Hydraulic diffusivity contract ratio	534		
Reservoir rock porosity distribution system			
analysis	522		
Matrix pore volumes calculation	424		
Fracture pore volume calculation	424		

Index terms**Links**

Heterogeneous reservoir systems (<i>Continued</i>)					
Partitioning coefficient estimation	424				
Well skin effects	582				
Pressure buildup analysis	425				
Use of pressure transient tests to describe reservoir heterogeneity	524				
Detecting fracture trends	536				
Procedures and guidelines	537				
Fracture orientation	536				
Approaches to detect fracture trends	540				
Homogeneous isotropic reservoir systems	540				
Interference tests	541				
Pulse tests	542				
Anisotropic reservoir systems	545				
Calculate system permeability	545				
Estimate product $\phi\mu c_i$	445	457	458	459	460
	542	566	570		
Hall plot for injection well tests	464				
Horizontal and vertical well drainage areas	62				
Horizontal well model in a fractured reservoir	279				
Hawkin's equation for estimating skin	179				
Hydraulic diffusivity	492				
I					
Injection well testing	463				
Under steady state	463				
Rate schedule and pressure responses	464				
Hall plot	464				
Water flood reservoir with M.R. = 1.0.	465				
Liquid filled unit mobility ratio reservoir	470				
Prior to reservoir fill-up unit mobility ratio	482				

Index terms**Links**Injection well testing (*Continued*)

Prior to reservoir fill-up non unit mobility ratio	488
Water and oil banks	489
Two rate injectivity test	492
Two rate injectivity test	492
Step rate injectivity test using Felsenthal method	496
Formation fracture pressure	497
Interference and pulse tests	429
Field application of interference and pulse tests	430
Pulse test analysis method-two well system	435
Horizontal pulse test and analysis	437
Kamal and Brigham techniques	437
Vertical pulse test design calculation	445
Nomenclature for vertical and pulse test	448
Pulse test designing method	453
Region for pulse testing	430
Rate schedule in pulse testing	434
Pressure responses	434
Pulse test responses	435
Pulse test analysis methods	435
Two well systems	435
Rate history and pressure response	436
Horizontal pulse test	437
Vertical pulse test design	445
Design and analysis of unequal pulses	448
Pulse test nomenclature	448
Pulse test terminology	449
Pulse test designing	453

Index terms**Links**

Interference and pulse tests (<i>Continued</i>)					
Pulse test analysis methods	457				
Infinite acting	108				
Interference test analysis	429				
Bounded systems	111				
Effect of wellbore storage and damage	287				
Estimating permeability	433				
Estimating porosity compressibility product	442	544			
Type curve matching	287				
Interporosity flow parameters	365	368			
Interporosity flow	368				
Interpreting flow tests, (<i>see</i> pressure drawdown tests)					
Interpretation of formation tester pressure buildup by Pollard-Pirson method	422				
Initial pressure	123	124	126	130	132
	180	204	206	237	240
	248	260	340	404	408
Influence of reservoir anisotropy on horizontal well	52				
Identifying flow periods in horizontal oil wells	278				
Infinite slab reservoir with slanting well	33				
Intermediate time linear flow	87				
Ideal pressure buildup graph	155				
Ideal productivity index	112	212			
Injectivity index	481				
J					
Jones <i>et al.</i> method	146	147			
Jones <i>et al.</i> Odeh method	146	147			
Joshi's method	45	47	48	49	51

Index terms**Links****K**

Kuchuk <i>et al.</i> method	75
Kumar and Ramey method	180
Kazemi method	257
Kamal and Bringam	435

L

Layered reservoirs	504				
Commingled	507				
With crossflow	505				
Line source solution	531				
Linear barriers	526				
Linear discontinuity	526				
Linear faults	526				
Linear flow period	339				
Log-log data plot	110	119	149	164	217
	227	268	279	295	298
	301	306	307	310	311
	320	323	326	327	323
Late-time radial flow (<i>see</i> Pseudoradial flow)					
Line source solution	531				
Log-log type curves for finite capacity vertical fractures, Constant wellbore pressure	288	299	306	315	316
Linear data plots					
Pressure drawdown test data plots	123	127	136	141	150
Pressure buildup data plots	189	206	209	212	217
	229	263			
Average reservoir pressure	245				
Type curve matching	296	328	334		
Drill stem test data plots	416				
Interference and pulse test data plots	443				

Index terms**Links**Linear data plots (*Continued*)

Injection well test data plots	465	497	501		
Logical well test data acquisition and analysis program	4				
Late time radial flow (pseudo-radial flow)	87				
Linear flow analysis-high conductivity fractures	384				
Late data parameter	312				
Layer fracture conductivity	509				
M					
Mathews-Brons-Hazebrook	236				
Miller-Dyes-Hutchison	237				
Muskat method	240				
Total mobility ratio	195	196	198		
Multiple-rate testing	463				
Analysis plot, slope, intercept	487	491	495		
Estimating permeability	469	470	473	477	487
	491	492	493		
Estimating skin factor	481	487	488	491	492
	496	499	502		
Estimating pressure drop across skin	469	475	481		
Radius of investigation	469				
Distance to well bank	471	471	487		
Radius of drainage	471				
Flow efficiency	471				
Injectivity index	481				
Calculate compressibility in swept zone	482				
Mobility ratio	488				
Volume of oil bank	489				
Volume of water bank	490				

Index terms**Links**

Multiple-rate testing (<i>Continued</i>)	
Fracture gradient	497
Multilayered reservoir systems	504
Classification of layered reservoir systems	551
Crossflow reservoirs	504
With crossflow	505
Without-crossflow reservoirs	506
Commingled reservoirs	507
Composite reservoir	507
Interlayered crossflow reservoirs	508
Two-layered reservoir without crossflow	512
Three layer without crossflow reservoirs	506
Four layer crossflow reservoir	505
Muskat plot characteristics	516
MDH method	516
Constant producing rate	511
Constant producing pressure	510
Determine degree of communication and types of crossflow	513
Pressure buildup behavior curve in two- layered gas reservoir	563
Factors affecting performance	520
Relative permeability	520
Pore size	520
Reservoir geometry	520
Permeability anisotropy	520
Reservoir n-layer system	521
Economic aspects	521
Most common gas well test interpretation methods	5
Major flow regimes in horizontal oil wells	86

Index terms**Links**

Methods of evaluating MHF oil wells	372	
Match of interference test data	433	
Muskat straight-line intercepts for two-layer reservoirs without cross flow	506	
Muskat plot for-layer reservoir with a permeability contrast of 2	518	
Mechanical skin factor	73	
Multiphase pressure buildup plot	197	
MDH drawdown pressure plot	237	
Muskat graph for average pressure	250	
Main characteristics of matrix block and fracture system	256	
Main characteristics and behavior of naturally fractured reservoir	260	
Mud gradient	392	
Model selection process or optimum selection	28	
Multi rate drawdown test plot	141	
MBH graph	180	
MDH graph	181	188
Muskat data plot	184	189
Multiphase pressure buildup data plot	197	
Multiphase and multi-rate pressure buildup data plot	217	
MDH dimensionless pressure for circular and square areas	237	
Main characteristics of matrix blocks and fracture systems	256	
Most common interpretation methods for naturally fractured reservoirs	259	

Index terms**Links**

Main characteristics and behavior of naturally fractured reservoirs	260	
Methods of evaluating MHF oil wells	373	
Matrix storage	274	
Matrix permeability	272	
Matrix block shape factor	369	
Mud gradient	408	
Matrix pore volume	424	
Matrix porosity	424	
Mobility ratio	488	
N		
Nomenclature	640	
No-flow barrier	342	526
Numerical models and their applications	26	
Solution of radial diffusivity equation	21	
Various dimensional flow geometry	24	
Linear flow	24	
Radial cylindrical flow	25	
Radial spherical flow	25	
Reservoir model development process	26	
Selection of numerical simulation models and their applications	27	
One-dimensional horizontal model	29	
One-dimensional dipping model	29	
Two-dimensional horizontal model	30	
Three-dimensional layered model	30	
Two-dimensional coning model	31	
Two-dimensional vertical model	31	
Three-dimensional continuous model	32	

Index terms**Links**

Numerical models and their applications (*Continued*)

Three-dimensional continuous (section)
model 32

O

Original reservoir pressure 234

One-dimensional coordinate systems 24

Linear flow 24

Radial cylindrical flow 25

Radial spherical flow 25

Oil saturation 432 554

Oil well test data acquisition, analysis, and
management 2

Oil well test analysis programs 2

Oil wells for optimum stimulation treatment 2

Odeh's equation for calculating skin factor due
to restricted entry 168

P

Pulse tests 429

Pressure buildup analysis methods 153

Single-rate 162

Two-rate test 173

Buildup following variable rate test 201

Production stimulation, (*see* stimulation)

Pseudo-steady state (finite) flow 17

Pseudo skin factor with a finite conductivity
vertical fracture 258 274 366

Pressure response in pulse test 434

Pulse test responses with flow and shut-in time 434

<u>Index terms</u>	<u>Links</u>				
Pressure derivative trends for common flow regimes	370	371			
Pressure derivative type curves	361	366	369		
Calculating interporosity flow parameter	258	259	263	265	269
	283				
Calculating ratio of matrix permeability to fracture permeability	264	258	267	271	273
Pulse test design procedure	453				
Pressure buildup for crossflow oil reservoir	505				
Pressure buildup curve for a layered reservoir system	513				
Pressure buildup behavior in a two-layer oil reservoir	520				
Porosity partition in heterogeneous porous media	424				
Partitioning coefficient estimation	427				
Procedures and guidelines to describe reservoir heterogeneity	537				
Pseudoskin factor	97	98	99	282	
Porosity-compressibility product:					
Estimating by type curve matching	293				
Estimating from interference testing	433				
Estimating from pulse testing	436				
Porosity-compressibility-thickness product:					
Estimating from interference test,					
Estimating from pulse test	445	457	458	459	460
	461				
Pressure drop due skin	123	122	124	128	132
	134	137	143	146	161
	186	193	216	398	401
	409	469			

<u>Index terms</u>	<u>Links</u>				
Pore volume	112	114	115	120	
Pseudoproducing time	163	265	326	328	338
	355	480			
Permeability:					
Estimating by type-curve matching of					
vertical oil wells	290	296	300		
Of fractured oil wells	314	317	319	323	
Estimating from drawdown testing of two-					
rate drawdown test	122				
Estimating from drawdown testing after					
short shut in	389				
Estimating from interference testing	431				
Estimating from multi-rate pressure buildup					
testing	210				
Estimating from pressure buildup testing	154	165	179	183	186
	190	193	200	204	207
	218	228	230		
Estimating from pulse testing	442	446	461		
Estimating in composite system	505				
Estimating permeability and thickness					
product	112	113	148	200	264
	268	392	482	487	566
Partial differential equations:					
One-dimensional model	24				
Linear flow	24				
Radial cylindrical flow	25				
Radial spherical flow	25				
Pressure buildup test and data	154	163	178	186	198
	194	196	201	202	205
	208	213	214	215	216
	222	223			

<u>Index terms</u>	<u>Links</u>				
Pressure buildup curves	155	156	164	165	174
	176	179	180	181	182
	184	187	188	189	193
	197	203	206	209	212
	217	223	227	229	230
	231				
Pressure drawdown test and data	118	127	131	135	140
	144	145			
Pressure drawdown curves	108	109	110	112	114
	119	120	123	127	131
	136	141	149	150	
Pressure data analysis	347				
Bilinear flow type of analysis	348				
Pressure data partially match curve for the transition period between bilinear and linear flow	350				
Pressure data exhibit a half slope line on a log-log graph	351				
Pressure data partially falling in the pseudo radial flow period	352				
Pseudo skin factor equation	168				
Calculating skin factor due to restricted entry	168				
PVT properties					
Oil PVT properties	607				
Saturation pressure	608				
Solution gas oil ratio	612				
Oil formation volume factor	613				
Total formation volume factor	616				
Oil density	616				
Oil viscosity	618				
Oil compressibility	622				

<u>Index terms</u>	<u>Links</u>				
PVT properties (<i>Continued</i>)					
Water PVT properties	624				
Gas free conditions	625	627	629	631	633
	635	637			
Gas saturated conditions	626	628	630	632	634
	636				
Pore volume	112	115	120	191	
Purpose and objective of reservoir simulation	26				
Pressure time histories for a const rate					
drawdown test	108				
Pressure buildup plot dominated by afterflow	199				
Pressure buildup curve in naturally fractured					
reservoir	258				
Pressure derivative type curves	264				
Pressure derivative applications in oil well					
testing					
Infinite-acting Homogeneous reservoir.					
Systems	361				
Fractured reservoir systems	365				
Pseudo-state interporosity flow	365				
Transient interporosity flow	368				
Pressure derivative trends for other common					
flow regimes	370				
Pore volume	17				
Productivity index	166				
Pseudo-steady state time	20	21	177	239	
Pressure drop due to skin	113	134	137	139	143
	186	187	210		
Calculating from drawdown testing	113	114	118	122	130
	132	134	137	139	
Calculating from buildup testing	186	187	210		

Index terms**Links**

Pressure chart interpretation for various testing conditions	391	
Fluid loss before packer	392	
Leak in drill pipe	392	
Leak in drill pipe	392	
Packer failed and could not be set	393	
Runaway clock. Clock spring released	393	
Tool failed to close, no buildup is obtained	393	
Effect of large seepressure. Pressure buildup during flow and buildup period	393	
Low permeability formation	393	
Gauge plugged after packer was set but before tool was opened	394	
Two-layer effects. Caused by two producing zones	394	
DST is usually too short to notice interference with today's well pacing	394	
Two tests with the same gauge	394	
Gauge gradually plugged during flow period	394	
Gauge plugged during flow and unplugged late in buildup	395	
Single test with two gauges	395	
Pressure drop through	595	
Hagedorn and Brown method	596	
Beggs and Brill method	602	
Computer flow diagram for the Beggs and Brill method	503	
Porosity estimation	410	433
Using DST Testing	410	
Using Interference testing	433	

Index terms**Links****R**

Reservoir oil flow analysis	13		
Steady state flow equation	13		
Radial flow	14		
Pseudo steady state flow	17		
Flow equations	18		
Unsteady state (transient) flow	21		
Radial diffusivity equation	21		
Various dimensionless flow geometry	24	25	
Linear flow	24		
Radial cylindrical flow	25		
Radial spherical flow	25		
Numerical models	26		
Reservoir model development process	26		
Reservoir model construction process	27		
Model solution process	28		
One-dimensional horizontal model	29		
One-dimensional dipping model	29		
Two-dimensional horizontal model	30		
Three-dimensional layered model	30		
Two-dimensional coning model	31		
Two-dimensional vertical model	31		
Three-dimensional continuous model	32		
Three-dimensional continuous (section) model	32		
Calculating pressure distribution in directional well	33		
Long time approximation	34		
Reservoir geometry	117		
Radial flow	25	86	
Rectangular drainage area	62	63	65

Index terms**Links**

Rate dependent skin factor (<i>see</i> Turbulent factor)			
Reservoir rock properties	623		
Formation compressibility	623		
Reservoir water PVT properties (<i>see</i> Water PVT properties)			
Radial cylindrical flow	25		
Radial spherical flow	25		
Reservoir system characterization flow chart	6		
Reservoir consisting of commingled zones and crossflow layers	509		
Radius of investigation	213	399	
Reservoir layer conductivity	509		
Reservoir Pressure	221	231	234
References:			
Fluid flow equations to oil systems	13		
Well testing techniques in horizontal oil wells	44		
Drawdown test analysis methods	107		
Buildup test analysis methods	153		
Type curve matching techniques	287		
Massive hydraulic fractured oil well behavior analysis	372		
Well behavior analysis by bilinear flow theory	339		
Multilayered reservoir systems	504		
Pressure behavior analysis in heterogeneous systems	523		
Field case studies	348		
Reservoir system characterization flow chart process using integrated approach	6		

<u>Index terms</u>	<u>Links</u>				
Reservoir modeling	26				
Russell after analysis plot	203				
Reservoir size	173	174			
Pressure drop due to damage	179				
Radial permeability	332	366			
Radius of investigation	117	116	409		
 S					
Selection of oil wells for optimum treatment	5				
Slider method	190				
Skin effect: <i>See</i> Skin factor					
Skin factor	52	53	54	63	71
	97	99	100	101	107
	110	113	114	118	122
	124	126	128	129	132
	133	134	137	139	142
	143	144	148	149	154
	155	160	166	167	169
	172	179	184	186	187
	191	193	195	198	201
	294	205	207	209	211
	219	220	227	228	230
	263	265	296	300	318
	322	324	327	348	362
	365	368	397	401	403
	410	413	469	475	481
	483	498	492	496	499
Estimating from DST in horizontal wells	397				
Estimating from drawdown testing in horizontal wells	112				
Estimating from buildup testing in horizontal wells	96				

<u>Index terms</u>	<u>Links</u>				
Skin factor (<i>Continued</i>)					
Estimating from drawdown testing	112	122	125	131	138
	141	143	144	148	
Estimating from buildup testing	154	159	165	179	183
	186	188	190	191	195
	198	200	204	207	209
	228	230			
Estimating by type curve matching	296	300	302	318	322
	324	327			
Shaped factor-dependent skin factor	68				
Schematic pressure time history for constant rate drawdown test	108				
Schematic late transient drawdown plot	112				
Semilog late transient analysis plot	114				
Shapes of buildup curves	174	175			
Selection of oil wells for optimum treatment	2	8			
Semilog plots					
Pressure drawdown test analysis	114	131	150		
Pressure buildup test analysis	155	165	179	182	184
	187	188	193	223	
Average reservoir pressure	244	250			
Naturally fracture reservoir	258	262	269	273	
Type curve analysis	295	321			
Bilinear flow analysis	355				
Hydraulic fractured oil well	383				
Drill stem testing	408	413	415	426	
Injection well testing	467	468	474	481	487
	491	495			
Shaped factor dependent skin factors	68				
Schematic of a horizontal well located in a rectangular drainage area	69				

Index terms**Links**

Shaped related skin factors	74				
Schematic late transient drawdown analysis plot	112				
Semilog late transient analysis plot	114				
Superposition based on logarithm of the approximation	150				
Semilog single rate buildup data pit	165				
Schematic representation of rate variation preceding a pressure buildup test	207				
Semilog type curves for early and late time data analysis	400				
Selecting proper straight-line limits	213				
Upper time limit	213				
Lower time limit	213				
Shape factor	367				
T					
Type curve matching	287				
Ramey's type curve	287				
Earlougher and Kersch type curve	289				
McKinley type curves	302				
Fracture type curves	313				
Type curve for vertical fracture well	317				
Type curve for horizontal fracture well	329				
Pressure drawdown test data for Type curve matching	284	297	305	309	319
	325	332			
Pressure drawdown test data matching curves	295	298	301	306	307
	310	311	323	326	333
Pressure derivative type curves	359				

Index terms**Links**

Type curve matching (<i>Continued</i>)			
Pressure derivative application	360		
Pressure buildup testing	361		
Pressure drawdown testing	362		
Fractured reservoir system	365		
Pseudo state interporosity flow	365		
Transient interporosity flow	368		
Pressure derivative trends	370		
Typical pressure drawdown behavior curve			
shapes for fissured reservoir	257		
Two rate drawdown test plot	127		
Technique to estimate average pressure			
Using modified Muskat method	241	244	250
Using Arps and Smith method	245		
Typical pressure drawdown behavior curves,			
shapes curves			
Using Warren and Root model	257		
Using Kazemi model	257		
Total system mobility	195	196	198
Total compressibility	195	198	212
True skin factor	179		
U			
Use of SI	577		
Unit-slope straight line	110	289	
Unit	11	577	
Units systems	577		
Unsteady-state (transient) flow	21		
Uses of interference tests in fissured and			
matrix formations	275		

<u>Index terms</u>	<u>Links</u>				
V					
Variable-rate testing: <i>See</i> Multiple-rate testing	269	283			
Vertical interference testing: <i>See</i> Interference	507				
Vertical permeability	335	336			
Vertical pulse testing	511				
Vertically fractured wells	423				
Estimating fracture length	323	324	327		
Estimating permeability	323	324	326	328	332
	335	336			
Finite-conductivity fracture	373				
Horner plot	384				
Infinite-conductivity fracture	372				
Interference testing	429				
Linear flow analysis	384				
Conventional method of analysis	382				
Pulse testing	511				
Reservoir Limit testing	511				
Type-curve matching	509				
Uniform flux fracture	416				
Estimating fracture skin factor	406	448			
Viscosity:					
Oil	618				
Water	624				
Values of dimensionless pressure as a function of dimensionless time	36				
Various methods to determine the distance to a linear discontinuity	526				
Various reservoir parameters and their uses	3				
Various pressure analysis methods to determine important reservoir parameters	7				
View of a skin near wellbore	55				

<u>Index terms</u>	<u>Links</u>				
View of fractured vertical well	65				
Variable rate drawdown test plot	131				
Variable rate-Odeh and Jones plot	136				
Various analysis techniques, their applications, and their limitations	147				
Variable-rate pressure buildup analysis plot	209				
Variable rate pressure buildup plot	212				
Various analysis techniques, their applications, and limitations	218				
Various flow periods and their identification in naturally fractured reservoirs	279				
 W					
Water PVT properties-gas free conditions	624				
Formation water compressibility	625	627	629	631	633
	635	637			
Gas solubility	625	627	629	631	633
	635	637			
Water formation volume factor	625	627	629	631	633
	635	637			
Formation water density	625	627	629	631	633
	635	637			
Density gradient	625	627	629	631	633
	635	637			
Water viscosity	625	627	629	631	633
	635	637			
Water PVT properties-gas saturated conditions	625				
Formation water compressibility	626	628	630	632	634
	636	638			
Gas solubility	626	628	630	632	634
	636	638			

<u>Index terms</u>	<u>Links</u>				
Water PVT properties-gas saturated conditions (<i>Continued</i>)					
Water formation volume factor	626	628	630	632	634
	636	638			
Formation water density	626	628	630	632	634
	636	638			
Density gradient	626	628	630	632	634
	636	638			
Wellbore damage Improvement (<i>see</i> stimulation)					
Wellbore storage	64	68	89	422	
Unit-slope straight line	109				
Wellbore storage coefficient	110	111	262	268	300
	302	349	362	365	401
	403	410			
Wellbore storage constant, (<i>see</i> wellbore storage coefficient)					
Wellbore storage effect	291				
Wellbore radius	315				
Well geometry	297				
Well test interpretation models for naturally fractured reservoirs	254				
Pseudo-steady state model	258				
Transient state model	261				
Pressure gradient models	261				
Streltsova and DeSwaan techniques	261				
Type curve matching techniques	262				
Pressure derivative method	263				
Wireline formation test data evaluation	414				
Open hole formation test	415				
Empirical interpretation charts	418	421			
Closed hole formation test	429				

Index terms**Links**Wireline formation test data evaluation (*Continued*)

Reservoir rock's porosity distribution				
system analysis	422			
Pollard plot	423			
Matrix pore volume calculation	424			
Fracture pore volume calculation	424			
Partitioning coefficient estimation	424			
Well skin effects	425			
Formation test pressure difference plot	426			
Porosity partitioning coefficient	427			
Wellbore storage and skin type curves in a				
double porosity reservoir	263			
Water permeability	195	198		
Wellbore storage constant	289	290	298	307
Wellbore storage coefficient	300	302	303	
Well transmissibility	307	311	312	
Wellbore volume	469			
Water permeability	480			